Durham University

Durham E-Theses

The effect of rotor and casing geometry on the performance of cross-flow fans.

D. J. Allen

How to cite:

Allen, D. J. (1981) The effect of rotor and casing geometry on the performance of cross-flow fans. Doctoral thesis, Durham University.

Use policy

The full-text may be used and/or reproduced, and given to third parties in any format or medium, without prior permission or charge, for personal research or study, educational, or not-for-profit purposes provided that:

- a full bibliographic reference is made to the original source
- a https://etheses.durham.ac.uk/id/eprint/953/ is made to the metadata record in Durham E-Theses
- the full-text is not changed in any way

The full-text must not be sold in any format or medium without the formal permission of the copyright holders.

Please consult the full Durham E-Theses policy for further details.

Academic Support Office, The Palatine Centre, Durham University, Stockton Road, Durham, DH1 3LE
e-mail: e-theses.admin@durham.ac.uk Tel: +44 0191 334 6107
https://etheses.durham.ac.uk

THE EFFECT OF ROTOR AND CASING GEOMETRY ON THE PERFORMANCE OF CROSS-FLOW FANS

by

David J. Allen B.Sc.

Thesis submitted for the degree of Doctor of philosophy in the faculty of science, University of Durham.

June, 1981

Durham University
SCIENCE
11 AUG 1981
SECTION
Library

The copyright of this thesis rests with the author. No quotation from it should be published without his prior written consent and information derived from it should be acknowledged.

Dedicated to my mother, Mrs M.M. Allen

and my father, Mr J.F.G. Allen.

For ever and everything.

Don't grab a leopard by the tail - but if you do
don't let go.

- AFRICAN PROVERB.

ACKNOWLEDGEMENTS

My gratitude is extended to all those who helped during the entire period of preparation of this thesis; especially Pete Watson, Mrs J K T Allen, relatives and friends.

Particular thanks are due to Dr. M J Holgate, for conceiving and supervising the project and to AIRSCREW-HOWDEN Ltd. for supporting the work.

I am indebted to the Science Research Council for financing the project, and extend my thanks to the technicians of the engineering science department and staff of the computer unit and science site library, for operating valuable services.

Dave Allen

ABSTRACT

Cross-flow fans are similar in construction to forward-curved centrifugal blowers, but they differ fundamentally from all other fan types in that the flow traverses the same blade row twice.

A blade passage experiences continually varying flow conditions through a single impeller revolution: it is this complex flow field which enables a small diameter cross-flow fan unit to achieve a high aerodynamic performance.

The fan casing geometry is important in determining the proportions of the suction and discharge arcs - and therefore governing the aerodynamic performance. Geometric parameters are defined, and extensive experimentation has determined their effect on performance. An optimum fan design must satisfy the requirements of quiet, stable and efficient operation; these three interdependent criterion are discussed in separate chapters, written with equivalent section identifiers for ease of cross-referencing.

The results presented show that a simple casing design produces the best overall performance; ranges of optimum casing geometry are indicated. A design procedure is presented which will enable the designer to produce an optimum fan design for a given duty. However, there are a relatively large number of casing design parameters and some mutual dependence between these. It is therefore suggested that a first-guess design could be further improved by finessing elements of casing design.

Analytical methods have been developed to model the impeller flow conditions and to theoretically determine the effect of casing design on the aerodynamic performance, sound power level and impeller flow field.

LIST OF CONTENTS

Heading		Page
Acknowledgements		(i)
Abstract		(ii)
List of contents		(iii)
Symbols		(x)
CHAPTER ONE		
1.1	INTRODUCTION	1
1.2	HISTORY OF THE DEVELOPMENT OF CROSS-FLOW FANS	1
	Figures	9
CHAPTER TWO		
2.1	GOAL OF THE INVESTIGATIONS	10
2.2	EXPERIMENTAL APPARATUS - THE TEST RIG	10
2.2.1	THE ROTOR UNIT	10
2.2.2	CASING AND DUCTWORK	10
2.2.2.1	THE VORTEX WALL	11
2.2.2.2	THE REAR WALL	11
2.2.2.3	THE DISCHARGE DUCTING	11
2.3	MEASUREMENT APPARATUS	11
2.4	EXPERIMENTAL PROCEDURE	12
2.4.1	SPEED MEASUREMENT	12
2.4.2	MEASUREMENT OF VOLUMETRIC FLOWRATE	12
2.4.2.1	THE PLENUM CHAMBER	12
2.4.2.2	20-POINT TRAVERSE	13
2.4.2.3	5-POINT TRAVERSE	14
2.4.3	MEASUREMENT OF STATIC PRESSURE	15
2.4.4	DETERMINATION OF AERODYNAMIC EFFICIENCY	15
2.4.4.1	METHOD OF MEASUREMENT OF APPLIED TORQUE	15
2.4.4.2	CALIBRATION OF THE UNIT	16
2.4.4.3	MEASUREMENT PROCEDURE	16
2.4.4.4	CALCULATION OF EFFICIENCY	17
2.4.5	PULSATION ANALYSIS	17
2.4.6	DETERMINATION OF SOUND POWER	18
2.4.6.1	INTRODUCTION TO NOISE MEASUREMENT	18
2.4.6.2	EXPERIMENTAL INSTALLATION	19
2.4.6.3	MEASUREMENT PROCEDURE	20
	Figures	24

Heading		Page
CHAPTER THREE		
3.1	THE ENIGMA OF THE CROSS-FLOW FAN	31
3.2	CROSS-FLOW FAN THEORY	31
3.3	DEVELOPMENT OF A FLOW MODEL	37
3.3.1	GEOMETRICAL CONSIDERATIONS	38
3.3.2	CALCULATION OF INLET RADIAL AND TANGENTIAL VELOCITIES	38
3.3.2.1	COORDINATES OF THE FAN OUTER PERIPHERY	39
3.3.2.2	CALCULATION OF FLOW FIELD RADIAL AND TANGENTIAL VELOCITIES	39
3.3.2.3	TRANSFORM OF FIELD VELOCITIES TO FAN PERIPHERAL VELOCITIES	39
3.3.3	ESTIMATION OF DISCHARGE FLOW CONDITIONS	40
3.3.4	CALCULATION OF PERFORMANCE	41
3.3.5	REAR WALL DESIGN	42
3.3.6	VORTEX LOCATION	43
3.3.6.1	TOTAL PRESSURE VARIATION	44
3.3.6.2	TANGENTIAL VELOCITY DISTRIBUTION AROUND THE CORE BOUNDARY	45
3.3.6.3	RESULTANT FORCE ON THE VORTEX CORE	45
3.3.7	EVALUATION OF THE MODEL FLOW FIELD PARAMETERS, Γ AND M	46
3.3.8	ESTIMATE OF THE MAGNITUDE OF INLET 'SHOCK' LOSSES	49
3.3.9	CONDITIONS APPROACHING ZERO FLOW	49
	Figures	51
CHAPTER FOUR		
4.1	INTRODUCTION TO SOUND PRODUCTION MECHANISMS	63
4.1.1	MONOPOLE SOURCE	63
4.1.2	DIPOLE SOURCE	63
4.1.3	QUADRUPOLE SOURCE	64
4.2	DEVELOPMENT OF FLOW-ACOUSTIC THEORY	65
4.3	THEORY OF SOUND PRODUCTION BY CROSS-FLOW FANS	68
4.3.1	DETERMINATION OF THE IMPORTANT SOUND PRODUCTION MECHANISMS	68
4.3.2	SOUND GENERATED BY BLADE LOADING	72
4.3.2.1	EXISTING THEORY	72
4.3.2.2	APPLYING THE THEORY	74
4.3.2.3	PROCEDURE FOR THE SOLUTION OF THE THEORY	75

Heading		Page
4.3.3	SOUND GENERATED BY WAKE/STATOR INTERACTION AND DISCHARGE FLOW TURBULENCE/STATOR INTERACTION	76
4.3.3.1	EXISTING THEORY	76
4.3.3.2	APPLYING THE THEORY	82
4.3.3.3	PROCEDURE FOR EVALUATION OF THE THEORY	83
4.3.4	STATOR LIFT FLUCTUATIONS CAUSED BY EDDIES SHED FROM THE BLADE TIPS	84
4.3.4.1	EXISTING THEORY	84
4.3.4.2	APPLYING THE THEORY	87
4.3.4.3	PROCEDURE FOR THE SOLUTION OF THE THEORY	88
4.3.5	POTENTIAL FIELD INTERACTION	89
4.3.5.1	EXISTING THEORY	89
4.3.5.2	APPLYING THE THEORY	93
4.3.5.3	PROCEDURE FOR THE SOLUTION OF THE THEORY	94
CHAPTER FIVE		
5.1	SOME RESULTS FROM THE PERFORMANCE AND NOISE ANALYSES, INTRODUCTION	96
5.2	GENERAL RELATIONSHIPS	98
5.2.1	VARIATION OF PERFORMANCE WITH ROTATIONAL VELOCITY	98
5.2.2	VARIATION OF PERFORMANCE WITH FLOWRATE	99
5.2.3	POWER INPUT	99
5.2.4	ENERGY TRANSFER	100
5.3	★EFFECT OF ROTOR AND CASING DESIGN ON THE THEORETICAL FLOW PATTERNS, PERFORMANCE AND NOISE CHARACTERISTICS	100
5.3.1	VORTEX WALL CLEARANCE, E	100
5.3.2	REAR WALL CIRCUMFERENTIAL ANGLE, δ	101
5.3.3	VORTEX WALL DECLINEATION, B	102
5.3.4	DIAMETER RATIO, d/D	102
5.3.5	OUTER BLADE ANGLE, β_2	102
5.3.6	BLADE NUMBER, Z	103
5.3.7	TONGUE THICKNESS, T	103
5.3.8	ARCUATE DAMPER	104
5.3.9	VARIATION OF VORTEX LOCATION	105
	Figures	106

Heading			Page
CHAPTER SIX			
6.1		INTRODUCTION TO PERFORMANCE DETERMINATION	128
6.1.1		ROTOR AND CASING DESIGN VARIABLES	128
6.1.2		DETERMINATION OF REAR WALL SHAPE	128
6.1.3		SCALING	129
6.2	★	EFFECT OF ROTOR AND CASING DESIGN ON THE AERODYNAMIC PERFORMANCE	130
6.2.1		INFLUENCE OF PRIMARY CASING DESIGN ON AERODYNAMIC PERFORMANCE	130
6.2.1.1		VORTEX WALL CLEARANCE, E	130
6.2.1.2		REAR WALL CIRCUMFERENTIAL ANGLE, δ	132
6.2.1.3		DUCT HEIGHT, H	133
6.2.1.4		VORTEX WALL DECLINEATION, B	134
6.2.1.5		DIAMETER RATIO, d/D	135
6.2.1.6		REAR WALL CLEARANCE, E_2	136
6.2.2		INFLUENCE OF NOVEL CASING DESIGN ON AERODYNAMIC PERFORMANCE	136
6.2.2.1		TONGUE THICKNESS, T	136
6.2.2.2		IRREGULAR BLADE SPACING AND SLOTTED ENDPLATES	137
6.2.2.3		INCORRECT REAR WALL DESIGN	137
6.2.2.4		SLOPING THE VORTEX WALL	137
6.2.2.5		WEDGE ANGLE, α°	138
6.2.2.6		PERFORATED VORTEX WALL	138
6.2.2.7		OUTLET DIFFUSER	139
6.2.2.8		ECK-TYPE VORTEX WALLS - AND A PLAIN WALL WITH AN ARCUATE DAMPER	140
6.2.3		MISCELLANEOUS ROTOR AND CASING DESIGN MODIFICATIONS	141
		Figures	144
CHAPTER SEVEN			
7.1		INTRODUCTION TO MECHANISMS OF INSTABILITY	167
7.1.1		STALL AND SURGE	167
7.1.2		CROSS-FLOW FAN INSTABILITY	168
7.2		PROBLEMS CAUSED BY OPERATION IN A PULSATING FLOW	170
7.3		PULSATION ANALYSIS	170
7.3.1		ANALYSIS IN THE TIME DOMAIN	171
7.3.2		ANALYSIS IN THE FREQUENCY DOMAIN	173
7.3.2.1		PERIODOGRAM	173

Heading		Page
7.3.2.2	$\hat{F}$ (w) FREQUENCY ANALYSIS	174
7.3.2.3	ACCURACY AND REPEATABILITY	174
7.4	CHARACTERISTICS OF CROSS-FLOW FAN PULSATIONS	175
7.4.1	SIGNAL COMPOSITION	175
7.4.2	DEPENDENCE OF STABILITY ON AERODYNAMIC PARAMETERS	177
7.4.2.1	DEPENDENCE UPON FLOWRATE	177
7.4.2.2	DEPENDENCE UPON EFFICIENCY	178
7.5	★EFFECT OF ROTOR AND CASING DESIGN ON THE PERCENTAGE PRESSURE PULSATIONS	178
7.5.1	INFLUENCE OF PRIMARY CASING DESIGN UPON STABILITY	178
7.5.1.1	VORTEX WALL CLEARANCE, E	178
7.5.1.2	REAR WALL CIRCUMFERENTIAL ANGLE, δ	179
7.5.1.3	DUCT HEIGHT, H	179
7.5.1.4	VORTEX WALL DECLINEATION, B	179
7.5.1.5	DIAMETER RATIO, d/D	180
7.5.1.6	REAR WALL CLEARANCE, E_2	180
7.5.2	INFLUENCE OF NOVEL CASING DESIGN ON STABILITY	180
7.5.2.1	TONGUE THICKNESS, T	180
7.5.2.2	IRREGULAR BLADE SPACING	180
7.5.2.3	INCORRECT REAR WALL DESIGN	181
7.5.2.4	SLOPING THE VORTEX WALL	181
7.5.2.5	WEDGE ANGLE, α°	181
7.5.2.6	PERFORATED VORTEX WALL	181
7.5.2.7	OUTLET DIFFUSER	182
7.5.2.8	ECK-TYPE VORTEX WALLS - AND A PLAIN WALL WITH AN ARCUATE DAMPER	182
7.6	SECONDARY CONTROL OF OPERATIONAL INSTABILITY	183
	Figures	184
CHAPTER EIGHT		
8.1	INTRODUCTION TO THE STUDY OF FAN NOISE	197
8.2	ABSTRACT OF EXISTING WORK ON CENTRIFUGAL AND CROSS-FLOW FAN NOISE	198
8.3	EFFECT OF CASING ON THE SOUND PRODUCED BY ROTATING MACHINERY	199

Heading		Page
8.4	GENERAL RELATIONSHIPS BETWEEN SOUND POWER, ROTATIONAL SPEED AND PERFORMANCE, FOR CROSS-FLOW FANS	202
8.5	★EFFECT OF VORTEX WALL LOCATION ON THE RADIATED SOUND POWER OF AN UNSHROUDED ROTOR	204
8.5.1	VARIATION WITH VORTEX WALL CLEARANCE, E	205
8.5.2	VARIATION WITH VORTEX WALL DECLINEATION, B	207
8.5.3	VARIATION WITH DIAMETER RATIO, d/D	207
8.5.4	VARIATION WITH TONGUE THICKNESS, T	207
8.6	★EFFECT OF ROTOR AND CASI NG DESIGN ON THE RADIATED SOUND POWER	208
8.6.1	INFLUENCE OF PRIMARY CASIGN DESIGN ON RADIATED SOUND POWER	209
8.6.1.1	VORTEX WALL CLEARANCE, E	209
8.6.1.2	REAR WALL CIRCUMFERENTIAL ANGLE, δ	210
8.6.1.3	DUCT HEIGHT, H	211
8.6.1.4	VORTEX WALL DECLINEATION, B	211
8.6.1.5	DIAMETER RATIO, d/D	212
8.6.1.6	REAR WALL CLEARANCE, E_2	212
8.6.2	INFLUENCE OF NOVEL CASING DESIGN ON RADIATED SOUND POWER	213
8.6.2.1	TONGUE THICKNESS, T	213
8.6.2.2	IRREGULAR BLADE SPACING	213
8.6.2.3	INCORRECT REAR WALL DESIGN	214
8.6.2.4	SLOPING THE VORTEX WALL	215
8.6.2.5	WEDGE ANGLE, α°	216
8.6.2.6	PERFORATED VORTEX WALL	216
8.6.2.7	OUTLET DIFFUSER	217
8.6.2.8	ECK-TYPE VORTEX WALLS - AND A PLAIN WALL WITH AN ARCUATE DAMPER	217
8.7	SECONDARY NOISE REDUCTION TECHNIQUES	218
Figures		219

Heading		Page
CHAPTER NINE - CONCLUSIONS		
9.1	DISCUSSION OF RESULTS	232
9.2	FAN SELECTION PROCEDURE	233
9.3	FUTURE WORK	236
REFERENCES		238 -
APPENDICES		A 1 -

SYMBOLS

a	Fourier constant.
a_o, a_n	Fourier constants.
$\bar{a}$	Mean pulse amplitude.
A	Rear wall radial cross-section.
A_n	Constant (ILBERG and SADEH).
A	Distance of forced vortex centre to blade inner periphery. (Fig 3.7)
b	Fourier constant.
b	$\frac{1}{2}$ wake spacing (HANSON).
$\bar{b}$	Mean pulse interval.
B	Vortex wall declineation.
B_n	Constant (ILBERG and SADEH).
c	Orifice plate coefficient.
c	Speed of sound.
C	Blade chord.
C_o	Fourier constant.
C_V	Stator chord.
C_L	Lift coefficient.
C_D	Coefficient of drag.
C^*	Fan flow field location parameter.
d	Orifice plate diameter.
d	Fan inner diameter.
d	Fourier coefficient.
D	Fan outer diameter.
D'	Characteristic dimension.

e	Strain.
e	Fourier constant.
E	Orifice plate expansibility factor.
E	Vortex wall clearance.
E_2	Rear wall clearance.
f	General frequency.
f_o	Lower limiting frequency.
F	Force on vortex.
F ( )	Generalised function.
F_L	Lift force/unit span.
$\hat{F}$ (w)	Truncated autocovariance function.
g ( ), G ( )	Generalised functions.
G	Typical eddy diameter.
h	Pressure drop across orifice plate.
h	Span length (Chapter 4).
h^*	Busemann correction factor.
H	Duct height.
H ( )	Generalised function.
He	Helmholtz number.
i	$\sqrt{-1}$
I	Sound intensity.
J	Integer number.
J_n	Bessel number.

k	Material torsional strength.
k	Pressure loss factor.
k_o	Fourier constant.
K	Vortex constant (m^2/s)
l_s	Spanwise correlation length for fluctuating dipoles.
L	Rotor length.
M, M^*	Sink strength, dimensionless sink strength
M	Mass of fluid within an acoustically correlated volume.
M	Real number eddies within the active volume (potential interaction).
M_c	Multiplying factor.
M_t	Blade tip Mach number.
N	Fan RPM.
N	Any number.
$\tilde{N}$	Number of blades cutting through an eddy in time G/U'r.
P, p	Pressure.
Δp, $\bar{p}$	Acoustic pressure.
$\bar{p}_o$	Reference acoustic pressure.
PWL_a	Aerodynamic sound power level.
PWL_{na}	Non-aerodynamic sound power level.
Q	Volumetric flowrate.
Q	Fluid torque.

r, R	Polar coordinate.
r	Radius of vortex core.
r_{sp}	Radius of sphere.
R	General radius.
R 1	Outer radius.
R 2	Inner radius.
R_{eff}	Effective radius.
t	Time identifier.
T	Vortex wall thickness.
T	Shaft applied torque.
T	Fluid thrust.
T	Period of rotation.
T_{ij}	Stress tensor.
Δ T	Temperature change.
T_{dw}	Dwell time.
U	Blade tip rotational velocity.
U	General instantaneous velocity.
$\bar{U}$	Time - averaged component of velocity.
U'	Fluctuating component of velocity.
U_{∞}	Mean streamwise velocity.
$\bar{U}_a$	Fluid absolute velocity.
U'_a	Ultimate discharge absolute velocity.
U_c	Eddy correction velocity.
$\bar{U}_r$	Fluid radial velocity.
U'_r	Turbulent radial correction velocity.

V	Room volume.
v	Instantaneous velocity.
V	Rotor to stator axial velocity (HANSON).
$\bar{V}$	Time - averaged component of velocity.
V'	Fluctuating component of velocity.
V_S	Shock velocity.
V (t)	Pulse form, time domain.
V (w)	Pulse form, frequency domain.
VOL	Potential interaction volume.
W	Duct width.
W	Acoustic power.
W	Rotor to stator normal velocity (HANSON).
W_0	Reference acoustic power.
W_1, W_2, W_3 and W_4	Eddy direction velocities.
W	Fluid velocity relative to the tongue.
x	Cartesian coordinate.
x'	Streamwise coordinate.
x^*	Fan flow field coordinate.
y	Cartesian coordinate.
y^*	Fan flow field coordinate.
Y	Number of stator vanes.
$\hat{Y}$	$\frac{1}{2}$ wake width (HANSON).

Z	Blade number.
Z	Orifice plate Reynolds number coefficient.
Z_{ij}	Direction of oscillation.
$Z_1 - Z_5$	Flow zones (Section 3.3).
α	Wedge angle.
α	General exponent.
α	General velocity exponent.
α	Angle of incidence (HANSON).
α	Absolute flow angle (MOORE).
$\alpha(t)$	Variation of angle of incidence with time.
β	General exponent.
β_1	Inner blade angle.
β_2, β_4	Relative flow angles (MOORE).
β_2	Outer blade angle.
$\hat{\beta}$	Relative flow angle.
γ	Sound power/vortex wall clearance exponent.
$\gamma_{\bar{U}a}$	Turbulence velocity.
Γ	Circulation.
Γ^*	Dimensionless circulation coefficient.
δ	Rear wall circumferential angle.
$\delta_{(t)}$	Variation of pulse velocity with time (HANSON).
δ_{ij}	Delta - diriac function.
ϵ	Arc angle.
ζ	Potential field circumferential angle.
ζ	Polar coordinate.

η	Efficiency of energy conversion.
η	Angle, Section 3.3.
η_{rad}	Acoustic radiation efficiency.
$\bar{\eta}$	Eddy viscosity.
θ	Angle of twist.
θ	Polar coordinate.
θ	General angle of rotation ($0 \leq \theta \leq 2\pi$).
λ	Power.
λ	Dimensionless power coefficient $\phi \psi / \eta$
λ	Wavelength.
λ	Integer blade loading harmonic number.
λ	Ultimate discharge flow angle.
$\Delta\lambda$	Sector length.
λ_o	Lower limiting wavelength.
λ_d	Discharge arc length.
λ_s	Suction arc length.
λ_{brg}	Power to overcome bearing resistance.
λ_{aero}	Aerodynamic power.
μ	Vortex core angle.
μ'	Vortex core displacement angle.
μ_c	Velocity defect (HANSON).
ν	Fluid viscosity.

Ψ	Dimensionless pressure coefficient $P/\frac{1}{2}\rho U^2$
Ψ	Polar coordinate.
$\tilde{\Psi}$	Peak to peak percentage pulsation level.
ρ	Fluid density.
σ_a	Standard deviation of pulse amplitudes.
σ_b	Standard deviation of pulse intervals.
τ	Angle, Section 3.3.
τ	Time taken for a sound wave to cross an eddy.
τ_{xz}	Turbulent shear stress in the xz plane.
ϕ	Dimensionless flow coefficient Q/LDU
ϕ	Potential function (ILBERG and SADEH).
ω	General radian frequency.
Ω	Fan rotational frequency.
Ω	Angle of action on the forced vortex, Section 3.3.
Ω	Ohms.

Subscripts

a	Absolute.
d	Discharge.
i, j	Vector directions.
i	Integer counter.
r, R	Radial.
s	Suction.
st	Static.
t	Total.
t, T	Tangential.
v	Velocity.
λ	Blade loading harmonic number.
	Integer discrete counter.

Abbreviations

BPF	Blade passing frequency. (RPM/60 x Z)
dB	Decibels.
He	Helmholtz number.
m	Metre.
Ma	Mach number. (U/c)
PWL	Sound power level.
Re	Reynolds number.
RPM	Revolutions per minute.
RPS	Revolutions per second.
Se	Sears function.
St	Strouhal number. (f/ BPF: ie f=BPF; St=1)
SPL	Sound pressure level.
s	Seconds.

upstream downstream.

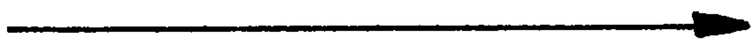

CHAPTER ONE

1.1 INTRODUCTION

The duty of a fan operating for the purposes of ventilation is to deliver a quantity of fluid at some requisite pressure head.

A cross-flow type fan consists structurally of a multi-bladed rotor, and an external casing (Figure 1.1) . When the rotor is in motion and above some threshold velocity it generates a potential vortex, with the vortex core located away from the fan axis of rotation and within the inner blade circumference. Since the vortex core is eccentrically located, zones of suction and discharge occur around the rotor periphery. This describes the principle of operation of a cross-flow fan. The existence of suction and discharge arcs implies that an element of fluid must traverse the rotor interior,and to do so must cross a single blade row twice, see Figure 1.2 .

The task of a designer is to optimise the pressure characteristics and the channelling of fluid from free space into a duct. Aerodynamic optimisation is dependent on five parameters: flowrate, static pressure rise, efficiency of energy conversion, noise and stability of operation. There may also be constraints on cost, materials, size, weight or strength.

1.2 HISTORY OF THE DEVELOPMENT OF CROSS-FLOW FANS

Early development of the cross-flow fan was carried

Durham University
SCIENCE
11 AUG 1981
SECTION
Library

out by individuals, rather than formal research establishments. Consequently, few of the results of this work are available, although the conclusions are documented in the form of patents.

A patent is sought by an inventor because it grants exclusive rights to an invention, for a limited period of time. A patent also affords protection of the 'principle' of an invention; thus, producing a structurally similar but operationally identical device, unlicensed, still constitutes an infringement of the patent laws. One necessary attribute of a patent is novelty, although this alone is insufficient. For a patent to be granted the invention has to be able to work and be manufacturable. However the more truly novel an invention the less it may be compared with functionally similar existing inventions. Thus; the viability of a conceptually new invention is not simple to assess — it may work, but work poorly.

DE-FRIES (22) reports that models built to some of these early patent specifications were noisy, of low efficiency and performance and unstable in operation.

MORTIER (55) was responsible for the first cross-flow fan patent and, therefore, for the first recognised design. He had realised that air enters and crosses the fan interior. He also noted the presence of some recirculating flùid and appreciated that in places the air speed was greater than the speed of rotation. The design of MORTIER includes inlet and discharge ducting, with a diffuser outlet to regain some of the velocity head: it also includes an

internal guide body located adjacent to the rotor inner periphery which, with the close fitting casing, is intended to reduce recirculation. The rotor has a throughgoing shaft, but no endplates; all casing is close and arc-shaped, designed to prevent leakage from high to low pressure zones.

In following years MORTIER patented other cross-flow fan designs and units incorporating them. The main use of these machines was for ventilation in european coal mines, but within fifteen years of his initial patent date they had been completely superseded by the more efficient axial machines. Axial fans had become the superior fan type because of the extensive research being done on air-screw and propeller design.

The rotor design of SCHARMJE (68) in 1910,also illustrates this secondary influence of a current popular technology on other technologies. His 60-bladed impeller included 12 blades of aerofoil profile; these having the shape of a wing section as used in powered flight. SCHARMJE also mentions that flow traverses the impeller interior, and may have included this factor in his decision to remove all internal fittings — except the solid shaft. His patent of 1914 (69) is for a draught inducer and makes no reference to his rotor design.

In 1923, the Frenchman PRAT (64) filed a patent for a cross-flow fan draught inducer, basing his claim for good operation on the fact that the air travels almost straight through the rotor, with little or no deflection. His work added little to the existing technology, indeed his fan

includes the internal body favoured by another Frenchman, MORTIER. However, the internal body of PRAT could be rotated about the driveshaft and used as a arcuate damper; the casing was, again, close fitting.

There subsequently followed a number of machine designs employing cross-flow fans, each designed for application in a particular branch of engineering. For example; DALIN (19), in 1927, patented a machine for drying grain and six years later in the U.S.A. BUCK(11) developed a machine for feeding pulverised fuel to a burner. The rotor design of BUCK was itself patented three years later in 1936 (12). Both the rotors of DALIN and BUCK incorporated approximately radial blades to avoid growth of particulate matter. DALIN incorporated a recirculation channel on the vortex wall side of the fan. He had not, though, recognised the nature of the flow field, but included the channel to even the discharge velocity profile and ' improve the efficiency of the machine '.

ANDERSON, in the U.S.A. , assessed accurately the principal attributes of cross-flow fans, and between 1929 and 1933 was granted a number of patents, see for example (2), (3), (4) and (5). At this time he was employed by a large engineering corporation and would have presumably have had access to the relevant preceeding patents. His early designs were based on engineering practicality and the need to design an easily manufactured unit. Thus; he removed all internal fittings and increased running clearances. The internal shaft was retained for strength and to enable a cross-flow blower to be made from existing

forward-curved impellers, so eliminating the high tooling costs of a new product. By the time of his final patent ANDERSON had made some significant advances in the machine design. He recognised the region of recirculation, although he thought this to be approximately oblong in shape. The rear-wall now diverged towards the discharge ducting, and the vortex wall clearance had been increased.

ANDERSON suggested many applications for these fans, applications which employed their advantages of size and shape. In particular; their ability to change flow direction, be of any shape and produce a straight airstream was thought to be ideal for draught induction, air heating and drying applications. Nevertheless, there is no record of any of these designs being widely employed, preference would have been given to the more efficient centrifugal fans.

The relative importance of scientist and engineer in the development of new equipment depends primarily on the nature of the task and the stage of development. It is clear, though, that a successful enterprise will require both the conceptual skills of a scientist plus a judicious appraisal of the constructional difficulties. The first patent was granted in 1893, it was not until 1938 that the first cross-flow fan performance characteristics were published by an academic research institute.

In 1937 SPRENGER, when a student in Zurich, considered the problem of cross-flow blowers and aimed to improve upon the design of MORTIER. Using water-table flow-vis-

ualisation experiments SPRENGER discovered the existence of a free vortex. Having recognised the mechanism of the vortex, his improvements to the MORTIER fan were to remove all internal fittings, including the shaft, and to include a gradually diverging rear wall profile. The result of these modifications was improved efficiency, flow rate , pressure rise and noise level. SPRENGER concluded that if substantial further improvements were to be made the vortex would have to be stabilised. This was the legacy of SPRENGER, the number of beneficiaries being unfortunately limited as his results were not widely circulated outside his institute.

By 1950 ECK, working in Cologne, and DE-FRIES, of the same institute, had taken an interest in cross-flow blowers (it was ECK who introduced the term ' cross-flow '). A model was constructed which had no external casing, but relied on an internal guide to stabilise the vortex; this model included a number of internal bodies. The idea was sold to a West German company, giving these fans their first practical application since the turn of the century. ECK published an article on this fan type in 1952, in his comprehensive text on fans (23,second edition onwards). An American patent was filed in 1955, for a fan with re-movable guide vanes (25). Meanwhile, in Europe, he was developing a more marketable unit.

Because of the accelerated flow induced by the vortex, cross-flow fans operate with higher fluid velocities than conventional fans at the same rotational velocity; this makes them relatively more effective in size-restricted applications. There are obvious disadvantages in constr-

ucting a fan with internal guide bodies, not only directly by increasing manufacture costs but indirectly, by reducing tolerances on rotor alignment. This is especially evident in the small, cheap fan unit market; where cross-flow fans find their predominant application.

By combining the dual requirements of innovative skill and workshop pragmatism, ECK and LAING developed an efficient cross-flow blower, ideal for use in low Reynolds number applications and cheap to manufacture through the absence of any filler bodies and the larger running clearances. Following substantial performance evaluation and flow - visualisation work, ECK established that the vortex could be stabilised by sloping a shaped vortex wall in the direction of rotation — producing a convergent 'nozzle'. The vortex itself acts as an aerodynamic seal, preventing leakage from the higher pressure discharge side. A shaped rear wall was fitted which had a relatively large radial clearance from the impeller outer periphery, the precise shape of this wall would have been determined by analysis and experiment. Increasing both the rear wall and vortex wall clearances also had the advantage of making the fan quieter.

It is this increased vortex wall gap and the profiled shape of the vortex wall which distinguishes the ECK fan from those of his predecessors. The design was patented in 1954 (24). BUSH(13) is of the opinion that, as a direct result of the work by ECK, cross-flow rotors are established for applications requiring impeller diameters of 62.5 mm or less.

Subsequent patents of interest include those of COESTER (15) and DATWYLER(20),(who was a graduate of the same institute as SPRENGER). DATWYLER produced a fan with a deep rear wall which ' allows the vortex to stabilise itself within the ducting '. COESTER attempted to produce a mathematical model of the flow through a cross-flow fan, which he based on the twin vortex model. His designs aim to strengthen and stabilise these analytical vortices by physically incorporating recirculation passages. Most of the more recent innovation has been in vortex wall design , well illustrated in the block patent of FIRTH-CLEVELAND(28), or in equipment utilising their unique behaviour, for example BENNINGER(7) and HEINE-GELDERN.(36).

Industry has tended to avoid the more complex units such as those of COESTER. Presently the ECK unit is unsurpassed as a viable module and prospective manufacturers await the expiry of his original and re-issued patents.

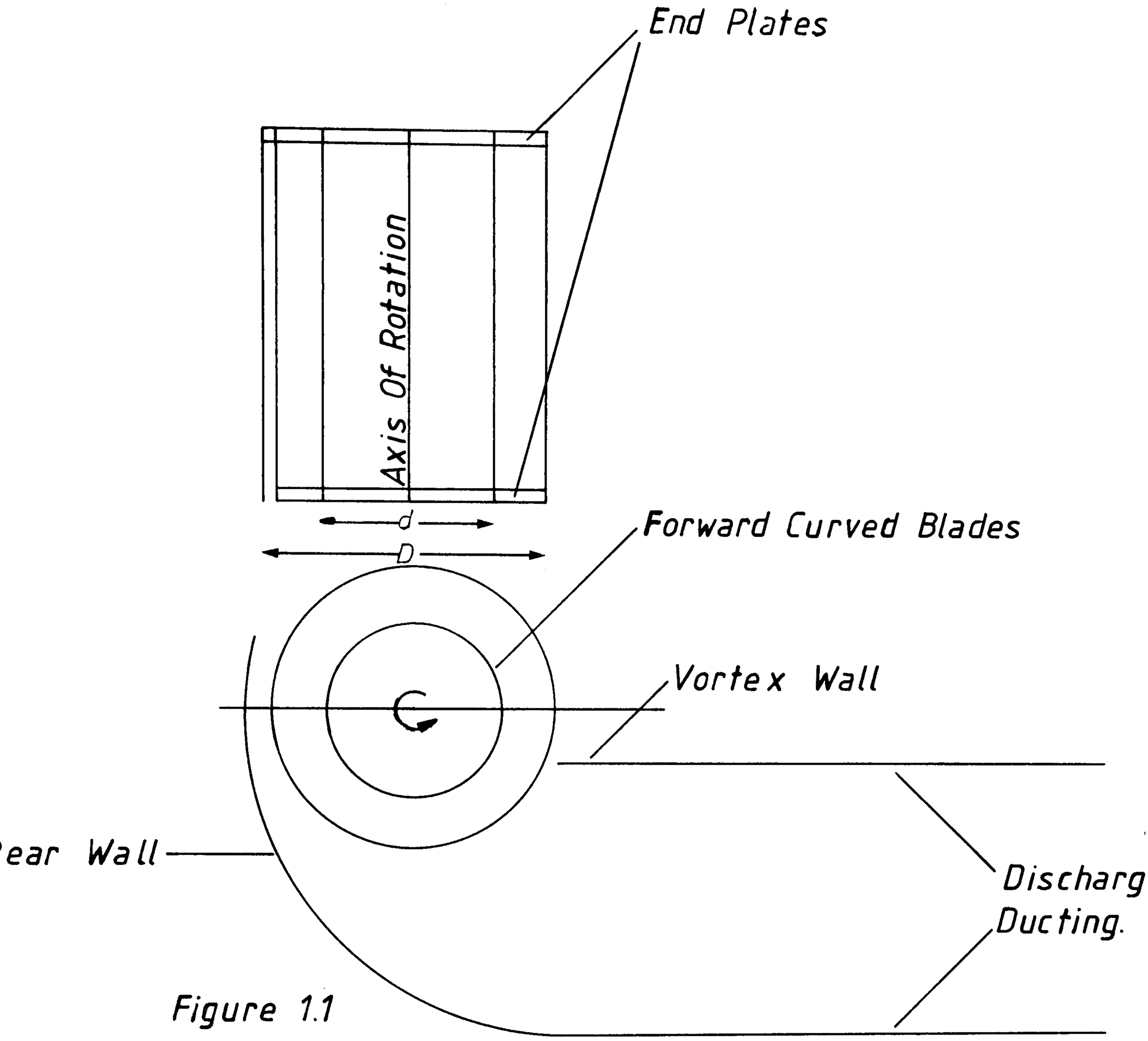

Figure 1.1

GENERAL ARRANGEMENT OF A CROSS-FLOW FAN.

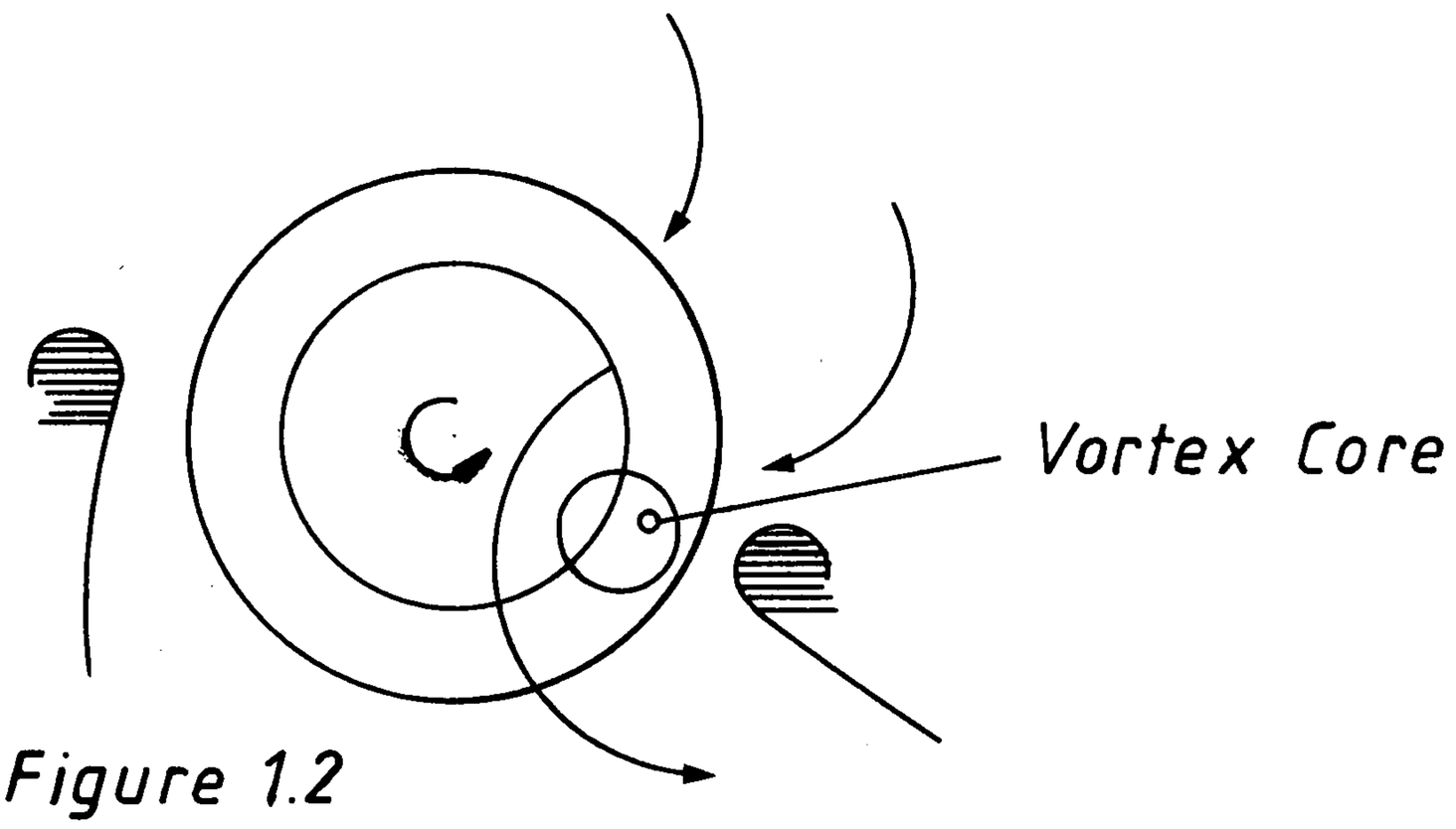

Figure 1.2

FLOW THROUGH A CROSS-FLOW FAN.

CHAPTER TWO

2.1 GOAL OF THE INVESTIGATIONS

The aim of this project is to determine the dependence of cross-flow fan performance on aspects of casing design. In order to do this a rotor and connected ductwork were built which enabled a wide range of fan designs to be tested.

For each fan configuration a complete performance test, aimed at determining volumetric flowrate, pressure head, aerodynamic efficiency, noise and stability, was made.

2.2 EXPERIMENTAL APPARATUS - THE TEST RIG

2.2.1 THE ROTOR UNIT

Figure 2.1 depicts the general rotor/drive arrangement. The rotor has been designed to enable fans of different diameter ratios to be tested. The end-plates are slotted (Figure 2.2) to enable the blades and blade fixings (Figure 2.3a and 2.3b) to move radially, but remain at a constant stagger angle.

The whole rotor may be removed from the drive system by uncoupling two plane-faced flanges. This allows variation of blade number and blade type if required. The rotor length is 320mm and the slotted end-plates enable the fan diameter to vary from 95mm to 195mm. There are 24 blades on the rotor, of a design shown in Figure 2.3c. The end-plate slots are sealed when the fan is operating.

2.2.2 CASING AND DUCTWORK

Figure 2.4 shows the composite features of the casing and discharge ducting.

2.2.2.1 THE VORTEX WALL

The vortex wall module is made of perspex and is slotted vertically to allow movement of the vortex wall and of the duct 'transition' piece. These slots also enable sloping of the vortex wall and make possible the use of more than a single vortex wall. A vortex wall support allows horizontal movement of the tongue and the attachment of various tongue types.

2.2.2.2 THE REAR WALL

The rear wall is laminated, made of 1.5mm gauge wooden slats. It is formed to shape by modelling from a template and the stepped finish smoothed by covering with plastic film.

Before construction of this unit a similar variable profile design was tested on another cross-flow fan. The result is shown in Figure 2.5, indicating a small decrease in performance using the variable wall but no change in the overall shape of the curves.

2.2.2.3 THE DISCHARGE DUCTING

Approximately 750mm of wooden ducting is placed downstream of the vortex wall. The duct height and shape may be varied to provide a smoothe transition from the vortex wall module. This discharge ducting may be connected to an outlet plenum/ diffuser unit, as represented in Figure 2.6.

2.3 MEASUREMENT APPARATUS

All pressure tappings used in the ductwork are of 2 mm internal bore and fit flush with the duct internal surface.

The manometers used for pressure measurement are sensitive

silicon-oil filled micromanometers; the vernier scale enables reading to 0.01mm. Problems in reading these manometers occur only when the flow is pulsing severely.

Pitot-static tubes used in the velocity traverses are commercially available types and satisfy the relevant British Standard requirements.

All other equipment discussed will be mentioned in the context of the experimental procedure.

2.4 EXPERIMENTAL PROCEDURE

2.4.1 SPEED MEASUREMENT

Speed is measured using a hand tachometer. Speed fluctuations are not generally large and the method itself is accurate, the overall speed measurement error is considered to be within 1% of the true value.

2.4.2 MEASUREMENT OF THE VOLUMETRIC FLOWRATE

There are three different methods adopted to determine volumetric flowrate. Lower flowrates are found using a plenum chamber on outlet (Figure 2.6) , this is removed and a full 20-point traverse is made in the ducting. One other 20-point traverse is made at the highest flowrate and between these two full traverses two 5-point traverses are made.

2.4.2.1 THE PLENUM CHAMBER

The plenum chamber is cubic, each dimension being 1.2m. The enclosed volume is sufficient to ensure negligible flow velocity within the chamber, and negligible dynamic pressure. Located in opposite walls of the plenum chamber are two orifice plates of 139.7mm internal diameter, these are made

of mild steel and manufactured to B.S. specifications of smootheness, flatness and paralellity, see Figure 2.6. There are no walls or obstructions closer than 4 x 139.7mm and no downstream piping - the system satisfies B.S 1042 (part one) for an orifice plate separating two infinitely large spaces. The plenum chamber may be used with one or two active orifice plates.

Flowrate is related to the pressure drop across the orifice plates by the following formula:

$$Q = 0.01252\ C\ Z\ E\ d^2 \sqrt{\frac{h}{\rho}} \qquad 2.1$$

Q = Volumetric Flowrate (m^3/s)

h = Pressure drop across orifice plates (mm H_2O)

ρ = Density of fluid (kg/m^3)

Z = f(Reynolds Number)

The lower limiting Reynolds Numbers occur at ϕ-values of 0.2 - 0.3 with two active orifice plates and 0.1 - 0.15 with one active orifice plate, depending on performance and fan rotational velocity. Above these values the correction for Reynolds Number is small, leading to an error of the order of 0.6% if Z is assumed to be unity.

For Z=1 equation 2.1 reduces to:

$$Q = 0.08090 \sqrt{\frac{h}{\rho}} \quad \text{for two orifice plates} \qquad 2.2a$$

$$\text{and } Q = 0.04045 \sqrt{\frac{h}{\rho}} \quad \text{for one active orifice plate.} \qquad 2.2b$$

2.4.2.2 20-POINT TRAVERSE

At a section about 620mm upstream of the vortex wall edge, two 20-point velocity pressure traverses are made on a regular grid. The velocity at each point is related

to the velocity pressure by equation 2.3

$$V = \sqrt{\frac{2\ P_v}{\rho}} \qquad 2.3$$

V = Ducted air velocity

p_v= Point velocity pressure

W = Duct width

H = Duct height

The mean velocity is the arithmetic mean of the point velocities (equation 2.4). The volumetric flowrate is given by equation 2.5.

$$\bar{V} = \frac{1}{20} (V_1 + V_2 + ... + V_{20}) \qquad 2.4$$

$$Q = \bar{V} \times W \times H \qquad 2.5$$

Statistical analysis of the 20-point traverse method, using spatially-dependant, regionalised variable theory, shows the measurement error to be less than $\pm$ 3% - within 90% confidence limits.

A comparison of a 20-point traverse and a 30-point traverse showed that the difference between estimates is small. This result indicates that the velocities are quite regular until very close to the duct walls, and that the error estimate of 3% is tenable.

2.4.2.3 5-POINT TRAVERSE

Between full traverses, two 5-point traverse approximations to the 20-point traverses are made. The mean velocity is approximated by equation 2.6.

$$\bar{V} = \bar{V}_5 \times M_c \qquad 2.6$$

$\bar{V}_5$= Mean velocity value from a 5-point traverse

M_c= Multiplying factor

M_c values are determined exactly at the two full-traverses, a ϕ-weighted interpolation procedure is adopted to approximate the M_c value for each 5-point traverse. M_c values are found to be consistent with with flowrate and independent of rear-wall shape.

A maximum error using this restricted traverse procedure is about 5.25% above the full traverse error. Consequently the method is used sparingly and not at salient points on the pressure characteristic. The location of the 20 points and 5 points within the duct are indicated in Figure 2.7.

2.4.3 MEASUREMENT OF STATIC PRESSURE

Static pressure is measured with a piezometer ring of four tappings, placed approximately 620mm upstream of the vortex wall tip. One limb of the manometer measures the atmospheric static pressure, yielding a pressure result independent of this value.

2.4.4 DETERMINATION OF AERODYNAMIC EFFICIENCY

2.4.4.1 METHOD OF MEASUREMENT OF APPLIED TORQUE

Torque in the driving shaft was determined by measuring the angle of twist in that shaft. These two variables are related by equation 2.7

$$T = k \times \theta \qquad 2.7$$

T = Applied torque

k = Function of material properties and machine design

θ = Angle of twist

The angle of twist was measured as a strain by using a full-bridge strain gauge circuit. Two gauges were mounted diametrically opposite each other on an unobstructed length of shaft, supported between two bearings.

A 'null-balance' reading system was adopted, the gauge signal being transmitted through an I.D.M. 8-channel slip-ring to a PEEKEL electronic strain indicator (type B103U). The minimum gauge lead resistance was found to be 200MΩ, it is considered that a resistance of at least 1MΩ is required for good results. The PEEKEL indicator needs to be zeroed before use, results are read directly in micro-strain (μe).

2.4.4.2 CALIBRATION OF THE UNIT

The rotor/shaft system as depicted in Fig 2.1 was calibrated in its assembled form. Using a torque arm manufactured within the department, a known torque was applied to the unit and the corresponding micro-strain equivalent read from the strain indicator. The resulting calibration chart is shown in Figure 2.8.

2.4.4.3 MEASUREMENT PROCEDURE

Due to shaft misalignment, there is some residual strain within the shaft; this causes the zero-torque micro-strain to vary sinusoidally with shaft angle. Zeroing the unit before and after a series of measurements requires, therefore, a polar plot of micro-strains.

There is also a zero-drift between commencing and completing a run, and because of this the torque measurements are taken before the measurements of pressure and flowrate. This keeps drift to a minimum and allows an elementary linear correction to be applied to the results.

At each predetermined throttle setting a microstrain reading is taken simultaneously with the speed of rotation.

The micro-strain result is converted to a torque equivalent by reference to the calibration chart.

2.4.4.4 CALCULATION OF EFFICIENCY

Total efficiency is related to the impeller power input by equation 2.8:

$$\eta_t = \frac{Q\, p_t}{\lambda_{aero}} \qquad 2.8$$

$$\lambda_{aero} = \lambda_t - \lambda_B \qquad 2.9$$

η_t = Total efficiency

Q = Volumetric flowrate (m^3/s)

p_t = Total pressure rise (Pa)

λ_t = Total power input (Watts)

λ_B = Power required to overcome bearing resistance

λ_{aero} = Power delivered to rotor

(λ_B is determined by experiment)

Measurement of efficiency is, as equation 2.8 indicates, vulnerable to an accumulation of errors. The exact accuracy depends upon the accuracy with which pressure and flowrate is determined.

2.4.5 PULSATION ANALYSIS

Any fan is subject to flow instability, generally due to separation and stall or an unequal peripheral pressure distribution. These are, apart from surge, high frequency pulsations, of the order of the fundamental blade passing frequency. Cross-flow fans are also subject to these instabilities, but they are superimposed upon high amplitude, low frequency pulsations due to vortex instability. The

pulsations must, to a varying degree, exist throughout the characteristic, and must be taken into account when designing a unit.

To quantify these; pulsing static pressures, at chosen flowrates, were converted to an analogue electrical output by a FURNESS micromanometer and fed to an X - Y plotter. The resulting trace was analysed in either the time-domain or the frequency-domain; see section 7.3..

Errors occur when the trace analysed is not representative or repeatable; a fairly large scan time (approx. 25s) was generally used. All results are taken at the same rotational speed or, for one fan diameter, the same rotational frequency. In this latter case, any bogus system resonances would be identified in the frequency plots as a constant feature. No such resonances were detected. Digitising of the trace results only in high frequency errors - well above the frequencies of interest. Also, the scan times used are small enough that the Nyquist frequency is well above prevalent pulsations frequencies.

2.4.6 DETERMINATION OF SOUND POWER

2.4.6.1 INTRODUCTION TO NOISE MEASUREMENT

Sound power is a fundamental property of any machine, it is independent of the location of the observer. Many attempts have been made to define a functional relationship between sound and fan operating characteristics (pressure, flowrate,power input, etc;). Although a similarity is evident for fans of the same type, the formulae derived are largely empirical and of little use to the designer. These will be discussed further in Chapter 8.

Sound is composed of pressure waves, emanating uniformly from a source. The unit of pressure is the Pascal, but it is convenient to express sound pressure and sound power on logarithmic scales.

$$PWL = 10 \log_{10}(W/W_0) \qquad 2.10$$

$$SPL = 20 \log_{10}(P/P_0) \qquad 2.11$$

PWL = Sound power level (dB)

SPL = Sound pressure level (dB)

$\bar{P}$ = Acoustic pressure

$\bar{P}_0$= Reference acoustic pressure

W = Acoustic power

W_0= Reference acoustic power

Reference pressure and power levels are standardised as those on the threshold of human hearing capability.

2.4.6.2 EXPERIMENTAL INSTALLATION

The acoustic measurements were taken in a chamber of high reflectivity and with a relatively diffuse sound field. Sound waves impingeing on the thick brickwork walls and concrete roof and floor are reflected back at various incidences, governed by the irregular shape of the room, see Figure 2.9.

If a room is small there is a danger of setting up standing waves, where the sound pressure will vary between node and antinode. The following empirical formula, suggested in the manual edited by BROCH(9), estimates the lower limiting central frequency.

$$V \geq 3 \times \lambda_0^3 \qquad 2.12$$

$$f_0 = C/\lambda_0 \qquad 2.13$$

V = Room volume (approx. $28m^3$)

λ_0= Wavelength of the central frequency of the lowest single octave band which may be accurately measured

C = Speed of sound (approx. 343m/s)

This gives a limiting centre frequency of:

$f_0 = 343/(28/3)^{\frac{1}{3}} = 163$ Hz

The BPF is, therefore, kept within or above the octave band centred at 250 Hz. The 250 Hz octave has lower and upper cut-off frequencies of 177Hz and 354Hz respectively.

To ascertain the diffuseness of the test chamber, a small centrifugal fan was placed in the chamber and used as a sound source. The fan spectrum was analysed in 22 1/3 octave bands (63Hz to 8000Hz), at 20 positions within the chamber. Between 177Hz and 250Hz the maximum spread of results decreased from 12 dB to 6dB, above 250Hz the spread was consistently within the permissible limit for a reverberant chamber (6dB between extreme values). Also, certain areas of the room were found to give spurious results; these zones were avoided when measuring noise.

2.4.6.3 MEASUREMENT PROCEDURE

Acoustic tests were performed using a BRUEL + KJAER sound power source (type 4205), connected to a loudspeaker unit (type HP1001). Sound pressure measurement involved single octave analysis using a BRUEL + KJAER sound level meter (type 2209), ½" condenser microphone (type 4133) and a single octave filter (type 1613). A full description of the operation of the 4205/HP1001 system is given in the manual, reference(10).

The particular test procedure adopted was determined by the twin facts that the fan may be stopped, but not altogether removed from the room. The method used was alternation and comparison, the second most accurate of the six alternative procedures, see reference (10).

The fan is run at some predetermined speed and flowrate. In a diffuse part of the sound field a single octave frequency analysis is made of the resultant sound pressure. The machine is then stopped, and the discharge ductwork removed. The loudspeaker is placed on a hard, reflecting base close to the rotor, giving it similar acoustic dispersion qualities to the fan. The sound power level in a particular octave band is adjusted on the sound power source until the sound pressure reading on the 2209 is the same as was originally determined. Sound power is then read directly from the meter on the facia of the 4205.

Noise testing is only performed when no other machines are operating in the vicinity of the measurement chamber. No correction is made for changes in air density, a simplification causing an extreme error of < 0.2 dB.

In determining the noise output, we are concerned only with the aerodynamic noise. Non-aerodynamic noise sources include motor hum, drive-belt slap and bearing noise. All casing components are made as stiff as possible so as not to vibrate and produce significant sound radiation. This non-aerodynamic sound power was determined by covering the rotor to prevent throughflow and running the fan at different speeds - the sound power was found to increase approximately as the

square of the rotor speed, for all frequencies.

The following equations outline the corrections adopted, such that only aerodynamic noise (PWL_a) was dealt with:

$$PWL_a = PWL_t - PWL_{na} \qquad 2.14$$

$$PWL_{na} = Ma^2 \times g(\hat{st}) \qquad 2.15$$

$$\hat{st} = f\ 60/N \qquad 2.16$$

$\hat{st}$ = Rotor Strouhal number. (freq./(RPM/60))

f = any frequency

N = Revolutions/minute

g = Generalised function

PWL_t = Total,measured sound power

PWL_a = Aerodynamic sound power

PWL_{na} =Non-aerodynamic sound power

$g(\hat{st})$ is assumed broad-band and has been determined experimentally. The resultant PWL_{na} - $g(\hat{st})$ relationship is approximated by a ninth-order polynomial, such that it may be incorporated in a computer program which solves equation 2.14. It is considered that the assessment of aerodynamic noise will be subject to large error when the total sound power is not 3dB above the non-aerodynamic sound power level: in this case the results are disregarded. However, the non-aerodynamic noise is relatively low and this latter condition occured only infrequently, and only with an uncased rotor. Non-aerodynamic noise was always negligible with cased rotors.

Motor noise is low frequency in nature and found to be comparitively small. No correction is made for the sound power output from a motor under load.

The largest source of error occurs when the machine sound power level fluctuates with time. However, all pre-

cautions are taken to ensure accuracy and repeatability of measurements. Although there may be inconsistencies at the lowest octave band, the overall estimate of the measurement error in all other octaves is $\pm$ 3dB.

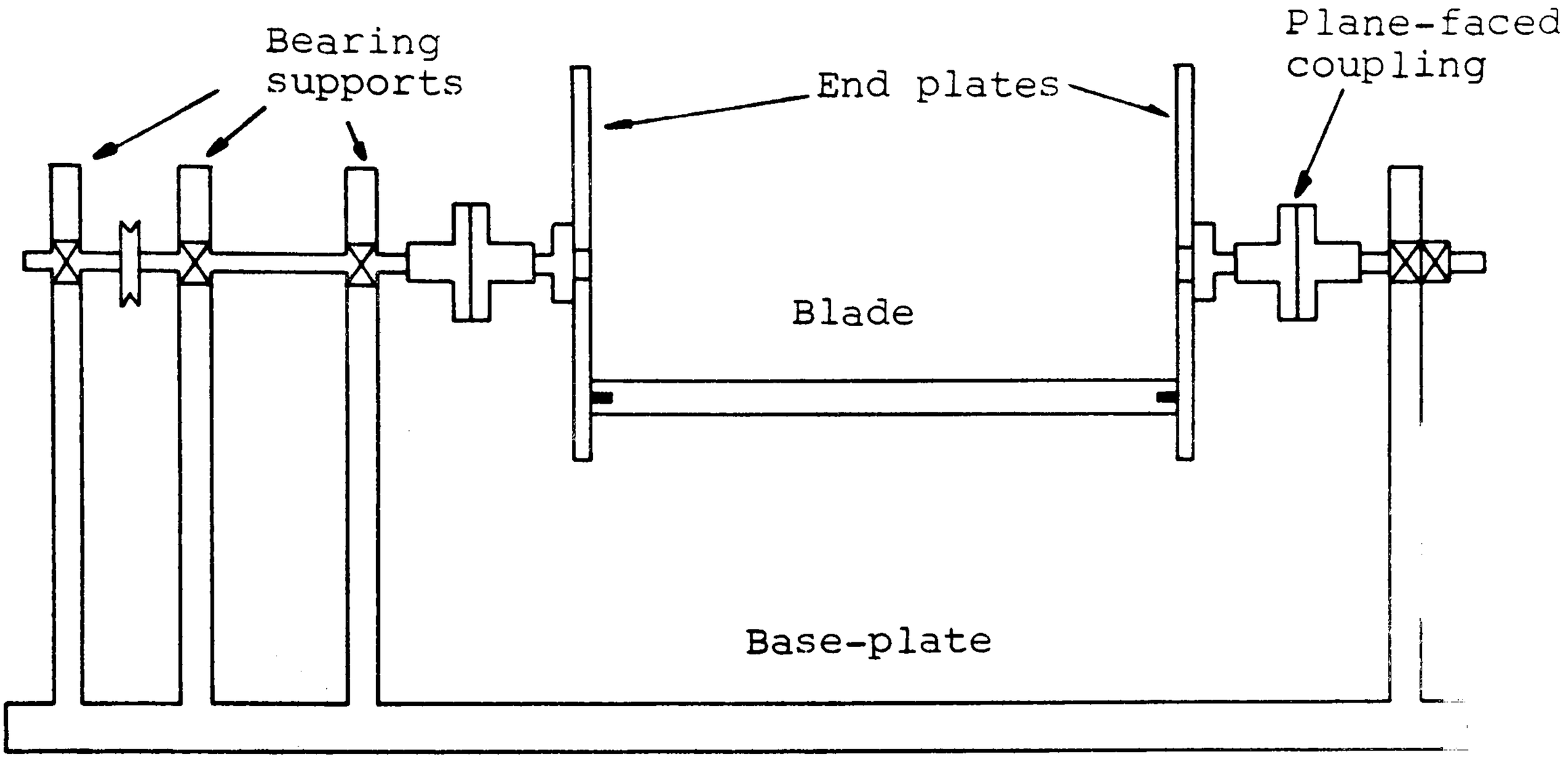

Figure 2·1 General arrangement of test rig

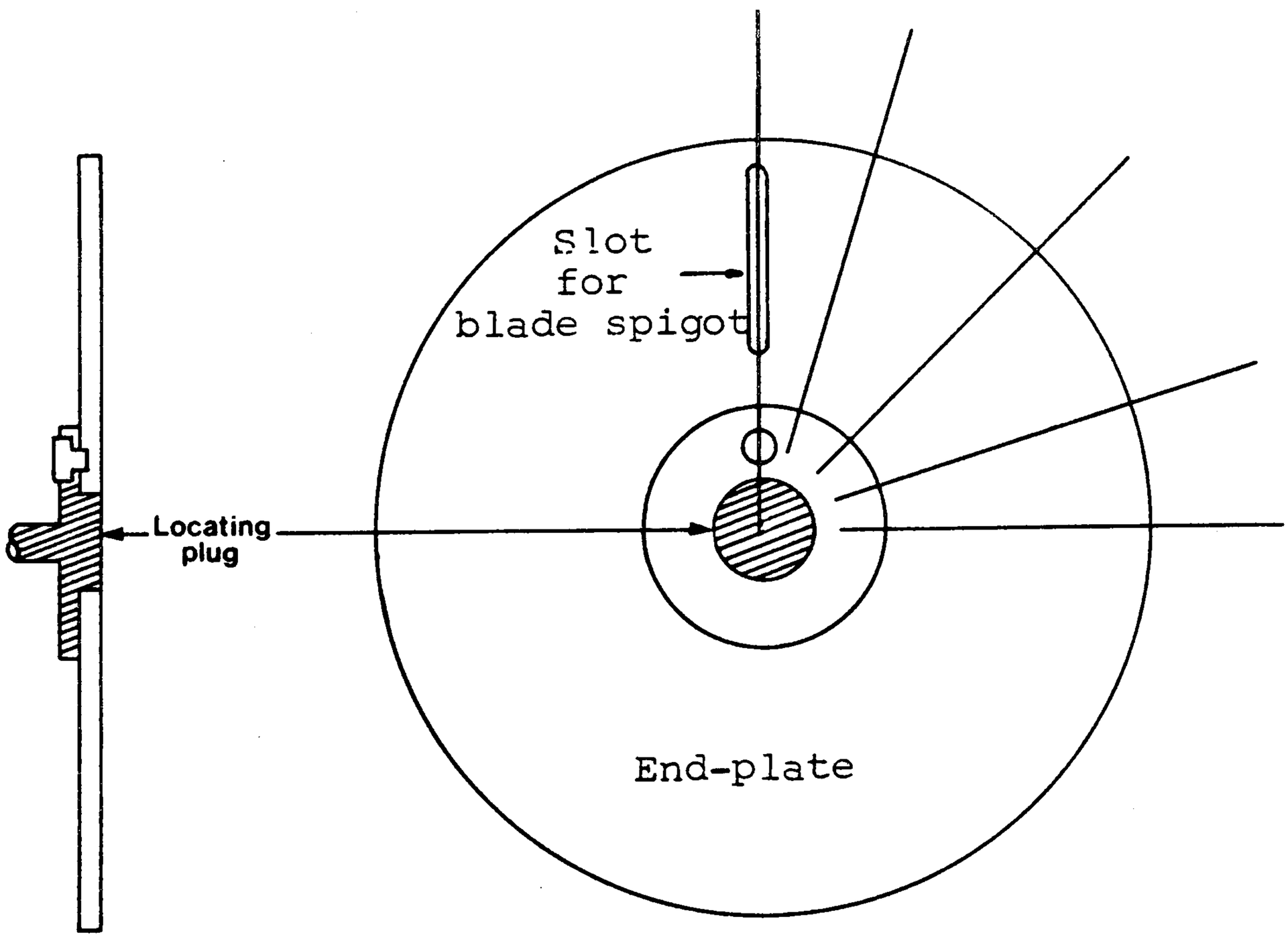

Figure 2·2 Side plate

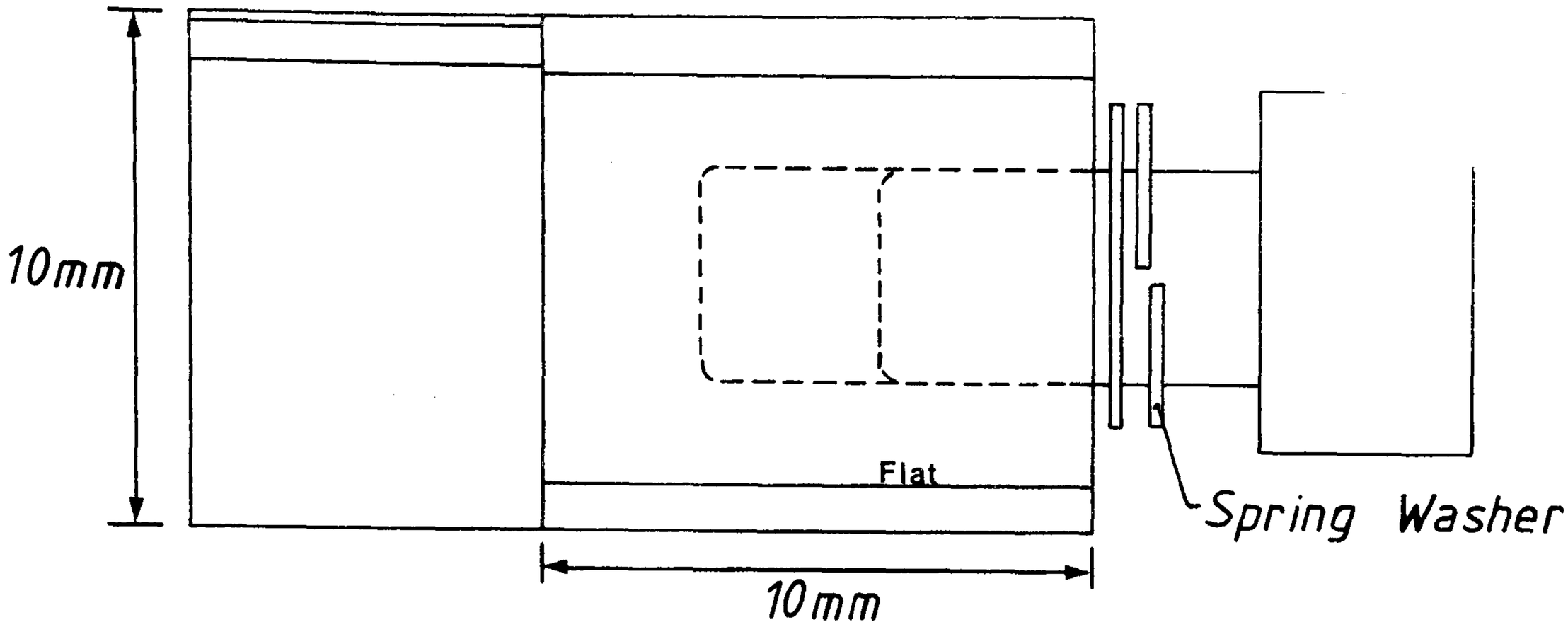

Figure 2.3a

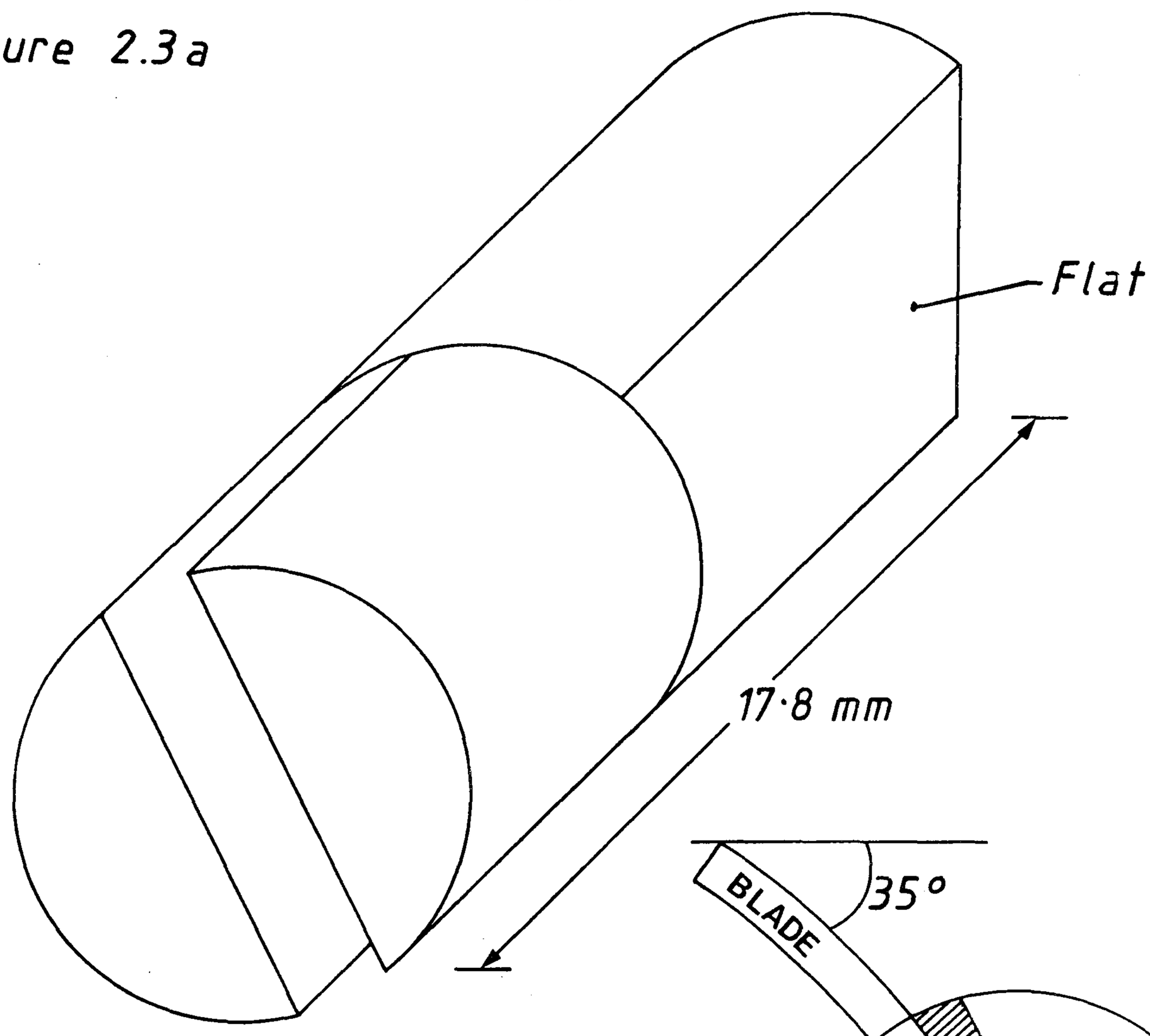

Figure 2.3 b

Blade Location Spigot

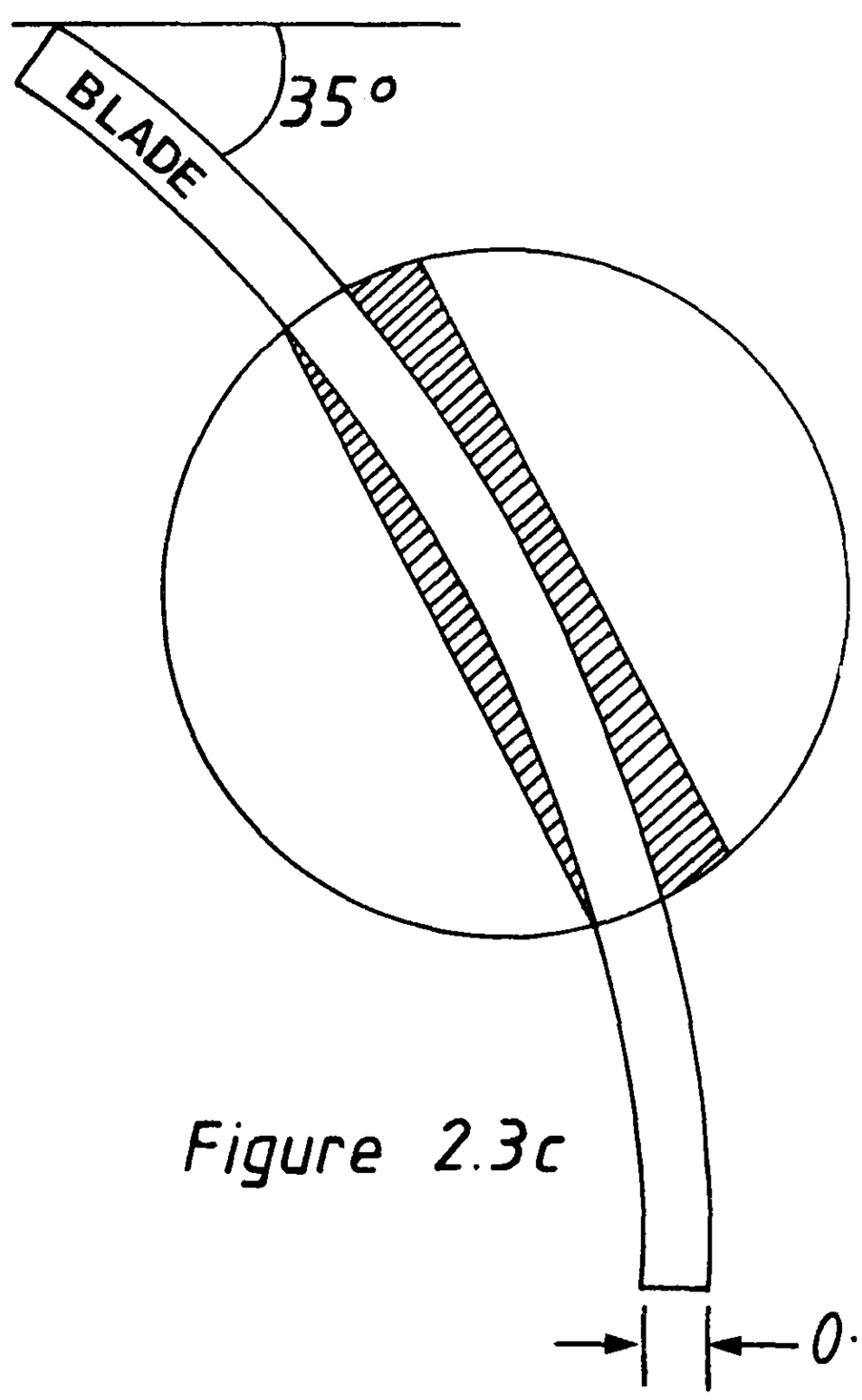

Figure 2.3c

BLADE DETAILS.

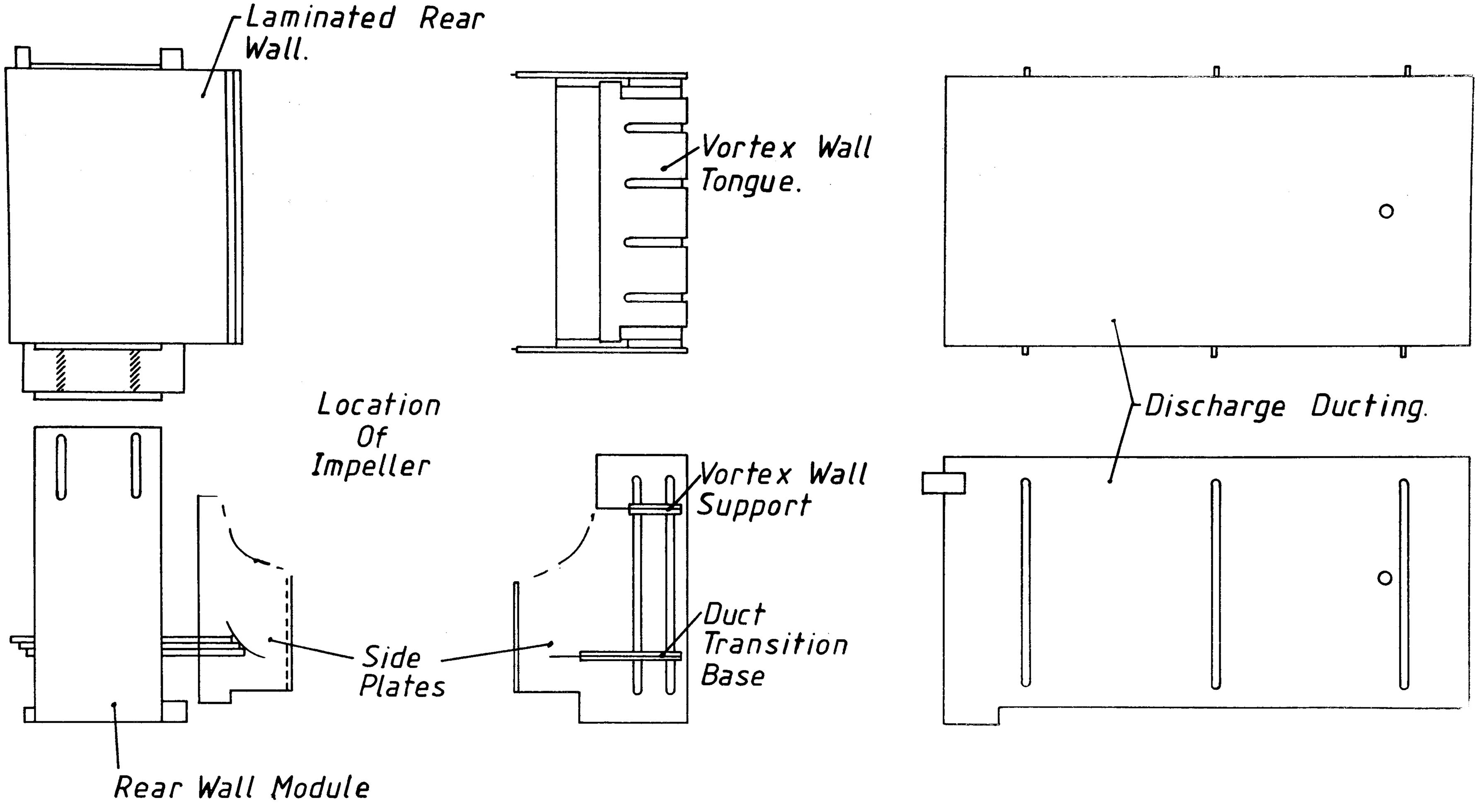
Laminated Rear Wall.
Vortex Wall Tongue.
Discharge Ducting.
Location Of Impeller
Vortex Wall Support
Duct Transition Base
Side Plates
Rear Wall Module

Figure 2.4

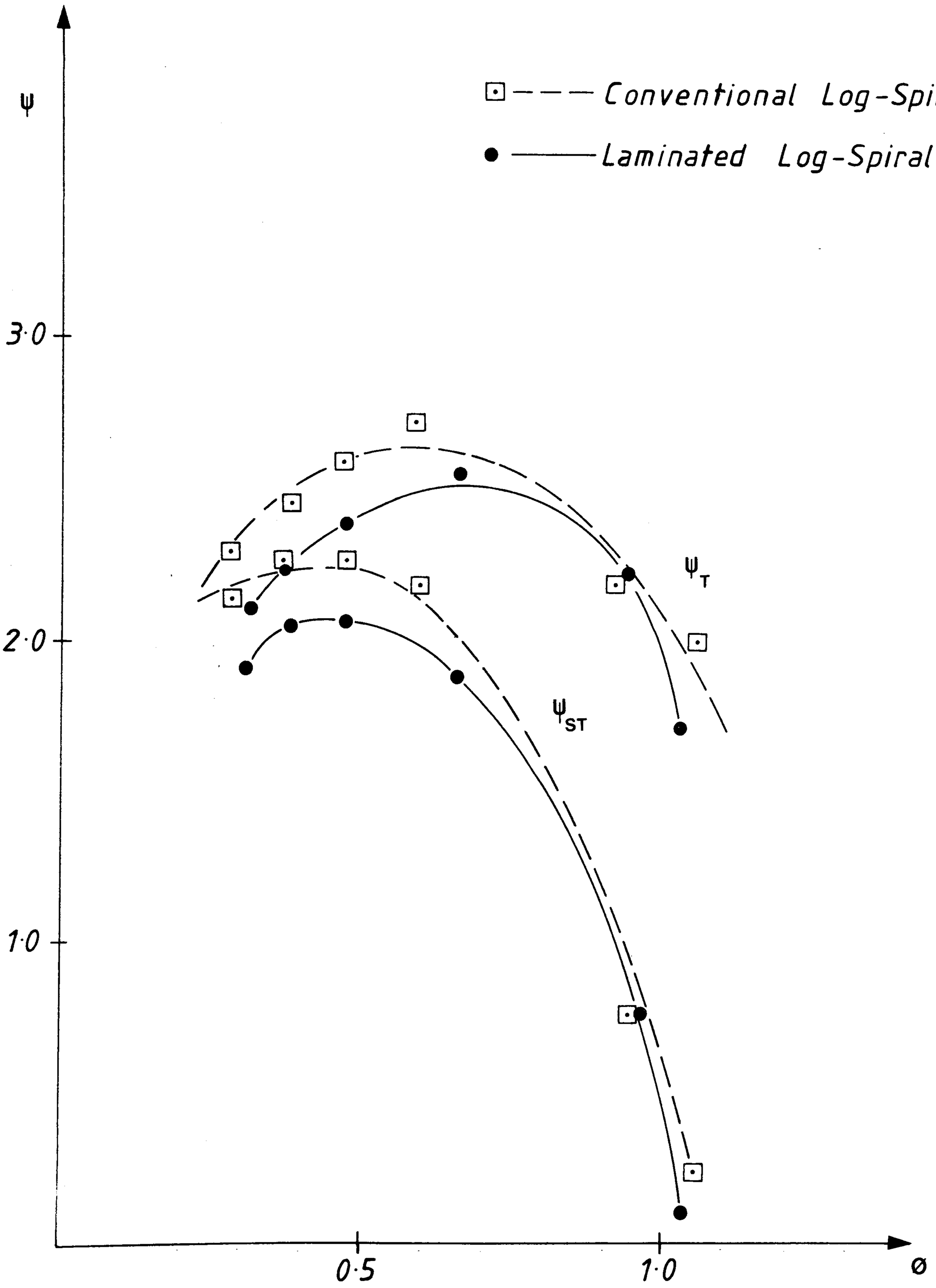

Figure 2.5

EFFECT OF A LAMINATED WALL

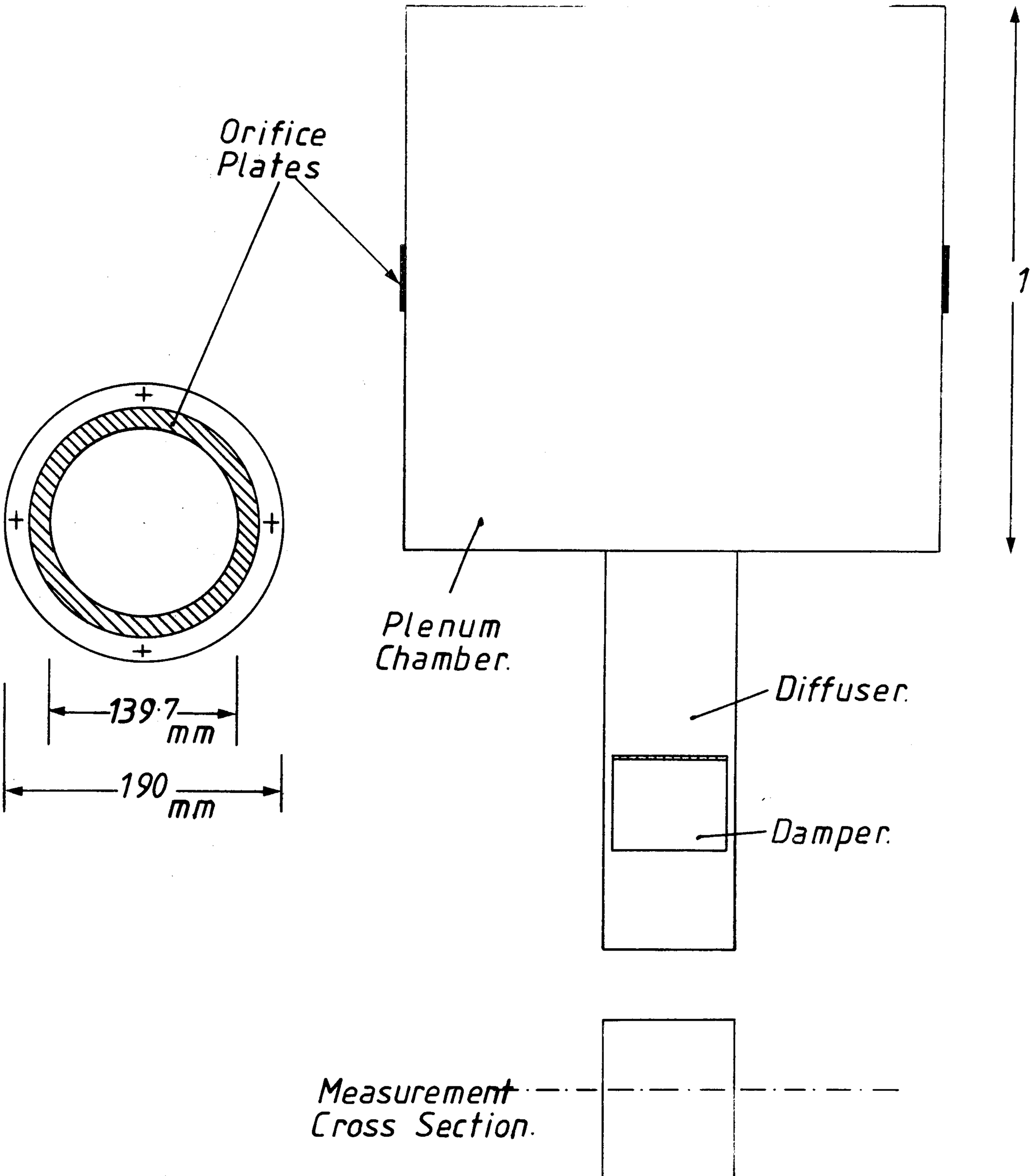

Figure 2.6

COMPLETE DUCTING ARRANGEMENT

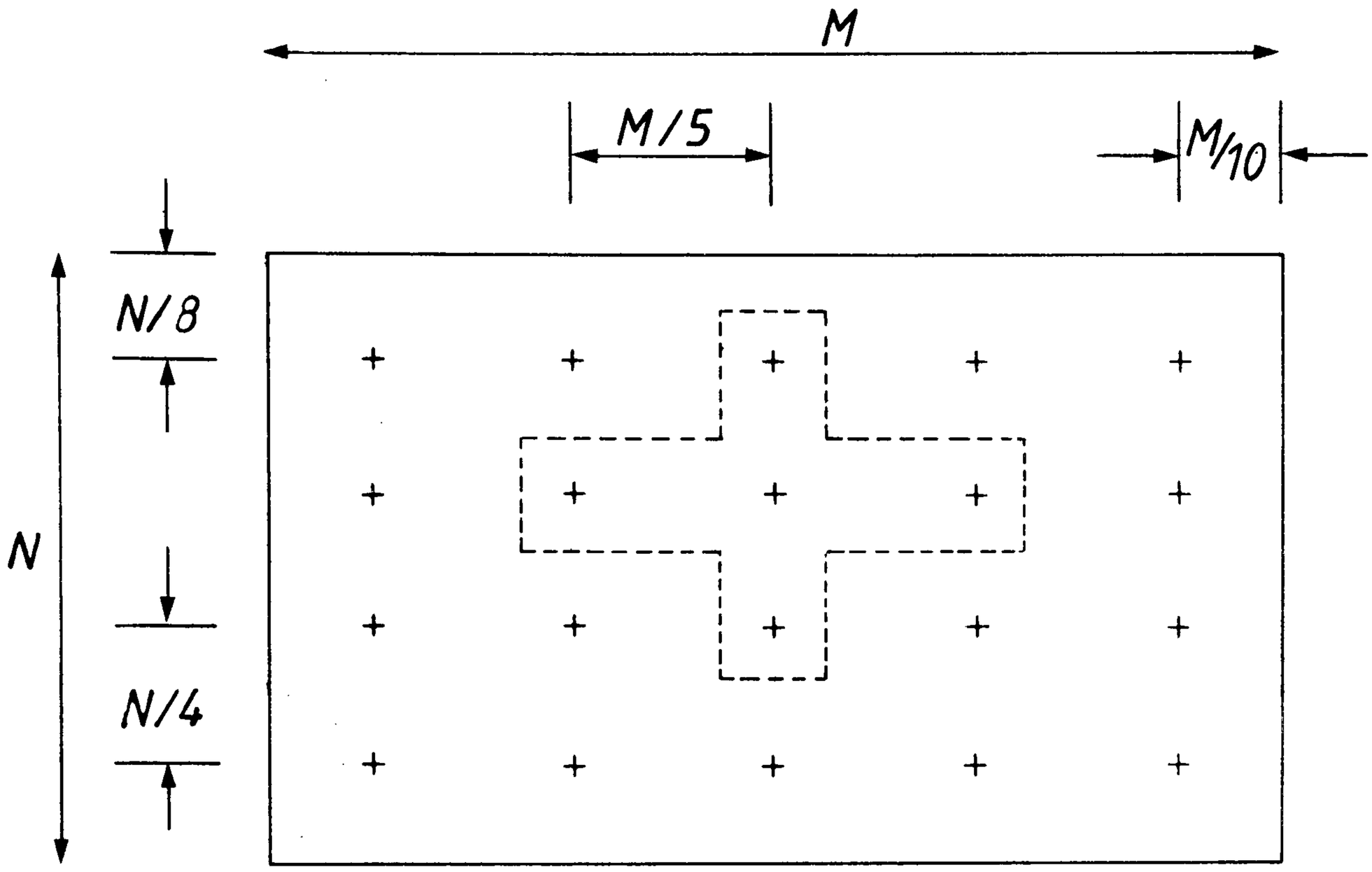

Figure 2.7

LOCATION OF TRA-VERSE POINTS

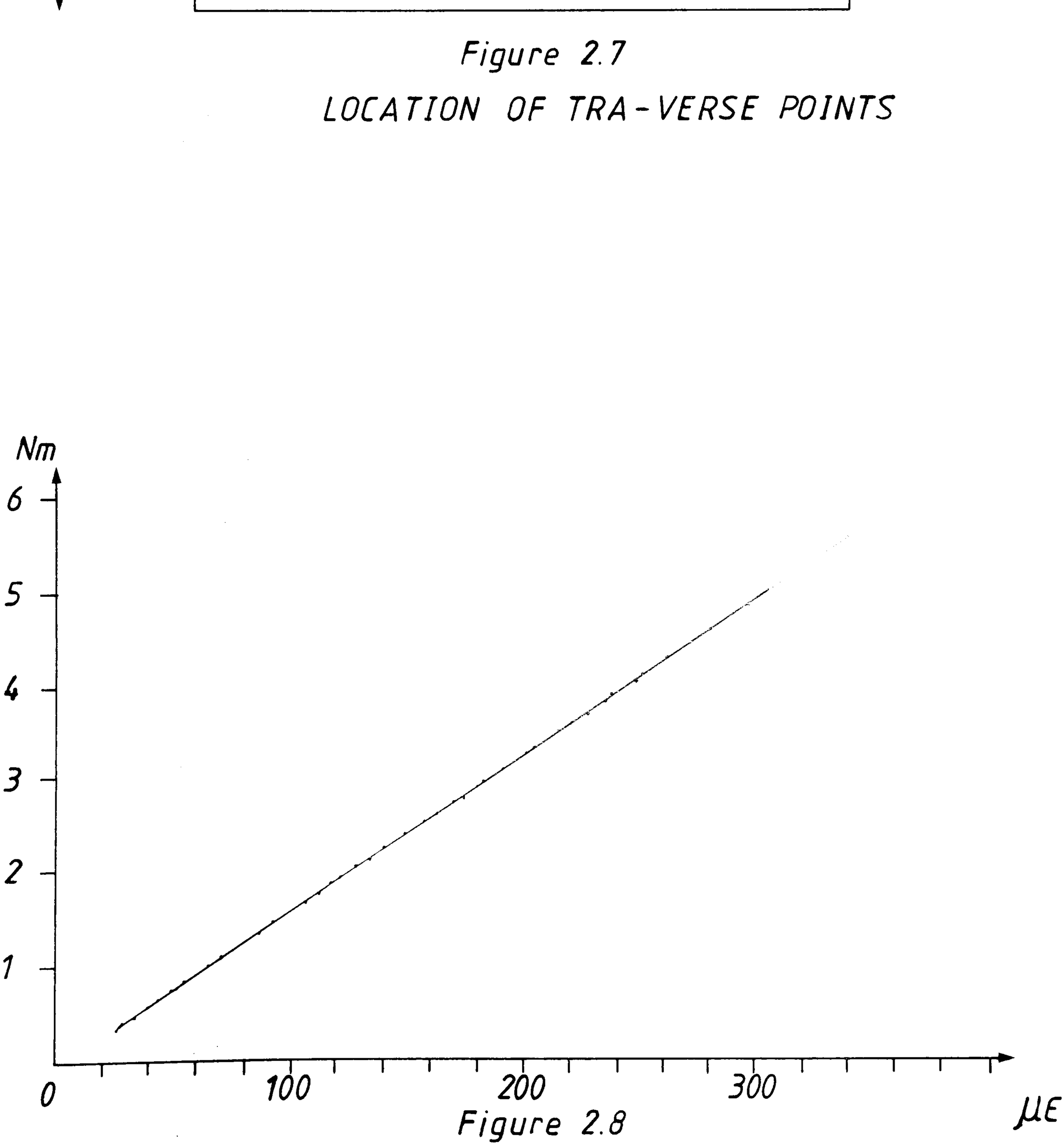

Figure 2.8

GAUGE CALIBRATION CHART

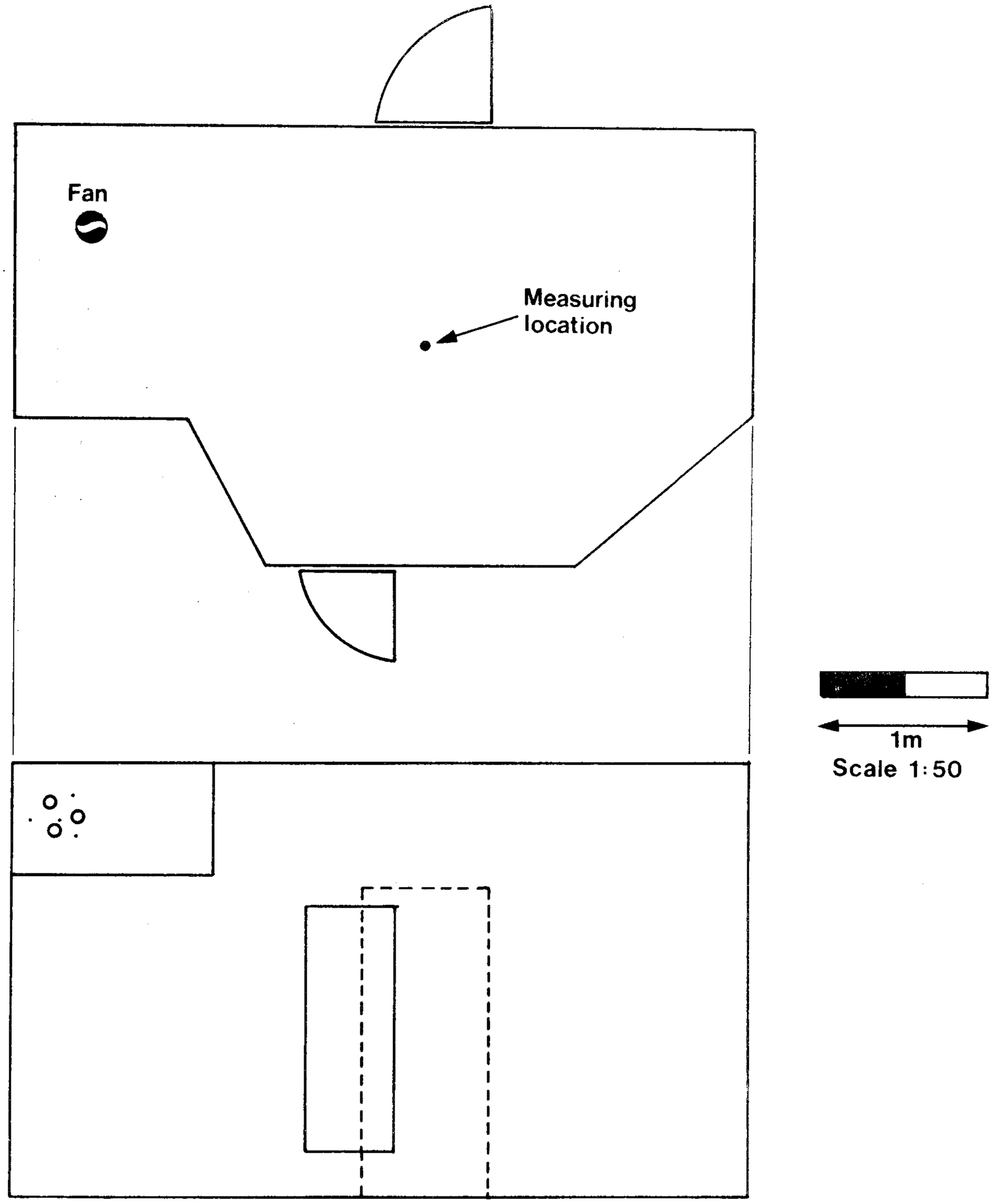

Figure 2·9 Noise measurement chamber

CHAPTER THREE

3.1 THE ENIGMA OF THE CROSS-FLOW FAN

If the flow regime of a cross-flow blower were known exactly, it would be possible to determine the 'ideal' total head characteristic; either analytically, by solution of stream functions or numerically, using velocity triangles. This latter technique is the procedure most commonly adopted to determine the 'ideal' characteristic of conventional fans.

Since SPRENGER recognised the mechanism of the internal vortex in 1937 a number of models have been proposed to explain cross-flow fan behaviour. The simplest of these analyses treat the internal flow field as a section from a potential vortex; but the models become necessarily more complex when modified to match quantitatively determined velocity values or qualitatively determined flow patterns.

3.2 CROSS-FLOW FAN THEORY

The most elementary approach is of the type used by TRAMPOSCH(71). Here, the postulated internal flow is that of a Rankine vortex; a potential vortex with a forced vortex core. The velocity distribution outside the forced vortex region is given by equation 3.1.

$$V_r = \text{Constant} \qquad 3.1$$

i.e The streamlines are considered concentric.

TRAMPOSCH determined the vortex constant by equating a point velocity value, diametrically opposite the vortex and on the inner circumference, as equal to the peripheral velocity, U.

$$K = U \times d \qquad 3.2$$

The flow is considered ideal and to satisfy Eulers equation of energy transfer. Thus; velocity triangles are used to express the total head in terms of flow-field and fan design parameters.

DE-FRIES (22), in his historical review, states that REINDERS also considered the throughflow to be a section from a potential vortex, where the law of speed distribution (3.1) applies. ECK and LAING adopted this conception of the flow field and developed an analysis using an 'eddy-field constant'. The report publishes a plot of the outer peripheral radial velocity distribution, determined by LAING. ECK and LAING considered this uneven velocity distribution to be directly related to velocities within the potential vortex (Figure 3.1). They approximate the vortex constant (K) by matching experimentally and analytically determined velocity distributions around the fan circumference. Applying velocity triangle theory between the suction and discharge arcs enabled an estimate of the aerodynamic performance, see Figure 3.2. It is also likely that their knowledge of the radial velocity distribution led to the development of a rear wall, by employing the 'constant mean velocity' premise. This procedure is discussed again later in the chapter.

MOORE (51) also attempted to determine the ideal performance of a cross-flow fan using the conventional velocity triangle procedure; that of equating the total head to the change in angular momentum between suction and discharge. He treats the flow field as a potential vortex of variable strength, and suggests that the throughflow may be adequately

represented by taking four points on a 'mean-line' through the rotor. His resulting equation is of the form of the functional relationship 3.3.

$$\Psi = f(\phi) \times G(R1, R2, \lambda_s, \lambda_d, \beta_2, \beta_4, \alpha, h^*) \qquad 3.3$$

R1 = Outer radius

R2 = Inner radius

λ_s = Suction arc

λ_d = Discharge arc

β_2 and β_4 = Relative flow angles

α = Absolute flow angle

h^* = Busemann correction factors

Figure 3.1 has indicated how irregular the flow distribution can be. This 'mean-line' approach can therefore be subject to great error by simplifying the flow field and ignoring the circumferential variation of a number of parameters.

This type of analysis may be considerably enhanced by treating the suction and discharge arcs as a number of segments, and choosing representative values for each segment. Boundary conditions may be determined experimentally and the total head calculated by numerical integration of values within paired suction and discharge segments. The author has developed a model using this approach, it is discussed in detail in section 3.3.

Between 1955 and 1957 COESTER (15), (16) deduced from experimental observation that the internal flow could be split into two zones:— a potential vortex of constant total pressure and an eddy of variable total pressure.

Working on the premise that only the potential vortex contributes to the performance, COESTER discarded the rotational flow zone from his analyses, by 'cutting away' this region of random, low-energy flow along a streamline of constant static pressure. The potential field was expressed as satisfying the two-dimensional Laplace equation.

$$\frac{\partial^2 \psi}{\partial x^2} + \frac{\partial^2 \psi}{\partial y^2} = 0 \qquad 3.4$$

COESTER's fundamental solution to 3.4 shows the flow to be a simple potential vortex, where the tangential velocity component is equal to the blade speed at all points on the impeller inner periphery; and the radial velocities follow a tangent law.

$$V_r = \text{Tan } (\xi/2) \qquad 3.5$$

$$V_t = U, \text{ for all } \xi \qquad 3.6$$

ξ = Potential field circumferential angle

We shall see that these two conditions have been challenged. COESTER extended this simple analysis to account for streamline convergence, which was observed to occur between suction and discharge. To simulate this qualitatively assessed condition of accelerated throughflow, yet allow for a dividing streamline of constant Pst ; COESTER analytically introduced a pair of vortices into the flow field, situated and centred within the impeller. Furthermore; he developed casings intended to enhance production of these postulated vortices (15) and claimed an improvement in performance over typical cross-flow blowers of the day.

Between 1965 and 1966 ILBERG and SADEH (40) investigated the flow through a cross-flow impeller. They made detailed internal and external traverses and proposed a theoretical

model which closely approximated to the measured flow field. Their investigations led them to question COESTER's three principal conclusions; namely :-

1 Flow within the impeller may be described as a free vortex, centred at the origin of the flow field coordinates.

2 Inner peripheral radial velocities satisfy equation 3.5, except where flow is distorted by unsuitable casing.

3 Inner peripheral tangential velocities satisfy equation 3.6, except where flow is distorted by unsuitable casing.

Figure 3.3 illustrates the order of disagreement between COESTER's theoretically determined velocities and the observed equivalents of ILBERG and SADEH. To improve on this, ILBERG and SADEH proposed a flow regime consisting of a forced vortex core surrounded by a potential field. They suggested that the potential field could be modelled by hydrodynamic superposition of a potential vortex and a periodic potential (period of 2π);

$$\text{Potential function } \phi(r/r_2) = \frac{\Gamma}{2\pi}\varepsilon_n + \sum_{n=1}^{n=\infty} (r/r_2)^N \quad 3.7$$

$$\times (A_n \cos n\varepsilon + B_n \sin n\varepsilon)$$

The forced vortex core has tangential velocities governed by equation 3.8 :

$$V_t = r\omega \quad 3.8$$

r = Generalised radius

ω = The angular velocity of the core

For a particular casing they experimentally determined the following quantities:

1 Circulation, Γ

2 Location of the vortex centre in relation to the combined flow field, $(r/r_2^*, \xi^*)$

3 Forced vortex angular velocity, ω

4 Radius of the forced vortex core, R

Equation 3.7 was solved and the potential function determined by invoking continuity requirements between the zones and including the preceeding four terms. Their results indicate a close agreement between the calculated potential function (Figure 3.4) and the measured static pressure (Figure 3.5). ILBERG and SADEH do not calculate the performance of their machine analytically. This would have been possible using velocity triangles, but it is probable that computing facilities which would enable lengthy numerical analyses were not available at that time.

Finally, IKEGAMI and MURATA (38) have demonstrated the possibility of developing a model enabling a purely analytical solution of the internal and external flow fields. Their analysis allows total head characteristics to be calculated and also permits some grossly simplified casing. This work is reviewed by PORTER (62) and extended by TUCKEY (73).

However, these complex analyses assume Laplacian fields within the rotor; satisfying a boundary condition on the inner blade edge of tangential velocities equal to blade speed. This condition must be met or a singularity will occur; but experimental work, traversing the impeller interior, has implied non-Laplacian conditions and a high-order 'drift' in velocities close to the blades.

3.3 DEVELOPMENT OF A FLOW MODEL

For the purposes of the model the internal flow field is considered to consist of two zones :-

i) A forced-vortex type 'recirculation zone', where the radius of the vortex is the distance between the vortex centre and the vortex wall tip.

ii) A potential field.

Radial and tangential velocities close to the outer suction periphery have been determined experimentally for one fan type and three flow conditions. The proposed model matches these observed values as closely as possible, by manipulating the constituent parameters of a combined hydrodynamic field. This is determined by superposition of a free vortex and a line sink; the resulting stream function is expressed, in cartesian coordinates, as :-

$$\psi = \frac{\Gamma}{2\pi} \ln \sqrt{(x^2+y^2)} - \frac{M}{2\pi} \tan^{-1}(y/x) \qquad 3.9$$

Γ is positive in the direction of rotation of the fan.

M is positive left to right.

The origin of the flow field coordinates occurs at the centre of the free vortex.

This sink/vortex combination is also a 2-D mathematical representation of the flow between the guide vanes and runner of a hydraulic turbine. The proposed model is concerned only with predicting flow velocities along the outer suction periphery of the impeller.

Theoretical radial and tangential velocities are found at representative segments around the suction arc by differ-

entiating equation 3.9. These 'flow field' velocities are then transformed into equivalent 'fan' radial and tangential velocities.

Knowledge of the suction velocity distribution enables the discharge flow field to be solved, and aerodynamic performance to be calculated using velocity triangles. Ideal conditions are assumed in the analysis; principally this implies no pressure loss and that relative velocities follow the blade angles.

The flow field constants, Γ and M , are approximated by matching with experimentally observed results, for one fan type only. They are assumed to be scaleable and independent of all rotor and casing design parameters, except blade chord. Particular details of the analysis are given in succeeding sections.

3.3.1 GEOMETRICAL CONSIDERATIONS

Using elementary geometry; λ_s, λ_d, μ', r, x^* and y^* (see Figure 3.6) may be determined. The design input data are: R1, R2, B, E, δ, μ and β_2 (see Figure 3.7). No account is taken of the inner blade angle or the rear wall clearance, these are certainly design parameters but optimum values and their effect on performance shall have to determined experimentally. The flow field centre of coordinates is generally taken as the point opposite and in the plane of the vortex wall, on the inner blade circumference.

3.3.2 CALCULATION OF INLET RADIAL AND TANGENTIAL VELOCITIES

There are three steps involved in the evaluation of radial and tangential velocities, with respect to the fan system of coordinates (centred on the axis of rotation).

i) Determine the cartesian coordinates of the fan suction periphery, with respect to the flow field origin.

ii) Calculate velocities at these coordinates.

iii) Transform the 'flow field' velocities into 'fan' velocities.

These steps are explained in sections 3.3.2.1, 3.3.2.2 and 3.3.2.3 respectively.

3.3.2.1 COORDINATES OF THE FAN OUTER PERIPHERY

See Figures 3.6, 3.7 and 3.8 for an explanation of the variables.

For all ϵ_i

$$X_i = -(x^* + R1 \cos\epsilon_i) \qquad 3.10(i)$$

$$Y_i = y^* + R1 \sin\epsilon_i \qquad 3.10(ii)$$

Where; i = 1,2,3.....N

N — Number of sectors

3.3.2.2 CALCULATION OF FLOW FIELD RADIAL AND TANGENTIAL VELOCITIES

Differentiation of the stream function (equation 3.9), enables tangential and radial velocities to be found in a sector $\Delta\lambda_s$, represented by a circumferential angle ϵ_i.

$$V_{ti} = \frac{\partial}{\partial y}(\psi) = \frac{\Gamma y \quad -Mx}{2\pi(x^2 + y^2)} \qquad 3.11$$

$$V_{ri} = -\frac{\partial}{\partial x}(\psi) = \frac{-\Gamma x - My}{2\pi(x^2 + y^2)} \qquad 3.12$$

3.3.2.3 TRANSFORM OF FIELD VELOCITIES TO FAN PERIPHERAL VELOCITIES.

See Figure 3.9.

T, R - Flow field subscripts

t, r - Fan-centre subscripts

$$c^* = /(x^{*2} + y^{*2}) \qquad 3.13(i)$$

$$\sigma_i = \pi + \mu' - \epsilon_i \qquad 3.13(ii) \quad \text{For } \epsilon_i > \delta$$

$$V_i^2 = c^{*2} + Rl^2 - 2c^* Rl \cos(\sigma_i) \qquad 3.13(iii)$$

$$\eta_i = \cos^{-1} \frac{V^2 + Rl^2 - c^{*2}}{2 V Rl} \qquad 3.13(iv)$$

2 ZONES:

a) $\epsilon_i \geqslant \pi$

$$V_{tli} = V_{Rli} \sin\eta_i + V_{Tli} \cos\eta_i \qquad 3.14(i)$$

$$V_{rli} = V_{Rli} \cos\eta_i - V_{Tli} \sin\eta_i \qquad 3.14(ii)$$

b) $\epsilon_i < \pi$

$$V_{tli} = V_{Tli} \cos\eta_i - V_{Rli} \sin\eta_i \qquad 3.14(iii)$$

$$V_{rli} = V_{Rli} \cos\eta_i + V_{Tli} \sin\eta_i \qquad 3.14(iv)$$

The absolute flow angles, λ_{li} and relative flow angles, $\hat{\beta}_i$ may then be calculated:

$$\lambda_{li} = \tan^{-1} (V_{rli}/V_{tli}) \qquad 3.15$$

$$\hat{\beta}_i = \tan^{-1} (V_{rli}/ U - V_{tli}) \qquad 3.16$$

3.3.3 ESTIMATION OF THE DISCHARGE FLOW CONDITIONS

Because the total head characteristics are determined using velocity triangles, this model is concerned primarily with the rotor outer circumference. Nevertheless, many researchers have observed the phenomena of a forced vortex and throughflow where the streamlines are not concentric circles. ECK(23 page 164,figure 141), shows a commonly observed internal flow pattern where the streamline curvature is greater towards the vortex wall; flattening and eventually reversing towards the rear wall. This flow field described does not exclude accelerated throughflow, which COESTER, ECK

and others have observed.

The presence of a forced vortex is accounted for in this model by eliminating a recirculation zone from the performance evaluation, thus treating a portion of the fan circumference as redundant with respect to throughflow and energy transfer. The existence of convergent streamlines and reversal of streamline curvature are accounted for by adopting an 'equivalent sector' hypothesis. This hypothesis states that each sector on the suction arc has an equivalent on the discharge arc; the radial velocities in each arc are related by the ratio of the suction and discharge arcs. These paired sectors are also geometrically equivalent, for example; the sector on the suction arc closest to the vortex wall is paired with the discharge arc sector closest to the vortex wall.

Discharge radial velocities are, then, given by equation 3.17:

$$V_{r2i} = V_{r1i} \times \frac{\lambda_s}{\lambda_d} \qquad 3.17$$

This condition implies non-concentric streamlines and also accelerated throughflow where $\lambda_s > \lambda_d$.

Knowing the discharge radial velocities enables the complete discharge flow pattern to be calculated from velocity triangles.

$$V_{t2i} = U + \tan(\pi/2 - \beta_2) \times V_{r2i} \qquad 3.18$$

$$\lambda_{2i} = \tan^{-1}(V_{r2i}/V_{t2i}) \qquad 3.19$$

3.3.4 CALCULATION OF PERFORMANCE

The volumetric flowrate is calculated by summing the radial velocities over the suction arc, λ_s.

$$Q = L \sum_{i=1}^{n} V_{rli} \qquad 3.20$$

Total head is determined from the difference between suction and discharge moments of momentum.

$$\Delta p_t = \rho (U_2 V_{t2} - U_1 V_{t1}) \qquad 3.21$$

With cross-flow fans air enters and leaves at the same radius. The numerical solution to equation 3.21, which accounts for a peripheral variation in velocity values is;

$$\Delta p_t = \frac{\rho U}{N} \sum_{i=1}^{n} (V_{t2i} - V_{t1i}) \qquad 3.22$$

Where; N is the number of sectors around λ_s and λ_d. Equations 3.20 and 3.22 converge quite rapidly with increasing N. Using N=150 gives a computation error of less than 5% in the evaluation of total head, and rather less in the evaluation of volumetric flow rate.

3.3.5 REAR WALL DESIGN

In conventional centrifugal fan design, the ideal volute areas at each cross-section are determined by the principle of 'constant mean velocity',see, for example, STEPANOFF (70, page 159). So far in this model the only rear wall parameter considered is δ, the angle of the rear wall tip above the rotor cross-sectional centre-line. This point is important because it divides the suction and discharge arcs.

Although the rear wall is not involved in the energy transfer, the importance of a sound design should not be underestimated. A poor design can lead to large pressure differences within the volute, giving rise to high viscous losses and flow instability. WORSTER (76) cites a case where a 300% improvement in centrifugal pump performance was achieved simply by changing the volute shape. See also BOWERMAN and

ACOSTA (8).

Knowing the discharge radial velocity distribution and specifying the duct depth, H, enables a rear wall to be designed using the principle of 'constant mean velocity', see Figure 3.10.

$$\tau = \tan^{-1}(H+B/(B/\tan\theta)) \qquad 3.23$$

$$A_m = H+B/\sin\tau - R1 \qquad 3.24$$

$$\bar{V} = Q_m/A_m \qquad 3.25$$

A_m - Extreme diffusion cross-section

$\bar{V}$ - Mean velocity through cross-section, m. ($1 \leq m \leq N$)

At each radial cross-section:

$$A_i = Q_i/\bar{V} \qquad 3.26$$

$$Q_i = \lambda_d/N \sum_{k=1}^{k=i} Q_k \qquad 3.27$$

Figure 3.11 shows four rear walls designed using equations 3.23 - 3.27.

Figure 3.12 shows the small variation in the calculated rear wall shape with flow coefficient.

3.3.6 VORTEX LOCATION

To complete the model, a routine is included in the algorithm which estimates the resultant 'force' on the recirculation zone. This is an expression of the irregular pressure distribution which surrounds the rotational core. This facility is available but not generally employed; the flow field centre of coordinates being taken at the point opposite, and in the plane of, the vortex wall, on the inner blade circumference.

Since the discovery of the internal vortex, designers have recognised the need to suppress its movement. DATWYLER(20) considered the vortex centre to be mobile and designed a rear

wall which had broad radial cross-sectional areas to 'allow the vortex to take up its most stable position'.

In an attempt to allow for vortex movement the core is treated as a solid body of radius, r and centred at some defined location (c^* ,μ') relative to the fan axis of rotation. The initial location is specified, usually as the point on the inner blade periphery opposite, and in the plane of, the vortex wall edge. The pressure distribution around the vortex core boundary is determined and the corresponding 'force' on the core is calculated. The vortex core is then 'moved' in the direction of this resultant force - this procedure is repeated a number of times at new (c^*, μ') locations, see Figure 3.8, and the position of least resultant force is found. Total head characteristics may be determined at this 'most stable' location.

Figure 3.13 illustrates the five zones(Z1 through Z5) considered in this part of the analysis. The core periphery is divided into J arcs, and at each arc the static pressure is determined by applying Bernoullis equation. Neglecting viscous forces the core is considered to have no influence on the surrounding fluid.

3.3.6.1 TOTAL PRESSURE VARIATION

The total pressure rise across the fan is estimated as 1 % of the ambient pressure. Assuming approximately 20% total energy transfer across the first blade row and 80% across the second, the total pressure distribution is estimated at the core boundary.

3.3.6.2 TANGENTIAL VELOCITY DISTRIBUTION AROUND THE CORE BOUNDARY

ZONE

Z1 Tangential velocities may be determined from equation 3.8.

Z2 Assessed as approximating to a linear change between the bordering velocities in zones Z1 and Z3.

Z3 Flow is assumed to be tangential to the forced vortex periphery. The velocity distribution is represented as a linear change in the absolute velocities, from the suction inner blade periphery to the discharge blade periphery.

Z4 Assessed as approximating a linear change between the bordering velocities in zones Z3 and Z5.

Z5 The flow distribution is treated as equivalent to flow round a cylinder, as in 'ideal' fluid theory. U, the free-stream velocity is calculated using field parameters, as determined in section 3.3.3. The tangential velocities at specific sectors in this zone may be calculated from equation 3.28.

$$\hat{V}_{t\theta'} = 2\ U \sin\theta \qquad 3.28\ (0^\circ \leq \theta \leq 80^\circ)$$

3.3.6.3 RESULTANT FORCE ON THE VORTEX CORE

The static pressure distribution is determined by applying Bernoullis equation:

$$P_{st}(\theta) = P_t(\theta) - \tfrac{1}{2}\rho V_t(\theta)^2 - kV_{abs}^2 \qquad 3.29$$

k - A factor which may be used to account for static pressure reduction due to viscous losses within the flow. If unspecified, this is assumed zero.

The resultant force on the vortex, F and the angle of

action Ω are calculated from equations 3.30 - 3.33.

$$\text{TOTAL FORCE, } F_x = J^{-1} \sum_{i=1}^{J} P_{st}(i) \cos\theta_i \, r \, d\theta \qquad 3.30$$

$$\text{TOTAL FORCE, } F_y = J^{-1} \sum_{i=1}^{J} P_{st(i)} \sin\theta_i \, r \, d\theta \qquad 3.31$$

$$F = \sqrt{(F_x^2 + F_y^2)} \qquad 3.32$$

$$\Omega = \tan^{-1}(F_y/F_x) \qquad 3.33$$

The vortex core is moved in the direction by an amount dependent on the magnitude of F, see Figure 3.14.

3.3.7 EVALUATION OF THE MODEL FLOW FIELD PARAMETERS, Γ^* AND M.*

To determine which combinations of circulation Γ, and sink strength, M are tenable it was necessary to fit the model to available experimental data. The Γ,M values were determined by 'trial and error', matching observed radial velocities for one fan type and three flowrates to theoretically determined equivalents, calculated using a conjectured Γ,M combination.

An undergraduate project within the department had studied the flow field external to the impeller by traversing the suction arc of a large, 625mm diameter, cross-flow fan impeller, see PELHAM(60). These three-hole yaw-probe traverses gave the radial and tangential velocities around 120^{o} of suction arc, for experimentally determined flow coefficients of $\phi = 0.3$, $\phi = 0.6$ and $\phi = 0.91$.

Figures 3.15 - 3.16 compare these observed velocities with their equivalents, calculated using the model outlined.

The approximations (3.15 - 3.16) are considered to be reasonably close throughout, particularily at the lowest flowrate where the waning radial velocity trend towards the vortex wall is well predicted. At higher flowrates there is some discrepancy, and particularily to the rear wall side of the suction arc.

Most of the disagreement between the calculated and observed values will be due to adopting an imperfect model, but there also errors of measurement; caused primarily by taking measurements in unsteady flow and through inaccuracies of location of the probe in an irregular field. Tangential velocities will be considerably more disturbed than the radial velocities, particularily close to the blades. Air close to the impeller will be subject to viscous distortions, manifest in the air rotating conformably with the fan. Figures 3.15 - 3.16 show that, over the major portion of the suction arc, the experimentally observed tangential velocities are generally greater than those predicted by the model. Some of this discrepancy may be explained by conformable rotation of the air - also; flow turbulence increases close to the rear wall and vortex wall which alters 'ideal' velocities and increases the problems associated with traversing.

The author considers these approximations to be as close as is it possible to achieve using a model consisting solely of an irrotational vortex and a line sink. The radial velocities need to be more accurately assessed than the tangential velocities because of their influence in determining discharge conditions (section 3.3.3).

By extrapolating the observed radial velocities and integrating, it was possible to calculate an 'inferred' flow coefficient. At all flow conditions these 'inferred' coefficients are greater than the measured flow coefficients (ϕ = 0.3, 0.6 and ϕ = 0.91). The three-hole probe traverses were taken around an arc close to the fan longitudional centre; the differences between observed and 'inferred' flowrates indicates some 3-D

asymmetry, also observed by BUSH(13), as well as a reduction in throughflow, probably due to stalling of the blade row.

The model developed is a 2-D analysis, not accounting for flow with a component in the axial direction or any axial variation of conditions; neither can the model account for losses: thus the flow field parameters need to be corrected for 3-D asymmetry and stall. The previously determined values of Γ and M are corrected by division by an 'exaggeration factor'; which is the ratio of the integrated,'inferred' flow rate to the experimentally determined flowrate, see Table 3.1.

model parameters Γ	M	experimental ϕ	integrated ϕ	exaggeration factor	corrected parameters Γ	M
6.35	14.61	0.3	0.4446	1.48	4.29	9.87
11.07	14.10	0.6	0.6690	1.115	9.93	12.65
15.00	19.50	0.91	0.9280	1.02	14.71	19.12

Table 3.1.

The corrected flow parameters are plotted, see Figure 3.17, from which six further values are interpolated. These nine values are non-dimensionalised through division by the product of rotor diameter an tip-speed.

$$\Gamma^* = \Gamma^* / U D \qquad 3.34$$

$$M^* = M^* / U D \qquad 3.35$$

Total head characteristics are determined from these nine dimensionless field parameters. Some theoretical per-

formance results are discussed in Chapter 5, and these may be compared with experimentally determined performance results presented in Chapter 6.

3.3.8 ESTIMATE OF THE MAGNITUDE OF INLET 'SHOCK' LOSSES

See Figure 3.18 for an explanation of the terms.

From Figure 3.18

$$V_s = U - V_t - V_r / \tan\beta \qquad 3.36$$

V_s - 'Shock' velocity; the prerotation velocity required for the relative flow angle to follow the blade angle.

ECK(23) suggests the following relationship between static pressure loss and 'shock' velocity. Although the factor μ has been determined for conventional centrifugal fans, it is considered that if it remains a useful estimator for both forward-curved and backward-curved centrifugal fans, it will also apply to cross-flow rotors.

$$\Delta P_{loss} = \mu \rho/2 \, V_s^2 \qquad 3.37$$

μ = 0.8 for a finite number of blades.

Figure 3.19 shows some efficiency curves determined by accounting for this 'shock' loss, equation 3.37, and indicates that this loss component accounts for only about 10% of the ideal total pressure.

3.3.9 CONDITIONS APPROACHING ZERO FLOW

Results from applying the model indicate a theoretical minimum flow coefficient of about ϕ = 0.45, Figure 3.2 indicates that ECK and LAING may have found a similar minimum. These results support the conclusion that it is not possible to achieve zero flow when the VORTEX is centred away from the fan axis of rotation.

Experimentally determined zero flow is not truly a cond- of no flow through the impeller, because inflow still occurs and air recirculates within the duct. Reducing the flowrate below some threshold level causes the flow to surge violently, with a large temporal pressure variation. Figure 3.20 helps illustrate that the immense pressure variations experienced are due to mass movement of the fluid within the impeller, responding to a periodic evacuation of the duct - mechanisms of flow instability are discussed further in Chapter 7.

The author has measured flow coefficients as little as $\phi = 0.15$ for low efficiency fans.

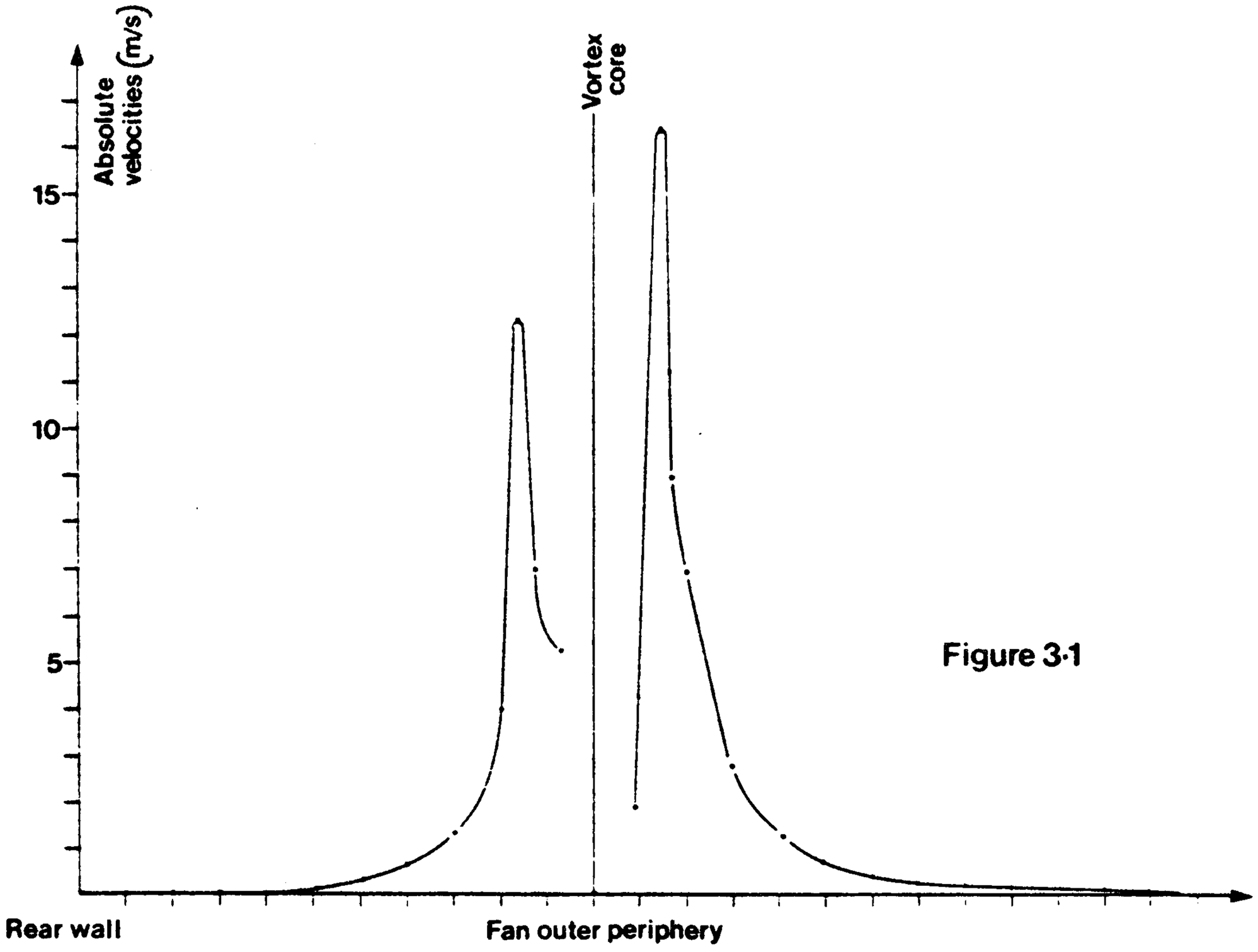

Figure 3·1

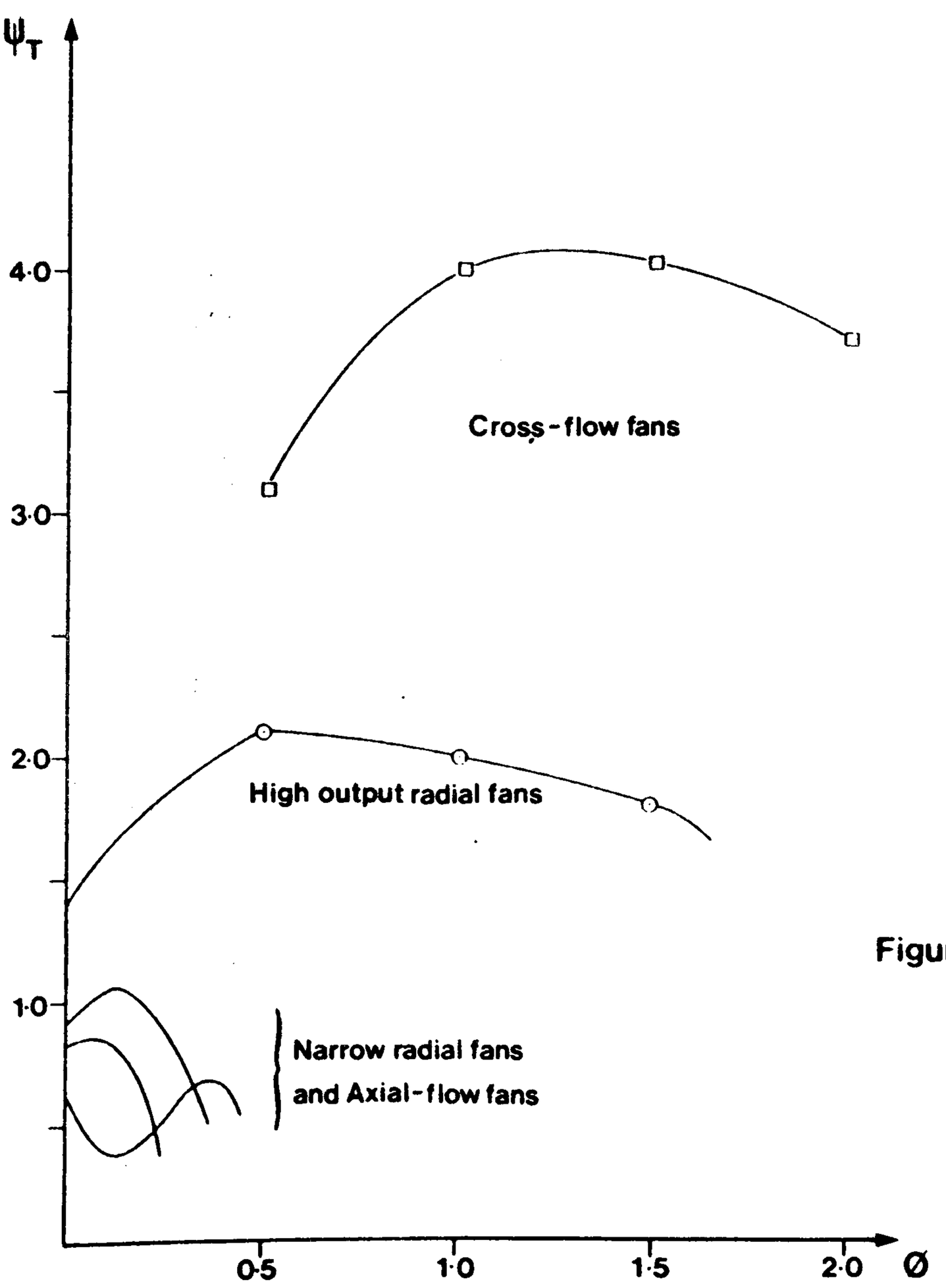

Figure 3·2

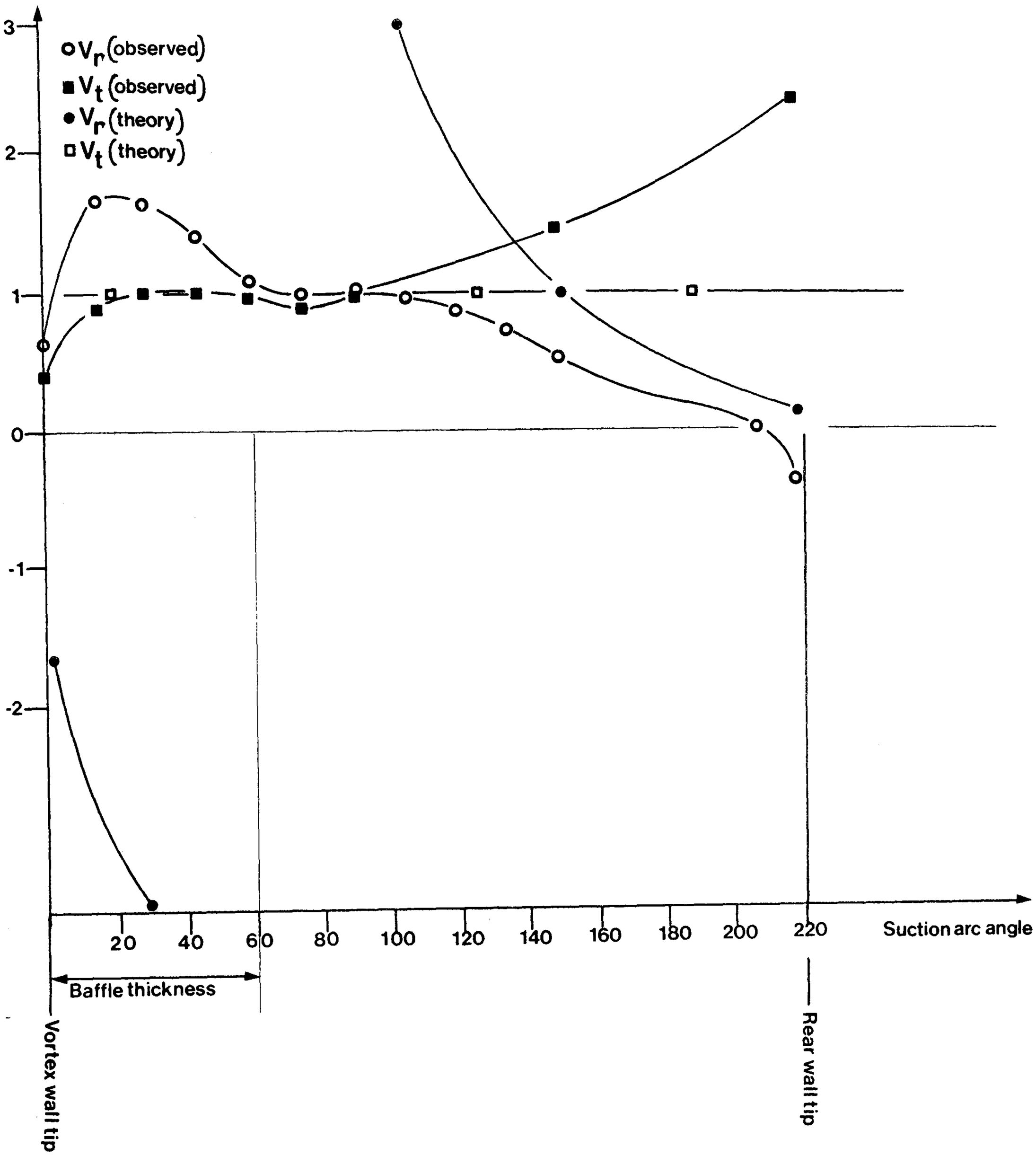
v m/s
3
2
1
0
-1
-2
V_r (observed)
V_t (observed)
V_r (theory)
V_t (theory)
20
40
60
80
100
120
140
160
180
200
220
Suction arc angle
Baffle thickness
Vortex wall tip
Rear wall tip

Figure 3·3

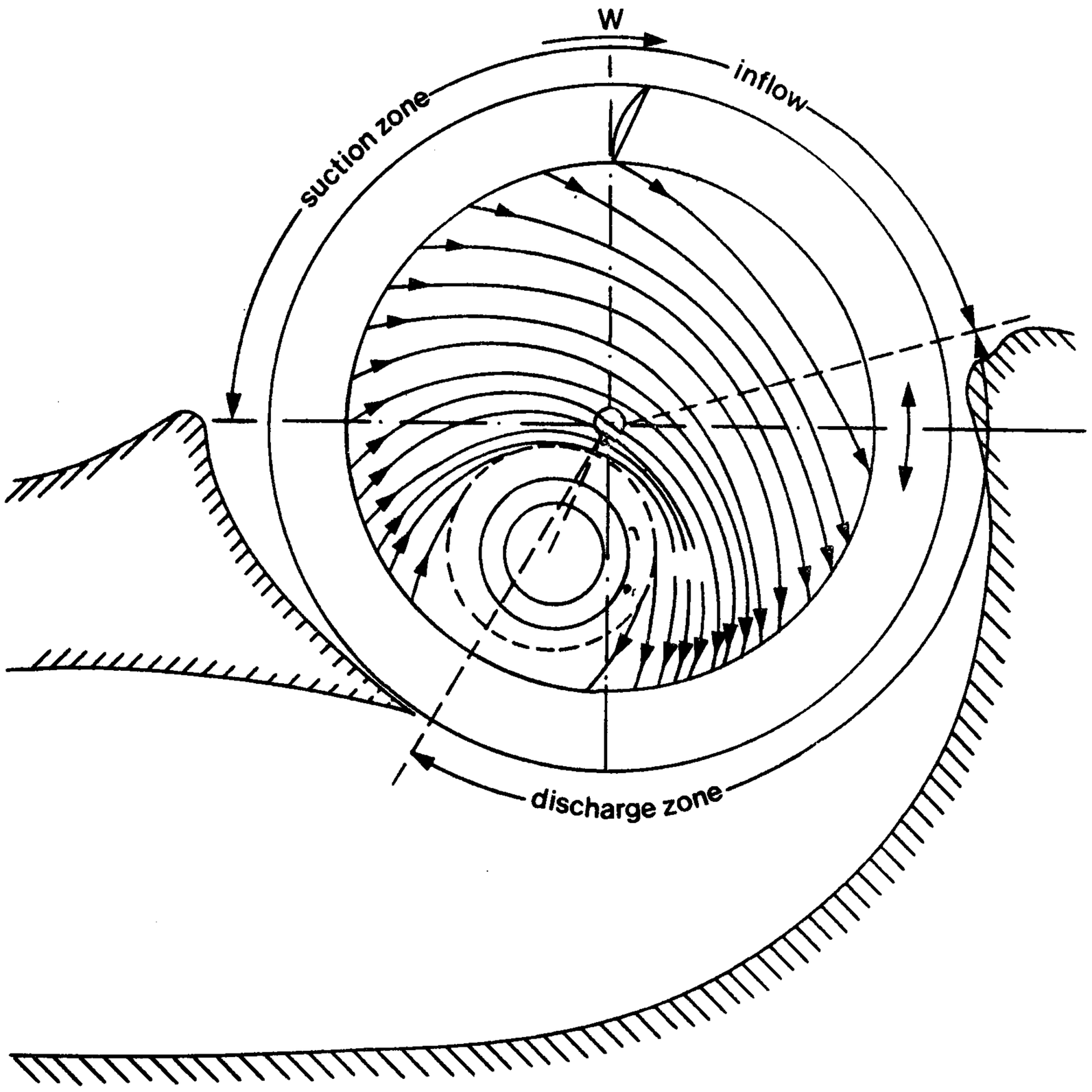

Figure 3·4 Calculated stream function (Ilberg & Sadeh)

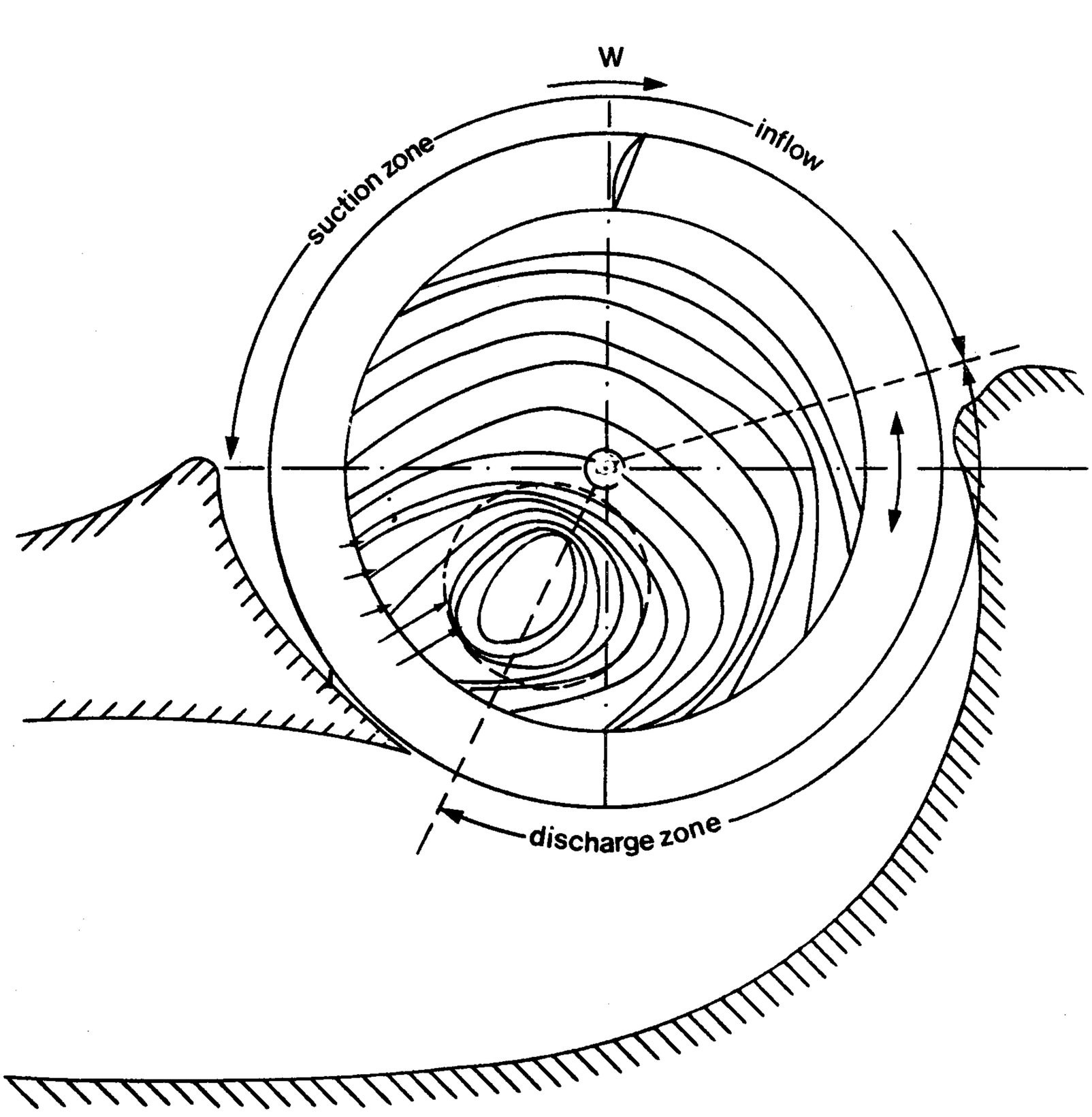

Figure 3·5 Measured isostatic pressure lines (Ilberg & Sadeh)

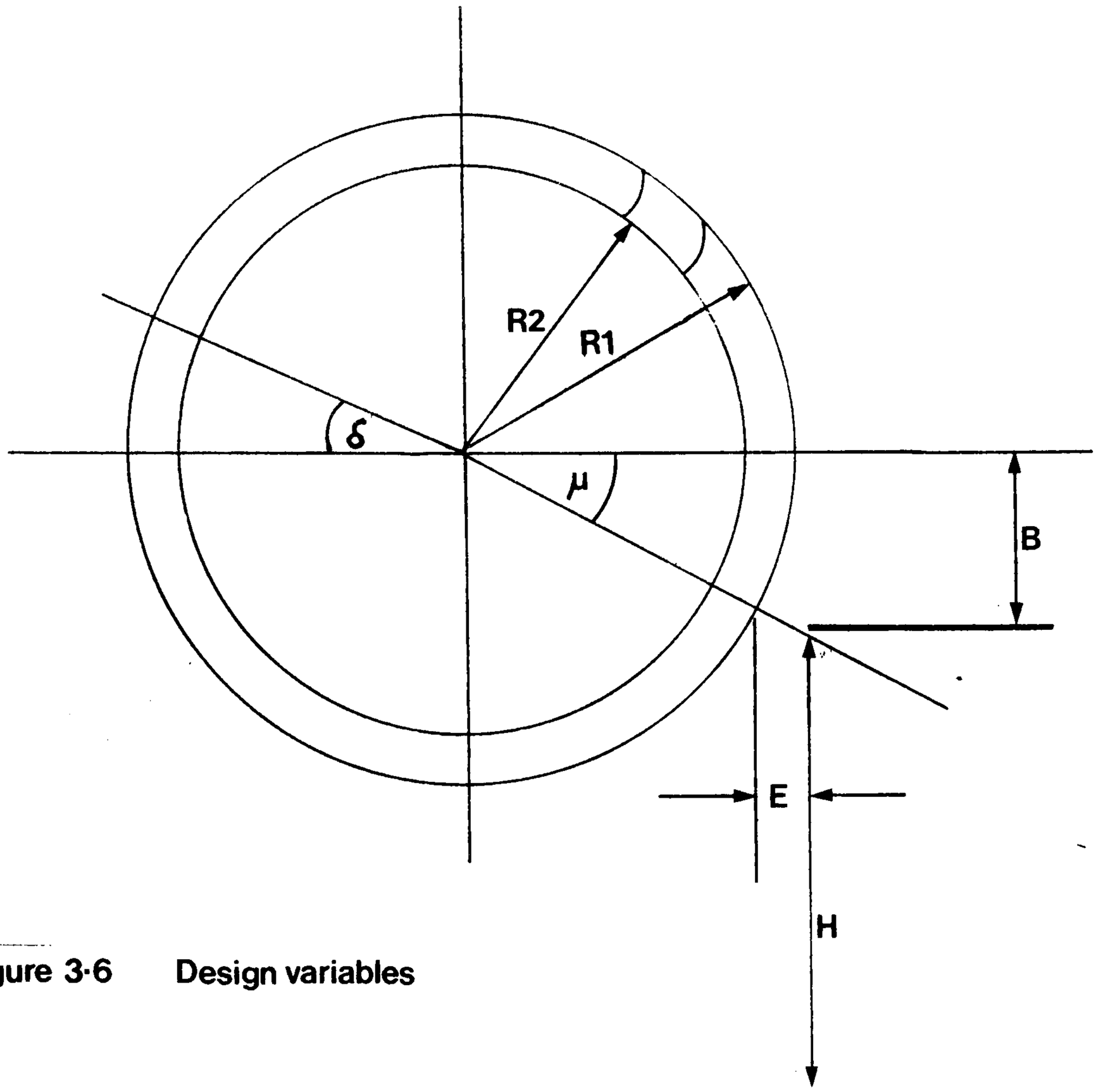

Figure 3·6 Design variables

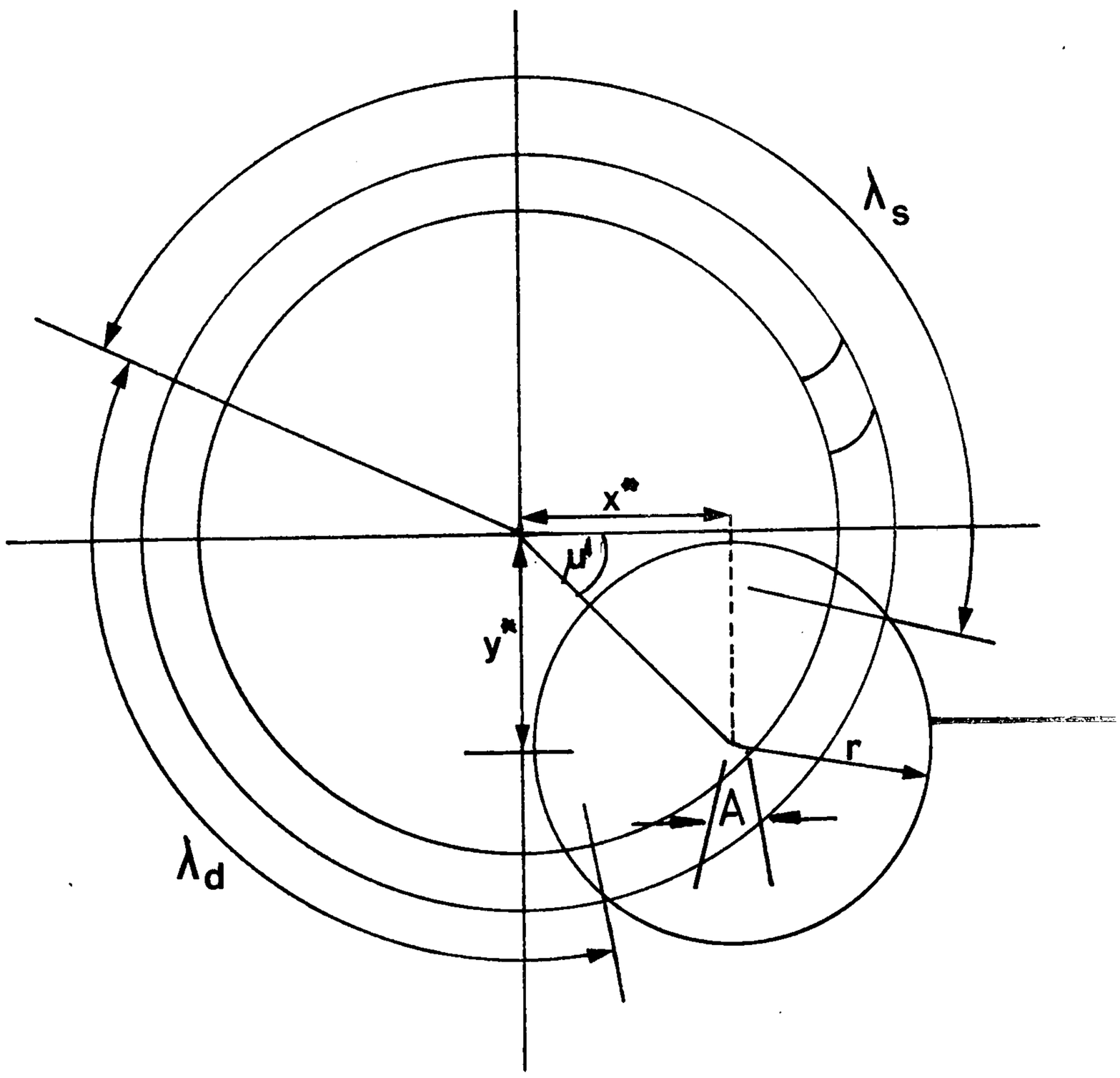

Figure 3·7 Vortex location variables

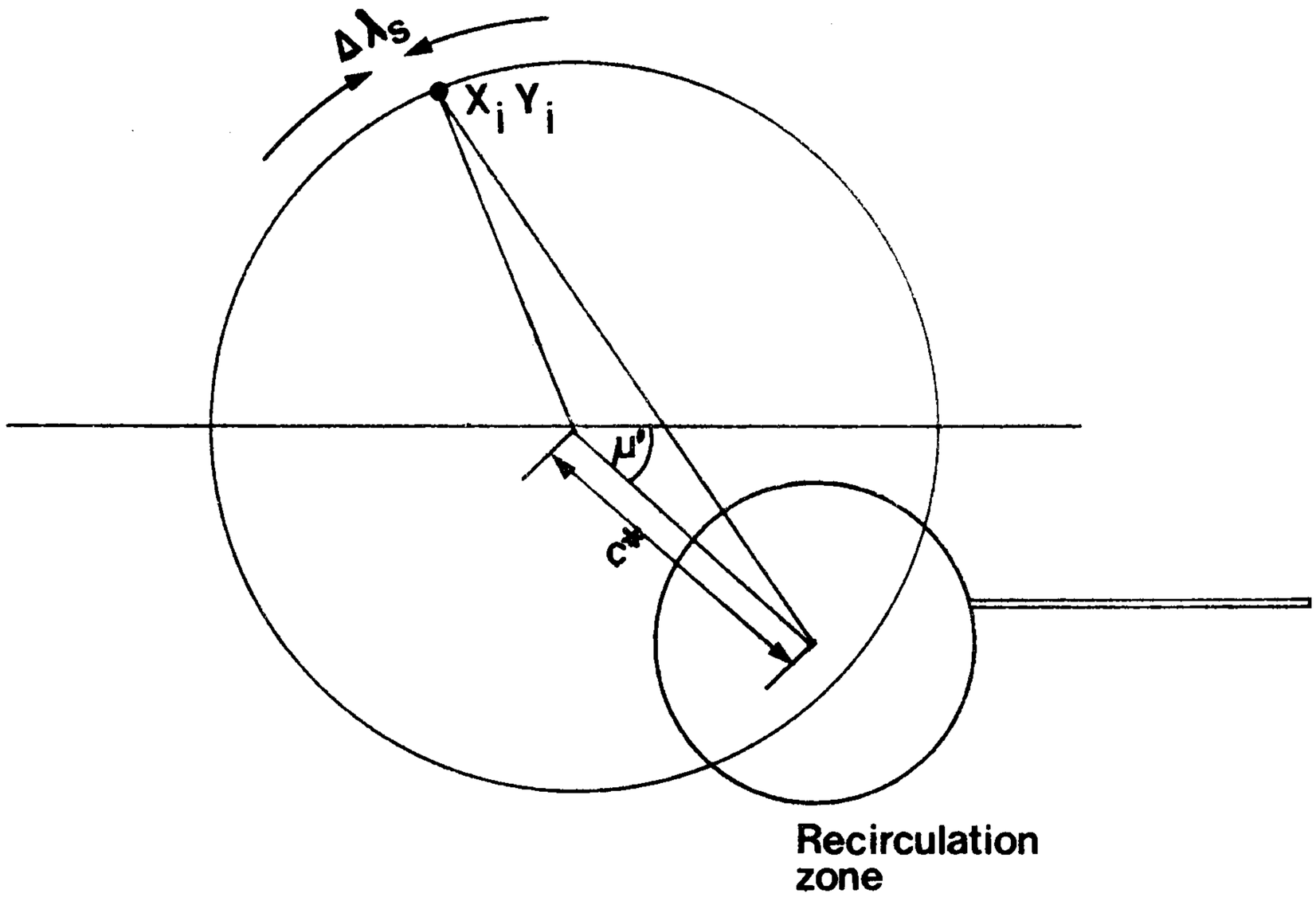

Figure 3·8

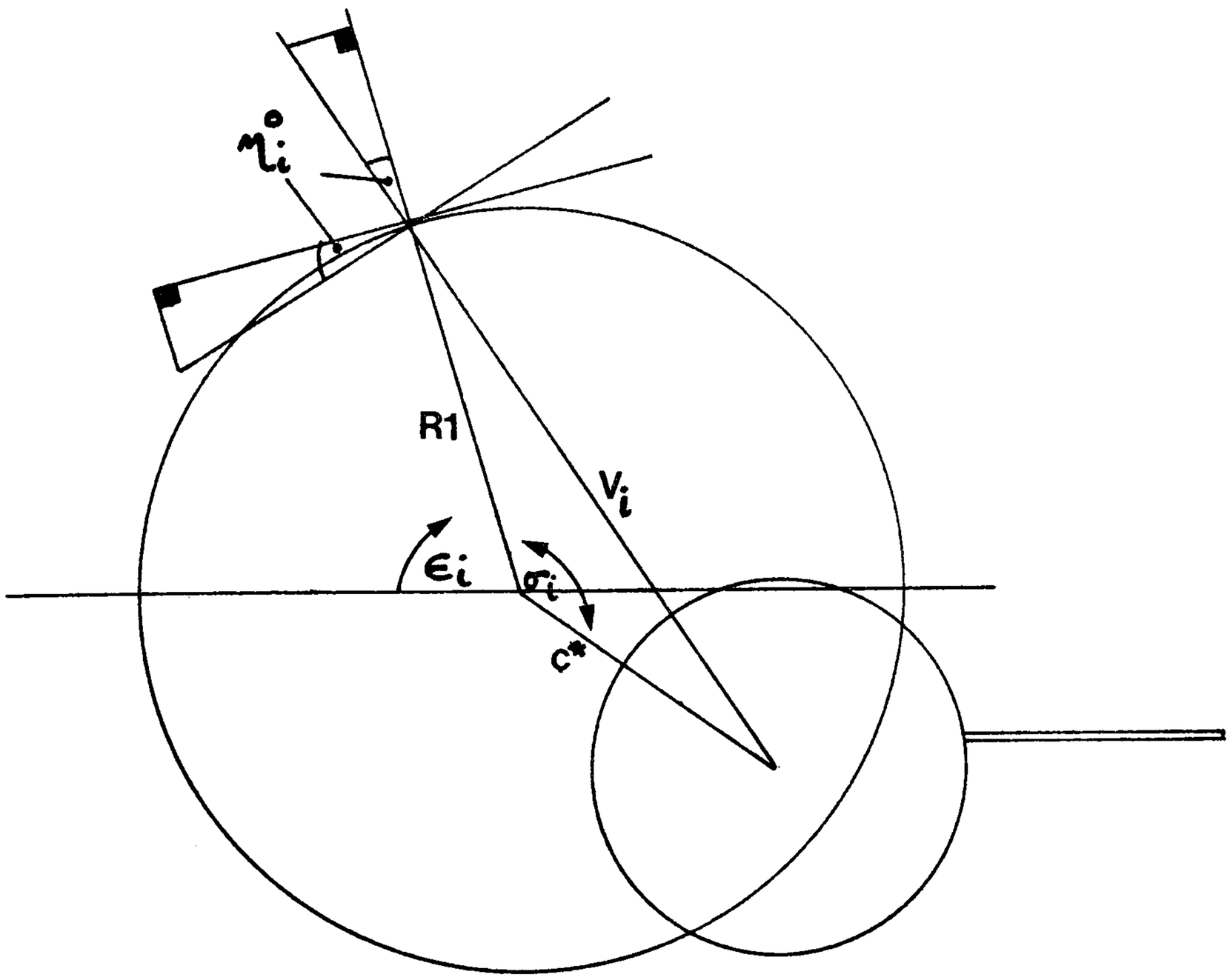

Figure 3·9

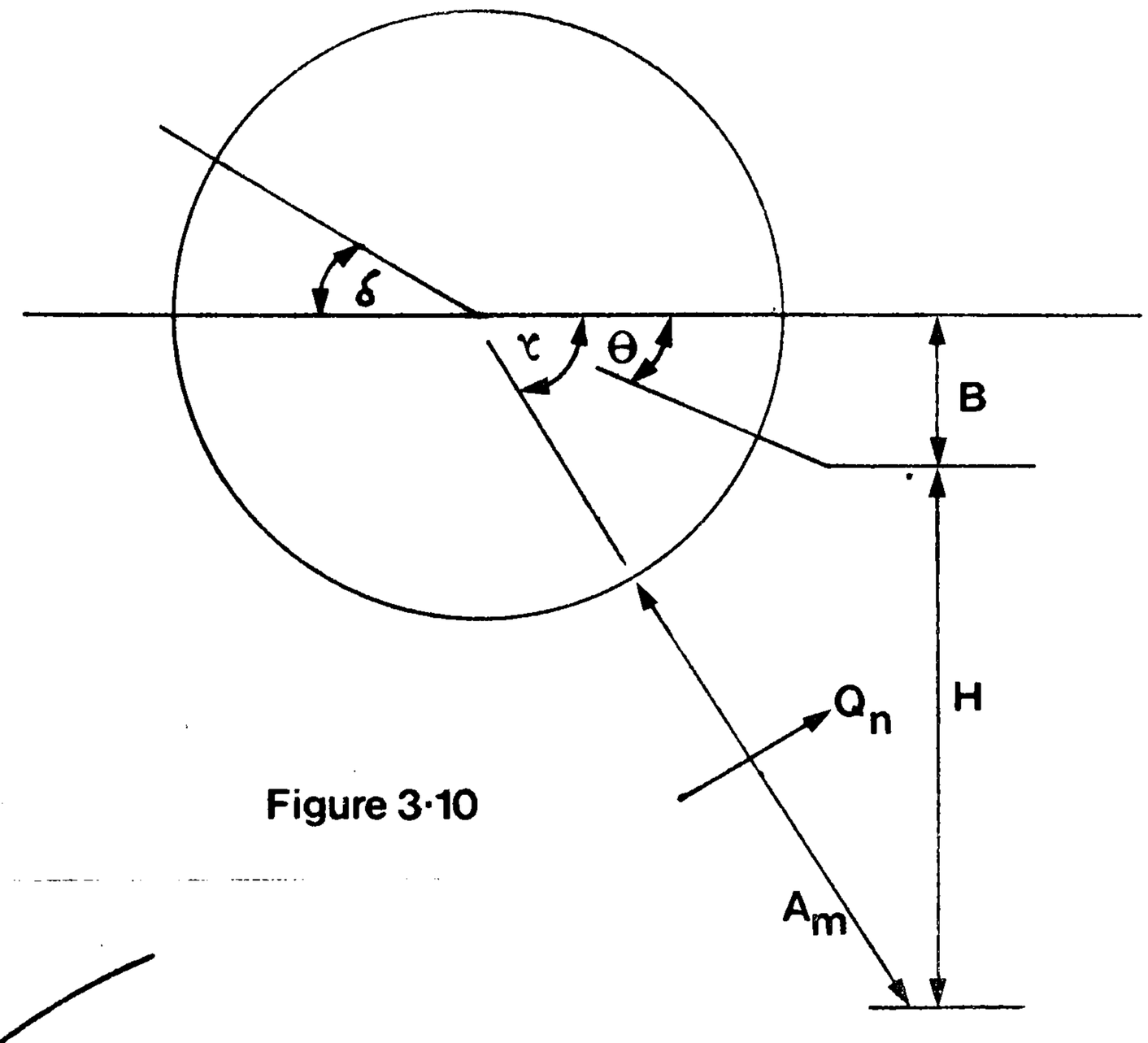

Figure 3·10

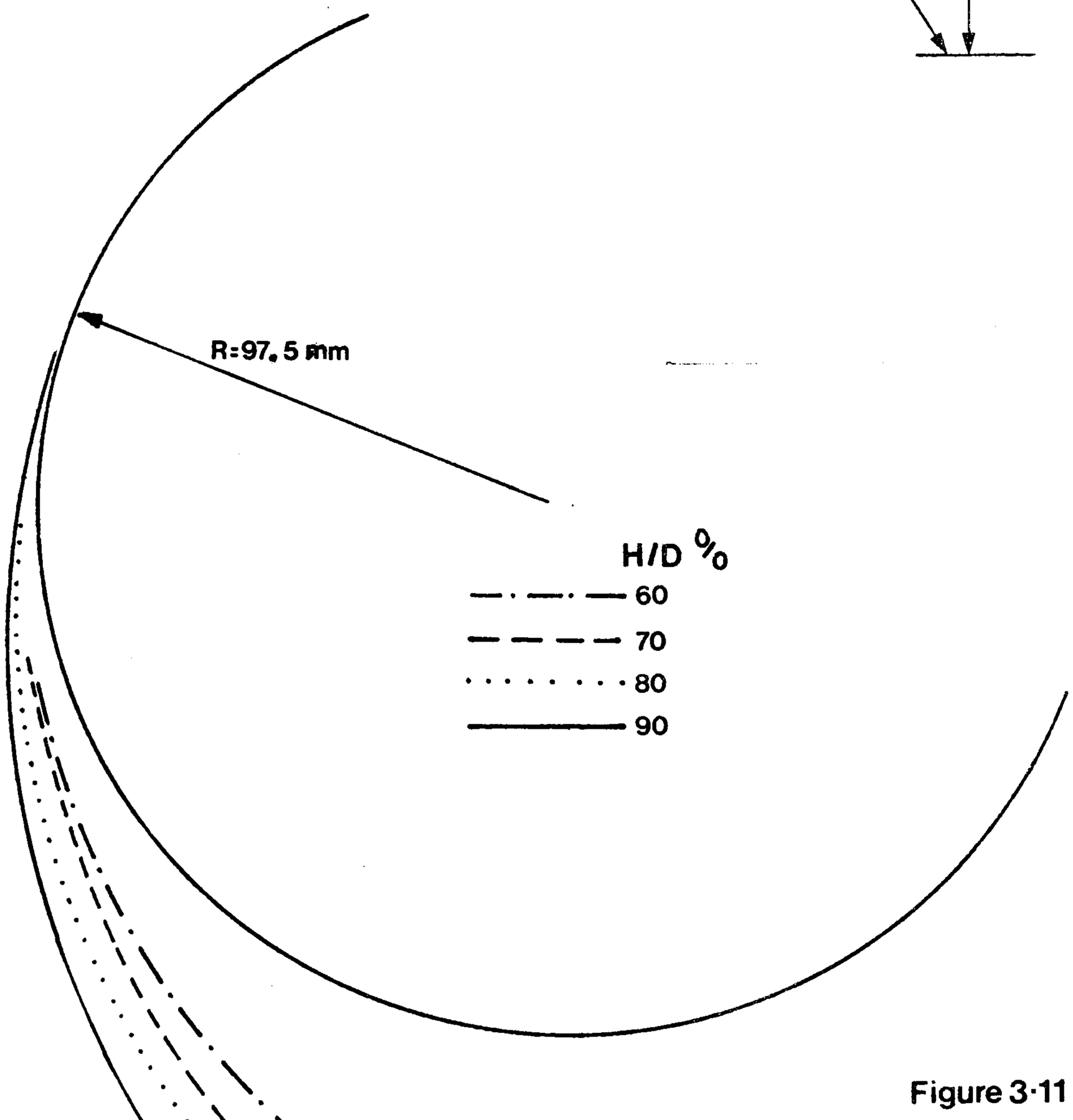

Figure 3·11

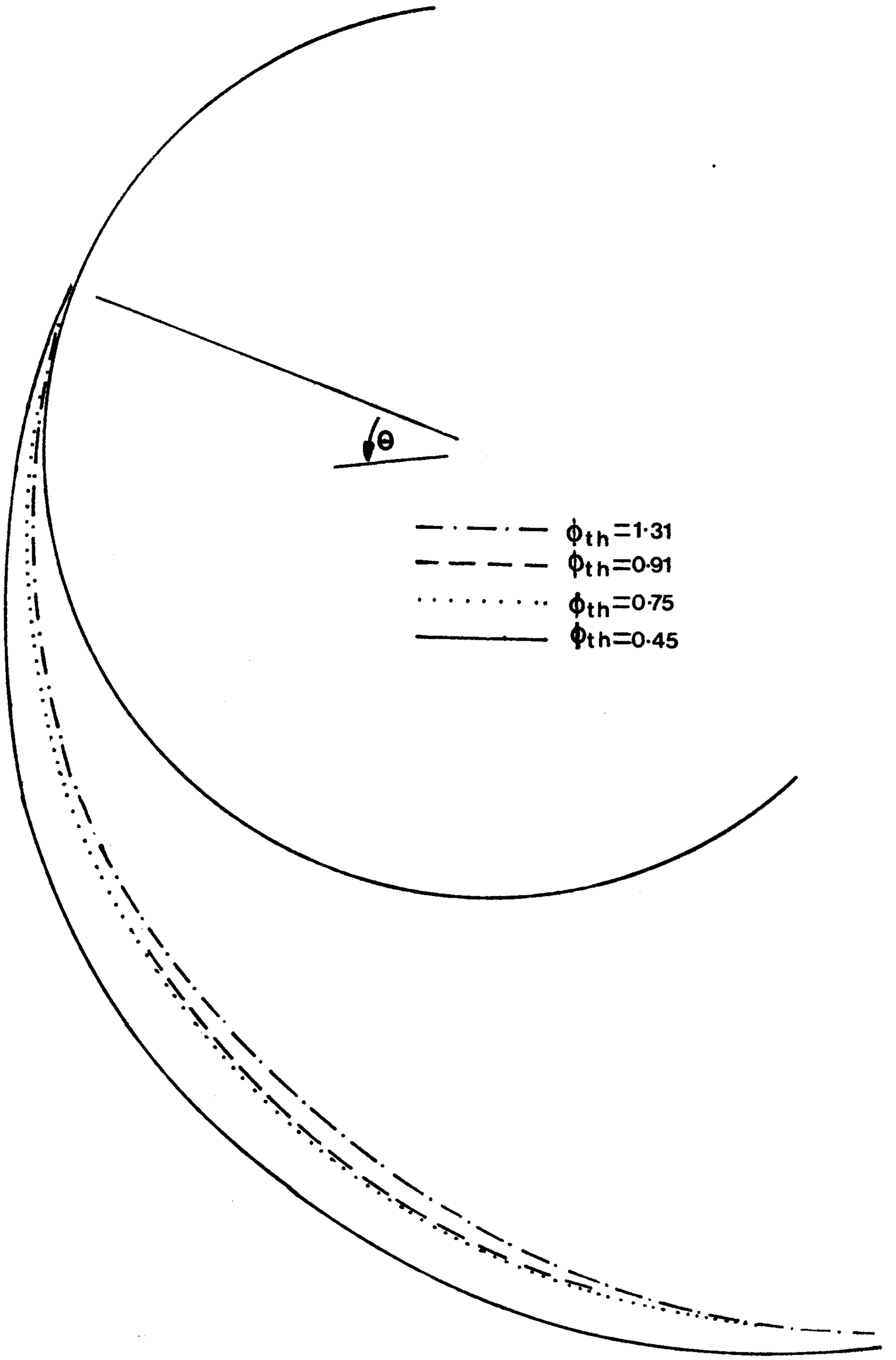

Figure 3·12 Effect of theoretically determined flowrate on the rear wall profile design, determined using the principal of 'constant mean velocity'.

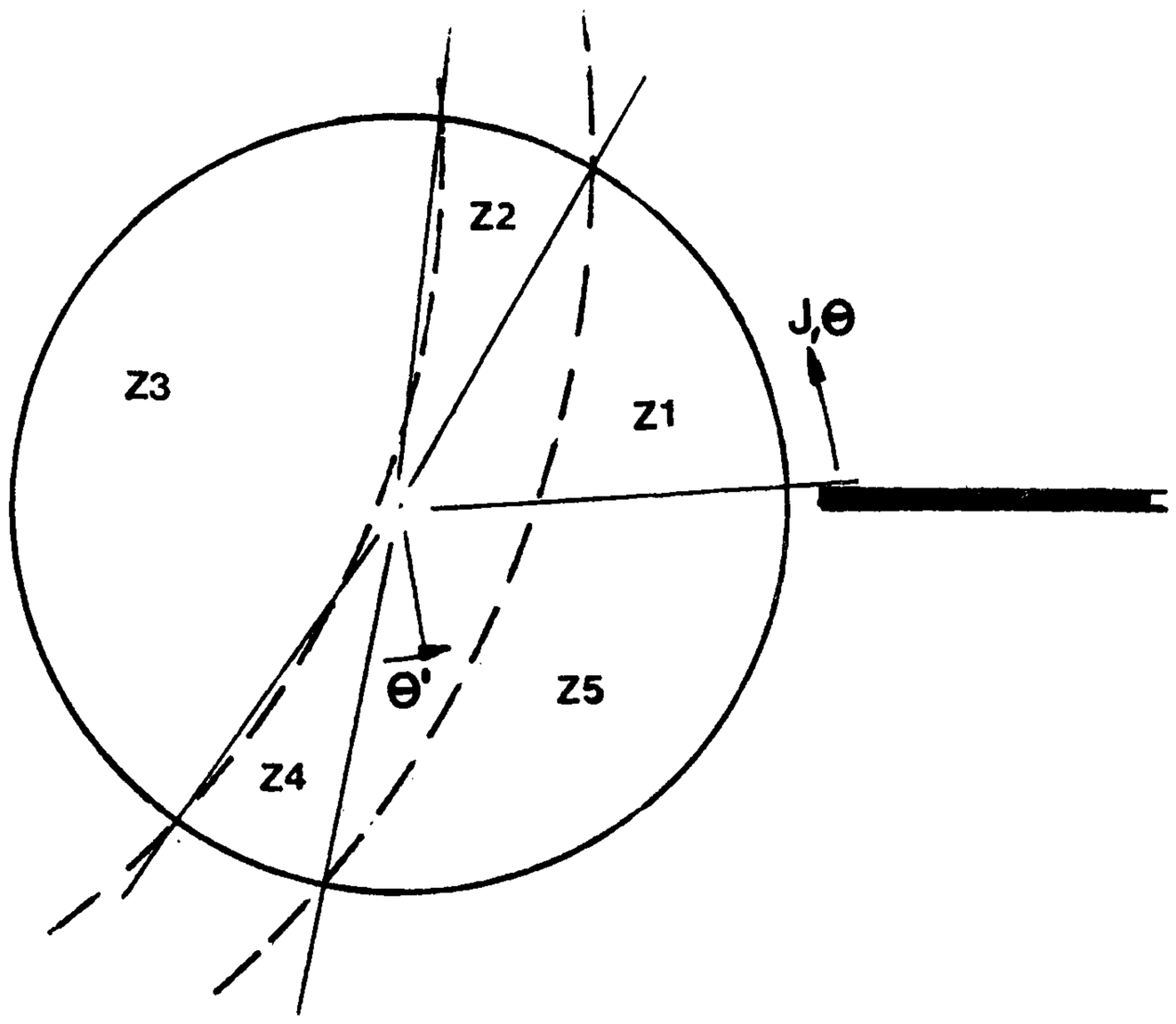

Figure 3·13 Forced vortex zones (Z1~Z5)

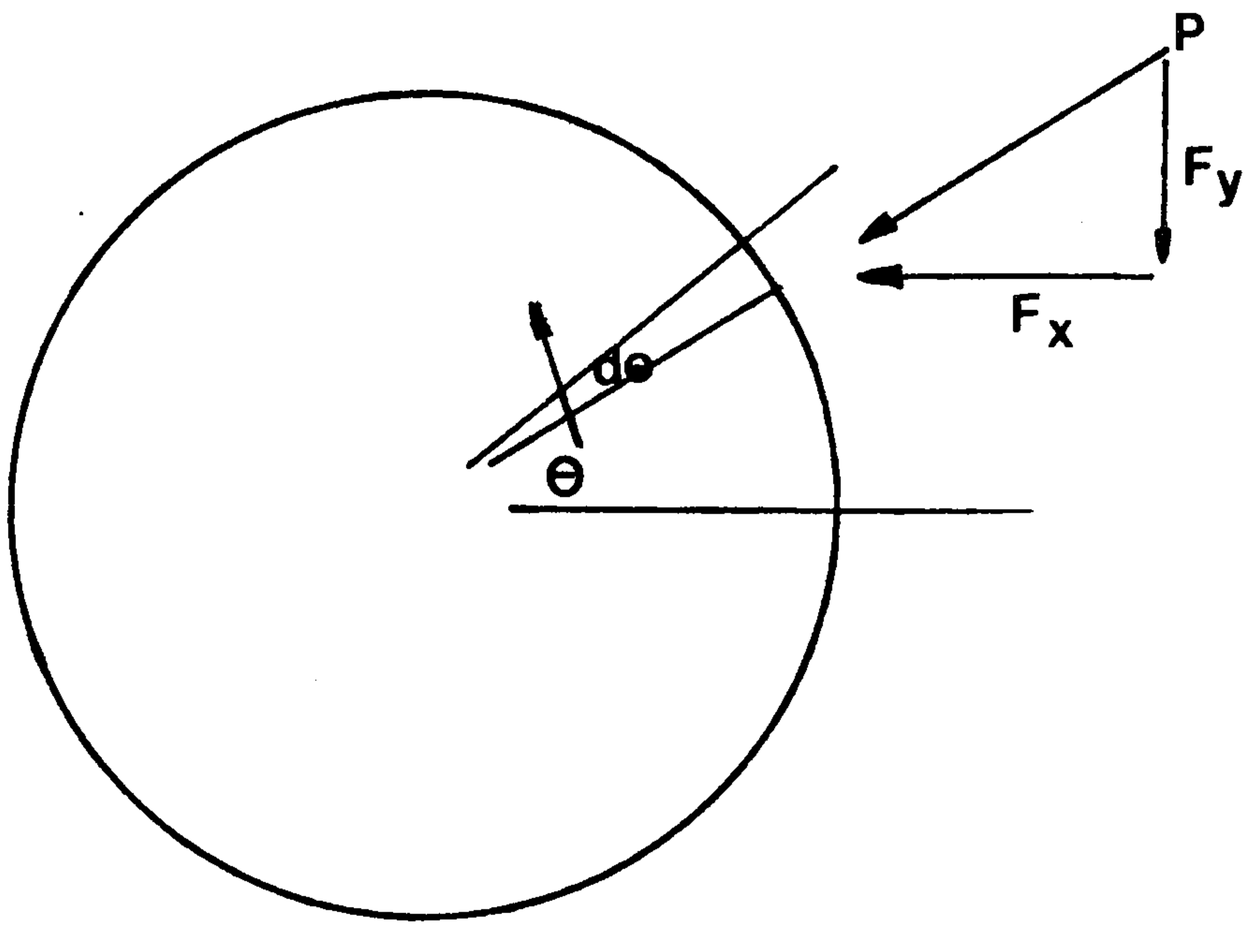

Figure 3·14 Resultant force on the postulated vortex 'core'

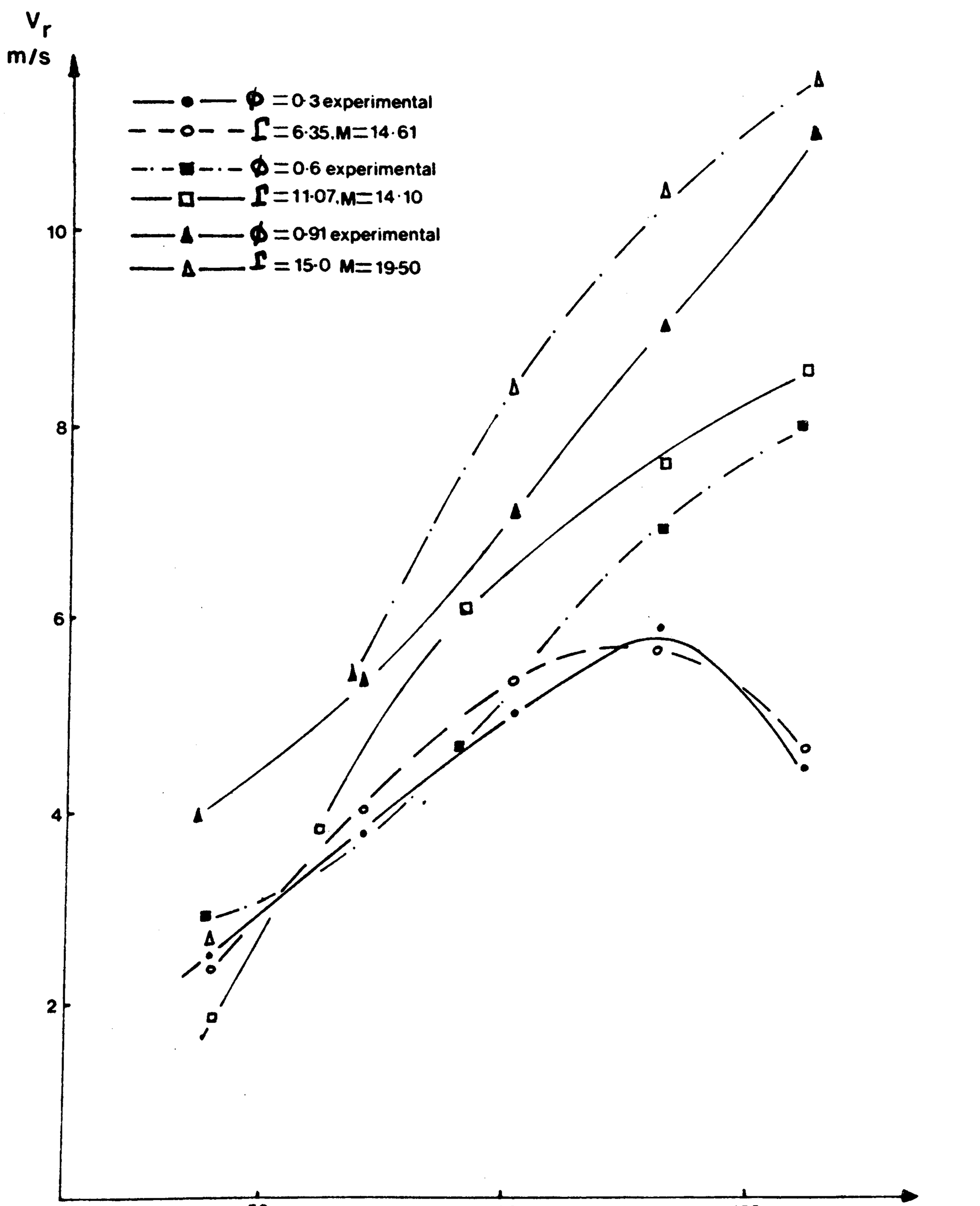

Figure 3·15 Observed and modelled radial velocities

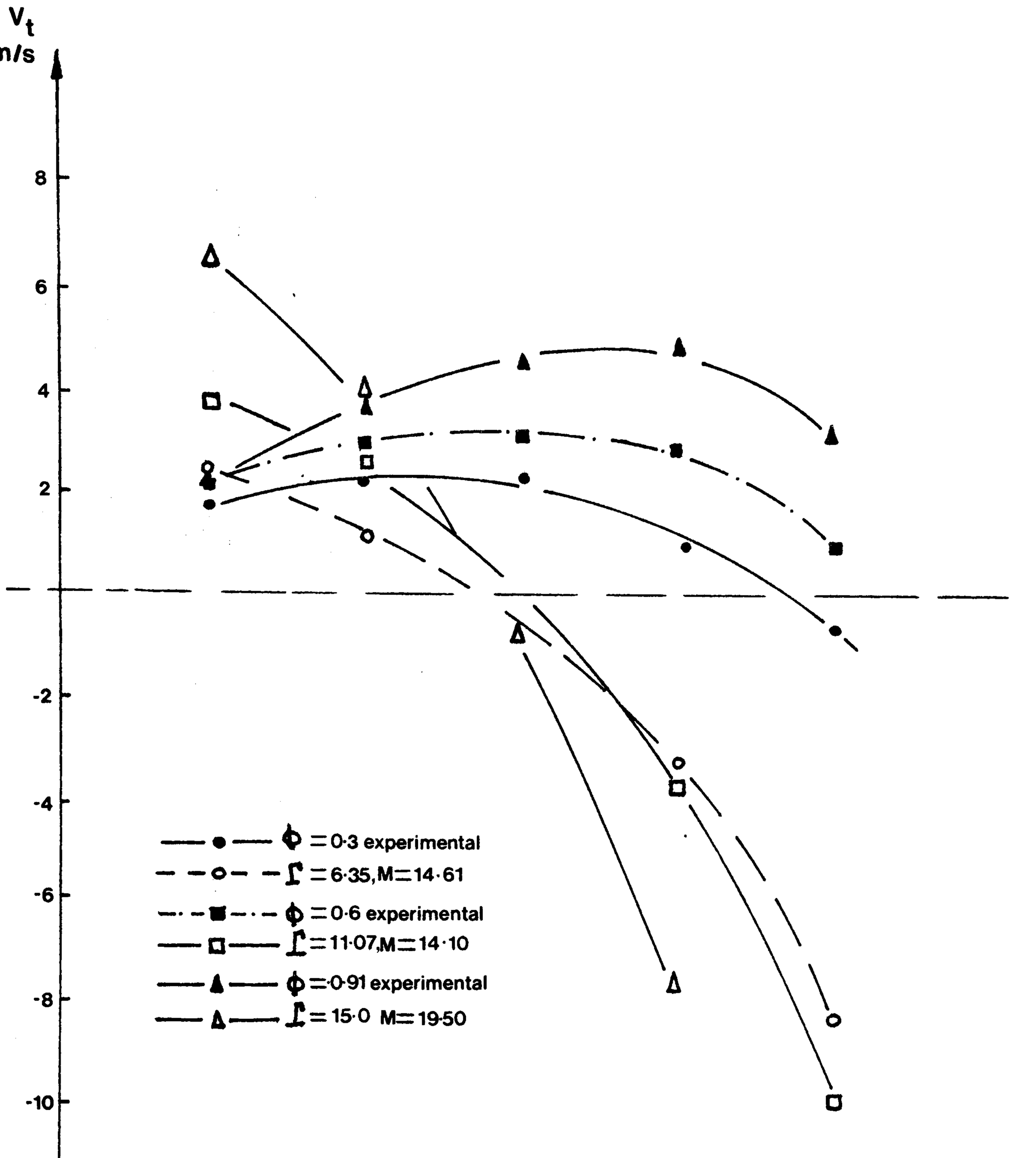

Figure 3·16 Observed and modelled tangential velocities

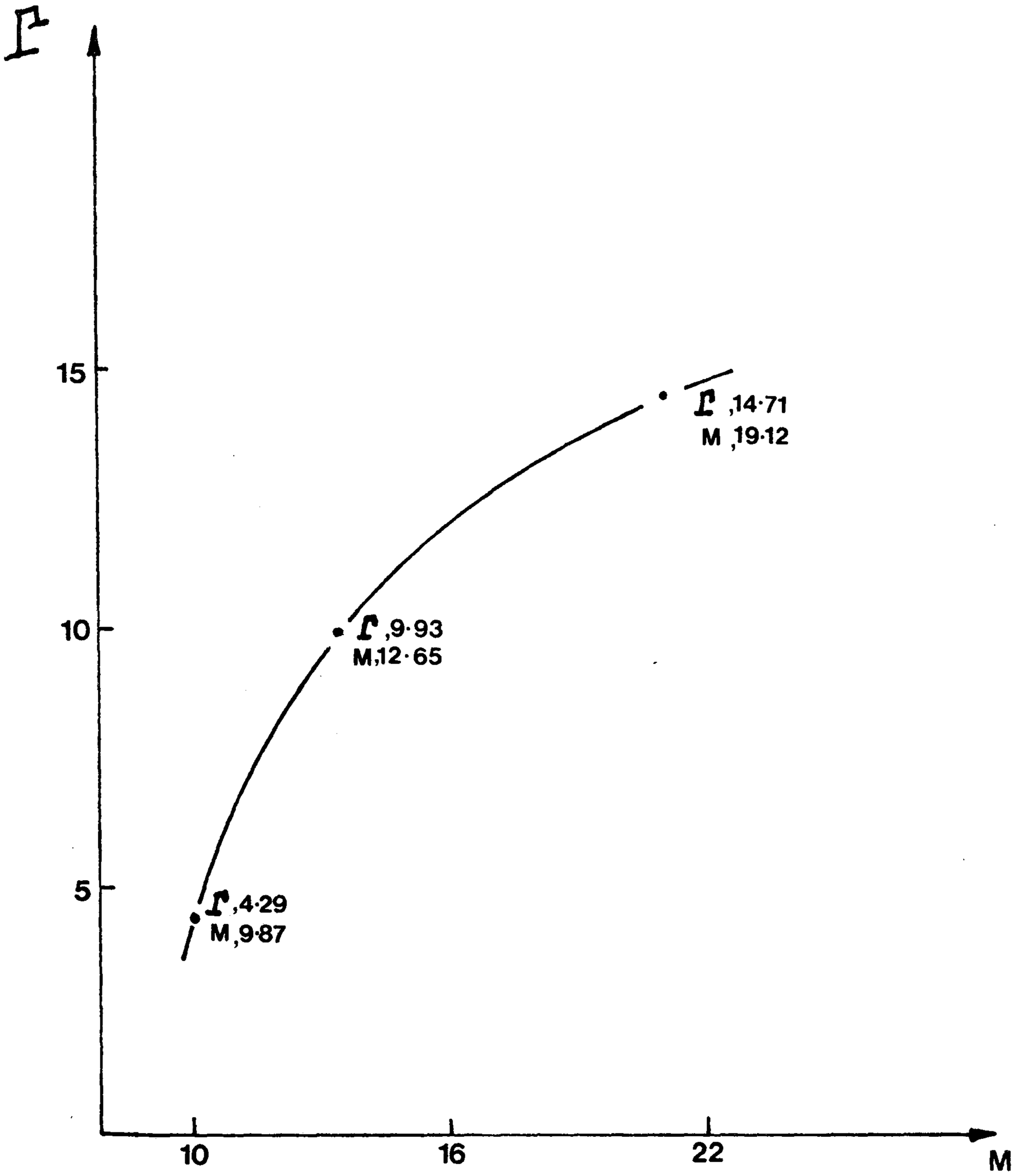

Figure 3 17 Flow field parameters

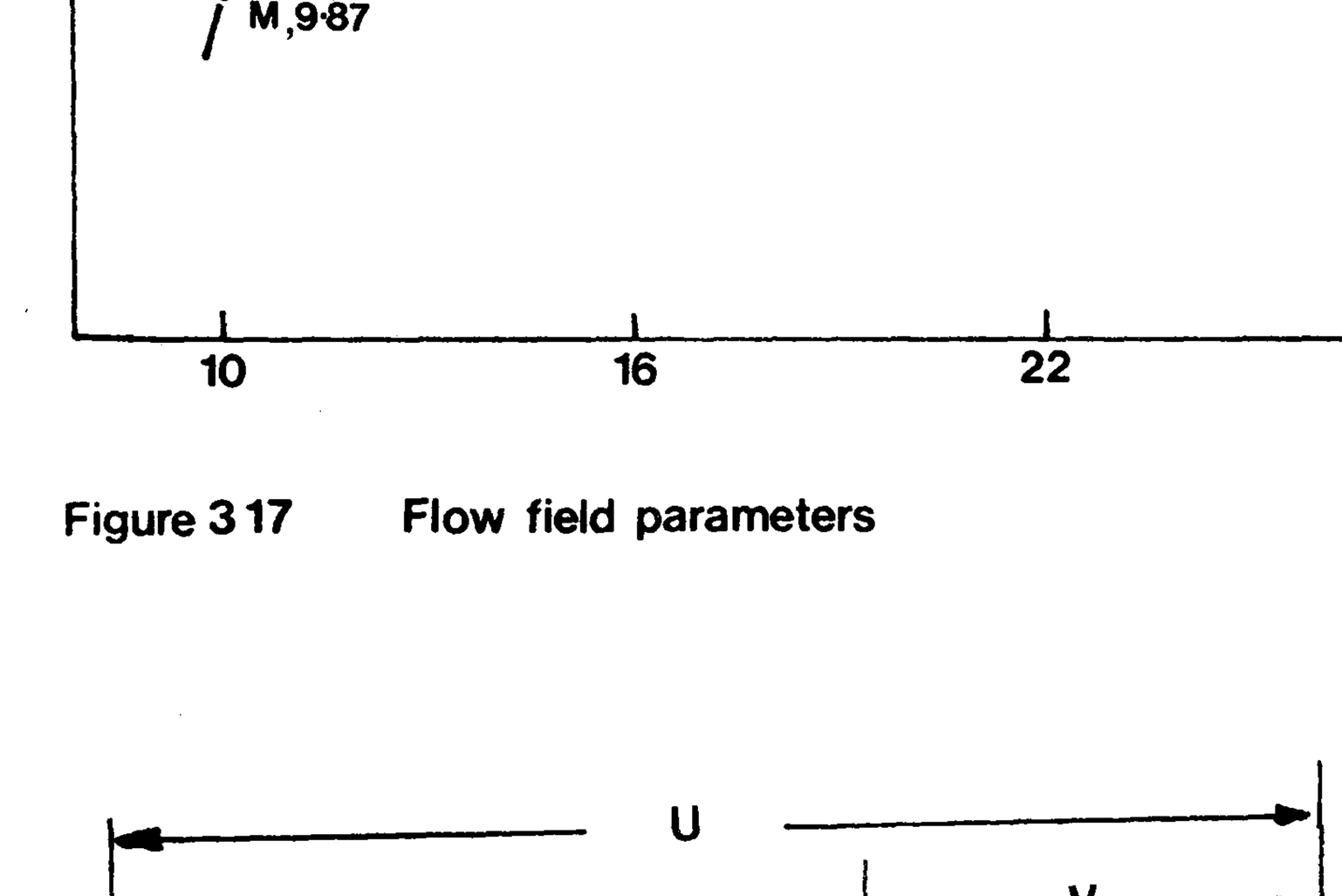

3·18 'Shock' velocity triangle

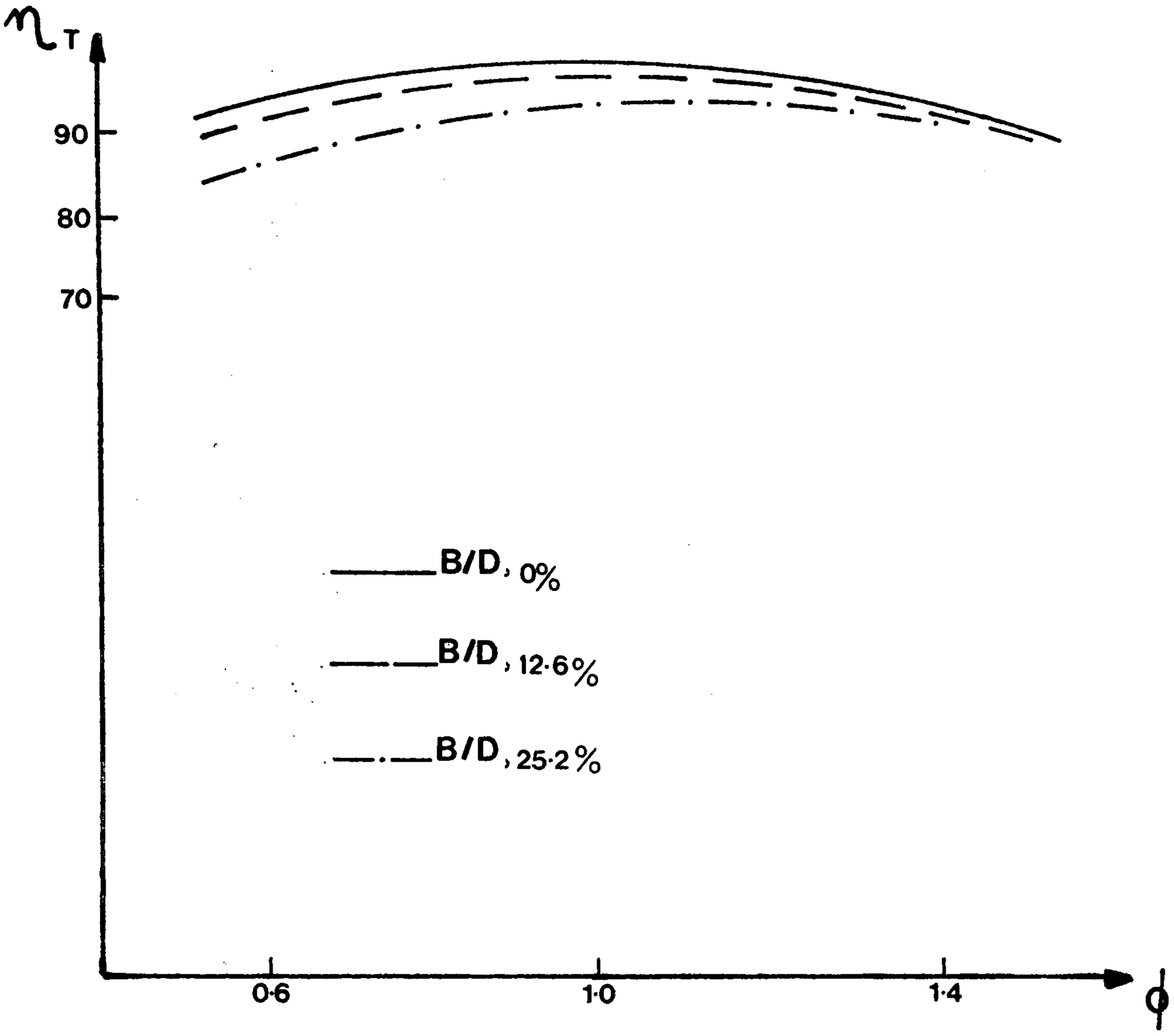

Figure 3·19 Theoretical efficiencies

Figure 3·20 Low flowrate temporal pulsations

CHAPTER FOUR

4.1 INTRODUCTION TO SOUND PRODUCTION MECHANISMS

There are three recognised ways in which acoustic energy may be derived from kinetic energy; they are, in descending order of efficiency, monopole, dipole and quadrupole sources. These terms are encountered repeatedly in the study of sound generation, for clarity these terms are discussed briefly below; more information is available from the text edited by RICHARDS and MEAD(67).

4.1.1 MONOPOLE SOURCE

The most efficient generating mechanism ; conversion from kinetic to acoustic energy is by forcing the mass within a fixed region of space to fluctuate. This may be visualised as a uniformly, radially pulsating sphere surrounded by a perfectly homogeneous material of infinite extent (such that no end reflections occur). The acoustic pressure $\tilde{\Delta}P$, is given by equation 4.1:

$$\tilde{\Delta} P_{mono} \propto 1/r \frac{\partial M(t)}{\partial t} \qquad 4.1$$

M(t) - Rate of addition of mass from the neighbourhood of the source to the surroundings.

r - Polar distance to the observer.

4.1.2 DIPOLE SOURCE

This is the predominant sound generating mechanism in low speed turbomachinery. Energy conversion requires the momentum within a fixed region of space to fluctuate. This process is equivalent to a uniformly pulsating sphere, oscillating in the Z-direction as a rigid body. Thus, the dipole is vibrating

along one axis; which accounts for the directional nature of sound generated by a dipole source - by virtue of the normal particle velocity on the sphere surface being a function of its polar location.

$$\tilde{\Delta} P_{dipole} \propto \frac{\partial}{\partial Z}\left\{\frac{r_{sp}}{r}, \frac{\partial M(t)}{\partial t}\right\} \qquad 4.2$$

r - Observer location.

r_{sp} - Radius of sphere.

Z - Direction of oscillation.

4.1.3 QUADRUPOLE SOURCE

The least efficient energy conversion mechanism. Sound is generated aerodynamically with no motion of solid boundaries, for example, in the mixing region in the exhaust of a jet. Within a fixed region of space there is no change of either mass or momentum; energy conversion is by forcing the rates of momentum flux across fixed surfaces to vary. Momentum flux is the rate at which momentum in the Z_i direction is being transported in the Z_j direction, with corresponding velocities V_i and V_j. A quadrupole source may be modelled as a double dipole, both oscillating along the same axis. Quadrupole generated noise exhibits complex directionality.

$$\tilde{\Delta} P_{quad} \propto \frac{\partial}{\partial Z_i}\frac{\partial}{\partial Z_j}\left\{\frac{1}{r} V_i V_j \rho_0 D'^3\right\} \cdot F(\nu, \Delta T) \qquad 4.3$$

D' - Characteristic dimension.

ρ_0 - Ambient density.

ν - Fluid viscosity.

Δ T - Temperature change across the region.

Generally the dissipation of acoustic energy into heat

by viscosity and heat conduction is negligible over short distances (<100m). In this case the viscosity and temperature defect terms in equation 4.3 may be neglected.

4.2 DEVELOPMENT OF FLOW-ACOUSTIC THEORY

Equations 4.1 - 4.3 may be applied to single sources, but within an acoustic field the degree of radiation will depend also on the level of phase cancellation between adjacent sources.

In the following sections the term 'disk' refers to the volume swept by the blades (not to be confused with an actuator disk) ;'stationary', with axial fans implies no axial motion.

Dimensional analysis by LIGHTHILL(45) has shown the acoustic power radiated by a quadrupole source, to be approximately proportional to the eighth power of some typical flow velocity. Similarily, the dipole source velocity exponent is approximately six and the monopole exponent, four. Overall sound power radiation for any fan type or homologous series of fans, will have a sound power / rotational velocity relationship which depends on the relative contributions of the three sources. However, it is not simply a matter of how an acoustic mechanism varies with a typical speed, rather how the flow conditions related to that acoustic mechanism vary with speed.

A considerable amount of work has been done attempting to define a consistent relationship between fan rotational speed and the generated sound power, this is particularily the case with centrifugal fans. But, unless strict similarity

is ensured and design variations are accounted for the empirically derived equations can give considerable error when applied. Consequently, results from various researchers differ, with the power - velocity exponent generally in the range: $4 \leq \alpha \leq 6$; where $PWL = k\ U^{\alpha}$.

The first theoretical study of noise from rotating machinery was that of GUTIN(33) in 1948, on the sound produced by a stationary, two-bladed propeller. His basic equation was developed for a 'steady-load' case, where the blade loading distribution is independent of time. Here, an element of fluid within the rotor disk is considered to recieve an impulse periodically with the passing of a blade. These impulses are treated as a series of dipole sources distributed throughout the disk, and of constant strength at each radius. The dipole source amplitudes are obtained from the thrust and torque loading conditions (see appendix A1) and the fundamental frequency is $Z\Omega$.

Where: Z - Blade number.

Ω - Rotational frequency (Revs/sec).

The resultant sound field can be analysed into a series containing the fundamental frequency and its' integer harmonics.

One assumption used in this formulation is that the acoustic pressure satisfies the homogeneous wave equation, 4.4.

$$\frac{\partial^2 p}{\partial t^2} - c^2 \frac{\partial^2 p}{\partial x^2} = 0 \qquad 4.4$$

Equation 4.6 holds for the general case of an unbounded fluid. When solid boundaries are present, certain modifications to the theory are necessary to account for reflections at the surfaces and an uneven quadrupole distribution - quadrupole sources may only exist external to the blades, for example. LIGHTHILL's formulation was extended by CURLE(18), who replaced fixed boundaries with surface force distributions, and further by FFOWCS-WILLIAMS and HAWKINGS(27) with a more permissive treatment enabling moving boundaries to be considered.

4.3 THEORY OF SOUND PRODUCTION BY CROSS-FLOW FANS

4.3.1 DETERMINATION OF THE IMPORTANT SOUND PRODUCTION MECHANISMS

Sound power generation is governed by LIGHTHILL's equation (4.6), the practical applicability of which depends on how accurately the components of source strength can be specified, with no prior knowledge of density variations within the fluid. There are two primary steps in formulating a sound power model: the first is to isolate mechanisms of sound production; which are tenable and which are likely to dominate in the fan type under consideration. Once the mechanisms have been determined, the equations are solved using available theoretical and experimental data. Where data are unavailable intuitive approximations have to be made to enable solution.

In the forthcoming analysis, one fundamental assumption made is the impeller runs unshrouded, but with unimpeded performance. This condition will certainly give less realistic

For equation 4.4 to hold, the fluid surrounding the blade surfaces must, everywhere, have velocities which are small compared to the speed of sound; such that acoustic waves can travel radially from their source. However, for high speed rotating machinery and turbomachinery with unsteady internal flow, there may be fluid velocities induced which are not negligible compared to the speed of sound.

It was LIGHTHILL(45) who resolved this, in 1952, by treating the fluid as a perfect acoustic medium containing quadrupole sound sources of strength T_{ij} - equation 4.5.

$$T_{ij} = \rho U_i U_j + p_{ij} - c^2 \delta_{ij} \qquad 4.5$$

As mentioned in 4.1.3, the last two terms in the above stress tensor may usually be neglected. The quadrupole strength density then becomes equal to the 'fluctuating Reynolds stress' of the fluid surrounding the blades.

With this corollory to the homogeneous wave equation, it is possible to itemise the source components of the whole radiation field: sound produced by a machine may be regarded as being generated by quadrupoles of strength density T_{ij} distributed throughout the surrounding fluid, plus dipoles distributed over the machine surfaces and monopole sources related the volume displacement.

LIGHTHILL's acoustic analogy was to regard density variations within the fluid as being driven by a source distribution Q.

$$Q = \frac{\partial^2 \rho}{\partial t^2} - c^2 \nabla^2 \rho \qquad 4.6$$

results than if all the casing was accounted for in the calculations, but the influence of casing on sound radiation and generation would be far too complex to model, and poor assumptions could quite possibly yield less satisfactory results than those for an unshrouded rotor.

The only part of the casing considered in the following analysis is the vortex wall: the importance of casing and ductwork resonances and reflections must, though, be appreciated.

It would be very difficult to determine all the separate noise generating processes which contribute to the overall discrete and broad-band noise. It would be even more difficult to numerically evaluate the importance of each effect. Table 4.1 lists the most important sound generating processes; grouping is by order of the generating mechanism and whether the effect is a tongue-interaction mechanism or whether it occurs within the impeller flow-field region.

	MONOPOLE	DIPOLE	QUADRUPOLE
TONGUE INTERACTION	1. Mass transfer across stator.	1. Lift fluctuations from shed vortices. 2. Lift fluctuations due to wake interaction. 3. Random lift on tongue due to turbulent outflow	1. Irregular inflow causing turbulent interaction with potential field of rotor. 2. Wake/wake interaction.
IMPELLER AND/OR FREE-FLOW REGION	1. Blade motion - thickness displacement.	1. Blade-slap. 2. Boundary layer turbulence. 3. Force dipoles due to blade loading.	1. Turbulence within disk.

Table 4.1

Monopole radiation, although efficient, is generally considered small compared to other sources.

Blade-slap is primarily an axial rotor phenomenon and is caused by the rapidly fluctuating angle of incidence which occurs when a trailing blade intercepts vortices cast by its predecessor. Blade-slap may be neglected with cross-flow fans, by virtue of the nature of the flow, which is substantially radial, and because of the damping effects which occur within the impeller flow-field, see section 8.3.

MORFEY(54) suggests that fluctuating shear stresses on the blade will generally be 10 - 20 dB down on pressure fluctuation, dipole sources. Considering this, and the difficulty of evaluating boundary layer turbulence, the effect is disregarded in the analysis.

Of the quadrupole radiation mechanisms; only potential field interaction will be considered. Turbulent mixing within the rotor disk will not radiate at the low Mach numbers generally encountered with cross-flow fans, and wake / wake interactions are probably unimportant with these fan types, particularily because of the aerodynamic seal formed by the forced vortex.

The remaining mechanisms are evaluated as far as possible by modifying existing theories developed for axial machines, and making estimates of the variables wherever possible. There are a large number of approximations used, both in the original and derived theories. This reflects the complex nature of the study and the lack of substantial experimental results.

The computer program written to evaluate the theoretical sound power levels for different fan designs, requires an estimate of a number of aerodynamic values. These are supplied by another computer program, written to estimate the aerodynamic performance; the development of this predictive performance model is discussed in Section 3.3 - the inter-relationship between the two theories is further explained and evaluated in Chapter 5.

The noise analysis discussed in this Chapter must be viewed in light of its' originality, and as a first advance in attempting to understand the processes which govern cross-flow fan noise generation. Results given in Chapter 5 show that the analysis used goes some way to supplying an assessment of the dependence of noise upon fan design.

To simplify the analysis, sound power rather than sound pressure is dealt with. Directivity results, if required, will have to be experimentally determined. Particular mechanisms of noise generation will be discussed in subsequent sections; the four mechanisms considered are listed below, with the name of the principal authors from whose work the authors' own theory has been adapted, Table 4.2.

MECHANISM	AUTHOR
BLADE LOADING	S.E. WRIGHT (75)
WAKE/STATOR I'ACTION, TURBULENCE/STATOR I'ACTION	HANSON (35)
STATOR LIFT FLUCTUATIONS	CURLE (18b) and FUKANO et al (29)
POTENTIAL FIELD INTERACTION	FFOWCS-WILLIAMS and HAWKINGS (27)

4.3.2 SOUND GENERATED BY BLADE-LOADING

4.3.2.1 EXISTING THEORY

GUTIN(33) is accredited with the first modern work on aerodynamic noise generation. He showed that, for a stationary propeller, the aerodynamic forces on the blades could be rep-represented as a series of acoustic dipoles. In this early formulation the blade loading distribution is assumed steady, i.e. invariable with θ, where; θ = angle of rotation ($0 \leq \theta \leq 2\pi$).

Although the blade loading distribution is constant, a small volume of air within the swept disk is subject to a periodic loading, of fundamental frequency $Z\Omega$. The results of GUTIN's work predicted the first few rotational harmonics quite accurately; however , steady loading of a free running, stationary propeller is very much a special case in the study of machinery noise.

LOWSON and OLLERHEAD(48) and WRIGHT(75) extended GUTIN's theory to account for unsteady, θ - variant, loading. Typically with propellers, the loading irregularity may be either impulsive or distorted. Impulsive loading would include 'blade-slap', and distortion could be due to forward motion of the propeller, blade stall or inlet asymmetry.

The disk time - load plot consists of a series of rectangular pulses, the width of each being related to the blade chord and the interval between pulse centres being $1/Z\Omega$ secs. Overall noise is represented as the summation of these impulses over the whole disk, with corrections for phase relations. The situation is fundamentally the same whether the loading is steady or unsteady with respect to θ. WRIGHT(75) analysed

the blade time - load plot and developed a theory for sound radiation from an asymmetrically loaded rotor. The theory adopts the concept of 'blade loading harmonics'; it is general and covers GUTIN's model.

If the potential field varies with θ, as it does with cross-flow fans, a blade will experience a fluctuating force as it rotates. If the blade force pattern is repeatable over 2π it may be Fourier analysed into a constant term plus a series of blade loading harmonics; each discrete frequency harmonic is treated by WRIGHT as a rotating acoustic mode, radiating a discrete tone. The resultant sound at each harmonic of the rotational frequency is affected by ALL the blade loading harmonics. The steady load case of GUTIN includes no blade loading harmonics, merely the constant term in the Fourier series. WRIGHTs' result is expressed in its' most usable form by HUBBARD et al(37):

$$\text{(Real part) } P_n(r,\theta,\phi) = \frac{1}{2\pi c\, r} \left(nZ\Omega T_\lambda \cos\phi - \frac{\Omega\, Q_\lambda}{M_t\, R_{eff}}\right)$$

$$(nZ - \lambda))\; J_{nZ-\lambda}(nZ\, M_t \sin\phi)\; e^{i\lambda\theta} \qquad 4.7$$

P_n - Acoustic pressure of harmonic No. n.

r,θ,ϕ - Polar coordinates of the observer.

Z - Blade number.

c - Speed of sound.

λ - Blade loading harmonic number.

T - Thrust

Q - Torque

M_t - Blade tip Mach number.

R_{eff} - Effective radius.

$J_n(x)$ - Bessel number of order n, argument x.

Solution of a Bessel function of the first kind.

The Bessel function accounts for phase cancellation, radiation and directivity properties in the ϕ-plane.

4.3.2.2 APPLYING THE THEORY

From Appendix A-1 (equations A.1.1 - A.1.21) the blade load / θ distribution may be calculated in the form of its torque and thrust components. The blade loading harmonics, T and Q , may be calculated by expressing $T(\theta)$ and $Q(\theta)$ as a Fourier series. The analysis is restricted to the case of discrete data points, in which summations replace integrations, see Appendix A-4.

$$Q_\lambda(t) = k_0 + \sum_1^T (a_\lambda \cos\lambda t + b_\lambda \sin\lambda t) \qquad 4.8$$

$$T_\lambda(t) = c_0 + \sum_1^T (d_\lambda \cos\lambda t + e_\lambda \sin\lambda t) \qquad 4.9$$

Where:

$$k_0 = 1/2\pi \int_0^{2\pi} Q(t)\, dt \qquad 4.10$$

$$a = 1/\pi \int_0^{2\pi} Q(t) \cos\lambda t \, dt \qquad 4.11$$

$$b = 1/\pi \int_0^{2\pi} Q(t) \sin\lambda t \, dt \qquad 4.12$$

$$c_0 = 1/2\pi \int_0^{2\pi} T(t)\, dt \qquad 4.13$$

$$d = 1/\pi \int_0^{2\pi} T(t) \cos\lambda t \, dt \qquad 4.14$$

$$e = 1/\pi \int_0^{2\pi} T(t) \sin\lambda t \, dt \qquad 4.15$$

From WRIGHT(75), (equations 30 and 31), it may be deduced that:

$$T_\lambda = T_{-\lambda} \qquad 4.16$$

$$Q_\lambda = Q_{-\lambda}$$

Effective radius is generally taken as the mean area radius of the end-plate:

$$R_{eff} = \surd\left(\tfrac{1}{2}(R_2^2 + R_1^2) \right) \qquad 4.17$$

The Bessel function is evaluated and solved over a spherical surface, as demonstrated in Appendix A-2.

Sound power is obtained by integrating the intensity over a sphere, radius R. Sound intensity, in any specified direction (θ, ψ), is the sound energy transmitted through a unit area in a unit time.

$$\text{Intensity, } I = \frac{|P_n|^2}{\rho a_0} \qquad 4.18$$

$$\text{Power} = \int_s I(\psi, \theta)\, ds \qquad 4.19$$

4.3.2.3 PROCEDURE FOR THE SOLUTION OF THE THEORY

1) Using equations A.1.1 - A.1.21, calculate T and Q for all θ.

2) Calculate total thrust and total torque at any instant. This is the resultant of the individual loads on all Z blades.

3) Plot T_{total} and Q_{total} against time and Fourier analyse to find the blade loading harmonics.(eqns. 4.8 - 4.16)

4) Solve equation 4.7 analytically, see Appendix A-2.

For cross-flow fans (Z = 24) the summation in equation 4.7 was found to converge using $\lambda = \pm 240$, for the first ten harmonics.

5) Integrate intensity over the spherical surface, S formed by radius, R using equations 4.18 and 4.19.

Two important results to arise from the solution to equation 4.7 are:

A) The generated sound power is independent of thrust.

B) The sound power in even harmonics is zero.

Some results from this section of the analysis are given in Chapter 5, where this generation mechanism is referred to as **noise(A)**. The resulting noise spectra are fairly irregular but overall the sound power levels are of the same order as for stator lift fluctuations and for the potential interaction sound generating mechanisms.

The sound power levels diverge with increasing speed; for low speed operation (approx. 6m/s) the speed exponent is generally between 6 and 8, and is a function of frequency. This exponent rises sharply with increasing speed, particularily for the higher harmonics; for higher speed operation (approx. 75m/s +) the speed exponent may be in the range $30 < \alpha < 40$. All other mechanisms considered give simple speed-sound power relationships.

4.3.3 SOUND GENERATED BY WAKE/STATOR INTERACTION AND DISCHARGE FLOW TURBULENCE/STATOR INTERACTION

4.3.3.1 EXISTING THEORY

HANSON(35) developed a pulse modulation theory to calc-

ulate acoustic radiation from an axial fan stator upstream of the rotor. He states that rotor/stator interaction is due to two effects; the relative importance of each being dependent on the axial clearance between the rotor and stator rows. The first effect is due to the wake downstream of the blade having a velocity defect, this produces a non-steady discharge with respect to the stator, causing fluctuating lift on the stator equivalent to an array of acoustic dipoles. The second effect is smaller scale and due to turbulent flow behind the blade producing random fluctuating lift on the stator, resulting in broad-band noise production.

The theory of HANSON treats a wake/stator interaction as a pulse which repeats periodically and indefinitely, the pulse amplitudes being normally distributed, with mean $\bar{a}$ and standard deviation σ_a. A pulse train of constant interval, but varying amplitude he terms 'amplitude modulated', a pulse train of constant amplitude but varying intervals between peaks he terms 'position modulated'. In this latter case $\bar{b}$ is the mean interval, σ_b is the standard deviation of the normally distributed pulse intervals. σ_b should be small for a well made rotor of constant blade spacing.

If the pulse is expressed as V(t), the Fourier transform, $V(\omega)$ will have a characteristic shape depending on the waveform. Basically, the theory decomposes an irregular pulse into a periodic component, responsible for discrete frequency tones and a random pulse train, responsible for broad-band noise. By making various assumptions about the wake dimensions and convection velocities, and coupling these with experimental

results; HANSON obtained lift, velocity and shedding frequency estimates enabling calculation of the spectra of harmonic sound powers and the level of broad-band noise.

ASSUMPTIONS:

1) Wake transport velocity is much larger than the turbulent velocity - 'frozen turbulence'.
2) Pulse arrival times and pulse amplitudes are uncorrelated.
3) Variations in pulse amplitudes and pulse arrival times are uncorrelated from vane to vane. This requires that eddies within the wake must be smaller than the stator row blade spacing.
4) Pulse amplitudes and arrival times are normally distributed.
5) Pulses have the same 'shape', only amplitudes and arrival times vary.
6) 'Point-source' approximation is used, which assumes uncorrelated regions only across the stator vane (no correlated dipoles). This may be untrue for high frequency noise, with short wavelengths, say; > 10kHz.
7) Boundary conditions imposed by the blades and ducting are neglected. The distortion will be worse at high frequencies where wavelengths are less than typical blade dimensions.

HANSON used experimentally determined values for wake width, $2\hat{Y}$ and wake spacing, 2b.

$$2\hat{Y} = 1.36\ C\ C_D\ (\ (x'/C) + 0.15)^{\frac{1}{2}} \qquad 4.20$$

$$2b = 2\pi / Z\ R_{eff}\ (1 - (\frac{\Omega R}{V} - \frac{W}{V})^2)^{\frac{1}{2}} \qquad 4.21$$

Where;

C - Blade chord.

C_D - Blade drag coefficient.

x' - Streamwise coordinate.

W - Normal velocity between rotor and stator.

V - Axial velocity between rotor and stator.

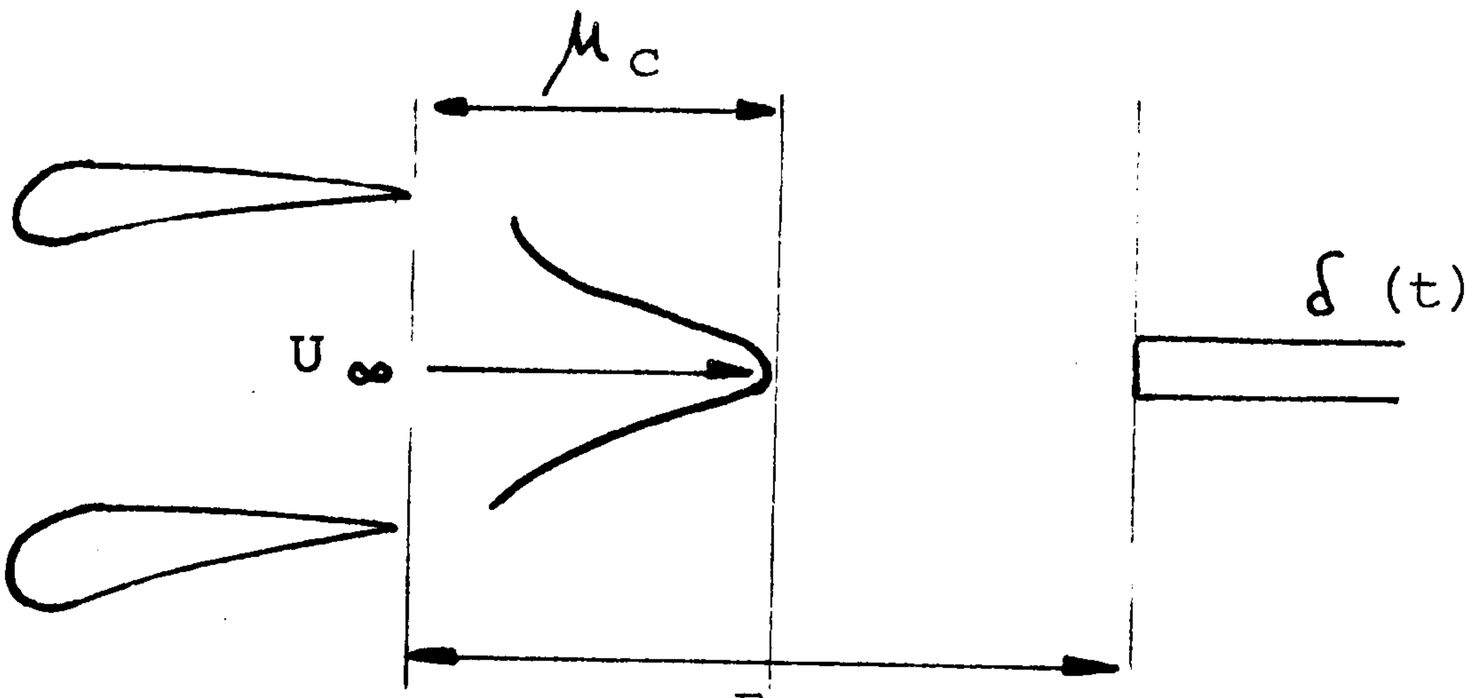

E

Figure 4.1

As well as the variation in velocity with time $\delta(t)$, there is also a variation in the angle of incidence with time $\alpha(t)$. HANSON assumes this variation of incidence on the stator to be a linear function of the velocity profile.

$$\alpha_{(t)} \propto \delta_{(t)} \qquad 4.22$$

The velocity defect comes from KEMP and SEARS(41) analysis (Appendix A-3, and Figure 4.1):

$$\delta(t) = \frac{\mu_c}{U\infty} \cos^2 \left(\frac{\pi Zb\ t}{\updownarrow T}\right) \qquad 4.23$$

Where;

U_∞ - Mean streamwise velocity.

T - Period of rotation.

The Fourier transform of $\delta(t)$ is $\delta(\omega)$:

$$\delta(\omega) = \underline{\mu_c}\ (1/2\pi\omega)\ (\sin(\underline{\hat{Y}}\ x\ \underline{\omega T})/\ (1-\ (\underline{\hat{Y}}\ x\ \underline{\omega T})^2)\ ) \qquad 4.24$$
$$U_\infty \qquad\qquad 2b \quad Z \qquad\qquad 2\pi\ b \quad Z$$

And the lift response equation is, from conventional aerodynamic theory:

$$\text{LIFT FORCE, } \hat{F}(\omega) = \tfrac{1}{2}\rho\, U_\infty^2\, C_V \langle \text{Span} \rangle \frac{dC_L}{d\alpha}\, \alpha(\omega)\, Se(\omega) \qquad 4.25$$

Where;

C_V - Stator chord.

C_L - Coefficient of lift.

$Se(\omega)$ - Sears function for time-unsteady lift, see Appendix A-3.

ω - Radian frequency, arbitrarily F(U).

Combining equations 4.22, 4.24 and 4.25 gives the broad-band lift force:

$$F(\omega) = \tfrac{1}{2}\rho V \omega R\, C_V \langle \text{Span} \rangle \frac{dC_L}{d\alpha}\, Se(\omega) \frac{\mu_c}{U_\infty}\ (1/2\pi\omega)$$
$$(\sin(\frac{\hat{Y}}{2b}\ x \frac{\omega T}{Z})/\ (1-\ (\frac{\hat{Y}}{2\pi b}\ x\ \frac{\omega T}{Z})^2)\ ) \qquad 4.26$$

BROAD-BAND SOUND POWER/ Unit frequency:

$$\frac{d\pi_B}{d\omega} = (\ Y\ \frac{d\pi_{dB}}{d\omega}\ )\ (\frac{\sigma_a^2}{\bar{a}^2} + (1-\ e^{-(\omega T \sigma_b)^2}) \qquad 4.27$$

Where; $\dfrac{d\pi_{dB}}{d\omega} = \dfrac{\omega^2\ Z\ \Omega |F(\omega)|^2}{6\pi\rho\, c^2}$

Y - Number of stator vanes.

$F(\omega)$ - Calculated from equation 4.26.

T - Period of rotation $(2\pi/\Omega)$.

DISCRETE FREQUENCY NOISE:

Here, the analysis is concerned with the regular part of the pulse; where the fluctuating lift will be modulated by the pulse amplitude - and amplitude is a function of the velocity defect. The variation of incidence is no longer random, but varies in a regular manner as the blade wake comes into contact with the stator vane. This variation of incidence is modulated by the blade passage and consequently contains discrete harmonics of Ω Z.

Because only integer harmonics are dealt with in this part of the analysis; $F(\omega)$ is equivalent to $F(nZ\Omega)$ since the lift force fluctuations are governed only by discrete frequency pulses.

HANSON defines the lift harmonics as:-

$$F(n) = 2\ Z\Omega\ F(nZ\Omega) \qquad 4.28$$

Substitute $nZ\Omega$ for ω and $2\pi/\Omega$ for T into equation 4.26:-

$$F(n) = \tfrac{1}{2}\rho V\Omega R\ C_V\ \langle Span\rangle \frac{dC_L}{d\alpha}\ Se(nZ\Omega)\ x\ \left(\frac{\mu_c}{U\omega\ n\pi}\right.$$

$$\left.\left(\frac{\sin(n\hat{Y}\pi/b)}{1-(n\hat{Y}/b)^2}\right)\right) \qquad 4.29$$

Equation 4.29 can solve the wake/stator interaction problem for all harmonics, n.

The sound power in the n-th harmonic is given by:-

$$\Pi_n = Y^2 \Pi_{dn} \eta_{rad} \exp(-(2\pi_n Z \sigma_b)^2) \qquad 4.30$$

Where;

η_{rad} = Radiation efficiency.

$$\Pi_{dn} \doteq \frac{(nZ\Omega \,.\, F(n))^2}{24\pi\rho c^3} \qquad 4.31$$

F(n), where n= 1,2,3,.....,N is obtained from equation 4.29.

4.3.3.2 APPLYING THE THEORY

As far as possible direct equivalents are substituted for the variables in equations 4.20 - 4.31; however other modifications are required:

$$x' \doteq \frac{2}{3}\pi r \qquad \text{(r - radius of forced vortex)} \qquad 4.32$$

$\langle$ Span $\rangle$ is equivalent to $\langle$ Length $\rangle$ 4.33

$C_V \doteq$ Tongue thickness 4.34

μ_c = Function of vortex wall clearance 4.35

The velocity defect, μ_c is 100% U_∞ at a distance zero chords downstream of the blades, and has been determined to be about 5% U_∞ 2 - 3 chords downstream of the blade tips. F(E) is calculated using these limits and an assumed square relationship between μ_c and x'.

Other variables are approximated as follows:-

C_D - A circular arc aerofoil is less efficient than a proper aerofoil profile: $C_D \doteq$ 0.03.

$dC_L/d\alpha$ - Ideally, 2π . Practically 5.6 - 5.7 for aerofoils, in this analysis; 5.0.

σ_b^2 - Ideally, 0.0. HANSON(35) used the approximation:

$$\sigma_b^2 = (0.03/Z)^2.$$

This approximation is adopted in the analysis.

$\sigma_a^2 / \bar{a}^2$ - Should be approximately 1.0.

η_{rad} - From HANSON, (Fig. 13): $0.003 \leq \eta_{rad} \leq 0.32$.

The higher acoustic efficiencies imply increased sound radiation. $\eta_{rad} \doteq 0.2$.

Se(ω) - This term is explained in Appendix A-3, which shows that time-unsteady lift is smaller than time-steady lift, under identical potential conditions. Se(ω) $\doteq$ 0.85.

There is a 3dB error for every halving or doubling of a variable in the preceeding list. A 'worst likely' combination of these variables yields, therefore, an error range of $\pm$ 18dB.

4.3.3.3 PROCEDURE FOR THE EVALUATION OF THE THEORY

To find the overall sound power in any frequency band, the discrete spikes are calculated from equation 4.30; these are superimposed upon the broad-band noise level calculated from equation 4.27. A vane number, Y, of 1 is adopted for a single vortex wall.

Some results from this section of the analysis are given in Chapter 5, where this generation mechanism is referred to as Noise(B). The resulting discrete frequency spectra are quite regular, increasing approximately as a square of the Strouhal number, although the exact power relationship depends on the fan design. The overall discrete sound power is usually at least 40 dB down on the next weakest mechanism, and the broad-

band component of the sound at least 100 dB down on the potential interaction, broad-band sound power levels.

Only the first 10 harmonics are calculated.

4.3.4 STATOR LIFT FLUCTUATIONS CAUSED BY EDDIES SHED FROM THE BLADE TIPS

4.3.4.1 EXISTING THEORY

One source of discrete frequency sound previously discussed is 'blade-slap'. An investigation into these impulsive aspects of overall rotor noise was performed by LEVERTON and AMOR(44), using gusts artificially introduced into the disk from nozzles beneath the rotor. Blade-slap is primarilly an axial fan phenomenon, where blades cast trailing vortices from their tips and leave spanwise wakes.

YEOW(78) artificially introduced turbulence into the entry flow of a centrifugal fan and detected no increase in the radiated sound power. This result is in contrast to results from CHANDRASHEKHARA(14), for axial fans, who found that inflow turbulence was a powerful dipole sound source, particularily at low Mach numbers (Ma. < 0.3). It would appear then, that blade/wake or blade/eddy interaction is not a powerful noise source in centrifugal fans. Flow from a centrifugal fan is essentially radial and vortices cast from the blades are convected downstream. The situation is slightly different with cross-flow fans, because blades active in the suction arc may shed vortices internally. But extending the results of YEOW(78) it may be assumed that internally cast vorticity produces no intense dipole fluctuation on the upstream blade row.

It has been known for some time that discrete frequency noise levels from centrifugal fans are strongly dependent on the shape, size and location of the tongue, see, for example, the review by NEISE(59). One mechanism which could account for this dependency has been discussed in 4.3.3; another would be an eddy/tongue interaction, where vortices shed up stream of the tongue impinge periodically upon its surface. These two mechanisms are quite distinct. If the eddies cast from the blades are of sufficient strength, the 'blade-slap' phenomenon has a 'tongue-slap' equivalent with cross-flow fans and centrifugal fans. The vortex shedding frequencies are modulated by the blade passing frequency and the noise produced is, therefore, discrete.

CURLE(18**b**) showed that the acoustic power generated by dipole radiation, from a solid surface experiencing fluctuating pressure loading, may be represented by the following surface integral:

$$W = \frac{1}{12\pi\rho c^3} \overline{\left(\int_S \frac{\partial p}{\partial t} \, ds \right)^2} \qquad 4.36$$

W - Acoustic power.

P - Instantaneous pressure.

This equation has been re-expressed in many ways, for instance by MUGRIDGE(56):

$$W = \frac{1}{12\pi\rho c^3} \left(\partial F_L(t)/\partial t\right)^2 h \, l_s \qquad 4.37$$

F_L - Lift force/ unit span.

l_s - Spanwise correlation length. The length over which all forces are in phase.

h - Span length.

Equation 4.36, and therefore all derived equations, assume that retarded time differences are negligible, ie that there is no phase cancellation within the acoustic field. This is true where the wavelength of interest is large compared to any blade dimension, other than span.

If it is assumed that the potential flow field is steady, the fluctuating force term in equation 4.37 will be due entirely to induced lift from shed vortices acting on the tongue. The situation may be visualised as a stationary impeller with the tongue rotating relative to a perfectly symmetrical flow field on discharge. The tongue cuts through one part of a train of vortices at an interval related to blade spacing.

Interval, $T = 1/Z\Omega$ seconds

The sound energy is concentrated at harmonics of the blade passing frequency.

$$W(\Omega_n) = \frac{1}{12\pi\rho c^3} \left(\partial F_L(t)/\partial t\right)^2 h\, l_s\, F(\Omega_n) \qquad 4.37(b)$$

FUKANO et al(29) used the following assumed condition to calculate lift induced by an eddy of diameter, G.

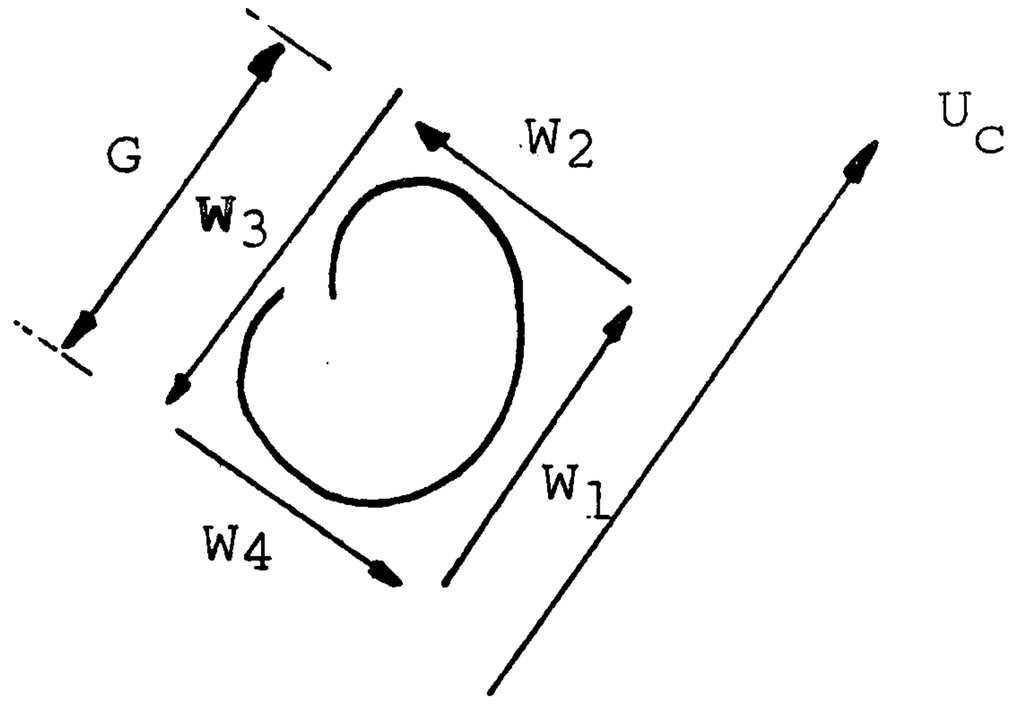

Figure 4.2

Where $W_1 \gg W_2$, W_3 and W_4.

See Figure 4.2.

$$\Gamma \doteq G\, W_1 \qquad 4.38$$

And, let $W_1 = U_c$; from Joukowski lift equation:-

$$F_L = \rho\, \Gamma\, W^* \qquad 4.39$$

W^* - Fluid velocity relative to the tongue.

$F_L(t)$ may be represented in the time domain as a series of rectangular pulses of a certain width, and period $1/Z\Omega$. It may be further represented by a Fourier series if the pulses are periodic and repeatible.

$$F_L(t) = \frac{a_0}{2} + \sum_{n=1}^{n=\infty}(a_n \cos(nt) + b_n \sin(nt)) \qquad 4.40$$

Where;

T is defined as an arbitrary period, equal to $1/\Omega Z$:-

$$F_L(t) = \frac{a_0}{} + \sum_{n=1}^{\infty}(a_n \cos(n\omega t) + b_n \sin(n\omega t)$$

$$a_n = 2\Omega Z \int_0^{1/\Omega Z} F_L(t) \cos(n\omega t)\, dt \qquad 4.41$$

$$b_n = 2\Omega Z \int_0^{1/\Omega Z} F_L(t) \sin(n\omega t)\, dt$$

$$\omega = 2\pi\Omega Z.$$

Differentiate 4.41 with respect to t, and square:

$$(\partial F_L(t)/\partial t)^2_{(n)} = (a_n^2 + b_n^2)\ n^2\omega^2 \qquad 4.42$$

For each harmonic, n.

4.3.4.2 APPLYING THE THEORY

The theory is concerned primarily with only a small surface area of the whole vortex wall, close to the impeller. To

enable numerical evaluation, the vortex wall is treated as an aerofoil having its' zero-incidence axis radial to the impeller, for all vortex wall locations. Hence:-

$$W^{*} = U_c' \cos\lambda \qquad 4.43$$

U_c' - Ultimate discharge absolute velocity.

λ - Ultimate discharge flow angle.

The dwell time spent by the tongue tip cutting through a train of vortices depends on the convection velocity and the eddy diameter, this specifies pulse width.

$$\text{Dwell time, } T_{dw} = \frac{2\,G}{U_c'} \qquad 4.44$$

combining 4.38, 4.43 and 4.39:-

$$F_L = \rho\, G\, U_c'^2 \cos\lambda \qquad 4.45$$

It is further assumed that the eddy diameter is reduced as it travels downstream and dissipates. This necessarily implies a relationship between G and the vortex wall clearance, E. Results obtained by the author suggest a weak dependence; of the order of the following relationship:

$$G/D = 0.06\ (E/D)^{-1/12} \qquad 4.46$$

l_s is obtained from KESHAHAVEN(42), who assumes an average spanwise correlation length of 0.025 C_V.

C_V is assumed equal to the tongue thickness.

The span length, in axial fans, is replaced by blade length for cross-flow fans. Sound power output only is considered.

4.3.4.3 PROCEDURE FOR THE SOLUTION OF THE THEORY

The fundamental equation to be solved is of the form of equation 4.37(b). The eddy circulation is estimated using the procedure of FUKANO et al(29), and this enables the lift force

on the tongue, due to eddy impingement, to be estimated. The lift force is a function of time and may be represented as a series of spikes, of width $2G/U_c$ and interval $1/Z\Omega$. The lift-time plot is Fourier analysed and the term $(\partial F_L(t)/\partial t)^2$ is solved from equations 4.41 and 4.42, for each harmonic.

Some results from this section of the analysis are given in Chapter 5, where this generation mechanism is referred to as Noise(C). Only the first ten harmonics are calculated and the general shape of the spectra is that of decaying sinusoids, usually with the predominant harmonic occuring between the third and seventh Strouhal bands. The overall sound power levels are theoretically determined to be the second weakest of the generation mechanisms considered, but there are a large number of approximations in the analyses and the mechanism may be an important one. Experimentally, the vortex wall clearance was found to have a strong influence on the radiated sound power, and this design parameter fundamentally affects the level of dipole fluctuations on the vortex wall.

4.3.5 POTENTIAL FIELD INTERACTION

4.3.5.1 EXISTING THEORY

Since LIGHTHILL(46) it has been recognised that an acoustic field contains quadrupole sources, distributed throughout the flow field, external to solid boundaries. These sources are inefficient radiators, but this fact alone cannot be invoked to dismiss them as insignificant contributors to the overall sound power from a machine. LIGHTHILL has shown that the quadrupole stress tensor may be approximated by:-

$$T_{ij} \doteq \rho V_i V_j \qquad 4.5(b)$$

It is generally argued that a blade rotating at speed, U induces velocities close to the blade surface of approximately the same order. Thus; velocities in the principal directions i and j approach U:

$$T_{ij} \doteq \rho U^2 \qquad 4.5(c)$$

From this elementary analysis it is already clear that quadrupole strength becomes increasingly significant at high speeds. LIGHTHILL states, in the same paper that; from tests on cold, subsonic jets discharging through an orifice, the acoustic power for $Ma < 0.3$ (relative to the mean jet velocity) was too low to measure.

The simple analysis represented by equations 4.5(b) and 4.5(c) fails to account for any non-regularities surrounding the rotor blades. The possible significance of these sources was first recognised by FFOWCS-WILLIAMS and HAWKINGS(27), who postulated that an interaction could be due to 'scattering' of an inlet flow distortion by a blade-to-blade non-uniformity. The acoustic source distribution is of the following form:-

$$\Delta p \propto \frac{\partial^2 (V_i V_j)}{\partial z_i \partial z_j} \qquad 4.3(b)$$

Where one velocity is the rate of momentum transfer due to inlet distortion and the other is associated with the blade potential field.

Equation 4.5(b) may be expressed in terms of its' time-variable components:-

$$\rho UV = \rho (\bar{U} + U')\ (\bar{V} + V')$$

$$\rho\, UV = \rho\, \bar{U}\, \bar{V} + \rho\, U'\, V' + \rho(\, \bar{U}\, V' + \bar{V}\, U') \qquad 4.47$$

Where; V, U - Instantaneous velocities.

V', U' - Fluctuating velocities.

$\bar{V}$, $\bar{U}$ - Time-averaged velocities.

Such that; $U = \bar{U} + U'$

$V = \bar{V} + V'$

The first term on the R.H.S of 4.47 is essentially the quadrupole source effect of the potential field. The second term is a purely turbulent source and the final term is an interaction between the potential and turbulent fields. It is this latter term which FFOWCS-WILLIAMS and HAWKINGS(27) isolated as being a potentially important quadrupole source.

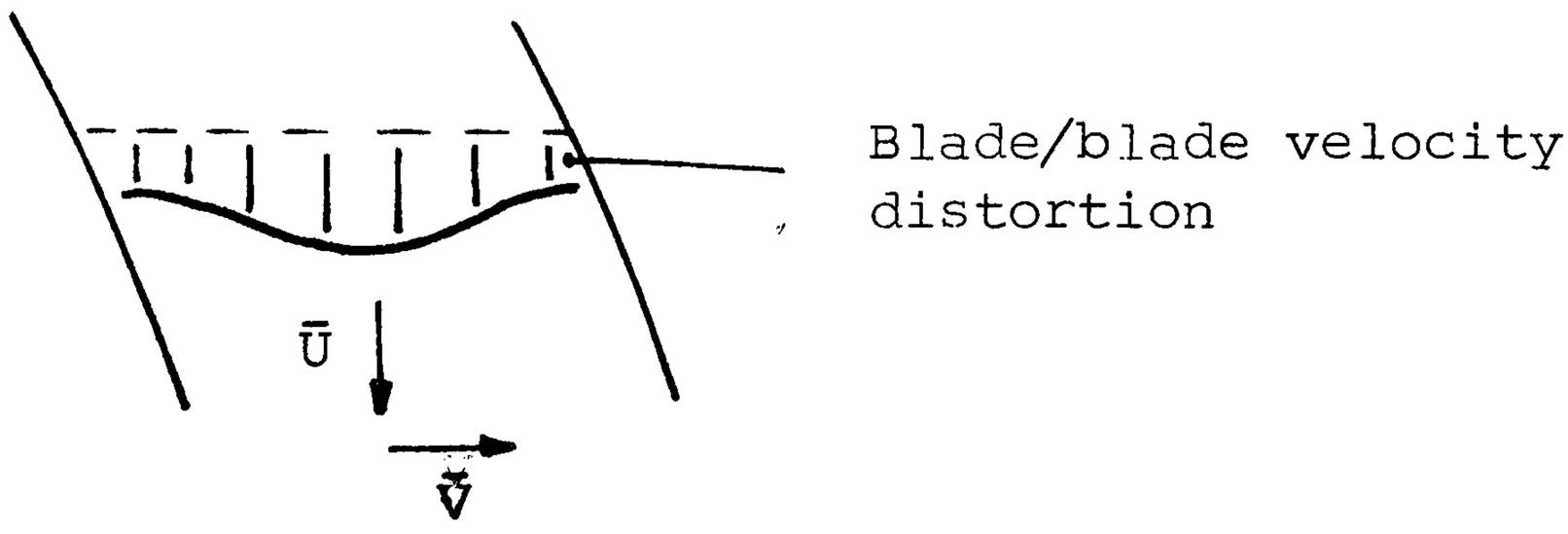

Figure 4.3

Considering a fan where the flow is essentially radial, the oscillatory motion caused by the blade constriction may be expressed as a low amplitude sinusoidal wave, fluctuating at a frequency ΩZ. Turbulence velocities are random in time and space and are convected downstream with a radial velocity U'_r. Where an eddy has a characteristic length, or dimension, G, the time taken for an eddy to pass a fixed point, radially, is G/U'_r seconds.

For a conventional fan, where the circumferential flow variation is generally small, the number of blades which chop

through a single eddy in time G/U_r' is:-

$$\tilde{N} = \frac{G}{U_r'} \frac{\Omega Z}{2\pi} \qquad 4.48$$

If $\tilde{N}$ is large a lot of blades will cut an identical eddy and the sound generation will be well correlated; modulated by a frequency ΩZ. Thus, $\tilde{N}$ is significant because it determines the nature of the radiated sound; for small N this will be predominantly broad-band and for large $\tilde{N}$ predominantly discrete frequency sound. $\tilde{N}$ becomes large for flows with a low radial component with respect to the rotational speed. In cross-flow fans the radial velocities induced by the eccentric vortex can be very large with respect to the rotational velocity. Also, each blade experiences a different flow condition and responds differently with varying θ. Because of these two latter effects it appears likely that the sound power output, for cross-flow fans and due to potential interaction, will be poorly correlated and broad-band in nature.

Sound pressure formed by a spherical quadrupole distribution, allowing for phase cancellation due to retarded-time effects, may be expressed as in Equation 4.49.

$$p(t)/\text{eddy} = \frac{1}{4\pi} \int_s \frac{\partial^2}{\partial^2 Y_i} (\rho U_i V_j) \frac{ds \; c \; \partial\tau}{r} \qquad 4.49$$

s - Sphere surface area.

τ - Time taken for sound to travel across an eddy.

r - c $(t-\tau)$ metres.

Let

$\bar{U}_a$ - Absolute velocity of the fluid.

$\gamma \bar{U}_a$ - Turbulence velocity.

FFOWCS-WILLIAMS and HAWKINGS' treatment allows the following approximation to be made to Equation 4.49.

$$\bar{P}^2 = M\left(\frac{\rho \bar{U}_a^2 \gamma c}{2 r \Omega Z}\right)^2 \qquad 4.50$$

$\bar{P}^2$ - Mean square sound pressure.

r - Observer radius.

M - Number of eddies involved in the interaction.

4.50 indicates a squared power relationship between a typical velocity and sound pressure, for the quadrupole mechanism considered.

4.3.5.2 APPLYING THE THEORY

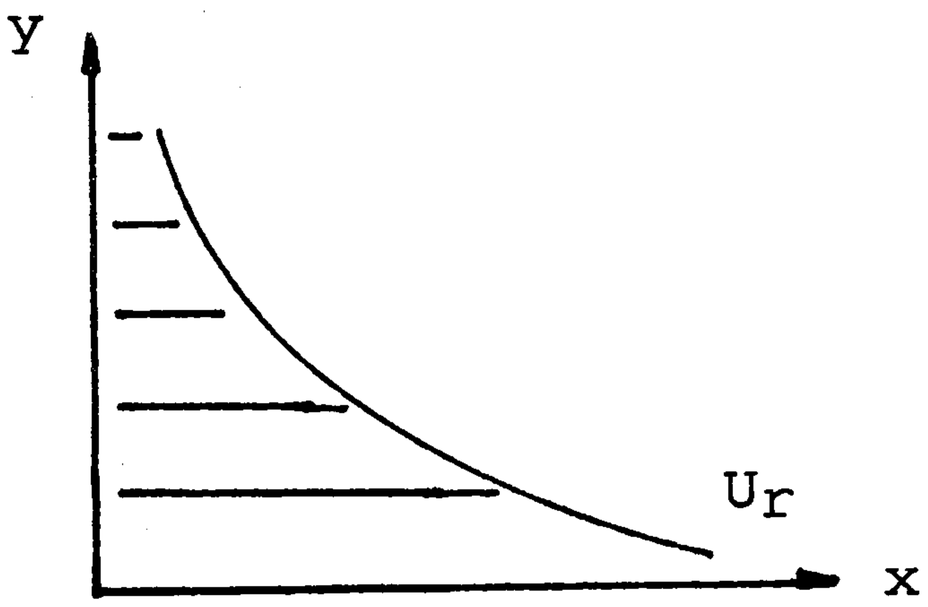

Figure 4.4

$$\text{Turbulent shear stress, } \bar{\tau}_{xz} = \bar{\eta} \frac{\partial \bar{U}}{\partial y} \qquad 4.51$$

Where;

η - Eddy viscosity.

Assume; - $\gamma \propto \bar{\tau}_{xz}$.

$$\gamma \propto \bar{\eta} \frac{\partial \bar{U}}{\partial y} \qquad 4.52$$

From FFOWCS-WILLIAMS and HAWKINGS, when the velocity distribution was approximately flat; $\gamma = 0.01$. Therefore:-

$$\gamma = 0.01 \frac{\partial \bar{U}_r}{\partial y} \qquad 4.53$$

When $\partial \bar{U}_r / \partial y$ is not linear, the noise produced is found by numerically integrating around the rotor periphery. It is possible that such a distribution could produce extra discrete harmonic tones, similar to the extension of GUTIN's work by WRIGHT(75). $\bar{U}_a$ is known around the rotor, calculated using the model outlined in section 3.3.

Assume an average eddy dimension, G to be the same as the blade chord, C; the eddy box area is C^2 and the box volume, C^3.

Where; C' = R2 -R1

Assume potential velocities to be well correlated for a distance C' each side of the rotor inner and outer peripheries, for D1/D2 approx. o.8. The volume under consideration, VOL is:

$$VOL = \left((R2 + C')^2 - (R1 - C')^2 \right) \times LENGTH \qquad 4.54$$

And the number of eddies, M, contained within this volume is:-

$$M = VOL / C^3 \qquad 4.55$$

Sound power is obtained by integrating the intensity over a spherical surface:

$$W = \frac{\bar{p}^2}{\rho c} 4\pi r^2 \qquad 4.56$$

W - Overall sound power.

$\bar{p}^2$ - Calculated from 4.50.

4.3.5.3 PROCEDURE FOR THE SOLUTION OF THE THEORY

Because the flow field varies around the impeller periphery, a numerical evaluation technique is adopted.

i) Find $\partial \bar{U}_a / \partial y_{(n)}$ where; n = 1,2,3,.....,N.

ii) Calculate γ (n) and smoothe.

iii) $$\bar{P}^2 = M\left(\frac{\rho c}{2r\Omega Z}\right)^2 \cdot \frac{1}{N} \sum \left(\bar{U}_a(n)^2 \gamma(n) \right)^2$$

iv) Calculate W; assume some likely frequency range and calculate the broad-band noise level per unit frequency, for the potential field interaction mechanism.

(The Author assumes a frequency range of 20 000Hz.)

Some results from this section of the analysis are given in Chapter 5, where this noise generation mechanism is referred to as Noise(D). The resulting sound power levels are consistently high compared to the average theoretical sound power, indicating a considerable degree of broad-band noise, for fans with an uneven peripheral velocity distribution.

CHAPTER FIVE

5.1 SOME RESULTS FROM THE PERFORMANCE AND NOISE ANALYSES,

INTRODUCTION.

A number of theoretical analyses have been attempted to determine the performance of cross-flow fans, these have been reviewed in Chapter 3. Generally, these analyses are inapplicable because they fail to account for the rotor or casing design: the cross-flow fan designer, therefore, has to rely either on flow visualisation techniques or modifications to existing designs.

The Author has developed a theoretical analysis of the cross-flow fan , which relates the aerodynamic performance and noise characteristics to aspects of fan design: these separate, but related theories are explained in sections 3.3 and 4.3 respectively. The theories have been expressed in algorithmic form and solved using the computer language, FORTRAN. The theory in both cases assumes 'ideal' conditions and does not account for pressure losses in the system or flow-rate reduction due to aerodynamic stalling of the blades. An estimate of the 'shock' loss on entry is attempted, see section 3.3.8, but the pressure characteristic is not modified by a loss term. Inevitably the theoretical results do vary, in absolute terms, from the experimentally determined results subsequently discussed in Chapters 6 and 8. The analysis is useful, however, in isolating the important design parameters and helping to supply an explanation to the observed relationships between fan design and performance. The performance evaluation theory does, in most

cases, successfully predict the relationships between fan design and aerodynamic performance. This is broadly the case with the noise analysis results also, although it would not be true to say that the problem is solved. The noise analysis does, at least, highlight some of the important sound generating mechanisms. In section 4.3.1 the Author explains the reasons for isolating the four mechanisms subsequently discussed in sections 4.3.2, 4.3.3, 4.3.4 and 4.3.5. These four mechanisms, defined in section 4.3, are given symbolic names in this Chapter, see Table 5.1:

Sound power generating mechanism	Symbolic name
Blade loading	Noise(A)
Wake/ stator interaction	Noise(B)
Eddy/ stator interaction	Noise(C)
Quadrupole noise generation (Potential field interaction)	Noise(D)

Table 5.1

The numerical evaluation of these mechanisms endorses their choice as important sound power sources. Noise(A), Noise(C) and Noise(D) yield sound power values of approximately the same order, wheras the Noise(B) results indicate that wake interaction mechanisms are likely of consistently lower magnitude than other sources, for cross-flow fans. In this Chapter the four mechanisms are discussed separately; scrambling the results together would lose information on the relative importance of particular mechanisms to aspects of fan design, and place too high a reliance on the absolute

values of the results from each mechanism considered.

This Chapter discusses some results from the performance and noise analyses.

5.2 GENERAL RELATIONSHIPS

5.2.1 VARIATION OF PERFORMANCE WITH ROTATIONAL VELOCITY

The aerodynamic performance characteristics; flow-rate, pressure rise, efficiency and power input, as determined in section 3.3, are scaleable and expressed as the dimensionless coefficients ϕ, ψ, η and λ, where $\lambda = \phi\psi_T/\eta_T$. An example of the variation in the peripheral velocity distributions with speed is illustrated in Figures 5.1 and 5.2.

The variation of noise level with speed depends on the noise mechanism being considered. Noise(B), Noise(C) and Noise(D) increase in a simple manner with increasing speed, but Noise(A) diverges with increasing rotational velocity, see section 4.3.2.3. The noise level variations produced by increased rotational velocities are illustrated in Figures 5.3(a) - 5.3(d), and indicate the PWL - U relationships listed in Table 5.2:

MECHANISM	EXPONENT, α
Noise(A)	Function(St, U and fan design) approx. $6.0 \leq \alpha \leq 40.0$ for $6\ m/s \leq U \leq 75\ m/s$
Noise(B) Broad-band:	3.0
Discrete:	6.0
Noise(C)	6.0
Noise(D)	8.0

Table 5.2

All subsequent theoretical results, discussed in this Chapter, are determined for U = 6.125 m/s.

5.2.2 VARIATION OF PERFORMANCE WITH FLOWRATE

The theoretical determination of performance is based on modelling the flow by adopting various combinations of circulation and sink strength, Γ and M. A discrete number of combinations are used, but these are just a sample of the large number of combinations possible. The variation of performance with flowrate depends upon the casing configuration adopted, a number of examples are discussed later in this Chapter. An example of the peripheral velocity variations with flowrate are illustrated in Figures 5.4 and 5.5, with the corresponding variations in noise level illustrated in Figures 5.6(a) - 5.6(d). These latter graphs indicate an increase in noise level with flowrate, for all the sound generation mechanisms discussed.

All subsequent theoretical results, discussed in this Chapter, are determined for the flow field combination :-

Γ = 2.0136, M = 2.5115; with U = 6.125 m/s and D = 0.195 m.

5.2.3 POWER INPUT

The theoretically predicted power input curves depicted in Figures 5.9, 5.13, 5.17, 5.21 and 5.24 highlight the fact that an improved performance is only gained at the expense of increased power, for constant total efficiency. This is also implied by the performance curves in Chapter 6, where the power demand, although not plotted, may be calculated from the flowrate, pressure and efficiency.

The power demand curves (for a forward-curved cross-flow fan) rise continuously with increasing flowrate, this is known

as an 'overloading' characteristic. If the motor is selected for duty at the maximum efficiency point of a cross-flow ventilating fan pressure characteristic, care must be taken to ensure that the system resistence is not greatly reduced, or the drive motor may overload.

5.2.4 ENERGY TRANSFER

It was determined from the performance analysis that, generally, between 18% and 20% of the total energy transfer occurs across the first blade row. The exact theoretical value will depend upon fan design and flowrate.

5.3 EFFECT OF THE ROTOR AND CASING DESIGN ON THE THEORETICAL FLOW PATTERNS, PERFORMANCE AND NOISE CHARACTERISTICS.

5.3.1 VORTEX WALL CLEARANCE, E

The variation in predicted performance with E is shown in Figure 5.9; which indicates a worsened total head characteristic for the narrowest clearance. The differences in pressure, power and efficiency are small in the range : $3\% \leq E/D \leq 7\%$. The efficiency is lowest with the narrowest clearance, for all ϕ.

Results illustrated in Figures 5.7 and 5.8 show that the performance evaluation must be very sensitive to flow conditions in the proximity of the forced vortex; a region in which aerodynamic stall of the blades and pressure losses are likely to occur. Because of this, trends predicted by the idealised model may not be experienced in practice. The experimental results discussed in section 6.2.1.1 suggest that performance varies little with small variations in the vortex wall clear-

ance.

Figures 5.10(a) to 5.10(d) predict a complex relationship between noise level and vortex wall clearance, for Noise(A) and Noise(C); but the trend indicated shows increased noise with E/D = 1% and generally reduced noise with an increasing vortex wall clearance. Noise(B), both discrete an broad-band, is consistently reduced with a widening of E.

Noise(D) remains approximately constant in the range: $1\% \leq E/D \leq 7\%$, but overall it decreases with increasing vortex wall clearance, for this particular generating mechanism.

5.3.2 REAR WALL CIRCUMFERENTIAL ANGLE, δ

Figures 5.11 and 5.12 illustrate the predicted variation in the radial and tangential velocity distributions, with δ. The performance, shown in Figure 5.13, is relatively insensitive to variations in the rear wall angle, but overall, the performance increases with reducing δ. The efficiencies remain approximately constant, especially at the lower flowrates, although it is enhanced by adopting a rear wall angle of either 0° or 20°.

The noise characteristics are depicted in Figures 5.14(a) to 5.14(d) and show, on average, increased noise with improved performance - although there exist strong frequency dependences. An interesting result is the dramatic decrease in Noise(D) with a rear wall angle of 40°; for a configuration found experimentally to produce quiet running conditions, with a cased impeller, see section 8.6.1.2. The dip at St = 8, for $\delta = 20^{\circ}$ is a feature of the cross-flow fan blade-loading noise

Durham University
SCIENCE
11 AUG 1981
SECTION
Library

and is not caused by non-convergence of Noise(A).

5.3.3 VORTEX WALL DECLINEATION, B

This geometric parameter has a significant effect on the peripheral velocity distributions, as indicated in Figures 5.15 and 5.16. The parameter must also, therefore, be fundamental in determining the pressure characteristic of the fan. This is supported by Figure 5.17, which predicts an increasing pressure characteristic and power input with increasing B/D, although the efficiences are correspondingly reduced, particularily for B/D = 30%.

Noise(A) and Noise(C) are highest overall for B/D = 20%. Noise(C) is lowest where B/D = 30% - a design condition also giving low blade-loading noise, Noise(A). Noise(B) is found to increase with increasing B/D for $0\% \leq B/D \leq 20\%$, but to be lowest where B/D = 30%; this mechanism consistently yields results considerably lower than the other three. Generally, the noisiest condition is predicted to occur with B/D = 20%, for Noise(D), dropping sharply where $B/D < 20\%$. These results are represented graphically in Figures 5.18(a) to 5.18(d).

5.3.4 DIAMETER RATIO, d/D

No allowance is made in the theoretical performance analysis for a modified power input with varying blade chord/diameter ratios. The experimentally determined relationships are discussed in sections 6.2.1.5, 8.6.1.5 and 8.5.3.

5.3.5 OUTER BLADE ANGLE, β_2

Figures 5.19 and 5.20 illustrate the profound effect of blade angle on the predicted discharge tangential velocities; the radial velocity distribution is unaffected. From momentum

transfer considerations it is clear that performance will be similarily affected. This assertion is supported by Figure 5.21, which demonstrates a large increase in the total head and power demand using a shallow blade angle, $\beta_2 = 10^\circ$. The variation in performance is less dramatic in the design range $30^\circ \leq \beta_2 \leq 70^\circ$, although the optimum predicted efficiency occurs with a blade angle of the order of 50° and drops with extreme blade angles.

The sound power levels for Noise(A) and Noise(C) increase as β_2 is reduced; Noise(D) is unaffected by blade angle and Noise(B) increases monotonically with increasing blade angle. These results are depicted in Figures 5.22(a) to 5.22(d).

5.3.6 BLADE NUMBER, Z

For an ideal fluid theory, blade number has no effect on the aerodynamic performance (Z is assumed infinite). However, blade number is an important parameter in the noise theory, the relationships being illustrated in Figures 5.23(a) to 5.23(d). These strongly indicate no optimum blade number for lowest aerodynamic noise. Noise(B) is highest for Z = 36, but Noise(A) and Noise(C) show no strong relationship and a complex frequency dependence. Noise(D) is reduced by increasing the blade number.

5.3.7 TONGUE THICKNESS, T

If the tongue does not obscure a significant portion of the suction arc, or cause the vortex location to vary, then the parameter, T, has no effect on aerodynamic performance, as calculated theoretically.

The term is included in the noise analysis as a variable, and influences the sound power level generated by tongue interaction mechanisms. The theoretical relationships are simple and imply a 3dB increase in Noise(C) and a 6dB increase in Noise(B) for a doubling of wall thickness, T.

5.3.8 ARCUATE DAMPER

The term 'arcuate damper' is applied to any component of the casing which causes a significant degree of the suction arc to be obscured. The theoretical calculations account for this by treating the velocities in an obscured zone as zero. This obviously reduces the maximum flowrate, but also affects the discharge velocity distributions and the efficiency of operation. Figure 5.24 illustrates the theoretical predictions that a 5^{o} damper affects the performance only marginally, wheras a 40^{o} damper severely reduces the pressure characteristic and power demand. In this latter case the operational efficiency is enhanced.

The effect of an arcuate damper on noise is illustrated in Figures 5.25(a) to 5.25(d). These results show that Noise(A) is increased using a 5^{o} damper although Noise(B) and Noise(C) are slightly higher with no damper. The overall noise level is greatly reduced by incorporating a 40^{o} suction damper.

The theoretical case of a 5^{o} damper is analogous to the experimental condition of a thick vortex wall or where a wedge is included on the vortex wall suction surface. The experimental results, discussed in section 8.6.2.5, indicate an increased noise level when incorporating a wedge on the vortex wall.

5.3.9 VARIATION OF VORTEX LOCATION

Figures 5.26 and 5.27 show how the circumferential velocity distributions are altered by varying the peripheral and radial location of the vortex centre. The effect on performance (for a constant Γ, M combination) is illustrated in Figure 5.28 and shows, in all cases, that performance is reduced with a displaced vortex, see Figure 3.7 also.

Figures 5.29(a) to 5.29(d) depict the predicted influence of vortex location on noise level. For Noise(A) the sound power is not reduced significantly with the vortex centre displaced only circumferentially; other vortex locations show a reduced noise level with a displaced vortex. Noise(B) decreases with increased vortex movement, but only a small change with the solely circumferential displacement. Noise(C) is highest with the circumferentially displaced vortex, rather lower with the vortex undisplaced and lowest with a radial displacement. Noise(D) tends to increase with increasing vortex displacement, although the variation is small.

ECK- type walls cause the vortex to migrate from its location established with a simple wall. The theoretical prediction is that the noise reduction will be greater where the vortex can be enticed to shift radially outward. In this case, the combination of a displaced vortex and the suction arc throttling effect leads to a theoretical prediction of a considerably reduced noise level using an ECK- type vortex wall.

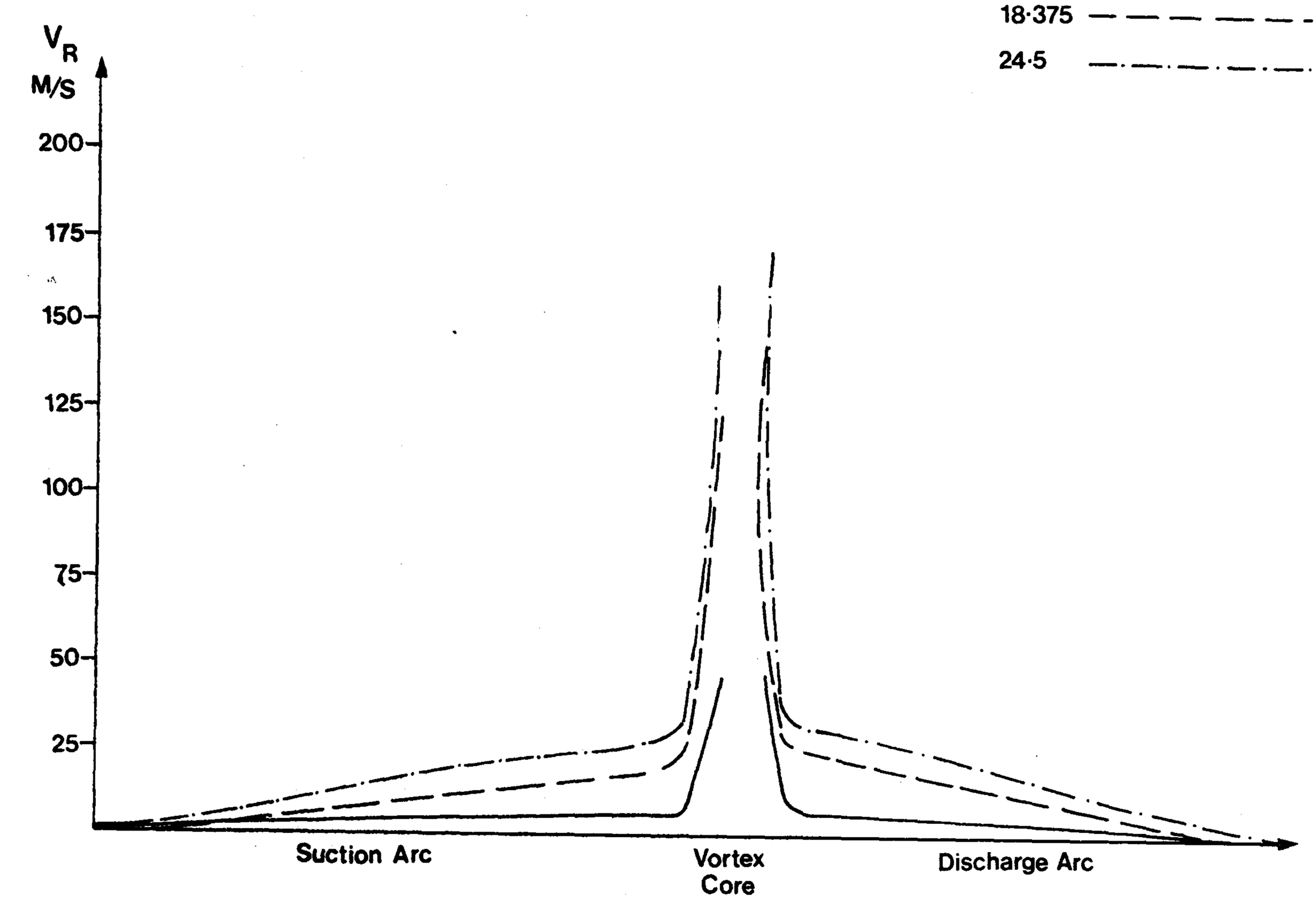

Figure 5·1

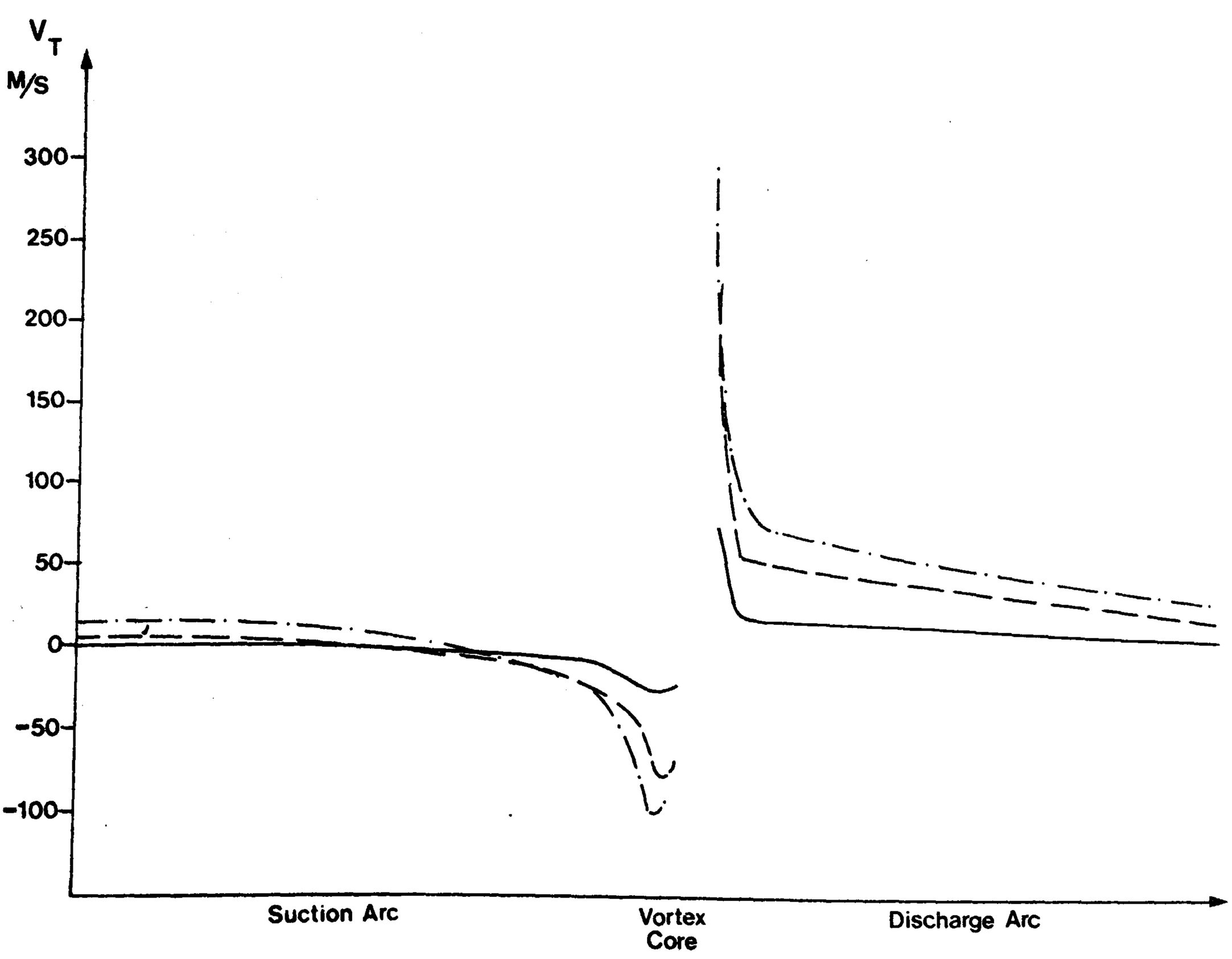

Figure 5·2

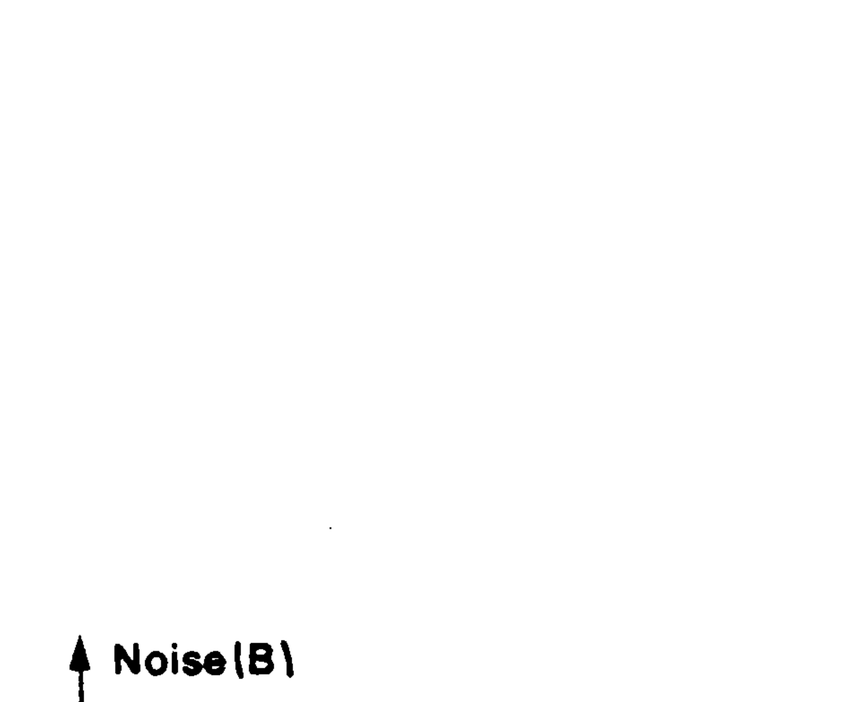

Figure 5·3(a)

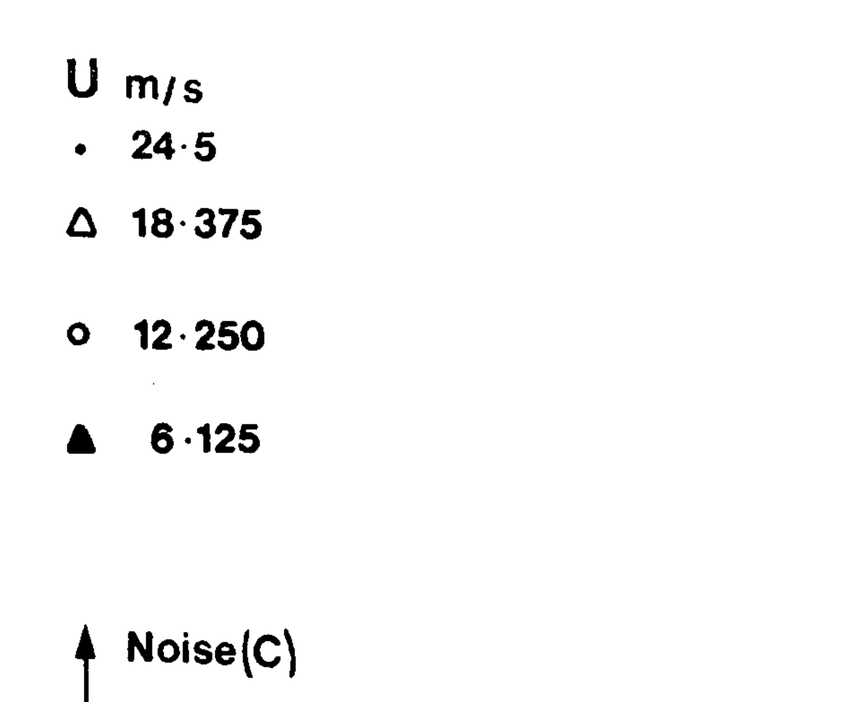

Figure 5·3(b)

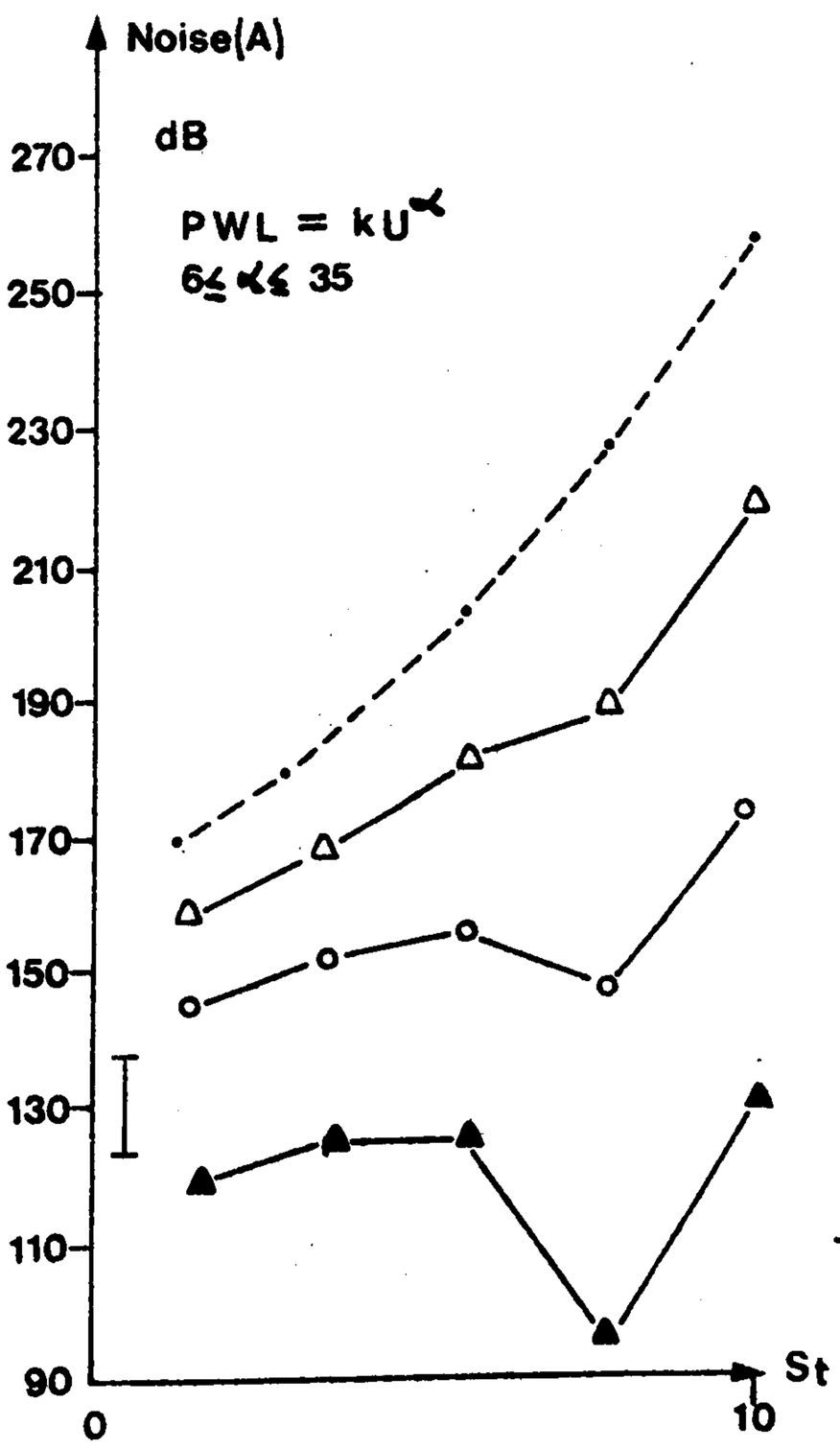

Figure 5·3(c)

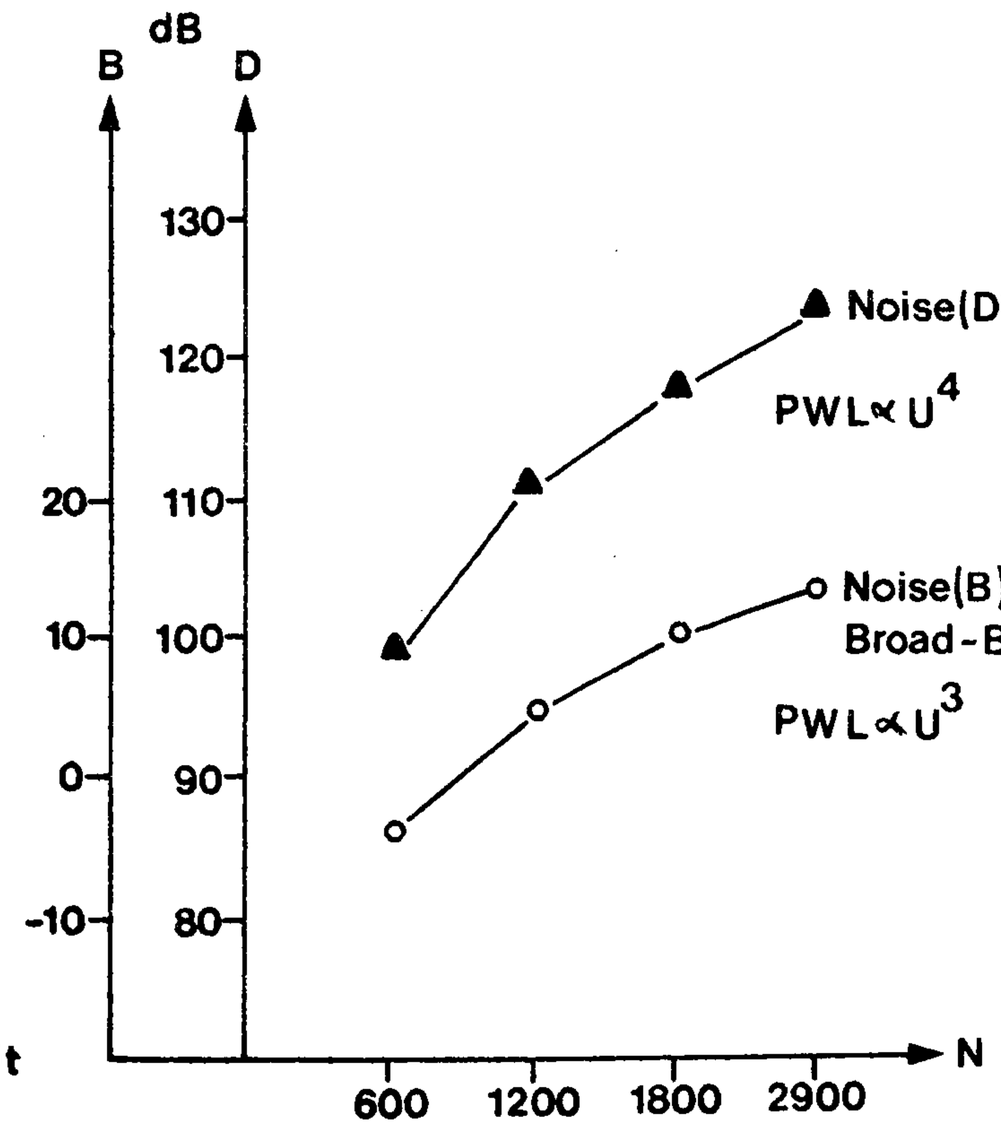

Figure 5·3(d)

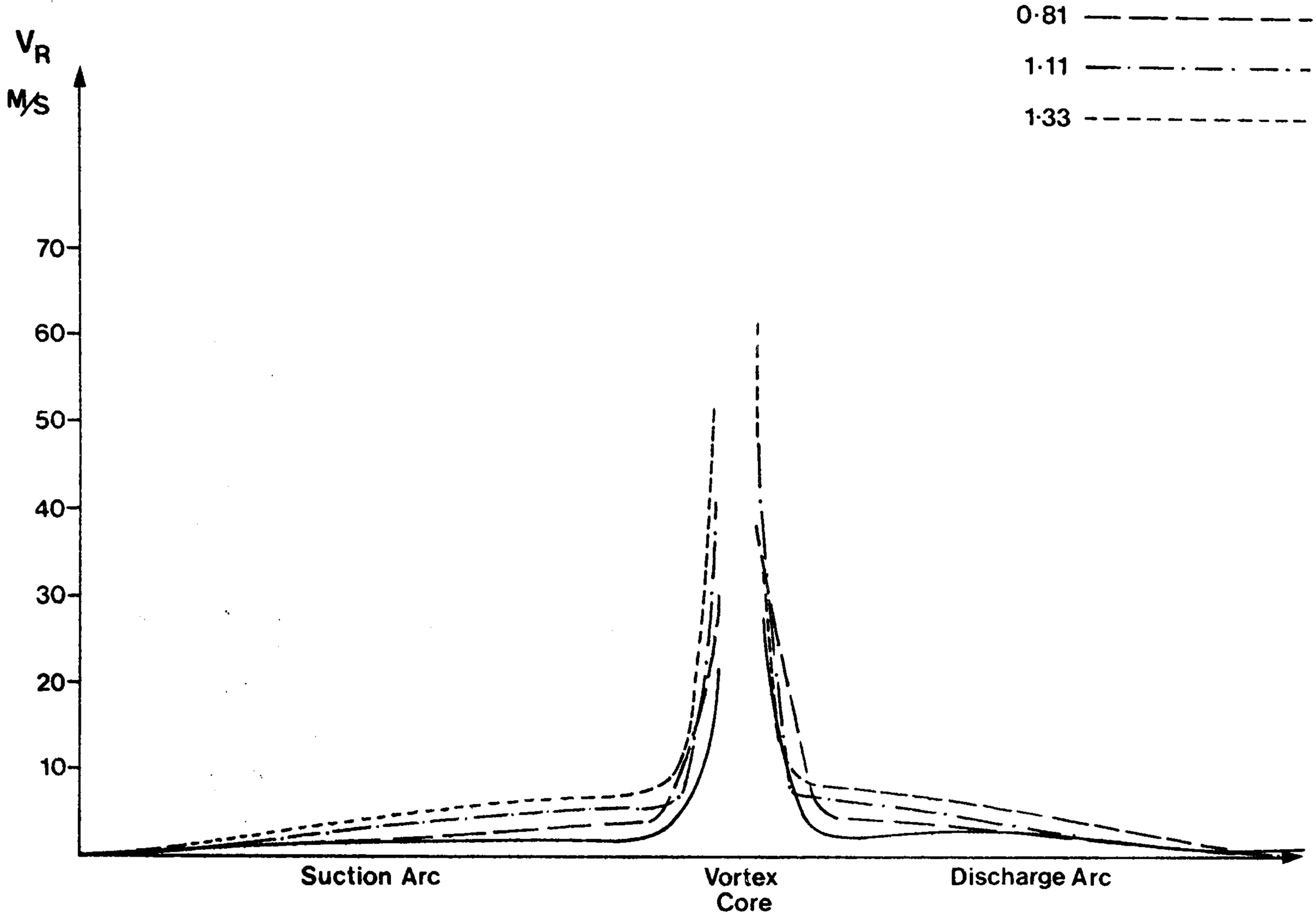

Figure 5·4

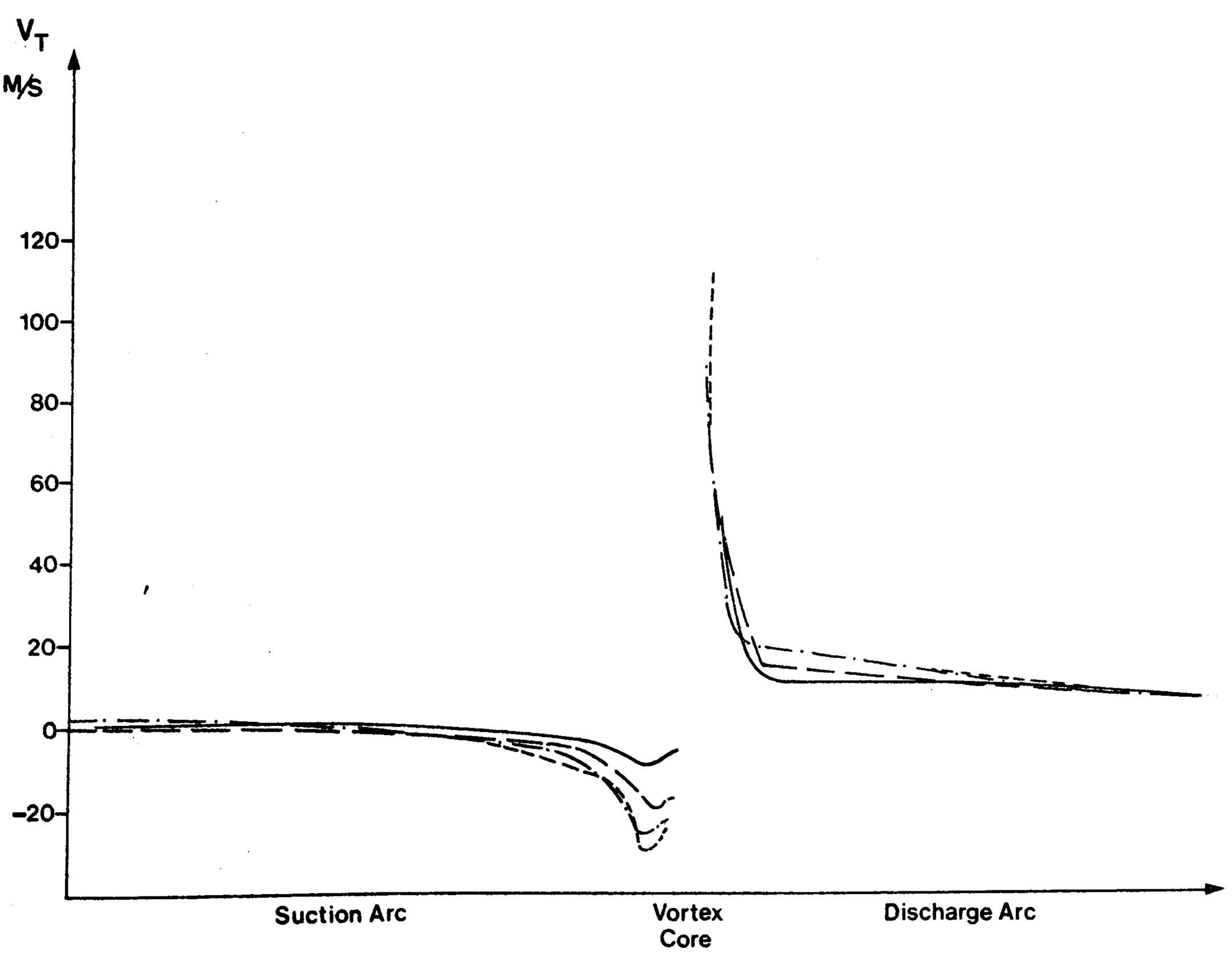

Figure 5·5

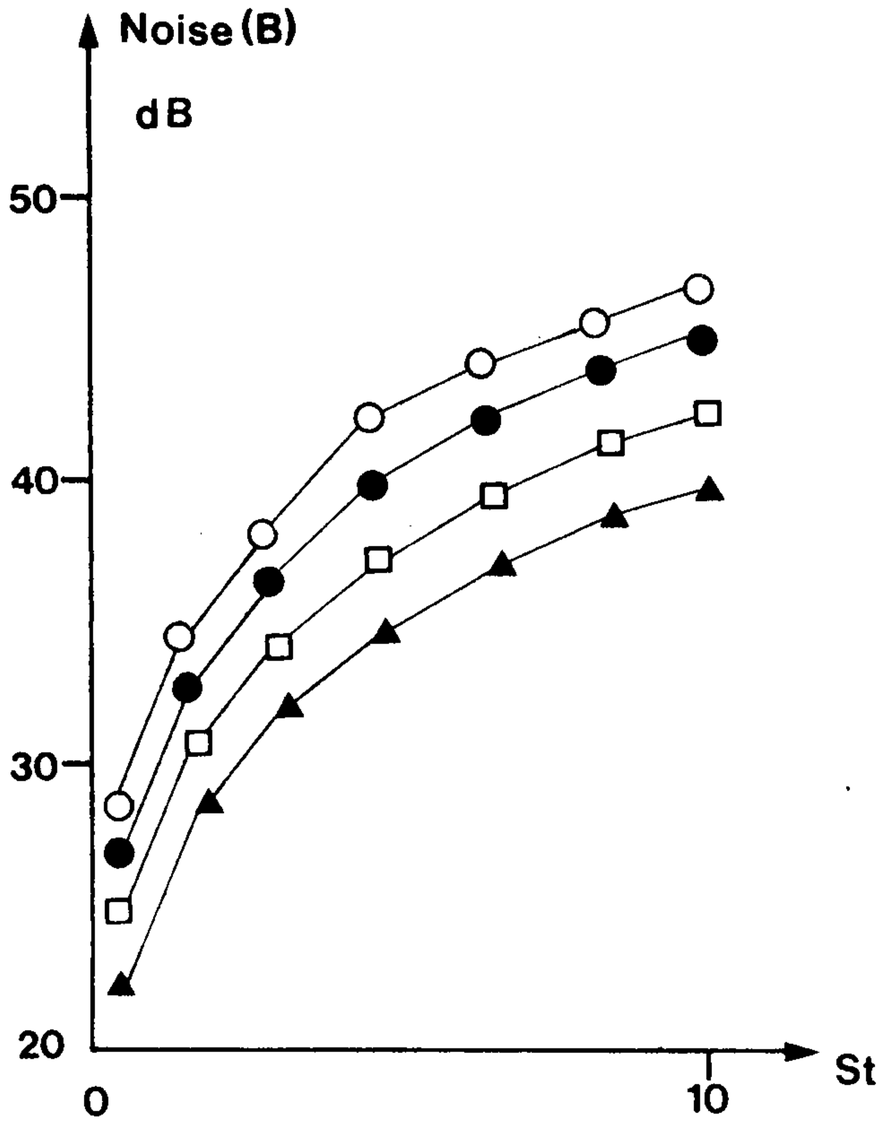

Figure 5·6(a)

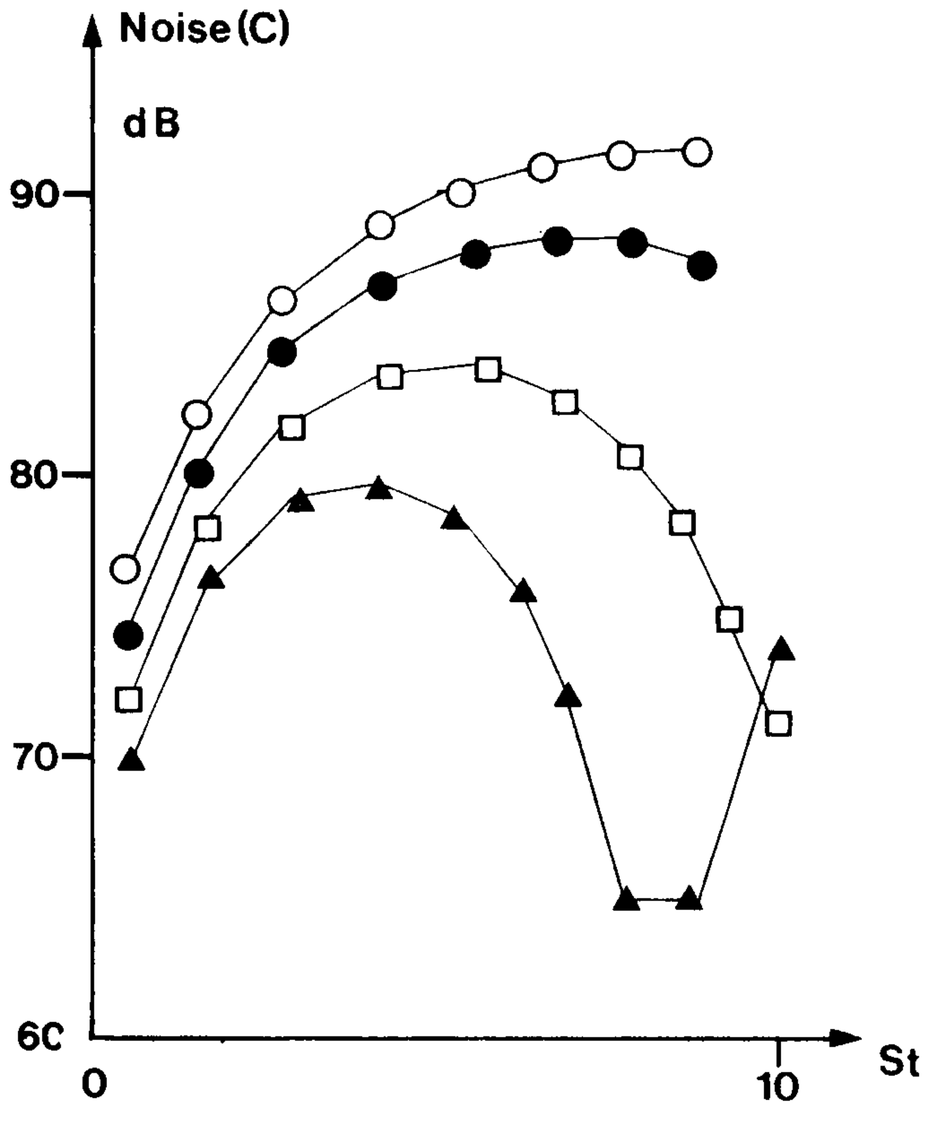

Figure 5·6(b)

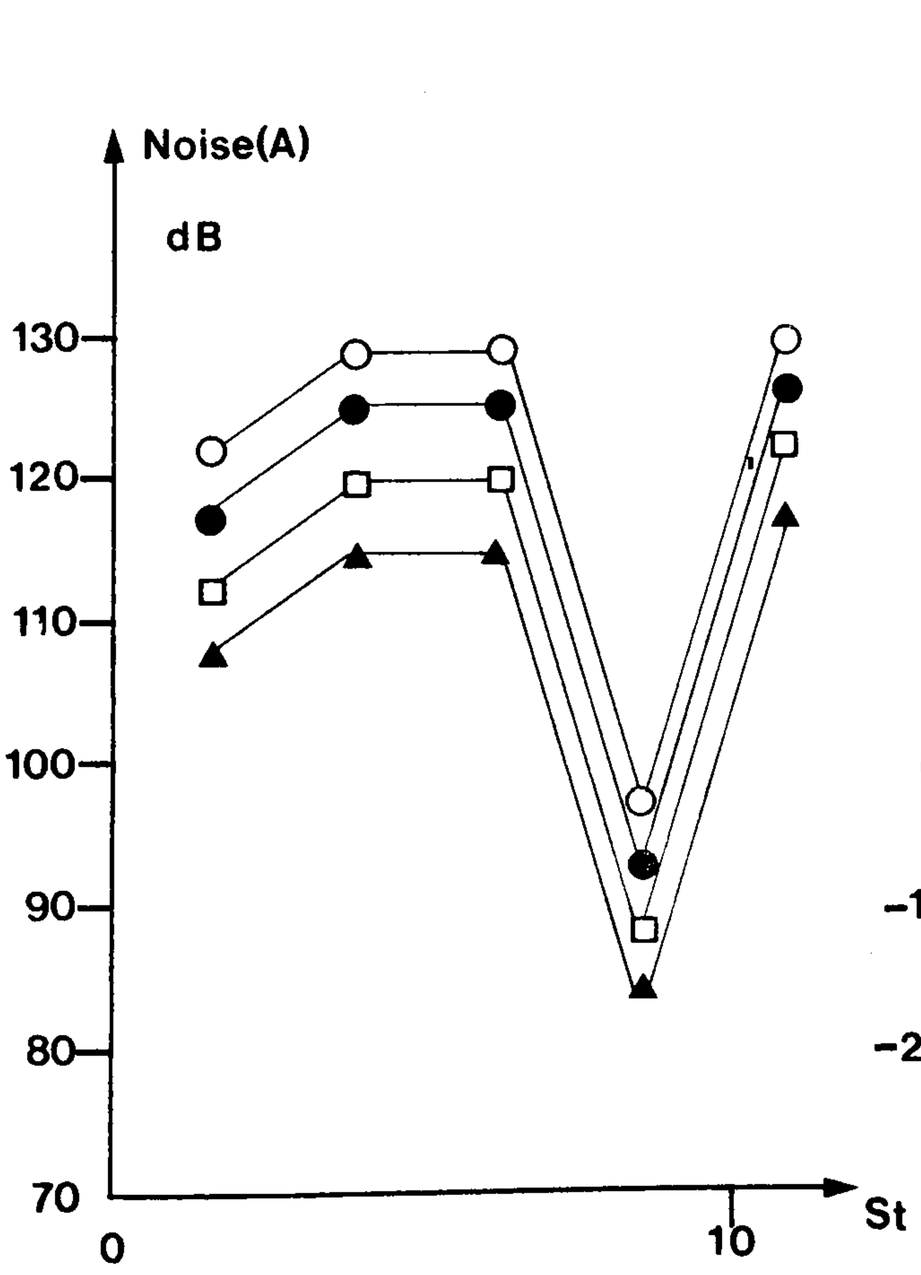

Figure 5·6(c)

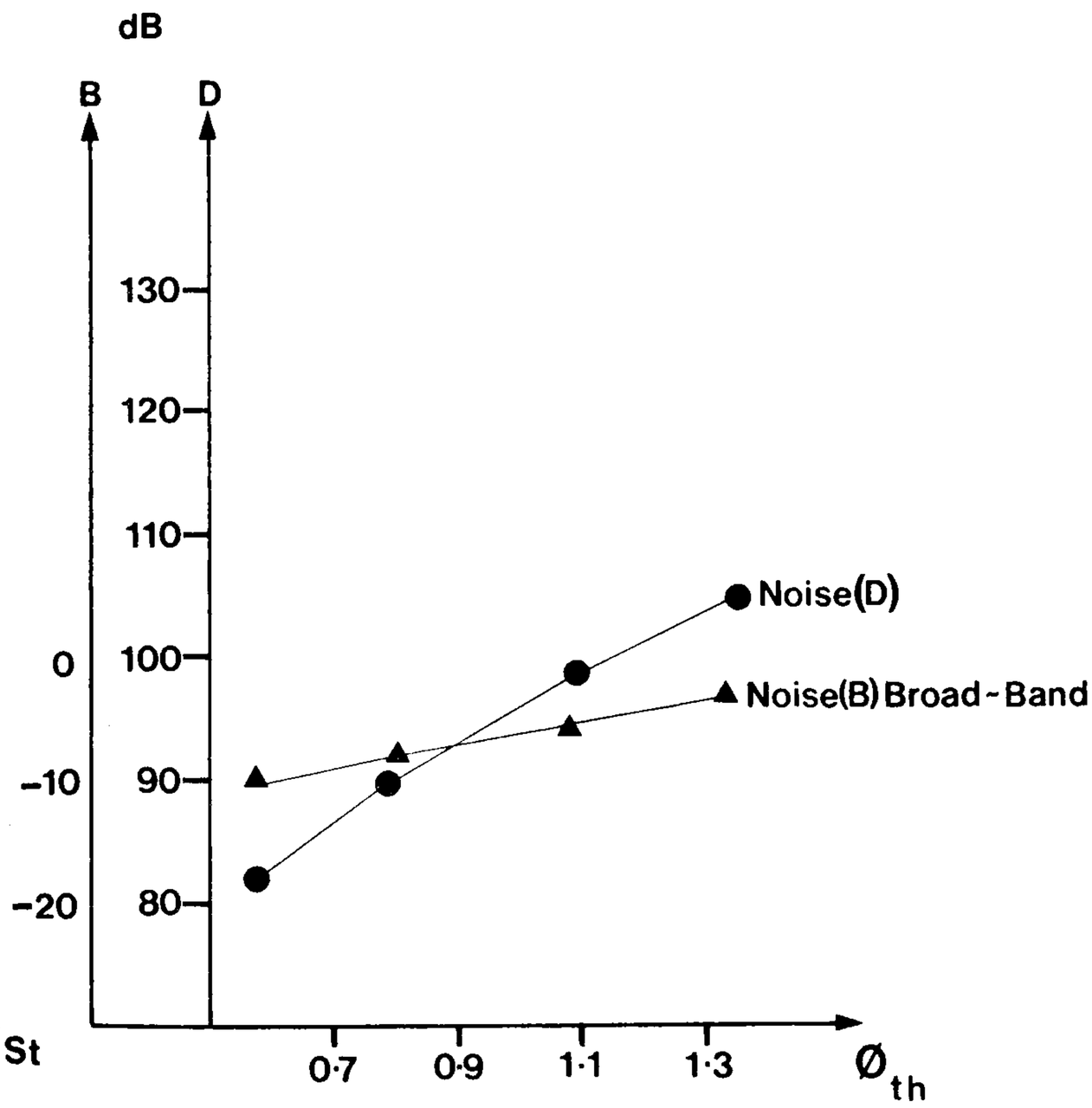

Figure 5·6(d)

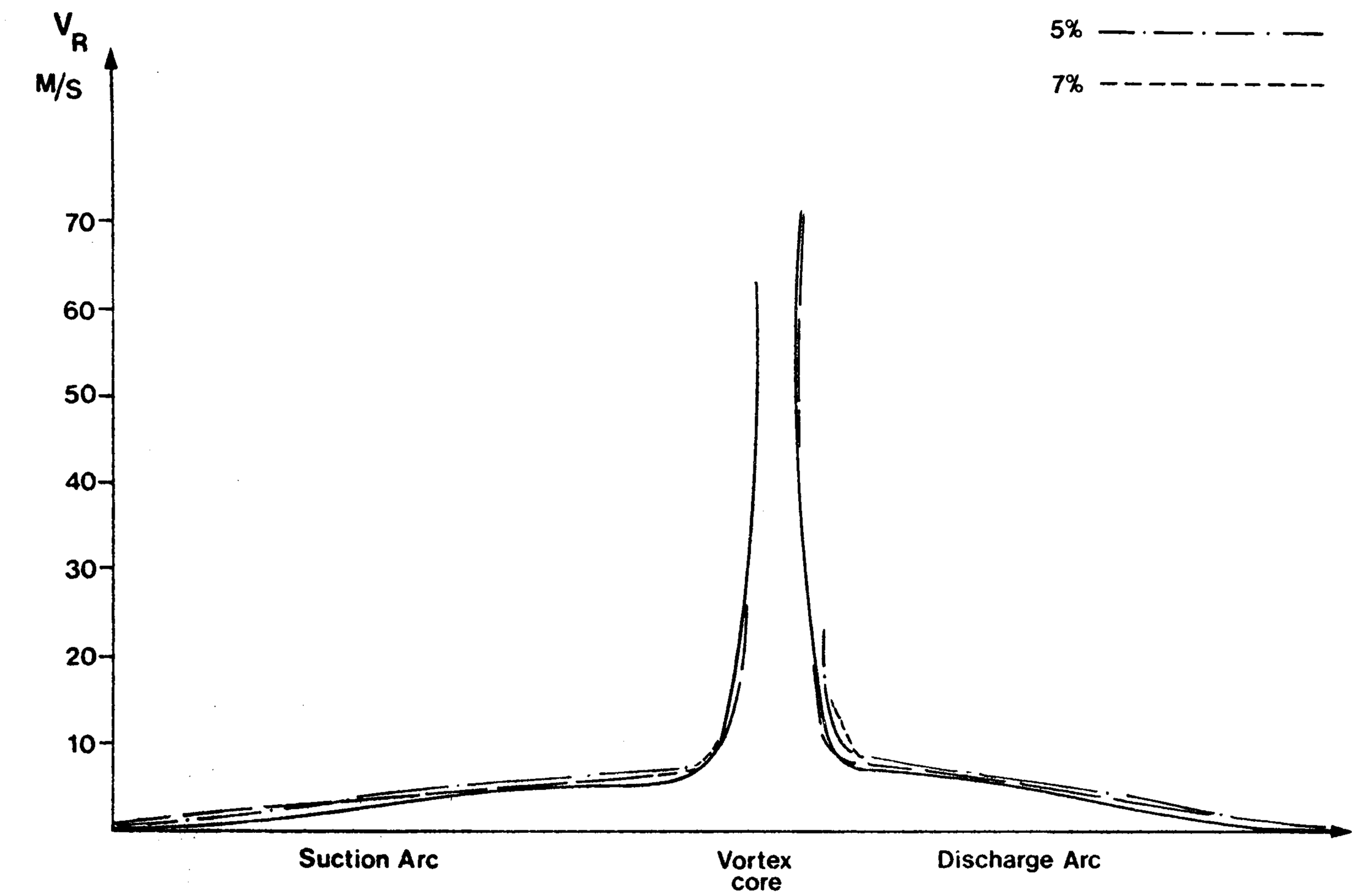

Figure 5·7

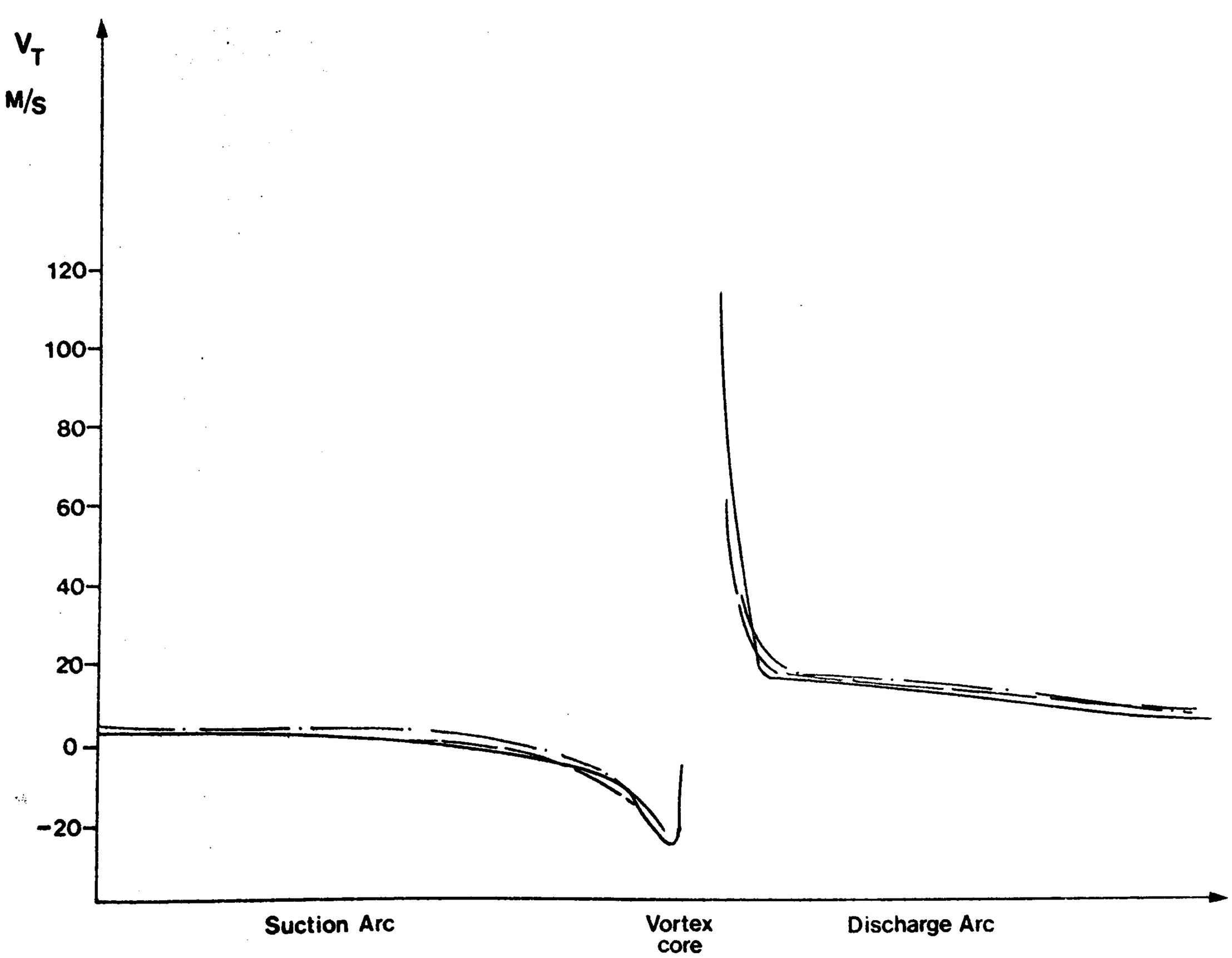

Figure 5·8

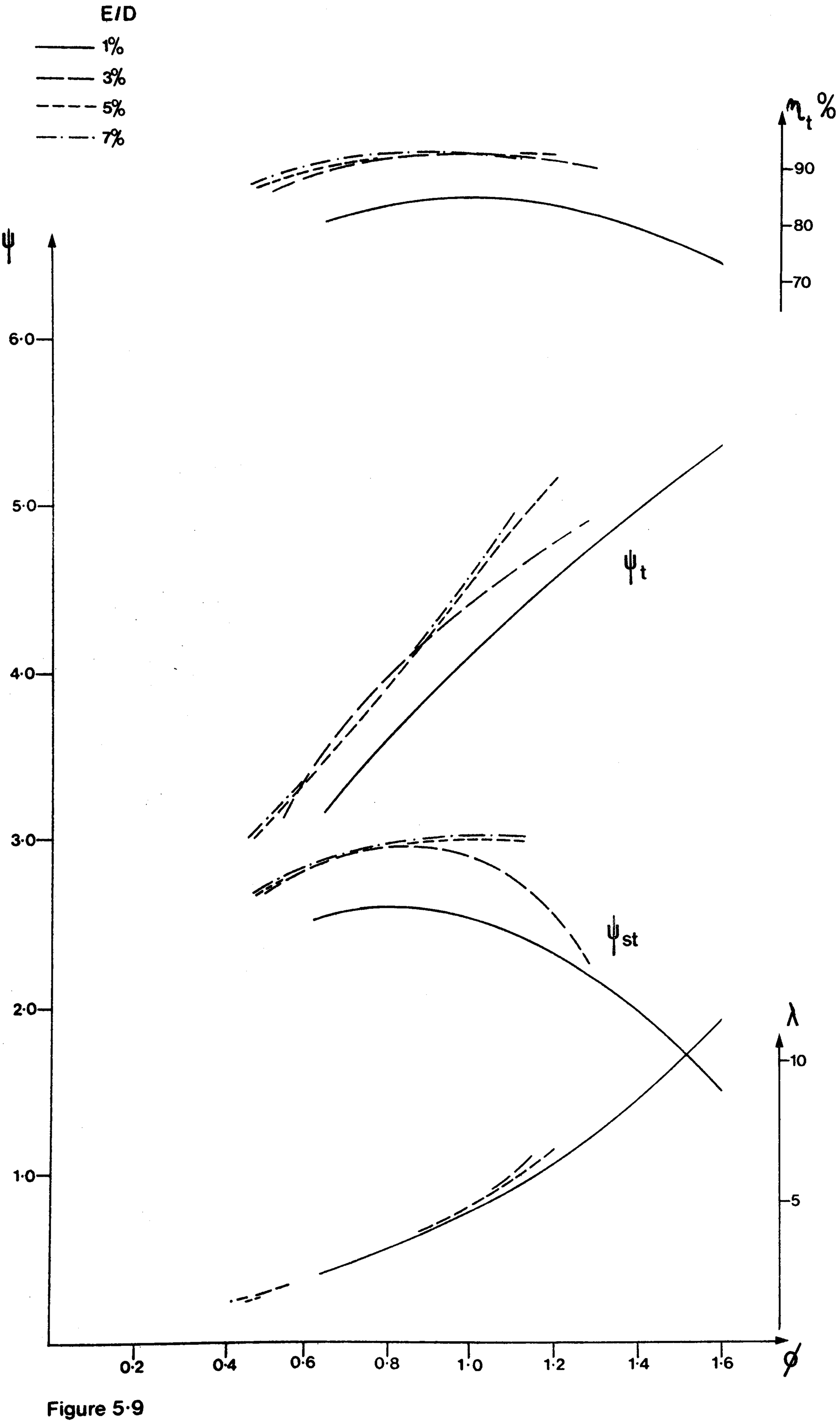
E/D
1%
3%
5%
7%
m_t %
90
80
70
ψ
6·0
5·0
4·0
3·0
2·0
1·0
ψ_t
ψ_{st}
λ
10
5
0·2
0·4
0·6
0·8
1·0
1·2
1·4
1·6
ϕ

Figure 5·9

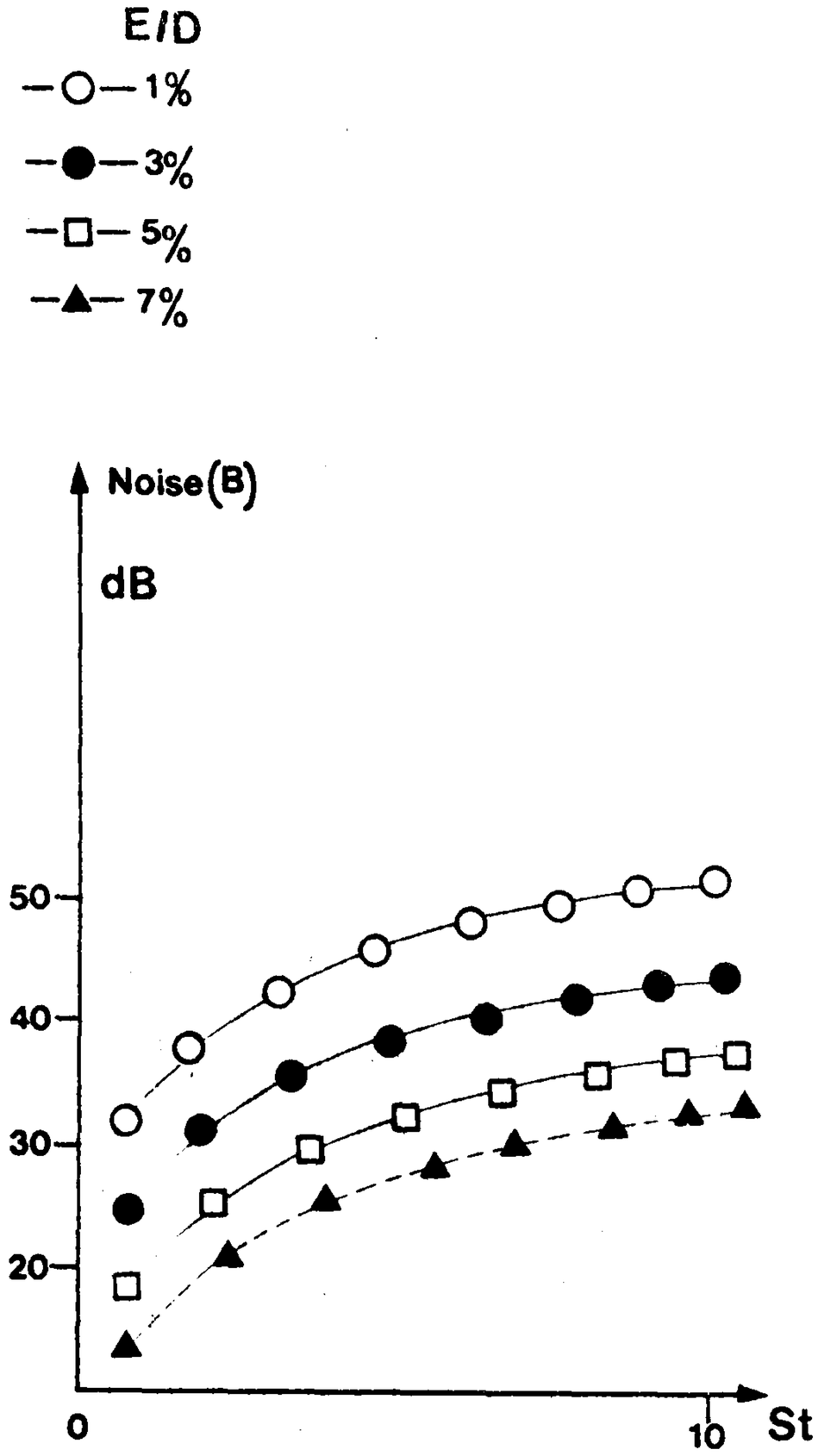

Figure 5·10(a)

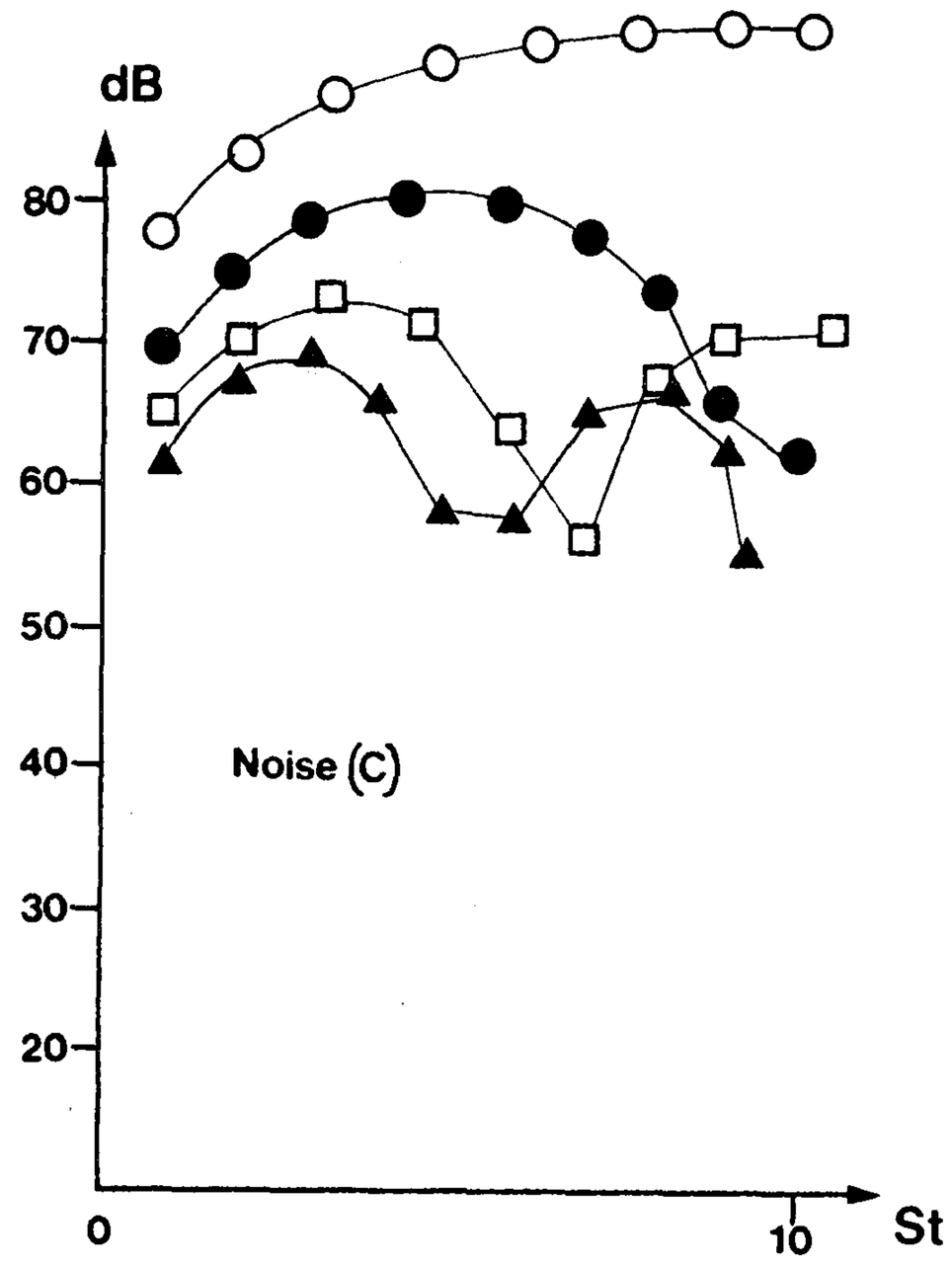

Figure 5·10 (b)

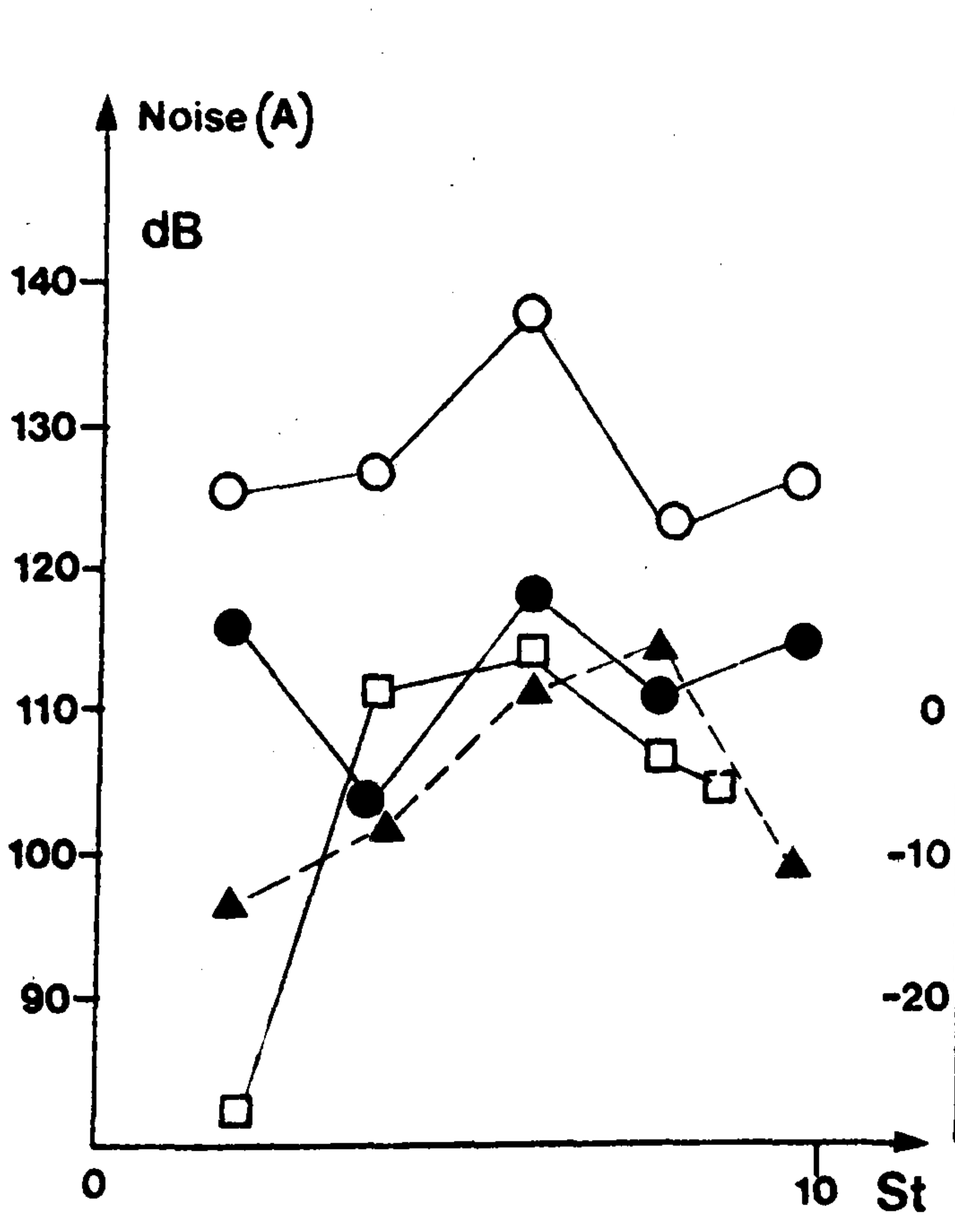

Figure 5·10 (c)

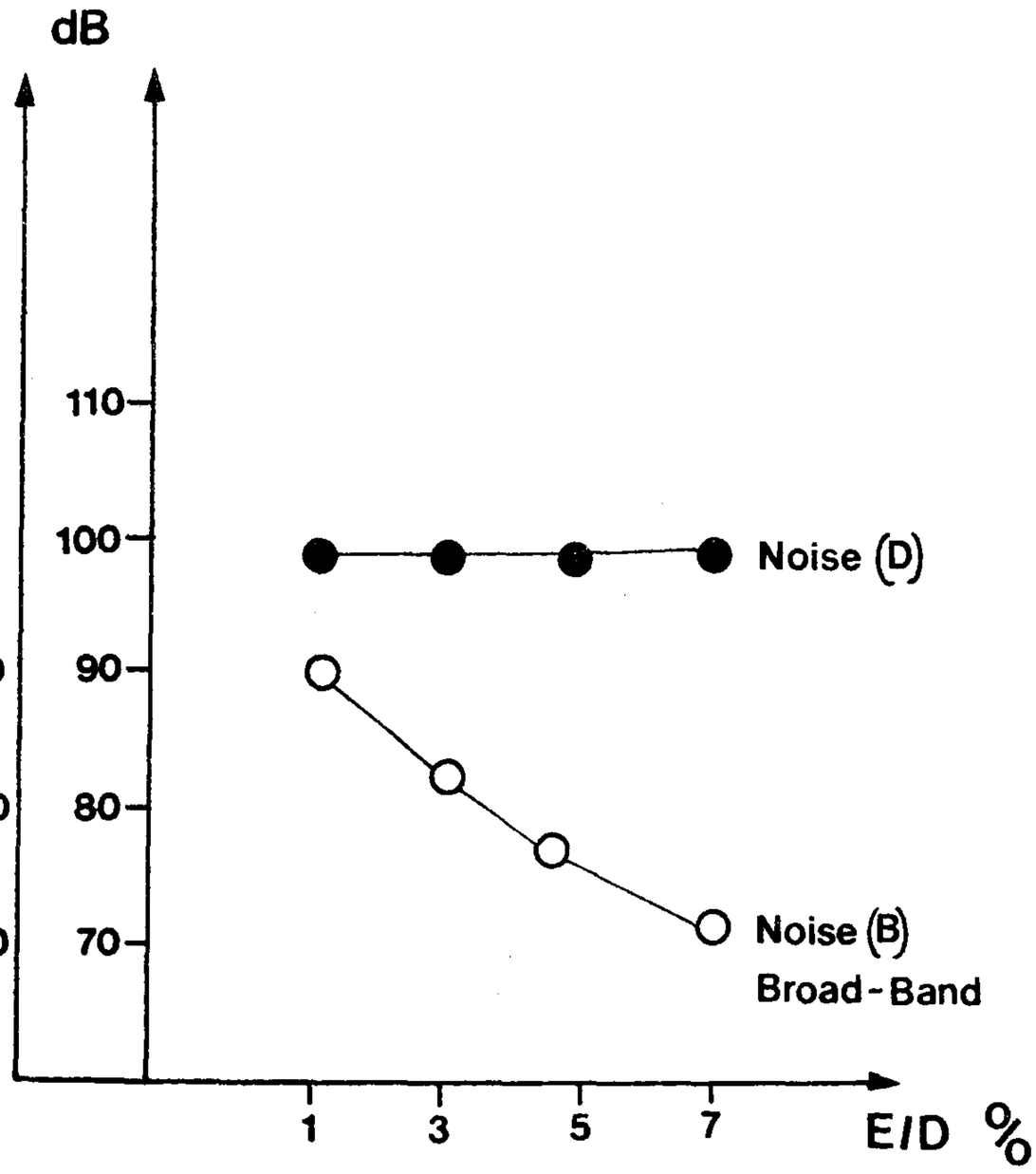

Figure 5·10 (d)

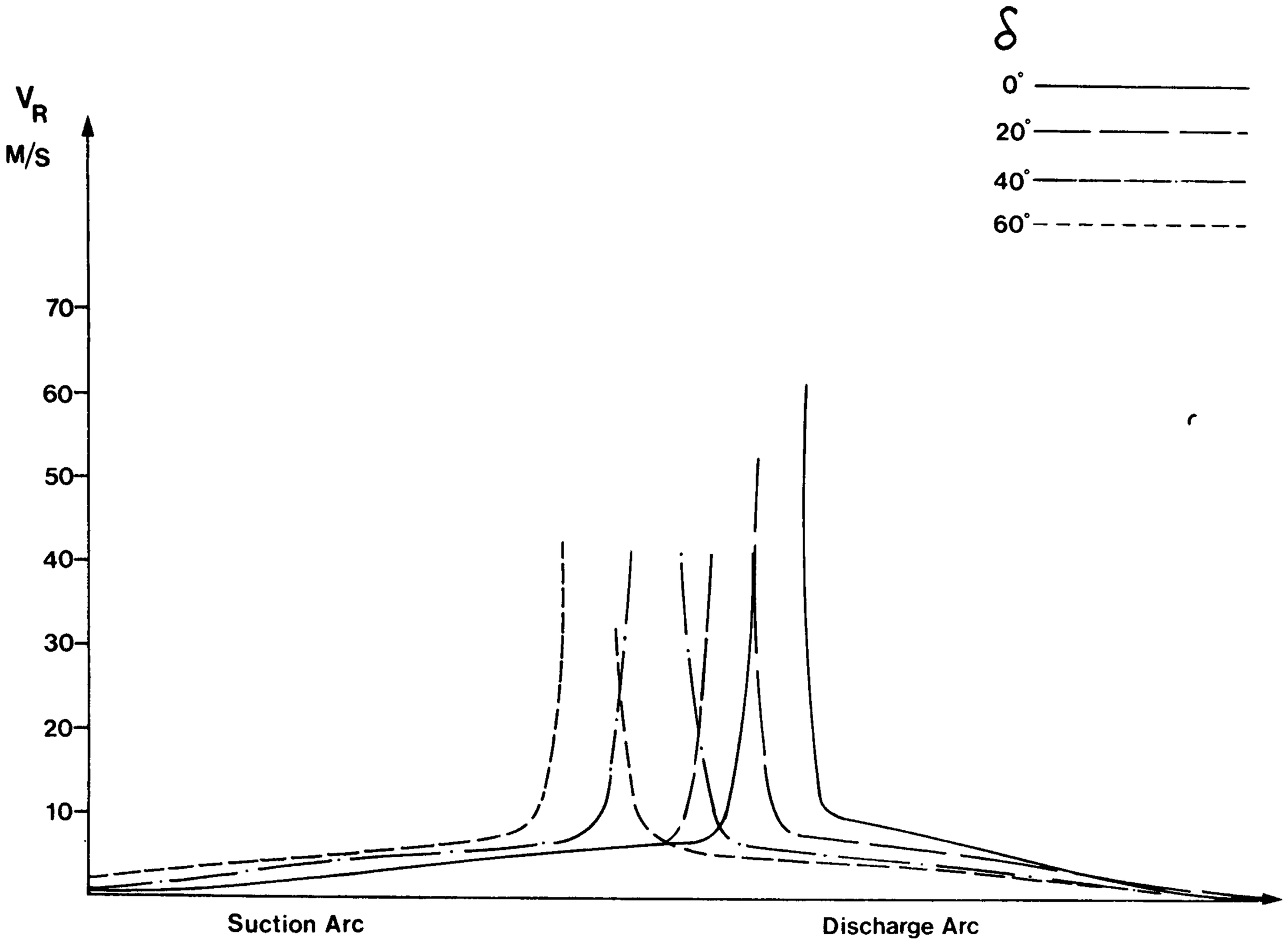

Figure 5·11

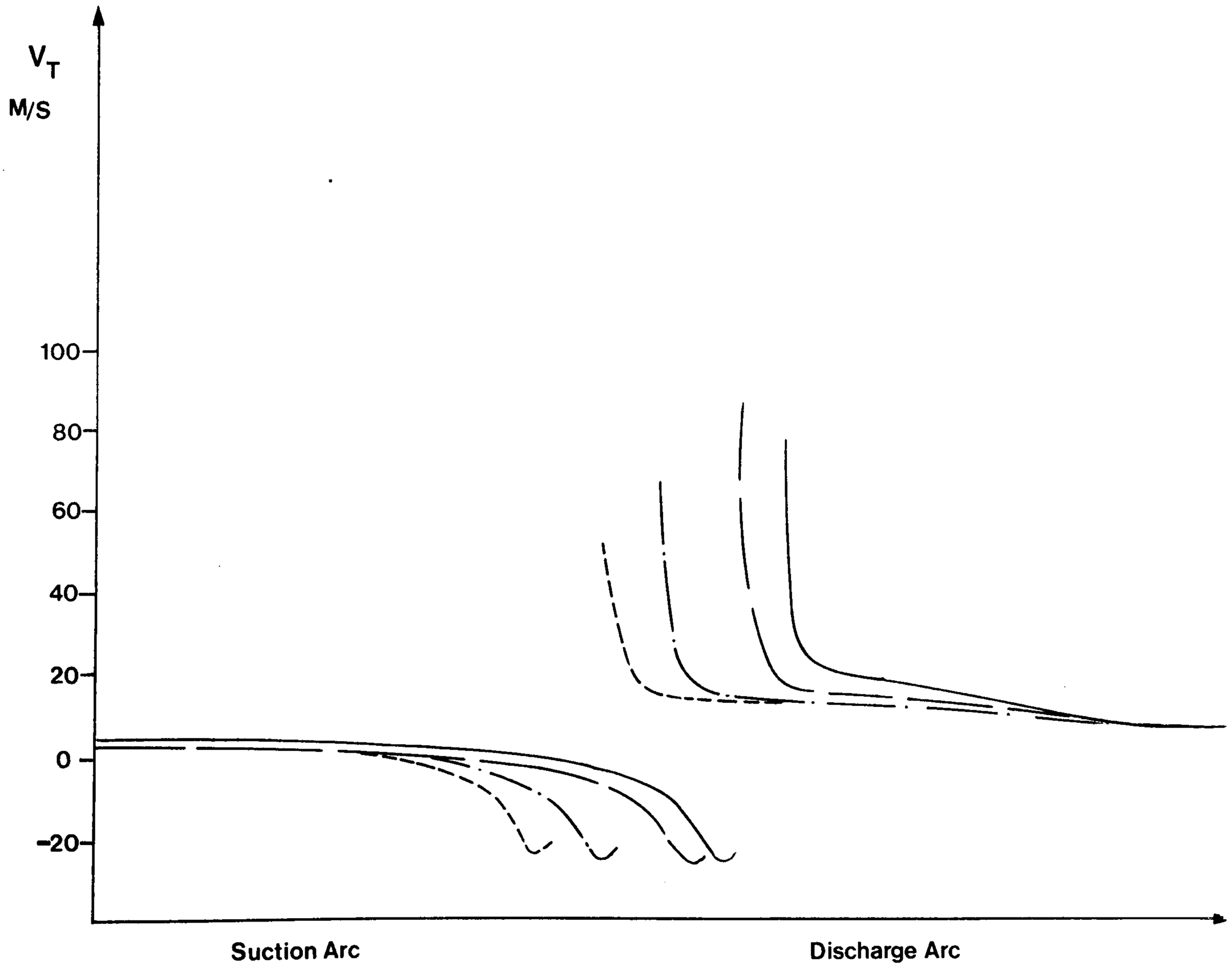

Figure 5·12

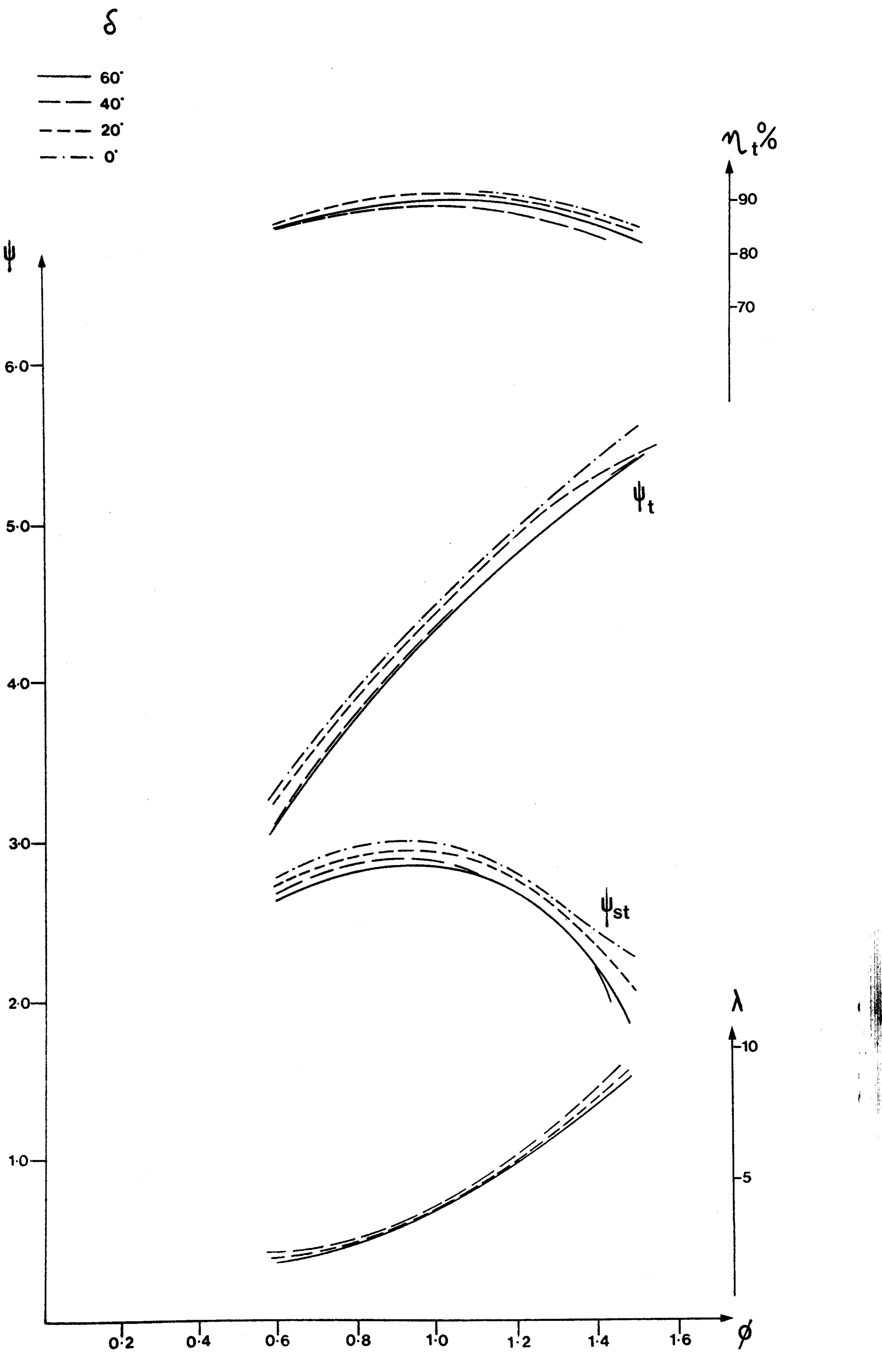
δ
60°
40°
20°
0°
ψ
6·0
5·0
4·0
3·0
2·0
1·0
ψt
ηt%
90
80
70
ψst
λ
10
5
0·2
0·4
0·6
0·8
1·0
1·2
1·4
1·6
ϕ

Figure 5·13

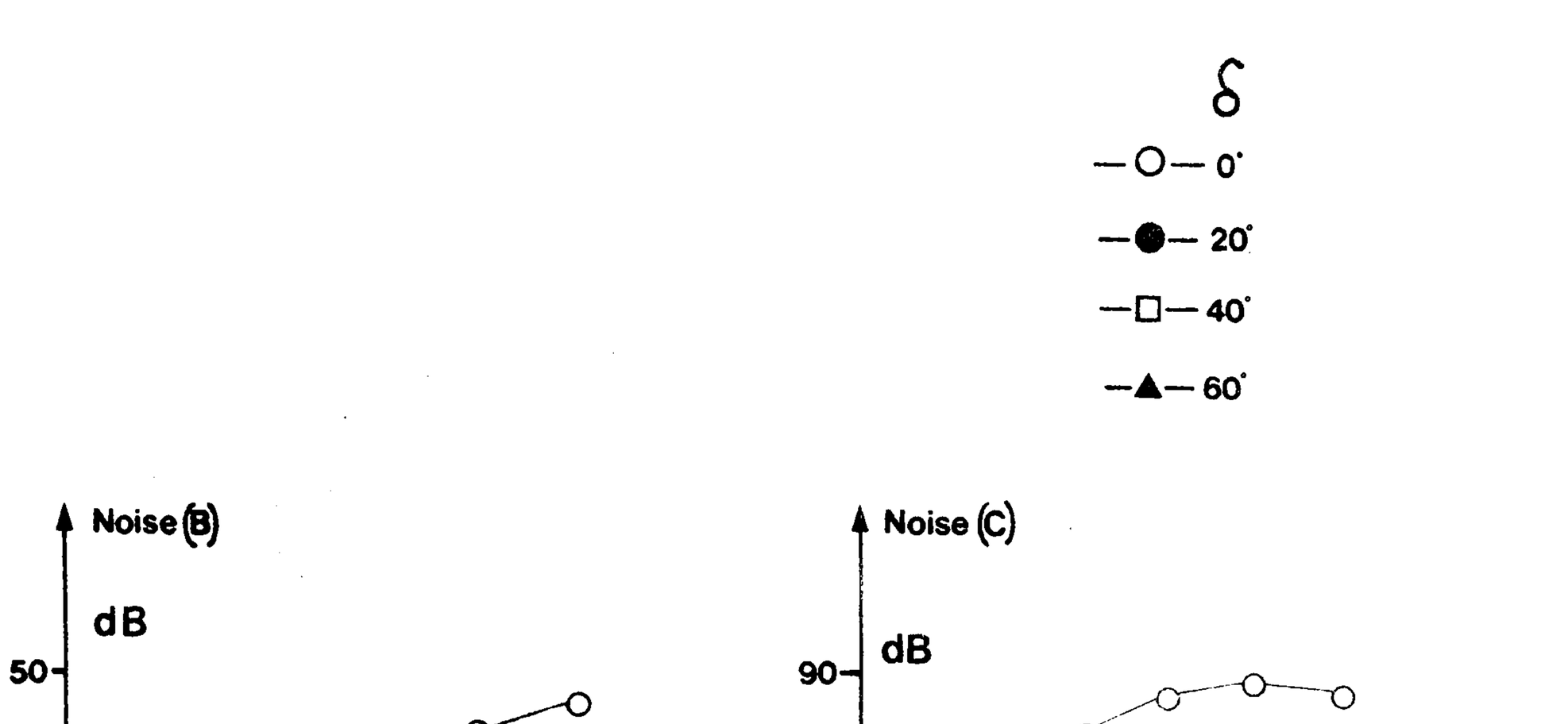

Figure 5·14(a)

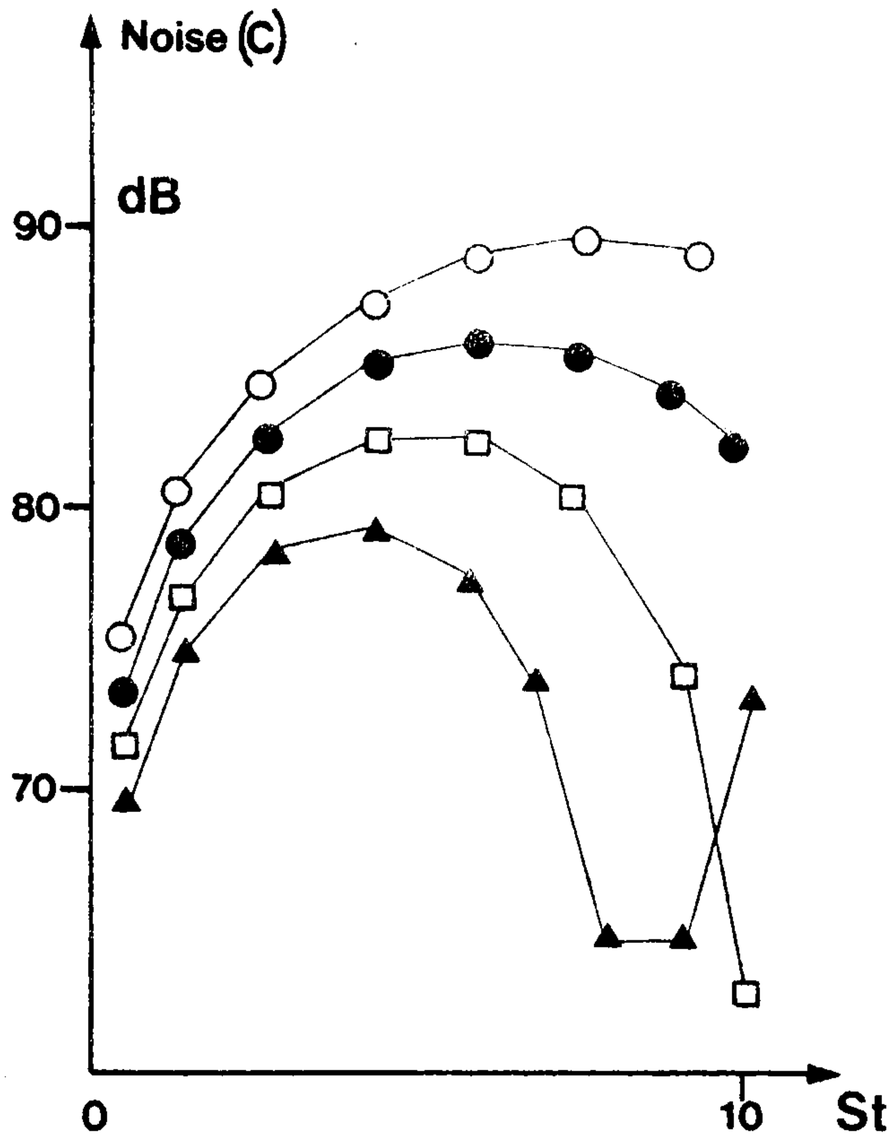

Figure 5·14 (b)

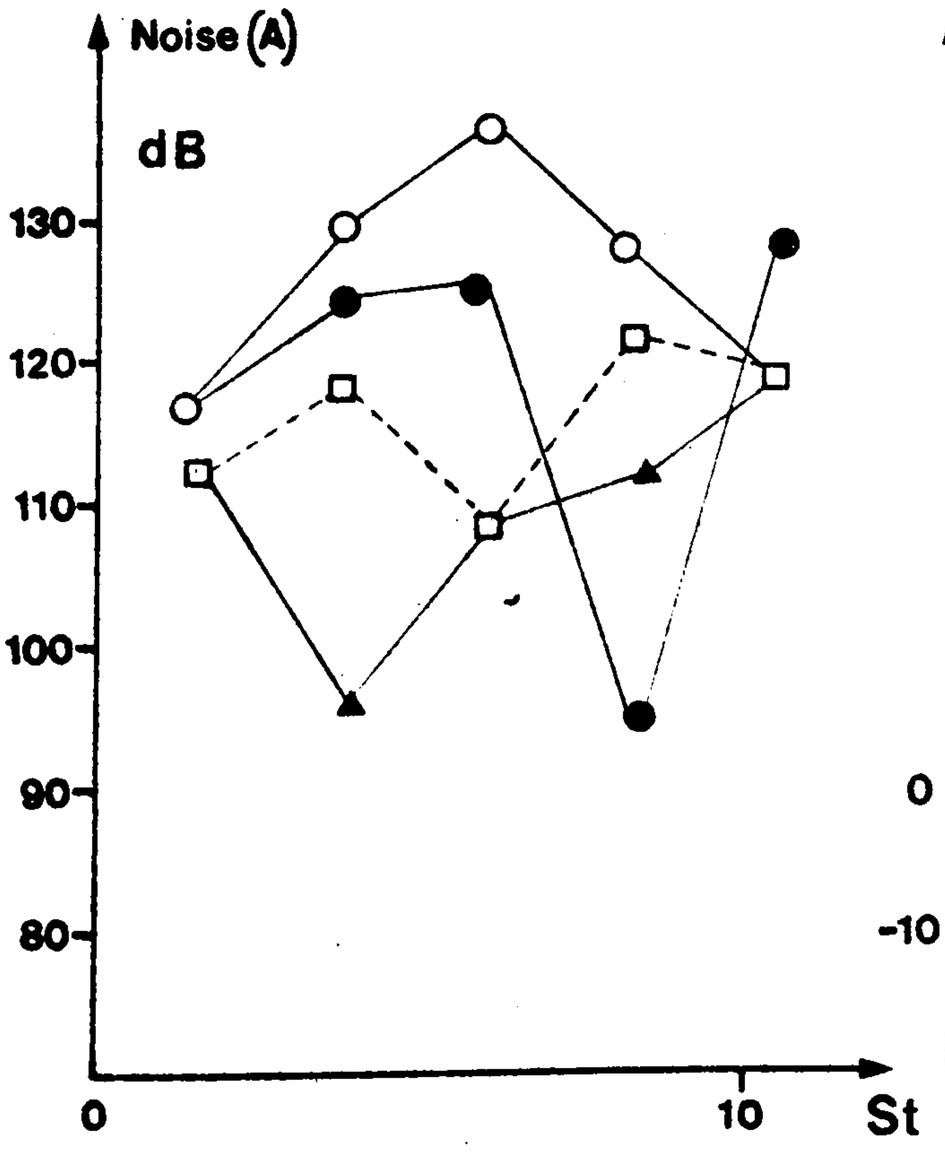

Figure 5·14(c)

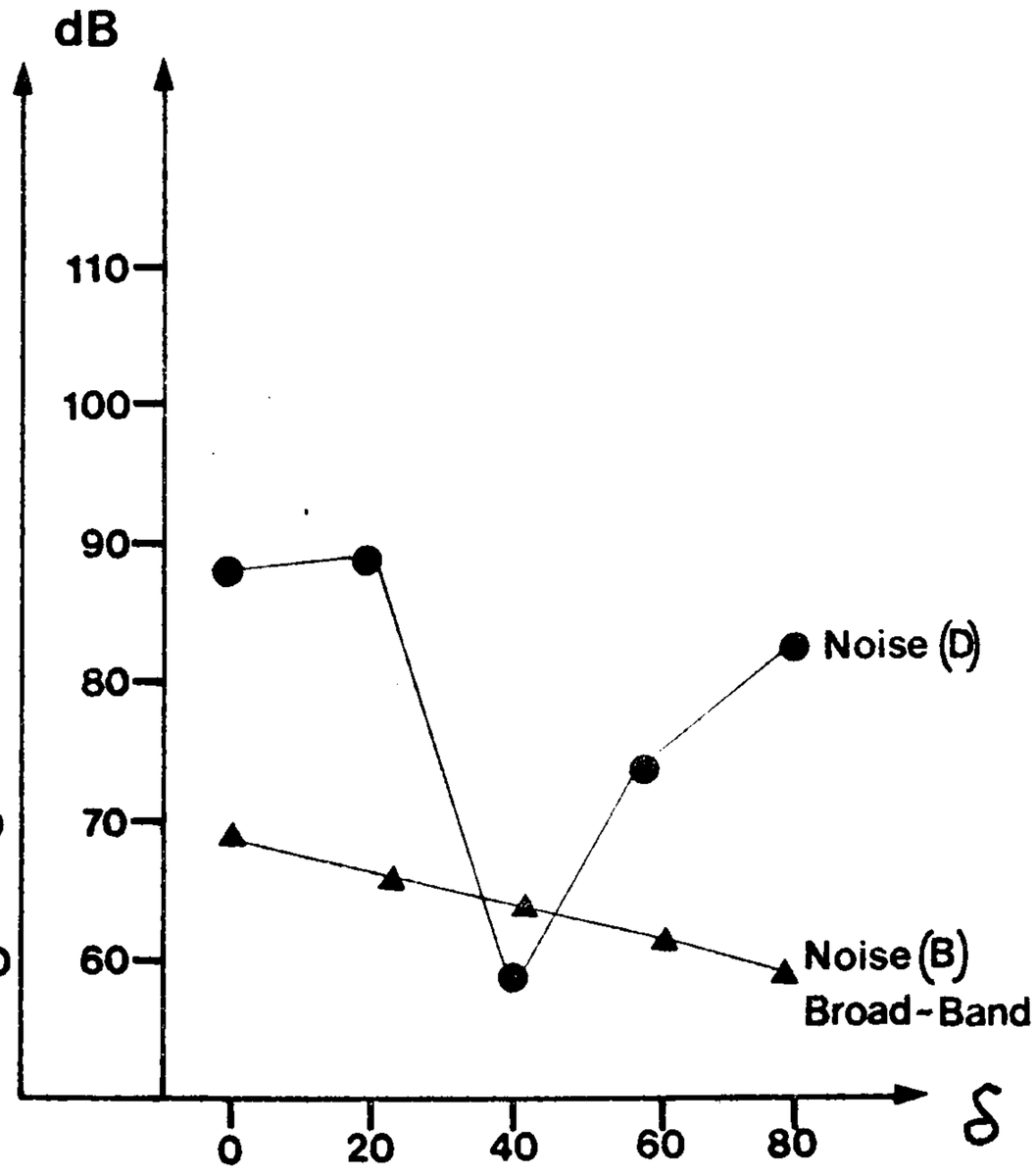

Figure 5·14 (d)

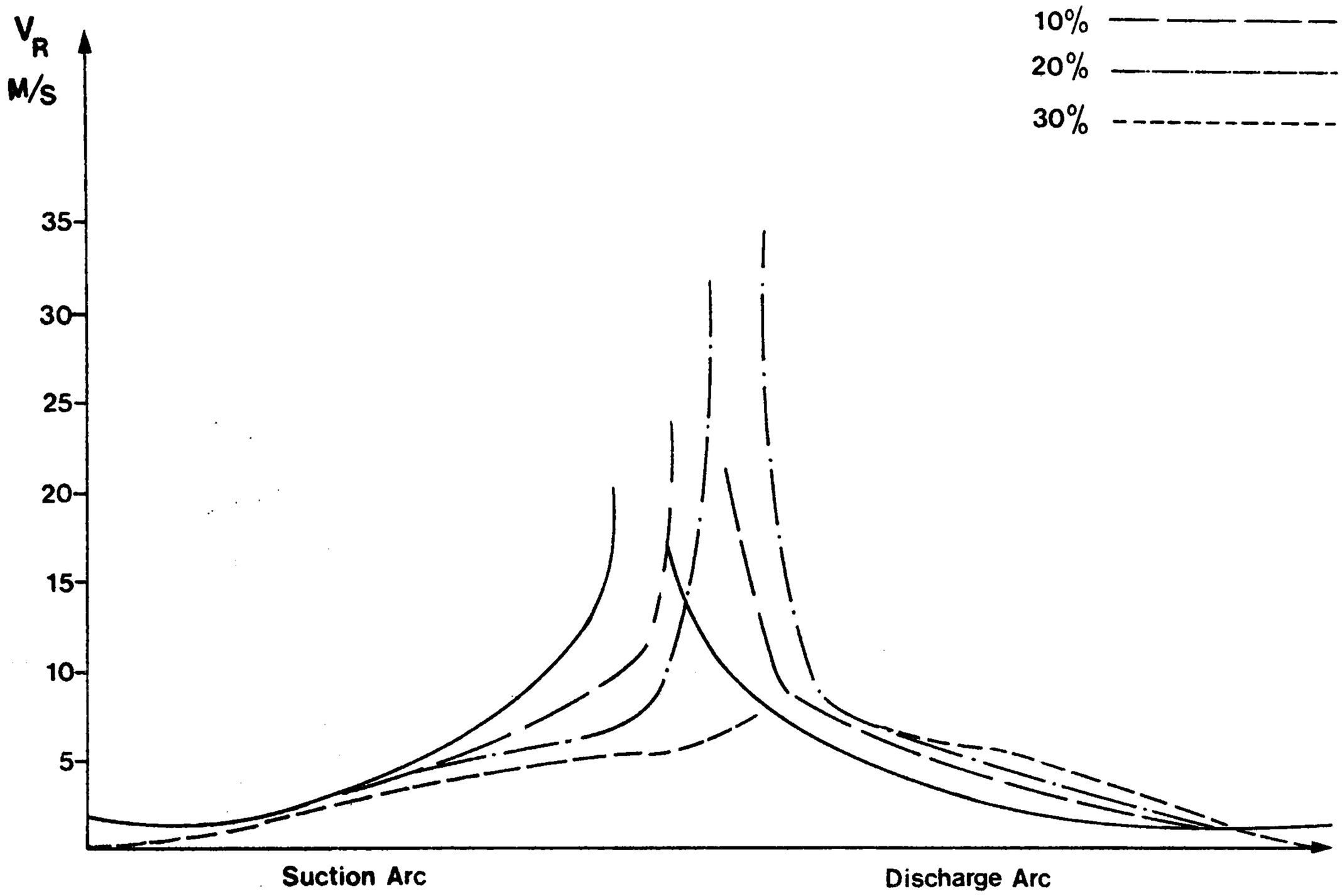

Figure 5·15

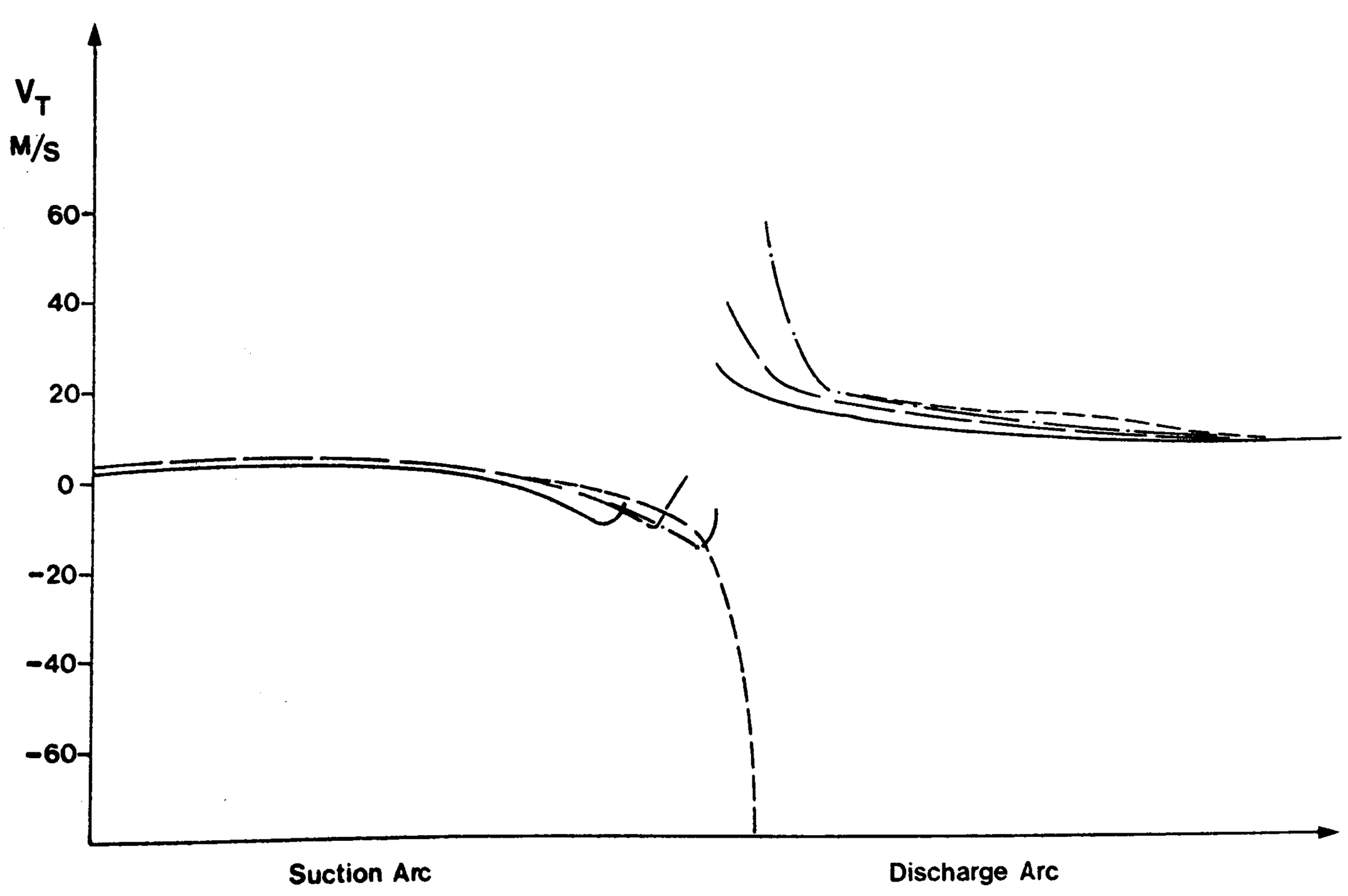

Figure 5·16

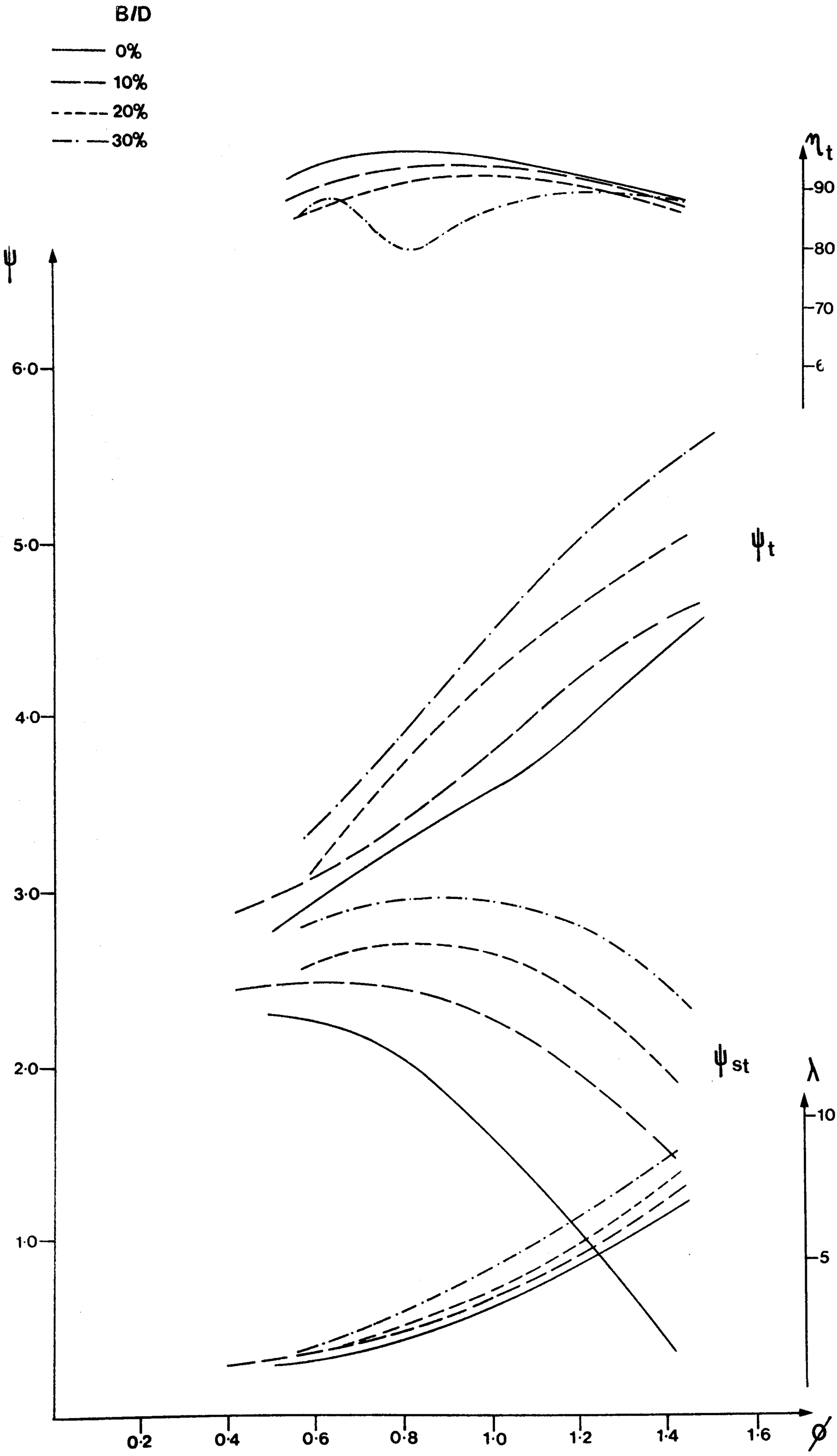
B/D
0%
10%
20%
30%
η_t %
90
80
70
60
ψ
6·0
5·0
4·0
3·0
2·0
1·0
ψ_t
ψ_{st}
λ
10
5
0·2
0·4
0·6
0·8
1·0
1·2
1·4
1·6
ϕ

Figure 5·17

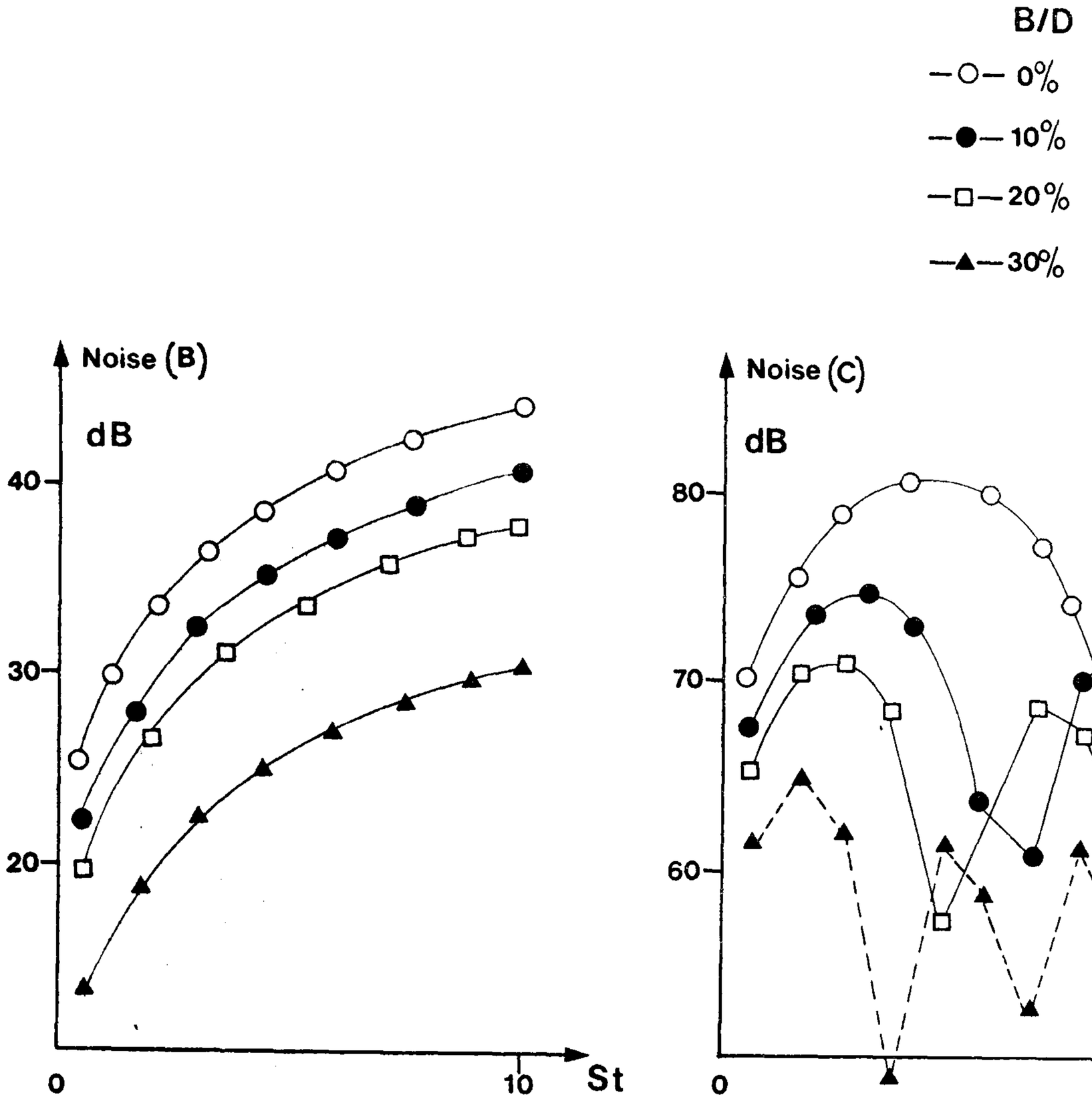

Figure 5·18 (a)

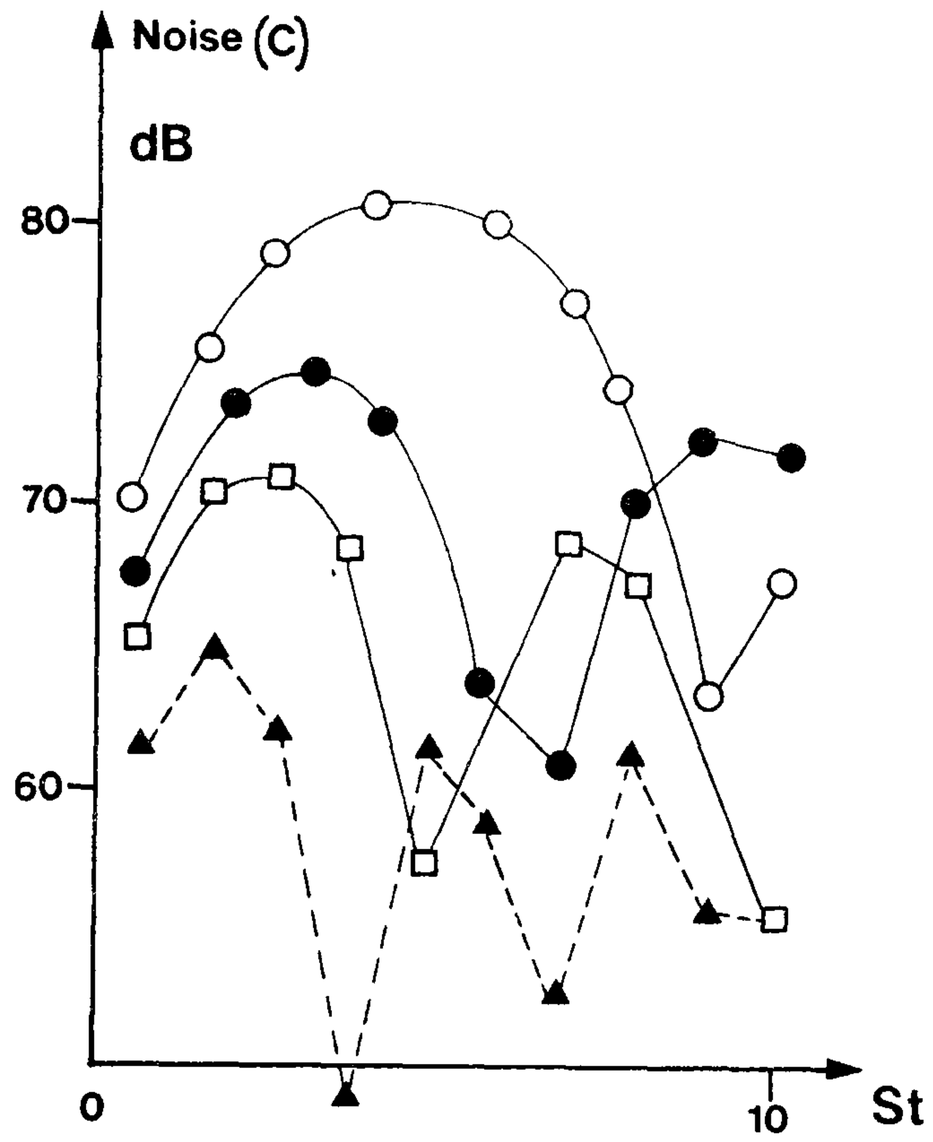

Figure 5·18 (b)

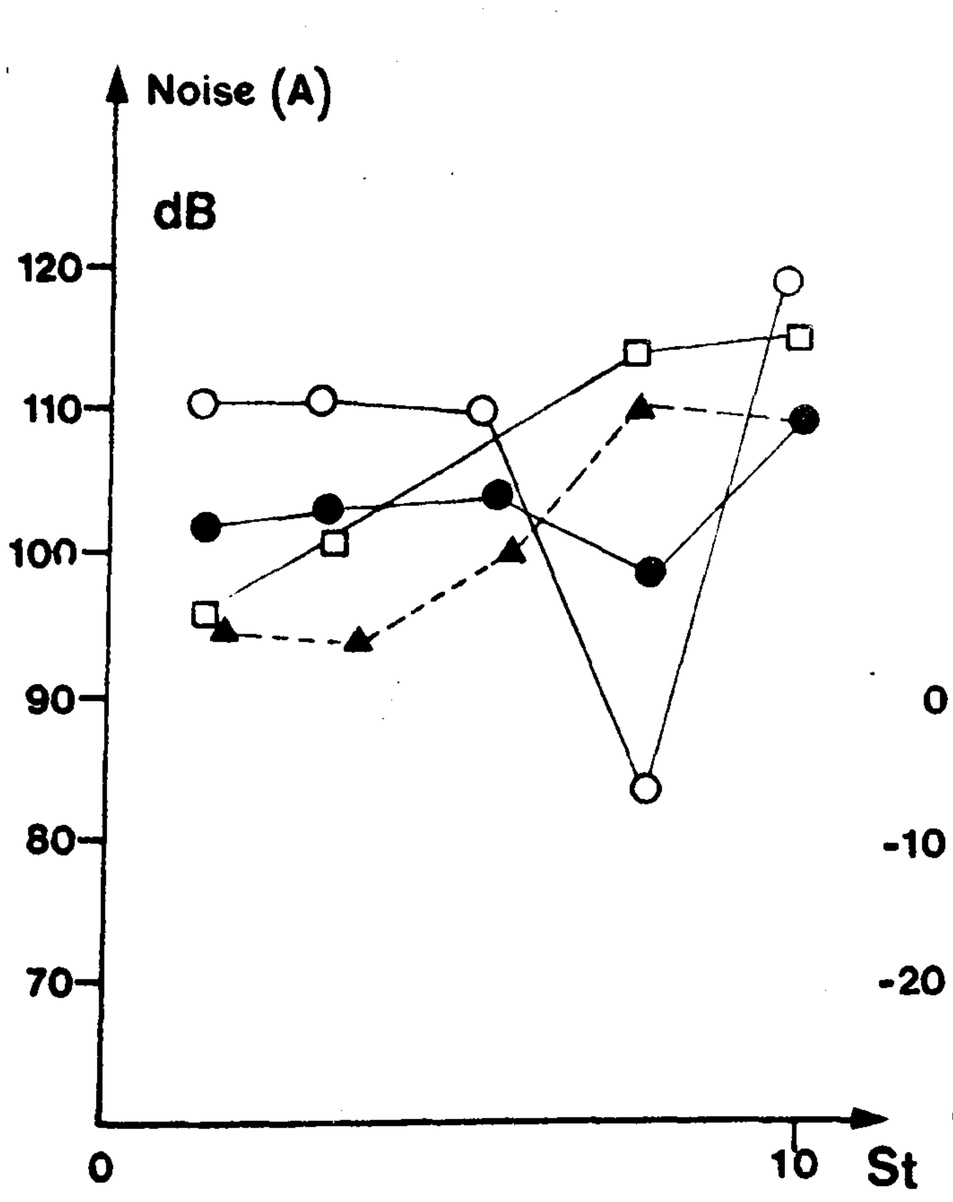

Figure 5·18 (c)

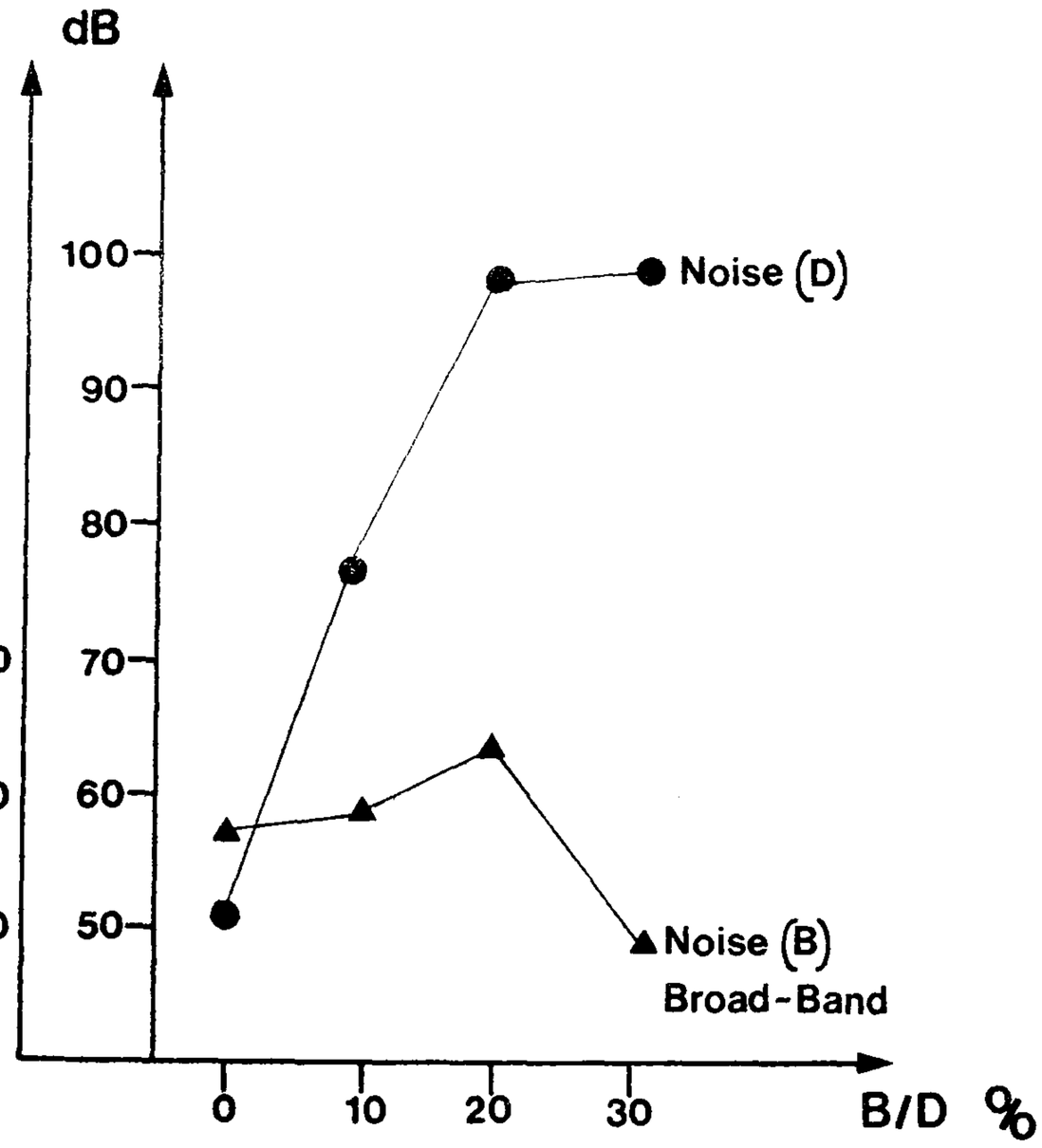

Figure 5·18 (d)

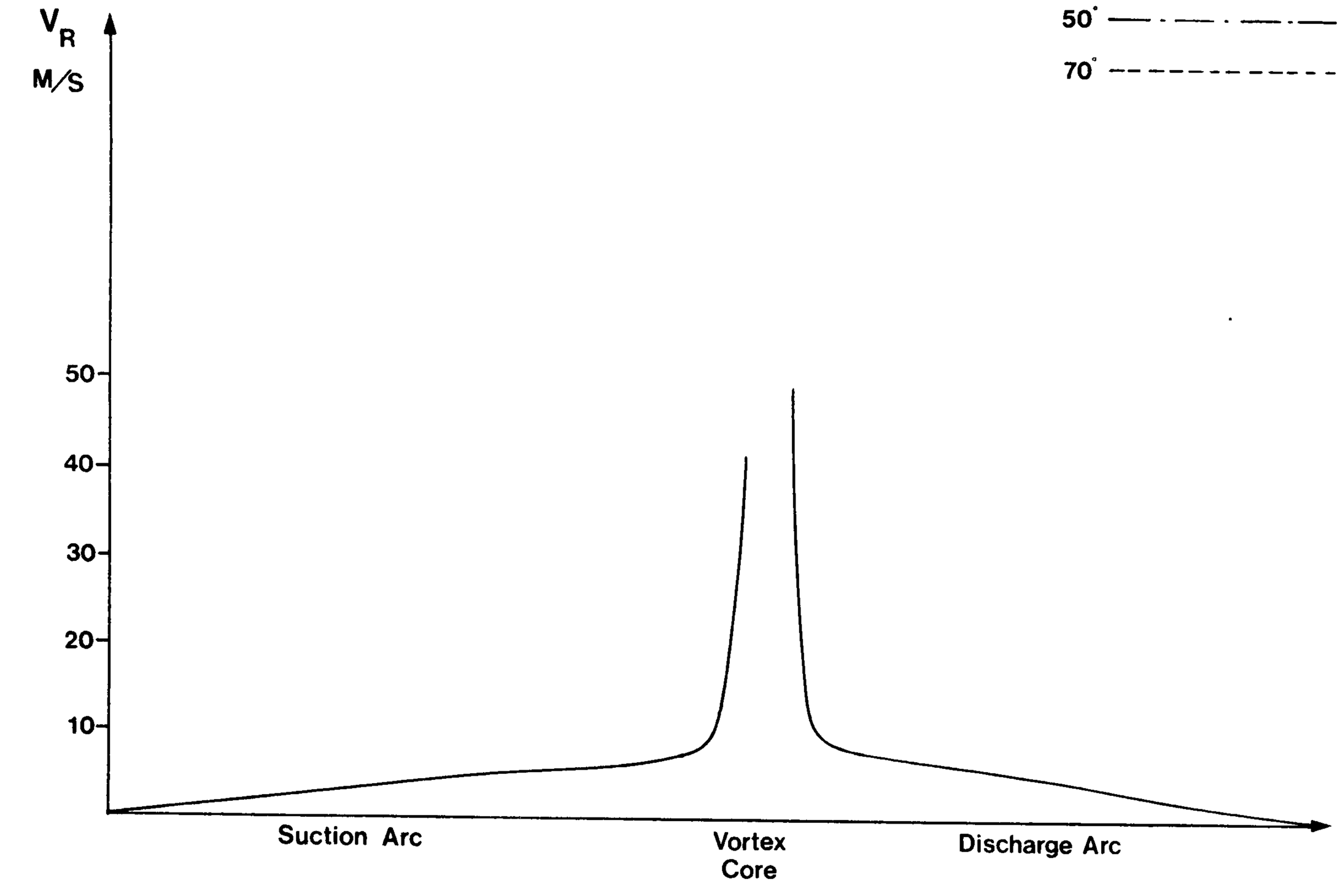

Figure 5·19

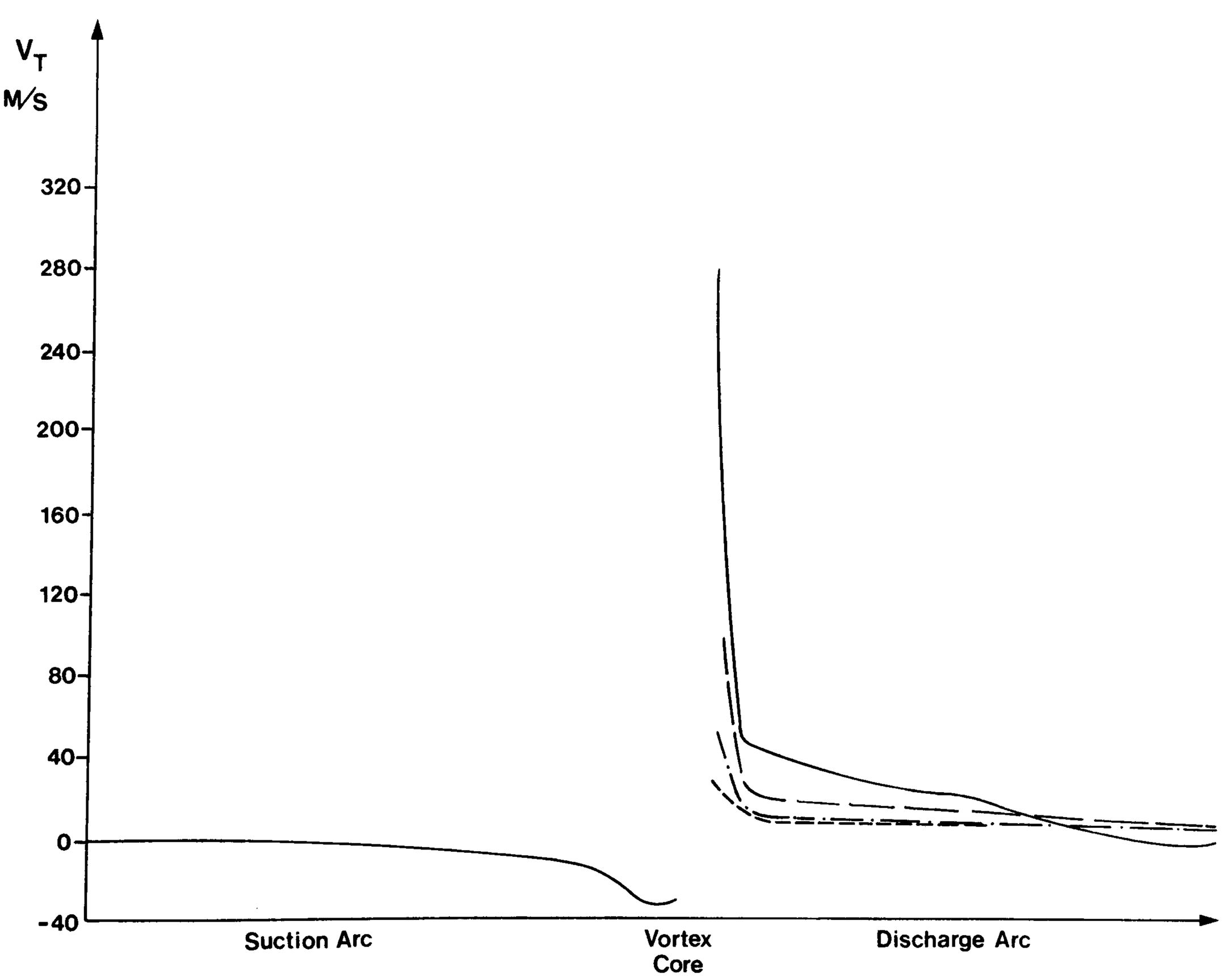

Figure 5·20

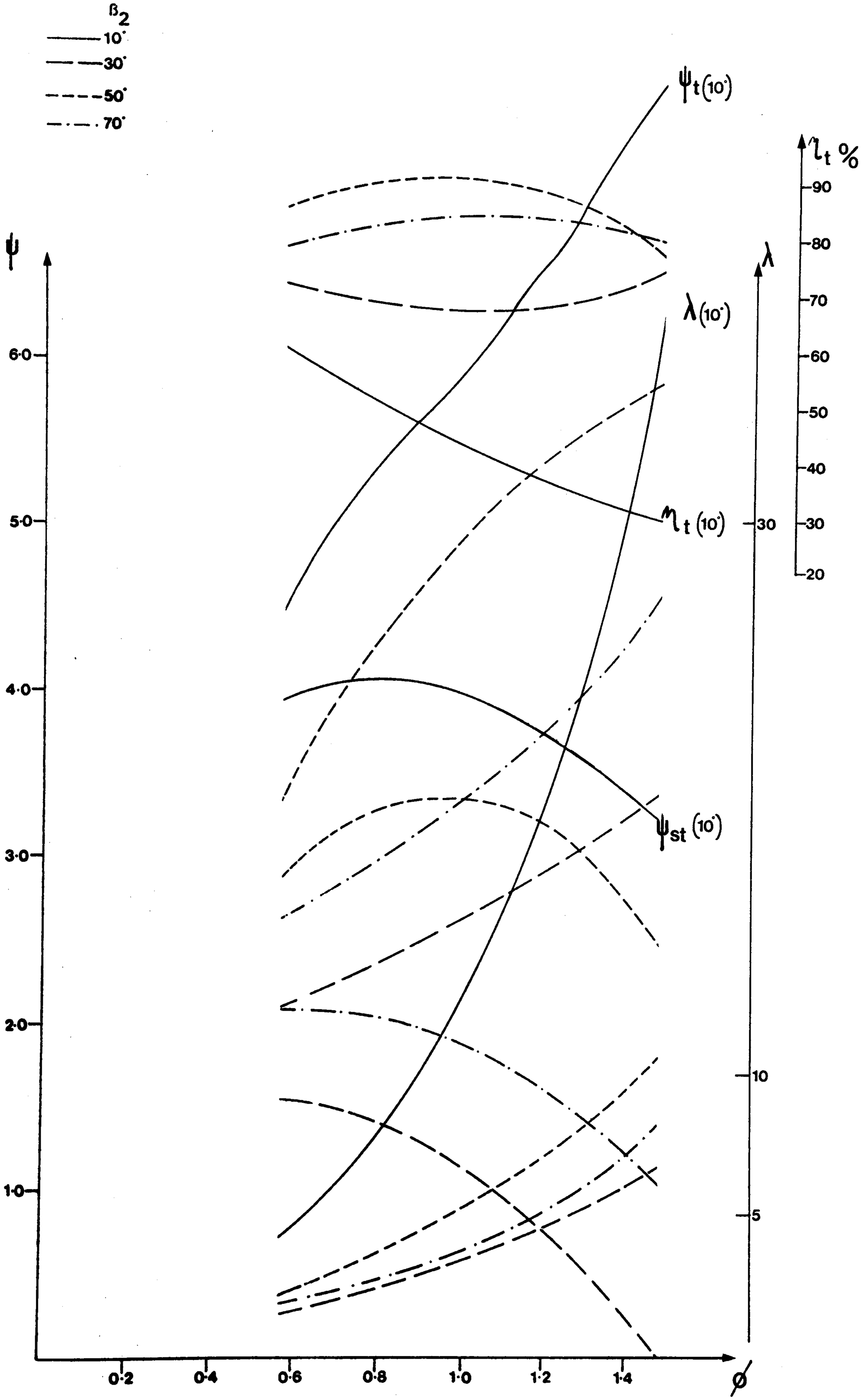
β_2
10°
30°
50°
70°
ψ
6·0
5·0
4·0
3·0
2·0
1·0
$\psi_{t(10^\circ)}$
$\lambda_{(10^\circ)}$
$\eta_{t(10^\circ)}$
$\psi_{st(10^\circ)}$
η_t %
90
80
70
60
50
40
30
20
λ
30
10
5
0·2
0·4
0·6
0·8
1·0
1·2
1·4
Ø

Figure 5·21

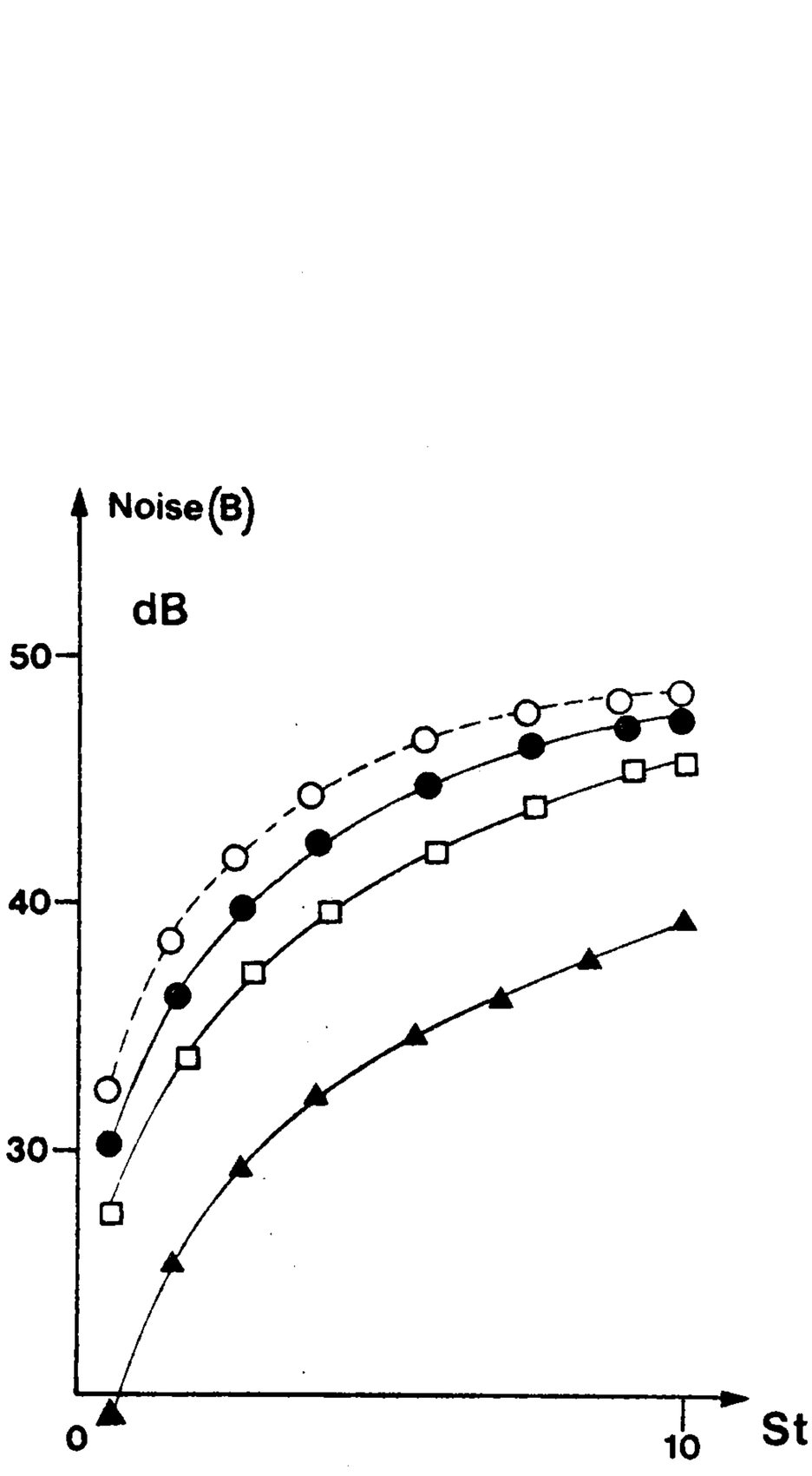

Figure 5·22(a)

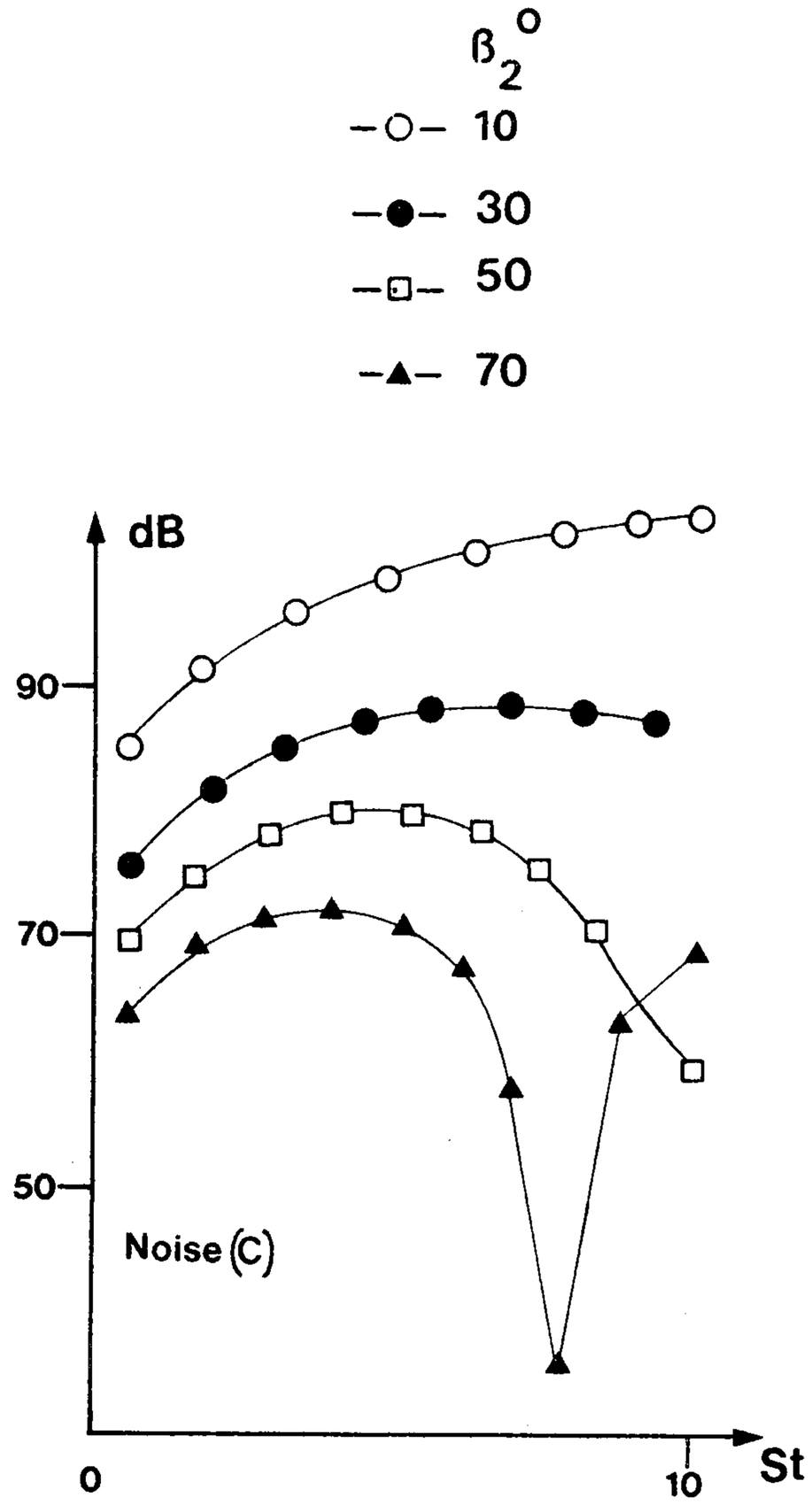

Figure 5·22(b)

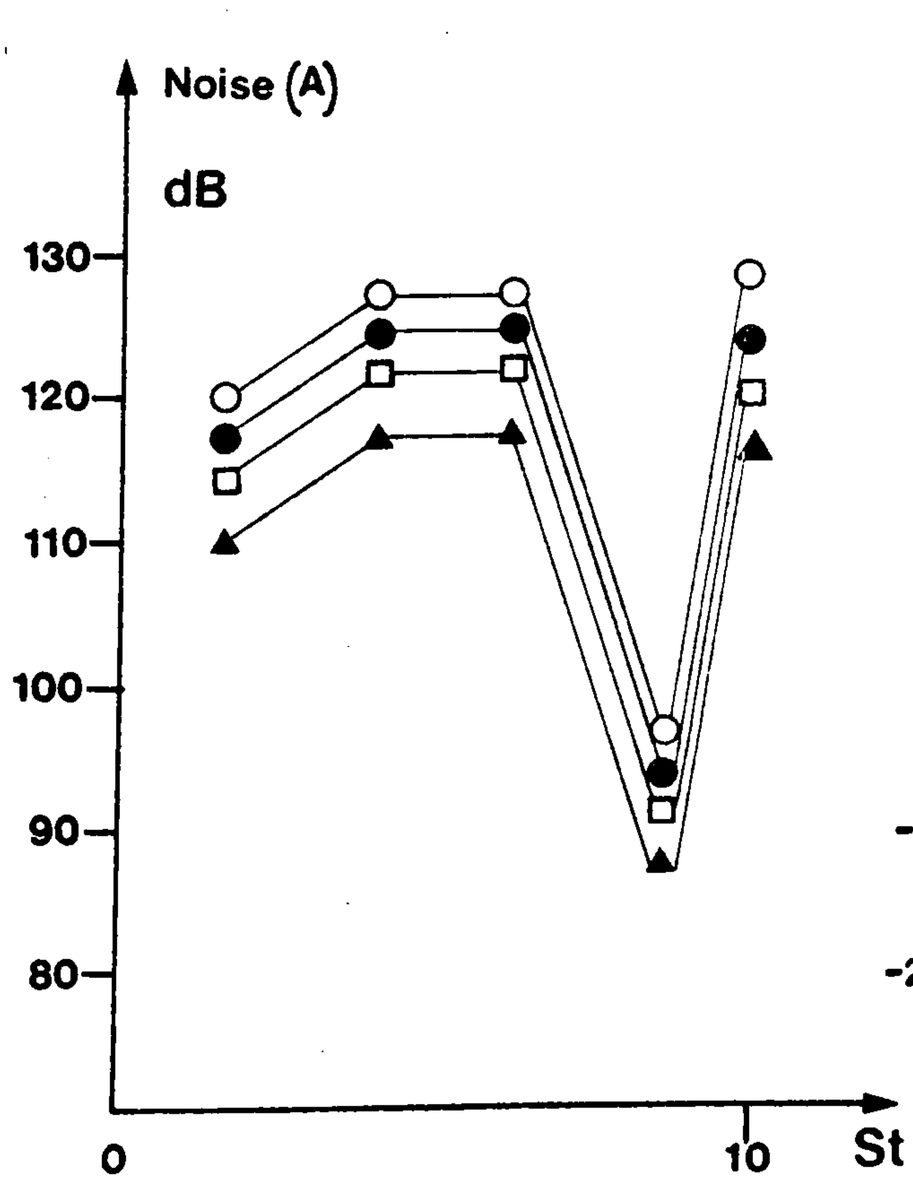

Figure 5·22(c)

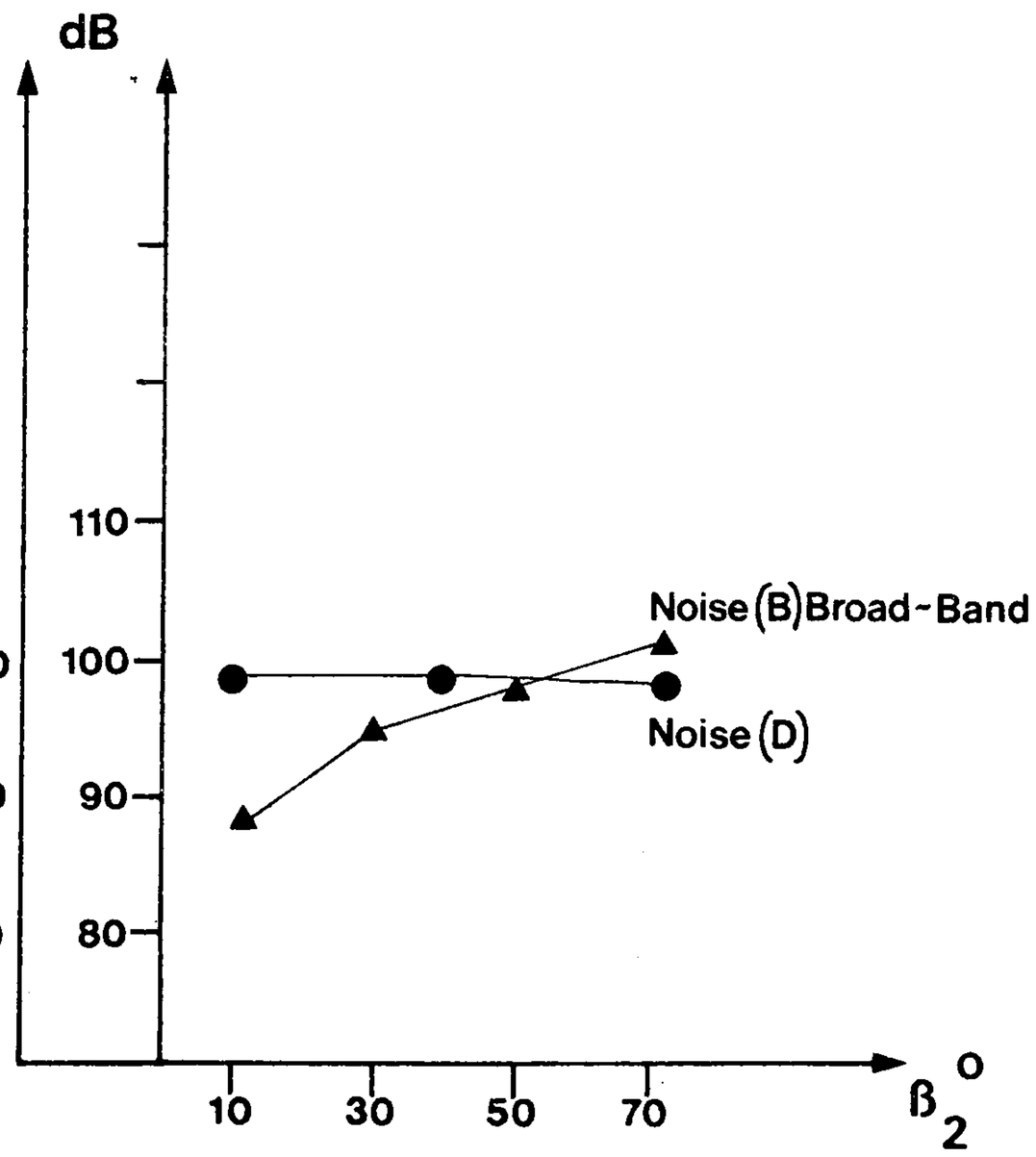

Figure 5·22(d)

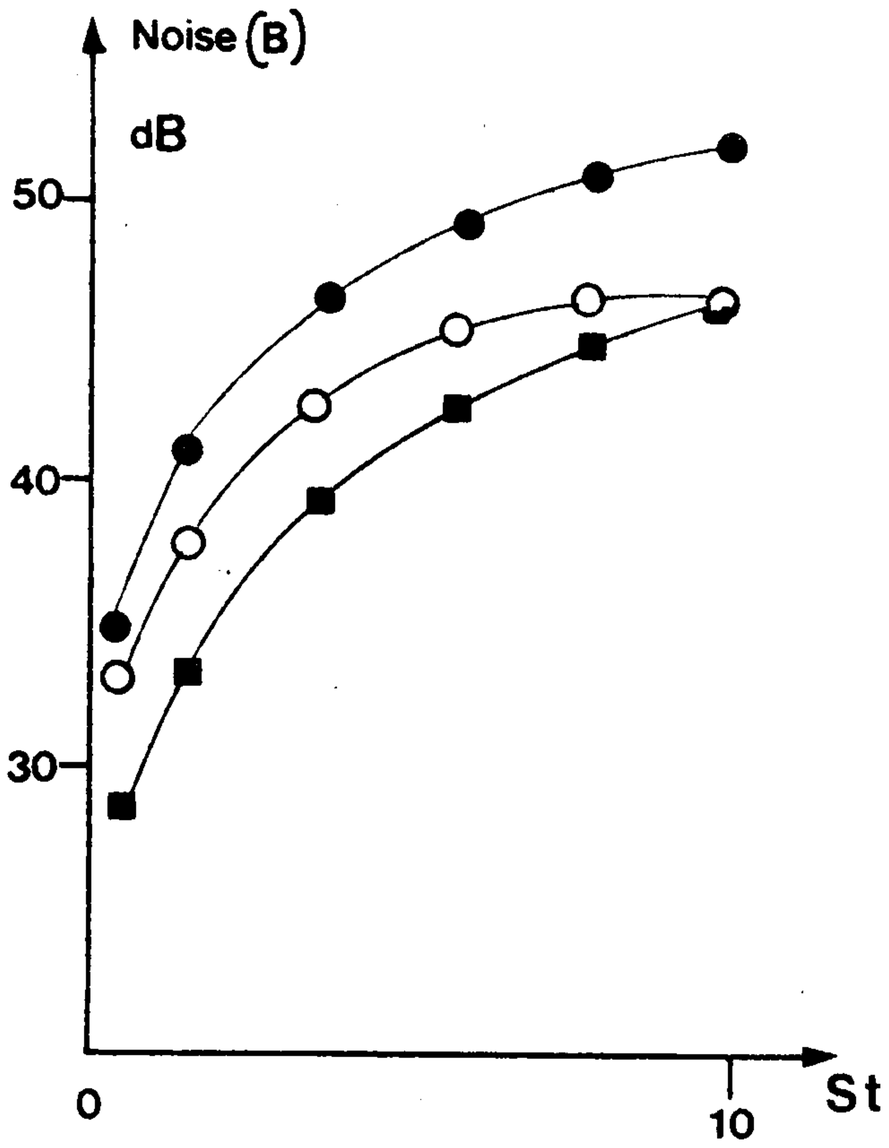

Figure 5·23 (a)

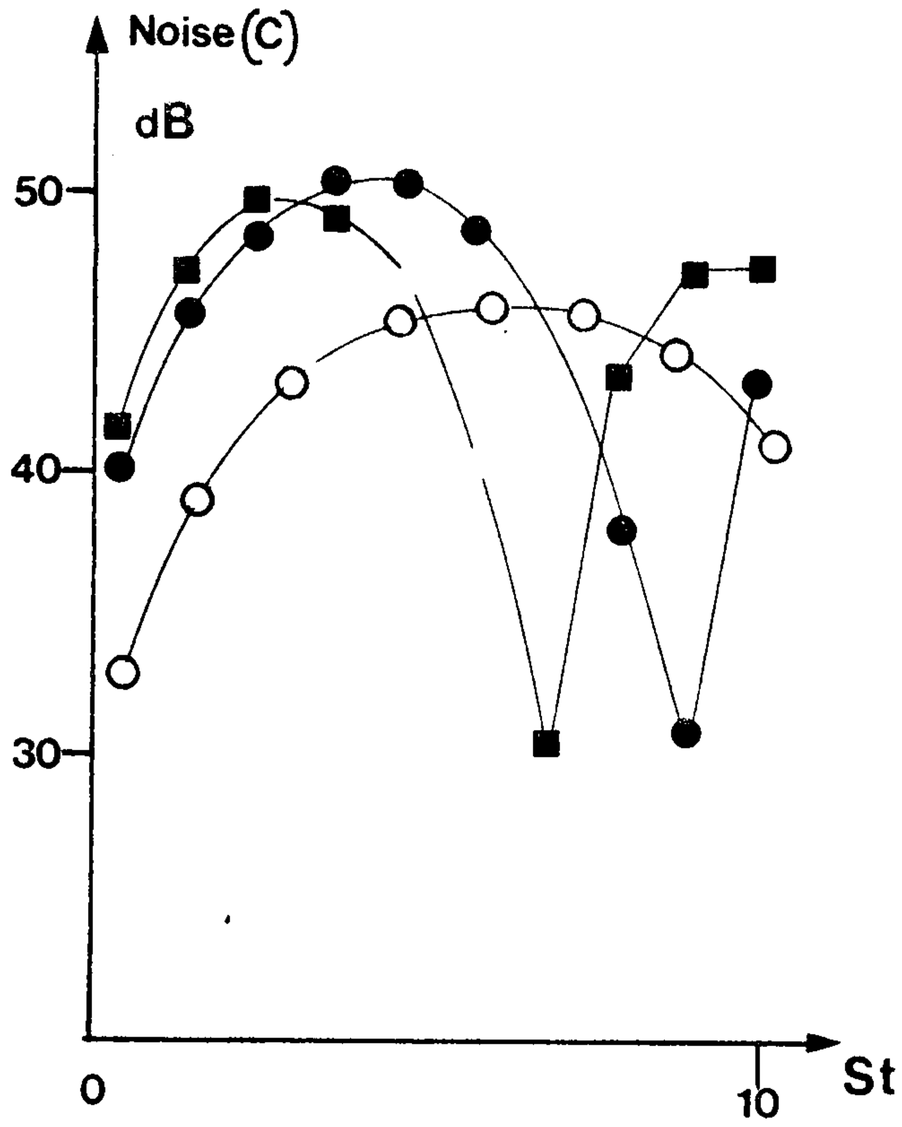

Figure 5·23 (b)

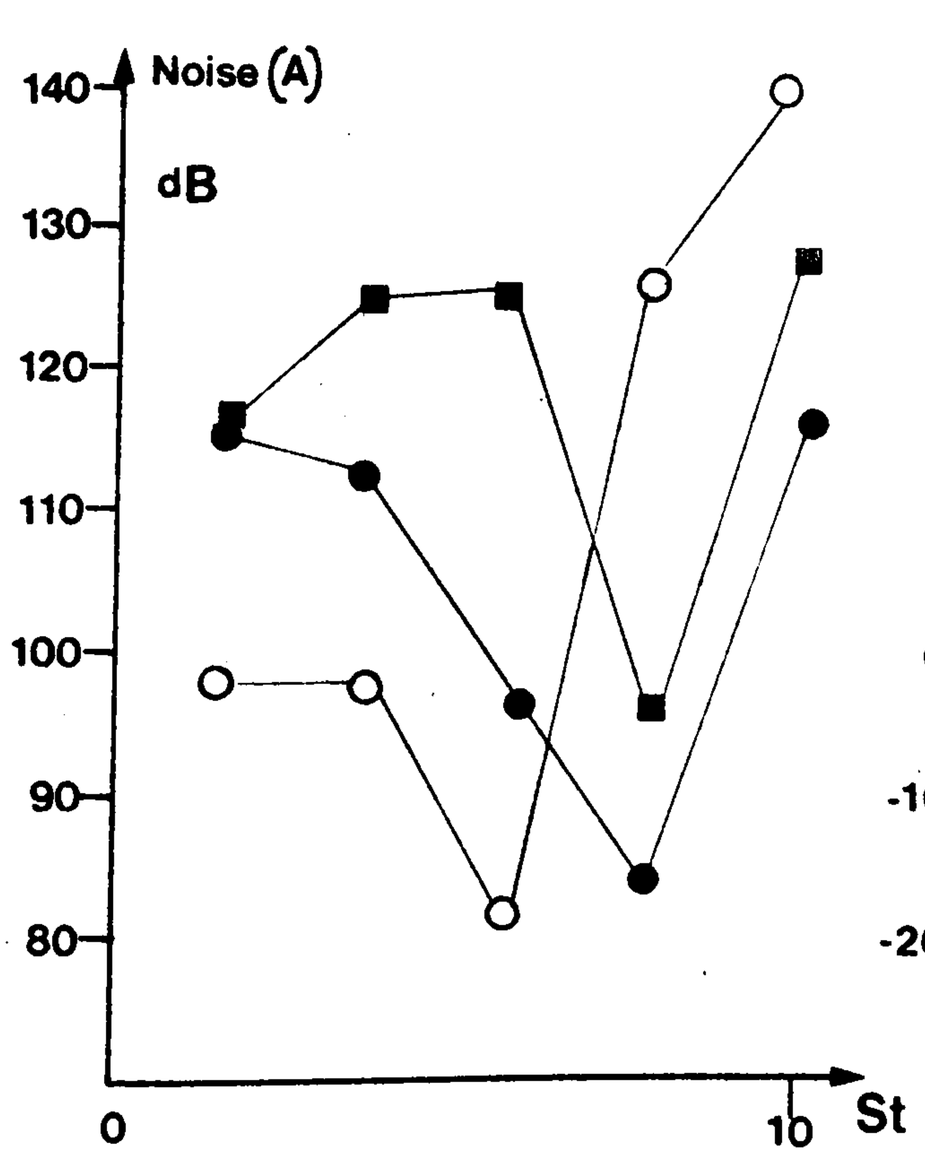

Figure 5·23 (c)

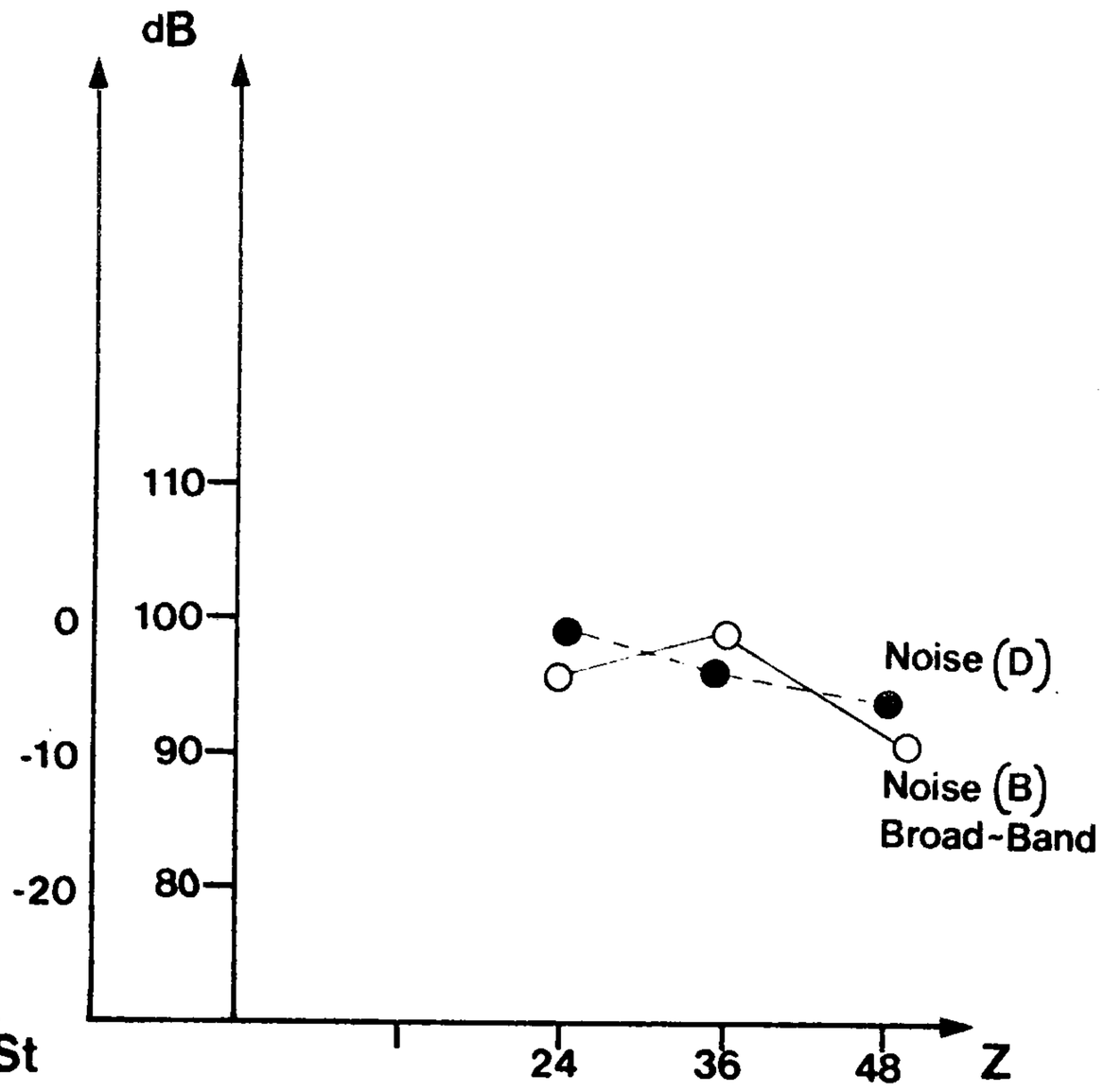

Figure 5·23 (d)

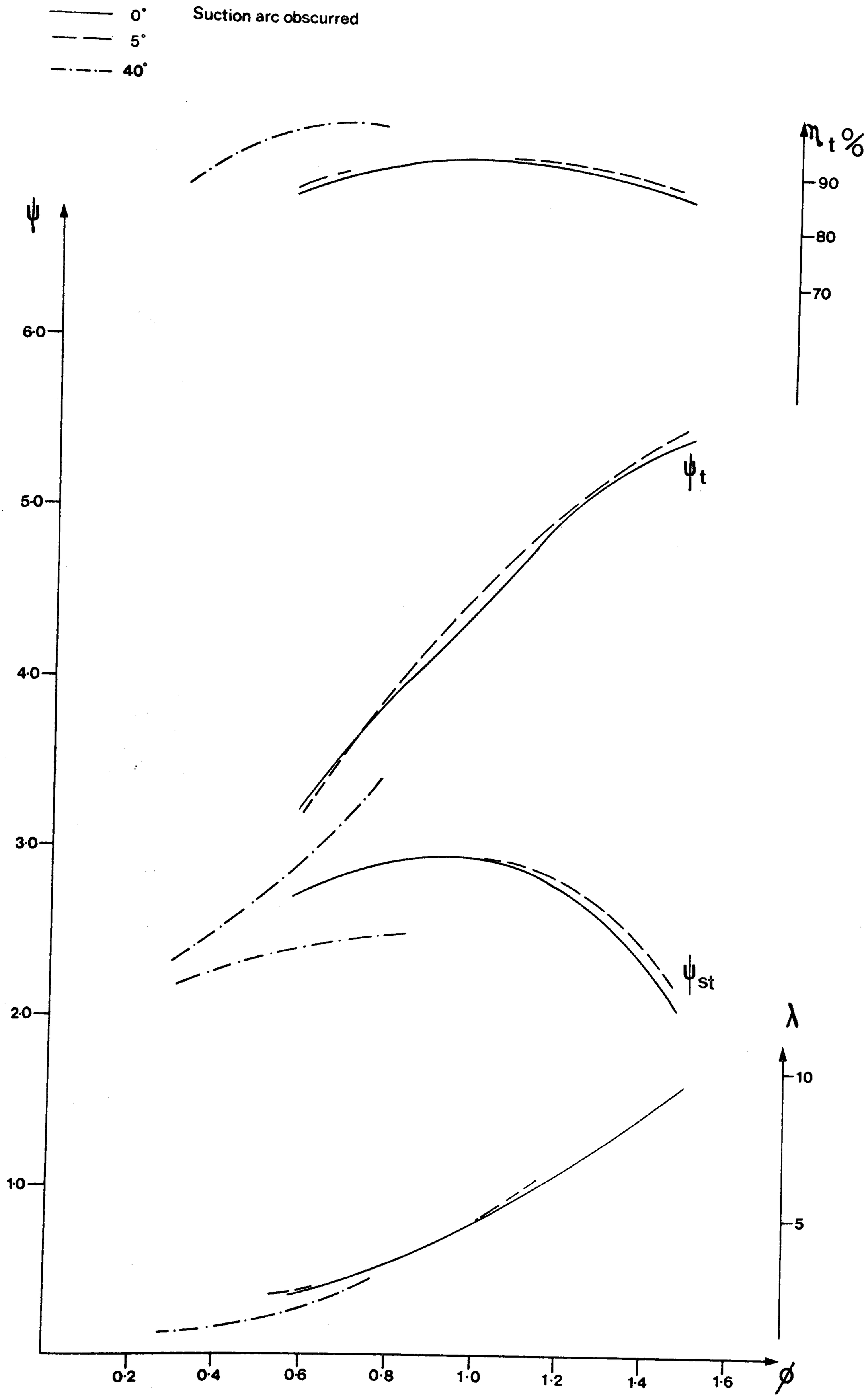
0°
5°
40°
Suction arc obscurred
ψ
6·0
5·0
4·0
3·0
2·0
1·0
ηt %
90
80
70
ψt
ψst
λ
10
5
0·2
0·4
0·6
0·8
1·0
1·2
1·4
1·6
ø

Figure 5·24

Suction Arc obscured

— ○ — 0°

— ● — 5°

— □ — 40°

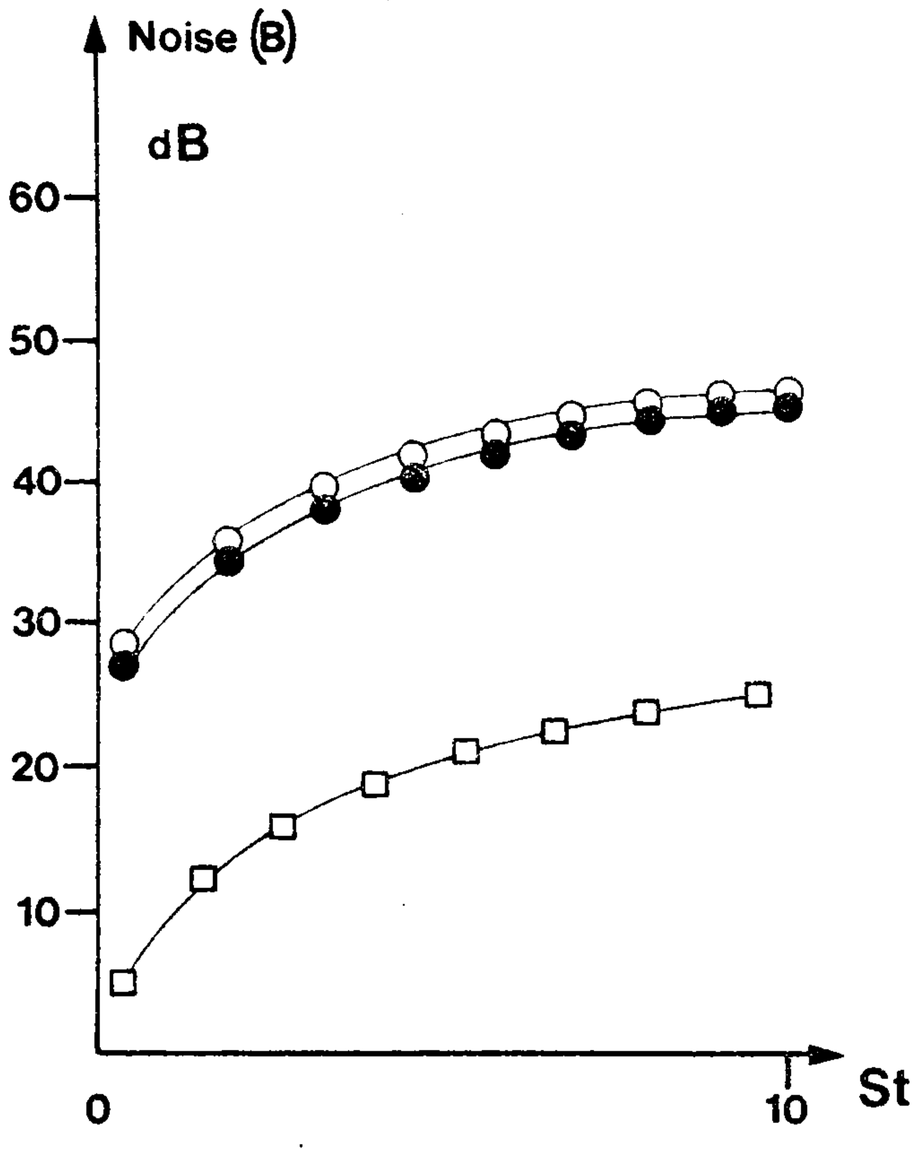

Figure 5·25(a)

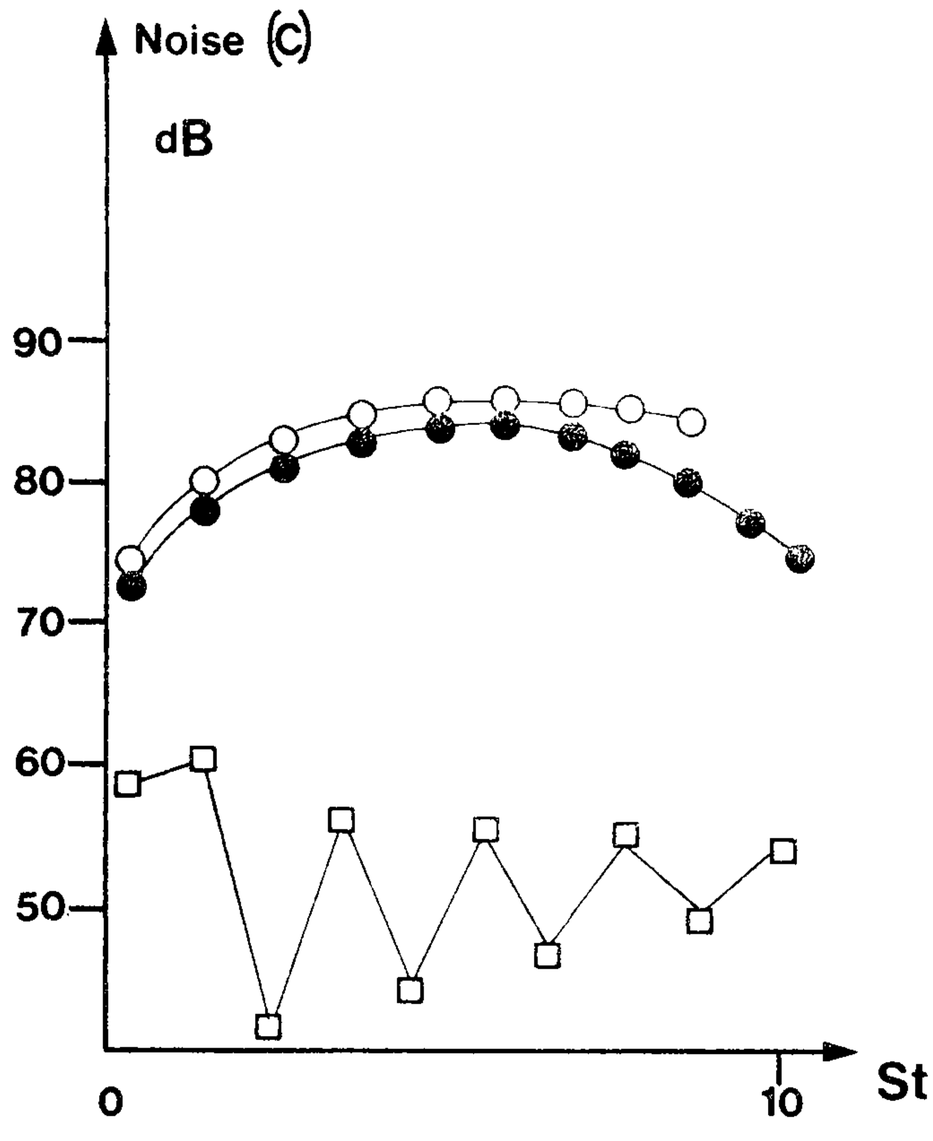

Figure 5·25 (b)

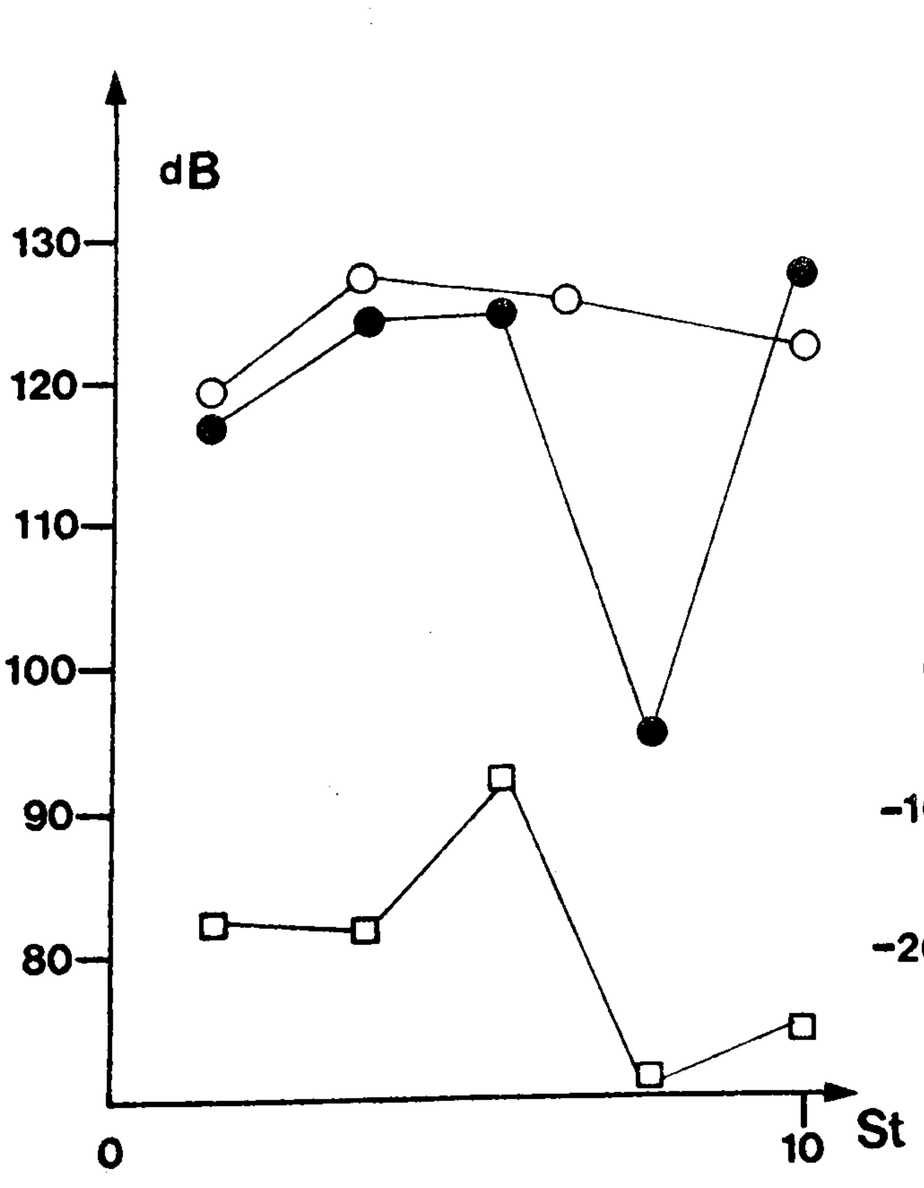

Figure 5·25 (c)

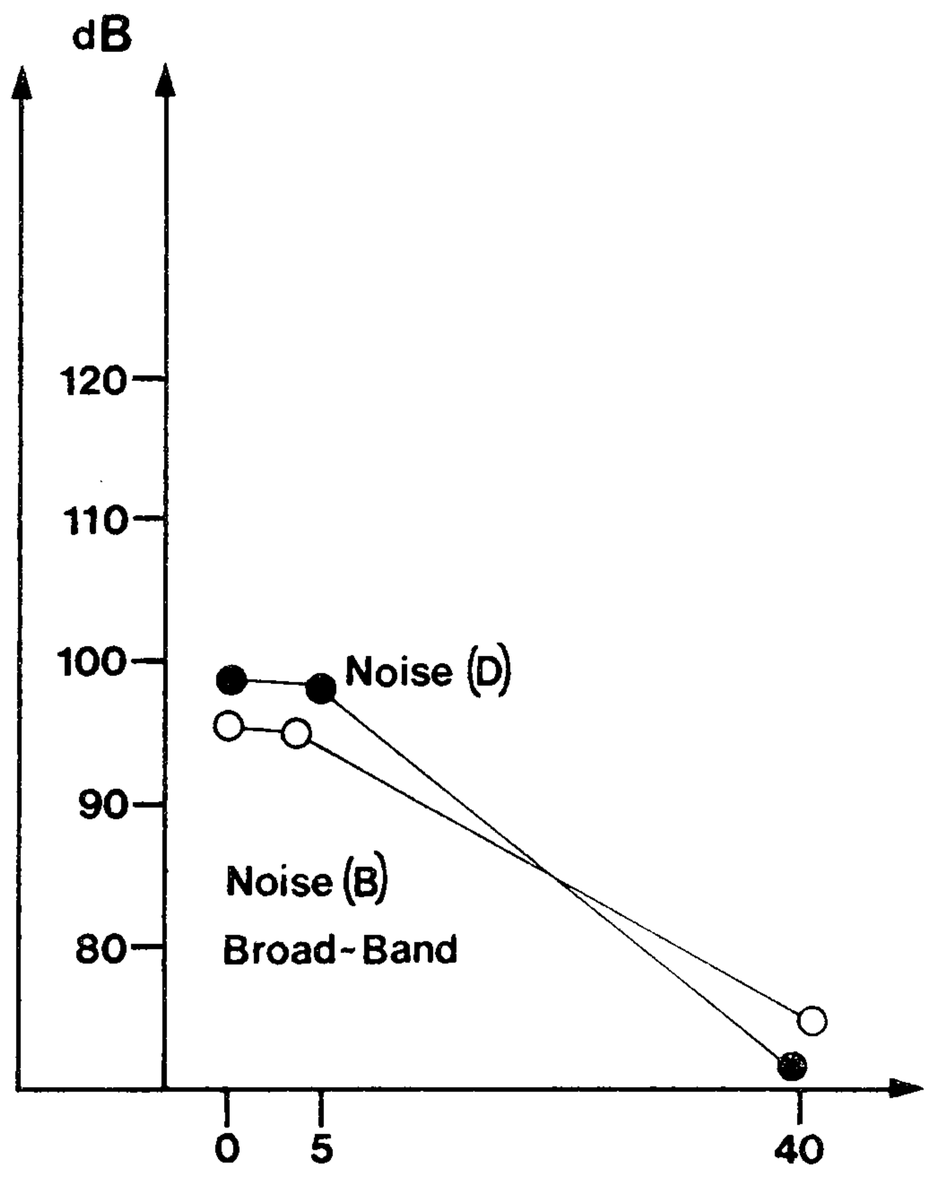

Figure 5·25 (d)

Vortex location 600mm Dia fan

μ, A

(10,20) ——————————

(0,20) — — — — — —

(10,0) —·—·—·—·—

(0,0) – – – – – – – –

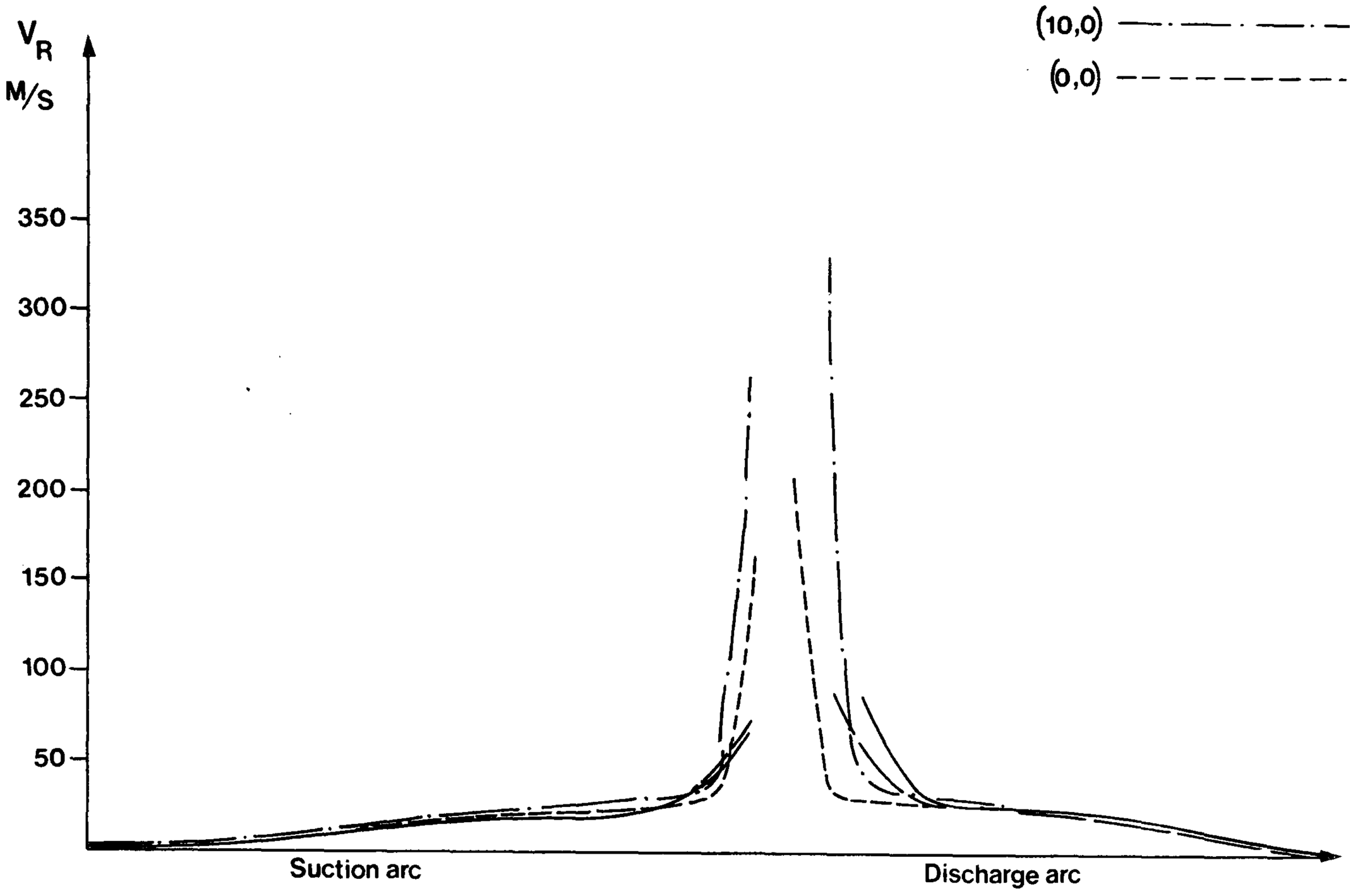

Figure 5·26

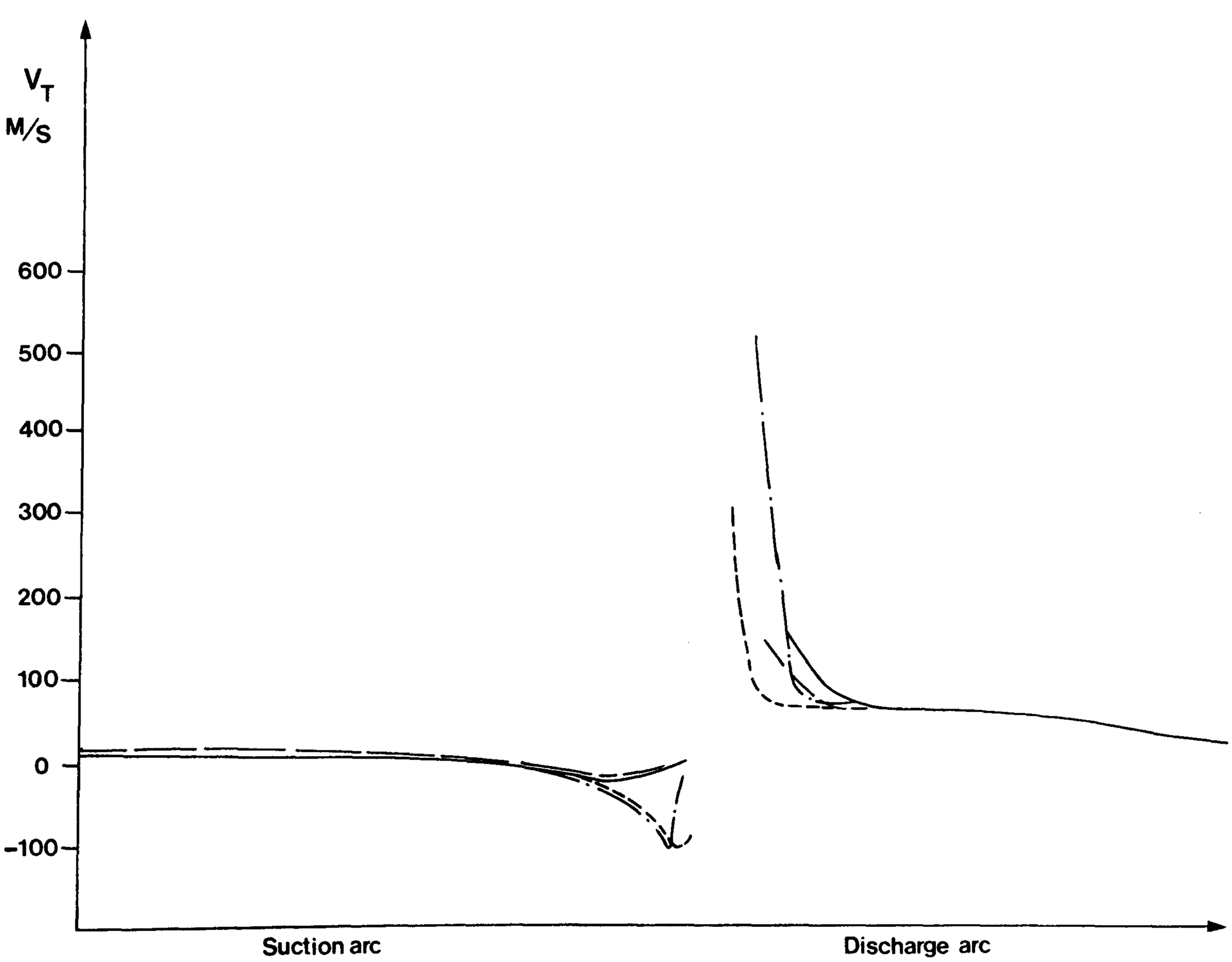

Figure 5·27

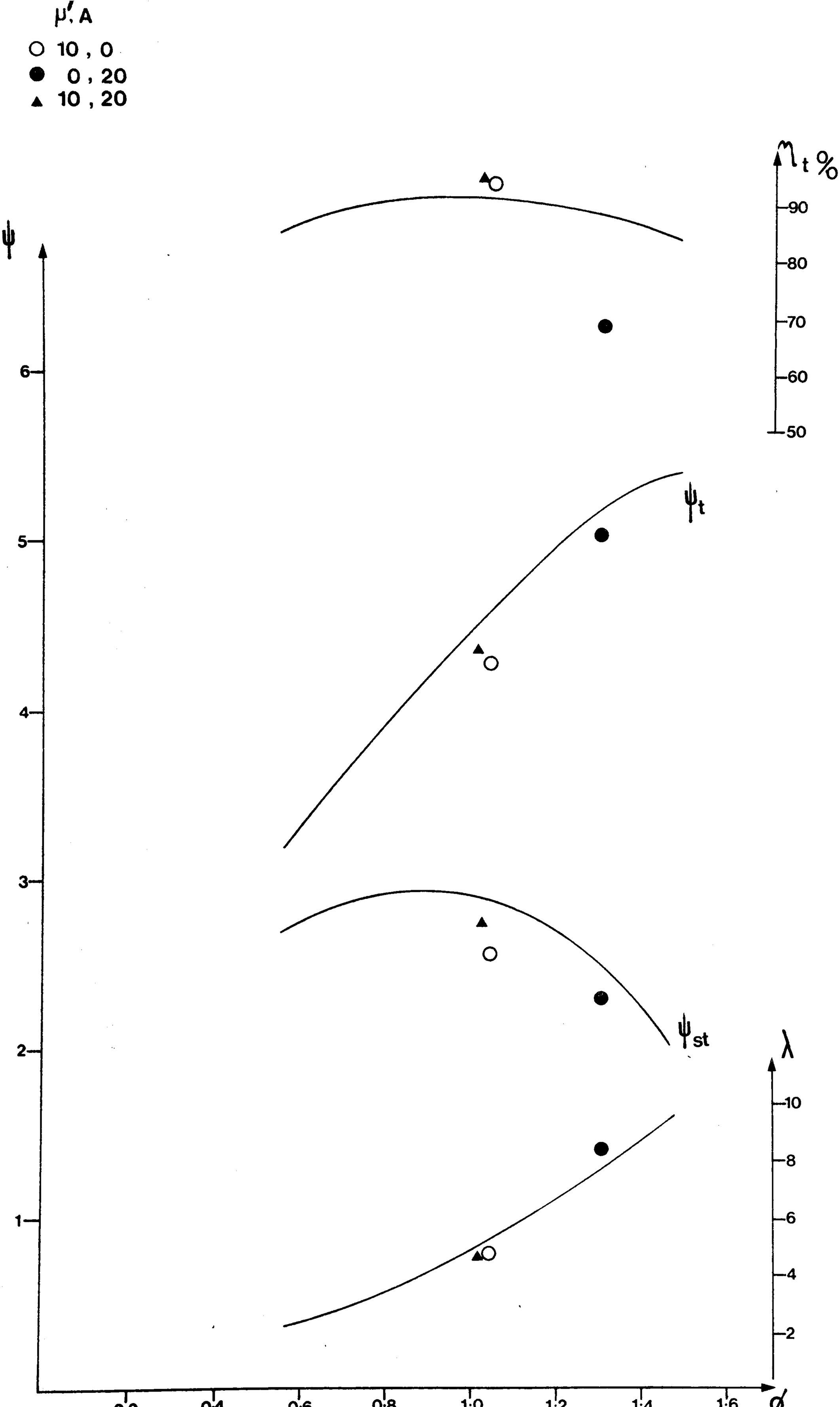
μ', A
10 , 0
0 , 20
10 , 20
ψ
6
5
4
3
2
1
ψt
ηt %
90
80
70
60
50
ψst
λ
10
8
6
4
2
0·2
0·4
0·6
0·8
1·0
1·2
1·4
1·6
ø

Figure 5·28

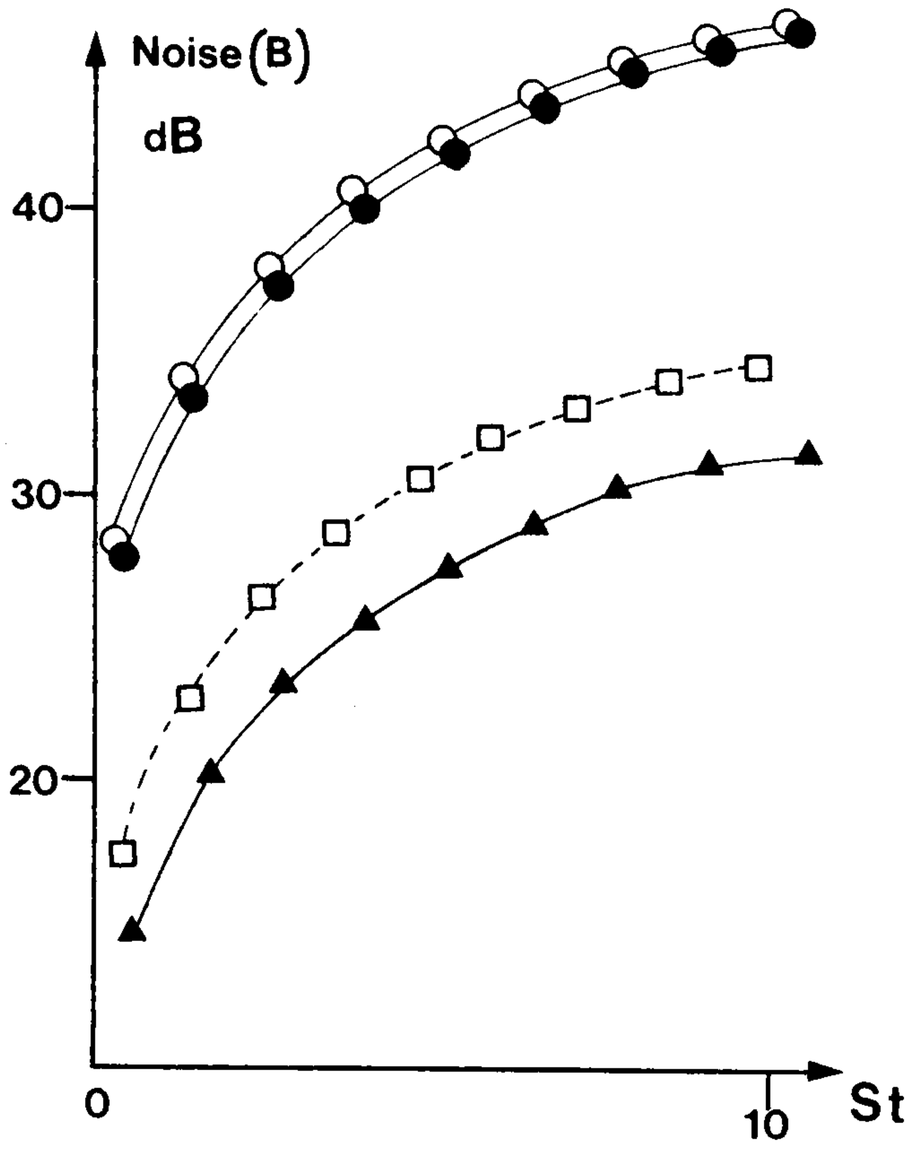

Figure 5·29(a)

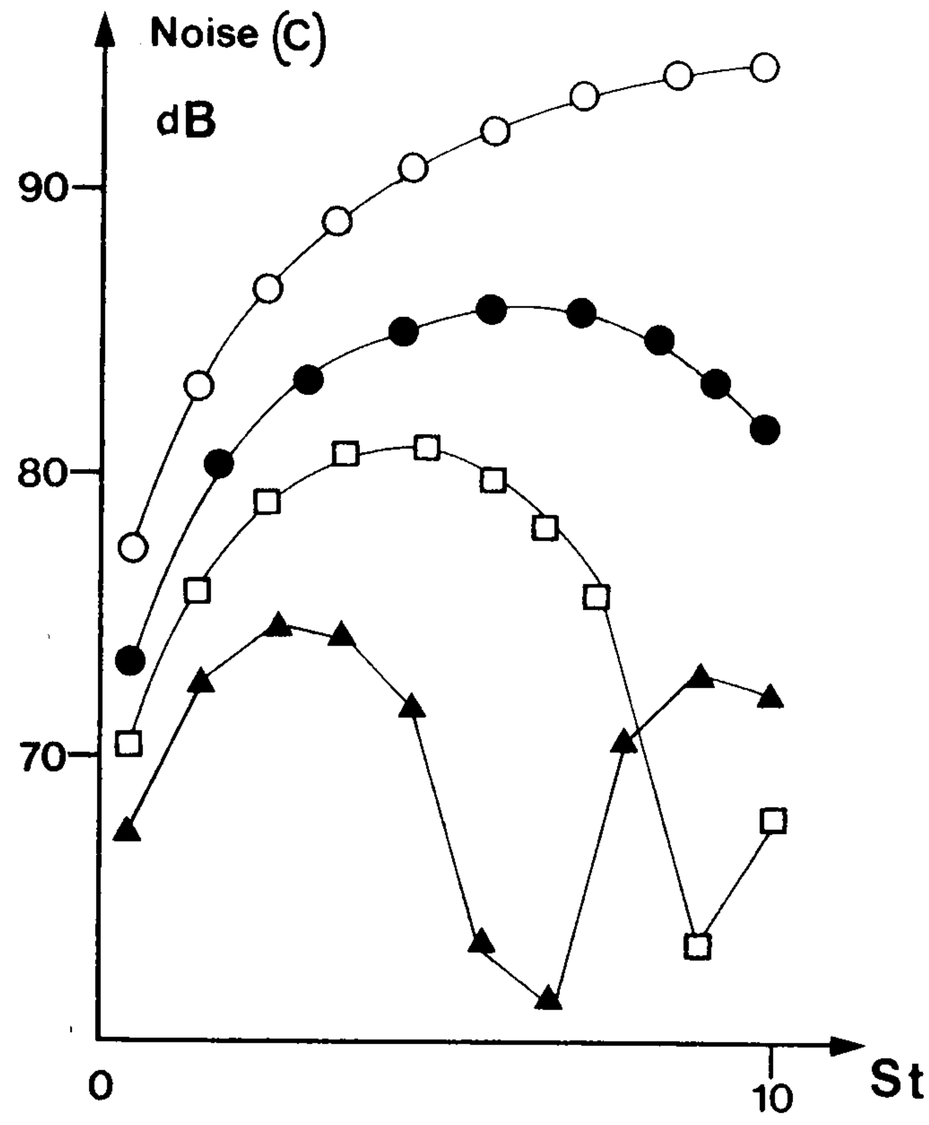

Figure 5·29(b)

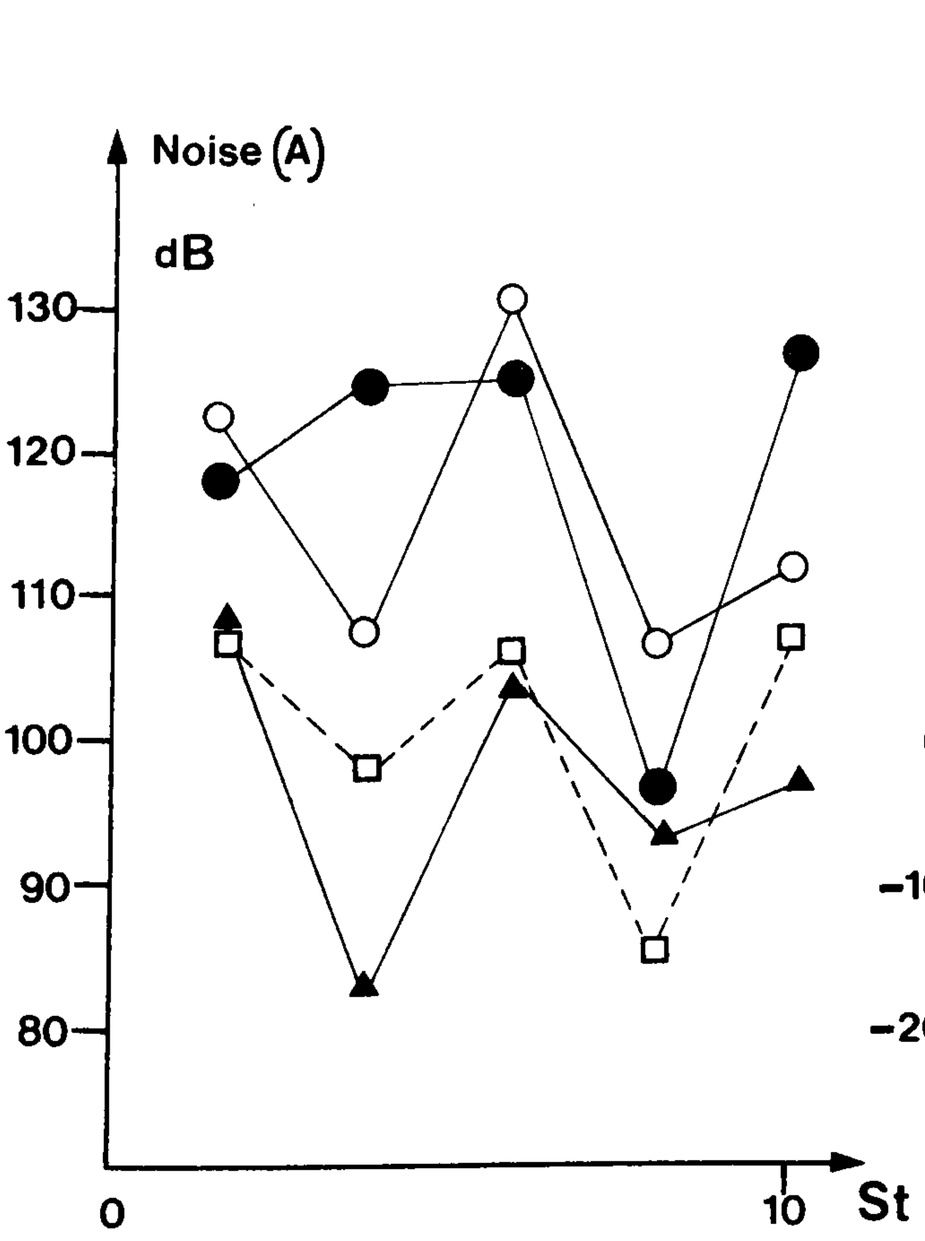

Figure 5·29 (c)

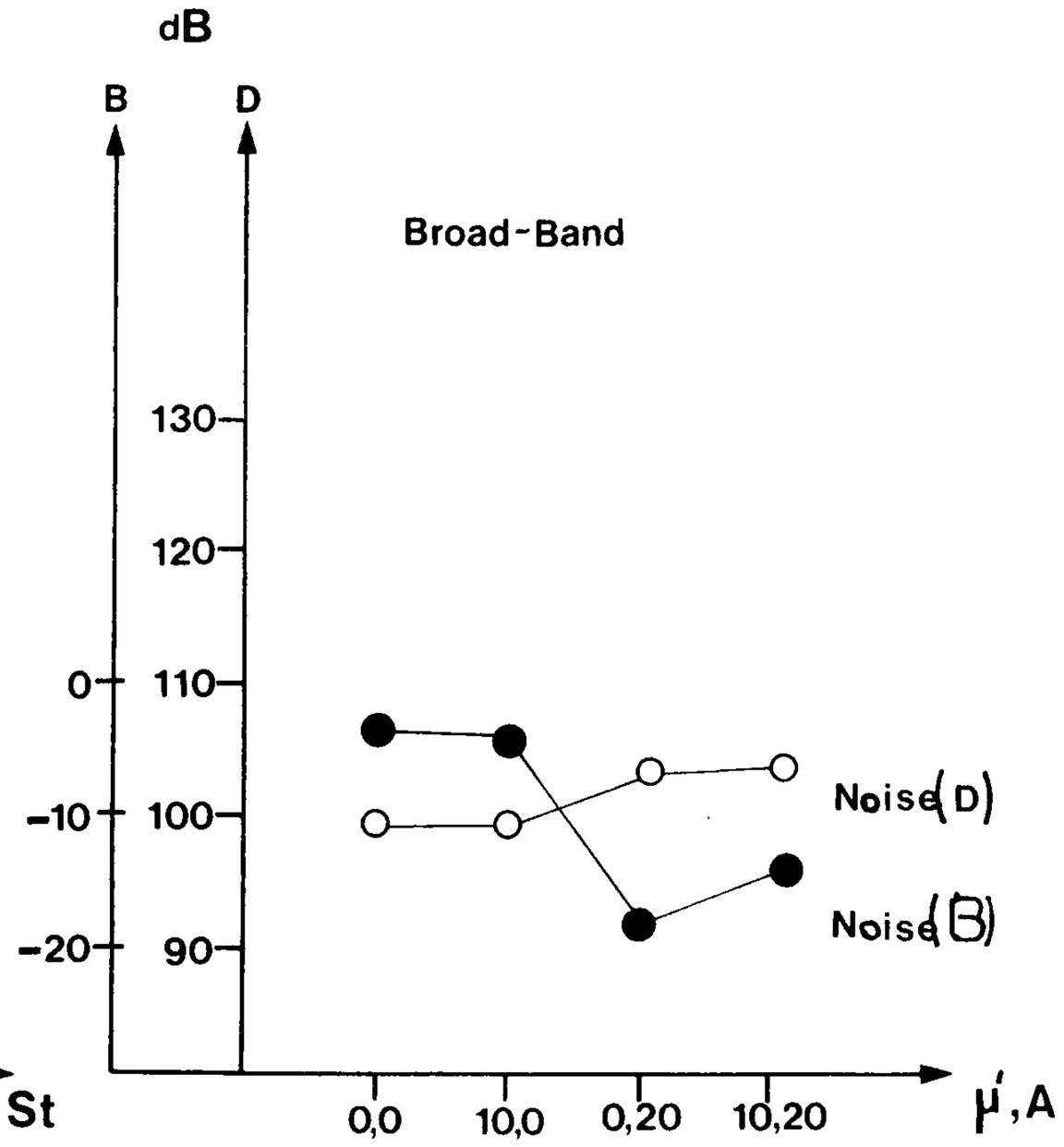

Figure 5·29 (d)

CHAPTER SIX

6.1 INTRODUCTION TO PERFORMANCE DETERMINATION.

6.1.1 ROTOR AND CASING DESIGN VARIABLES.

The design variables under experimental investigation are represented as two groups; 'primary' variables, which fundamentally determine the aerodynamic performance and 'Novel' design variables, which modify the flow conditions imposed by the primary casing. Primary design variables, for example, determine the vortex location, dictate the rear-wall shape and the lengths of the suction and discharge arcs. Novel designs include such items as flow-guides, Vortex stabilisers and modifications incorporated to suppress noise generation.

The results will demonstrate that aerodynamic performance is largely determined by a few basic geometrical parameters. Vortex wall 'shape' terms are neglected, because elaborate profiles generally do little more than relocate the vortex opposite some point on their leading face. Figure 6.1 illustrates the primary design variables and Figure 6.2 illustrates some of the design variants treated as novel. Other design variations, not dealt with experimentally, are discussed in Section 6.2.3.

6.1.2 DETERMINATION OF REAR WALL SHAPE.

For each variation in the primary design, see Figure 6.1, a new rear wall was constructed; the shape of each wall being determined using the 'constant mean velocity' principle. The walls themselves were of laminated construction, Section 2.2.2.2.

Conventionally, the best rear wall shape is considered to be a log-spiral - a casing design borrowed from centrifugal fan technology. Other walls frequently used are circular arcs, 'volute' types and sundry wall shapes governed more by the adaptability of the equipment than any aerodynamic criteria. The rear wall design procedure adopted by the author is an analytical method, details are given in Section 3.3.5. This procedure designs rear-walls with a 'flatter' profile than the conventional log spiral design, similar in shape to the ECK-Type rear walls.

A poorly designed rear wall will inhibit diffusion and lead to increased flow turbulence, the performance may thus be severely reduced by large pressure losses. The wall design procedure used is robust, the derived wall profile varying little with flow rate, see Figure 3.12; the rear wall is designed at a theoretical flow coefficient of approximately $\phi = 0.8$. Figure 6.3 demonstrates the order of improved performance using the computer-aided design procedure.

6.1.3 SCALING

The following aerodynamic results are expressed in non-dimensional form, implying that one set of performance curves may represent a homologous series of fans. BUSH (13) determined that cross-flow fans obey conventional fan laws, and that scaling must be valid within certain limits: he also notes however, the existence of three-dimensional effects. It is generally assumed that cross-flow fans are scaleable; but with vortex breakdown in Slim rotors and secondary effects in Short rotors (ILBERG AND SADEH (40)), there are limiting slenderness (L/D) ratios. The effect of Reynolds number on

cross-flow fan performance has been researched by HAINES and HOLGATE (34); their results indicate that cross-flow fans satisfy the accepted similarity relationships.

It is usually not possible to determine performance much below ϕ = 0.2; the immense pressure fluctuations in this zone make measurement difficult and the experimentation becomes inaccurate.

6.2 EFFECT OF ROTOR AND CASING DESIGN ON THE AERODYNAMIC PERFORMANCE

The following experimental results are expressed in non-dimensional form, where:

pressure coefficient $\psi = \frac{p}{\frac{1}{2}\rho U^2}$

flow coefficient $\phi = \frac{Q}{LDU}$

The modifications discussed are illustrated in Figures 6.1 and 6.2.

The results indicate that the maximum efficiency point generally occurs between 40% and 60% of ϕ max., and that the static pressure characteristics are almost always continuously rising.

6.2.1 INFLUENCE OF PRIMARY CASING DESIGN ON AERODYNAMIC PERFORMANCE

6.2.1.1 VORTEX WALL CLEARANCE, E.

The vortex wall clearance is defined not as the radial distance between the vortex wall tip and impeller, but as the distance between the vortex wall tip and the point on the

impeller outer periphery in the plane of the unsloped vortex wall. This is physically consistent with locating the vortex.

Although this is an important and obvious parameter, the gap is commonly increased to reduce noise, very few results have been published on the relationship between clearance and performance. PREZSLER AND LAJOS (65) discuss the effect of increasing radial E/D; their results indicate that performance is fairly consistent in the range $1\% \leq E/D \leq 4\%$, the performance decreasing quite rapidly with increasing clearance for $E/D > 4\%$. The efficiency they found to be reasonably constant for $2\% \leq E/D \leq 10\%$, falling at more extreme clearances. ECK (24), who advocated a large clearance, states that efficiency is unaffected by E; a result partially supported by IKEGAMI AND MURATA (39), who state that efficiency is independent of clearance for $E/D > 3\%$, but reducing E/D below this value enhances the efficiency.

Expanding the vortex involves an increased portion of the rotor in the rotational zone. The relationship, however, between momentum loss and the forced vortex volume is not a simple one, and depends also on the angular velocity and the shape of the recirculation zone. The angular velocity of the vortex decreases with increasing cross-sectional area and momentum loss decreases with decreasing rotational velocity. Also, a non-circular forced-vortex cross section increases the momentum loss, because a rotating element of fluid has to alter its radius during each revolution, see MOORE (51).

No consistent relationship between 'E' and efficiency is indicated in Figures 6.4 (a) - 6.4 (c). For $\phi > 0.4$ the static pressure characteristic remains fairly constant in the range $E/D \leq 4.5\%$, but increasing the clearance above this reduces the pressure characteristic. In the lower flow zone (approx. $\phi < 0.4$) the static pressure increases with decreasing clearance.

All the characteristics are stable (non-drooping), so that the maximum static pressure occurs at the minimum measured flowrate.

6.2.1.2 REAR WALL CIRCUMFERENTIAL ANGLE, δ

This value is important because it defines the extent of the suction and discharge arcs, for a fixed vortex wall location.

There is a zone of random, low-energy flow close to the rear-wall edge, due to the impossibly rapid changes in direction demanded by an abrupt suction arc/discharge arc division. The ratio $\lambda s/\lambda d$ is often considered important, but it is too simplistic a term. Defining the suction arc length independently of its position in relation to the vortex core, is to ignore a fundamental property of the cross-flow fan; the uneven velocity distribution governed by an eccentrically located vortex. Because of this the majority of inflow and energy transfer takes place over an arc close to the vortex wall. The spatial distribution of velocities over an arc is of considerably more importance to performance than the circumferential length of that arc.

PORTER (62) finds a reduction in performance with increasing δ ; Figure 6.5 illustrates his result. The corresponding efficiencies are not shown here, but were found to be independent of the rear wall angle.

Figure 6.6 indicates an optimum δ value of 20^{o}, this is consistent with results reported by HAINES & HOLGATE (34). Apart from this optimum value the trend is a gradually reduced pressure performance with increasing rear-wall angle. No obvious trend exists between δ and aerodynamic efficiency.

6.2.1.3 DUCT HEIGHT, H

Duct height is a design criterion governed by the dimensions of the ventilation ductwork. Previously the term has been dealt with indirectly by varying the depth of the rear wall; for example, volute-type walls and DATWYLER designs have a broad cross-section and therefore a greater duct height.

PORTER AND MARKLAND (63) suggest that rear wall design has a profound effect on performance. Although the rear-wall breadth may well be influential in determining the location of the vortex, the rear wall is essentially a flow channeller and not involved in the transfer of energy. Thus, for correctly designed rear-wall profiles the performance should not vary greatly with H.

The results, Figure 6.7 , depict an optimum H/D of about 80%, although the performance remains fairly constant in the range $70\% \leqslant H/D \leqslant 85\%$. Decreasing the duct height below this range causes a severe reduction in performance; increasing the duct height causes a reduction in the maximum flow-rate possible. An optimum efficiency with an H/D in the order of 80% is indicated.

6.2.1.4 VORTEX WALL DECLINEATION, B

This value proves to be the most important single parameter in cross-flow fan casing design. Its importance stems from the increased suction-arc velocities formed by lengthening the inlet arc over a spatially important sector - this has been discussed in Chapter 5.

Previously, little reference has been made to the importance of the vertical location of the vortex; generally B has been altered indirectly by using profiled vortex walls. An example of this is the 'best' baffle shape determined by PRESZLER AND LAJOS (65). In this case, as with other profiled wall shapes, optimum performance is achieved using the vortex wall which gives the largest effective 'B' and obscures the least suction arc. Other researchers have tended to treat the independent terms of B and E as a single value, represented by an angle. MURATA AND NISHIHARA (57) use this definition, but do not account for variations in duct height. Their results, however, (Figure 6. 8) illustrate the strong dependence of performance on vortex wall vertical location. They correctly conclude that vortex wall location is a main geometrical parameter. Figures 6. 9(a) and 6. 9 (b) clearly illustrate the improved performance possible by increasing the vortex wall declineation in the range $0.0\% \leq B/D \leq 28.2\%$. In general the efficiencies also improve with increasing B.

These results are broadly supported by those of Figure 6. 9 (c); which also demonstrates how important aerodynamic trends may be smothered by low performance, when rear walls of arbitrary shape are used.

6.2.1.5 DIAMETER RATIO, d/D

PORTER AND MARKLAND (63) suggest a lower limiting ratio of 70% and an upper limit of 85%. They state that satisfactory operation occurs between these boundaries, so that the influence of diameter ratio must be small. PORTER (62), used two experimental rotors and postulated that an increased diameter ratio would 'provide a greater space for the vortex to develop', improving the performance. His results contradicted this postulate however, and a decreased diameter ratio was found to improve performance for $\phi > 0.4$.

Figure 6.10 indicates a strong dependence of performance on diameter ratio. In particular that performance increases, within limits, with decreasing diameter ratio (or increasing chord/diameter ratio). Performance is acceptable in the range: $70\% \leq d/D \leq 80\%$ but optimal in the range: $72\% \leq d/D \leq 76\%$.

With the experimental rotor used by the author, decreasing the diameter ratio also increased the slenderness ratio (L/D). The reduction in performance with a d/D of 68% could be attributed to two causes; either axial vortex breakdown or increased flow curvature resulting in increased flow turbulence. Because of the suddenness of the onset of reduced performance, and the improved stability with increased diameter ratios, vortex breakdown is considered to be the most likely cause of the reduced pressure characteristic. The author attempted to detect a transverse non-uniformity using a smoke generator, but the flow-field could not be visualised clearly enough for any conclusions to be drawn.

The results further imply that increasing the blade chord/ diameter ratio increases the power input, under fixed design

6.2.1.6 REAR WALL CLEARANCE, E_2

It is important to adopt the rear wall clearance which will result in minimum pressure loss. With an ideal fluid the rear wall gap should be no more than a running clearance. But in the turbulent zone around the rear wall edge eddies may form which travel in the direction of flow and may considerably disrupt conditions within the volute, leading to a reduction in performance.

Figure 6.11 illustrates that there is usually a broad range of clearances where the pressure loss is tolerable, and that too narrow clearances are less desirable than too wide clearances. MURATA AND NISHIHARA (57) state that no change in performance is experienced in the range $2\% \leq E_2/D \leq 10\%$, and that the optimum value is a function of the external diameter. The author has also observed that the optimum rear wall clearance is a function of B, δ and H.

Because the rear wall clearance exhibits a complex, functional dependence on many other rotor and casing design parameters, it is recommended that the optimum value be determined for each fan-type tested. It should generally be in the range: $5\% \leq E2/D \leq 15\%$.

6.2.2 INFLUENCE OF NOVEL CASING DESIGN ON AERODYNAMIC PERFORMANCE

6.2.2.1 TONGUE THICKNESS, T

Only plane and flat vortex walls are considered. Previous researchers have tested this variable, but have portrayed the variation as a change in the shape of the

baffle. It may be significant if:

a) It reduces the effectiveness of the natural 'pneumatic' seal.

b) It affects the vortex location.

c) It is thick enough to obscure a significant portion of the suction arc.

The results depicted in Figure 6.12 demonstrate that the vortex wall thickness does not greatly affect performance in the range: $0.8\% \leq T/D \leq 4\%$. Increasing the thickness beyond this upper limit will decrease the performance, for all ϕ. Reducing the thickness below this range will not enhance performance but may necessitate strengthening of the tongue. The efficiencies appear approximately constant within the recommended range of tongue thicknesses.

6.2.2.2 IRREGULAR BLADE SPACING AND SLOTTED ENDPLATES

These contrived conditions represent extreme cases of manufacturing imperfection. The results, Figures 6.13, 6.14 show that poor manufacture can significantly affect the performance. This is especially so with unsealed endplates and a random, radially-irregular spacing of the blades. Efficiencies are similarly affected.

6.2.2.3 INCORRECT REAR WALL DESIGN

The principal relationships between rear wall design and performance are discussed in Sections 6.1.2 and 6.2.1.6.

6.2.2.4 SLOPING THE VORTEX WALL

This design modification is frequently proposed as a noise reduction technique. IKEGAMI AND MURATA (39) found that sloping the vortex wall longitudinally, up to 10^{o}, reduced the maximum total pressure only slightly.

The results in Figure 6.15 show that performance is unaffected by longitudinally sloping the wall at 0.9^{o}. Employing a vortex wall which gave a variable tongue clearance ($2\% \leq E/D \leq 4\%$), achieved by sloping the tongue radially, led to a significant decrease in performance and high amplitude vortex pulsations. The reduced performance is related to increased momentum loss induced by this vortex motion.

6.2.2.5 WEDGE ANGLE, α^{o}

Previous researchers have frequently incorporated wedge-shaped tongues in the casing design. MURATA AND NISHIHARA (57), for example, claimed that a wedge on the vortex wall would improve performance. Subsequent testing within the authors' department was, however, unable to prove their worth.

To be effective the wedge must function as an inlet guide vane, otherwise it acts only as a blockage to the high radial velocities which occur along the vortex wall upper surface.

Figure 6.16 shows that including a vortex wall wedge reduces the fan performance.

6.2.2.6 PERFORATED VORTEX WALL

No previous results are available for designs incorporating this modification, although a similar design has been adopted by some manufacturers with the aim of improving aerodynamic stability, and by ECK to improve diffuser effectiveness.

Figure 6.17 indicates a marginal increase in performance for $\phi \lesssim 0.6$, using a perforated wall.

6.2.2.7 OUTLET DIFFUSER

Because diffusers are included in conventional centrifugal fans, this has been one aspect of cross-flow fan design frequently studied.

With centrifugal fans the velocity profile to the diffuser can be fairly uniform, and under this condition the diffuser is most effective: increasing distortion of the velocity profile decreases the diffuser effectiveness. Cross-flow fans have a circumferentially variable, radial discharge flow distribution, and this generates a non-uniform velocity pattern in the discharge ducting. Where the flow has considerable velocity variation over a duct cross-section (high shear), there is a danger of increased flow turbulence. This is particularly true where a large regular variation of velocity occurs between opposite walls of a duct, and leads to flow separation on the low velocity wall.

Velocity contours within the discharge ducting vary greatly with changes in fan design and with variation of flowrate. PORTER (62) found that using a simple vortex wall gave a velocity profile peaked towards the lower duct wall; whereas an ECK wall gave a velocity profile peaked towards the upper duct surface. PORTER concludes that an ECK wall supplies a profile sufficiently uniform to enable performance to be enhanced by artificial diffusion (i.e. using a diffuser).

Figures 6.18a to 6.18 l represent the order of variability of the velocity profiles, and include results for fans using ECK-type walls. These latter contour plots do not enforce

PORTERS' conclusions, but indicate velocity contours as distorted as for any other design, and which peak towards the lower duct wall.

PRESZLER AND LAJOS (65) found that increasing the diffuser angle from zero gave some rise in static pressure but an overall reduction in total pressure.

Results depicted in Figure 6.19 illustrate that for $\phi < 0.6$ and a diffuser angle of less than 2.7°, the diffuser has little effect on performance. With a diffuser angle of less than 2.7° and $\phi > 0.6$ the static pressure is reduced. Increasing the diffuser angle from 2.7° to 5.6° caused a severe reduction in fan performance, at all measured flowrates.

The effectiveness of a diffuser depends upon the regularity of the discharge velocity pattern - a uniform velocity profile is required for successful diffusion. With cross-flow fans, the velocity profile is likely to be irregular in the discharge ducting close to the impeller, but a diffuser placed well downstream may increase throughflow.

6.2.2.8 ECK-TYPE VORTEX WALLS - AND A PLAIN WALL WITH AN ARCUATE DAMPER

ECK developed a profiled wall to improve the fan stability. Because he pioneered cross-flow fan research, many subsequent researchers have used walls of this type, for example LOCKLEY (47). PORTER AND MARKLAND (63) found that an ECK -wall reduced the performance compared to a simple wall, and further recommended that 'the vortex wall should cover the minimum possible arc', see Figure 6.20 .

The physical significance of these profiled walls, apart from acting as a recirculation channel, is that they lower the vortex vertical location. This increases the effective vortex wall clearance and also causes a section of the convergent arc to act as a damper over the suction arc.

The results plotted on Figures 6.21a and 6.21b illustrate the reduction in performance when using an ECK-type wall. The greatly reduced pressure characteristic (graph 'x') demonstrates the danger of obscuring a significant portion of the suction arc, close to the vortex wall.

6.2.3 MISCELLANEOUS ROTOR AND CASING DESIGN MODIFICATIONS

The following variables have not been tested experimentally by the author.

PARAMETER OR MODIFICATION	COMMENTARY
OUTER BLADE ANGLE, β_2	Because of the variable peripheral flow pattern, no obvious optimum blade angle exists. However, losses may be reduced if the relative flow angles and blade angles are matched over a portion of the suction arc where the throughflow is greatest. This gives usually: $25^\circ \leq \beta_2 \leq 35^\circ$, with higher performance at the lower blade angle.

PARAMETER OR MODIFICATION	COMMENTARY
INNER BLADE ANGLE, β_1.	The simple internal Rankine vortex model requires $\beta_1 = 90^\circ$. Whilst this is an imperfect model, there is no reason why the inner blade angle should not be approximately radial.
BLADE NUMBER, Z.	ECK suggest 36, but COESTER was most successful with 24. PORTER (62) experienced unstable flow conditions using 18 blades. $24 \leq Z \leq 36$
INTERNAL BLADES OR BODIES	The optimum location of such elaborations is a function of flowrate and basic fan design. There is little evidence to suggest that internal blades or bodies do locate or stabilise the vortex, but such additions would greatly complicate the fan manufacture and they are unlikely to find commercial acceptance.
INLET GUIDE VANES.	Again, the optimum vane settings could only be deduced by experiment and these would be a function of flowrate and basic fan design. PORTER AND MARKLAND (63) however, improved operating stability by including a single recirculation-vane towards the rear wall.

PARAMETER OR MODIFICATION	COMMENTARY
TONGUE SHAPING.	These can only vary the vortex location or act as a guide vane, usually they only obstruct the inflow. The best design is a simple, flat wall.
S-SHAPE, U-SHAPE AND L-SHAPE THROUGHFLOW.	Care must be taken to ensure the casing design is not compromised to suit the ducting - and that the suction flow field is not distorted by the proximity of casing.
SINGLE ROTOR FANS (IN SERIES).	See British patent 816,689. These are supposed to be compact and high-pressure units. Care must be taken to ensure that flow is not distorted on entry to successive rotors. There may be stability problems running a fan in series, see Section 7.2.
TWIN-ROTOR FANS (PARALLEL).	See GUNTON AND HOLGATE (32). This design has the advantage of a simplified casing. If the external inlet flow is not symmetrical about the duct C/L, there may be problems with 'windmilling'.

Generally, the simplest casing design is the best to use. Complicated modifications only decrease the commercial competitiveness of the fans, usually without improving the performance.

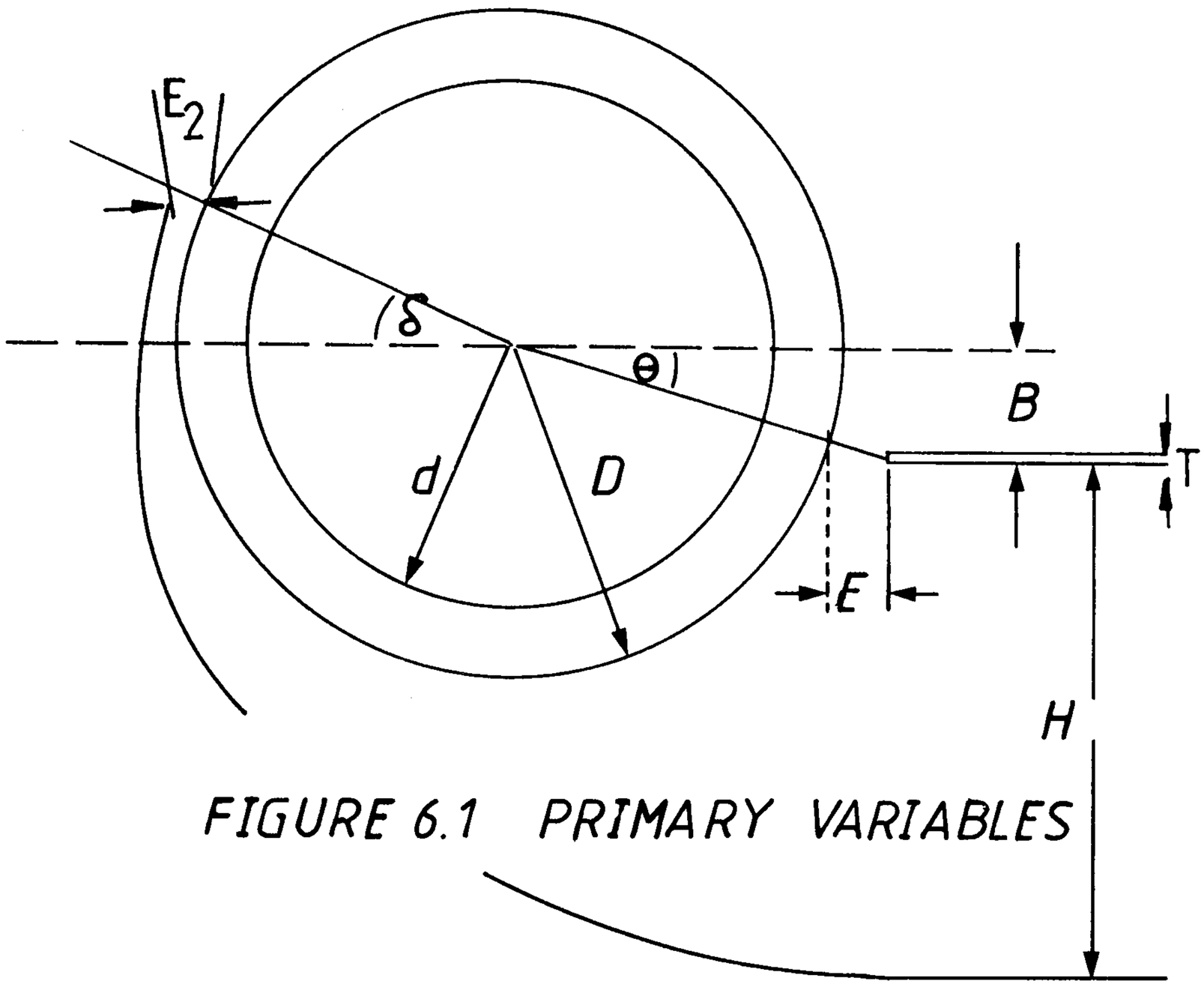

FIGURE 6.1 PRIMARY VARIABLES

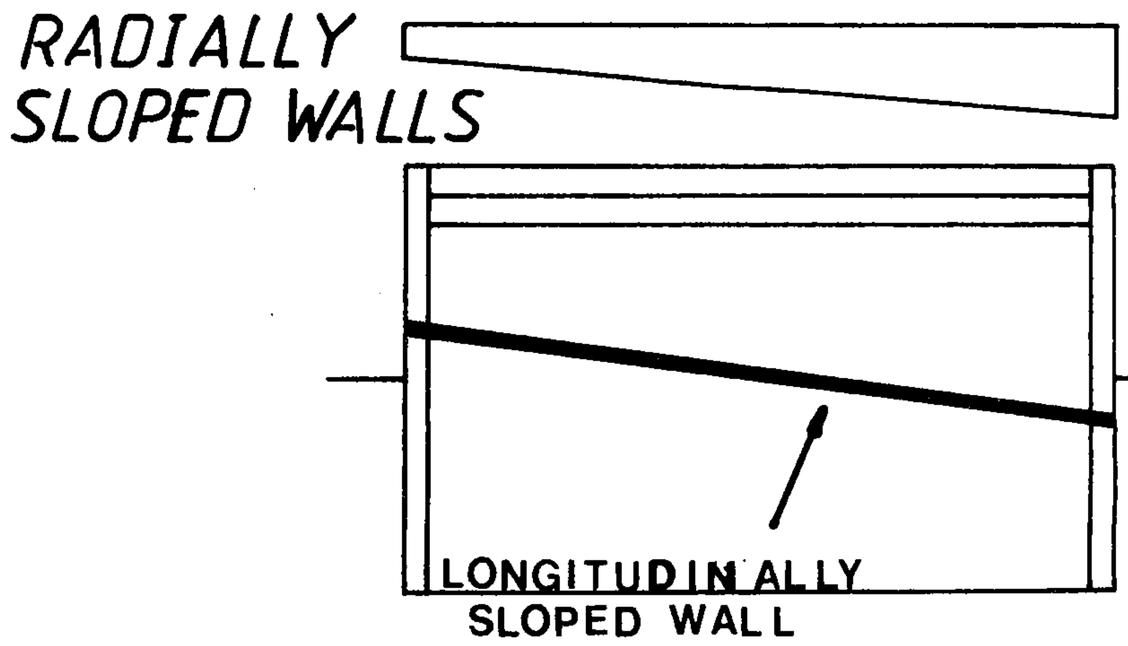

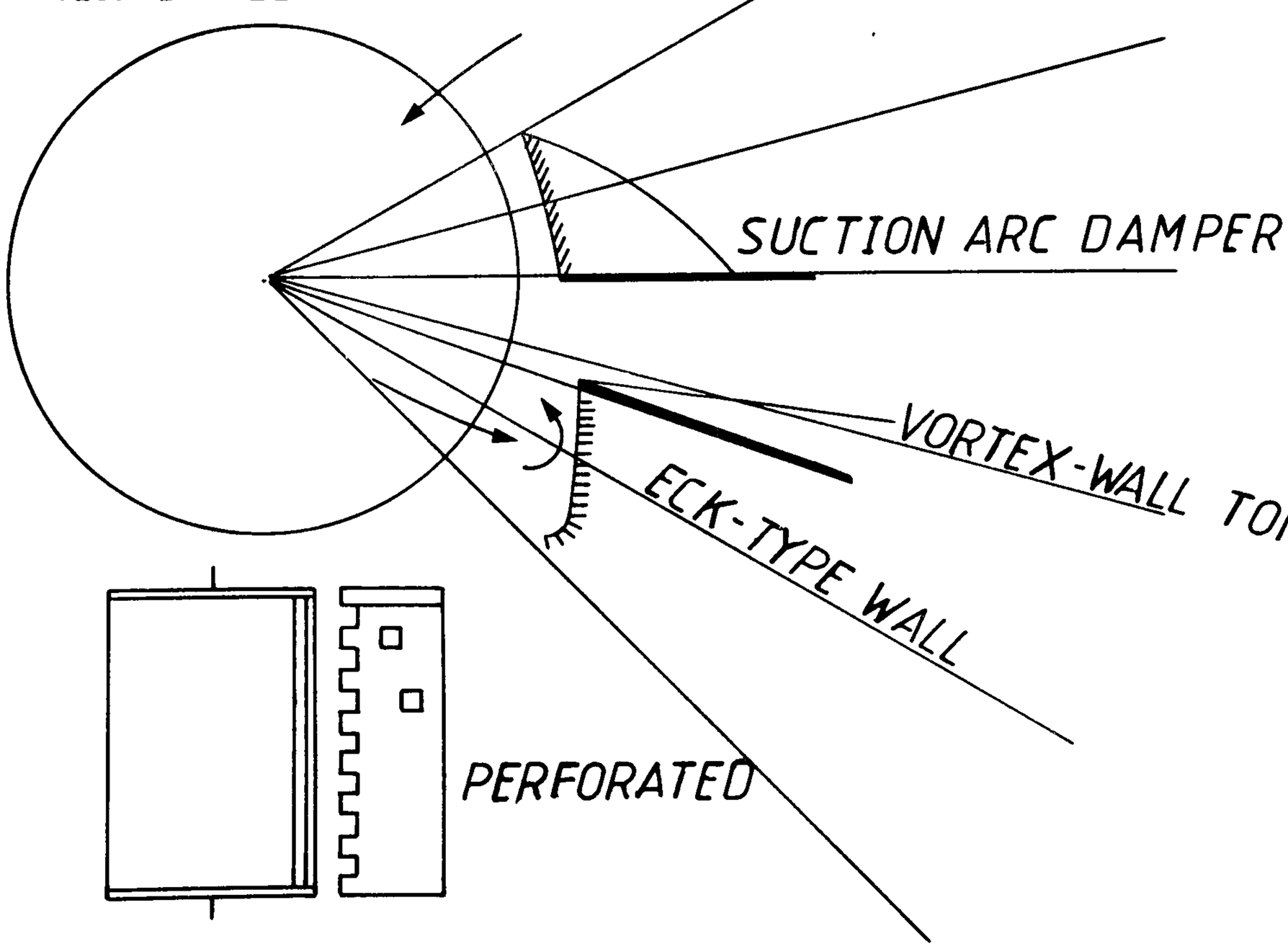

FIGURE 6.2 NOVEL DESIGN VARIABLES

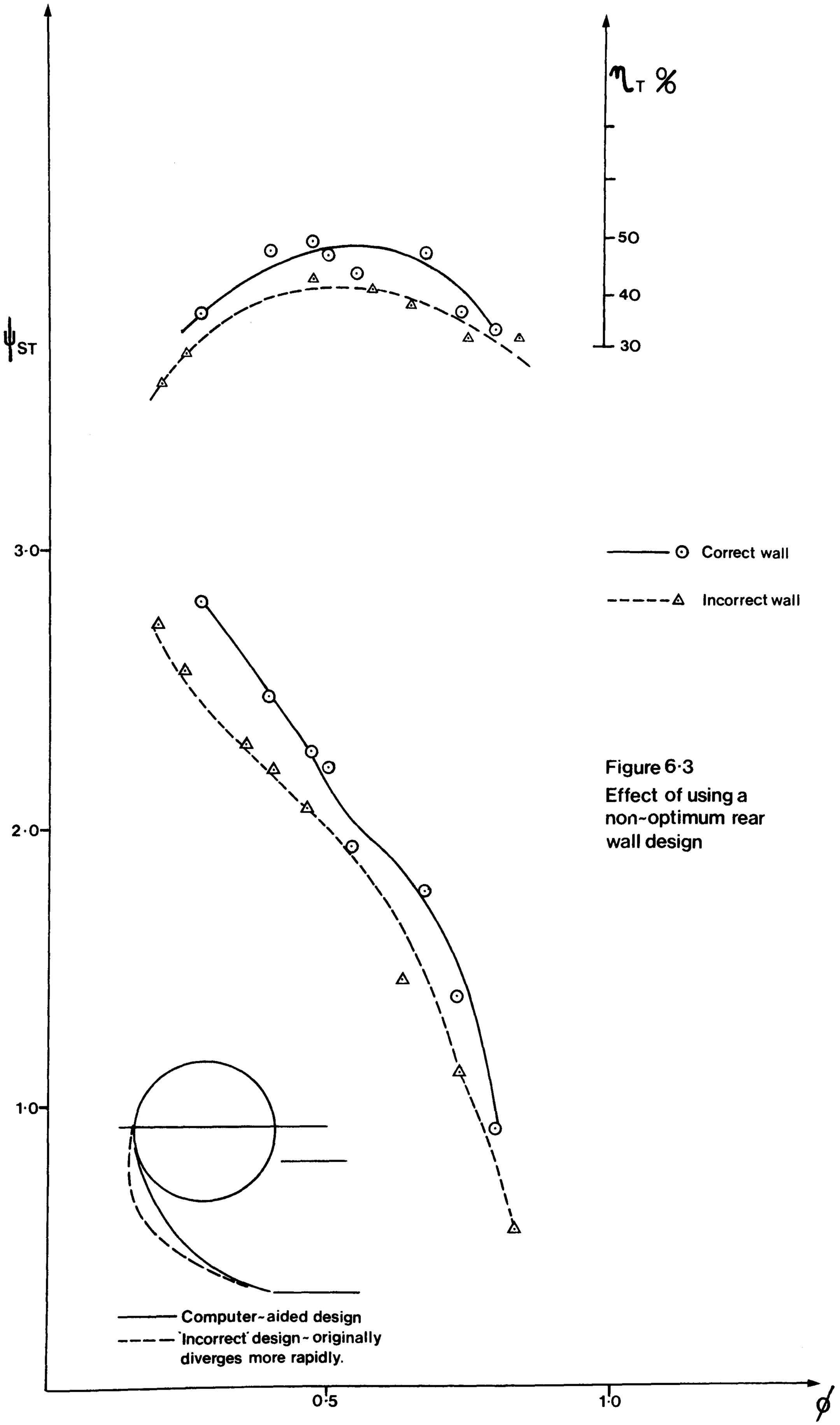

Figure 6·3
Effect of using a non-optimum rear wall design

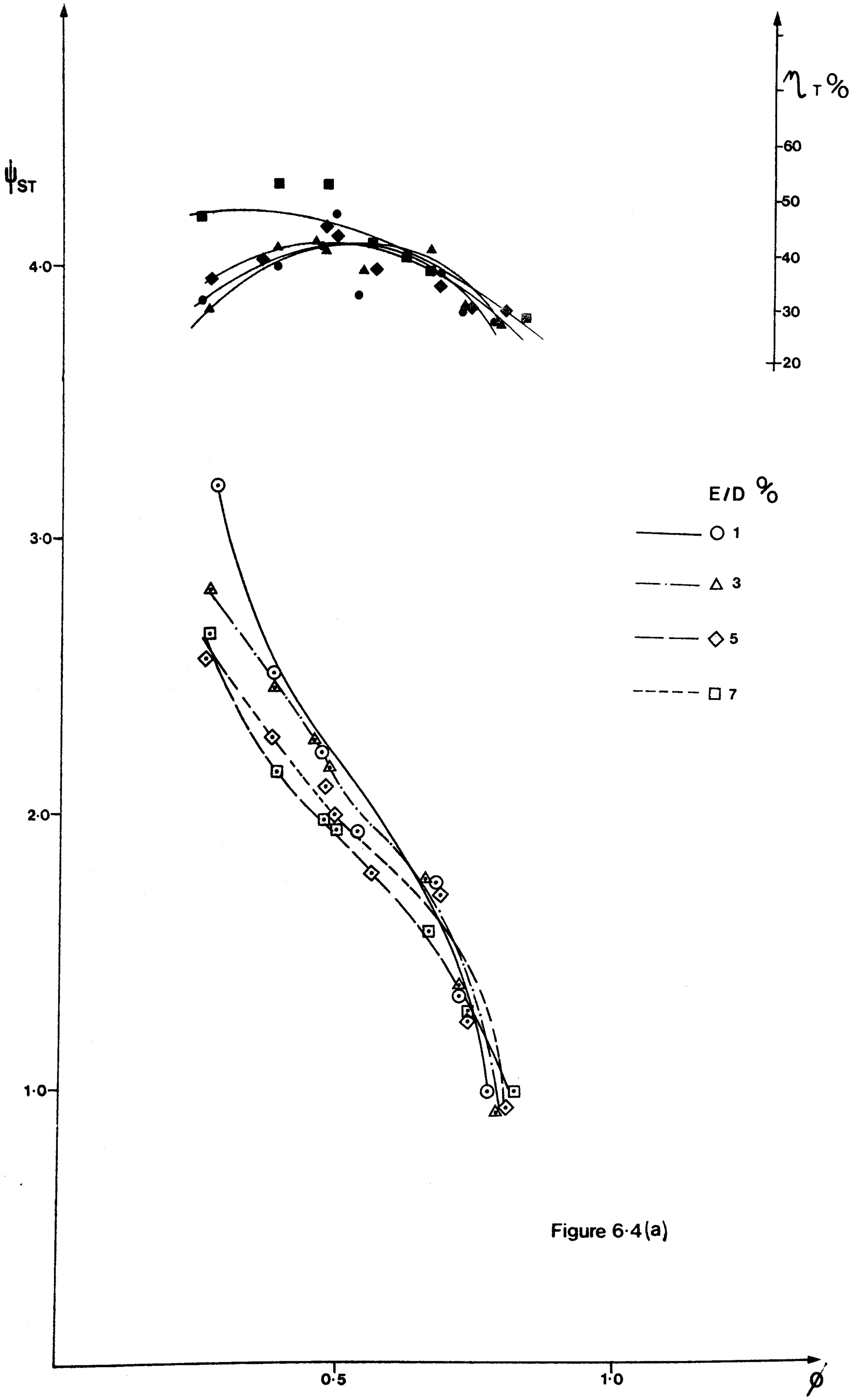

Figure 6·4(a)

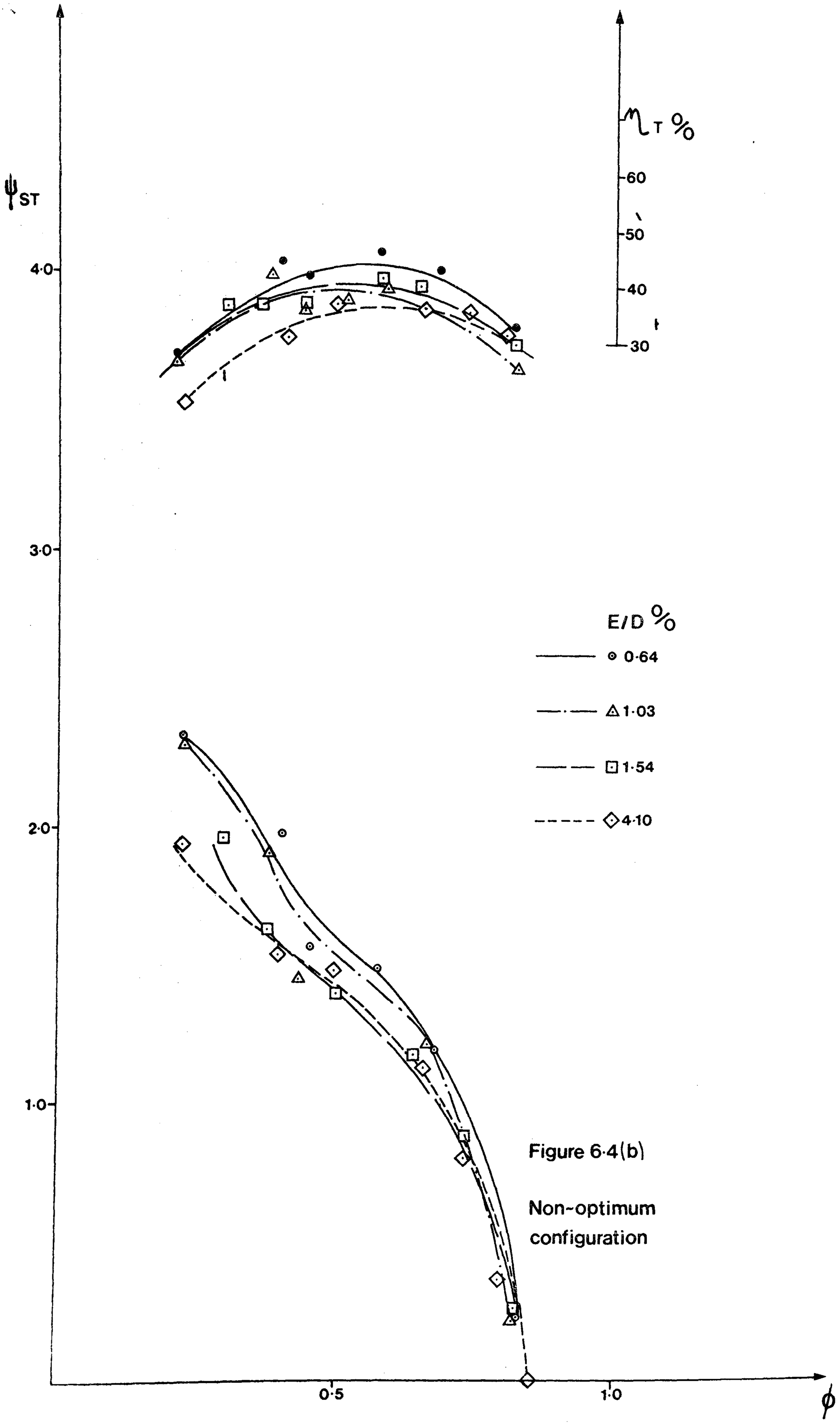
ψST
4·0
3·0
2·0
1·0
0·5
1·0
φ
ηT %
60
50
40
30
E/D %
0·64
1·03
1·54
4·10
Non-optimum
configuration

Figure 6·4(b)

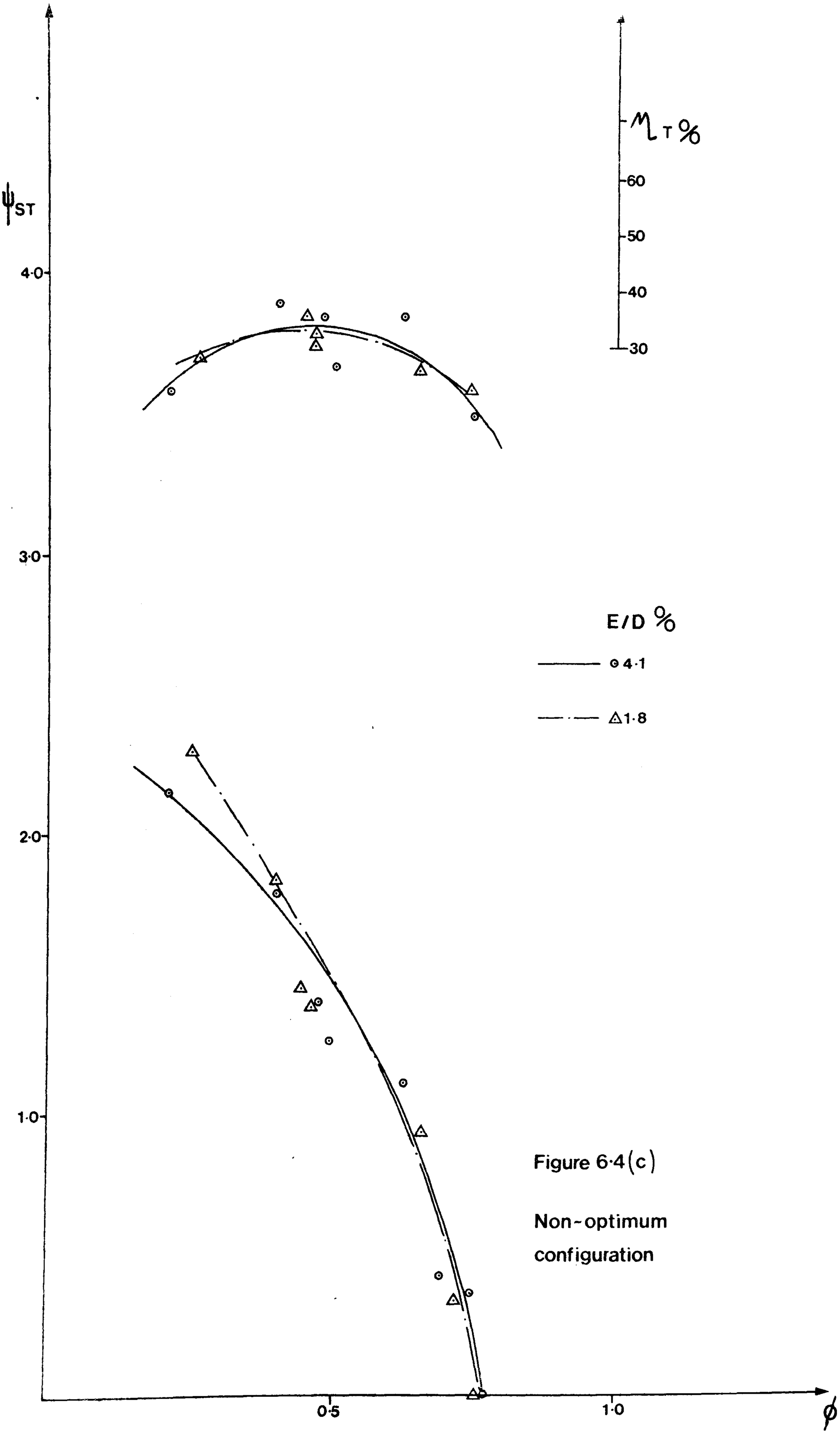

Figure 6·4(c)

Non-optimum configuration

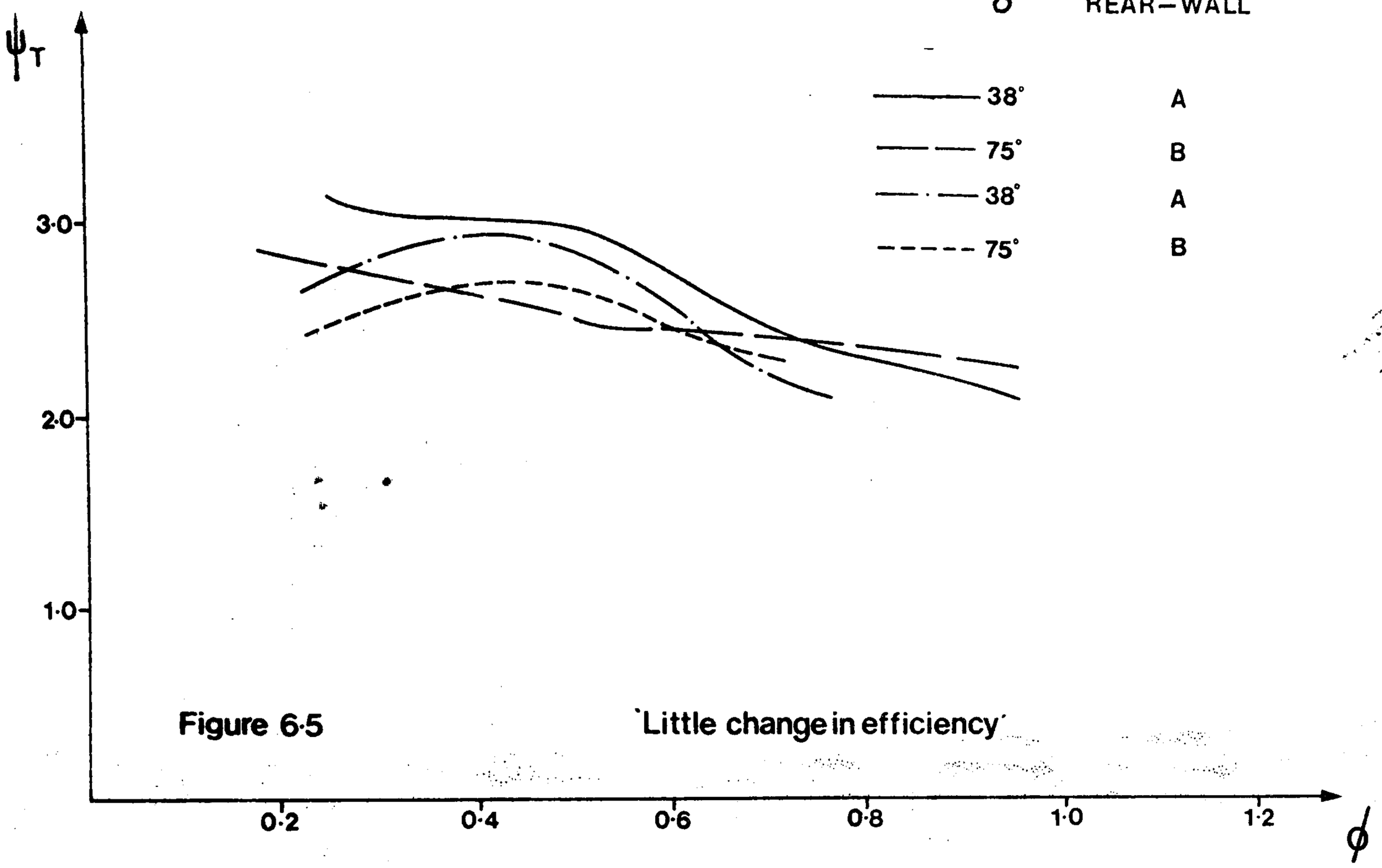

Figure 6·5 'Little change in efficiency'

Decreasing B
(MURATA and NISHIHARA)

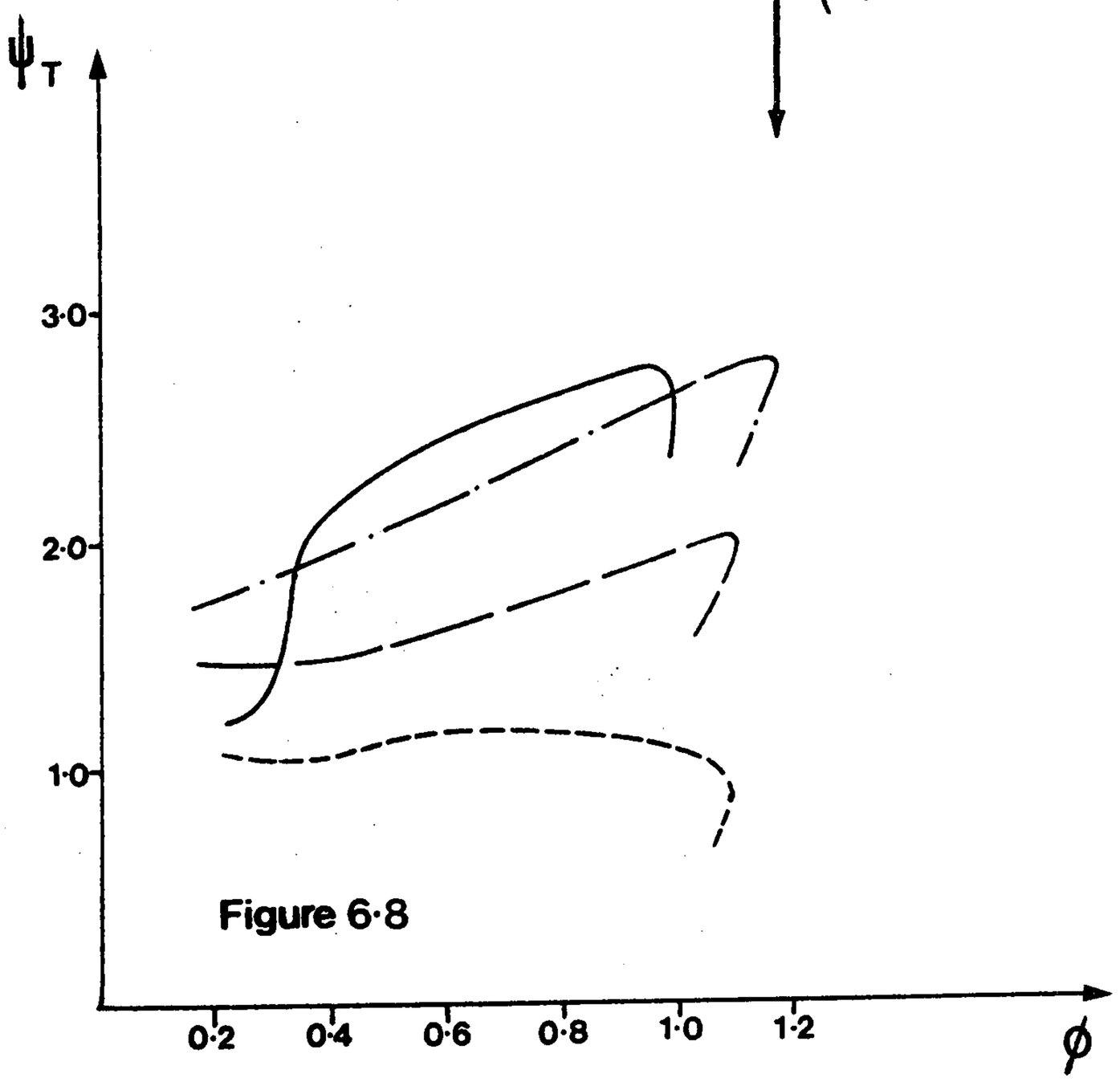

Figure 6·8

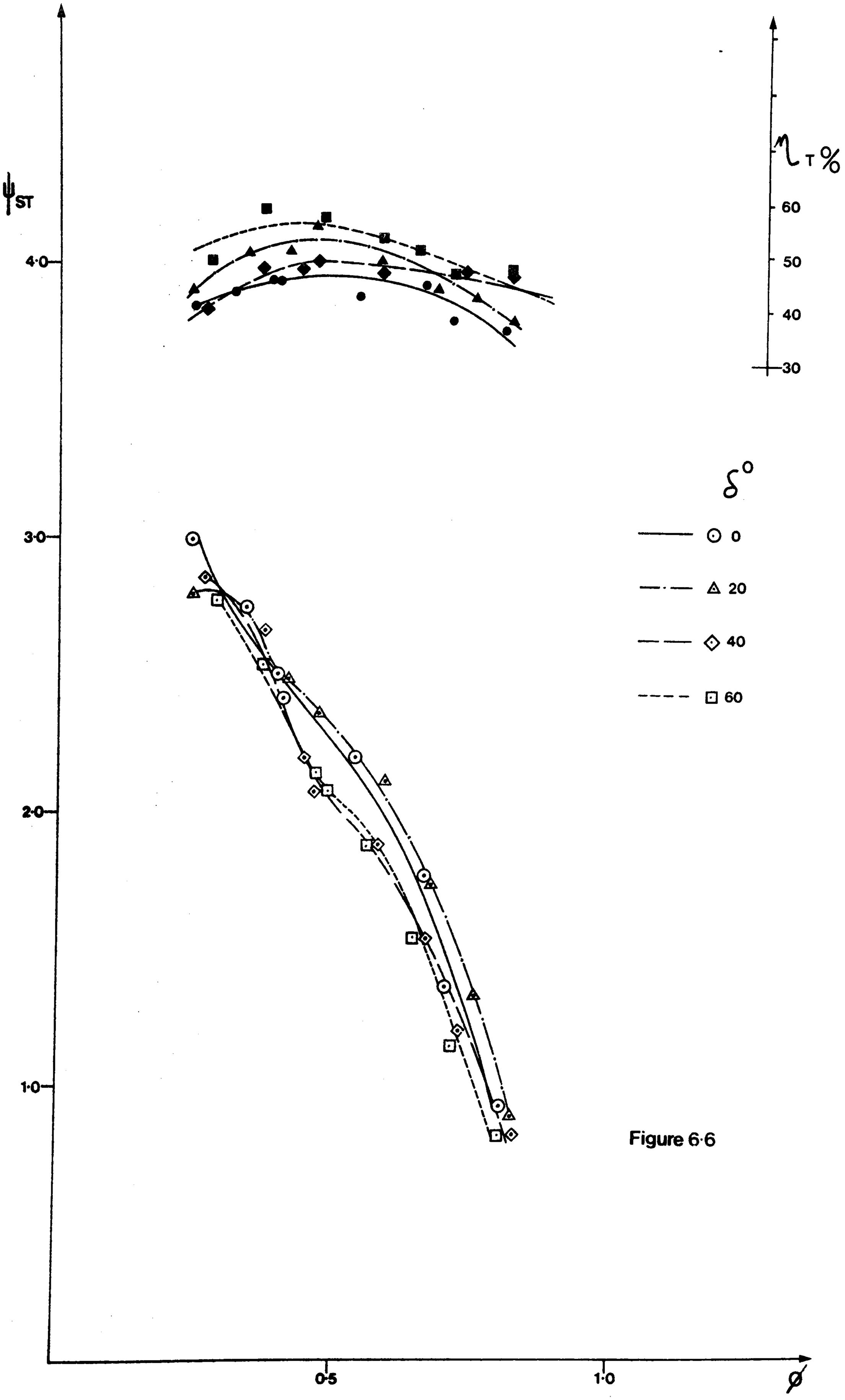

Figure 6·6

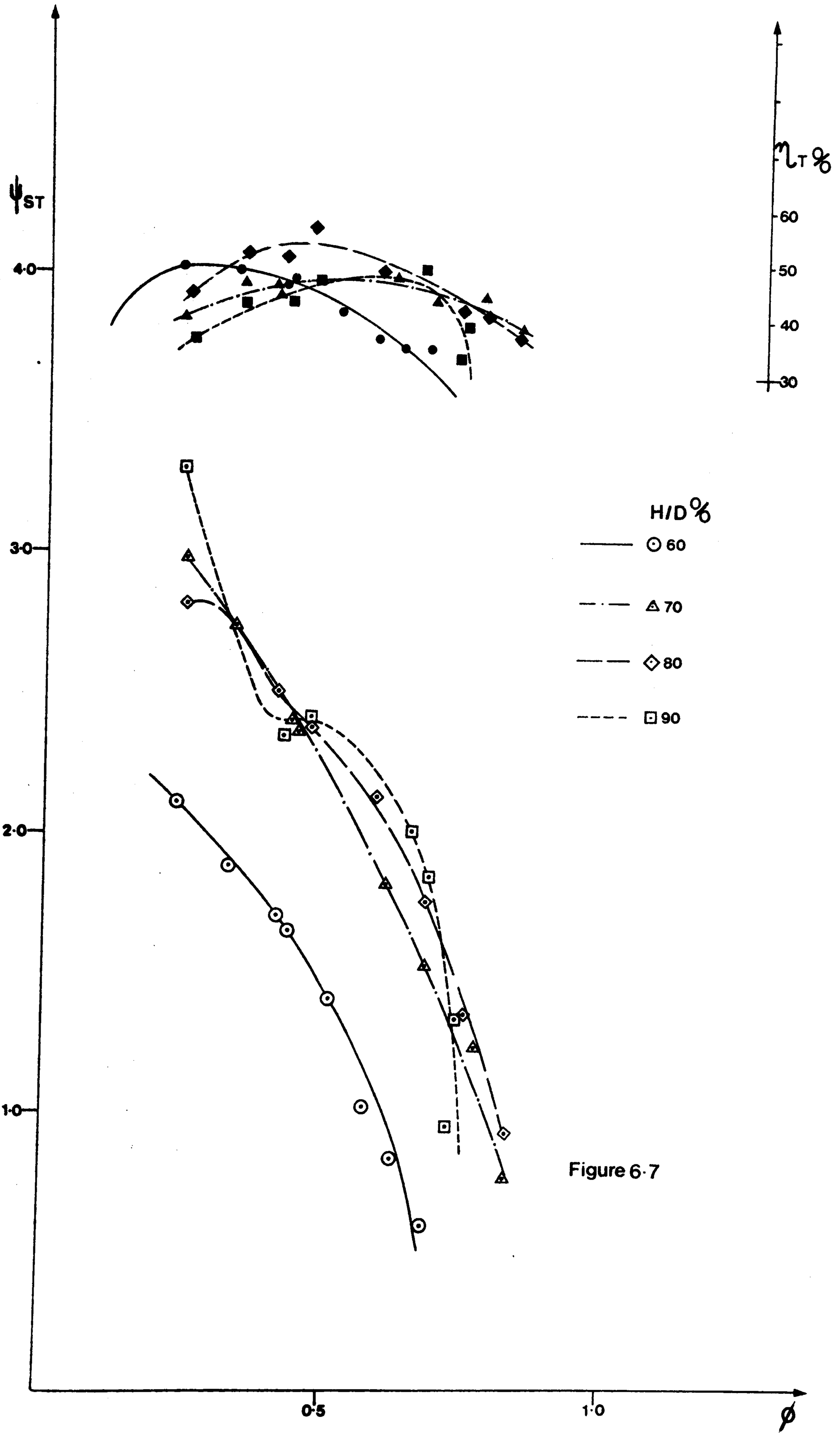

Figure 6·7

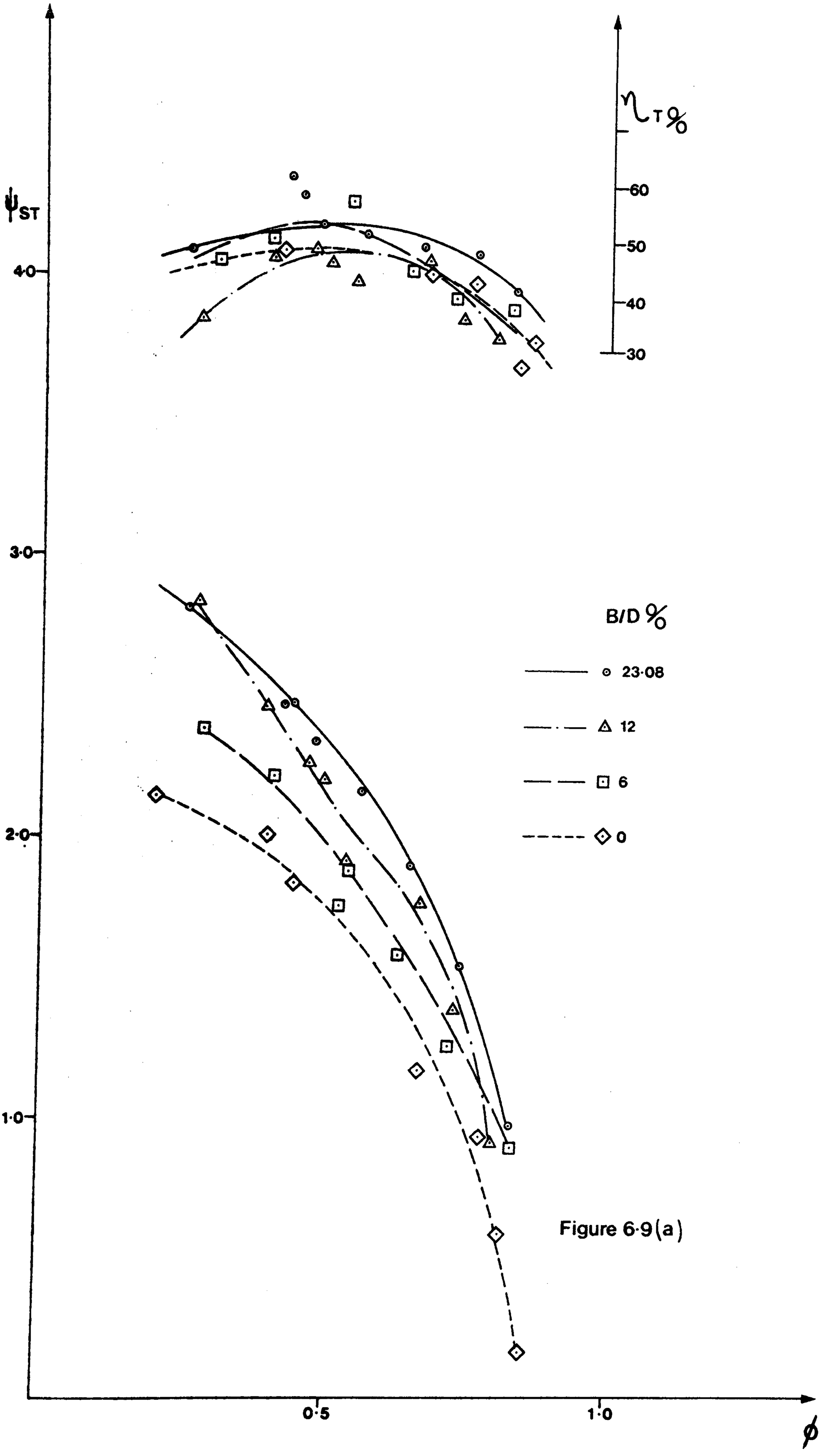

Figure 6·9(a)

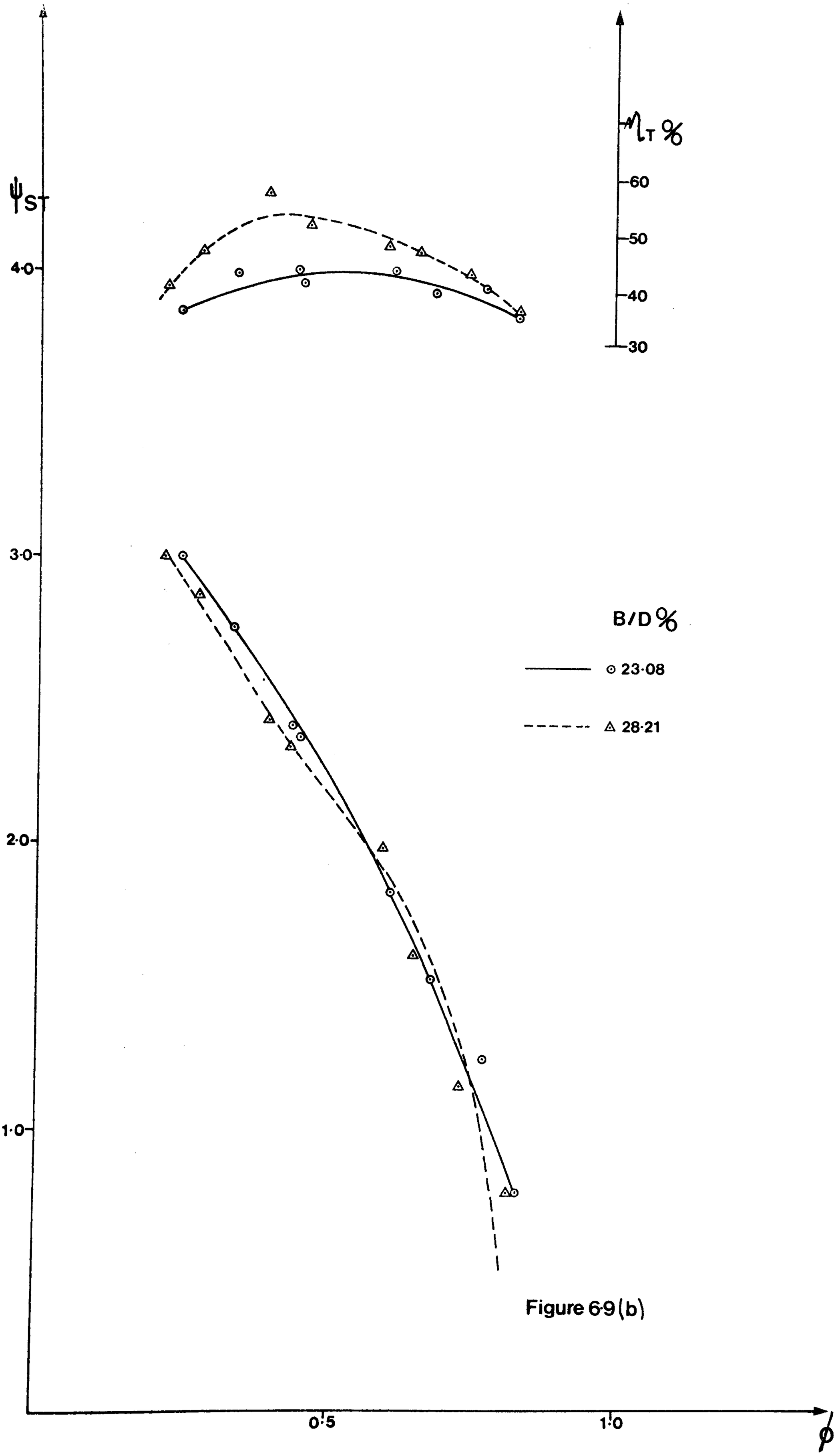

Figure 6·9 (b)

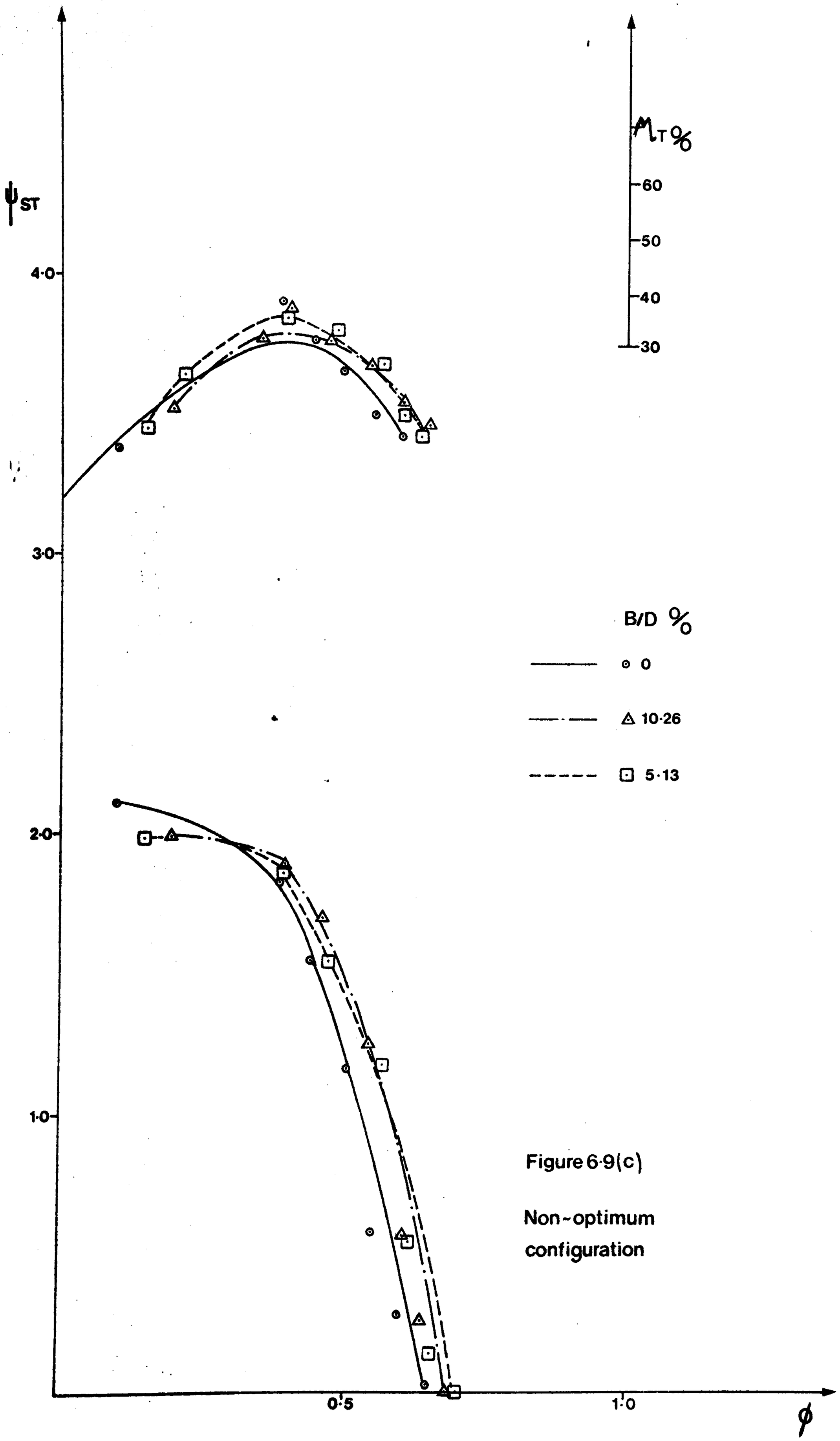

Figure 6·9(c)

Non-optimum configuration

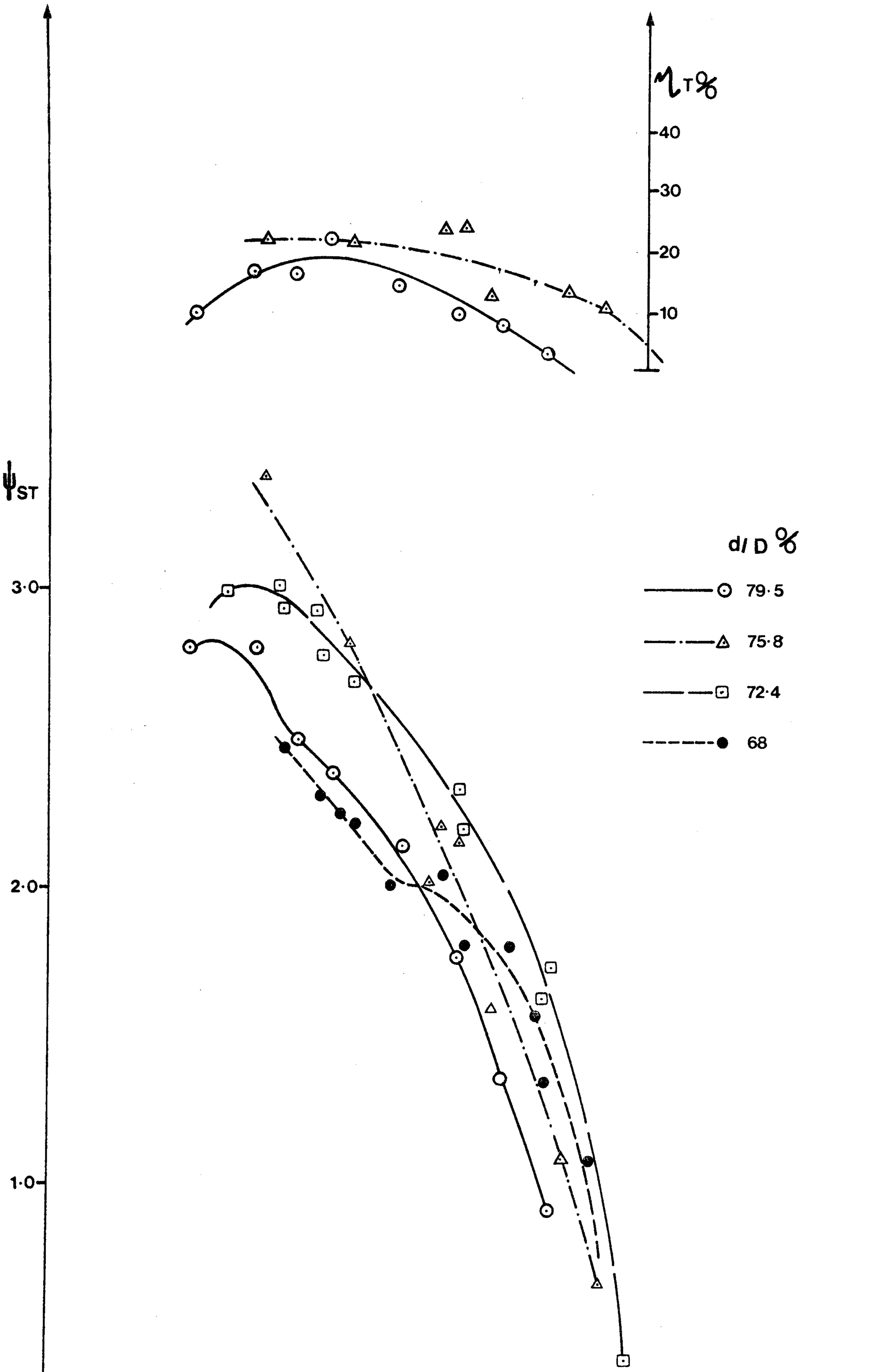

Figure 6·10 **Effect of d/D on performance**

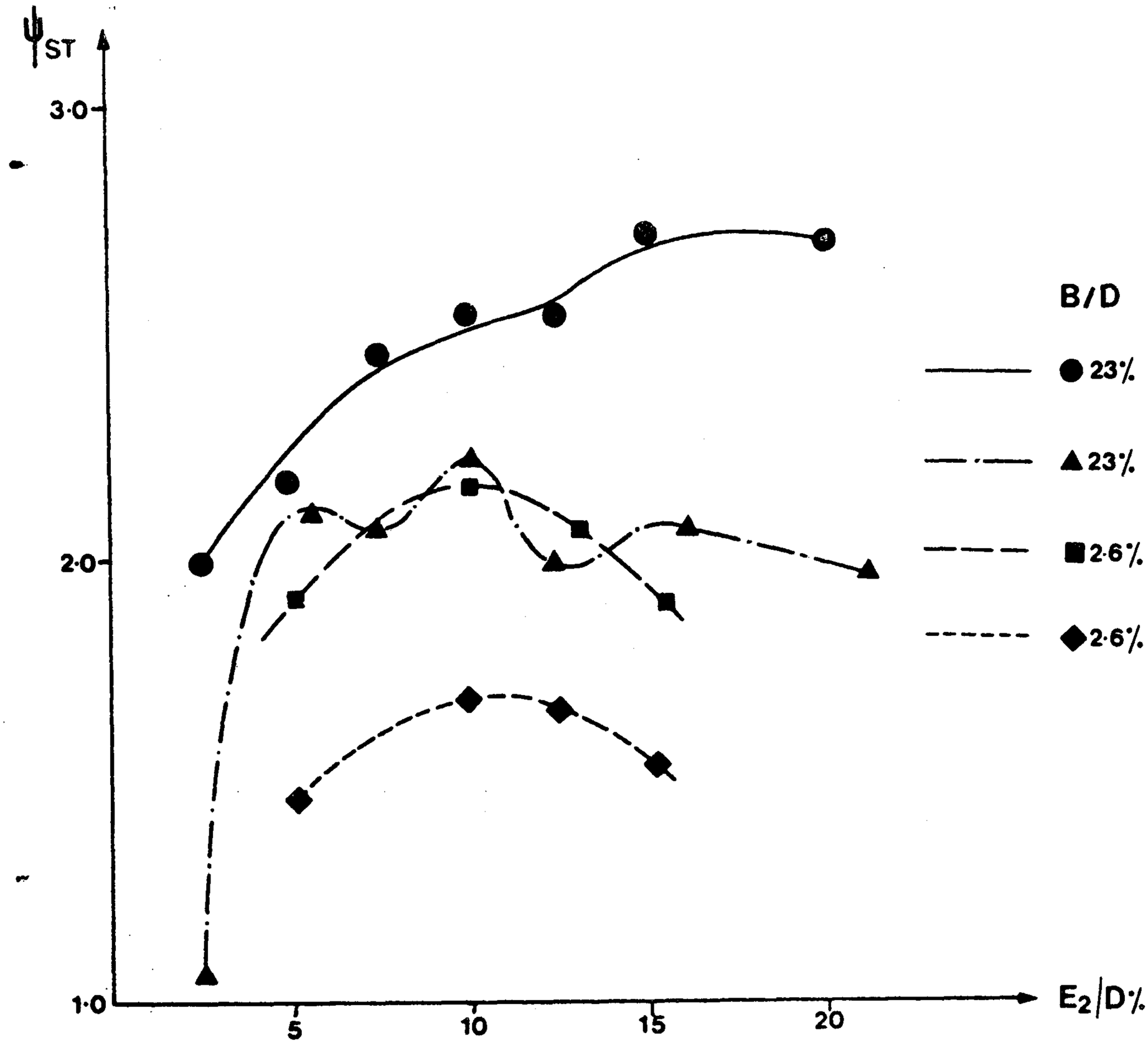

Figure 6·11

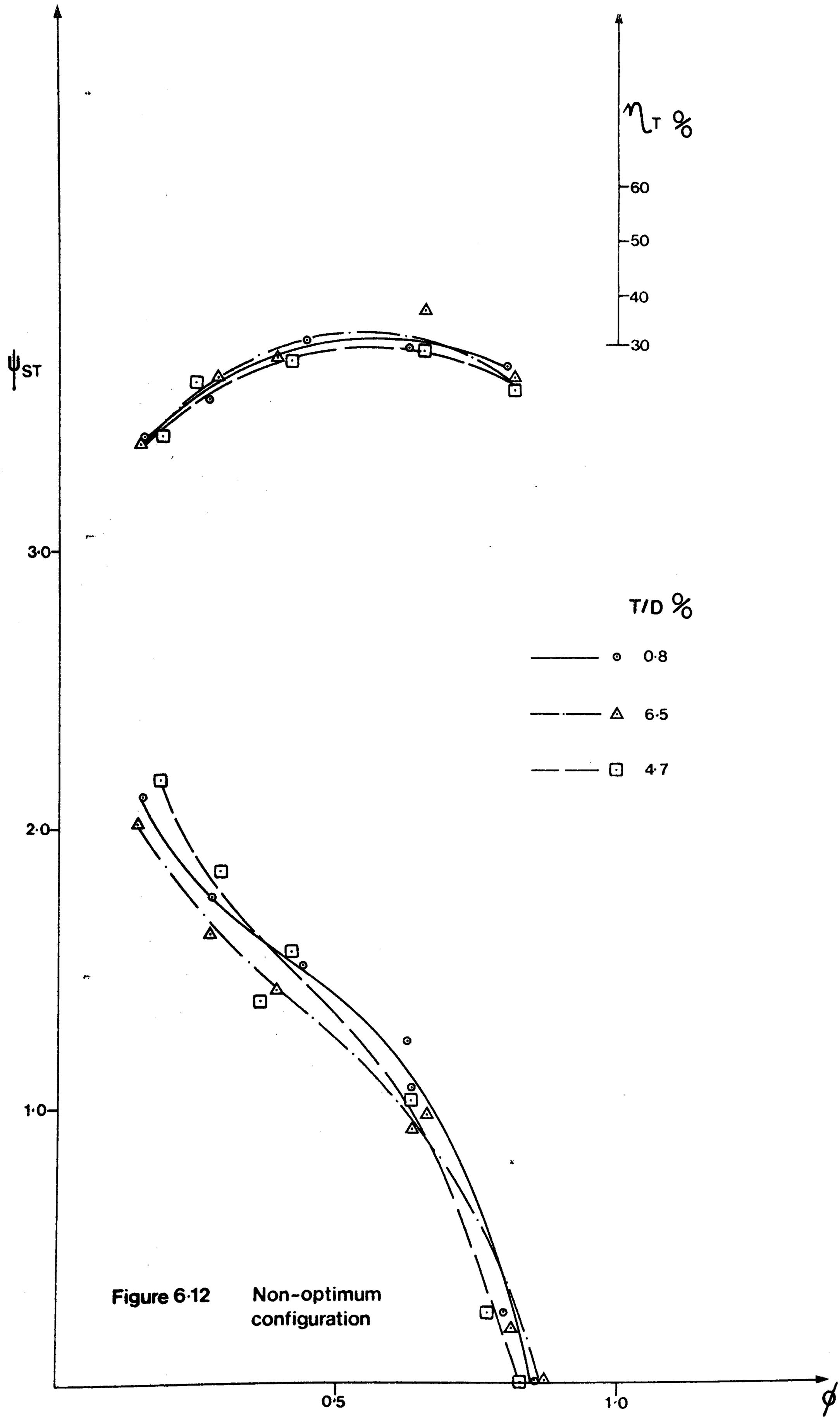

Figure 6·12 Non-optimum configuration

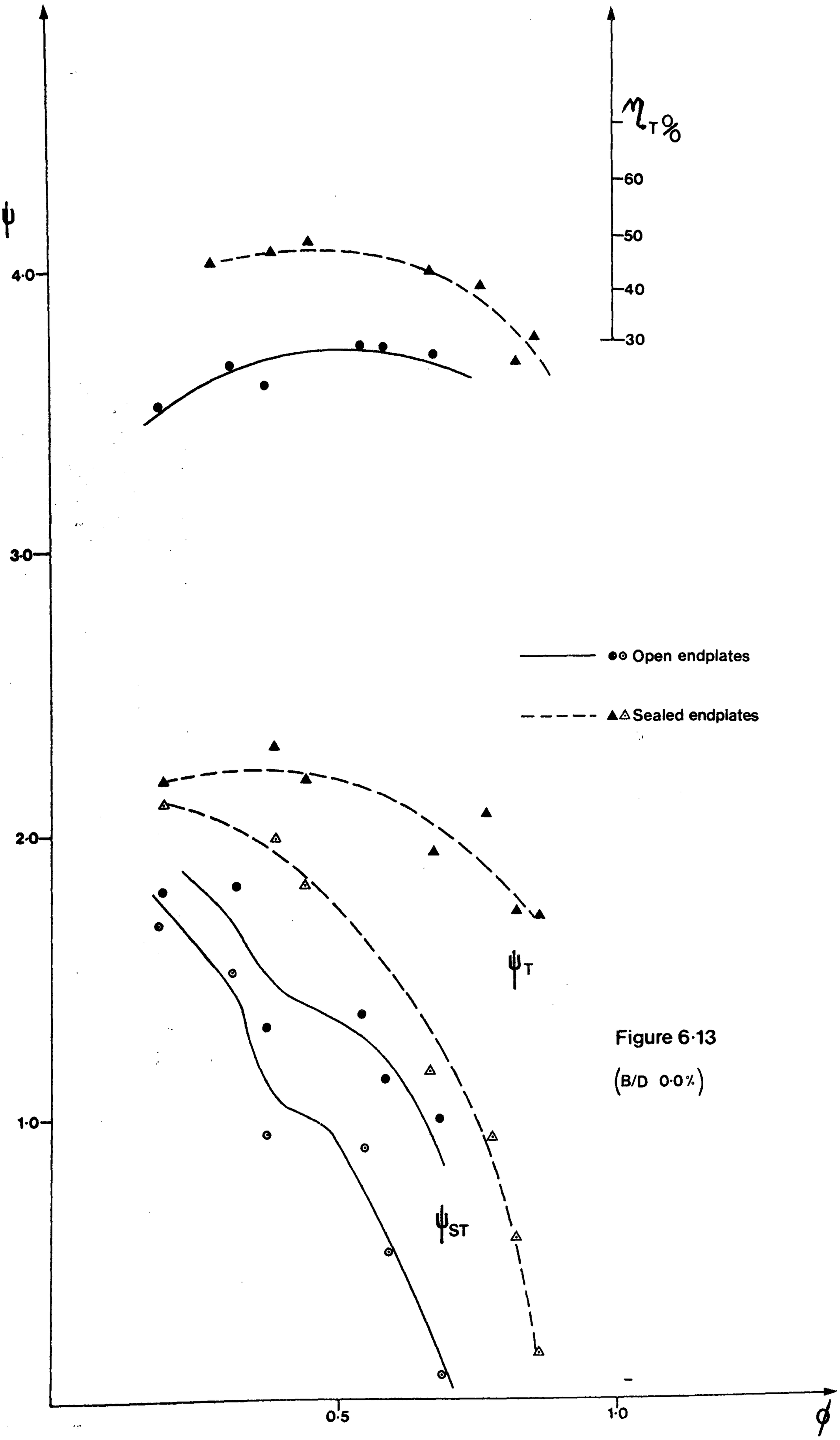

Figure 6·13

(B/D 0·0%)

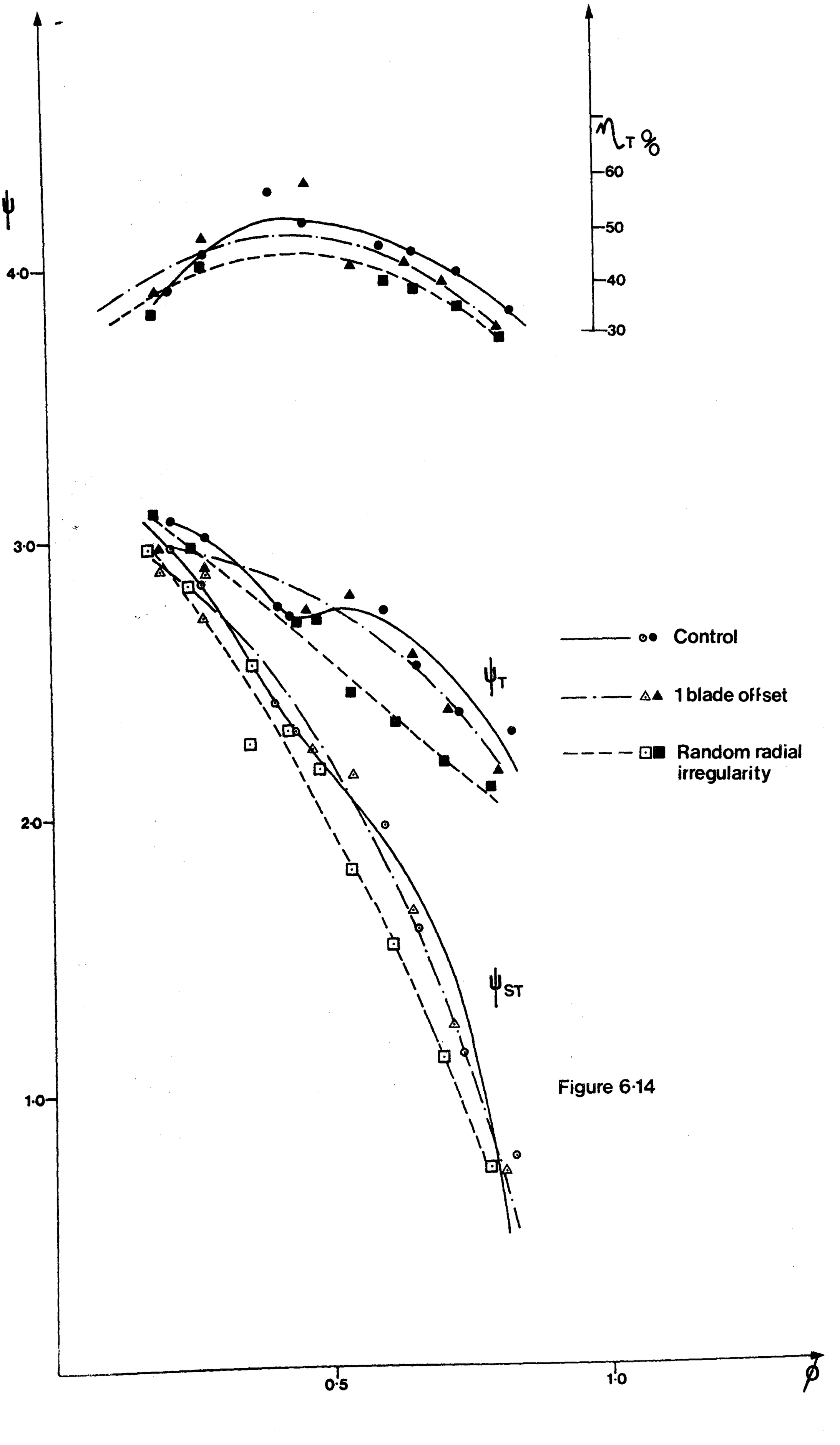
ψ
4·0
3·0
2·0
1·0
0·5
1·0
ϕ
ηT %
60
50
40
30
ψT
ψST
Control
1 blade offset
Random radial irregularity

Figure 6·14

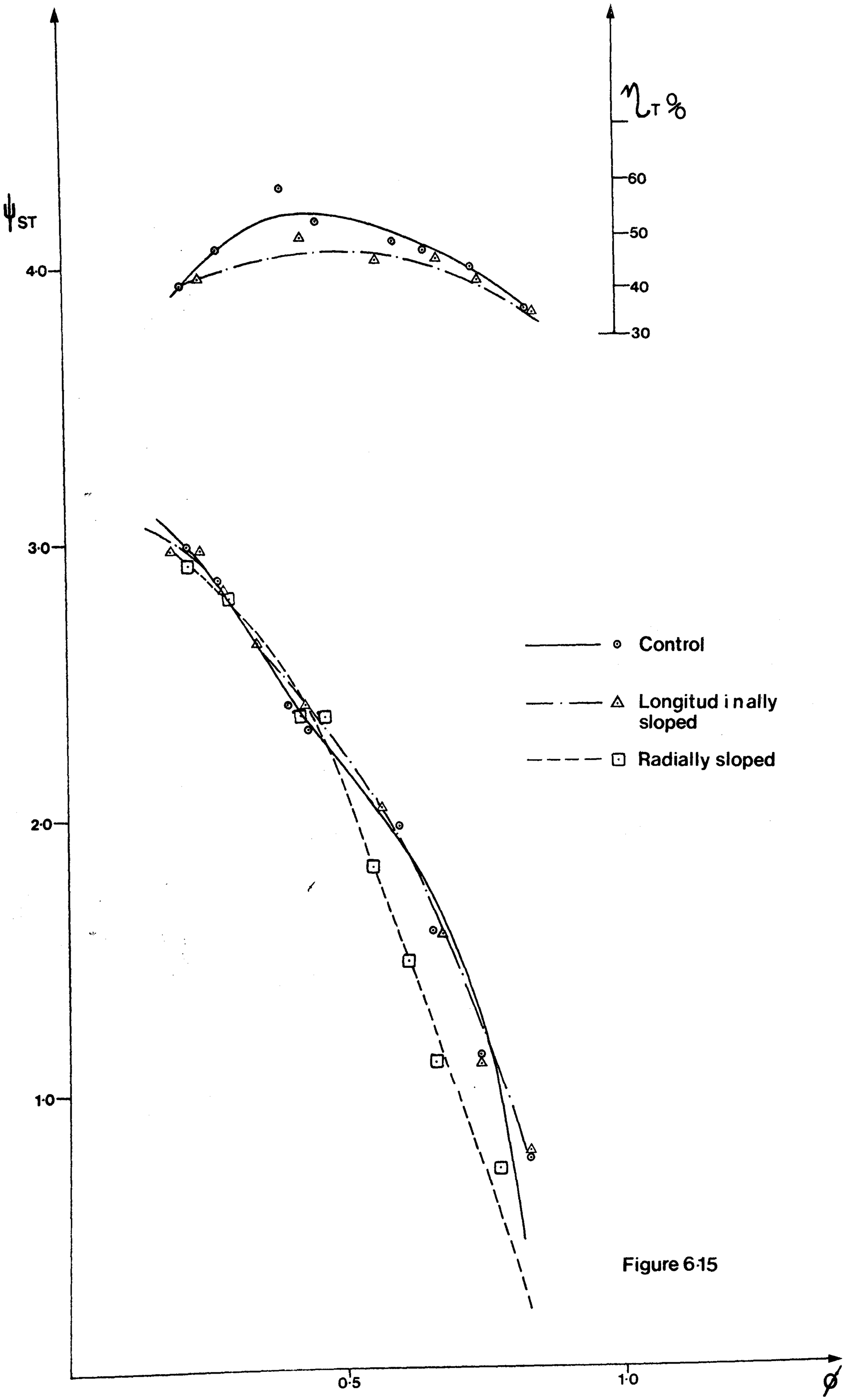
ψ_{ST}
4·0
3·0
2·0
1·0
0·5
1·0
ϕ
η_T %
60
50
40
30
Control
Longitud i n ally sloped
Radially sloped

Figure 6·15

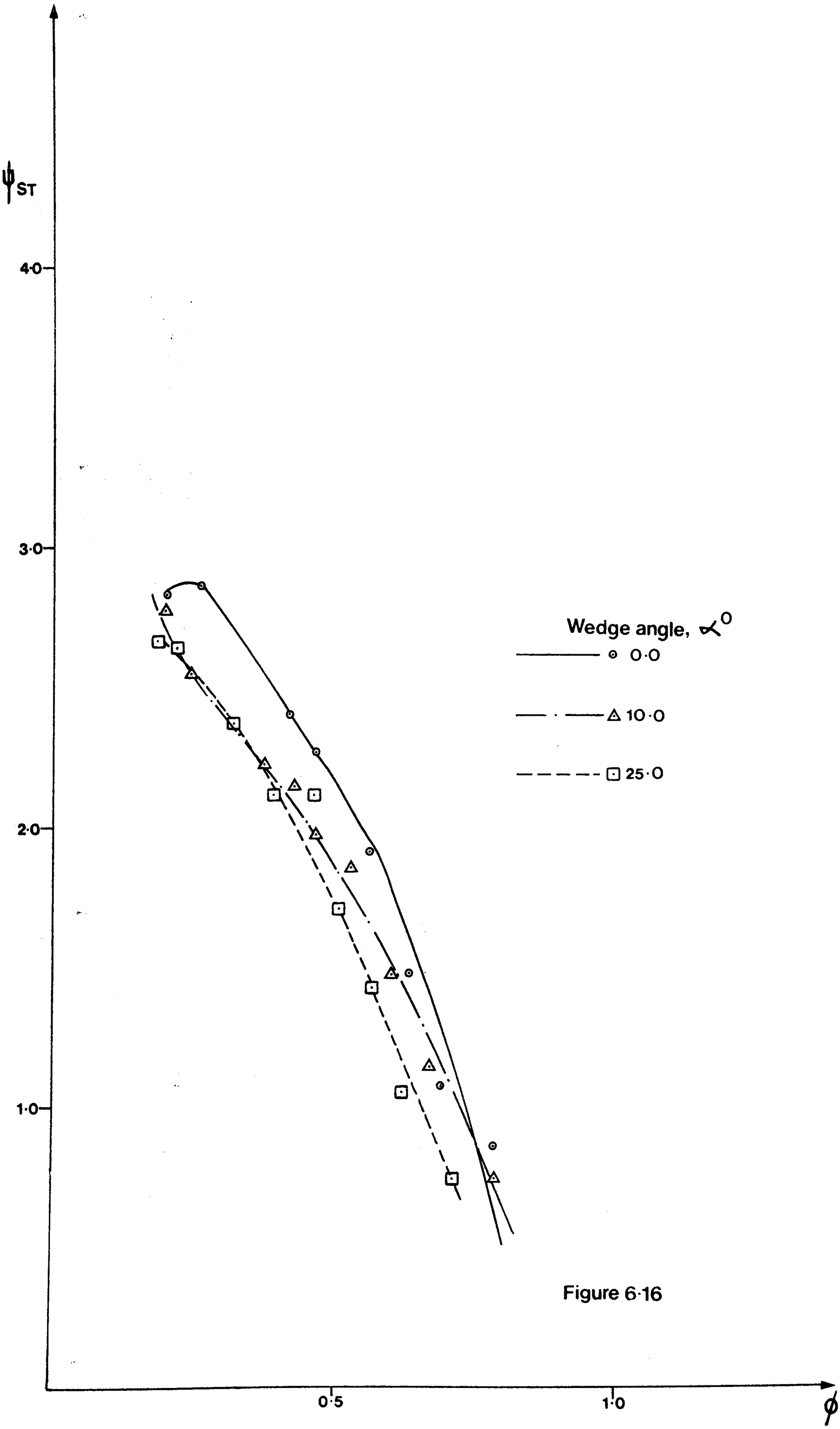

Figure 6·16

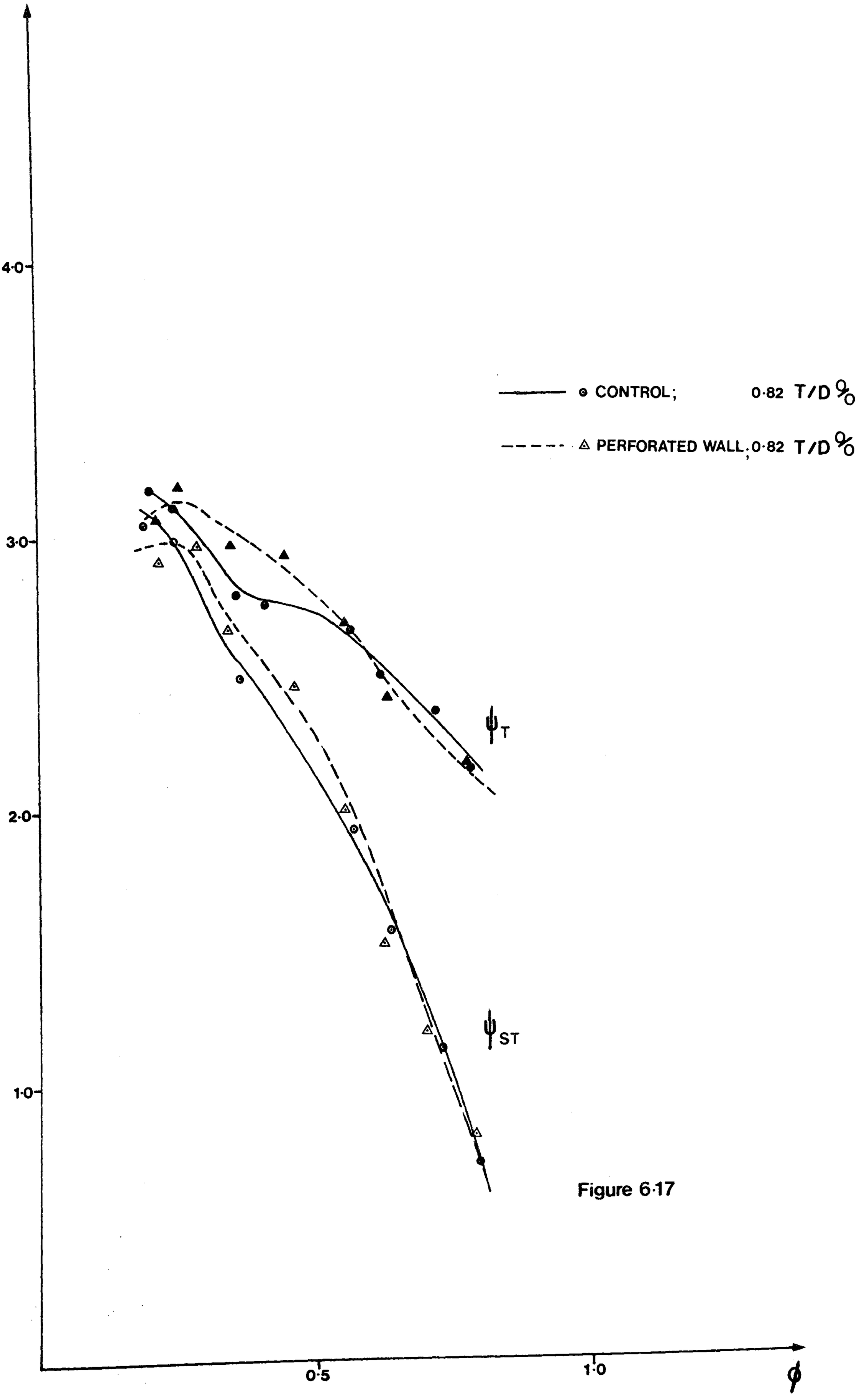
ψ
4·0
3·0
2·0
1·0
0·5
1·0
ϕ
ψT
ψST
—— ⊙ CONTROL; 0·82 T/D %
- - - - - △ PERFORATED WALL; 0·82 T/D %

Figure 6·17

FIGURE 6.18(a) TO 6.18(l) VOLOCITY PROFILES

a

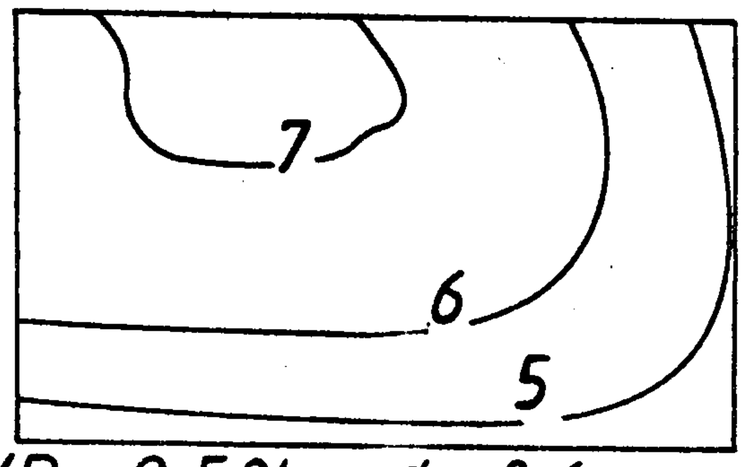

E2/D = 2·5% Ø = 0·6

b

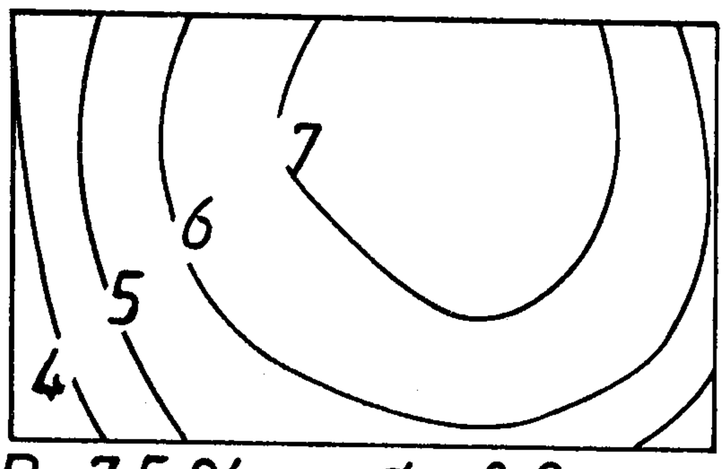

E2/D = 7·5 % Ø = 0·8

c

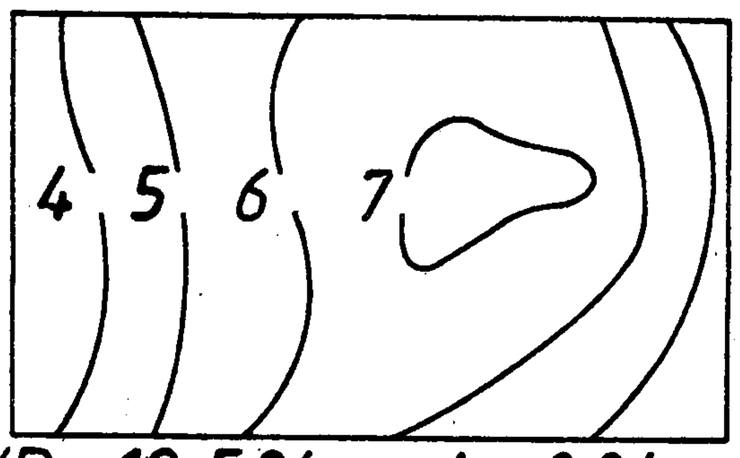

E2/D = 12·5% Ø = 0·84

d

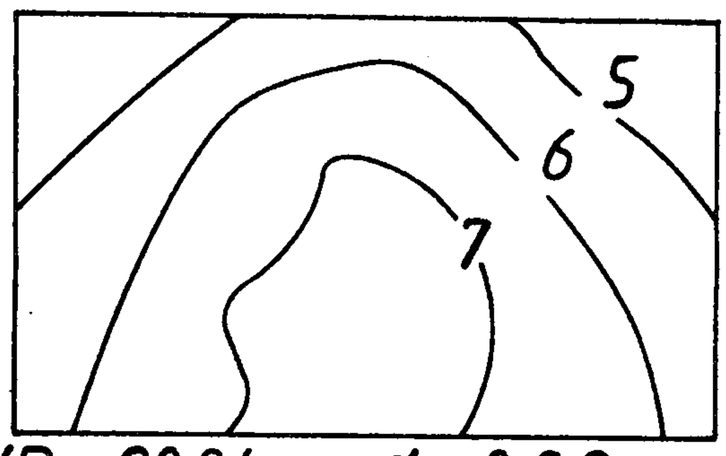

E2/D = 20 % Ø = 0·82

e

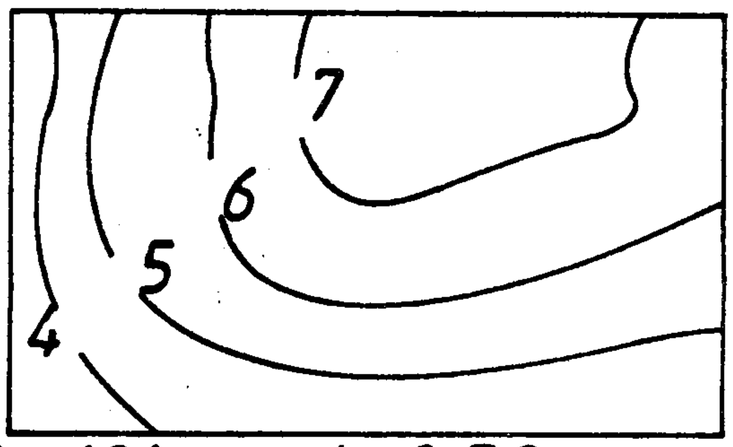

E/D = 1% Ø = 0·79

f

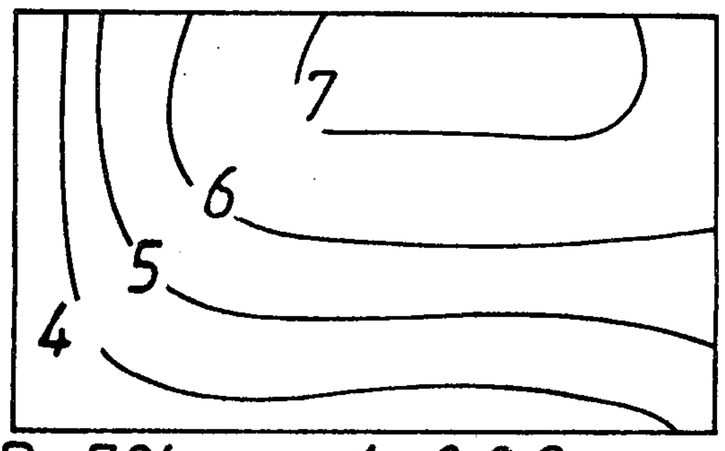

E/D = 7% Ø = 0·82

g

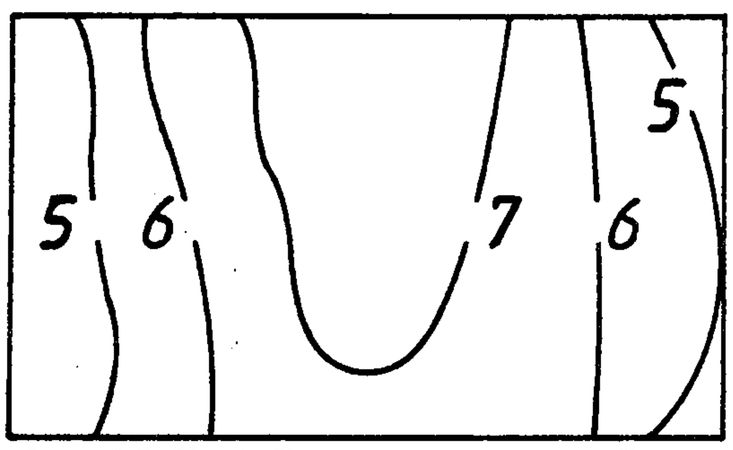

10° WEDGE Ø = 0·5

h

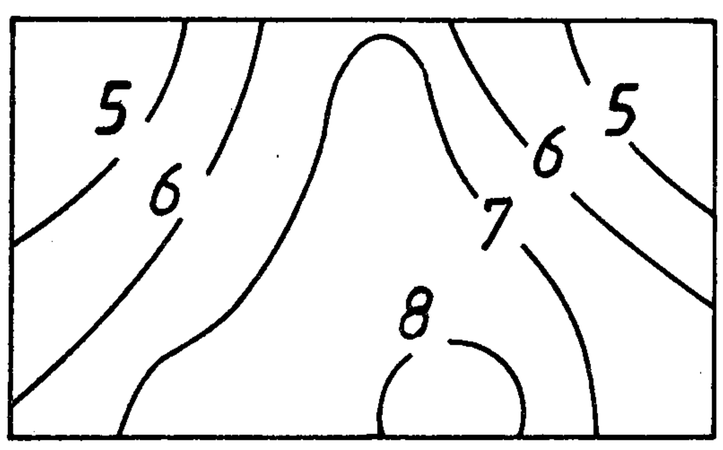

10° WEDGE Ø = 0·78

i

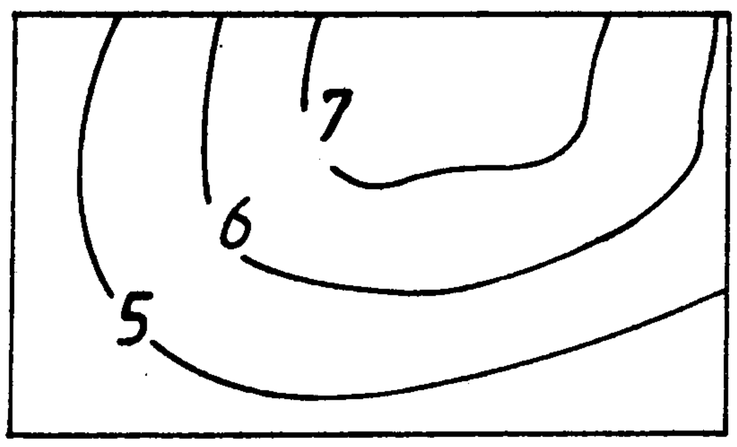

B/D = 12·8 % Ø = 0·8

j

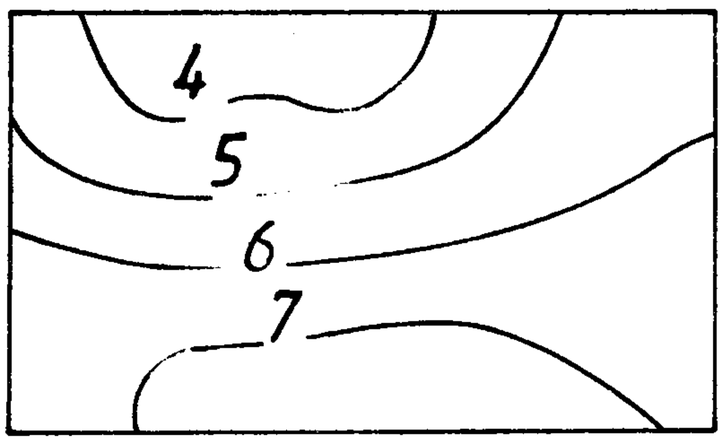

B/D = 12·8 % Ø = 0·76

k

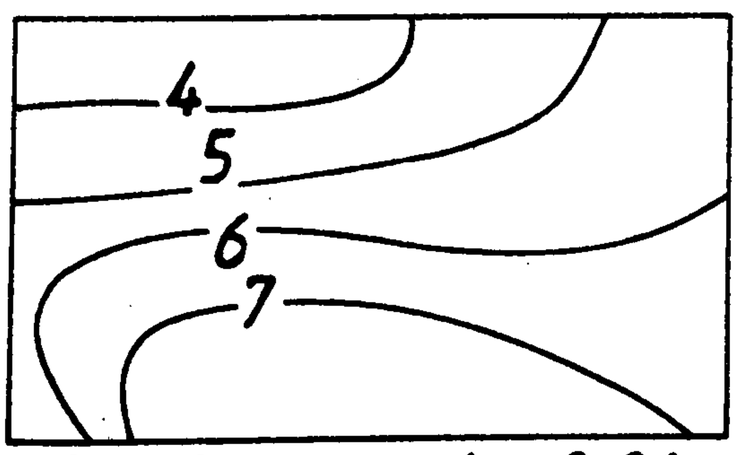

B/D = 28 % Ø = 0·81

CONVENTIONAL WALL

l

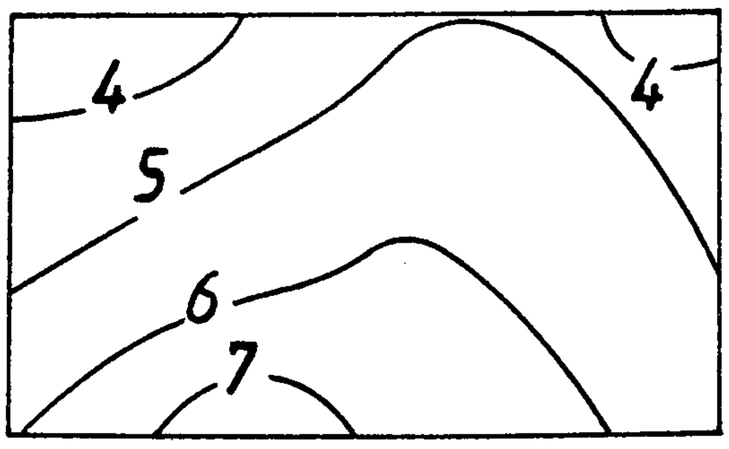

B/D = 28 % Ø = 0·77

ECK-TYPE WALL

HIGHER NUMBERS INDICATE HIGHER FLOW VELOCITIES

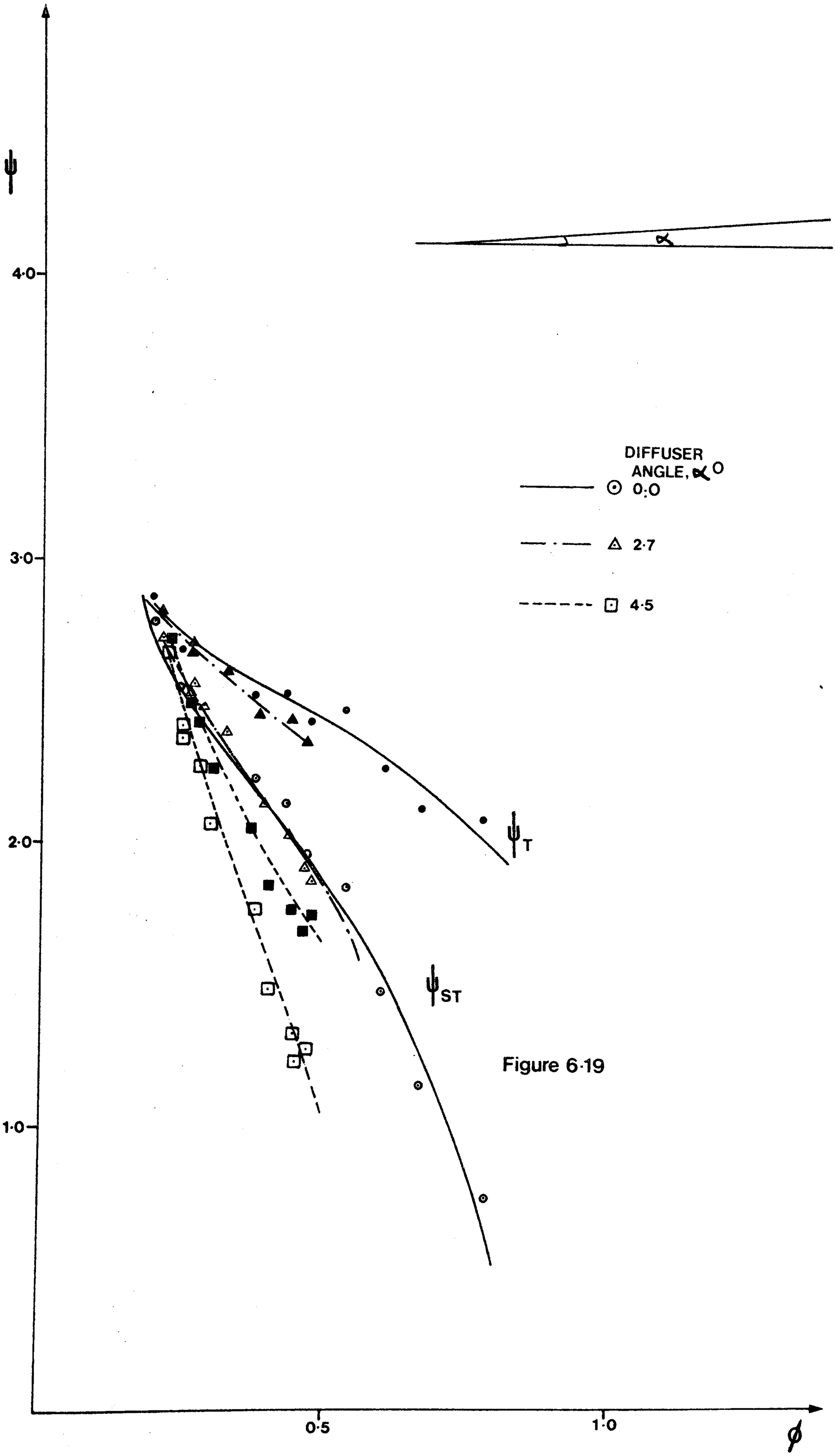

Figure 6·19

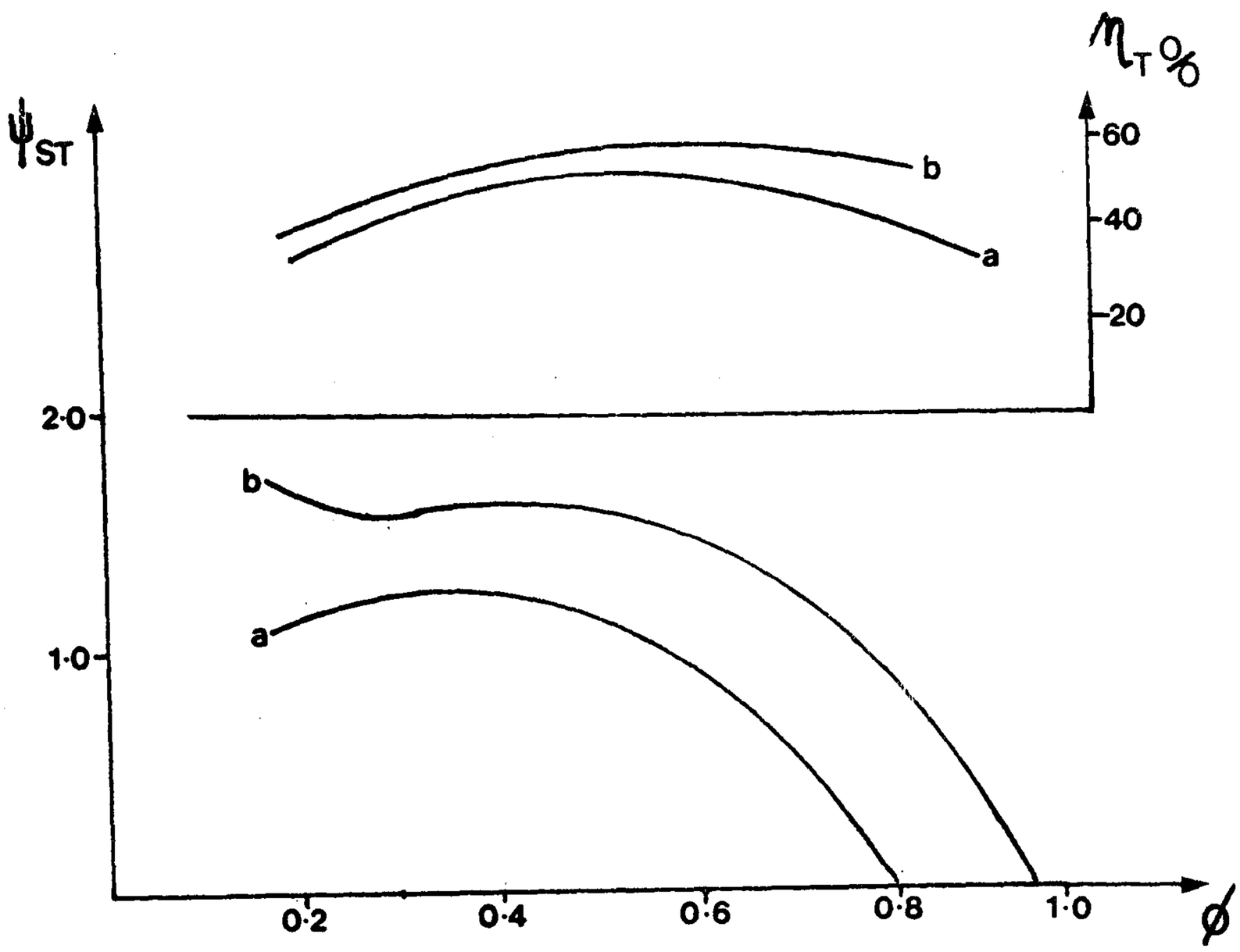

a - ECK WALL
b - SIMPLE WALL
(PORTER and MARKLAND)

Figure 6·20

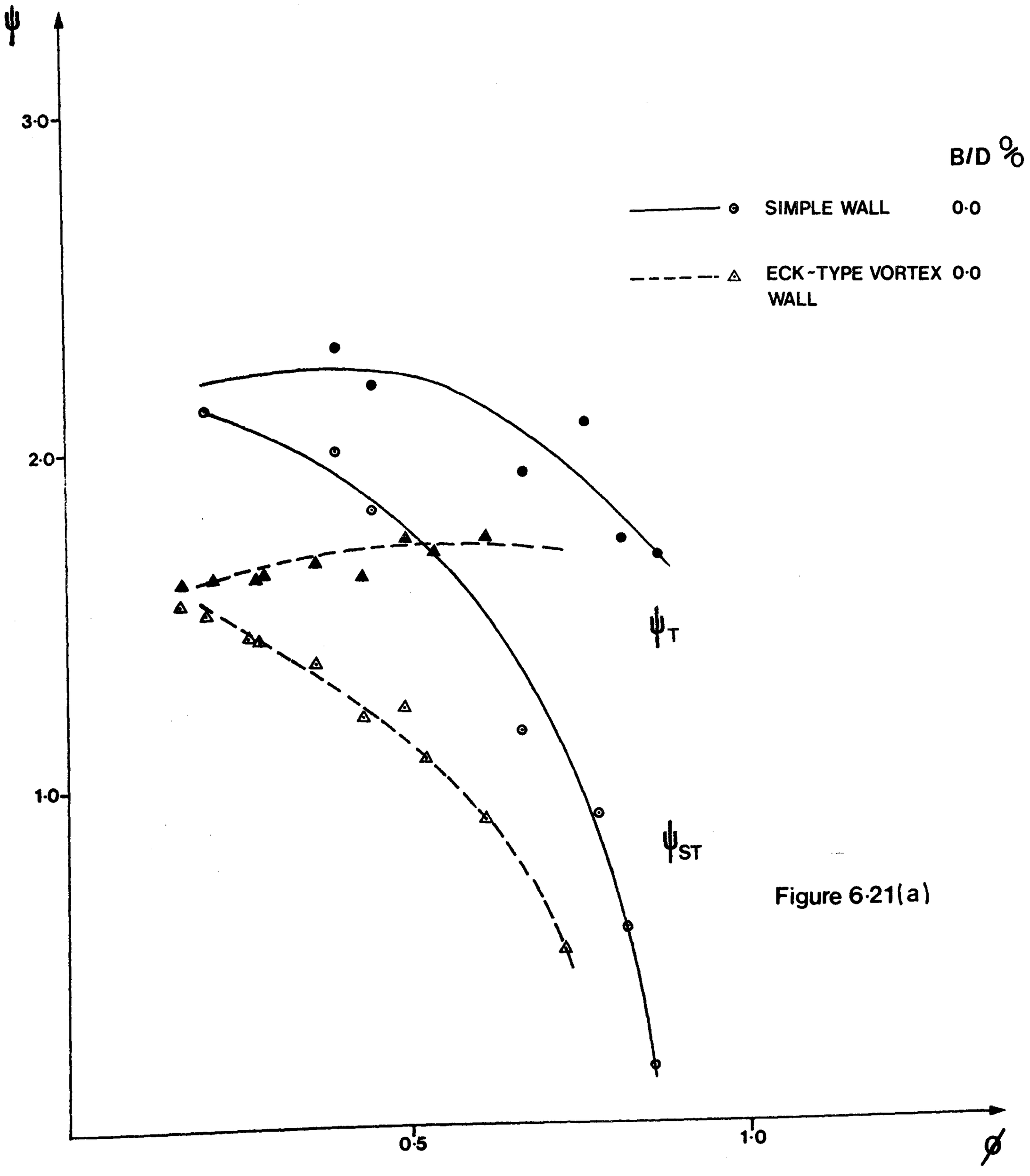

Figure 6·21(a)

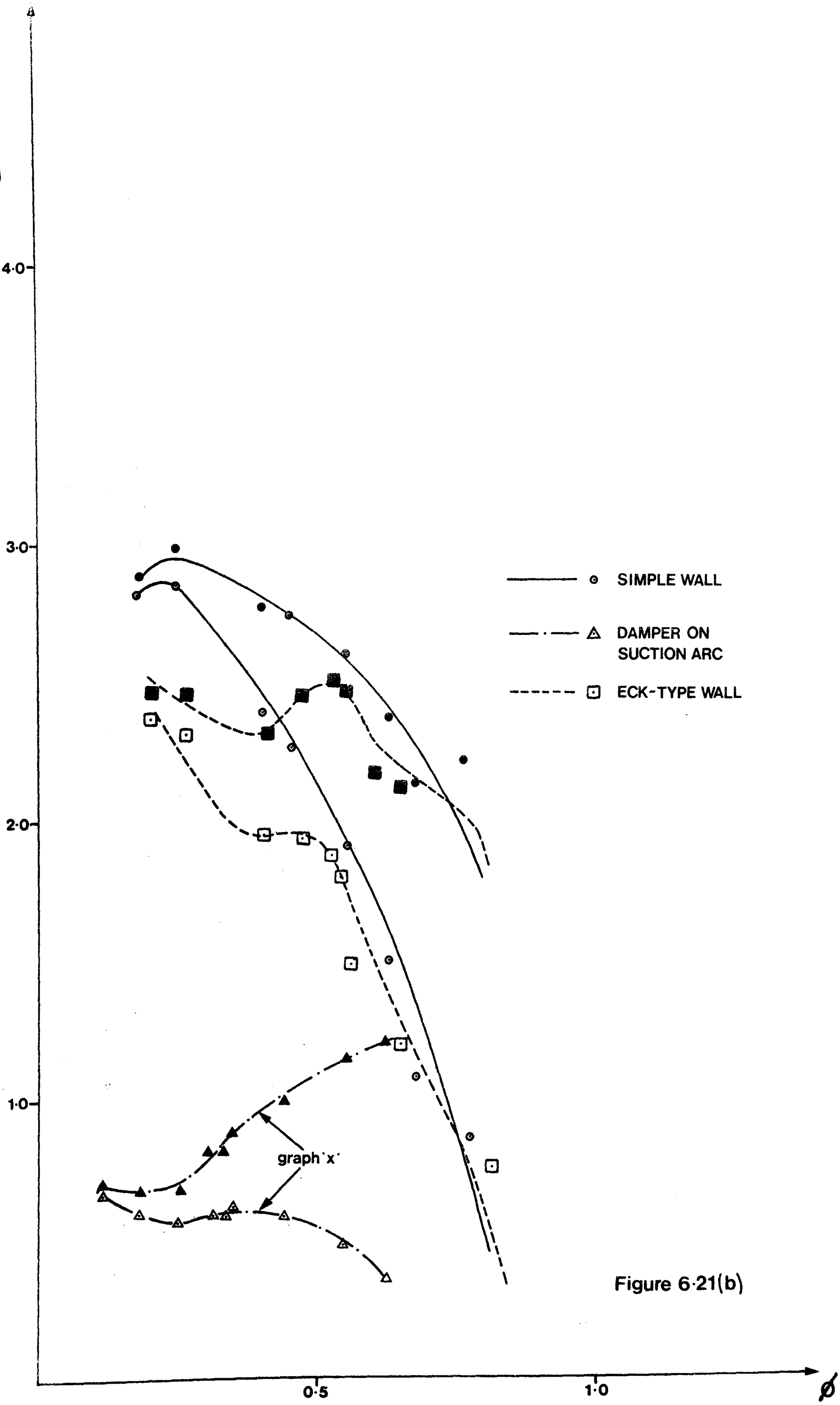
4·0
3·0
2·0
1·0
0·5
1·0
ϕ
graph 'x'
SIMPLE WALL
DAMPER ON SUCTION ARC
ECK-TYPE WALL

Figure 6·21(b)

CHAPTER SEVEN

7.1 INTRODUCTION TO MECHANISMS OF INSTABILITY.

7.1.1 STALL AND SURGE.

Stall and surge differ in scale. Stall is a flow-induced condition existing between adjacent blade rows, whereas surge is detected as a periodic variation in the mass flowrate and pressure.

Stall occurs where the relative flow angle and blade angle are poorly matched. If the counter prerotation of the fluid, required for flow alignment with the blades, proves to be physically impossible, separation will occur leading to the partial or complete blockage of a blade channel. Flow is then diverted through adjacent blade channels, which may as a result also become stalled. Where the stall propogates peripherally it is termed 'rotating stall'.

Cross-flow fans, due to the eccentrically located vortex, have a range of relative flow angles distributed around the suction arc: it is likely, therefore, that a cross-flow fan will always operate with some stalled blade passages, and that these will probably occur towards the vortex wall or rear wall boundaries of the suction arc.

A fan or compressor characteristic which droops is often called 'unstable'. To avoid confusion; the term 'stability' in this text refers to the temporal stability of the flow and not to the shape of the characteristic curve.

Surge occurs where some flow disturbance causes a reduction in flowrate coupled with a fall in static pressure. This momentarily leaves the duct static pressure above the impeller pressure, which results in a nett force acting on the impeller flow field. Generally, stable operating conditions can only be regained by increasing the flowrate, otherwise the fan operating point will oscillate between two points on the characteristic, Figure 7.1. Stall is commonly the disturbance which induces surging. Stall may be associated with a large drop in efficiency, surge is always intolerable from the point of view of system operation. Figures 7.1 and 7.2 demonstrate that surge is dependent on the shape of the characteristic curve. Stall and surge must also occur with cross-flow fans under the correct conditions, but the author suggests that they are not the primary mechanisms of cross-flow fan instability.

7.1.2 CROSS-FLOW FAN INSTABILITY.

Improvement of operational stability has long been an objective of cross-flow fan researchers. ECK (24), for example, called his profiled vortex wall a 'vortex stabiliser'. PORTER (62), though suggests that the vortex wall has less of an effect than ECK implies. However, although easy to detect the problem is not simple and most researchers have been able to do little more than acknowledge the presence of pulsating flow conditions.

BUSH (13), in his review, stresses the need to quantify levels of stability when dealing with cross-flow fans. One reason, he claims, for these fans not finding commercial acceptance is that superficially impressive performance

curves may be obtained at the expense of unstable operation. YAMAFUJI (77) found that, even with steady (speed invariant) rotation, the flow pattern varied cyclically.

There are a number of mechanisms capable of generating a periodic flow instability; stall and surge are two, another is the small hydraulic pulse experienced as each blade passes a close-fitting element of the casing. This latter effect and stall are considered relatively unimportant in cross-flow fans; they are related to the blade passing frequency (BPF) rather than the revolutions per second (RPS), and thus occur at frequencies considerably higher than the dominant pulsation frequencies. The author has been unable to detect pulsations occuring at BPF multiples.

Pressure around the forced vortex core can only be guaranteed uniform when there is a free-vortex velocity distribution; the existence of an eccentrically located vortex eliminates this possibility. Thus, in most cases the forced vortex must have an uneven peripheral pressure distribution, which may cause the vortex to migrate between quasi-stable locations. TRAMPOSCH (71), in 1964, was the first to observe a small oscillatory motion of the forced vortex centre along the impeller inner periphery. It is this mechanism which the author considers to be primarily responsible for the operational instability experienced with cross-flow fans.

7.2 PROBLEMS CAUSED BY OPERATION IN A PULSATING FLOW.

Apart from difficulties in measurement, the main problem is that a cyclic variation in loading can induce large vibratory stresses in the blading and casing. This could lead to impeller destruction or mechanical failure of the casing along seams or weaknesses. A certain level of instability must be tolerated but instability is increased by poor manufacture.

A ventilation fan is required to deliver a certain quantity of air at an average static pressure in a certain time, say J minutes. As far as fan rated duty is concerned frequencies above (1/60 J) Hz may be substantially ignored. Problems will be encountered when running the fan in combination; by amplifying pulsation frequencies (series operation) or by causing the fan to operate in an unstable zone of the characteristic (parallel operation). There are also increased noise problems associated with low frequency pulsations, which tend to modulate existing noise and increase the drone.

It is important to assess priorities when selecting a cross-flow fan. A large ventilating fan, for example, will be chosen for optimum aerodynamic performance, consistent with low noise and stability. Whereas a desk-top blower must be quiet and the main criterion with ground-effect applications (e.g. hovercraft) may be stability of operation.

7.3 PULSATION ANALYSIS.

Any fan is subject to flow instabilities, due conventionally to stall or unequal peripheral total pressure.

These are high frequency pulsations related to the fan BPF. Cross-flow fans are subject to these instabilities, but in addition have low frequency, large amplitude pulsations due to vortex instability.

Understanding the cause and nature of these low frequency pulsations is fundamental in restricting or eliminating them. The pulsations pervade the performance characteristic and are generally larger at extreme flowrates, Figure 7.3, although a mid-characteristic peak instability is commonly observed, Figure 7.4. Vortex instability is a feature of cross-flow fans and must be allowed for in fan design.

To deal with this problem, the pulsating total or static pressures are converted to an analogue voltage and this processed signal fed to an X-Y plotter. The resulting trace may be analysed in two ways; in the time domain and in the frequency domain. A scan time of 22 seconds was normally used.

It should be mentioned that because these pulsations are due to a global oscillation of the fan-entrained fluid, not only does the pressure vary periodically, but also the mass flowrate. The variations are mutually dependent and, in the analyses, mass flowrate is taken as the datum at which the pressure oscillates. Three specimen traces are given in Figures 7.5(a) - 7.5(c), Table 7.1 compares results from the two methods under review.

7.3.1 ANALYSIS IN THE TIME DOMAIN.

The mean pressure over a specified time is determined, and the percentage pressure fluctuation is defined as half the peak-to-trough pressure variation, Δ p.

$$\text{percentage pressure fluctuation } \tilde{\psi} = \tfrac{1}{2} \ (\Delta p/p) \times 100\%.$$

WITH PULSATION TRACES

TEST NO.	UNCASED ROTOR	B31	B12	B51
MAX. FOURIER COEFFICIENT	6679	23	1553	495
% RPS OF MAX. F.C.	6	6.4	21.4	20
$\bar{\Psi}$ %	89	14.7	68.3	32.3
ϕ	-	0.54	0.92	0.43
Ψ_{ST}	-	1.95	0.0	2.17
η_T%	-	37	Low	32

Table 7.1

This method has the advantage of giving single value results at each flowrate and makes the term most useful for comparing the stability of different fan types. $\tilde{\psi}$ is found readily, is robust (less than $\pm$ 10% error) and quantifies a physically sensible phenomenon. However, the measure is relatively insensitive and its' simplicity is gained at the expense of information on the nature of the pulsations.

One other time-domain analysis adopted was to determine the autocovariance function of a digitised signal. This procedure looks at neighbouring points on a trace, separated by various lags, and as with simple covariance picks out mutual trends. Autocorrelation coefficients are calculated by computing the series of autocovariance coefficients, and these are interpreted on a correlogram. Under correct conditions the correlogram is able to distinguish well-defined low frequencies. The analysis was applied to about 40 traces, but was unable to isolate any frequencies which could be regarded as significant.

7.3.2 ANALYSIS IN THE FREQUENCY DOMAIN.

The pressure-time trace is digitised using about 310 points; for a scan time of 6 seconds or more, this gives a Nyquist frequency well above the range of interest. The digitised signal is initially analysed using two independent procedures.

7.3.2.1 PERIODOGRAM.

The periodogram is a discrete Fourier transform of the autocovariance function. It transforms the signal into the frequency domain, the relative intensity of each frequency being expressed as a Fourier coefficient, a dimensionless term.

The periodogram is smoothed to exclude ghost frequencies and help isolate the important dominant frequencies. Further elaborations are included to filter drift, trim harmonics and magnify low intensity, higher frequency noise.

7.3.2.2 $\hat{F}(w)^{e}$ FREQUENCY ANALYSIS.

This method is used as a check to the periodogram analysis. It is a transform of a truncated autocovariance function, a method which makes use of an assumed waning correlation between points at increased lags. Closer points have a higher weight and all values outside a certain 'window' are zero-weighted, implying independence between these points.

7.3.2.3 ACCURACY AND REPEATABILITY.

Only frequencies determined by the smoothed periodogram, filtered periodogram and the $\hat{F}(w)$ periodogram approximation are considered to be significant. The analysis itself is inherently accurate; a test signal containing a predominant high frequency pulse was analysed to check the periodogram estimation procedure, the agreement was within 3% of the true frequency.

Unfortunately the behaviour of the pulsations is not as reliable as the pulsation analysis procedure. Pulsation frequencies and amplitudes are transient in nature and the analysis procedure is, ultimately, only as reliable as the representativeness of the trace. Figure 7.6 illustrates this temporal variation, the two plots are periodograms of different representative traces, taken under identical conditions and separated only in time.

e Pron. "F-CAP OMEGA"

A frequency analysis itself supplies much information on the nature of the pulsating flow. Flaws in the procedure stem from the temporal predictability of the pulses not being commensurate with the accuracy of analysis. Figure 7.7 and Table 7.1 illustrate the sensitivity of the procedure to what are superficially only small changes in the percentage pulsation.

So, although a frequency analysis is more refined, it is arguable whether, for a single case, the procedure yields any more technically useful information than a percentage pulsation.

7.4 CHARACTERISTICS OF CROSS-FLOW FAN PULSATIONS.

7.4.1 SIGNAL COMPOSITION.

It was mentioned previously that the pulsations tend to vary in amplitude and frequency with time. This variation is not merely non-stationarity but also includes a fundamental variation in the nature of the pulses. Non-stationarity is represented by the periodogram as 'drift'; very low frequency pulsations say, ~ 5% RPS.

BUSH (13) states that a reduction in flow from the maximum static pressure point results in a periodic pumping of random intervals up to several seconds. Although the illustrated drooping characteristic suggests surging rather than the inherent flow-field instability, it is interesting to note the duration of the pulse period and the random nature of these low frequencies. Frequency analysis by the author has generally established the existence of one or more predominant frequencies apart from drift. For one fan type

the pulsations are not random, although they are indeterminate in the sense of being unpredictable, Figure 7.8 illustrates the incidence of occurence of various frequency components. Apart from drift and a low peak around the rotational frequency, the pulsation frequencies are largely randomly distributed, with a preference to frequencies less than 50% RPS.

An attempt to isolate individual pulsation frequencies was also made on the 0.625 metre diameter fan in the department. The procedure adopted was a 'phase-lock loop system', which tracks from high to low frequencies 'locking' into dominant frequency components. The method failed to isolate BPF fundamentals but picked up a peak at the rotational frequency. The system also locked into a number of distinct frequencies below 45% RPS; which is in agreement with results from the periodogram analysis. A common feature observed using this procedure was a 'locking-in' to a frequency for several seconds before losing it altogether. This demonstrates one of the difficulties of analysing a time-transient signal.

Only in rare cases, (e.g. with a completely uncased rotor), did the pulsation trace transform into a single frequency, more often dominant components are obscured by other effects such as drift and recovery of stability. Recovery of stability is an oscillatory variation of pressure following large pressure pulses. Figures 7.9(a) and 7.9(b) illustrate this phenomenon, the latter signal exhibiting

secondary recovery. Transformation of such signals yields periodograms which, due to this relatively rapid oscillatory motion, display boosted high frequency 'noise'.

7.4.2 DEPENDENCE OF STABILITY UPON AERODYNAMIC PARAMETERS.

7.4.2.1 DEPENDENCE UPON FLOWRATE.

An approximate relationship between percentage pulsation and flowrate is expressed by the least-square-fit polynomial in Figure 7.3. This illustrates less stable conditions at extreme flowrates. The three flowrates; $\phi = 0.4$, $\phi = 0.6$ and $\phi = 0.8$ were chosen as conditions for determining the relationships between operational stability and fan design. Figures 7.11(a) to 7.11(m) indicate that conditions are generally most stable for $\phi = 0.6$, regardless of fan design.

Any simplified relationship between flowrate, stability and fan design may be misleading if it neglects the localised peaks of instability mentioned in Section 7.3, (Figure 7.4). These peaks may be narrow or broad; they have been detected in about 25% of cases, but the occurence may be more common if very localised peaks have been missed. It is not possible to draw any definite conclusions between flowrate and stability, but the pulsation level should always be checked to ensure the operating point does not lie within a zone of locally increased percentage pulsation level.

Figure 7.8 indicates a trend favouring increased high frequency pulsations for ϕ approx. = 0.5 and increased low frequency pulsations at reduced flowrates.

7.4.2.2 DEPENDENCE UPON EFFICIENCY.

Figures 7.10(a) to 7.10(c) indicate that there appears to be little or no correlation between operational stability and efficiency.

A strong dependence between these parameters would not be expected as their levels are governed by quite different processes. The correlation appears to be strongest at the highest flowrate (ϕ = 0.8), indicating static pressure pulsations related to frictional loss and the level of flow turbulence. For this reason the flowrates, in pulsation analysis, may be better represented as a percentage of ϕ max.

7.5 EFFECT OF ROTOR AND CASING DESIGN ON THE PERCENTAGE PRESSURE PULSATIONS.

The following experimental analysis is not concerned primarily with increasing the stability of the fan, rather in establishing relationships between stability and fan design. The relationships discussed are illustrated in Figures 7.11(a) through 7.11(m), respectively.

7.5.1 INFLUENCE OF PRIMARY CASING DESIGN ON STABILITY.

7.5.1.1 VORTEX WALL CLEARANCE, (E).

There is a consistent decrease in stability with increasing E for ϕ = 0.6 and ϕ = 0.8. For ϕ = 0.4 the lowest pulsation level occurs at the largest clearance.

Stability at the two higher flowrates may be regarded as substantially invariable in the range $1\% \leq E/D \leq 5\%$.

7.5.1.2 REAR WALL CIRCUMFERENTIAL ANGLE, (δ).

There is a small but consistent decrease in stability with increasing δ. For ϕ = 0.6 the pulsation level rises linearly from 6.5% to 8.5% between $\delta = 0^{\circ}$ and $\delta = 60^{\circ}$. This trend is reflected at the other two flowrates.

Assuming that increasing δ only affects the flow field locally, the result indicates a relationship between conditions towards the rear of the suction arc and stability. This may be due to unstalling a section of the suction arc blade rows. PORTER AND MARKLAND (63) tried to improve stability by installing an inlet guide vane, located to the rear wall side of the suction arc. They claim a great improvement in stability, with a modest improvement in performance and efficiency.

7.5.1.3 DUCT HEIGHT, H.

Decreasing H reduces the volute enclosed volume and improves the stability at ϕ = 0.4. This relationship is not reflected at ϕ = 0.6 or ϕ = 0.8, where the pulsation levels are found to be tolerable in the design range $70\% \leq H/D \leq 85\%$. If flow conditions within the volute are poor, the operational stability is likely to be impaired.

7.5.1.4 VORTEX WALL DECLINEATION, B.

This is the most important single casing parameter, increasing B within a certain range greatly improves the performance characteristic. Thus, the value of B will be determined more by performance than stability.

However, for ϕ = 0.6 and ϕ = 0.8 the stability also increases considerably with increasing B. For ϕ = 0.4 a minimum pulsation level occurring at B/D = 23% is indicated from the three points.

7.5.1.5 DIAMETER RATIO, d/D.

For ϕ = 0.6 and ϕ = 0.8 the pulsation levels are reduced monotonically with decreasing d/D; to below 5% for d/D $<$ 72.5%. All other major design ratios are constant, so the result indicates a strong dependence of flow stability on diameter ratio.

7.5.1.6 REAR WALL CLEARANCE, E2.

The pulsation levels are a function of too many other variables for any consistent relationship to be established.

Optimum rear wall clearance will not be determined by pulsation levels. E2 should be chosen for best efficiency operation and this itself should ensure reasonable stability. No results are given.

7.5.2 INFLUENCE OF NOVEL CASING DESIGN ON STABILITY.

7.5.2.1 TONGUE THICKNESS, T.

The results indicate, for all flowrates, a decrease in stability for T/D $<$ 1.5%. The optimum thickness appears to be T/D = 3%, but levels are acceptable in the range 1.5% $\leq$ T/D $\leq$ 5%.

7.5.2.2 IRREGULAR BLADE SPACING.

Pulsation levels are increased by having blades at various radii, although only by a small amount for ϕ = 0.6. At more extreme flowrates, at least, the results demonstrate the importance of good manufacture to stability. A single blade offset by N% gives less stable conditions than a number of blades randomly offset by a maximum of N%.

7.5.2.3 INCORRECT REAR WALL DESIGN.

Incorrect rear wall design has more of an effect on aerodynamic performance than stability. There is no significant decrease in stability by incorporating a non-optimum rear wall profile.

The apparent large decrease in stability at ϕ = 0.8 is more a result of the flowrates being different fractions of their respective maximum flowrates.

7.5.2.4 SLOPING THE VORTEX WALL.

The pulsations are consistently lowest with a flat, unsloped vortex wall. Longitudinal sloping of the vortex wall causes only small increases in instability, whereas radial sloping greatly reduces the stability of the flow field, especially at ϕ = 0.4. This reflects the aerodynamic performance relationship.

7.5.2.5 WEDGE ANGLE, α°.

For all flowrates tried a maximum pulsation level occurs with a wedge angle of approximately $\alpha = 12.5^{\circ}$. The most stable condition occurs where there is no wedge, although for $\alpha = 25^{\circ}$ the stability is only marginally decreased. The wedge length is 75% of the outer diameter.

7.5.2.6 PERFORATED VORTEX WALL.

It was hoped that perforating the vortex wall would improve stability by equalising pressures immediately above and below the wall. ZIEHL-ABEGG (West German fan manufacturers) include a perforated vortex wall section in their designs, which they claim 'stabilises an area of turbulence, resulting in a stable laminar flow through the rotor'.

This claim is not substantiated by the results shown in Figure 7.11(1), which indicate a decrease in stability, at all flowrates, when using a perforated wall.

7.5.2.7 OUTLET DIFFUSER.

Results are available only for $\phi = 0.4$, and indicate a slight improvement in stability when using a diffuser with a diffusion angle of between 2.5^{o} and 5^{o}. This improvement is not reflected in performance.

The dependence is weak, no improvement would be anticipated because the internal flow pattern must remain unchanged.

7.5.2.8 'ECK'-TYPE VORTEX WALLS - AND A PLAIN WALL WITH AN ARCUATE DAMPER.

These two modifications to the plain wall are classed together because they both feature arcs which obscure part of the impeller circumference. The vortex walls cover mostly discharge arc and the damper a considerable portion of the suction arc.

The results show that stability is improved by incorporating an ECK wall and forming a fluid 'recirculation' zone. Stability is decreased using an arcuate damper.

The improvement in stability persists at all flowrates and for both B/D values, but is impressive at the lower vortex wall declineation. These results endorse those of ECK.

7.6 SECONDARY CONTROL OF OPERATIONAL INSTABILITY.

The previous section expresses the relationships between stability and fan design. It indicates certain configurations which should not be used and other configurations which achieve good stability.

Stability of the internal flow is not achieved absolutely; the complex nature of the flow field, governed by an eccentric vortex, causes an irregular pressure distribution and intrinsic instability.

Secondary measures, such as settling boxes and damping by impedence may improve conditions within a ventilation network. Stability is always enhanced by avoiding operation at extreme flowrates.

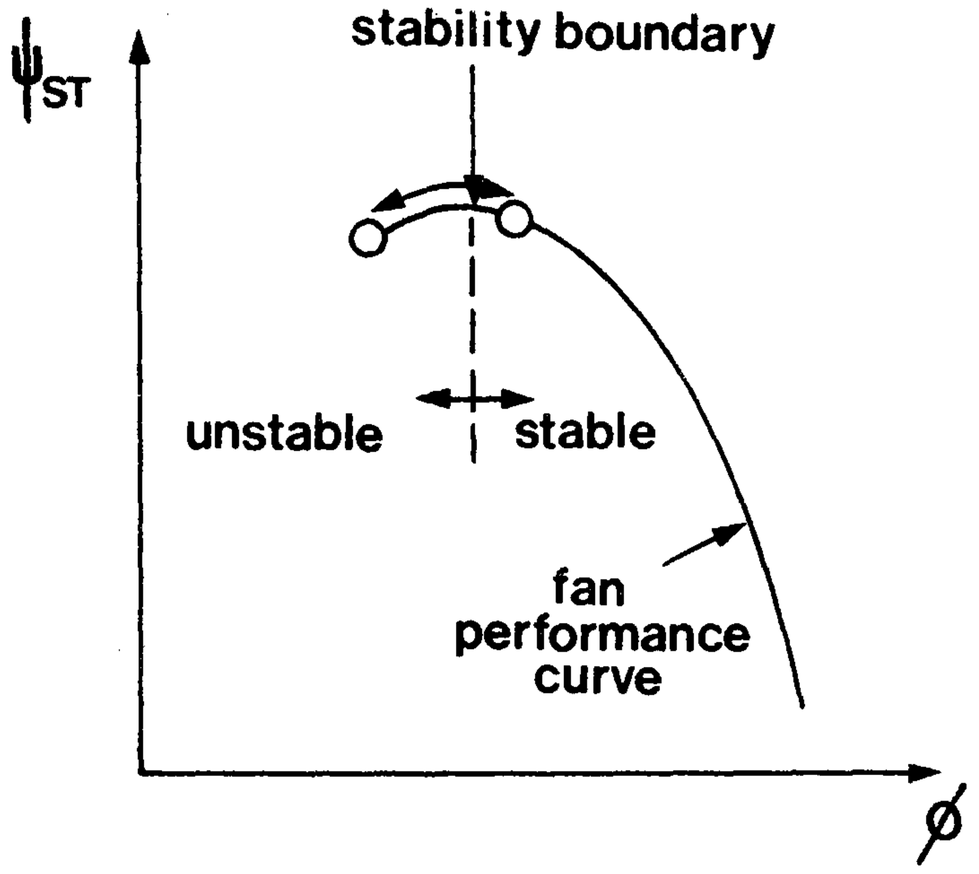

Figure 7·1

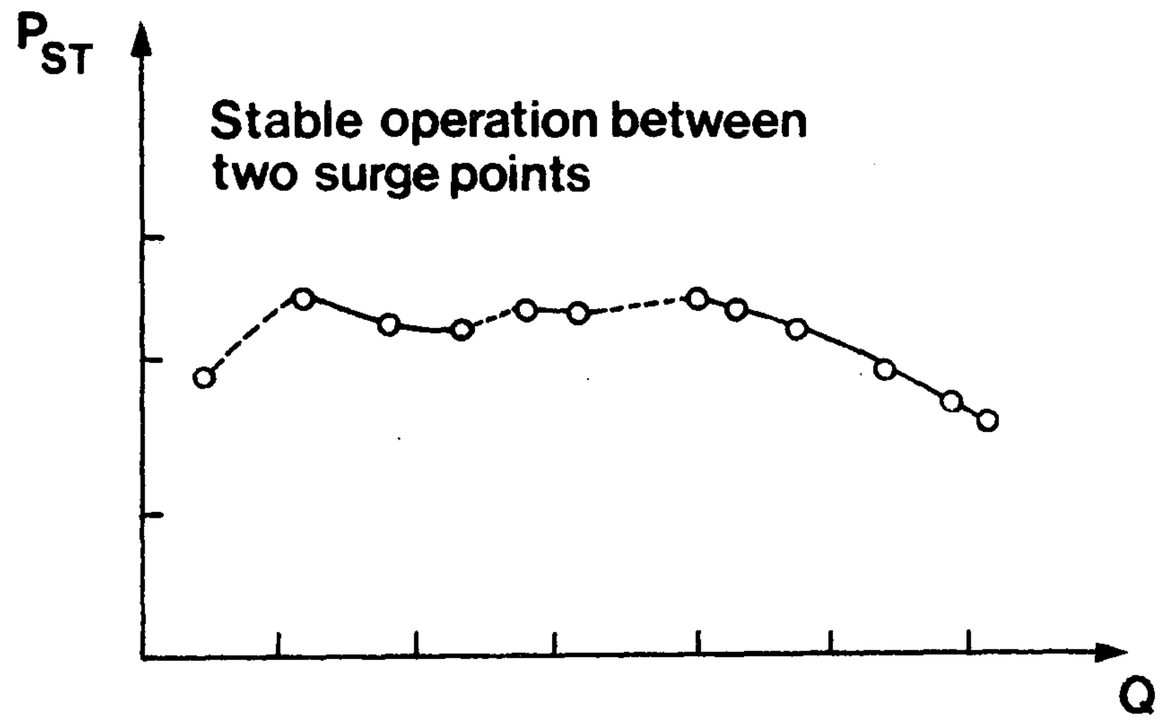

Figure 7·2

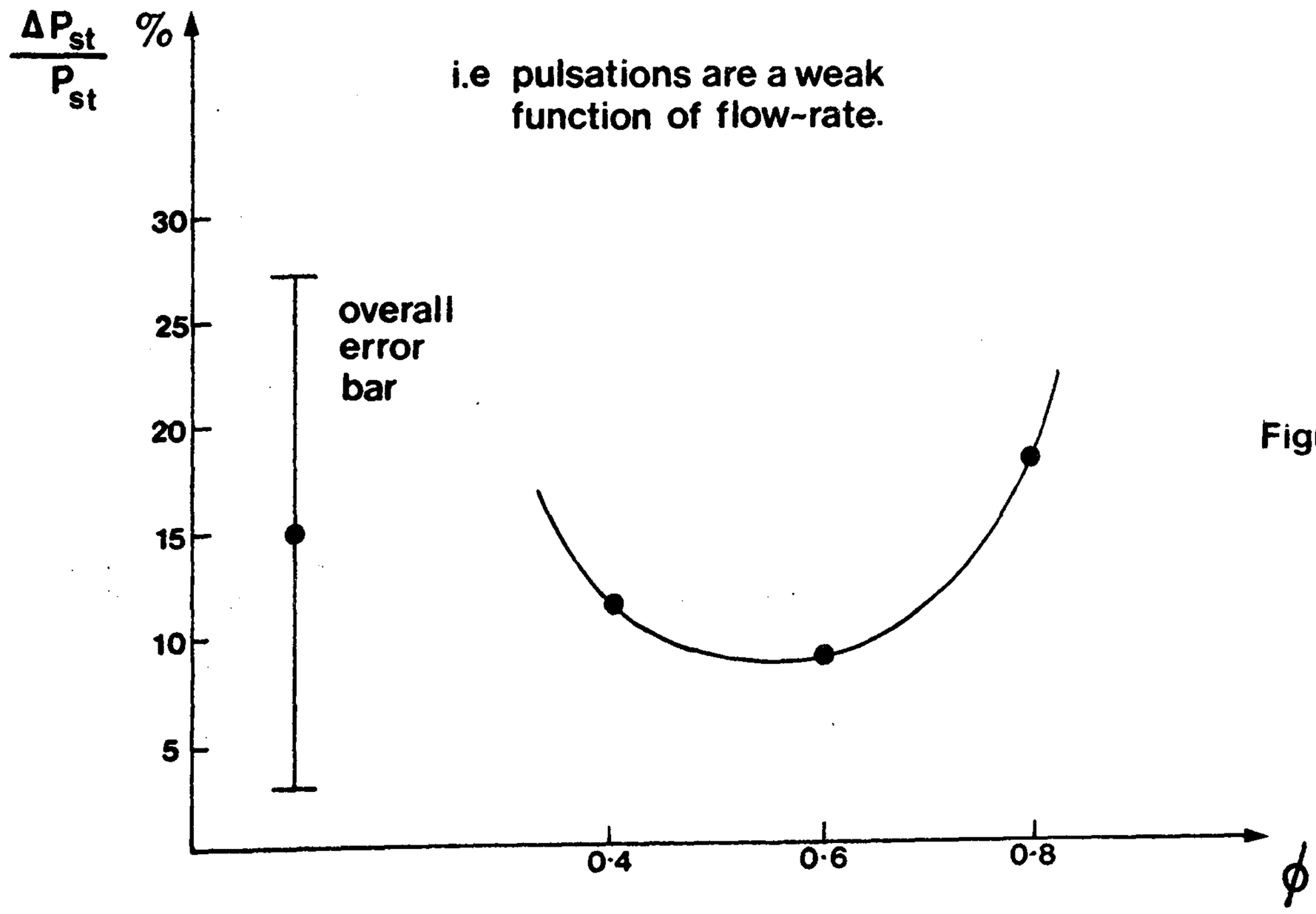

Figure 7·3

—second order least-square-fit polynomial

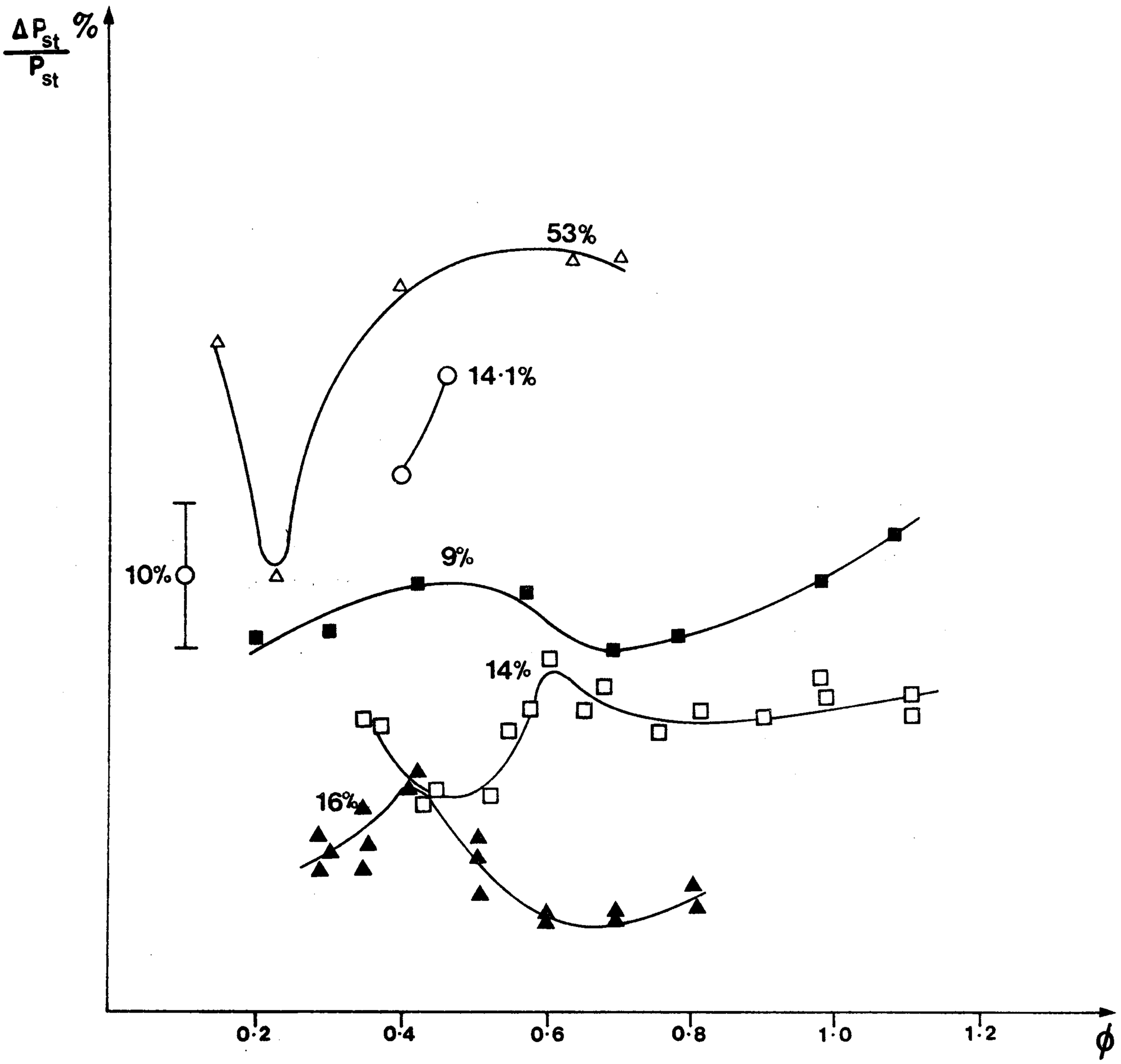

△ 200mm Diameter fan.

■ 150mm Diameter fan, $E_2/D = 20\%$.

□ 150mm Diameter fan, $E_2/D = 3{\cdot}3\%$.

▲ 625mm Diameter fan, internal traverse.

○ 200mm Diameter fan.

Figure 7·4

This graph illustrates the unpredictability of the behaviour of fan stability with flow-rate.

FIGURE 7.5 (a)

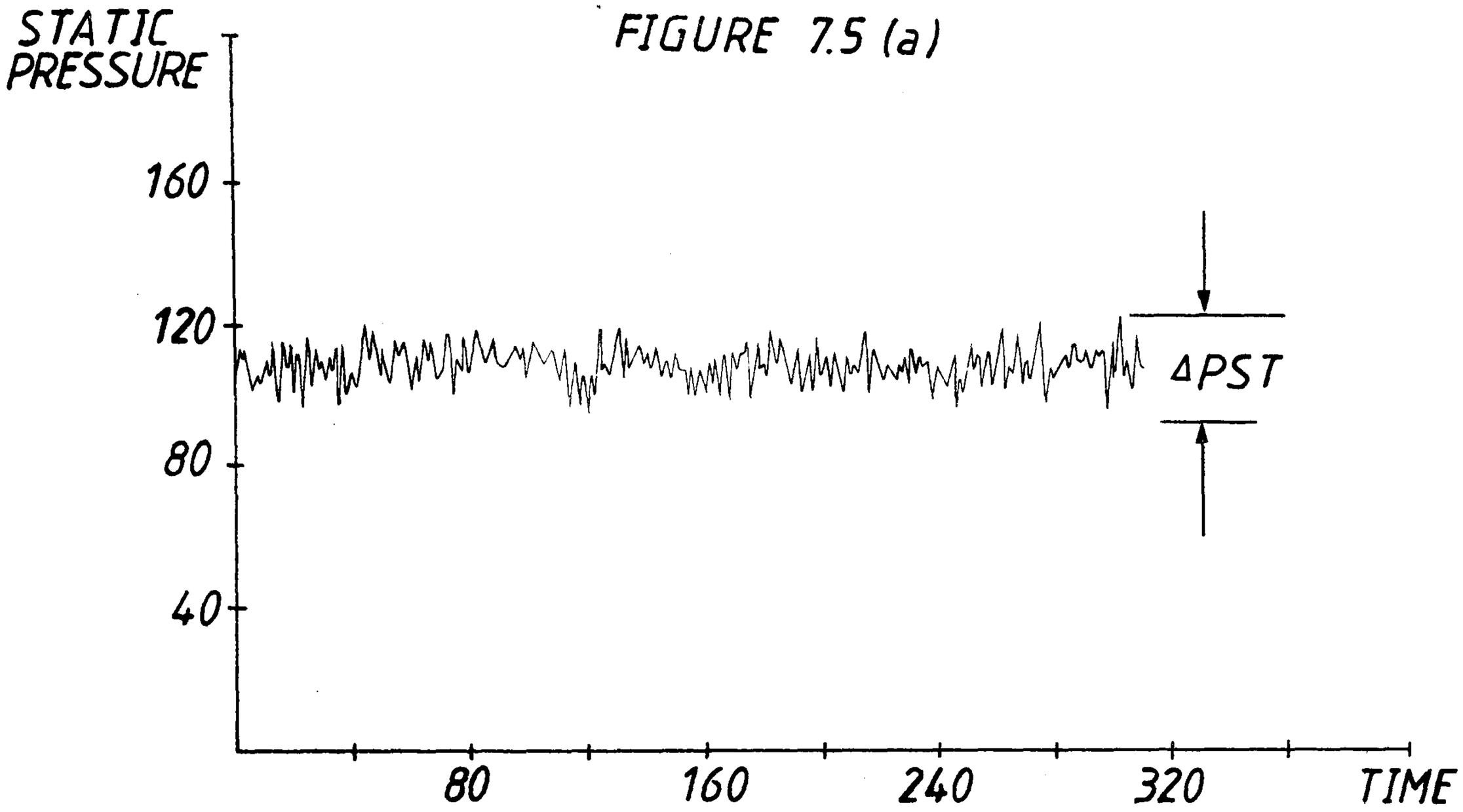

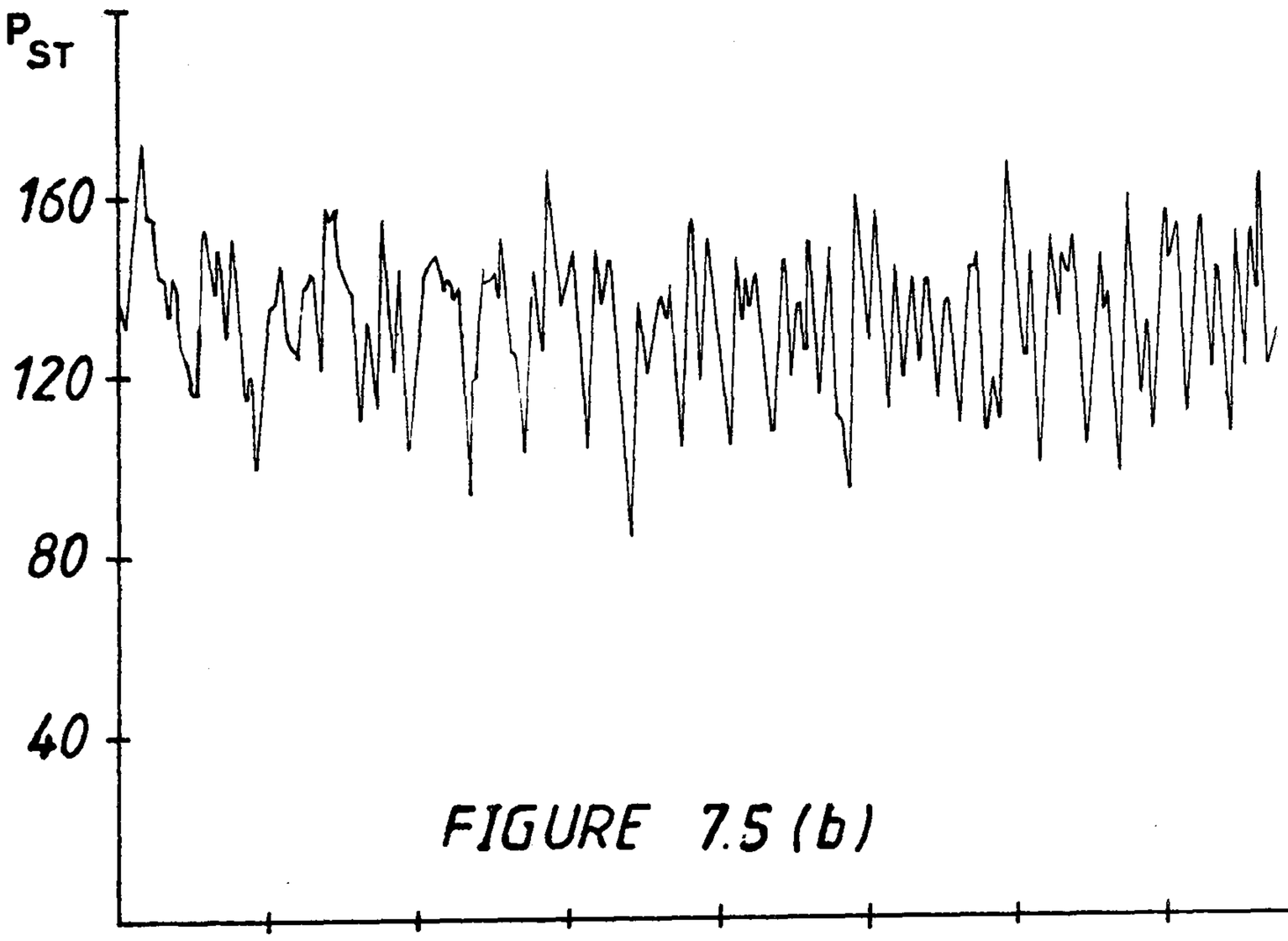

FIGURE 7.5 (b)

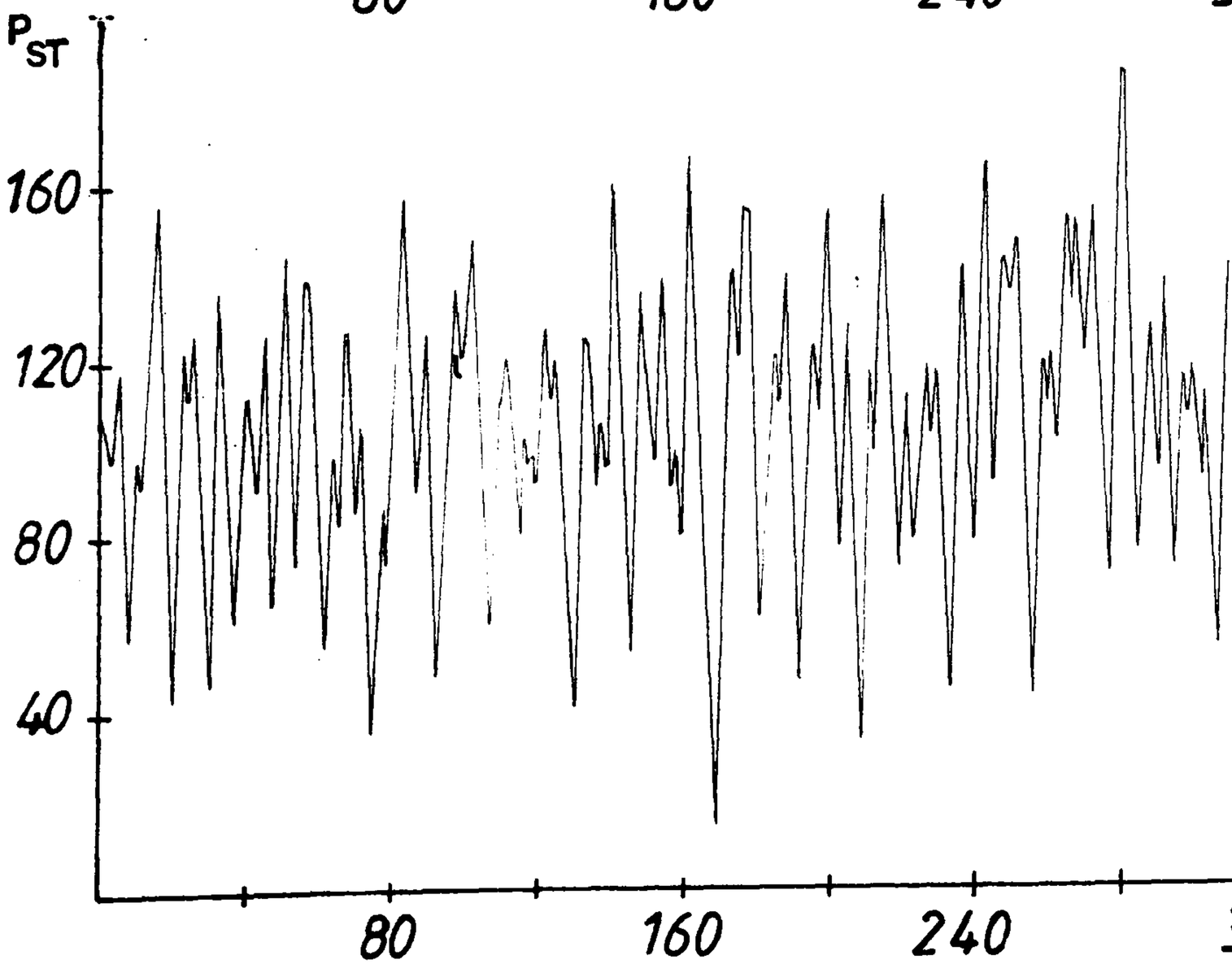

FIGURE 7.5 (c)

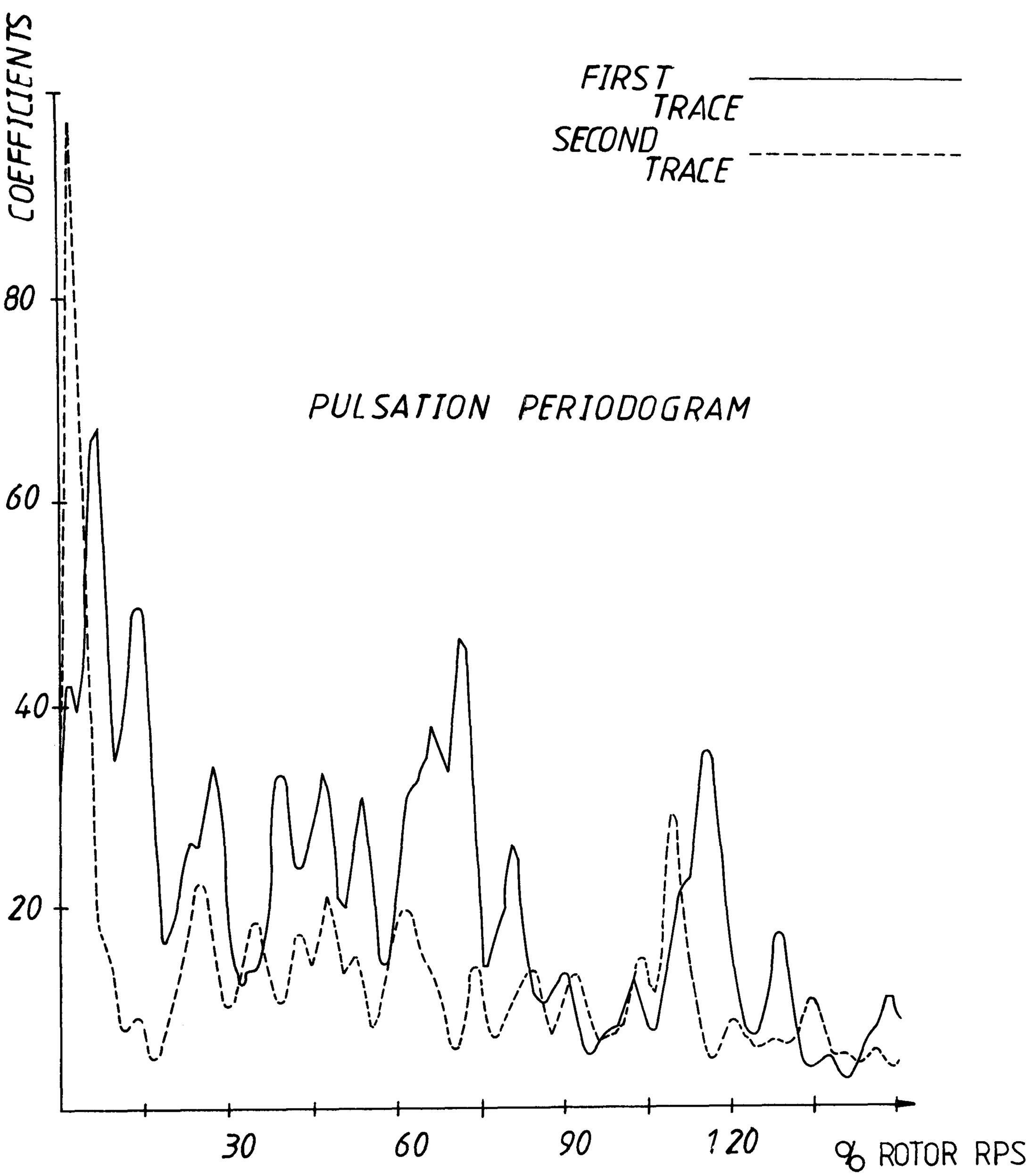

FIGURE 7.6

REPEATABILITY OF PULSATION TRACES.

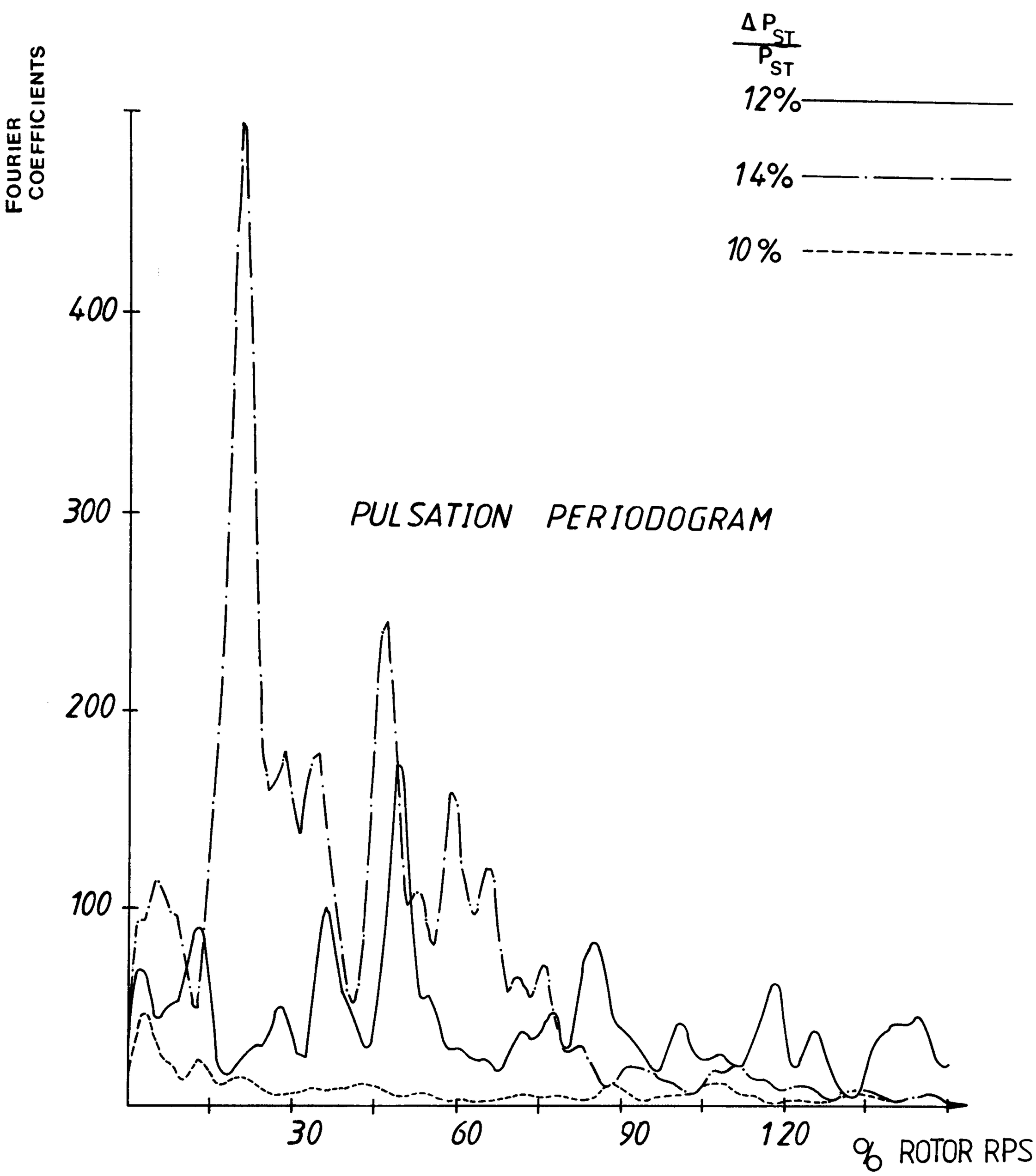
FOURIER COEFFICIENTS
400
300
200
100
PULSATION PERIODOGRAM
ΔP_SI / P_ST
12%
14%
10%
30
60
90
120
% ROTOR RPS

FIGURE 7.7

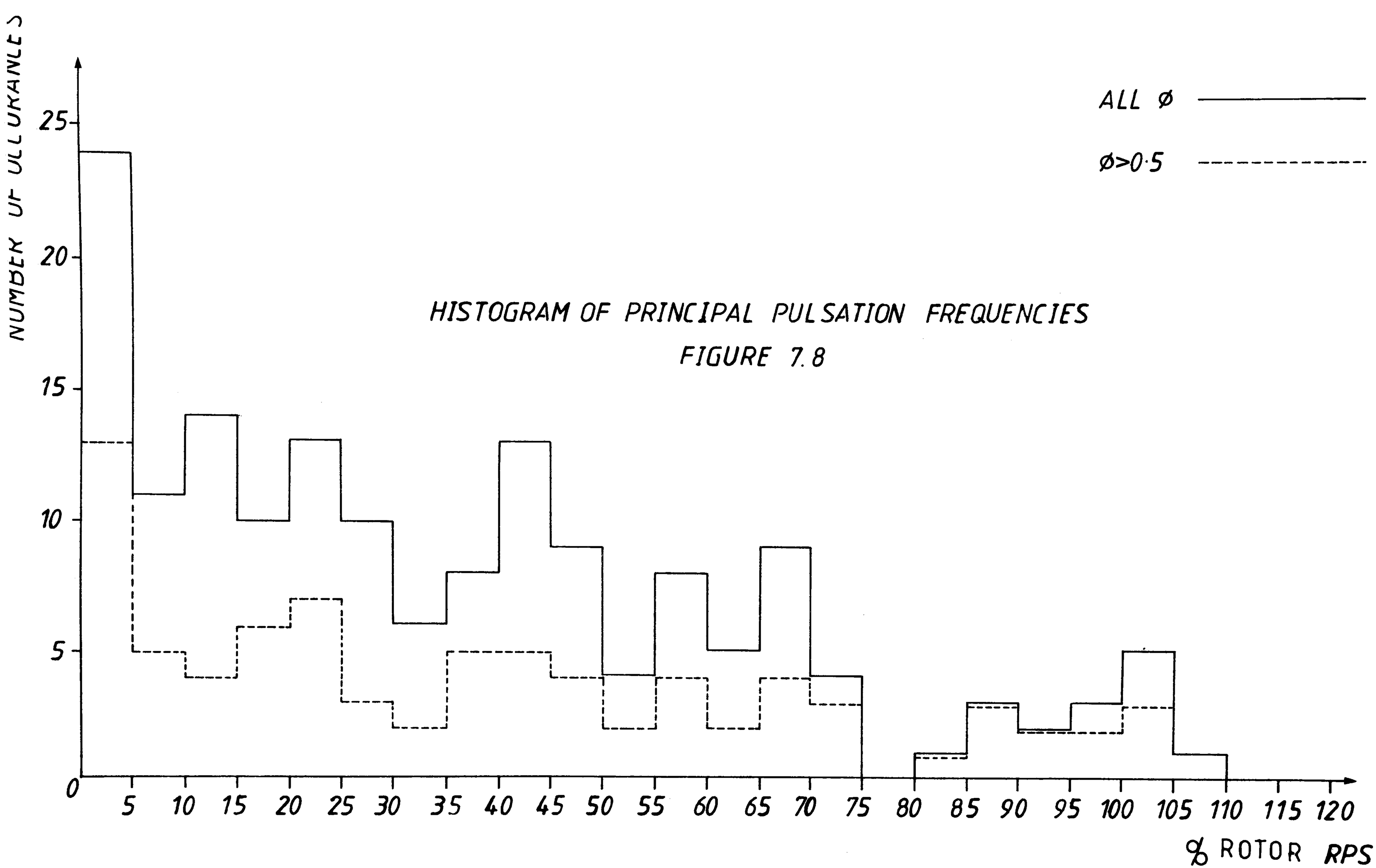

HISTOGRAM OF PRINCIPAL PULSATION FREQUENCIES

FIGURE 7.8

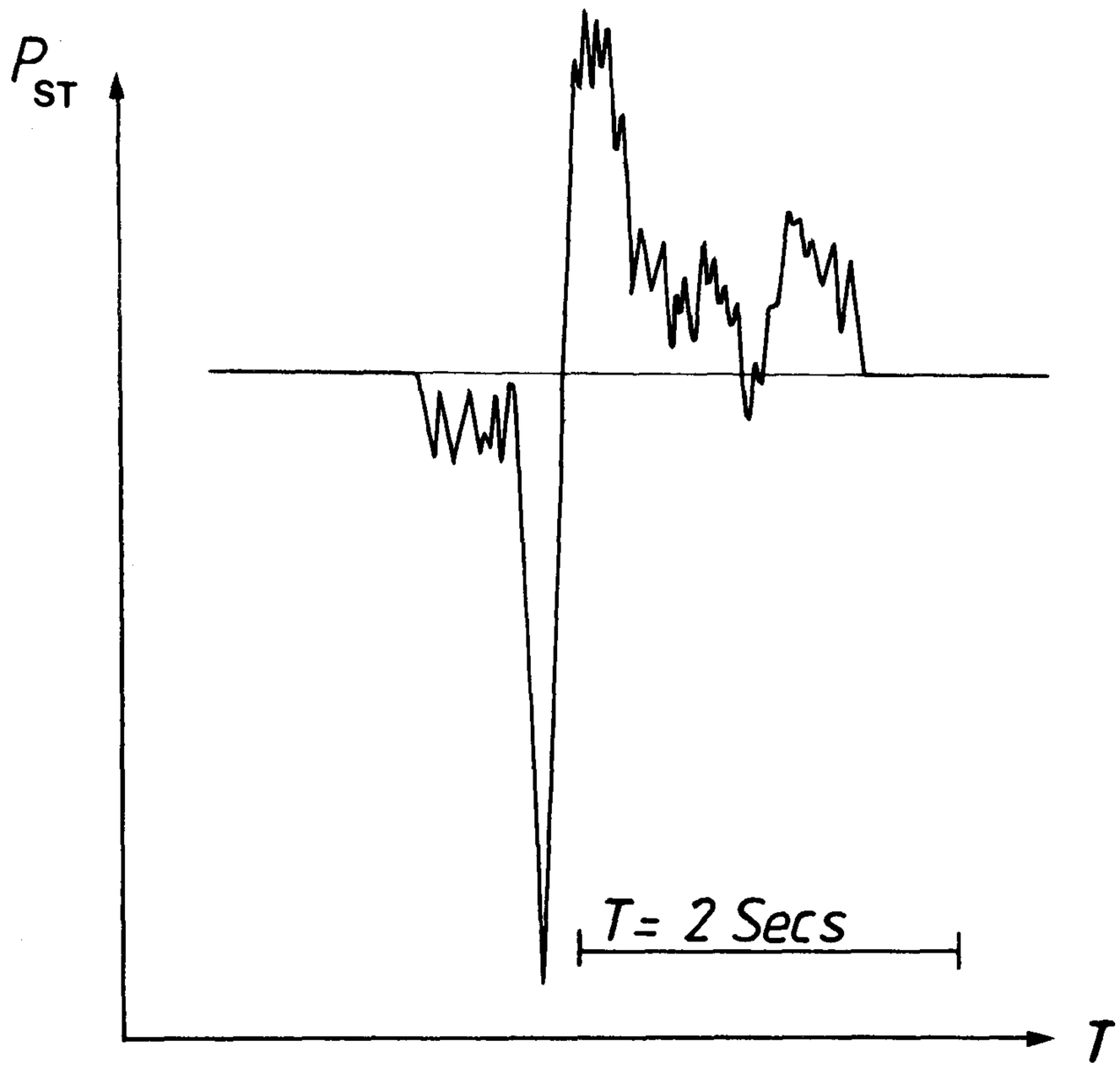

FIGURE 7.9 (a)

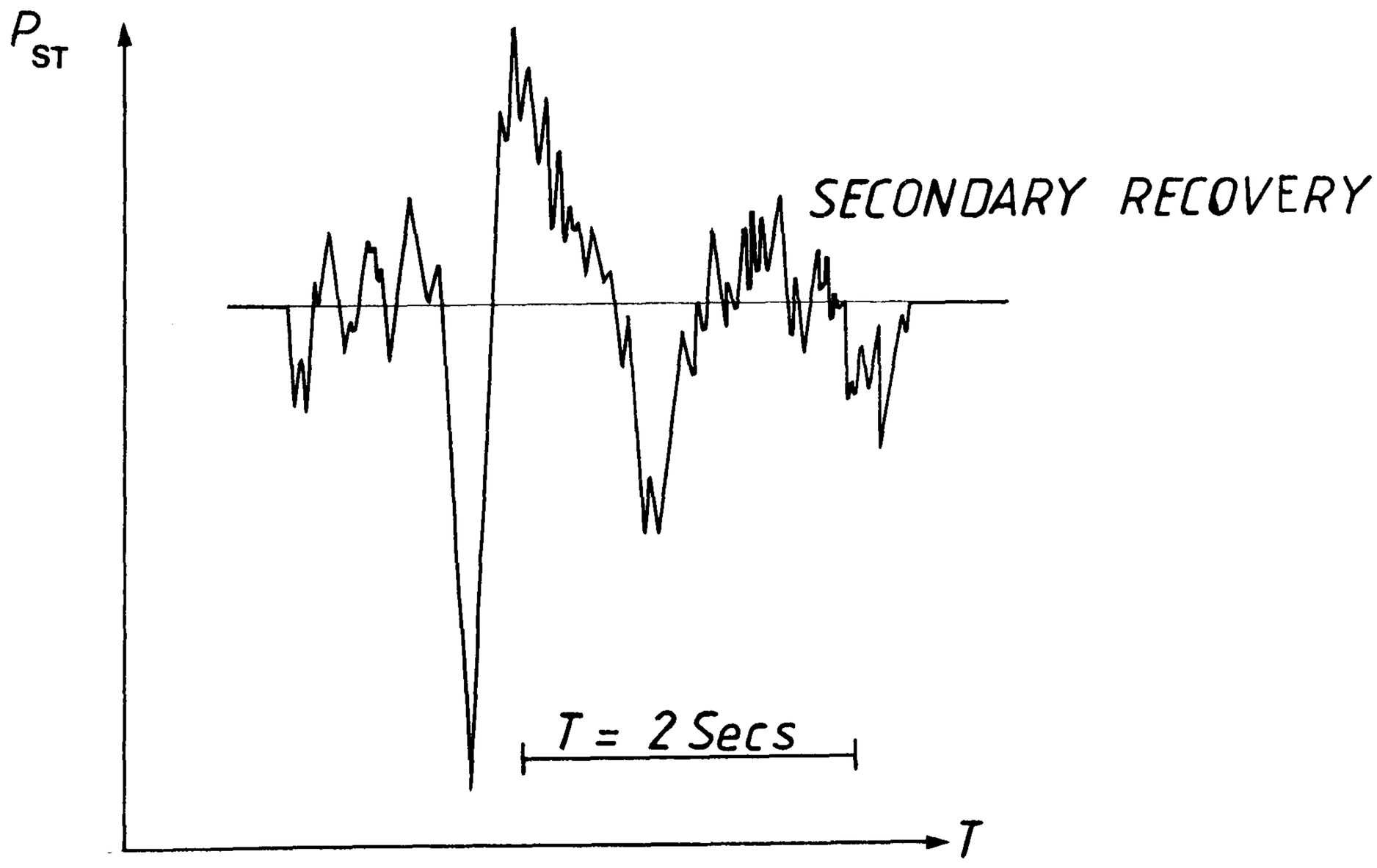

FIGURE 7.9 (b)

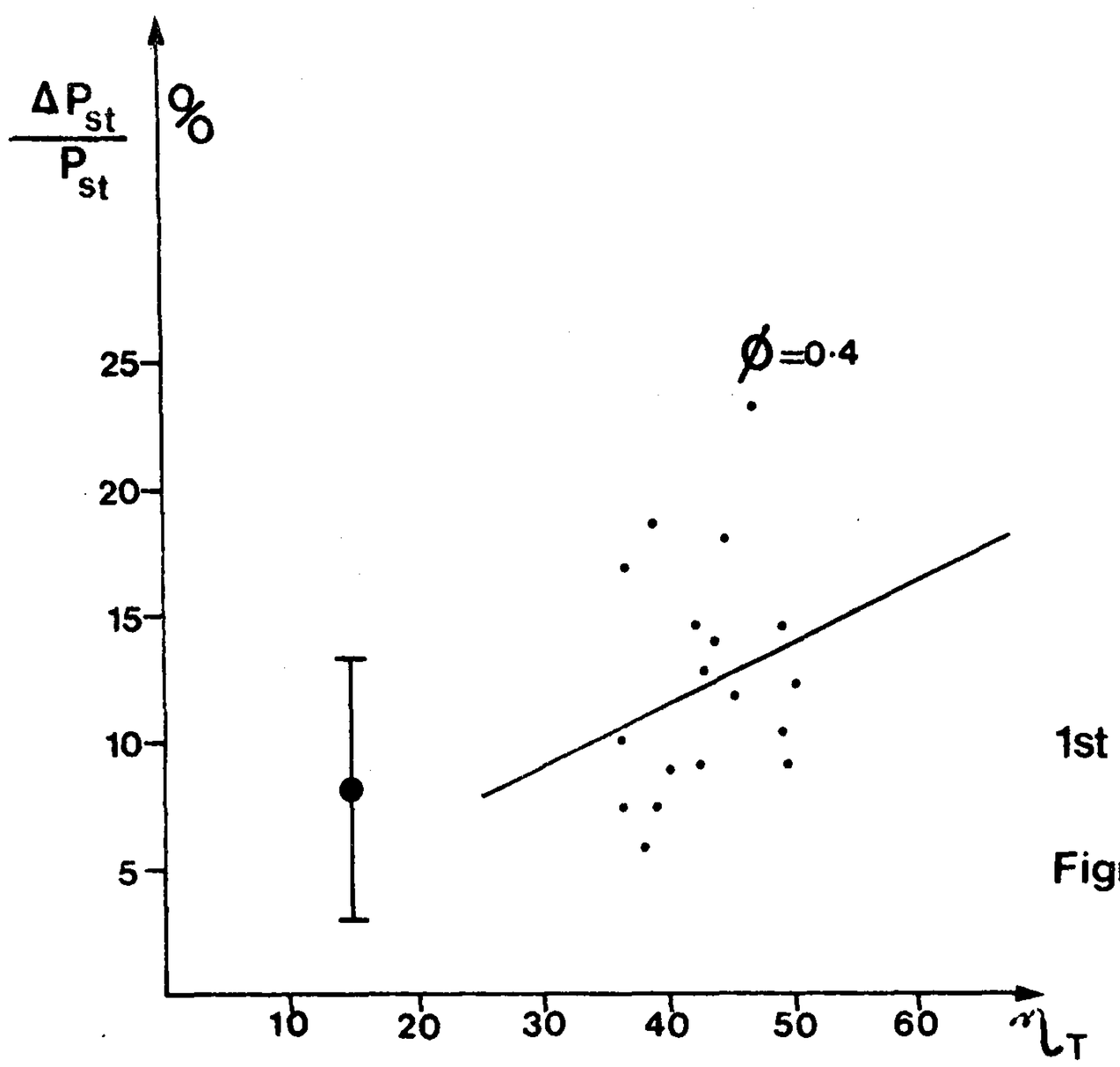

1st order polynomial fit

Figure 7·10(a)

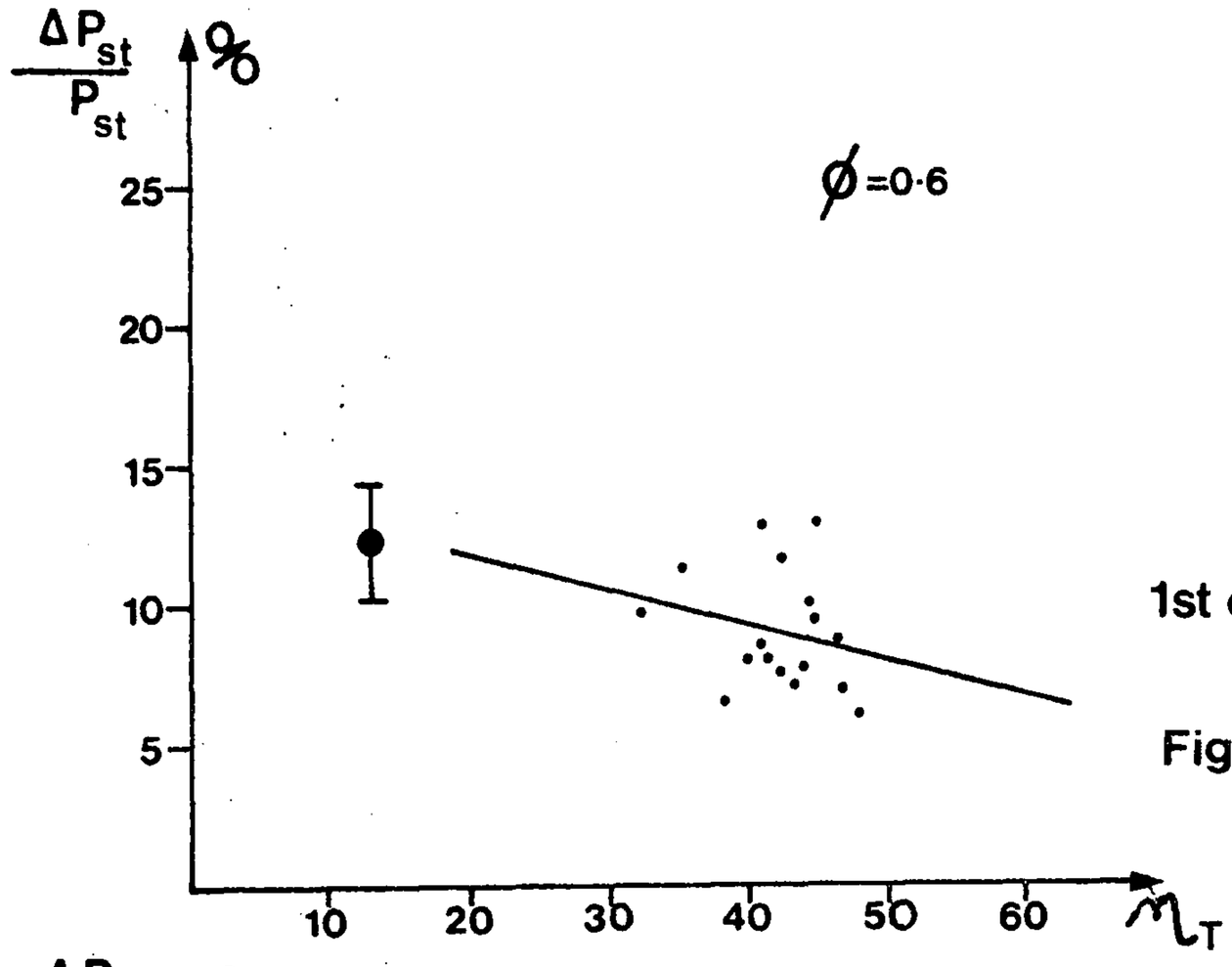

1st order polynomial fit

Figure 7·10(b)

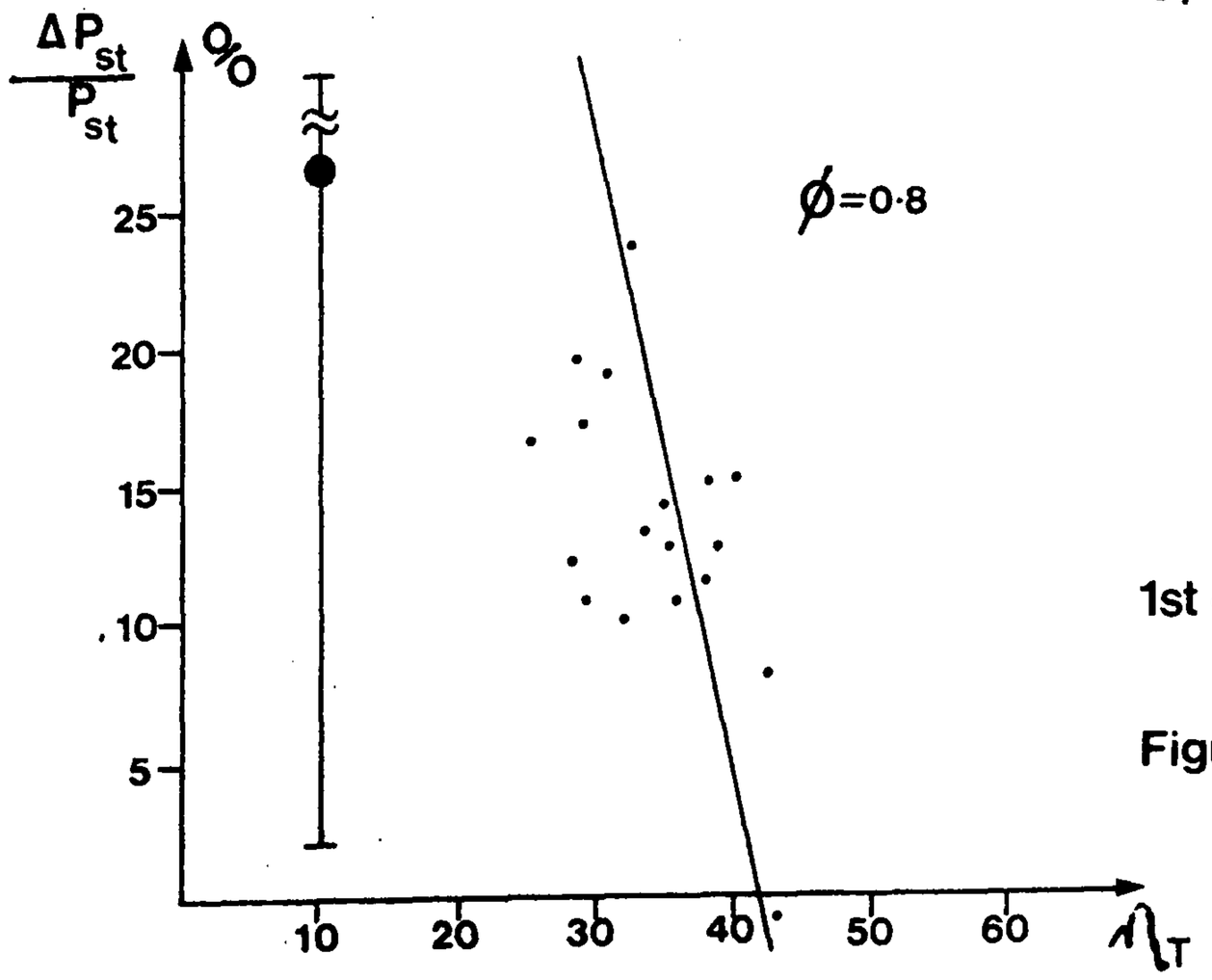

1st order polynomial fit

Figure 7·10(c)

RMS error bar

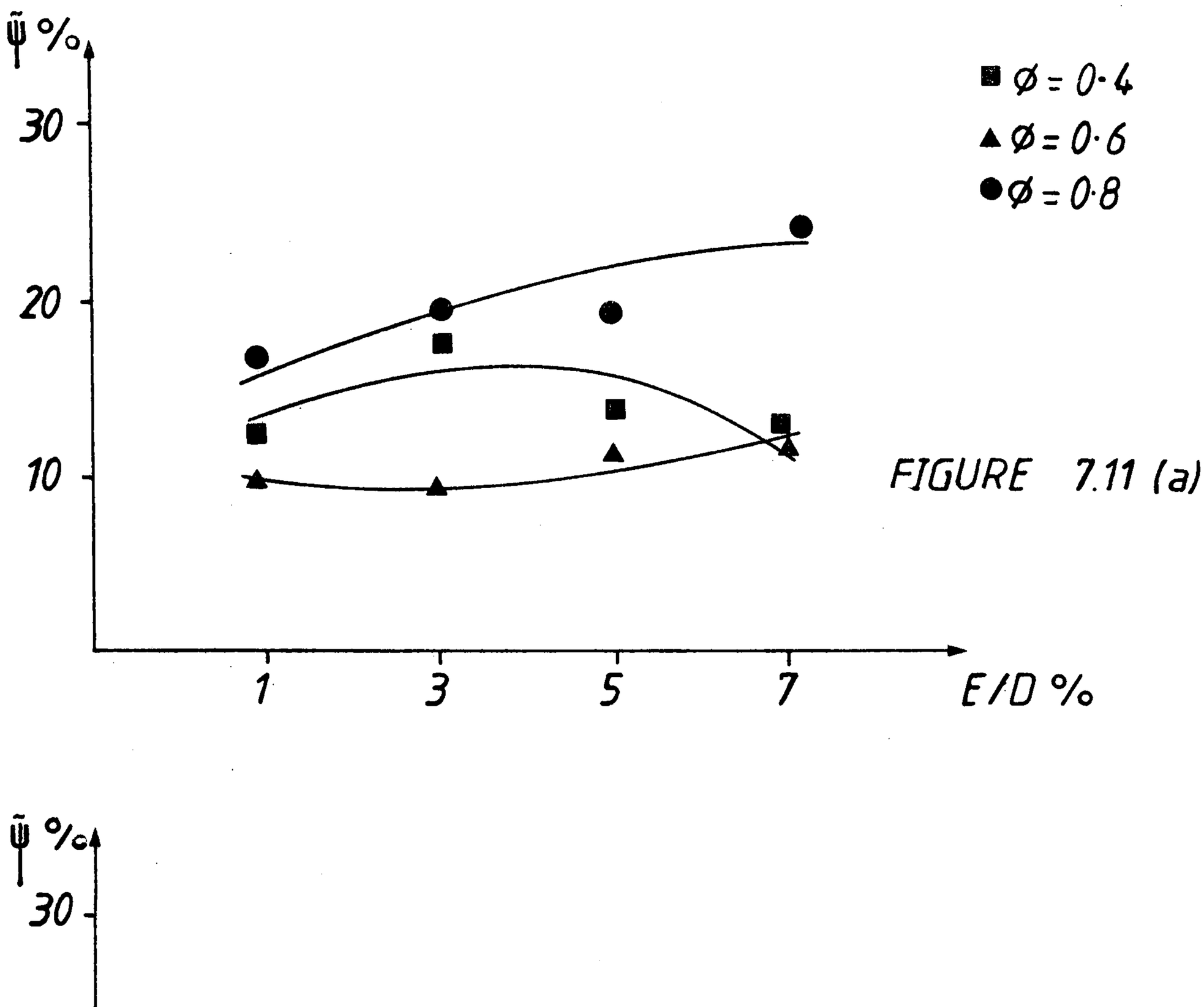

FIGURE 7.11 (a)

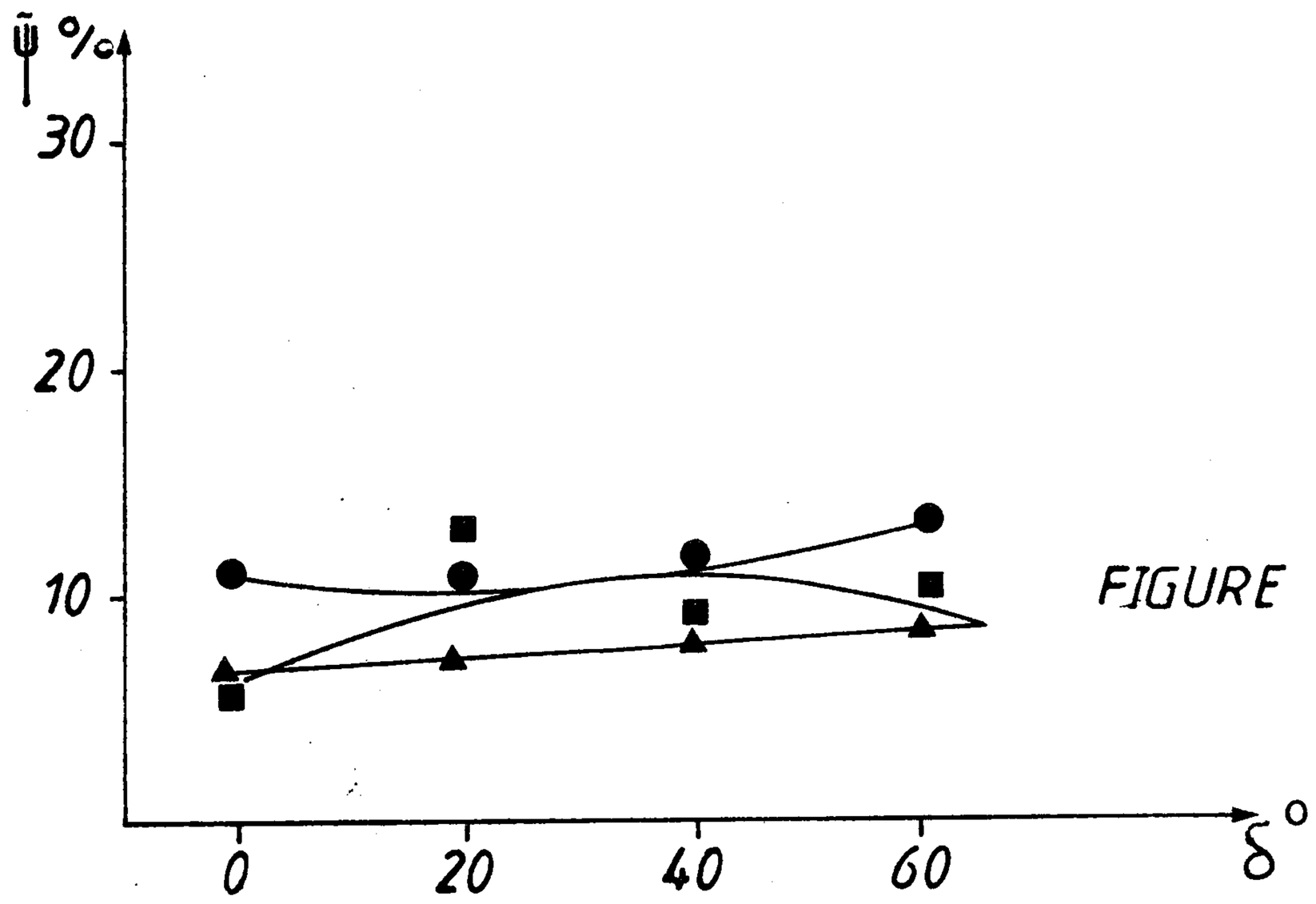

FIGURE 7.11 (b)

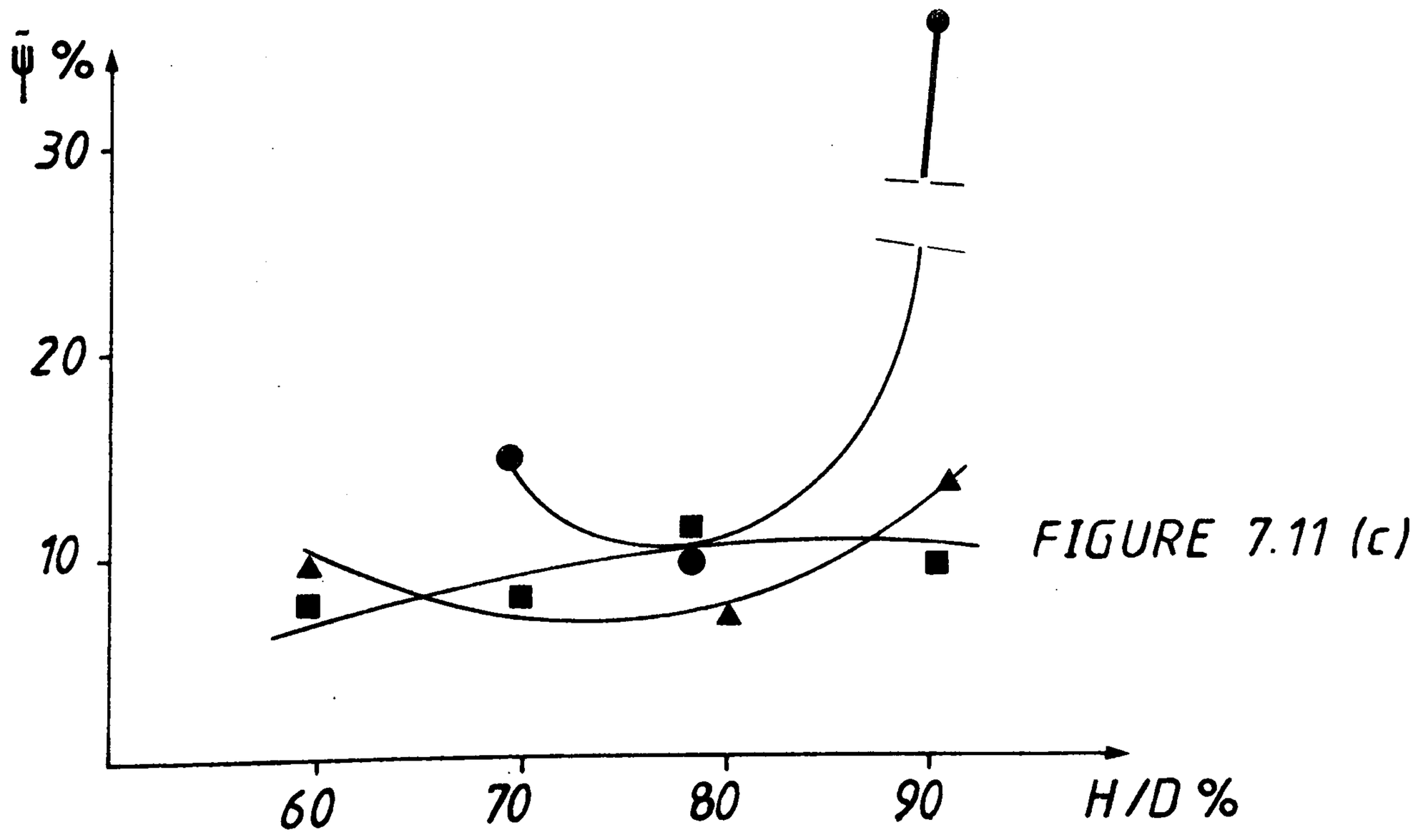

FIGURE 7.11 (c)

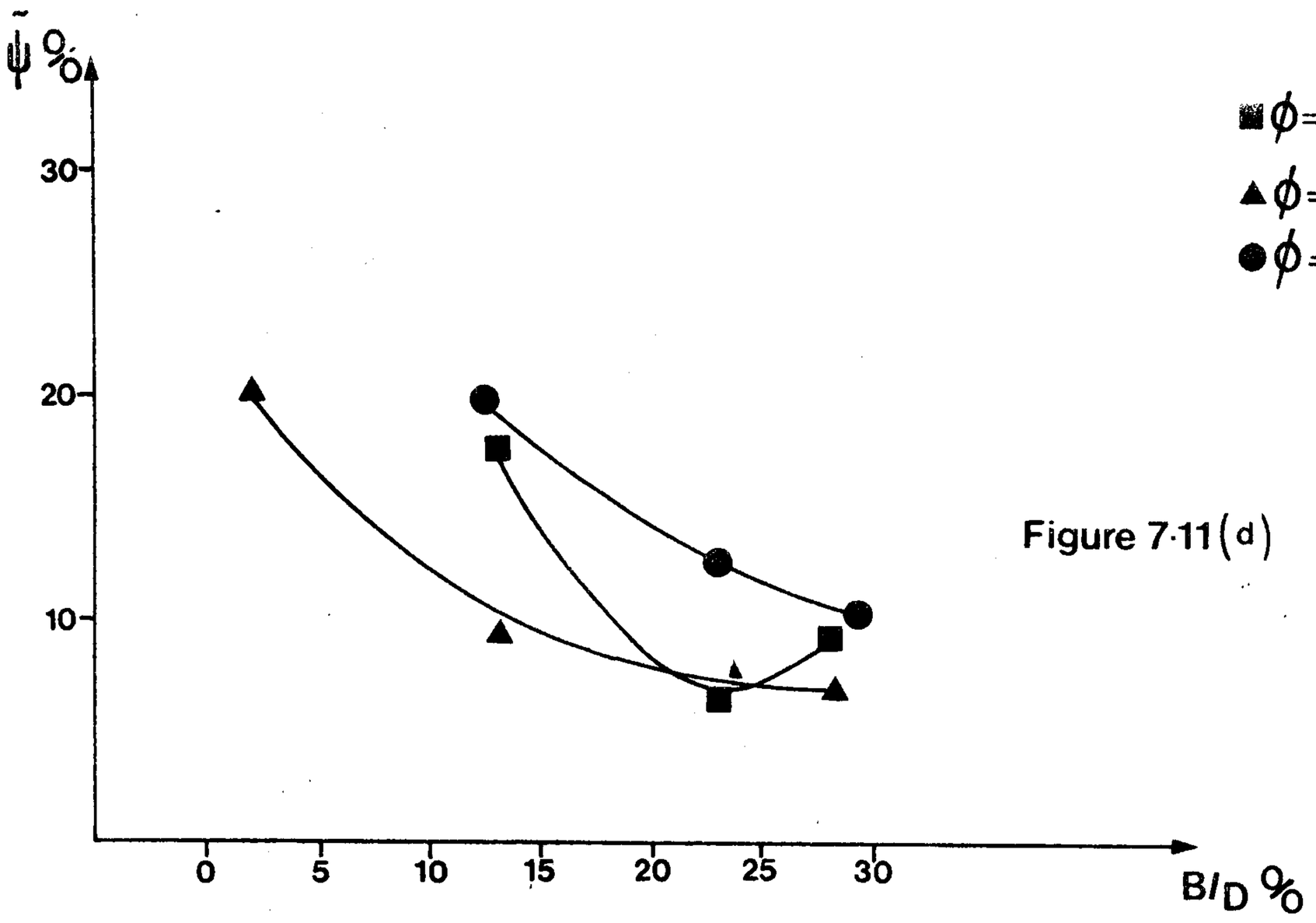

Figure 7·11(d)

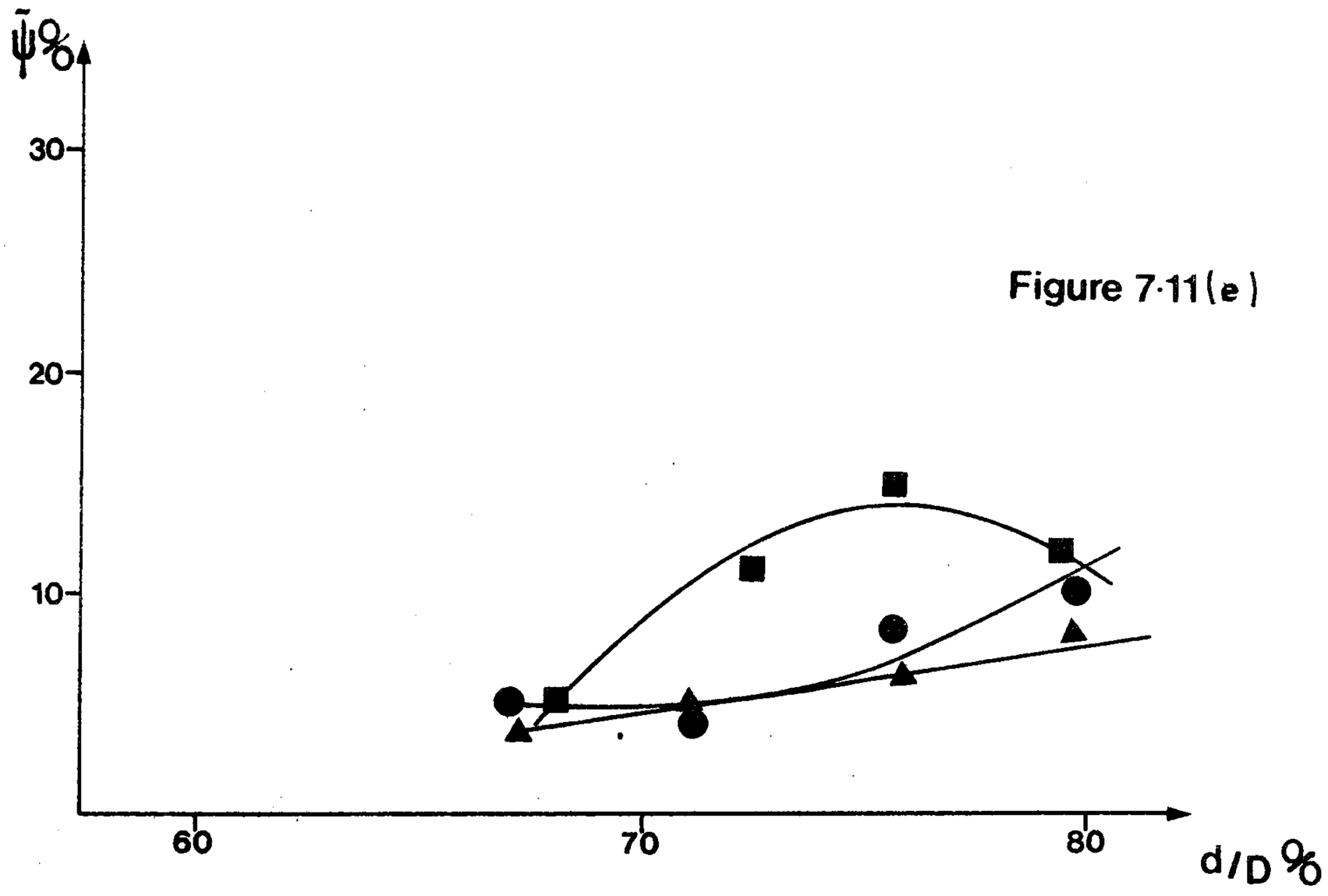

Figure 7·11(e)

An irregular function, E_2 should be determined optimally by aerodynamic performance.

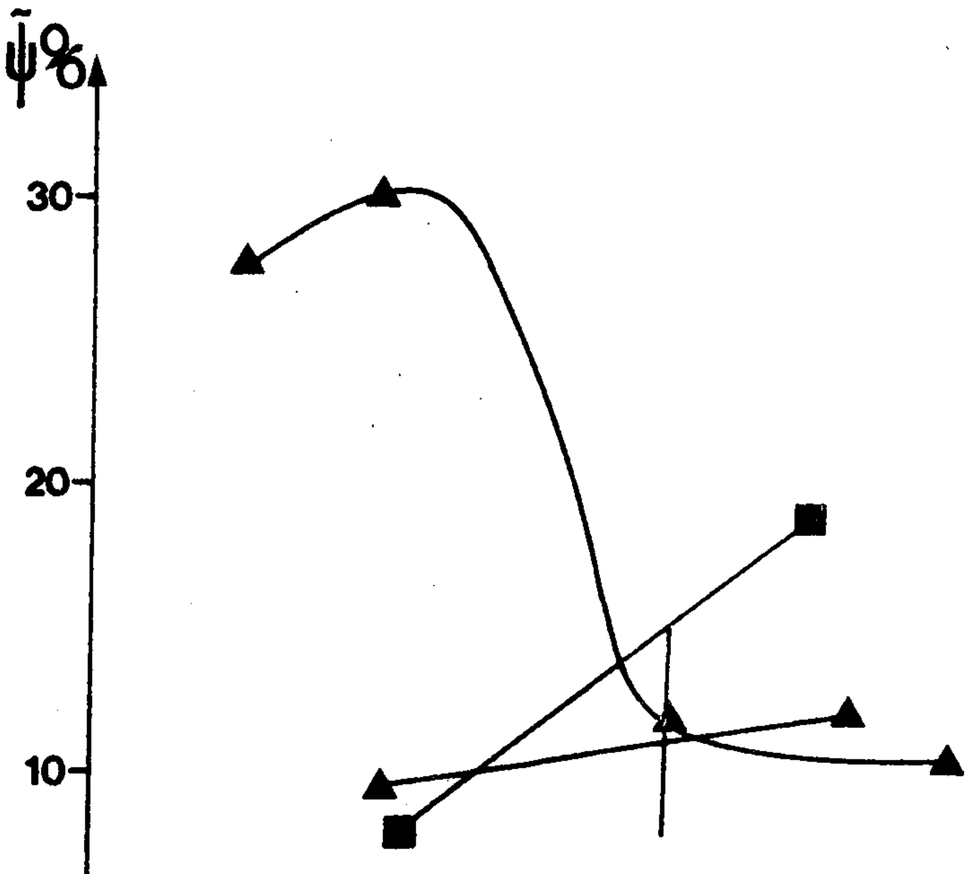

Figure 7·11(f)

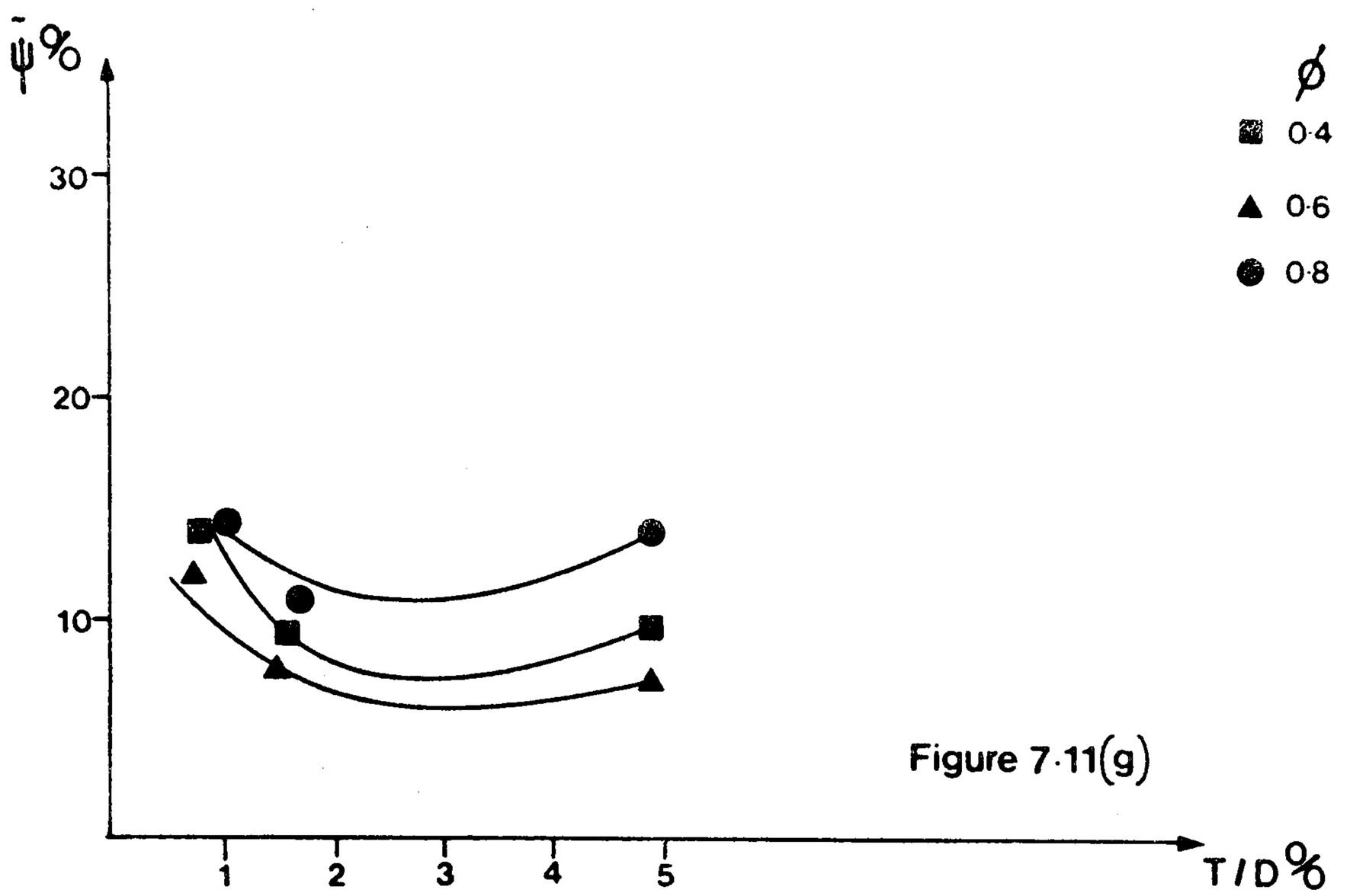

Figure 7·11(g)

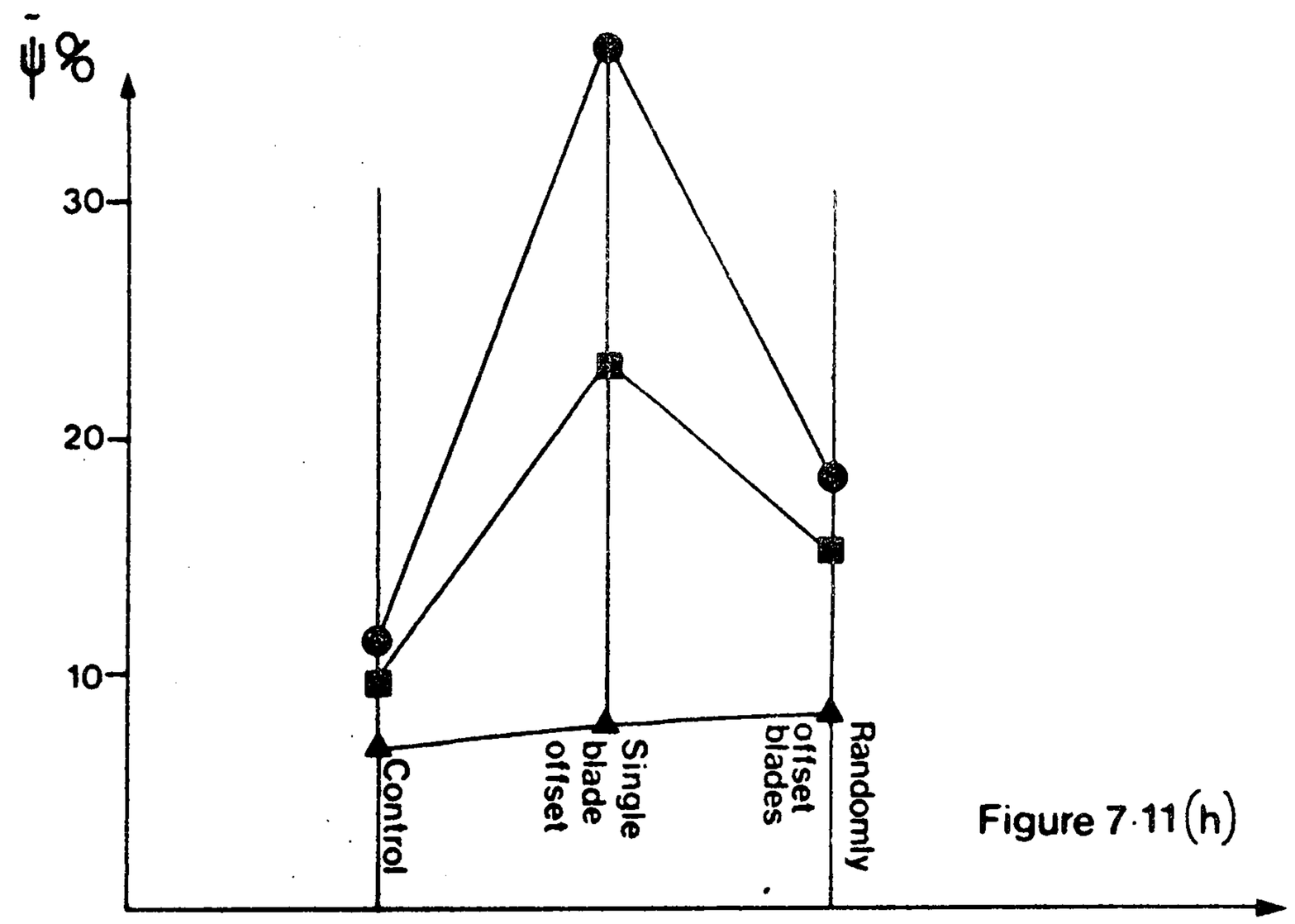

Figure 7·11(h)

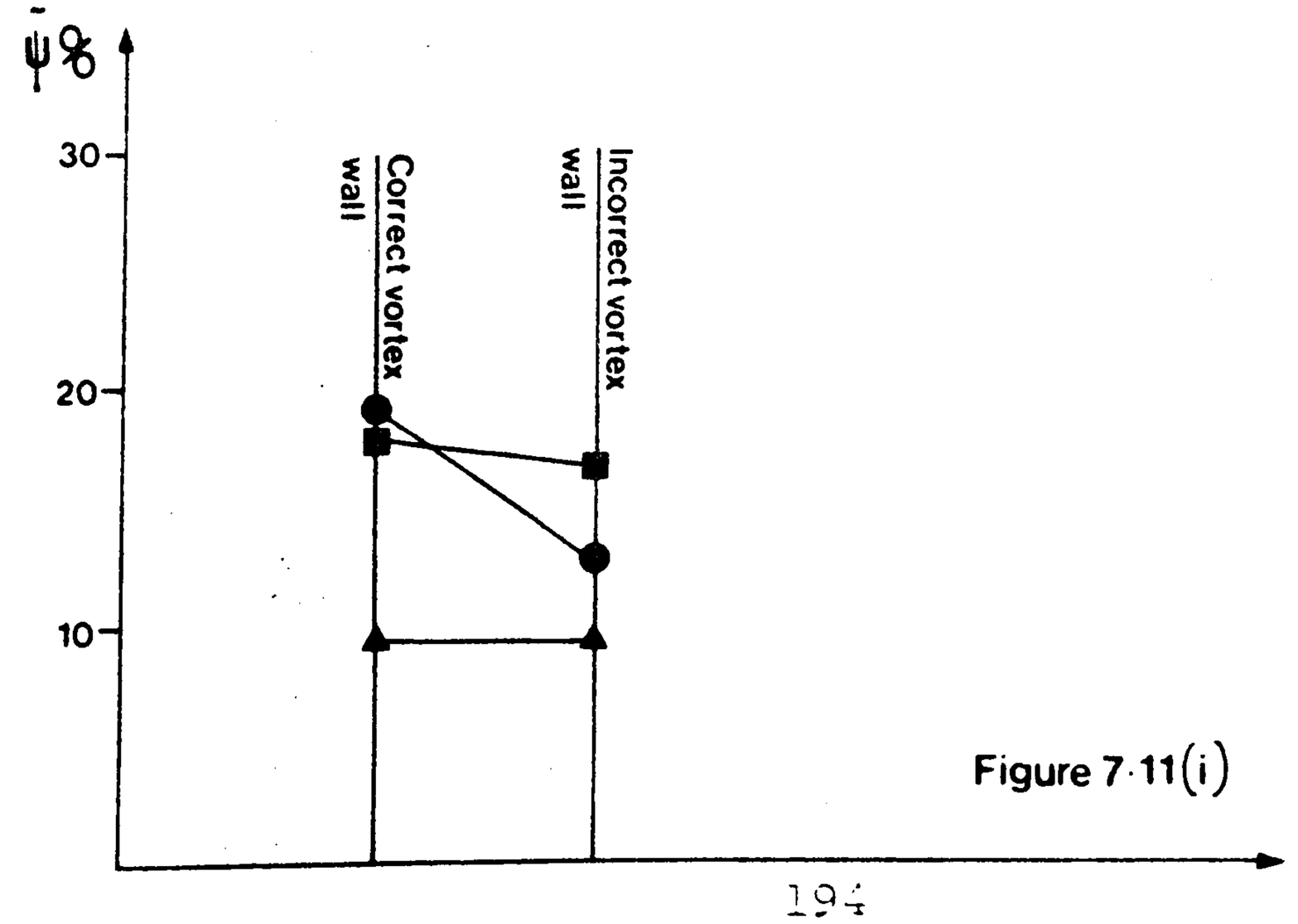

Figure 7·11(i)

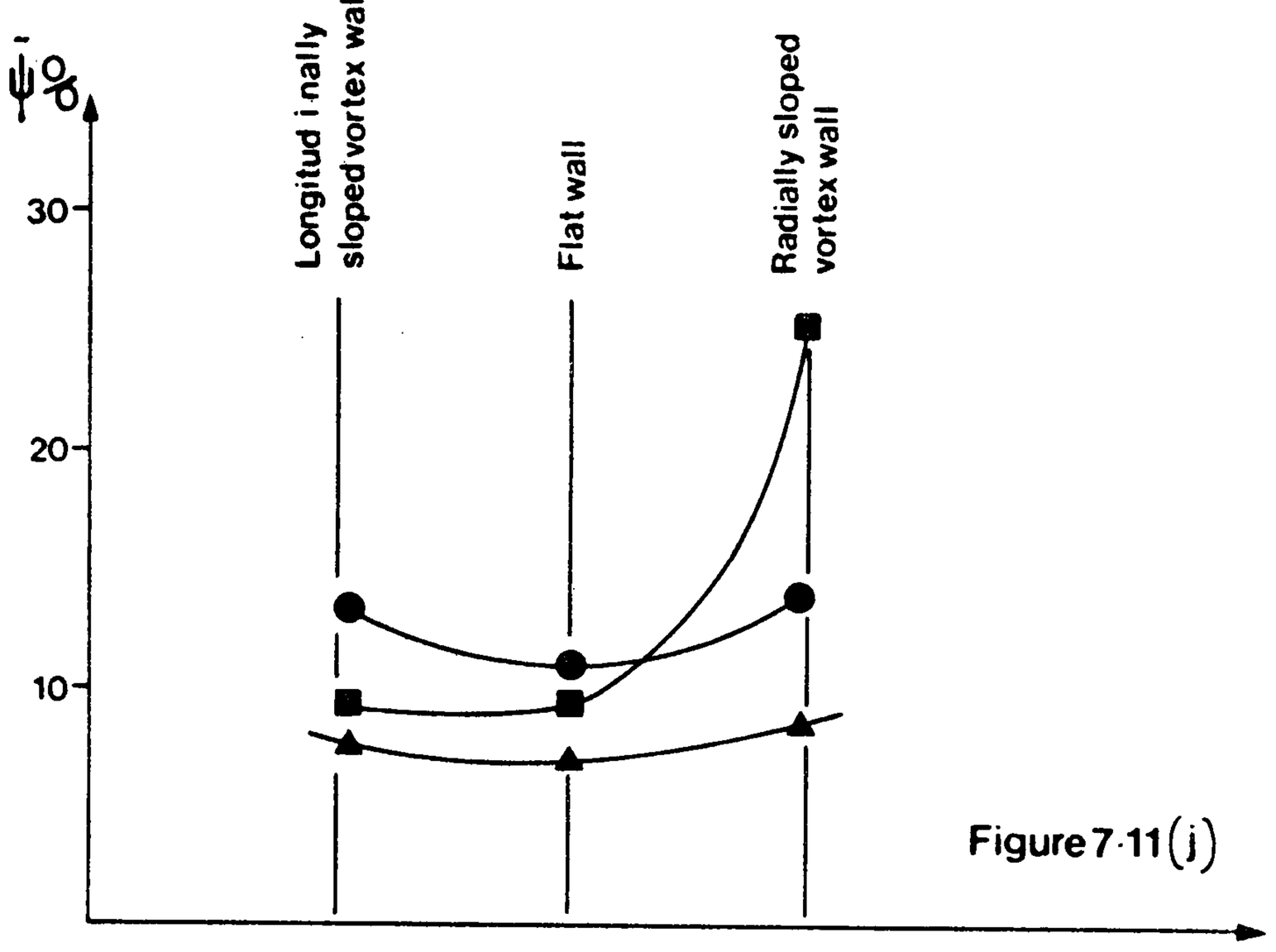

Figure 7·11(j)

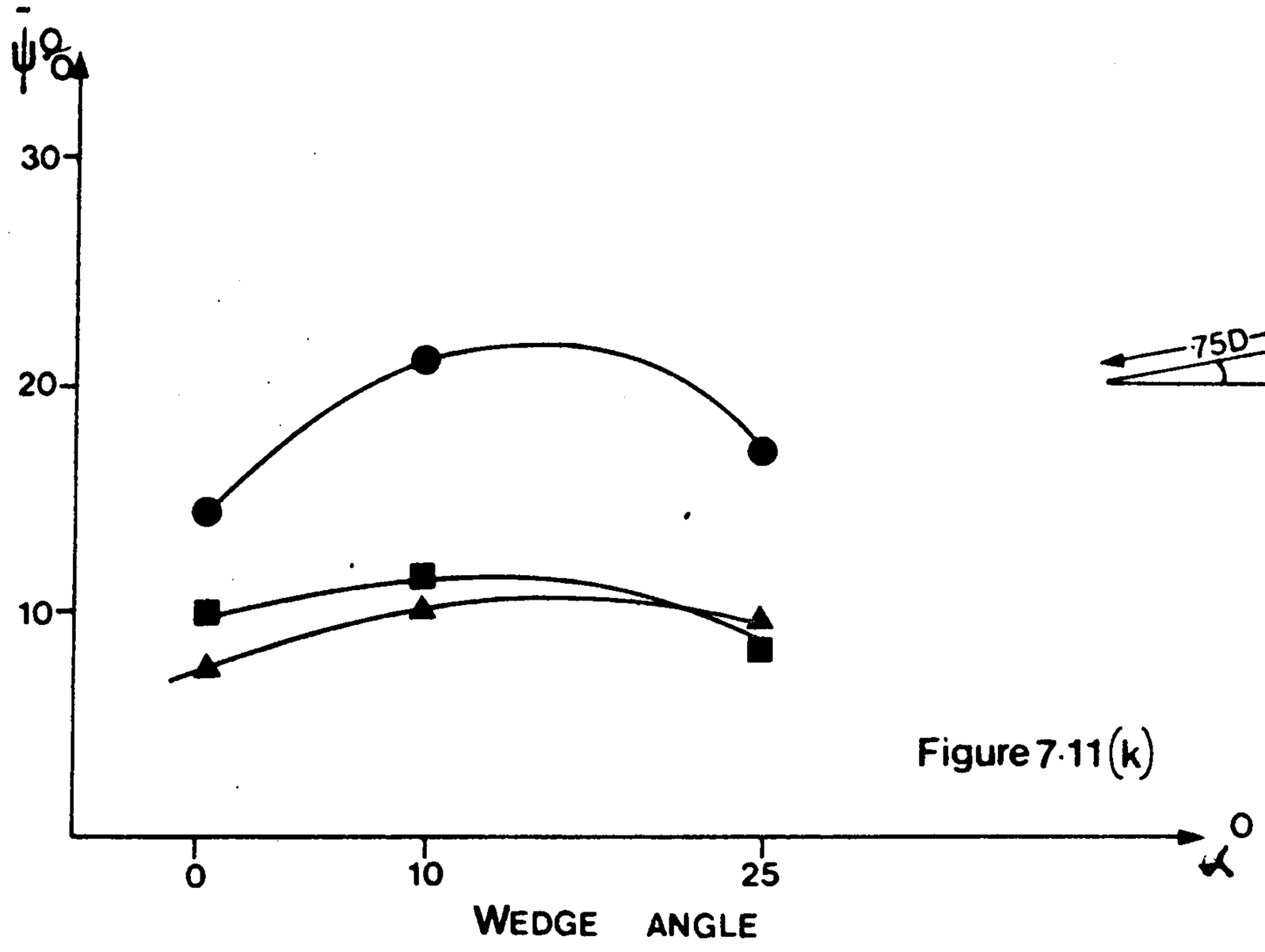

Figure 7·11(k)

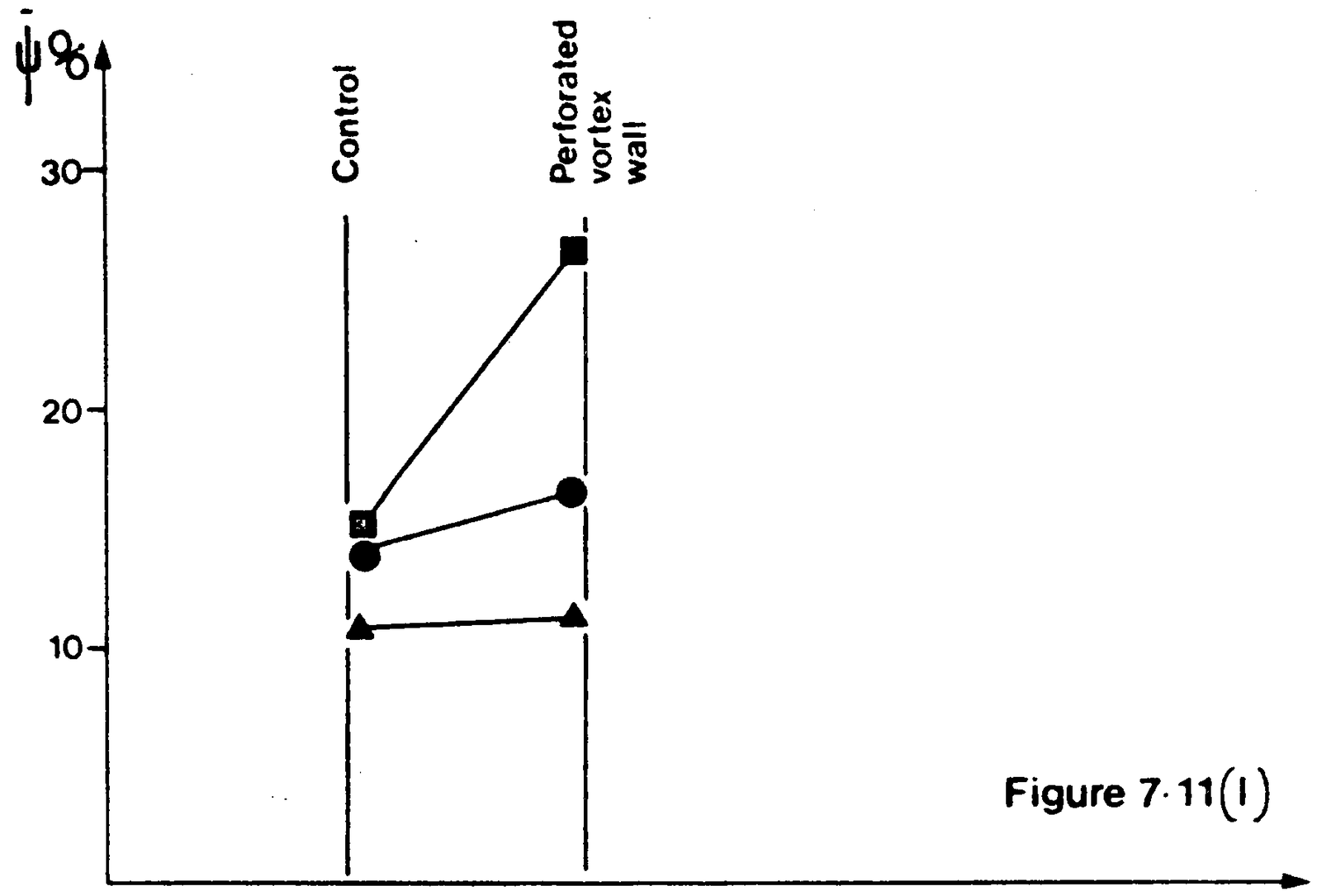

Figure 7·11(l)

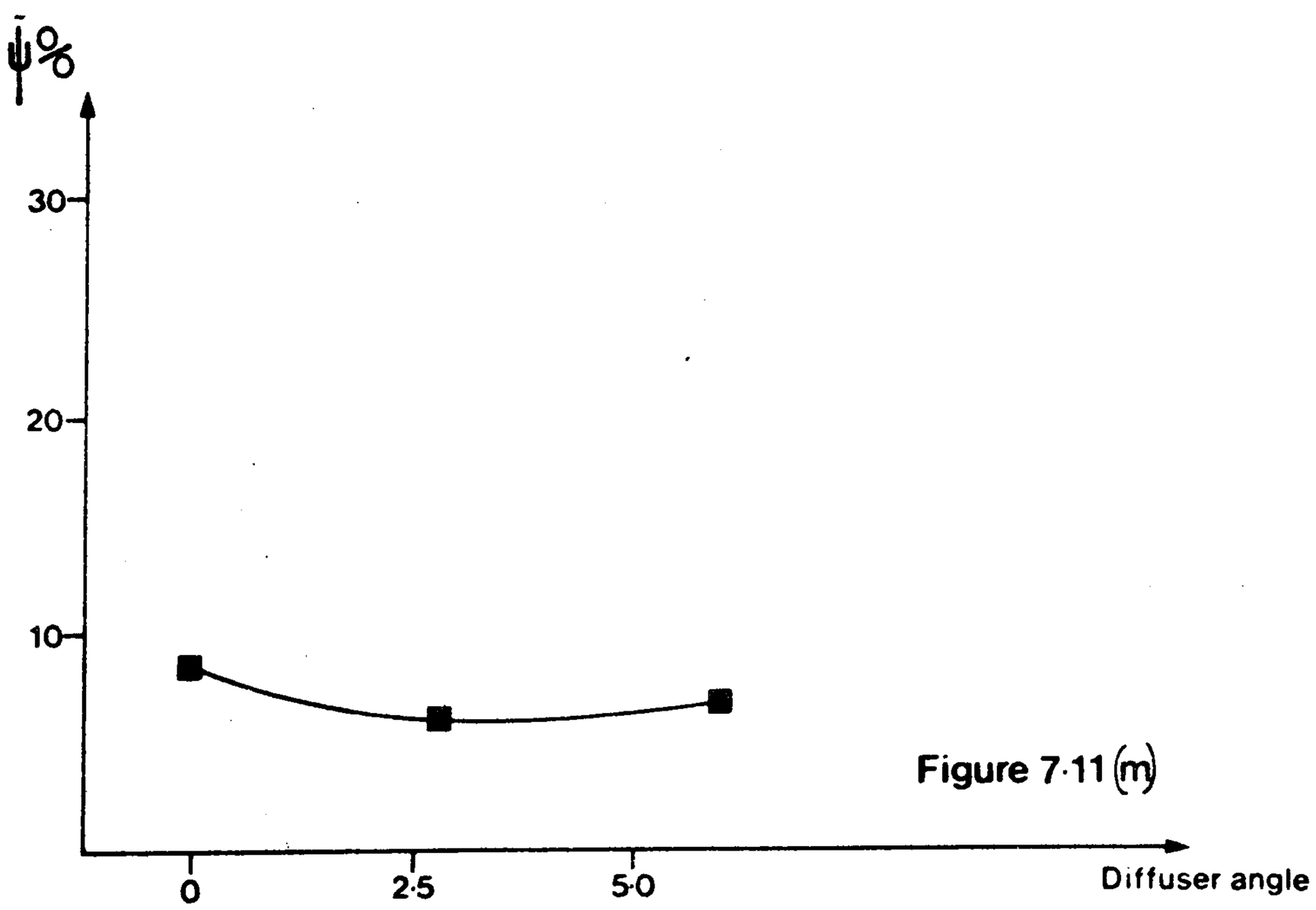

Figure 7·11(m)

CHAPTER EIGHT

8.1 INTRODUCTION TO THE STUDY OF FAN NOISE.

The study of fan noise was catalysed by the introduction of the high speed turbojet engine, where the predominant noise source was found to be in the axial flow compressor stage. A thorough review of the aerodynamic sound generating mechanisms in jet engines is given by MORFEY (54). The author has discussed and assessed some possible cross-flow fan noise production mechanisms in Chapters 4 and 5.

Annoyance is one problem with fan noise, but in extreme cases continued exposure of an individual to a noise source may lead to physiological damage. The danger of hearing loss is well understood, but a paper by MØLLER (50) asserts that the nervous system may also be affected; MØLLER tentatively suggests that exposure to noise increases the occurrence of cardovascular disease and diabetes, and may also be a cause of cancer. These dangers have led most industrialised countries to adopt codes of practice, which aim to reduce the chance of disability through noise. This is particularly so in countries where employers are under a constant threat of litigation.

Nowadays most fan manufacturers have some noise measurement facilities, and include noise performance in their product specification.

8.2 ABSTRACT OF EXISTING WORK ON CENTRIFUGAL AND CROSS-FLOW FAN NOISE.

Little has been published on aerodynamic noise generation by centrifugal fans, and considerably less on cross-flow fans. What work has been done may be grouped into three categories:

1. Variation of sound power or sound pressure with rotational speed.
2. Noise reduction by casing and rotor modification.
3. Empirical prediction of the sound power and spectral distribution; using performance criteria such as flowrate, static pressure or power input.

For centrifugal fans, work included in the first two groups has been reviewed by NEISE, in separate articles(58, 59).

Methods of empirical prediction are of varying complexity, but all suffer from the deficiency of not taking blade geometry or other design details into account. Because of these omissions it is not surprising that quite large errors can occur with prediction methods of this type. The usual range of error quoted is $\pm$ 4 to 5 dB, which gives results useful to an installation engineer but of limited worth to the designer. See, for example, ALLEN (1) and GORDON (30).

A number of cross-flow fan researchers have mentioned the problem of noise, and suggested casing modifications which may reduce sound output. However, to date no comprehensive results are known which allow noise levels to be estimated or which assess the relationship between sound power and fan design.

8.3 EFFECT OF CASING ON THE SOUND PRODUCED BY ROTATING MACHINERY.

Sound waves produced by a source within a duct will undergo some reflection, interference and decay - the degree of this being largely dependent on the frequency of the emitted wave. The study of duct acoustics is a distinct and complex field and the vast majority of work done has been related to noise from axial compressors. Any extension of this work to other fan or compressor types would be extremely difficult. CREMER (17) AND YEOW (79), however, have used one-dimensional analogue methods to treat ducted centrifugal fans.

Centrifugal fans and cross-flow fans typically run at much lower Mach numbers than axial fans; thus, the predominant tones have wavelengths larger than characteristic impeller or duct dimensions and the overall radiated sound power is greatly affected by reflection properties of the casing and ductwork. This can lead to some distortion of the sound power and directivity pattern, particularly at low frequencies. MORELAND (52) compared spectra from cased and uncased centrifugal impellers and found a consistent spectral enhancement at well-defined frequency bands, related to the geometry of the casing. An uncased impeller was observed to give a flat spectrum, but the addition of casing formed peaks in the sound spectrum, which he deduced were due to resonances within the volute. In a later publication (53), MORELAND found that flowrate variations did not significantly affect the overall shape of the cased spectra although the

magnitude in particular frequency bands could vary, for example: reducing the flowrate from 100% free delivery flow to zero flow, in 25% steps, gave a practically monotonic decrease in noise level in all 1/3 octave frequency bands.

Bearing in mind the complex geometry of centrifugal and cross-flow fans it is clear that the overall radiated sound power can be quite different from the generated sound power. Attempts have been made to include casing parameters in the study of noise radiation from centrifugal fans. WEIDEMANN (74), in a trial solution to the rotor radiated sound power, includes a purely geometric parameter to account for radiation and resonance properties of a system; in which an important frequency has a wavelength of the same order as some major casing dimension.

The quantity D/λ

where; D - typical dimension

λ - wavelength

is termed the 'Helmholtz number' - He.

The dependence of the radiated sound upon He is termed the 'system frequency characteristic' - F (He), and describes the sound radiation characteristics of the fan.

In another analysis of a ducted centrifugal rotor YEOW (78) states that the acoustic power radiated by a sound source is dependent upon the impedance against which it operates. YEOW further suggests that ducting can act as a low pass filter, restricting radiation at high frequencies. In a subsequent paper YEOW (79) investigated the effect of rotor internal impedance and found its' effect to be

negligible below ~ 160 Hz, and only small at any frequency. He also detected that the narrow volute opening combined with a large internal volume could cause the casing to act as a Helmholtz resonator, exhibiting a discrete resonance frequency. This latter result agrees with the hypothesis of MORELAND mentioned above.

In the first of his two companion papers YEOW successfully concluded that ducted turbulence is not an important noise source, also that artificially introduced turbulence in the entry flow had no discernible effect on the overall noise produced. This last result was found by MUGRIDGE (56), in a comparison of axial and centrifugal fans used in radiator cooling units. MUGRIDGE found that centrifugal fans, although inherently no quieter, may be quieter than its axial equivalent if the inlet flow is distorted. Axial fan noise performance is more sensitive to inlet flow distortion.

The importance of ductwork as an impedance and not as a source of turbulent noise, has also been determined by DAVIES AND FFOWCS-WILLIAMS (21). They found that quadrupole radiation, due to oscillating shear stresses within the flow, becomes a function of frequency for ducted flow. The effect may be sufficient to reduce the U^8-law for quadropole radiation to a U^6-law at low frequencies.

This variation of speed exponent with frequency is a well known phenomenon in centrifugal fan noise study, see ECK (23).

GROFF (31), when comparing different noise measurement techniques points out the importance of ensuring no standing waves form in the duct - these would greatly increase the noise output. Also, the noise produced by a sudden expansion can be significant and should be reduced as far as possible by fitting a divergent, horn-shaped termination, of correct design, to the duct ending.

To conclude; fluctuating vorticity within the flow itself can be a source of random quadrupole sound at high mach numbers (Ma > 0.2). Experimental investigations indicate though, that the primary role of the ducting, for low speed fans, is to supply an impedance to the generated sound. The measured sound power depends not only on the sound generating mechanisms but also on the sound radiation properties of the fan and associated ductwork. These properties are extremely difficult to assess and may vary with fan design.

8.4 GENERAL RELATIONSHIPS BETWEEN SOUND POWER, ROTATIONAL SPEED AND PERFORMANCE, FOR CROSS-FLOW FANS.

There exists no simple relationship between rotational speed and the sound power generated by a centrifugal fan; the noise output exhibits a complex functional relationship depending on frequency, efficiency, Reynolds number and fan design.

If there exists a variety of speed dependences for centrifugal fans, this is also likely to be the case with cross-flow fans, particularly as the flow conditions are strongly affected by alterations in the fan design. The author has performed a number of tests on an unshrouded cross-flow impeller, the only casing component being a vortex wall of variable location and the vortex wall supporting module. Figure 8.1, graph (a) strongly indicates a speed exponent of $\alpha = 7.24 \pm 0.53$ (90% CL's). Graph (b) suggests that this exponent value may also be a useful estimate with cased impellers. The exponent appears approximately constant for all Strouhal bands.

Theoretically, the noise generated should increase significantly with increased throughflow, see Section 5.2.2. Figures 8.7(a) to 8.21(c), though, indicate only a small decrease in noise level at reduced flowrates. One reason for this may be that noise levels at lower flowrates are increased by worsened stall conditions. Greatly increased noise at stall onset is a common feature with axial fans.

In Section 8.3 it was mentioned that increased flow turbulence had a negligible effect on the sound production of ducted fans. However, this result alone is insufficient evidence of there being no relationship between noise and efficiency. Stall, for example, may reduce efficiency and increase noise, leading to a weak, indirect relationship. The author considers it unlikely that there exists any strong, direct dependence between aerodynamic efficiency and the radiated sound power.

8.5 EFFECT OF VORTEX WALL LOCATION ON THE RADIATED SOUND POWER OF AN UNSHROUDED ROTOR.

It was mentioned previously that the sound generated by a cased rotating impeller will be distorted by the presence of the casing. In this part of the experimental program the effect of the housing and ductwork is eliminated by including only a simplified casing, consisting solely of a vortex wall tongue.

The sound power of a cross-flow fan may then be represented by the following functional relationship:

$$w \propto Ma^{\alpha} . \; Re^{\beta} . \; F(St) . \; G(He) . \; H(design) \quad 8.1$$

where w - sound power

F, G & H - generalised functions.

For an uncased cross-flow impeller, running at constant speed, the equation reduces to:

$$w \propto F(St) . \; H(design) .$$

The function H(design) is directly related to the aerodynamics of the impeller, and is not simply a geometric term. Although the aerodynamic performance of all uncased impellers will probably be similar (very low), the peripheral velocity distributions and blade loading patterns will vary greatly with changes in location of the vortex wall leading edge. The performance of a typical ducted impeller, with no rear wall is depicted in Figure 8.2; the operating point, using the simplified casing adopted, will approximately coincide with the maximum flowrate condition.

The study of an uncased impeller is only of limited practical interest - usually, but not necessarily exclusively, the rotor will be enclosed, even if the rear wall is quite

distant from the rotor and the unit includes just a short outlet duct. Nevertheless, the study offers an interesting comparison with results from cased impellers by concentrating on tongue interaction mechanisms in the absense of ducting.

Simplified casing produces less stable flow conditions than with a shrouded impeller, and because of these temporal fluctuations a large number of results are taken and the mean value chosen as representative. The casing is made as stiff as possible to reduce vibration and increased noise through additional monopole sound generation.

8.5.1 VARIATION WITH VORTEX WALL CLEARANCE, E.

In this study the vortex wall edge is kept parallel to the fan axis of rotation. Increasing the tongue clearance is a frequently adopted noise reduction modification with centrifugal fans, see, for example, the review by NEISE (59).

A number of cross-flow fan researchers have suggested that increasing the clearance should reduce noise, particularly multiple harmonics of the blade passing frequency. The results of a large number of tests by the author are illustrated in Figure 8.3, which shows that, for an unshrouded impeller, the dependence of noise level upon vortex wall clearance may be expressed as a simple power relationship. There is a frequency dependence to the results, which are reproduced in Table 8.1.

Where: $PWL \propto f(st) . (E/D)^{\gamma}$

Strouhal band	γ
St 0.5	0.00
St includes 0.5	-0.63
St includes 1.0	-0.88
St includes 2.0 & 3.0	-1.56
St includes 4.0	-1.61
St includes 8.0	-0.30

TABLE 8.1

In cases where the St=1 band predominates the equation:

$$PWL \propto (E/D)^{-0.9} \quad (1\% \leq E/D \leq 5\%) \quad - 8.2(a)$$

is a reasonable estimate of the relationship between sound power and vortex wall clearance, for an unshrouded rotor.

For unshrouded casing designs where the primary Strouhal band does not predominate (see Figures 8.4(a) to 8.6(f)), the equation 8.2(a) must be modified by a term accounting for the higher order harmonics.

$$PWL \propto (E/D)^{-1.6} \quad (1\% \leq E/D \leq 5\%) \quad - 8.2(b)$$

The degree of modification to 8.2(a) will depend on the relative magnitudes of the sound power levels in St=1 and in Strouhal bands including multiple harmonics of the blade passing frequency. For example, if the band including St=2 and St=3 is 10 dB above the band including St=1, the power relationship will be better approximated by 8.2(b).

8.5.2 VARIATION WITH VORTEX WALL DECLINEATION, B.

Varying the vortex wall declineation does not simply alter the angle of attack of a blade on the vortex wall, but fundamentally affects the peripheral distribution of velocities and forces.

Figures 8.4(a) to 8.4(f) show only a weak increase in sound power with increasing B, for some frequency bands and for low-performance, uncased rotors.

8.5.3 VARIATION WITH DIAMETER RATIO, d/D.

In Section 6.2.1.5 it was suggested that increasing the blade chord/diameter ratio also increased the power input to the fluid. This assertion is supported by the results in Figures 8.5(a) to 8.5(f) which show a practically continuous increase in sound power with decreasing diameter ratio. The results for d/D = 68% are less predictable, but this would be expected if vortex breakdown caused a transverse variation in the flow conditions across the vortex wall tongue.

8.5.4 VARIATION WITH TONGUE THICKNESS, T.

Increasing the tongue radius and shape is frequently suggested as a method of reducing the sound power output of centrifugal fans. The practical efficiency of this method in reducing the noise of an uncased cross-flow impeller is illustrated in Figures 8.6(a) to 8.6(f). Figure 8.6(a) indicates that the primary subharmonic is also reduced, implying that some low frequency noise may be due to tongue interactions.

These results disagree with those predicted theoretically in Section 5.3.7 and also with those determined experimentally with a cased impeller, Section 8.6.2.1. With the unshrouded impeller some of the noise generated may be due to vibration of the tongue.

8.6 EFFECT OF ROTOR AND CASING DESIGN ON THE RADIATED SOUND POWER.

For a cased cross-flow fan running at constant peripheral velocity, equation 8.1 reduces to:

$$w \propto f(st).\ H(design).\ G(He). \qquad - 8.3$$

which is the functional relationship for an uncased impeller, modified to account for cancellation, reflection and impedance properties, governed by the casing.

The casing designs used in this study commonly have an analogue in centrifugal fan technology. Because few results are available on cross-flow fan noise, some of these centrifugal analogies will be referred to. Tongue interaction mechanisms, for example, are likely to be similar for some centrifugal and cross-flow fans, although it is not certain that a proven centrifugal fan casing modification will also be effective in reducing the noise from a cross-flow blower.

If the fan designer is to apply secondary measures of noise reduction, not only is the overall noise level of interest, but more particularly the level of primary harmonics. Broad-band noise is generally not as easy to suppress.

All results in this section are taken at constant peripheral velocity, U = 6.125 m/s, which gives an identical frequency range in each strouhal band, in all cases except where the outer diameter varies. Table 8.2 lists the composition of the Strouhal bands.

St band \ d/D%	RANGE OF STROUHAL NUMBERS 79.5	75.8	72.4	68
1	0.37	0.31	0.27	0.24
2	0.74	0.62	0.55	0.47
3	1.47	1.25	1.10	0.95
4	2.95	2.49	2.19	1.89
5	5.89	4.98	4.38	3.78
6	11.78	9.96	8.76	7.55
7	23.57	19.92	17.52	15.11
	47.13	39.83	35.04	30.21

(St = f/BPF)

where St=1 represents the rotational frequency.

TABLE 8.2

8.6.1 INFLUENCE OF PRIMARY CASING DESIGN ON RADIATED SOUND POWER. (d/D = 79.5%, unless otherwise stated)

8.6.1.1 VORTEX WALL CLEARANCE, E.

EMBLETON (26), studied in detail the effect of increasing tongue clearance on the sound power produced by an 8-bladed, radial centrifugal impeller. His results were for clearances in the range $0.1\% \leq E/D \leq 4\%$, and he determined an optimum overall clearance of 1.7%, for minimum noise production. When using a sloped wall, however, the minimum was not found, but the sound power decreased monotonically

with increasing tongue clearance. NEISE (59) suggests that the optimum clearance of 1.7% has no universal significance but is a function of the directionality of the machine. This example serves to illustrate the difficulty of attempting to predict universally valid relationships between noise level and casing design.

Most other researchers have supported NEISE and assert that increasing the tongue clearance leads to a monotonic decrease in noise level.

PRESZLER AND LAJOS (65), working on cross-flow fans, determined that increasing the vortex wall clearance in the range $1\% \leq E/D \leq 4\%$ reduced the overall sound power by 10 dB. Increasing the clearance further had little effect on the level of noise radiation.

The results of Section 8.5.1 illustrated a simple, frequency dependent power relationship between clearance and sound level. The same trend is noted for a cased impeller. Figures 8.7(a) to 8.7(c) and 8.8(a) to 8.8(c) demonstrate that, generally, sound power is reduced with increasing vortex wall clearance, for Strouhal bands 2, 3, 4 and 5.

8.6.1.2 REAR WALL CIRCUMFERENTIAL ANGLE, δ .

The rear wall angle has a significant, though unpredictable, effect on the sound production properties, see Figures 8.9(a) to 8.9(c). In Strouhal bands 1, 5, 6 and 7 adopting a rear wall angle of 0^{o} or 20^{o} will cause the largest radiated sound power level. This increase in noise is commensurate with an improved aerodynamic performance. For the primary blade passing multiple harmonic (St-band = 2), a rear wall angle of

60^{o} gives the noisiest conditions for ϕ = 0.6 and ϕ = 0.8, this configuration also gives noisy operation at all flowrates, in Strouhal bands 2 and 3. Generally, the quietest operating conditions occur using a rear-wall angle of 40^{o}.

8.6.1.3 DUCT HEIGHT, H.

Closed boundaries are essential to a fan if the impeller is to deliver air at a useful pressure, in one direction. Because the rear wall acts only as a flow guide, any dependence of noise upon rear wall design will be related to the boundary turbulence or the internal impedance of the enclosed volume.

Although the sound powers are complicated functions of flowrate and frequency; the graphs, Figures 8.10(a) to 8.10(c), loosely indicate a reduction in sound power with increasing H/D: except for H/D = 70% which is the noisiest condition.

i.e. H/D|PWL: 70% > 60% > 80% > 90%.

8.6.1.4 VORTEX WALL DECLINEATION, B.

This geometric parameter has been shown to strongly influence the aerodynamic performance of a fan.

For an uncased impeller, the sound power output was found to increase weakly with increasing B, (Figures 8.5(a) to 8.5(f)). This relationship is broadly supported by Figures 8.11(a) to 8.11(c), for a simple wall design and strongly supported by Figures 8.12(a) to 8.12(c), using an ECK-type wall.

Although there is some disagreement within the results, it may be concluded that, in the Strouhal bands 2, 3 and 4 at least, the sound power level increases with B. To extend this result: the higher the performance of a cross-flow fan, the noisier it will be in operation. This result is implied in many of the experimentally determined relationships between radiated sound power and fan design.

8.6.1.5 DIAMETER RATIO, d/D.

For an uncased impeller the radiated sound power was found to increase steeply with an increase in the chord/diameter ratio, see Section 8.5.3. This trend is obscured by running the impeller cased, although an irregular relationship, see Figures 8.13(a) to 8.13(c), broadly implies increasing sound power with increasing d/D, for Strouhal bands 2, 3, 4 and 5.

The apparent weakness of the relationship for a cased impeller may be attributed to some feature of the experimental rig affecting sound radiation properties.

8.6.1.6 REAR WALL CLEARANCE, E2.

The results depicted in Figures 8.14(a) to 8.14(c) support the assertion of 8.6.1.4 that improved performance generally increases the radiated sound power. Overall, the noisiest operation corresponds to the optimum rear wall clearance. An increased clearance reduces the noise level, so, from sound power considerations, a too-large clearance is preferable to a too-narrow gap.

8.6.2 INFLUENCE OF NOVEL CASING DESIGN ON RADIATED SOUND POWER (d/D = 79.5%)

8.6.2.1 TONGUE THICKNESS, T.

The tongue thickness has been shown to have relatively little effect on performance, although an optimum of about T/D = 1.62% was determined. The importance of this parameter is limited to tongue-interaction mechanisms.

In centrifugal fan technology, the radius of the tongue has been shown on many occasions to affect the sound power of fundamental harmonics. LYONS AND PLATTER (49), for example, state that cut-off radius is one of the most important design parameters influencing pure-tone generation. With cross-flow fans, flow conditions in the proximity of the vortex wall are complicated by the existence of a forced vortex, so the effectiveness of increasing tongue thickness, as a noise reduction procedure, may not be so apparent.

Under the fairly artificial conditions with an uncased impeller, increasing the tongue thickness was found to be an effective noise treatment. The results for a cased impeller, Figures 8.15(a) to 8.15(c), show a reduction in noise production by increasing the tongue thickness from T/D = 0.81% to T/D = 4.88%. However, the highest noise level occurs at the maximum aerodynamic performance configuration of T/D = 1.62%.

8.6.2.2. IRREGULAR BLADE SPACING.

KUROSAKA (43), in a study on the noise from axial impellers, showed that non-regular blade spacing, and irregular staggering of the blades, increased the multiple pure tone generation. EMBLETON (26), sloped the blades of a sirocco

runner in a regular fashion and achieved a 9-12 dB drop in the primary harmonic; although he suggests that broad-band noise may be increased. Sloping of the blades acts in a similar fashion to sloping the vortex wall - this is discussed in a later section.

Irregular rotor manufacture has the effect of altering conditions between blades, and disrupting flow processes temporally governed by the blade passing frequency. This could lead to phase cancellation between sound power sources, but the increased instability may also modulate conditions and increase low frequency noise. The results of Figures 8.16(a) to 8.16(c) indicate that, in all Strouhal bands except the lowest, noise is significantly decreased by radially offsetting the blades. The magnitude of noise reduction is greatest at low multiple harmonics, decreasing towards the higher frequency bands. The degree of noise reduction is largest with a random radial irregularity of the blades, and may be up to 10 dB.

8.6.2.3 INCORRECT REAR WALL DESIGN.

It has been mentioned that increased ducted turbulence has a negligible effect on the overall radiated sound power. This is verified by results in Figures 8.17(a) to 8.17(c), which show a small increase in sound power using a 'correctly' designed rear wall. The increased sound levels are most apparant in the lowest Strouhal band; at other frequencies the relationship exists, but the difference in sound power is generally less than 2 dB.

8.6.2.4 SLOPING THE VORTEX WALL.

LYONS AND PLATTER (49) attempted to reduce the noise of a centrifugal fan by inclining the tongue; the theory of this technique being that two or more adjacent radiating sources can interfere and cause phase cancellation. LYONS AND PLATTER report a maximum pure tone reduction of 10 dB. Other centrifugal fan researchers have suggested splitting the wall longitudinally to produce these local pressure cancellations. PLONER AND HERZ (61), by stating that noise reduction techniques are not necessarily additive, sensibly imply that the effectiveness of these noise reduction techniques is dependent on the vortex wall clearance, and that they may only be significantly useful for small E/D.

IKEGAMI AND MURATA (39) claim a 10 dB reduction in overall sound pressure by sloping the wall longitudinally at 2^{o}, further sloping of the wall decreased the sound pressure only marginally. The results in Figures 8.18(a) to 8.18(c) indicate that radially sloping the wall may be effective in reducing the noise level by 1-4 dB, in some frequency bands. Radial sloping of the vortex wall is generally a more effective noise reduction technique than longitudinal sloping, but the procedure does not really prove its worth with cross-flow fans. One reason why the procedure is not very effective, may be that phase cancellation is counteracted by the reduction in wall clearance, which must occur with a sloping wall where $B > 0$. This being so; longitudinal sloping of the vortex wall may be more effective for low B.

8.6.2.5 WEDGE ANGLE, α°.

Figures 8.19(a) to 8.19(c) show that radiated sound power is increased by the inclusion of a wedge on the suction surface of the vortex wall. In the Strouhal bands 3, 4, 5, 6 and 7 the noisiest configuration is with the largest wedge angle, $\alpha = 25^{\circ}$. In the Strouhal bands 1 and 2, however, this wedge angle proves to be the quietest casing configuration. Operating the fan with no wedge gives consistently lower sound powers than with a 10° wedge.

Incorporating a wedge on the vortex wall has been found to produce a wake which passes through the impeller interior. This may affect noise generation by modulating existing conditions or increasing the level of the tongue interaction mechanisms. Obscuring the suction arc with a wedge also affects the theoretically determined noise levels.

8.6.2.6 PERFORATED VORTEX WALL.

The perforated vortex wall may be considered as two parts: (1) the castellated leading edge and (2) the perforated upper and lower surfaces, see Figure 6.2.

Self induced oscillations within the perforations may cause noise reduction through dipole source phase-cancellation; but, it is most likely that noise reduction is due primarily to interference between neighbouring sources on the castellated leading edge of the vortex wall. Figures 8.20(a) to 8.20(c) show a consistent noise reduction of $\sim$ 1-5 dB using a perforated vortex wall.

This modification, however, may not always be effective; for, with some combinations of flow conditions over the vortex wall and perforation area, viscous effects could prevent penetration of the gap, such that the wall perforations are ineffective.

8.6.2.7 OUTLET DIFFUSER.

No results are available for this casing modification, but it is conceivable that a divergent duct could affect radiation properties of the fan. Modifications to the outlet ducting are commonly included as silencing measures for ducted blowers.

8.6.2.8 ECK-TYPE VORTEX WALLS - AND A PLAIN WALL WITH AN ARCUATE DAMPER.

ECK (24), in a patent specification, states that the inclusion of a wall of his design eliminates the unpleasant whistling noise, which hitherto had limited the commercial acceptance of the cross-flow fan. Figures 8.21(a) to 8.21(c) support this claim and illustrate how the ECK-type wall successfully reduces the overall radiated sound power. This was also predicted in Section 5.3.9. The arcuate damper, which obscures the suction arc rather than, primarily, the discharge arc, but does not affect the vortex location, is not as effective as the ECK-type wall in reducing sound power levels.

It is to be expected that a reduction in aerodynamic performance will also reduce the radiated sound power, but the ECK-wall is considerably the more effective. Noise reduction with this modification is of the order of 4-10 dB in each Strouhal band, whereas the equivalent reduction using an arcuate damper is only 2-5 dB.

8.7 SECONDARY NOISE REDUCTION TECHNIQUES.

The previous section has indicated again that, for cross-flow fans, a reduction in the radiated sound power is usually accompanied by reduced aerodynamic performance. It is always possible, though, that shaped tongue designs may produce phase cancellation which significantly reduces the noise level; an example of this is the perforated vortex wall.

However, shaped walls apart, it is not necessary for a fan subjected to a noise control program to undergo a reduction in performance, if secondary techniques are used. Such techniques are common to all fan types and may broadly be categorised into three groups.

1. Absorptive Treatment.

For example, tuned resonators and the use of acoustic materials, see ARCTANDER (6) or the comprehensive review by PURCELL (66).

2. Ducted Silencers.

These aim to reduce pipework noise. There are numerous types and designs, the most exhaustive information available being in the form of manufacturers' literature.

3. Miscellaneous Noise Reduction Techniques.

For example, sprung vortex walls, see FIRTH-CLEVELAND (28) and porous blade surfaces, see TSEO (72).

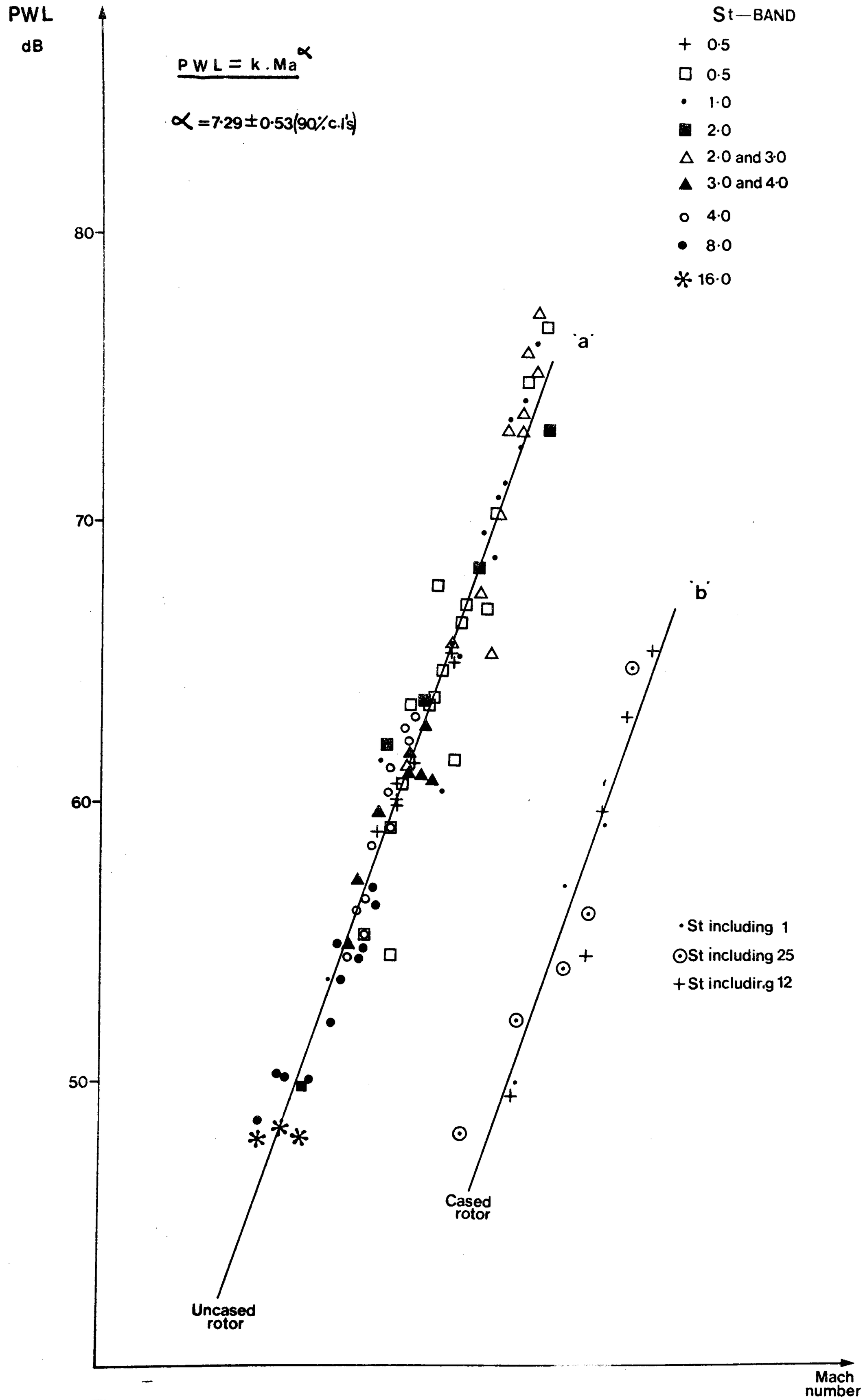
PWL
dB
PWL = k . Ma^∝
∝ = 7·29 ± 0·53 (90% c.l's)
80
70
60
50
St — BAND
+ 0·5
□ 0·5
• 1·0
■ 2·0
△ 2·0 and 3·0
▲ 3·0 and 4·0
o 4·0
● 8·0
✳ 16·0
a
b
• St including 1
⊙ St including 25
+ St including 12
Uncased rotor
Cased rotor
Mach number

Figure 8·1

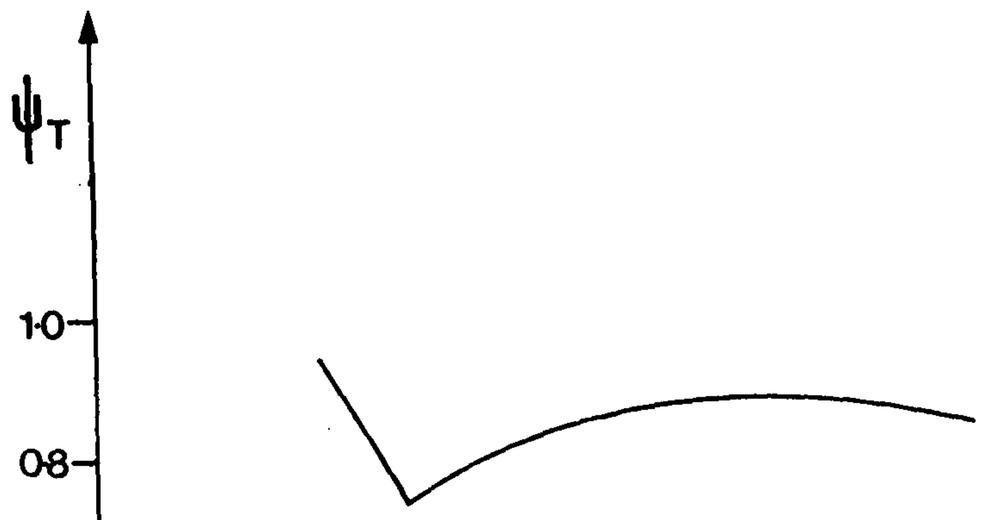

Performance of a cross-flow fan with no rear wall

Figure 8·2

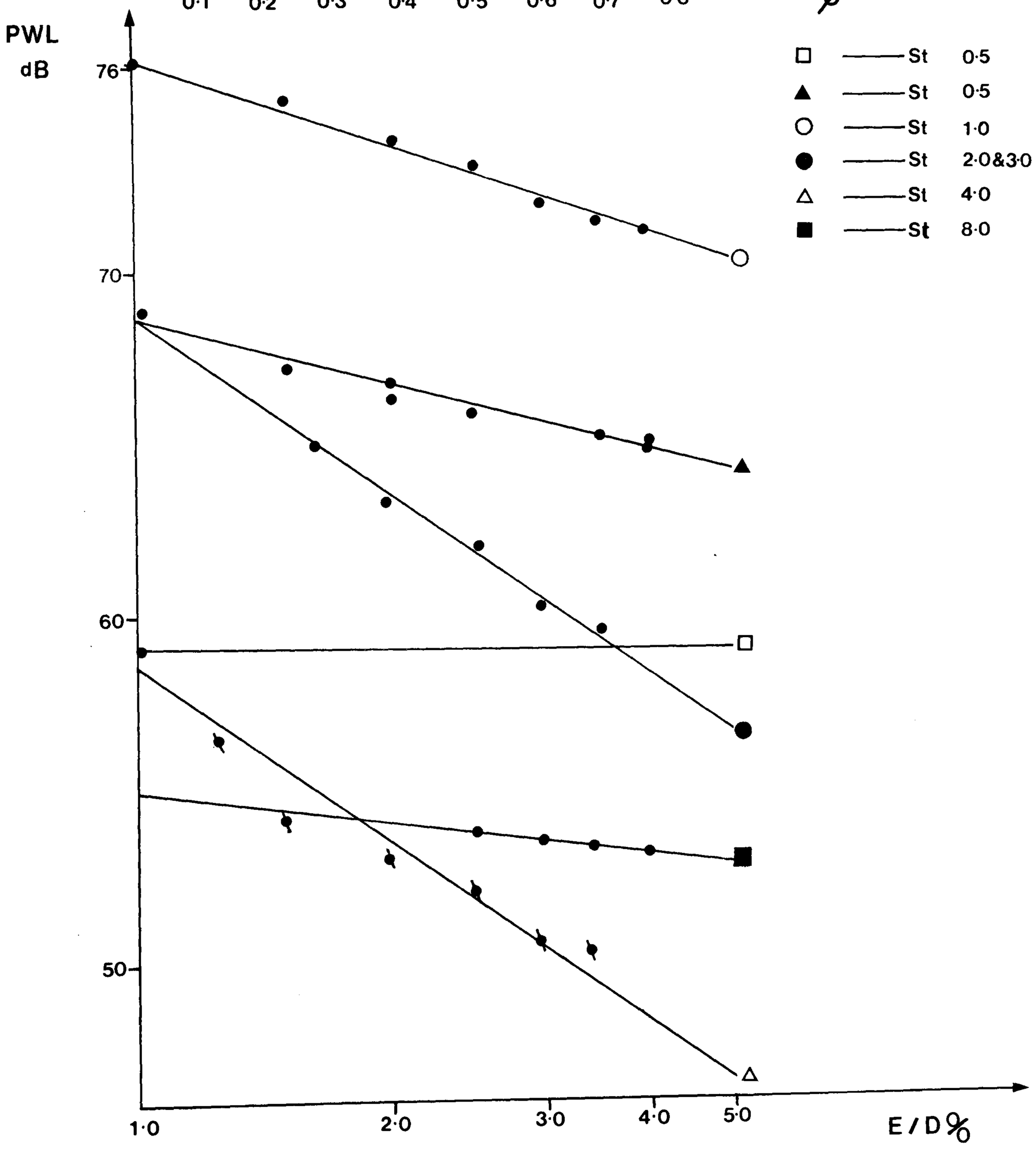

Figure 8·3

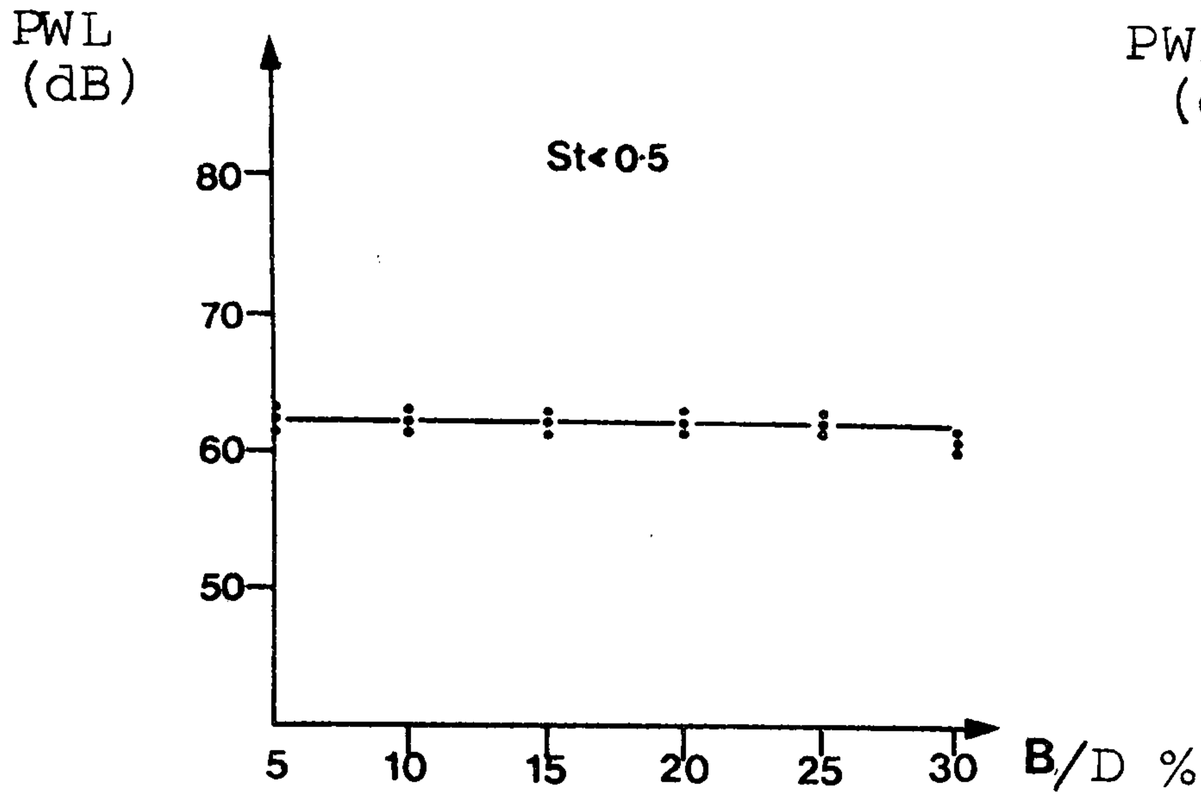

Figure 8·4 (a)

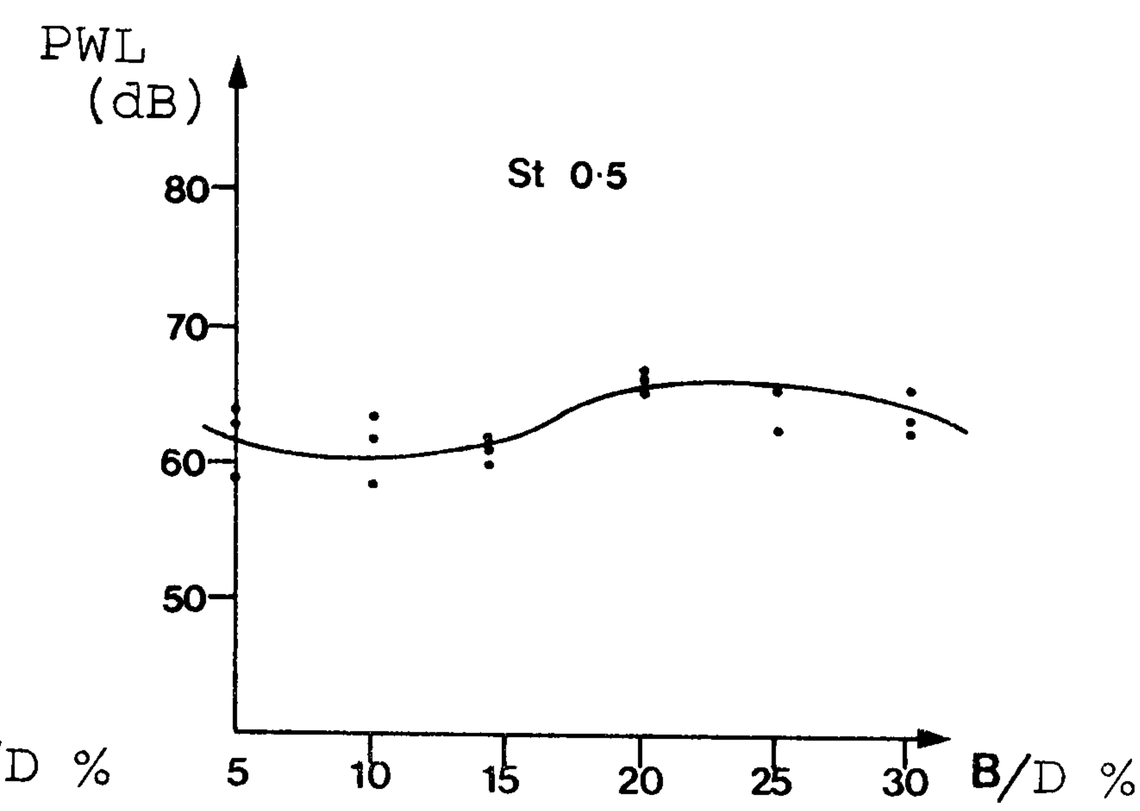

Figure 8·4 (b)

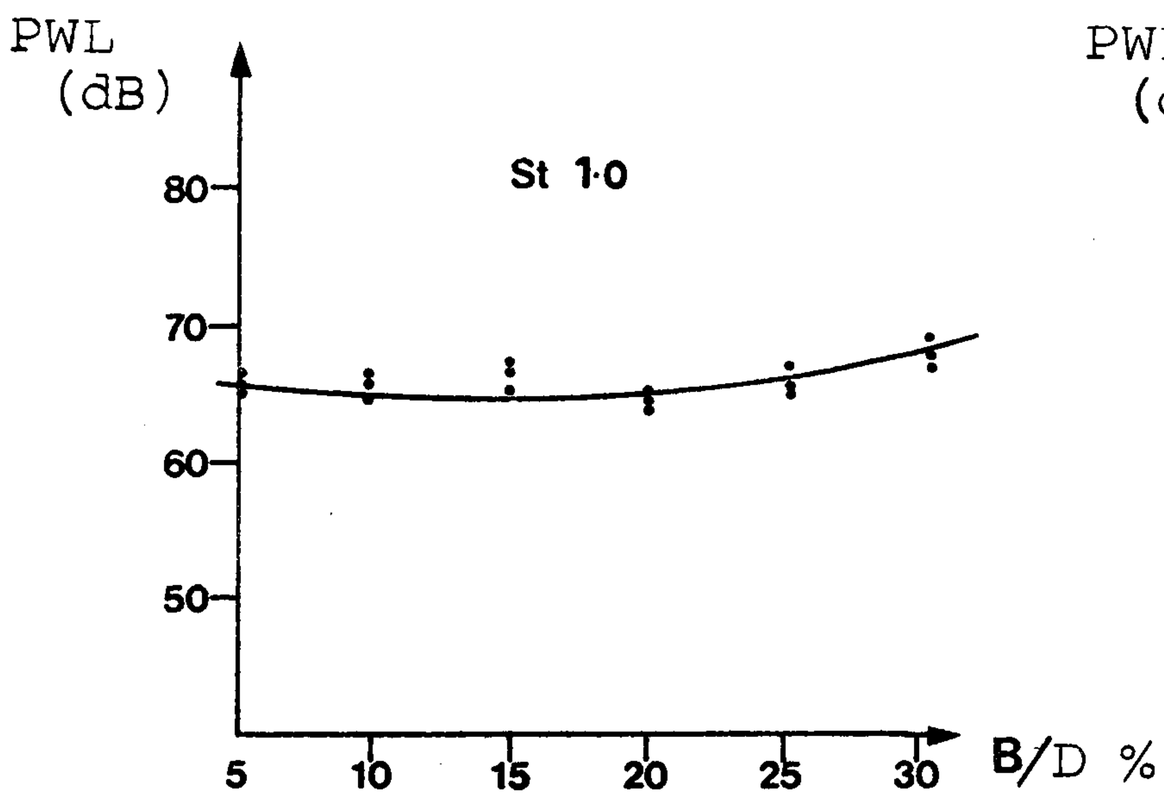

Figure 8·4 (c)

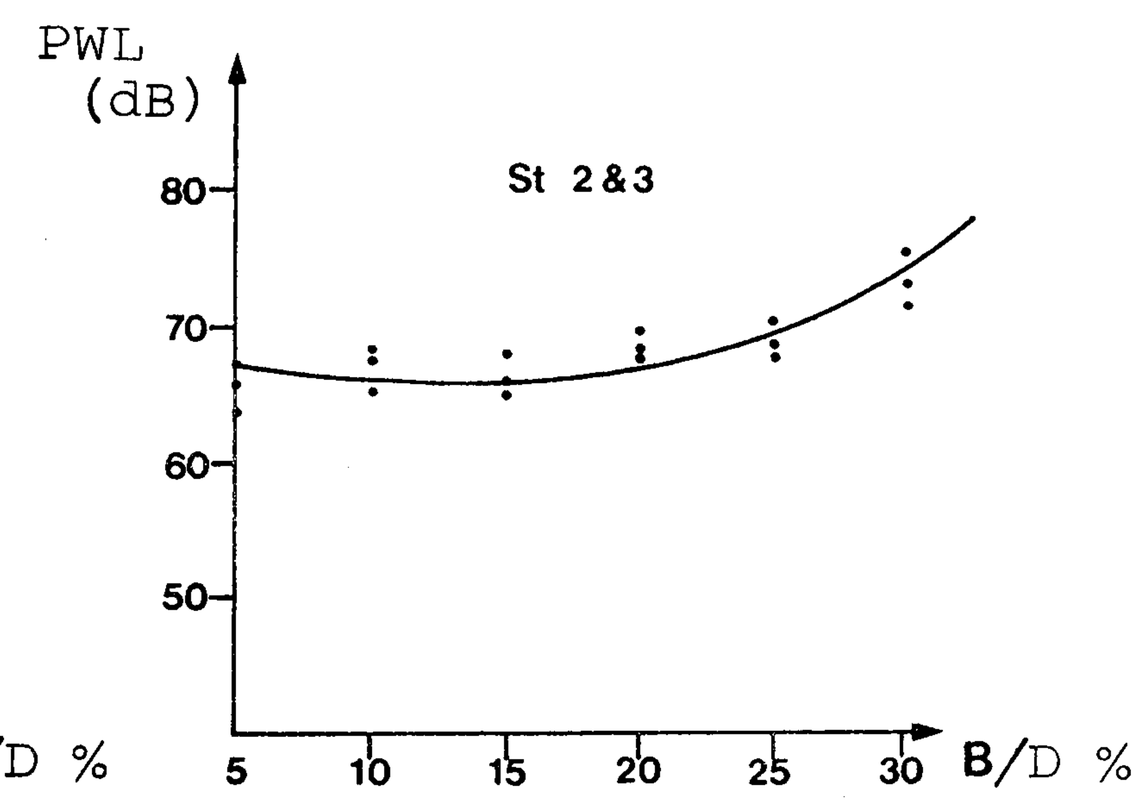

Figure 8·4 (d)

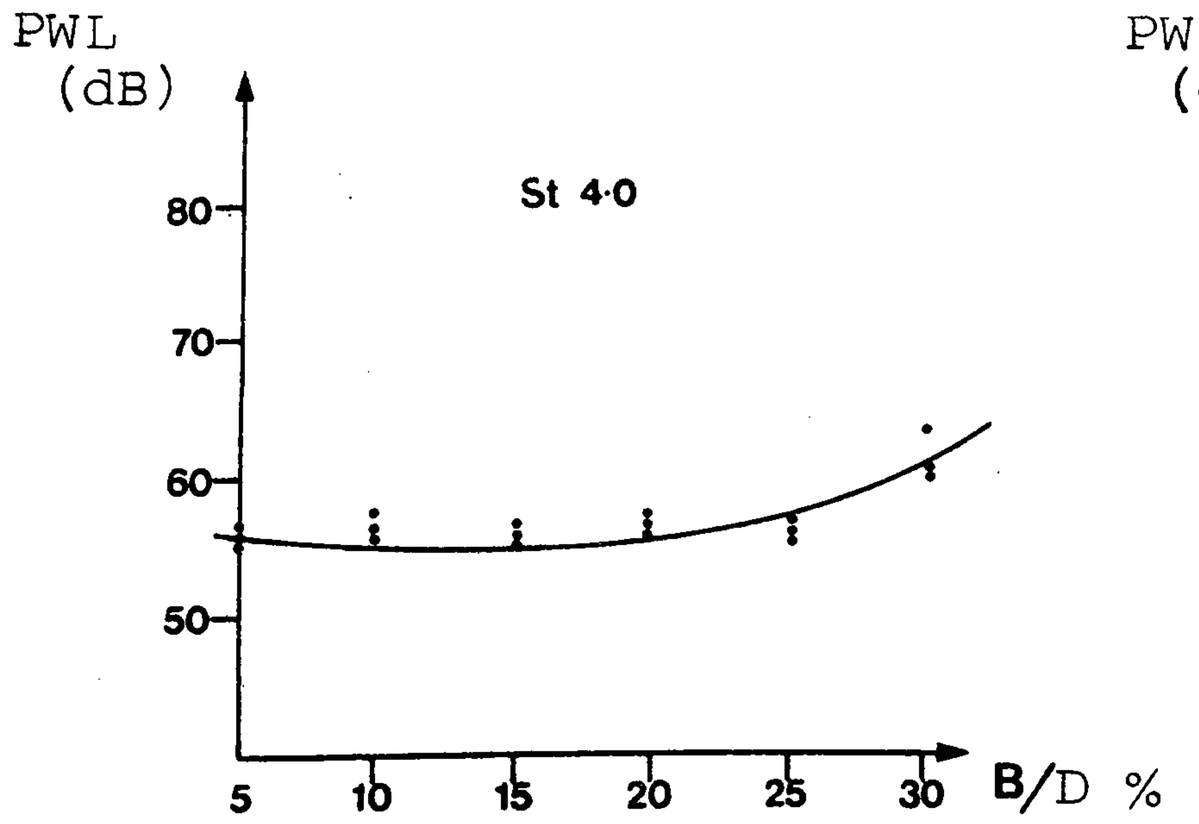

Figure 8·4 (e)

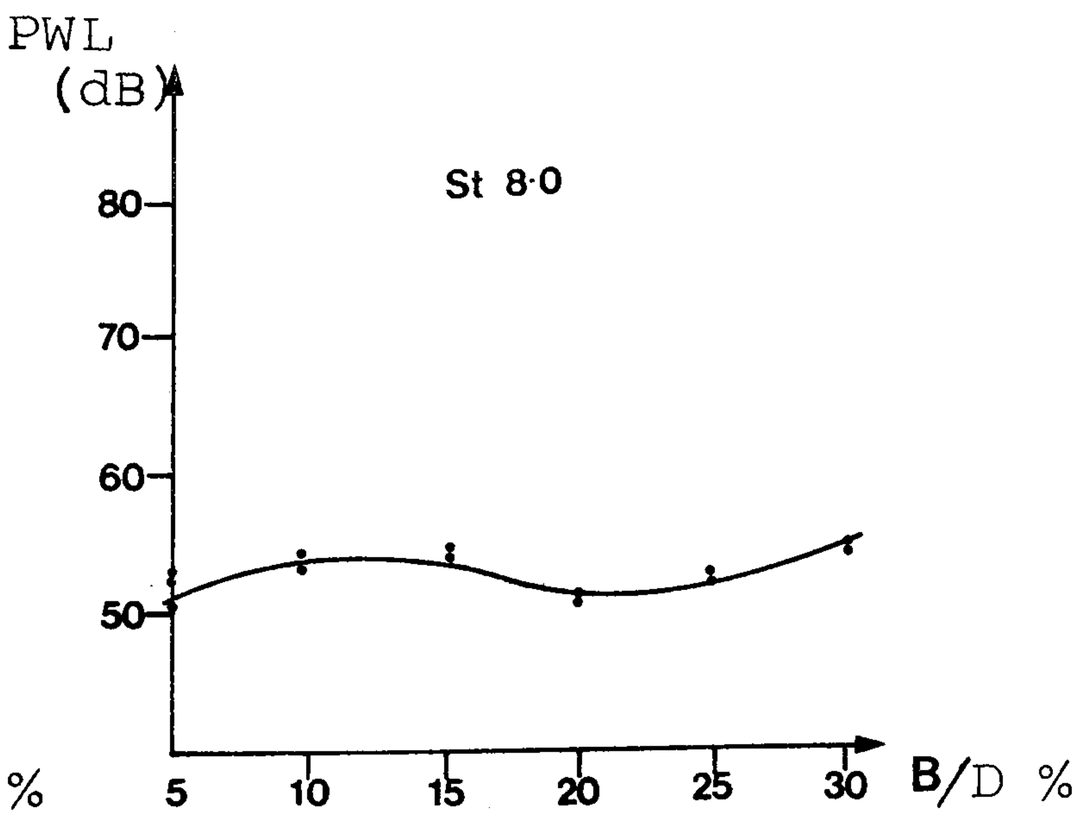

Figure 8·4 (f)

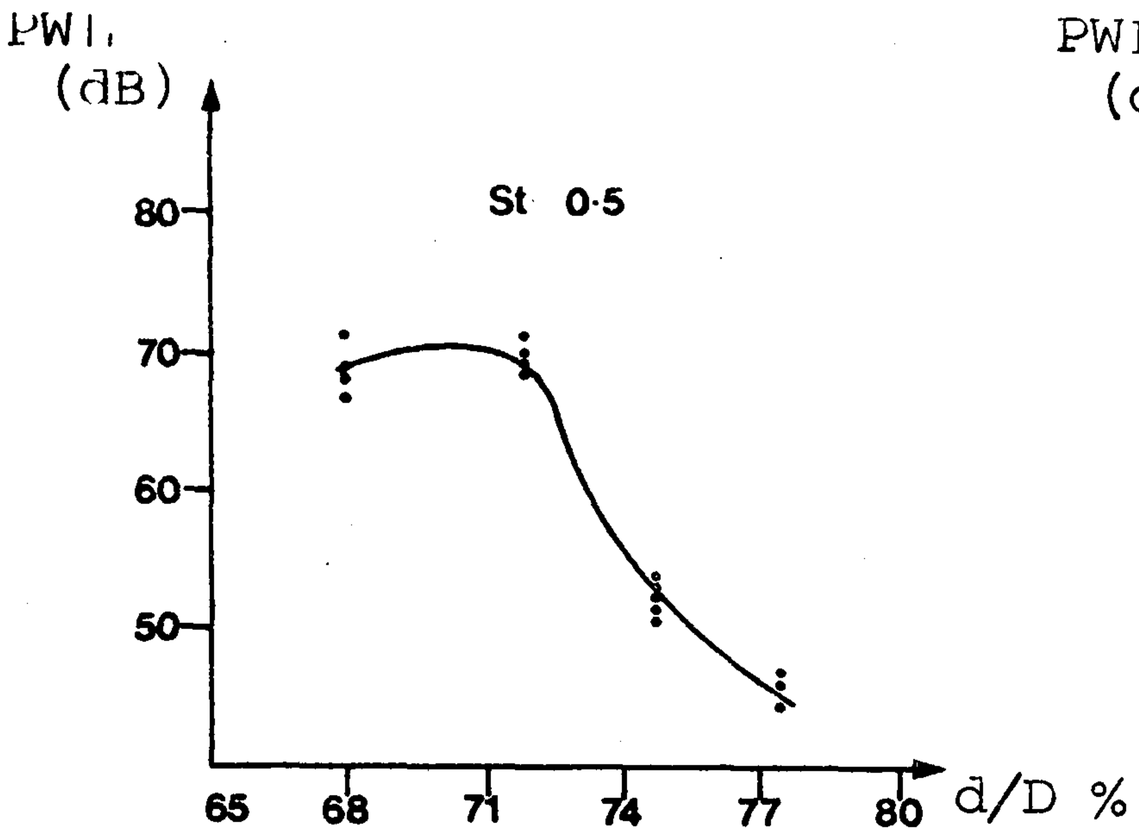

Figure 8·5(a)

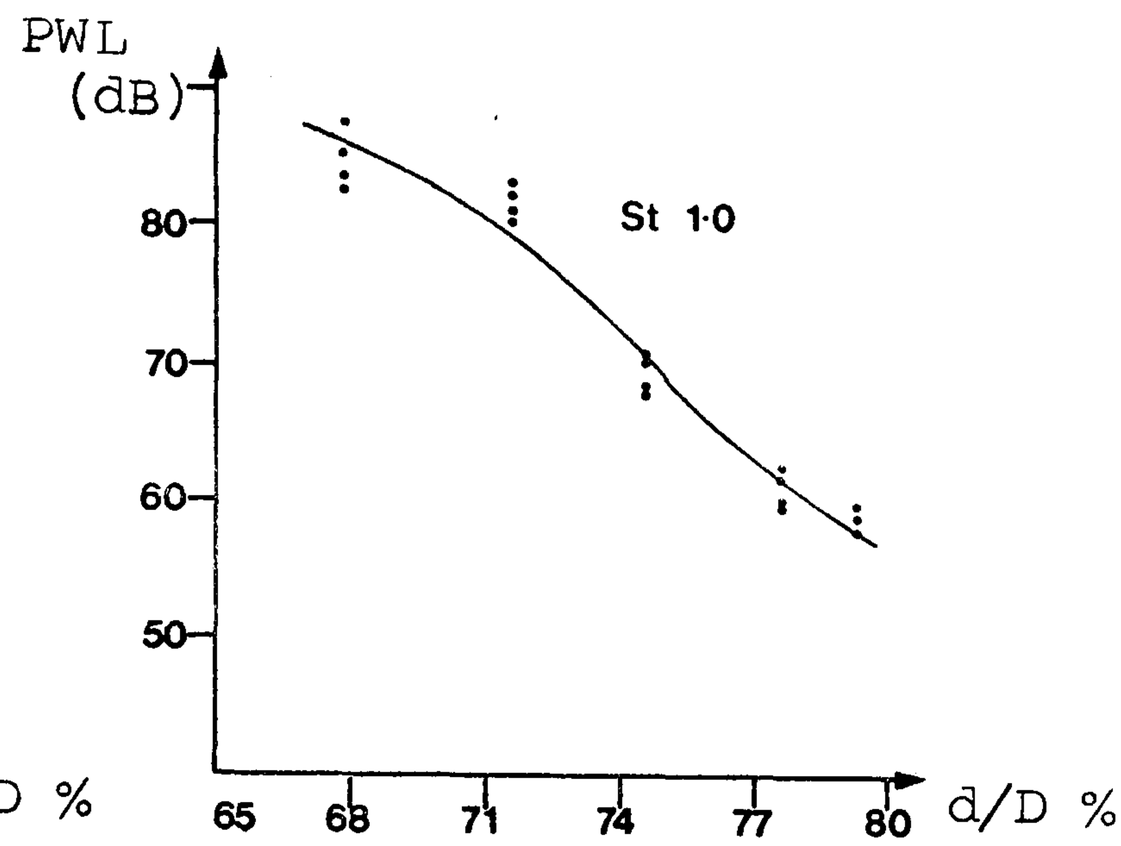

Figure 8·5 (b)

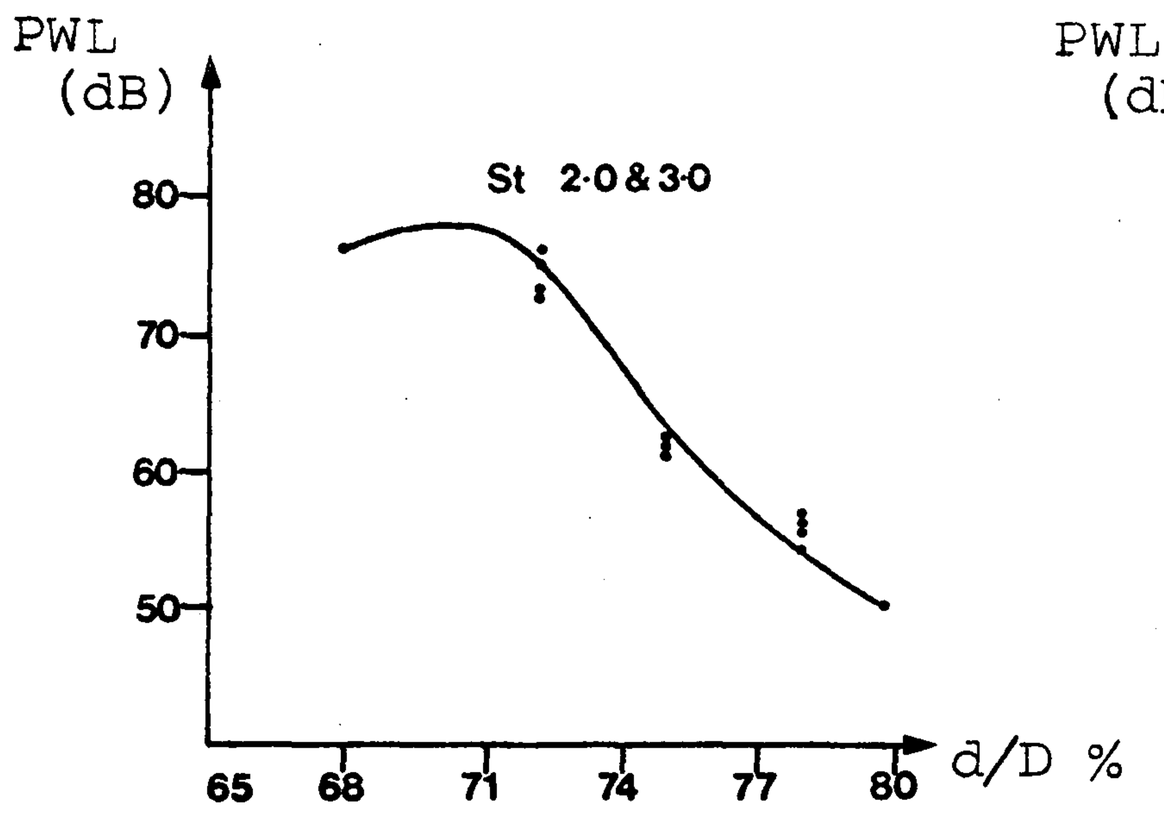

Figure 8·5(c)

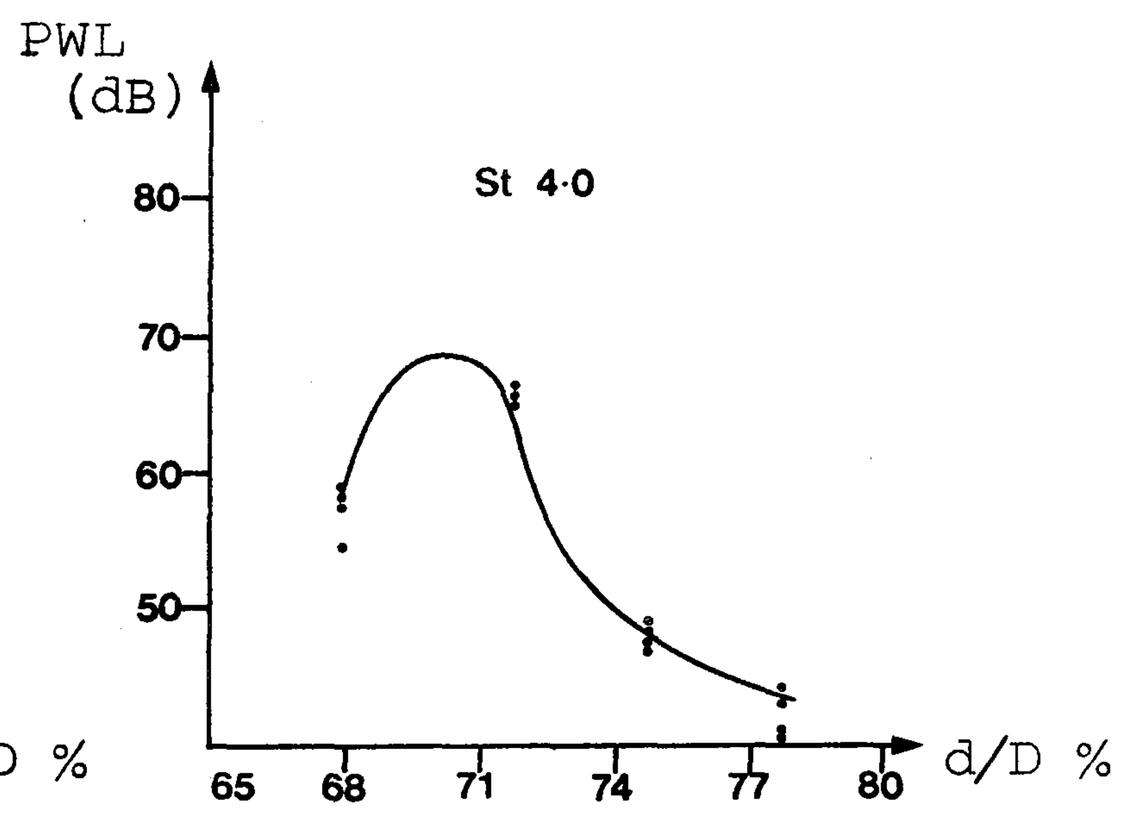

Figure 8·5(d)

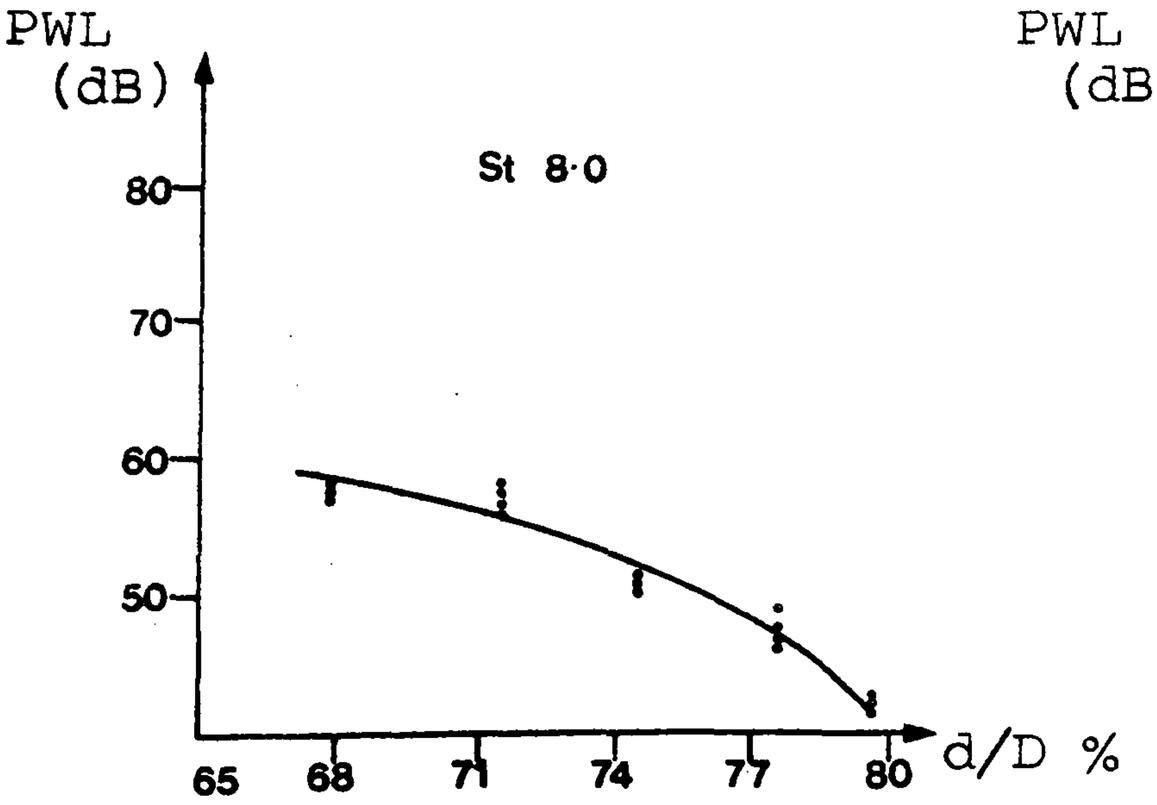

Figure 8·5(e)

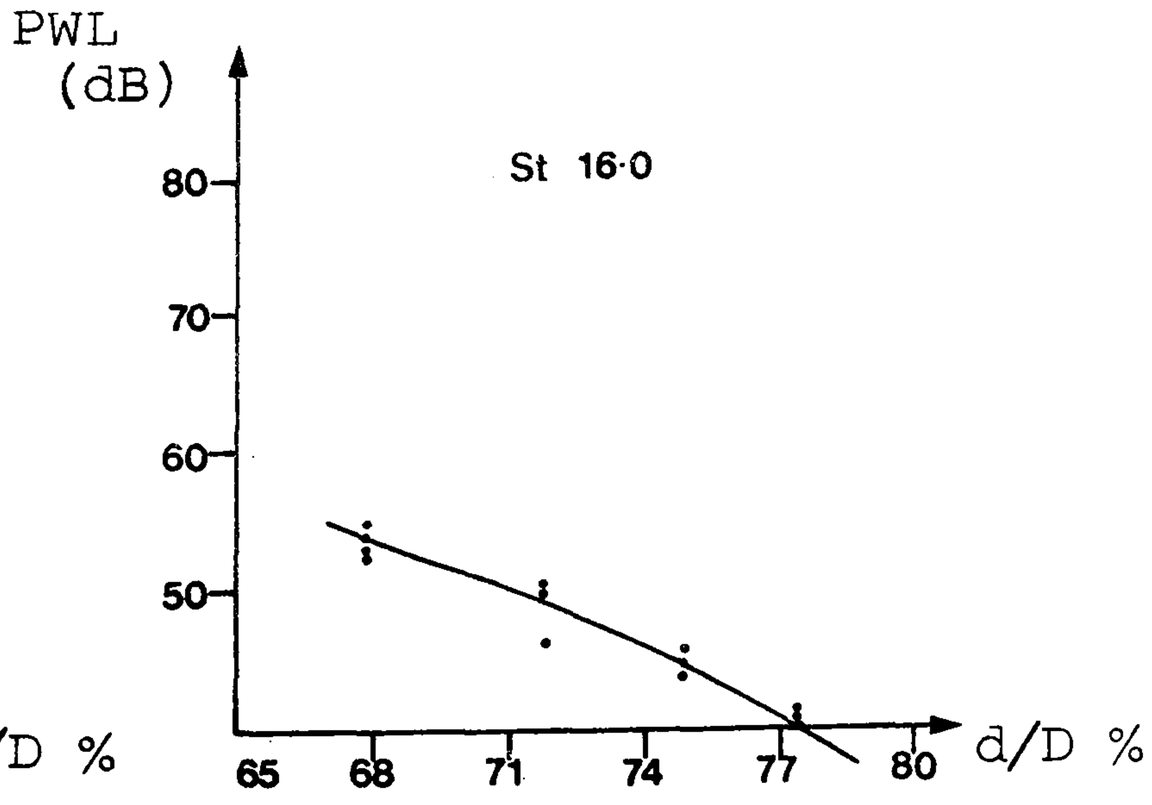

Figure 8·5(f)

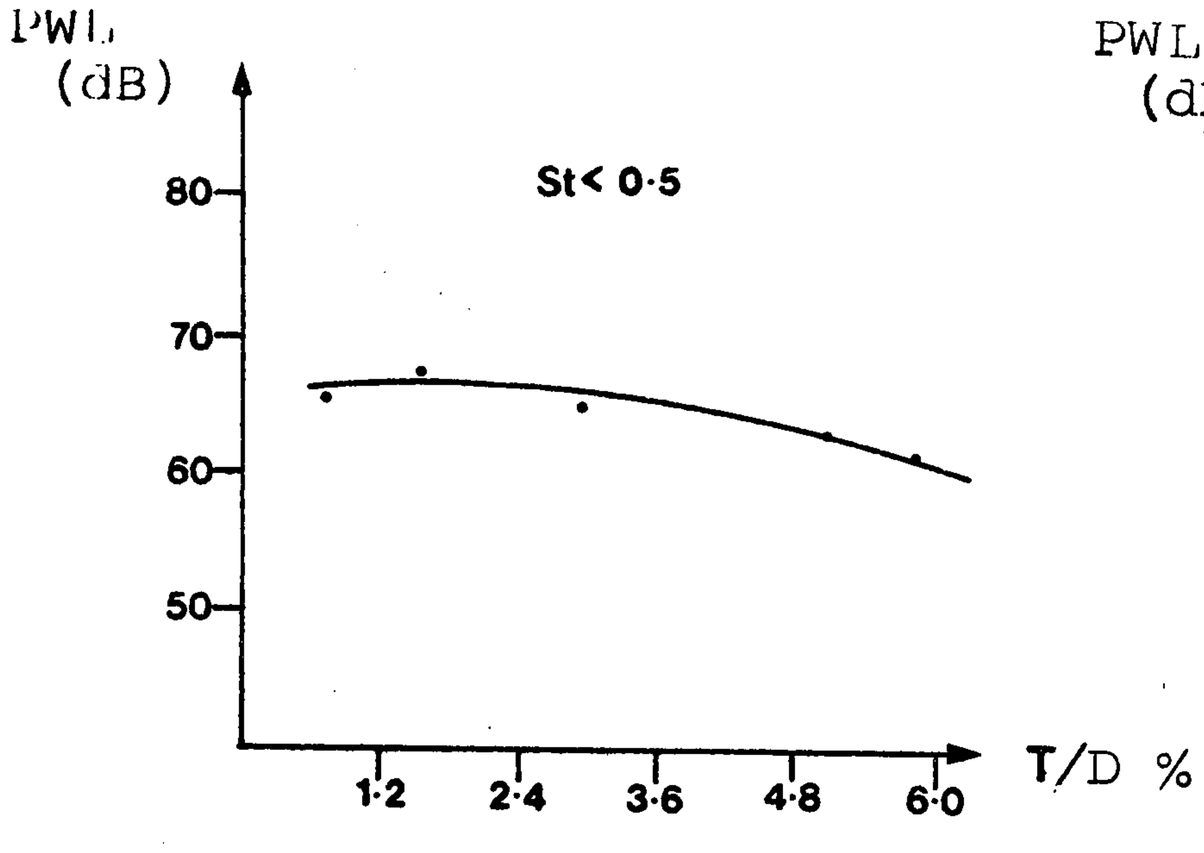

Figure 8·6(a)

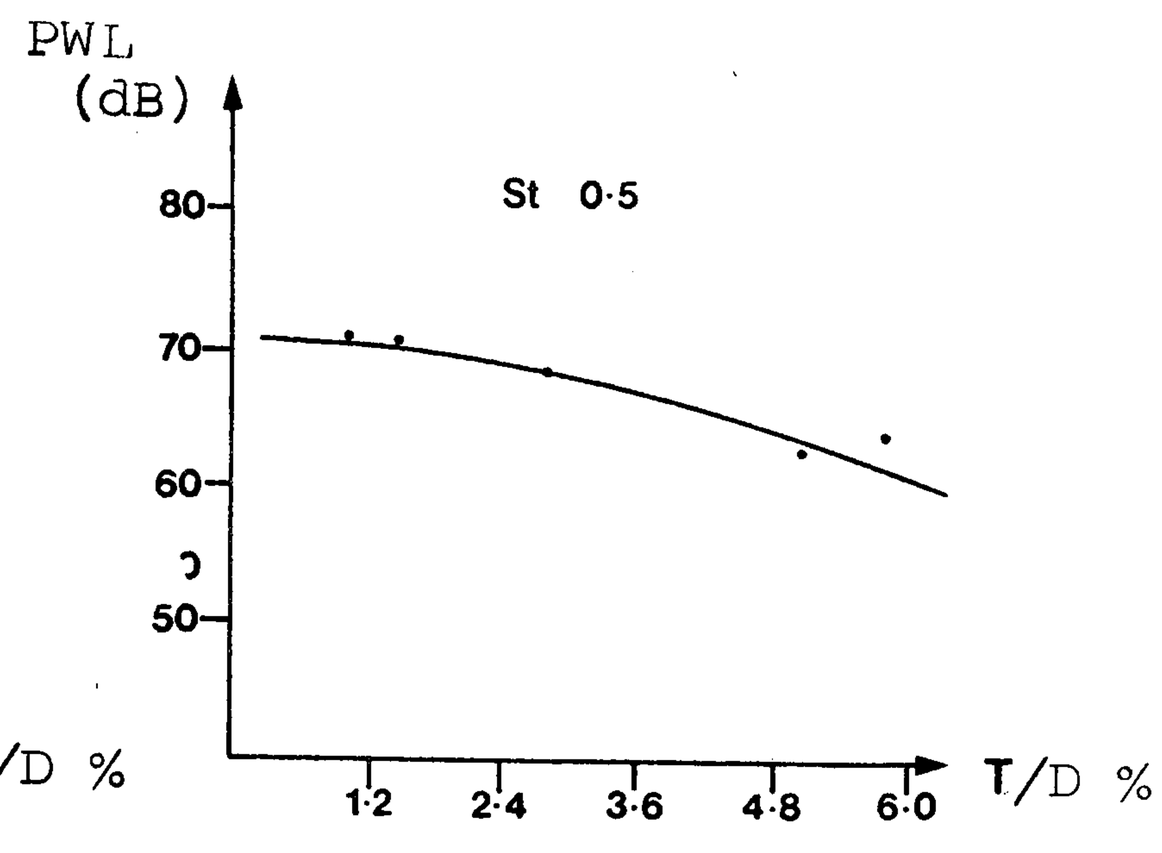

Figure 8·6(b)

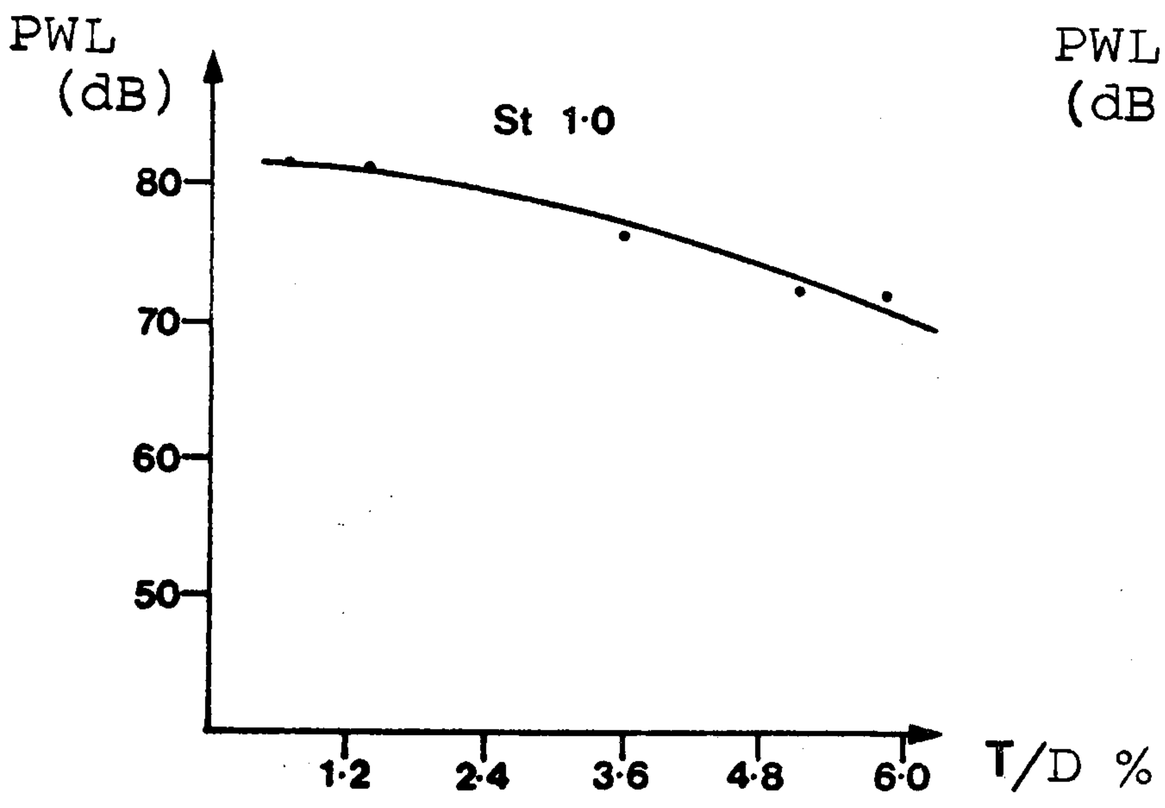

Figure 8·6(c)

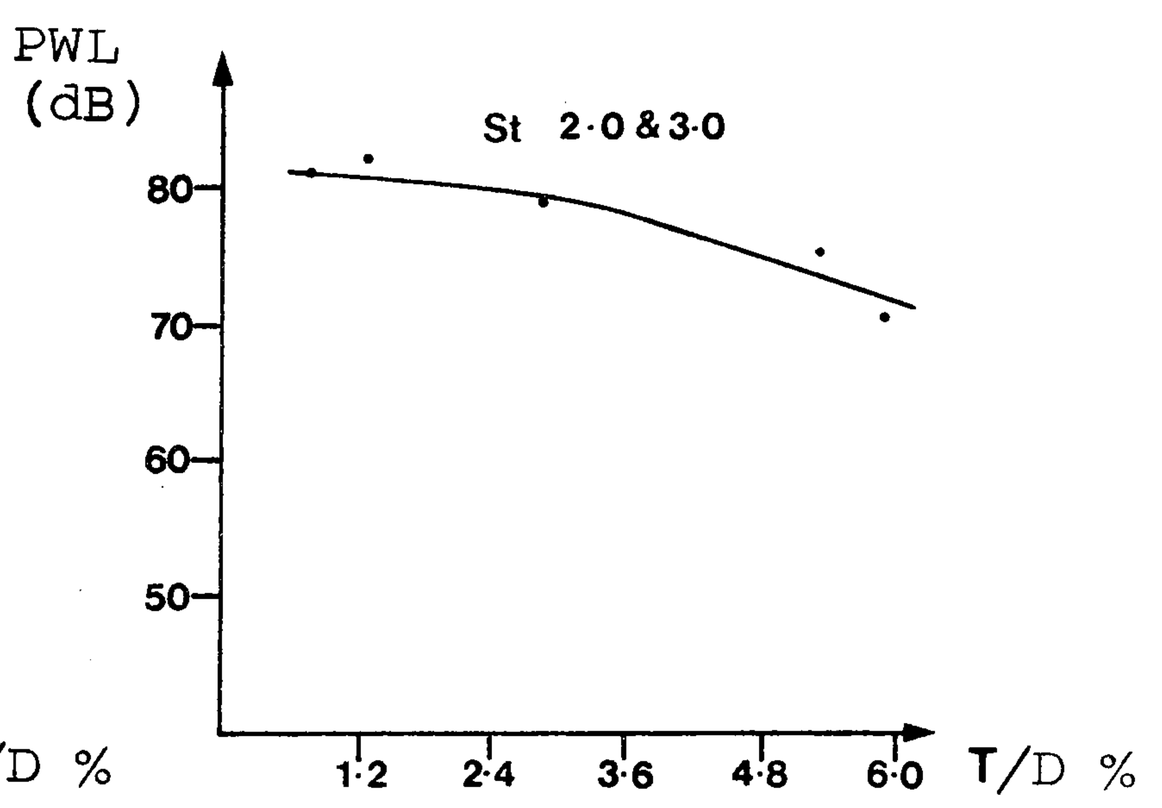

Figure 8·6(d)

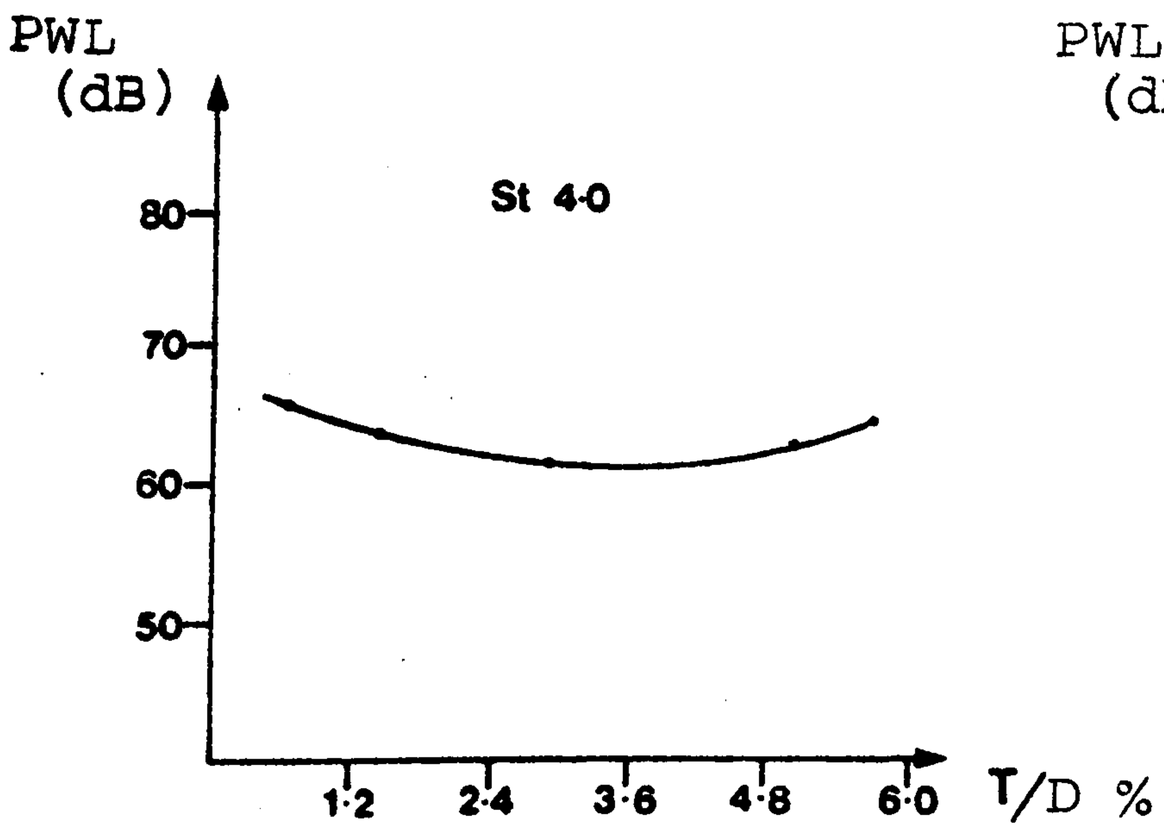

Figure 8·6(e)

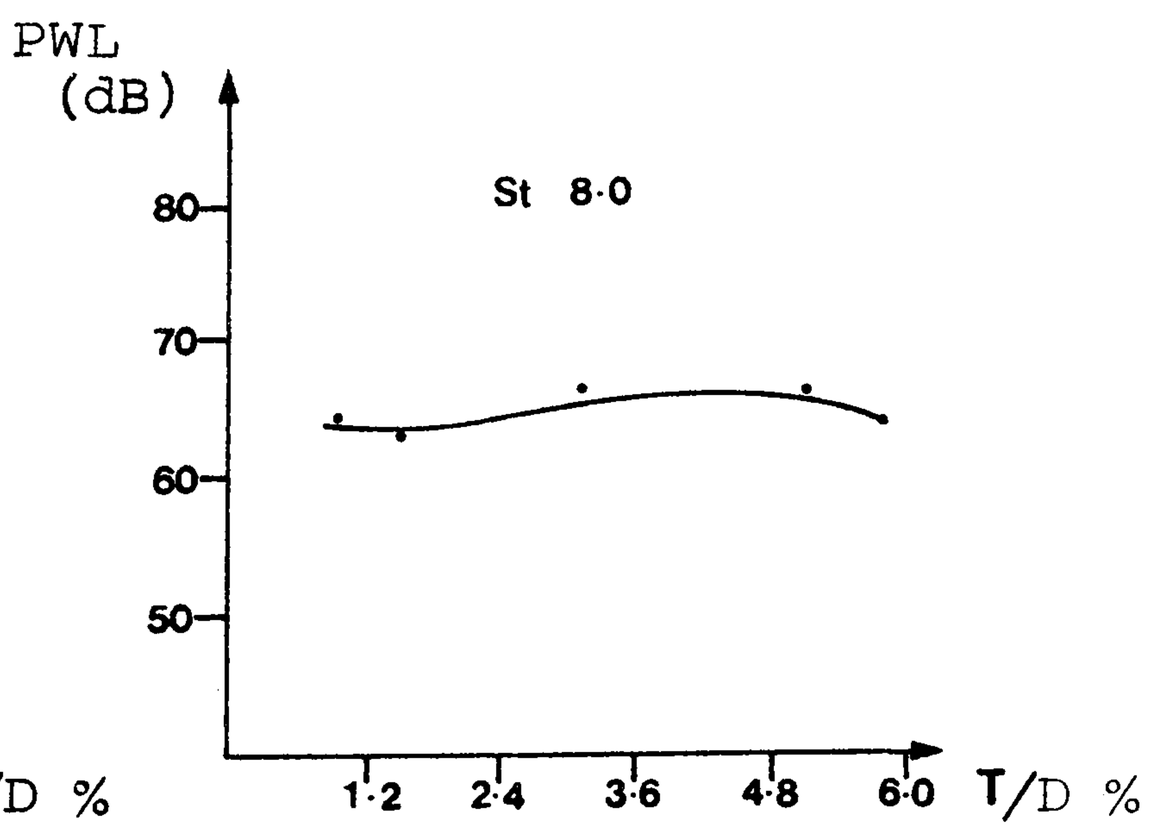

Figure 8·6(f)

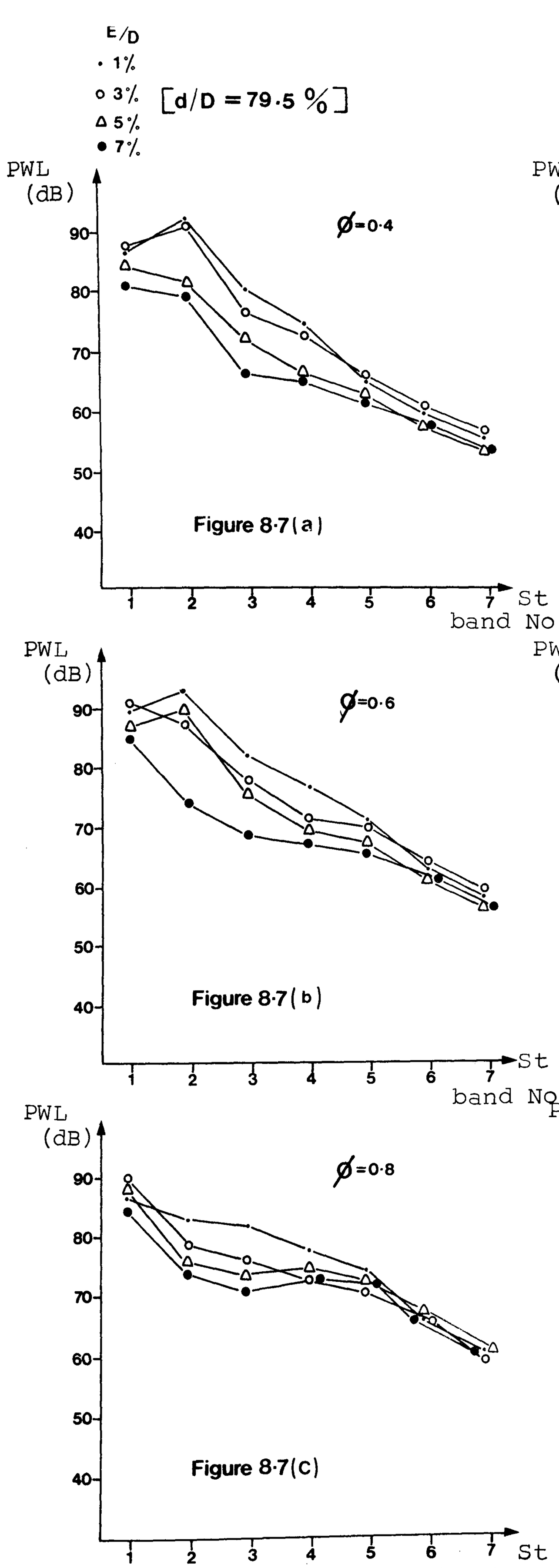

Figure 8·7(a)

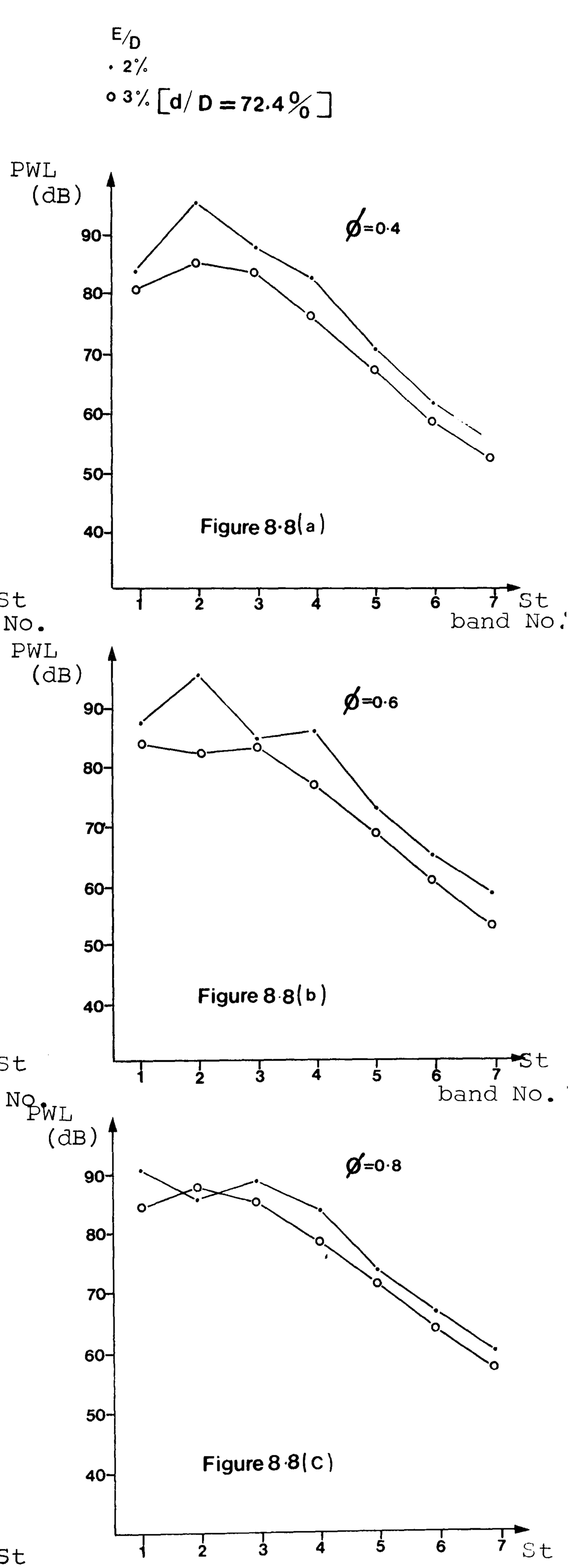

Figure 8·8(a)

Figure 8·7(b)

Figure 8·8(b)

Figure 8·7(C)

Figure 8·8(C)

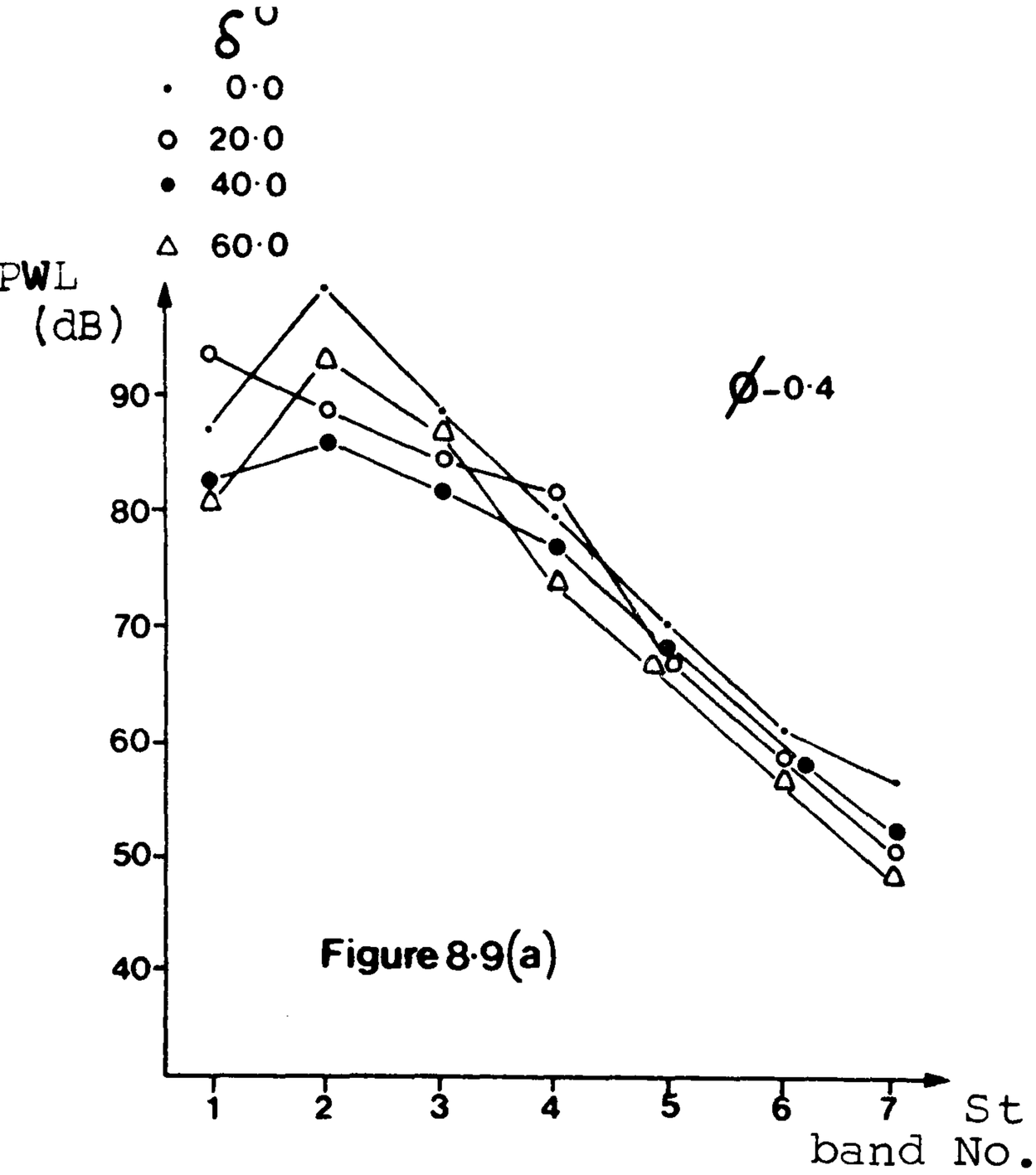

Figure 8·9(a)

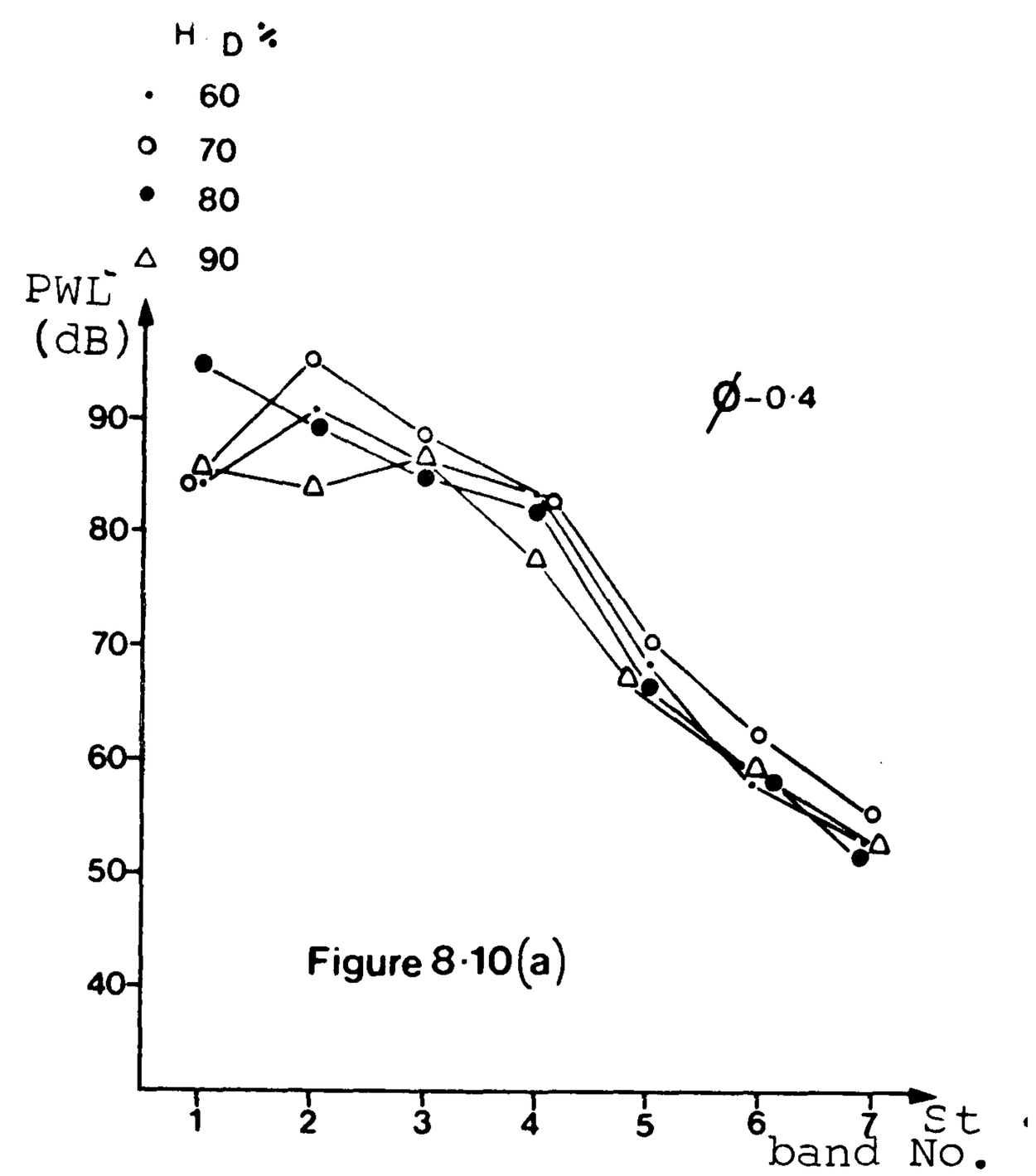

Figure 8·10(a)

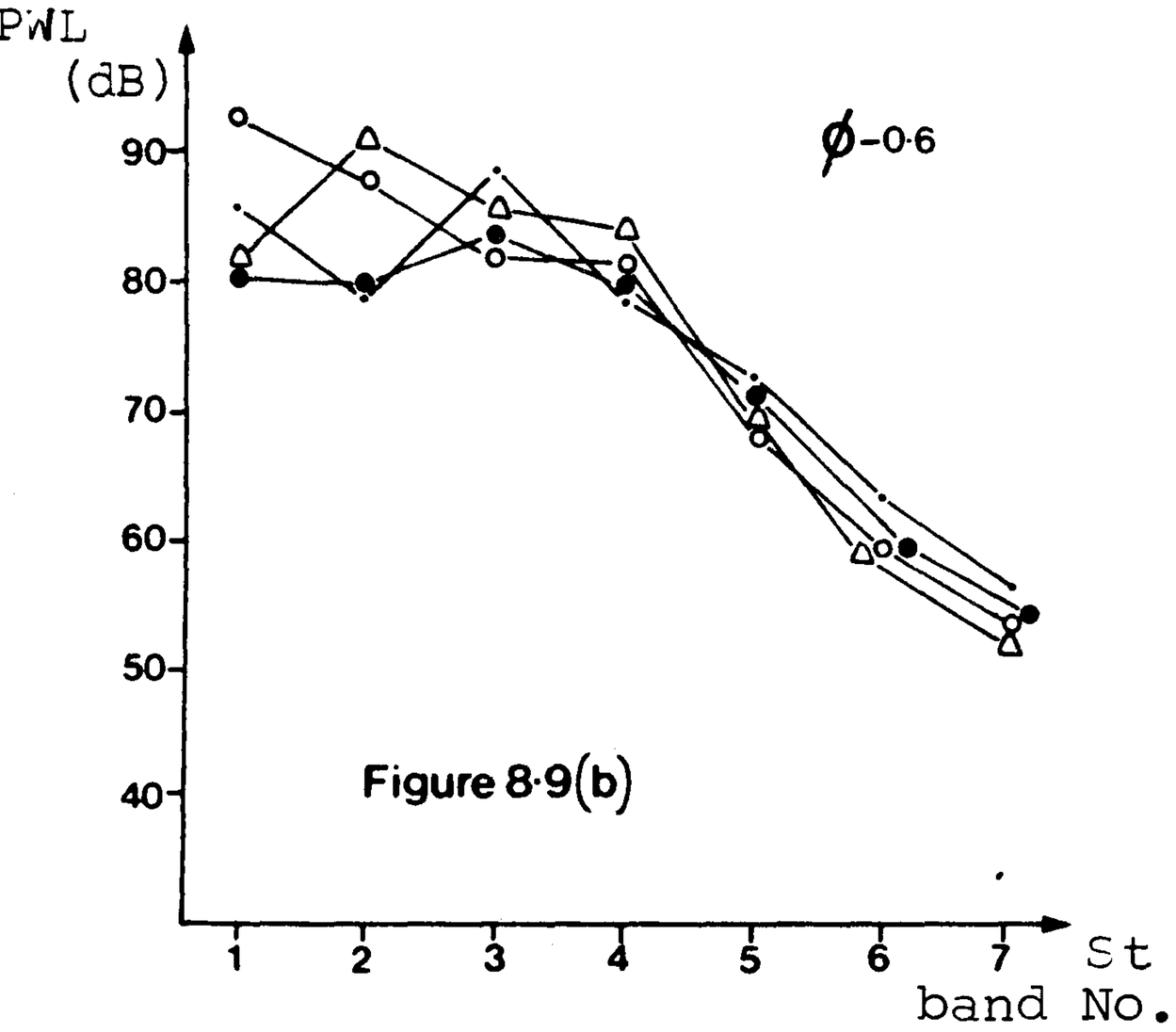

Figure 8·9(b)

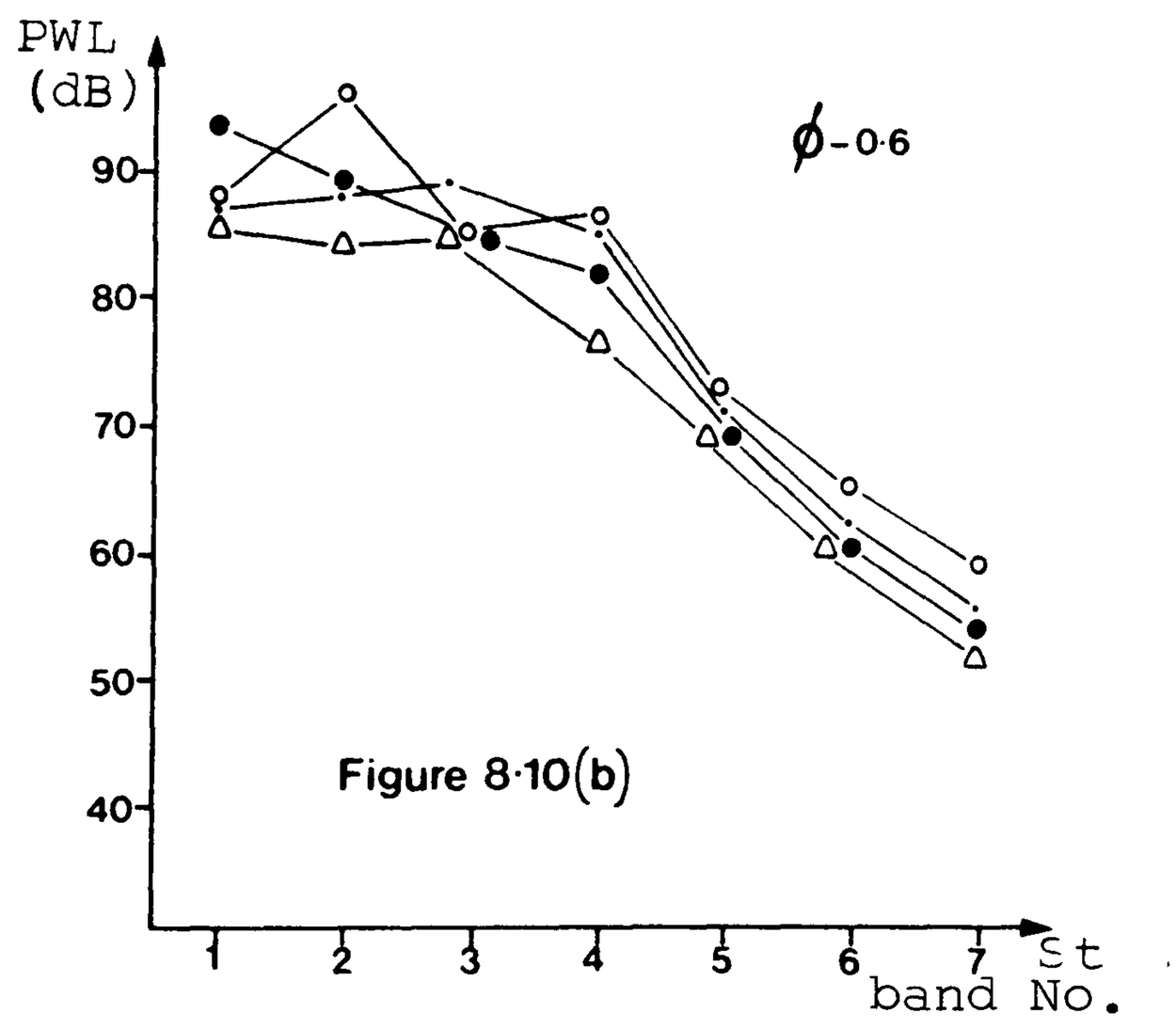

Figure 8·10(b)

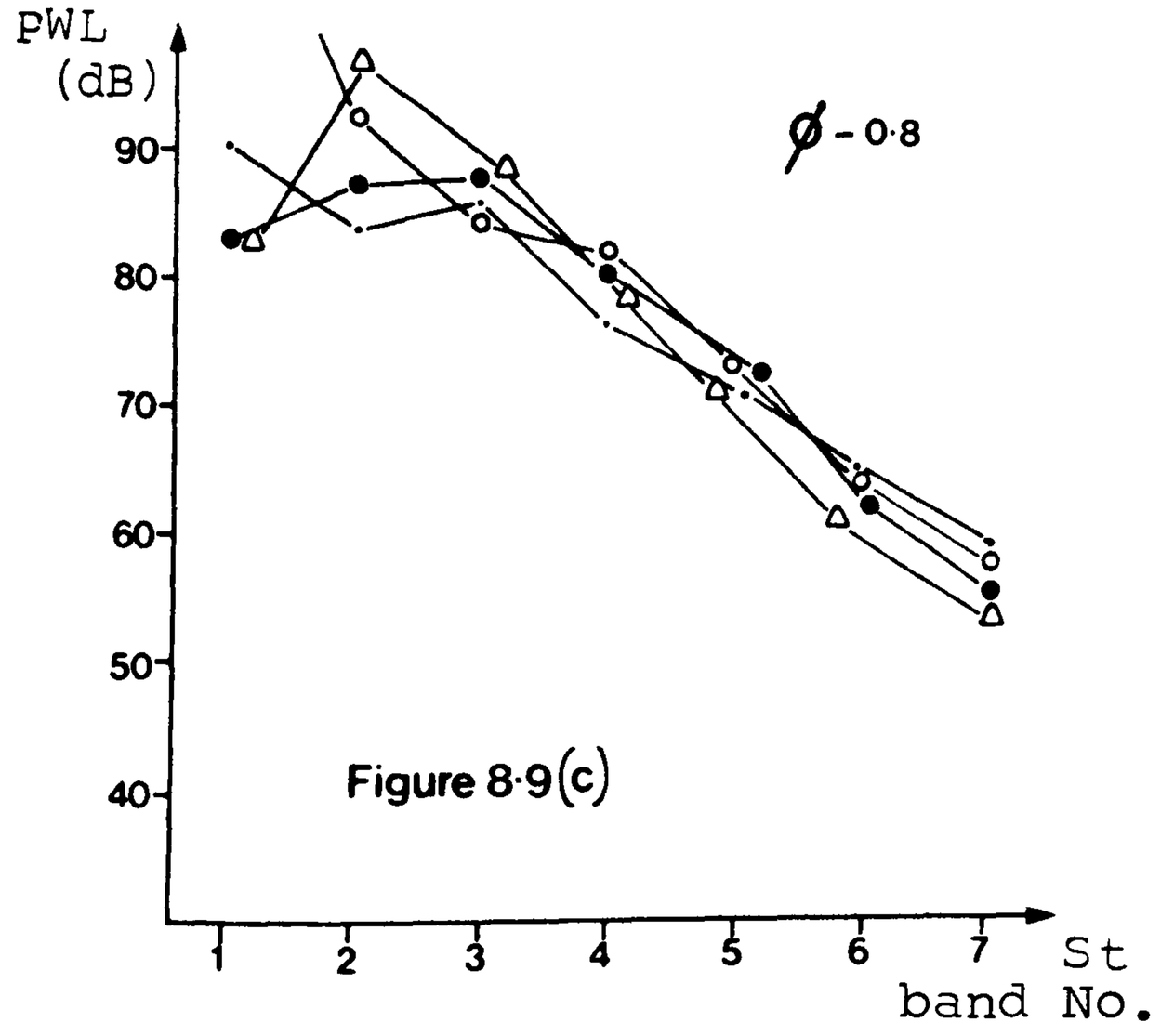

Figure 8·9(c)

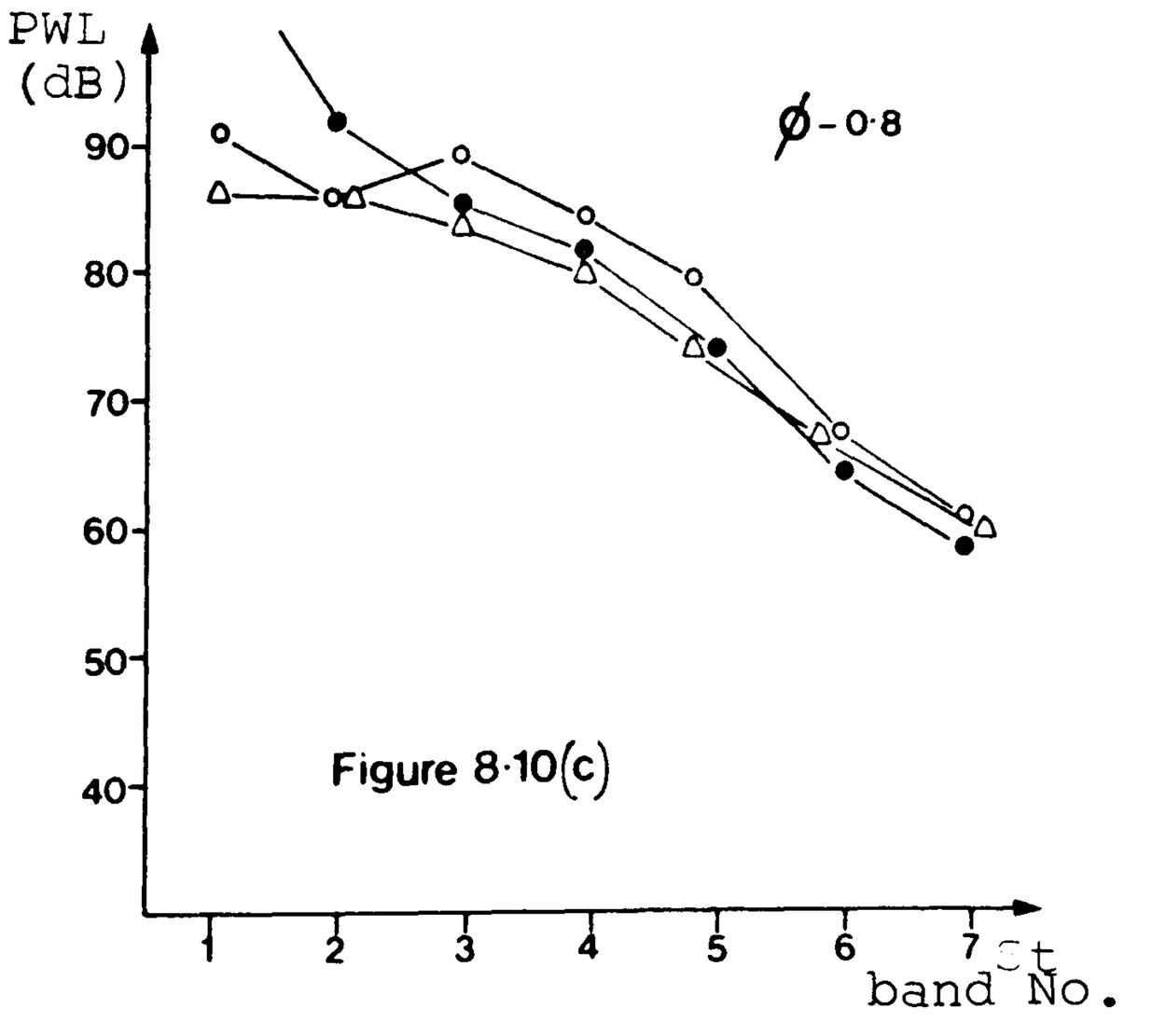

Figure 8·10(c)

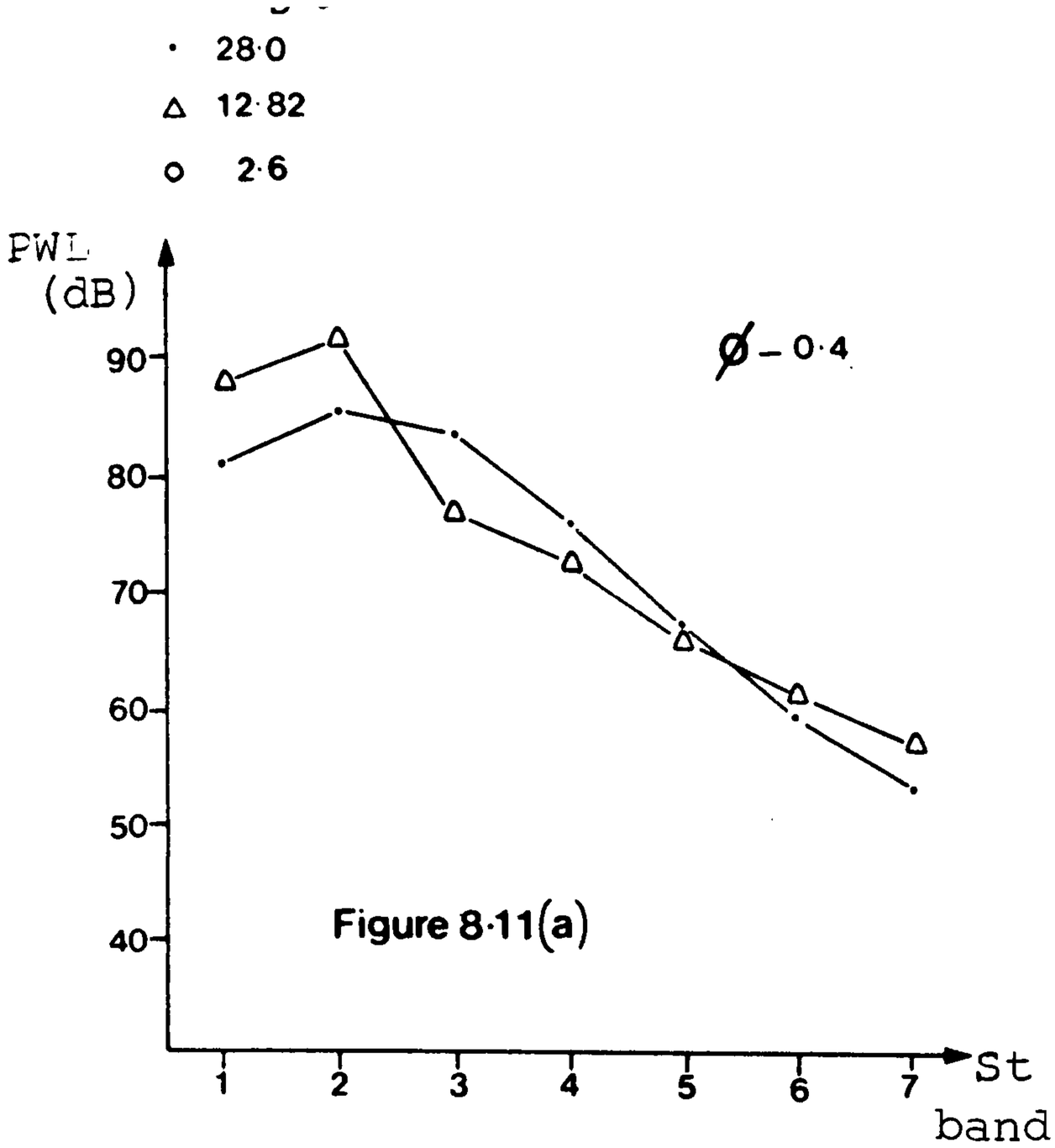

Figure 8·11(a)

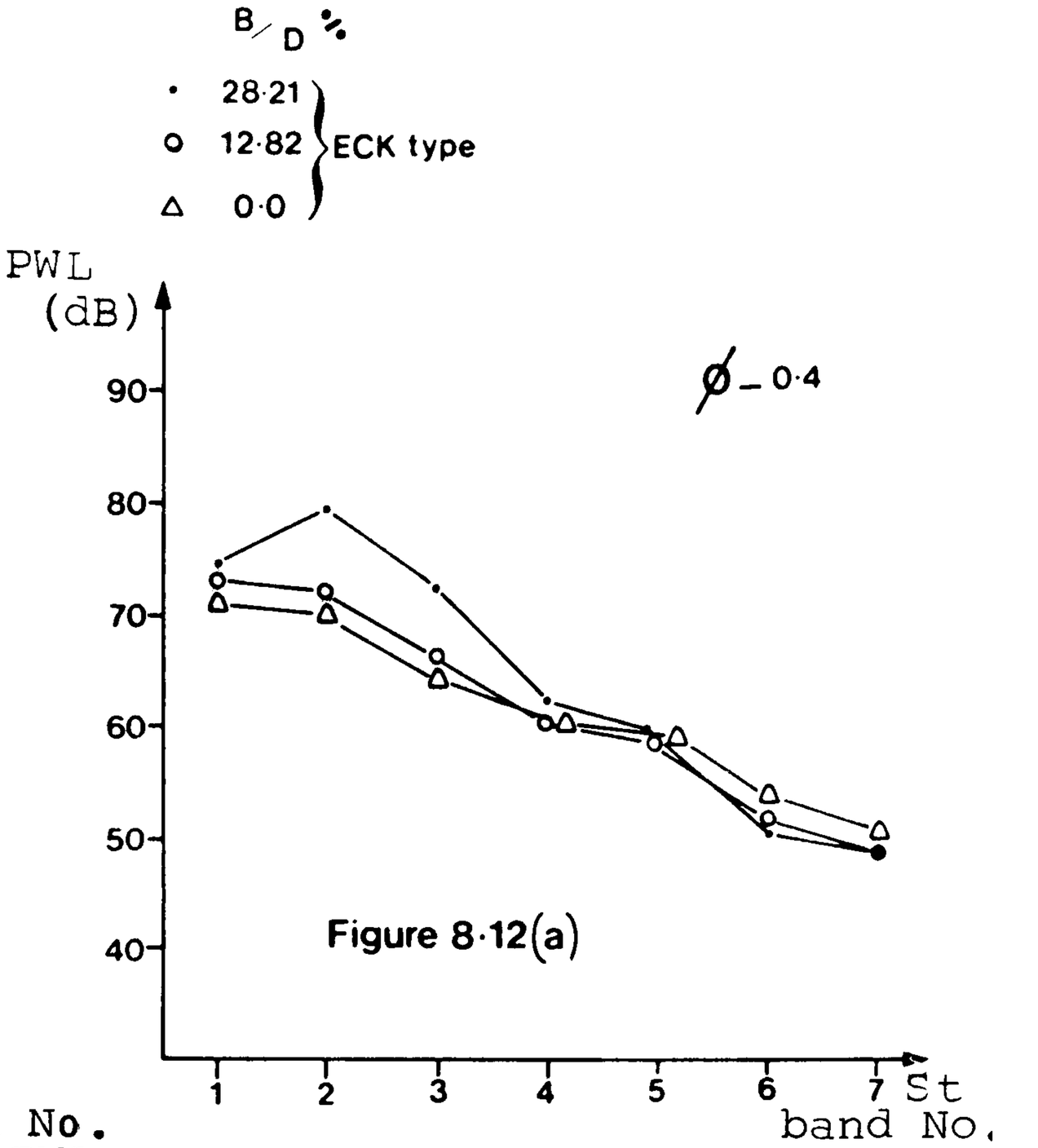

Figure 8·12(a)

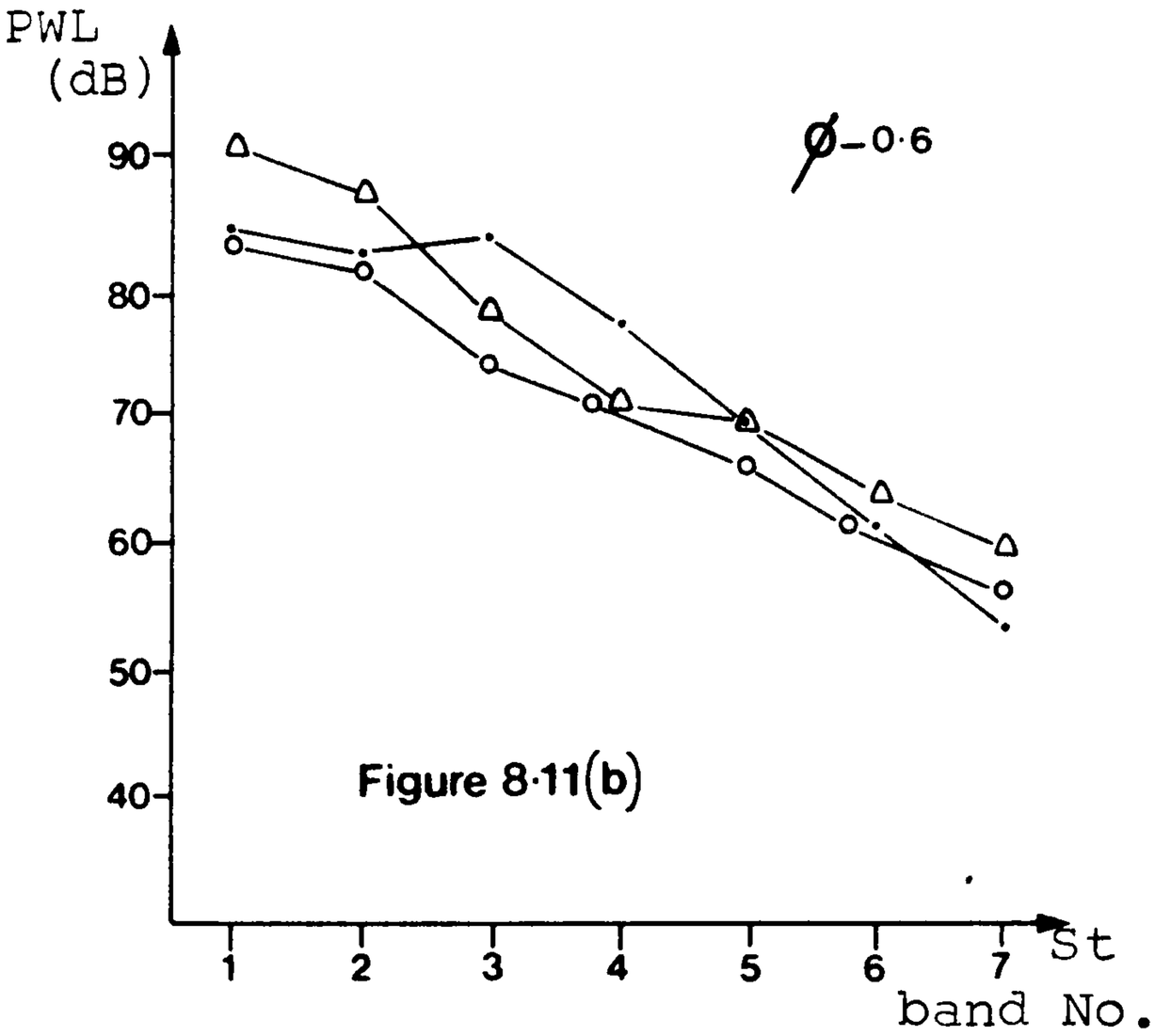

Figure 8·11(b)

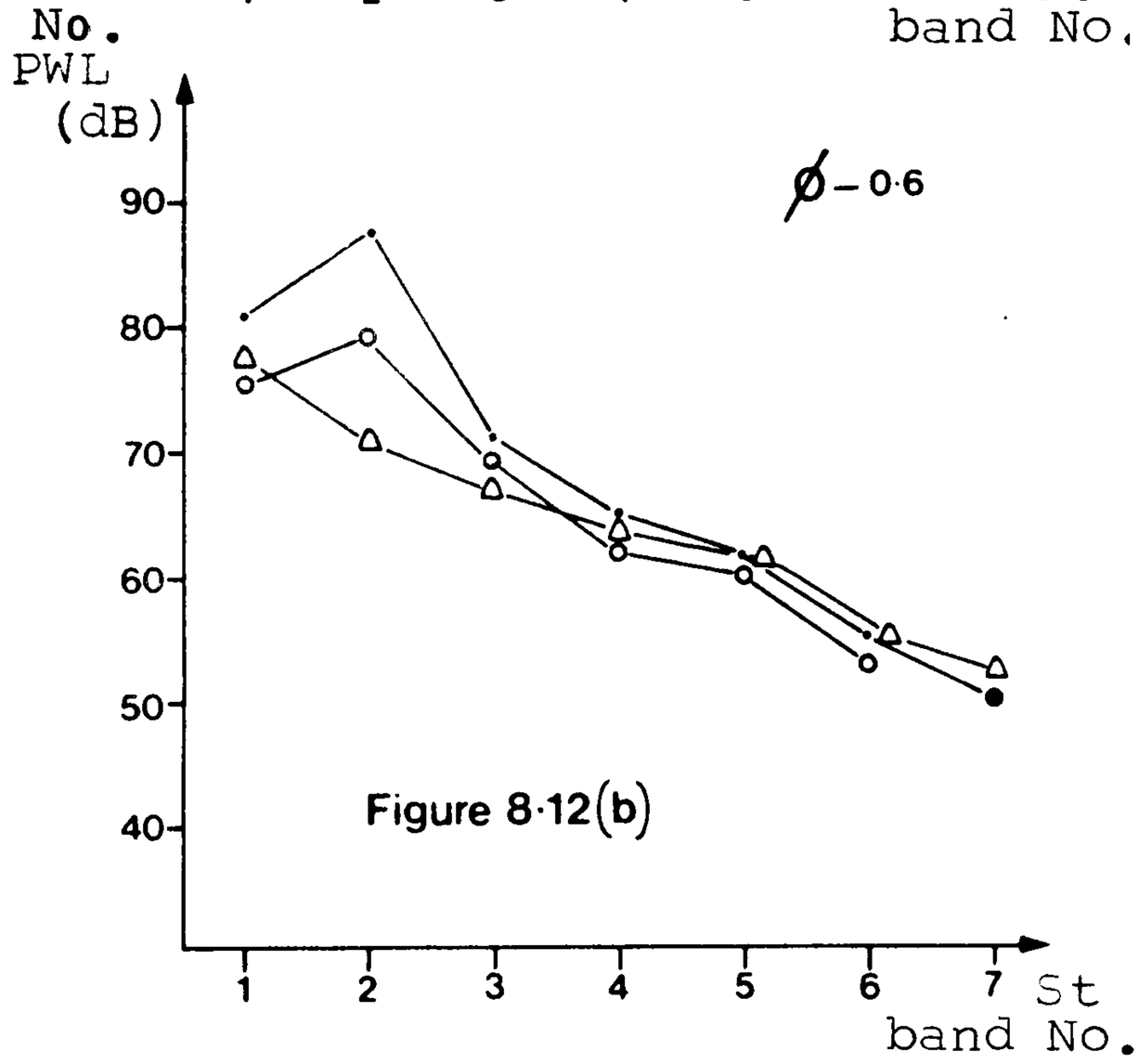

Figure 8·12(b)

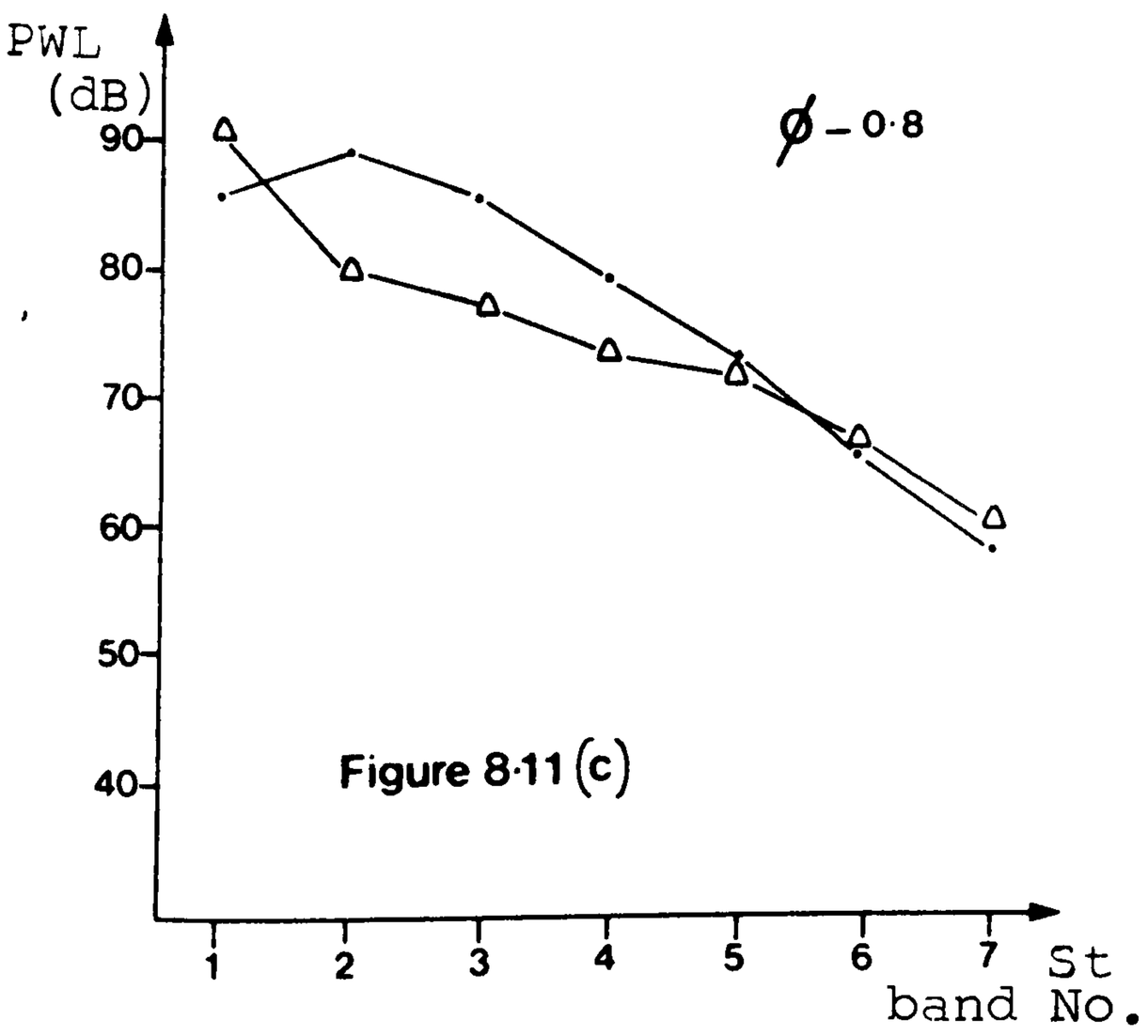

Figure 8·11 (c)

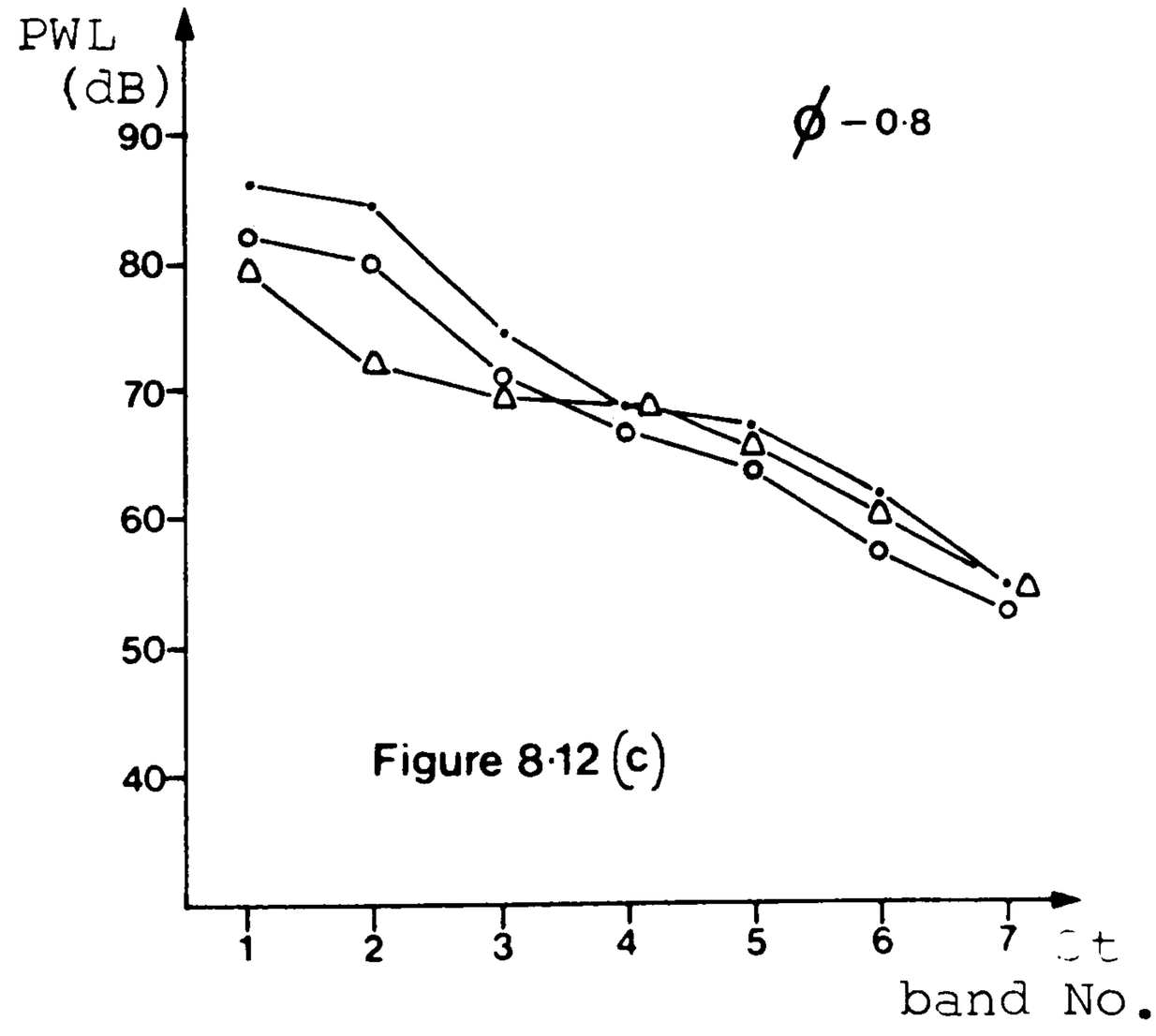

Figure 8·12 (c)

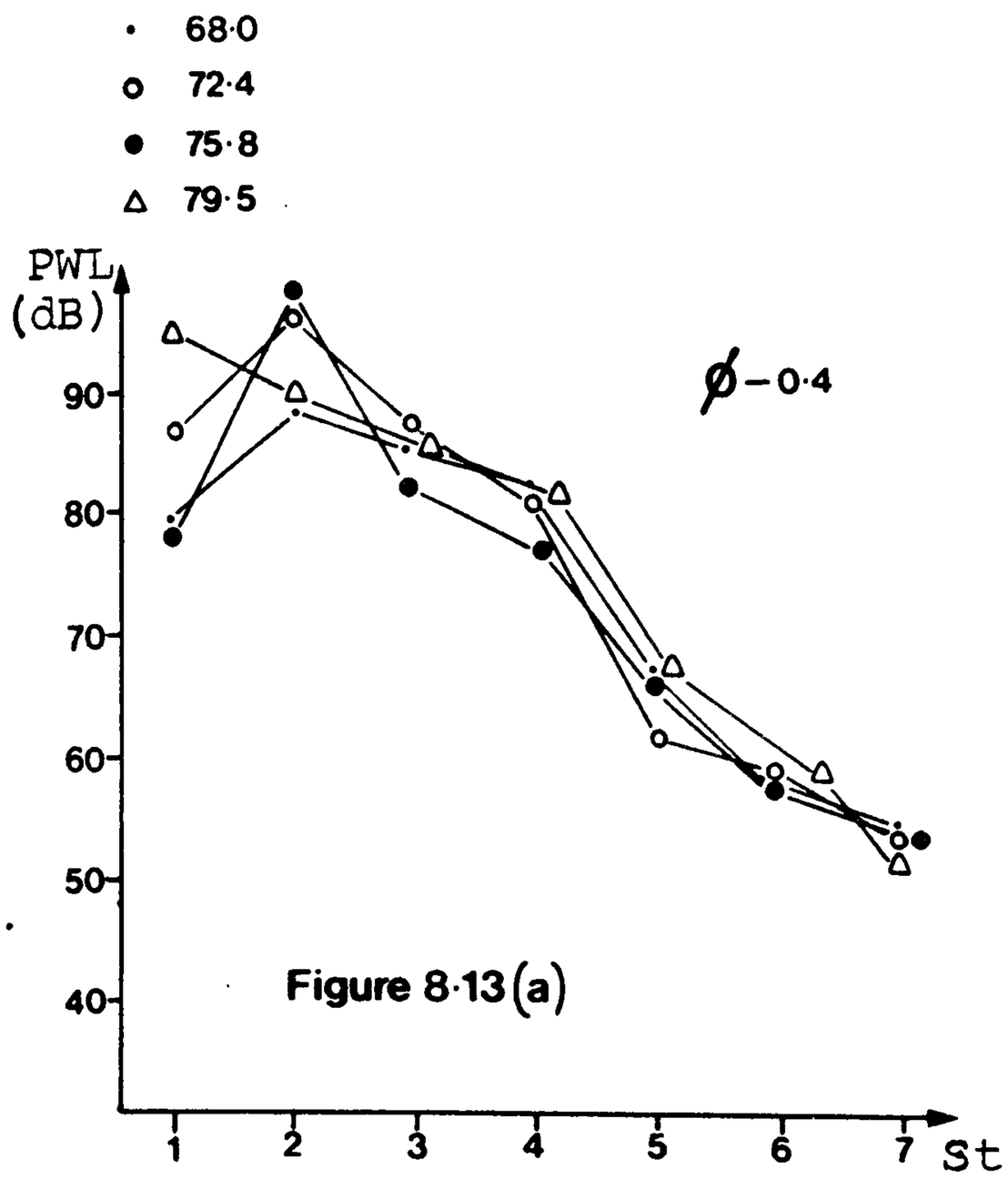

Figure 8·13 (a)

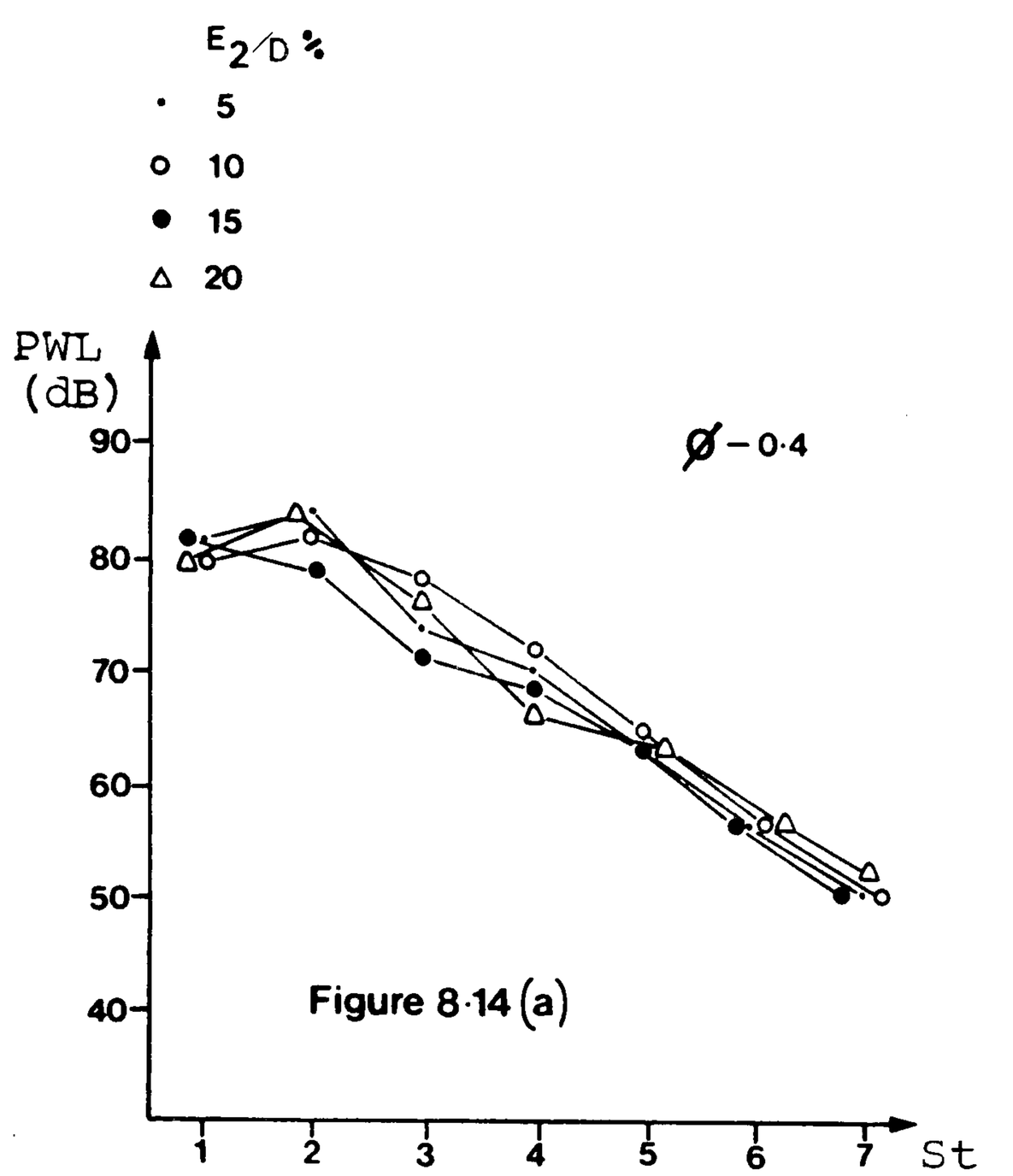

Figure 8·14 (a)

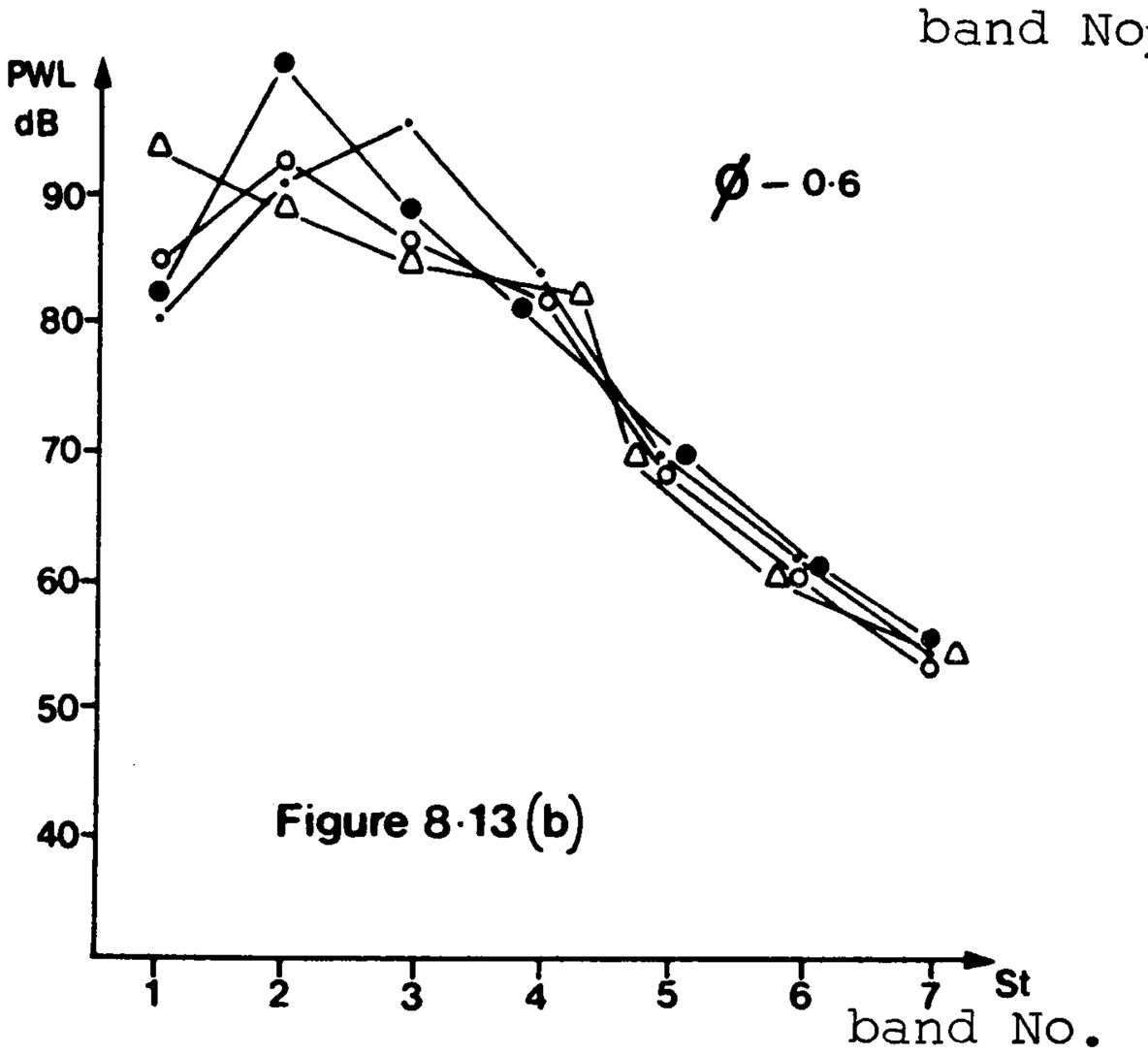

Figure 8·13 (b)

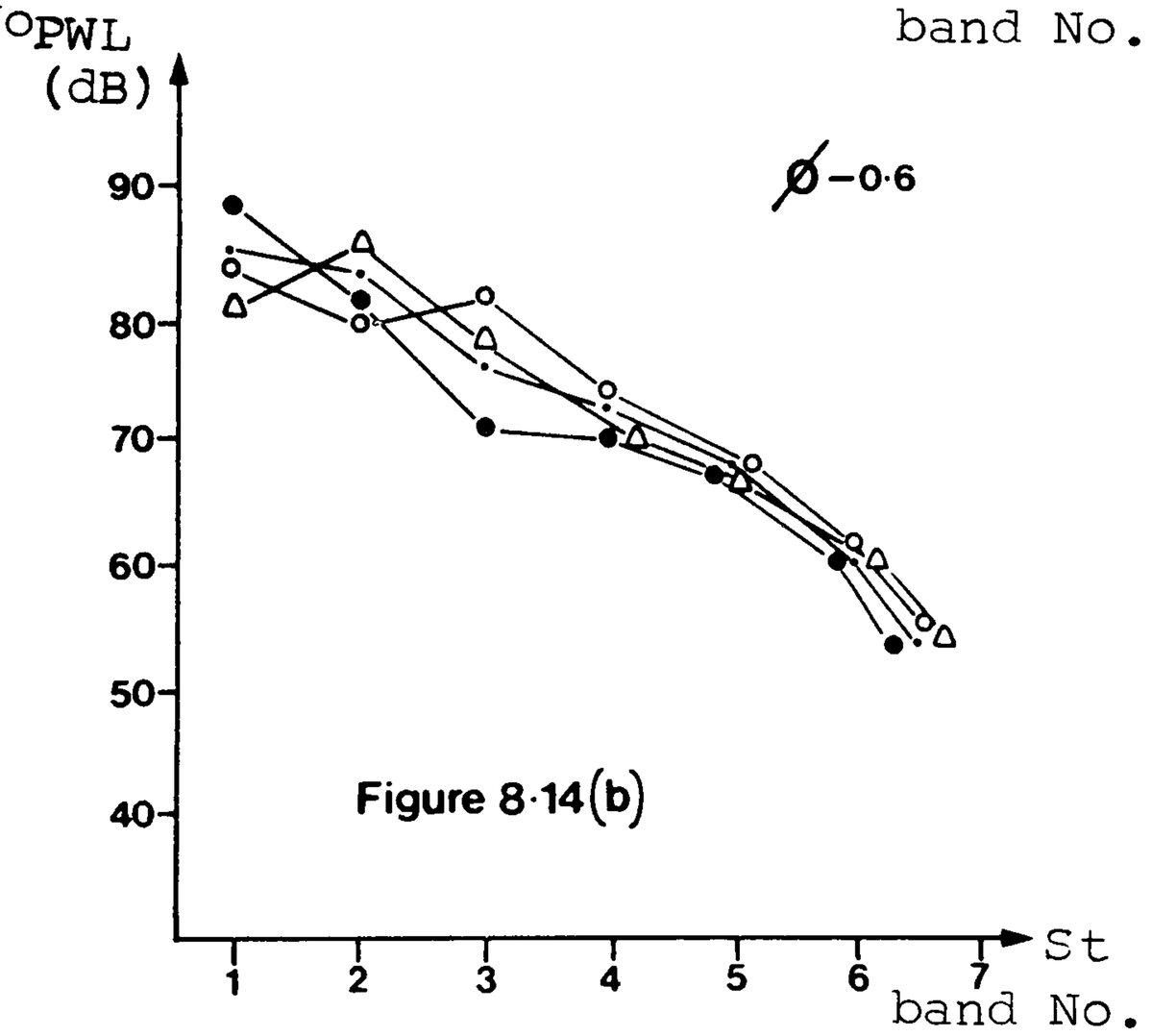

Figure 8·14 (b)

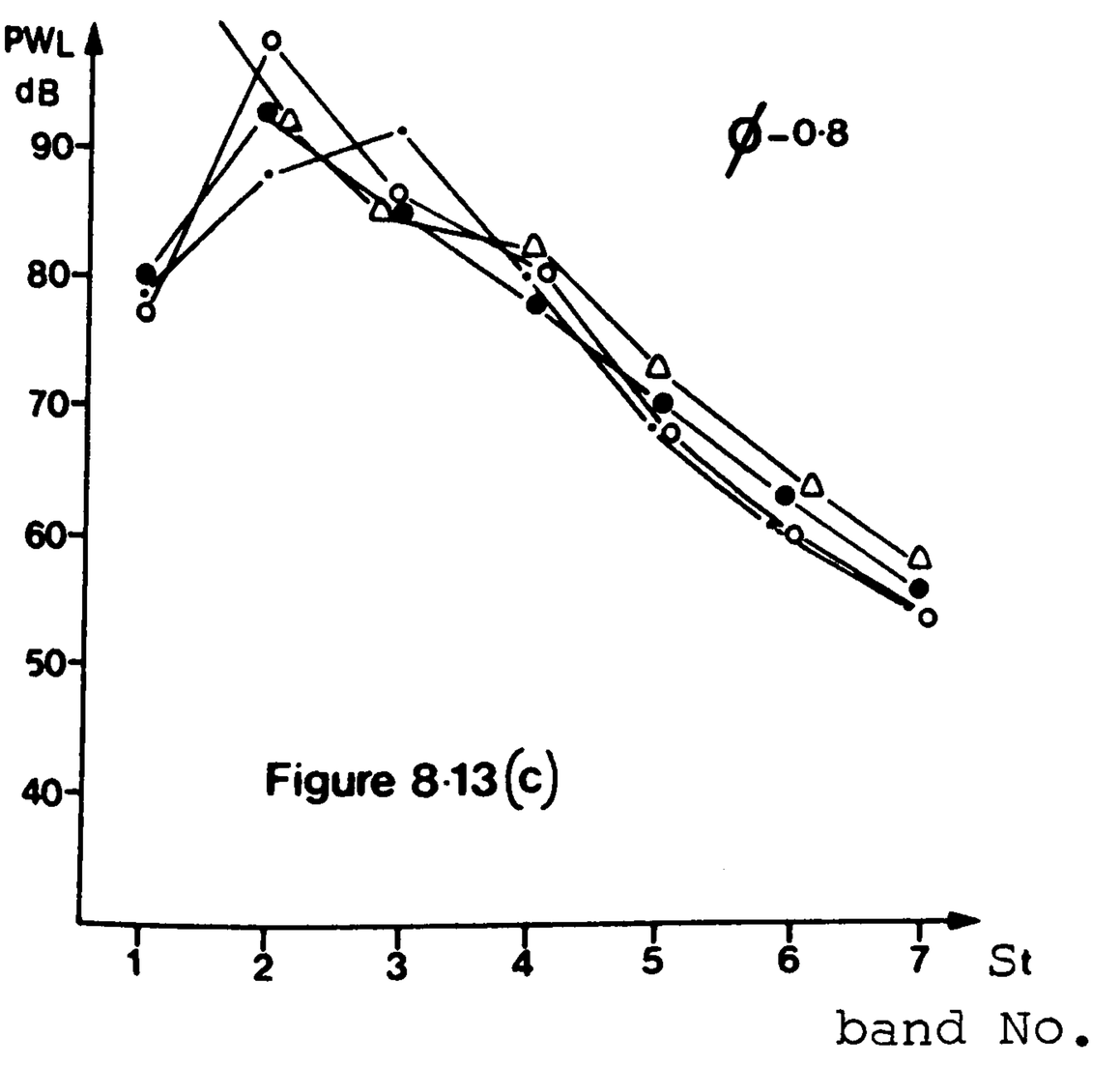

Figure 8·13 (c)

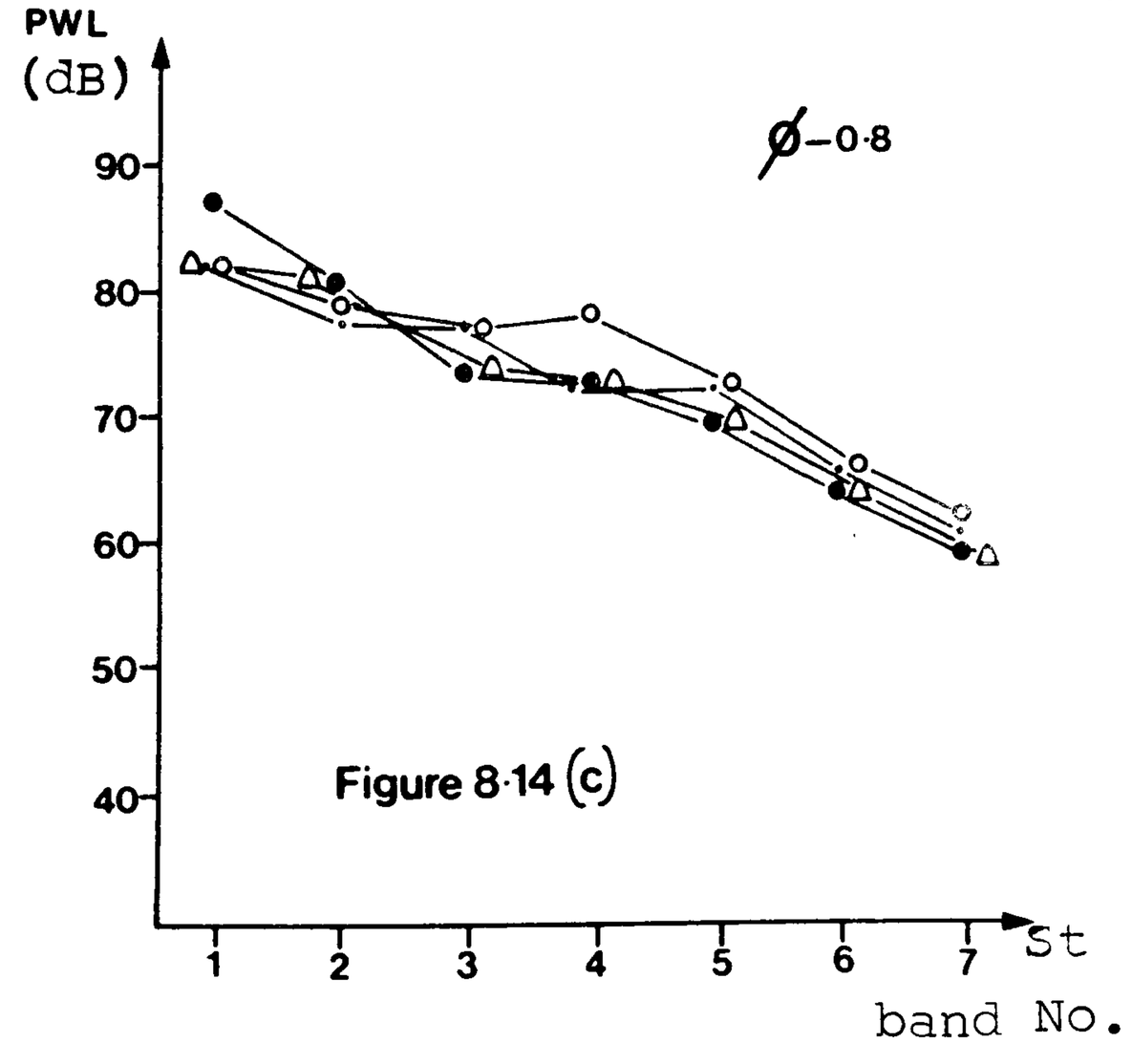

Figure 8·14 (c)

T/D %

• 0.81

o 1.62

△ 4.88

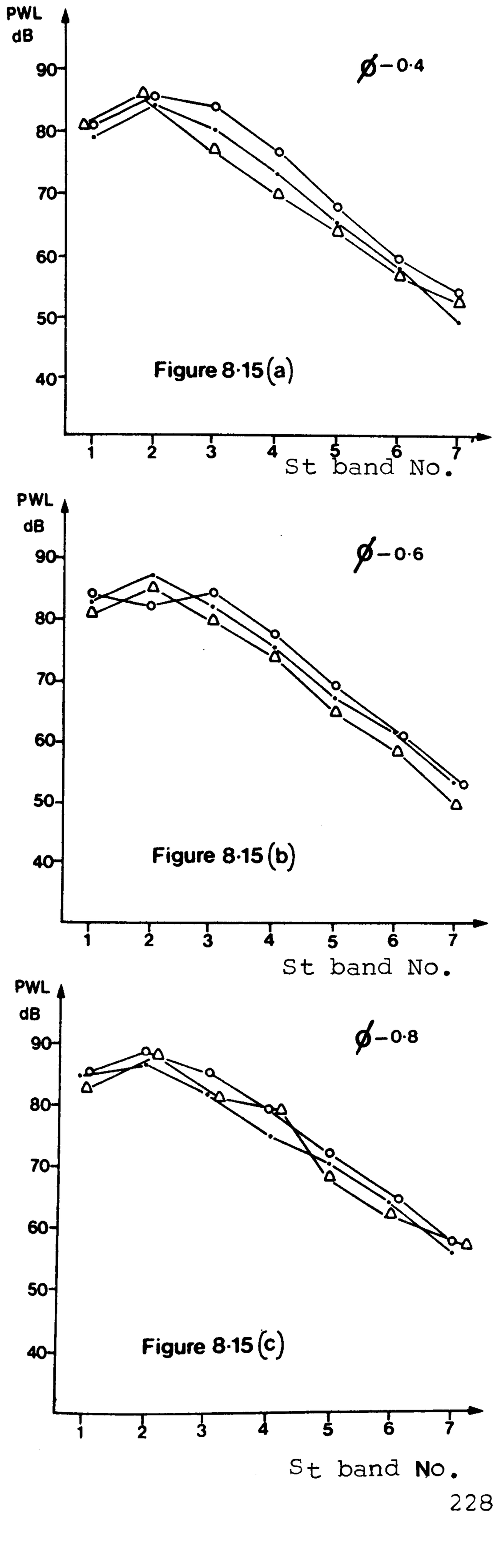

Figure 8·15(a)

Figure 8·15(b)

Figure 8·15(c)

• Control

o 1 blade offset

△ Random irregularity

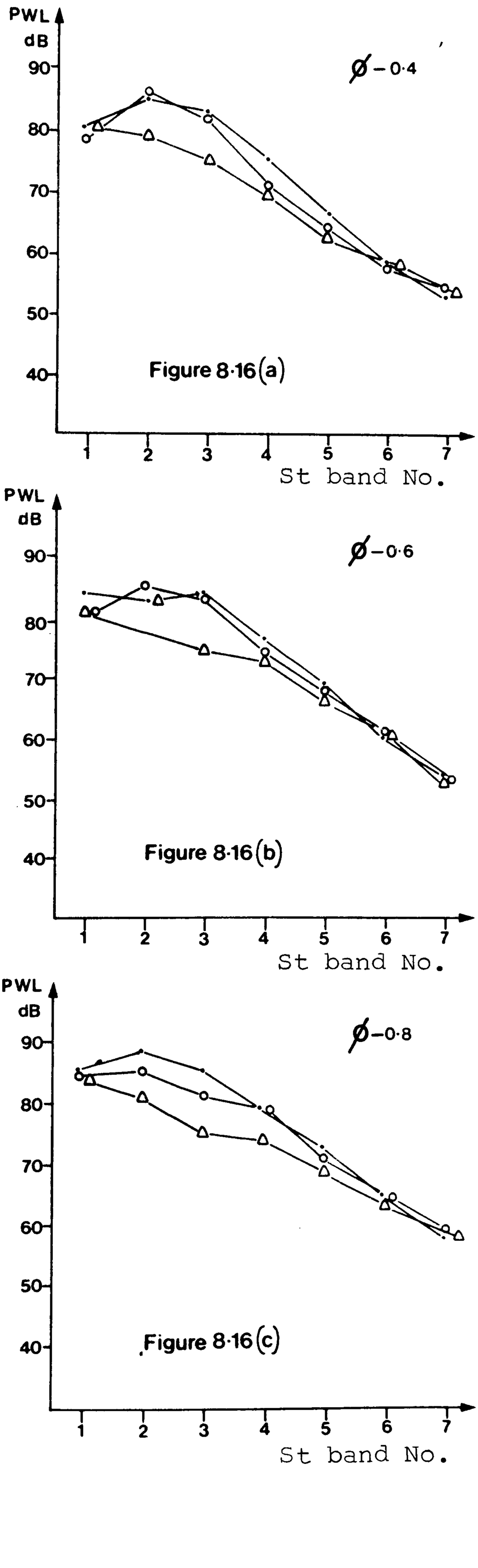

Figure 8·16(a)

Figure 8·16(b)

Figure 8·16(c)

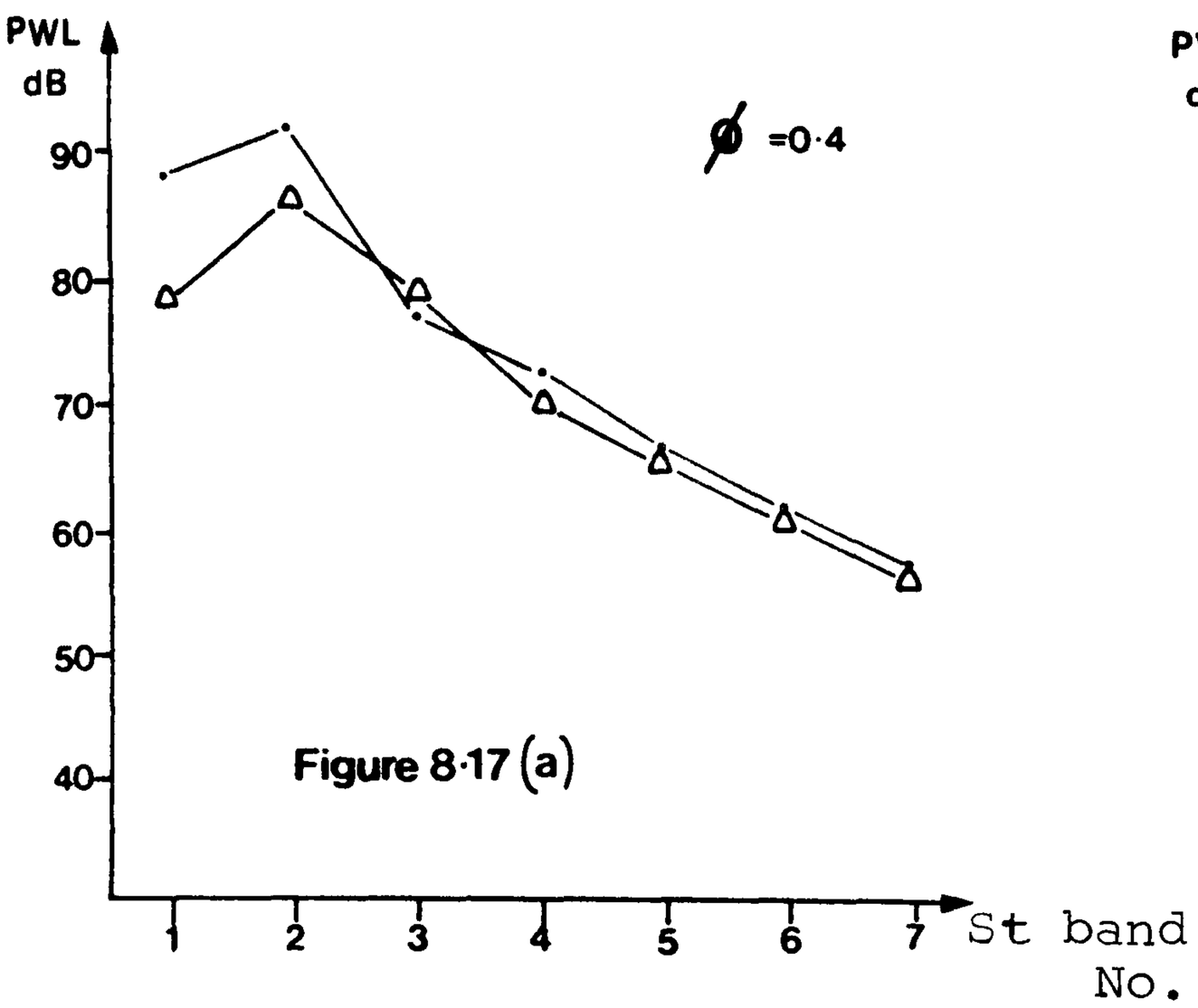

Figure 8·17 (a)

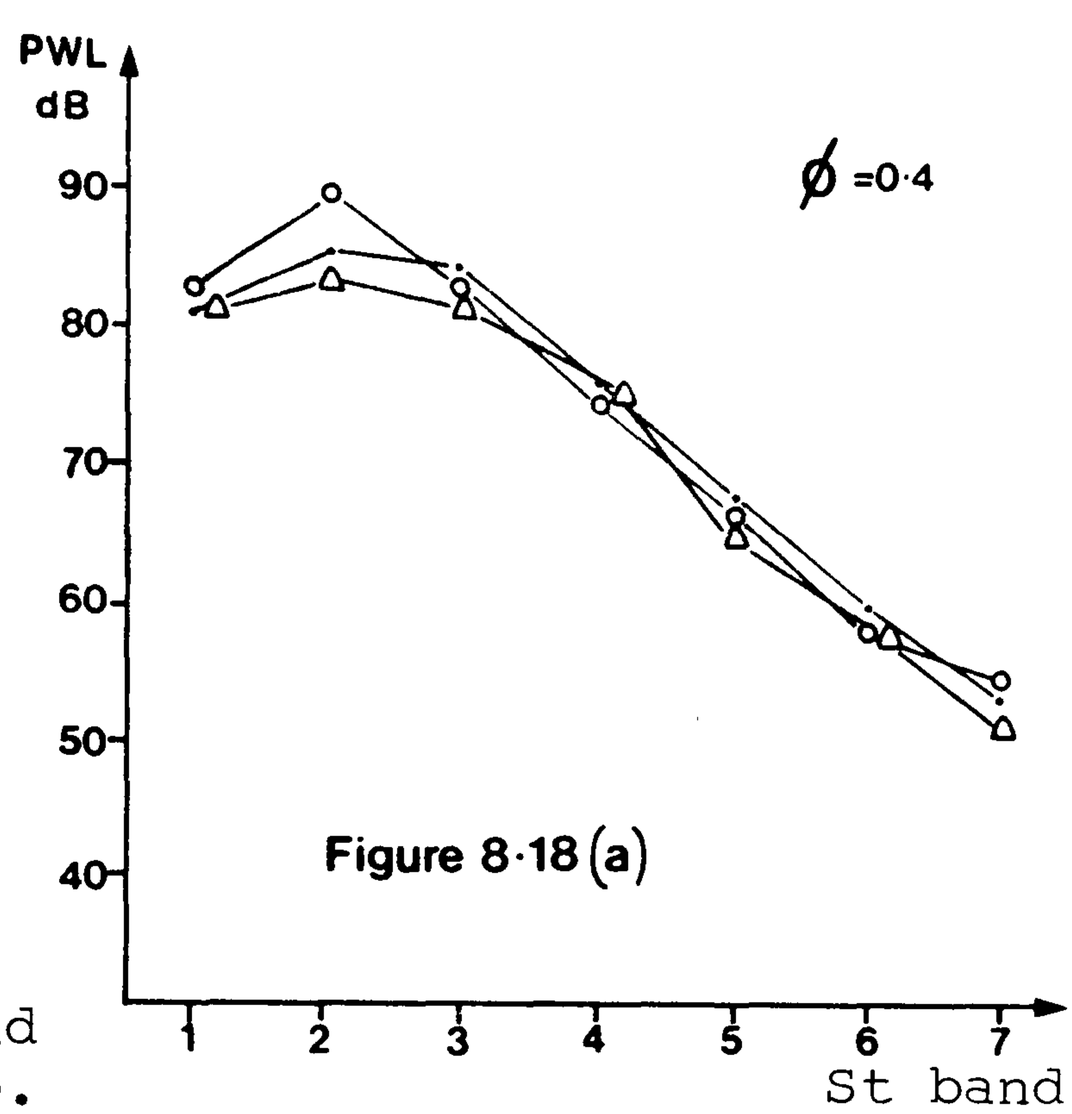

Figure 8·18 (a)

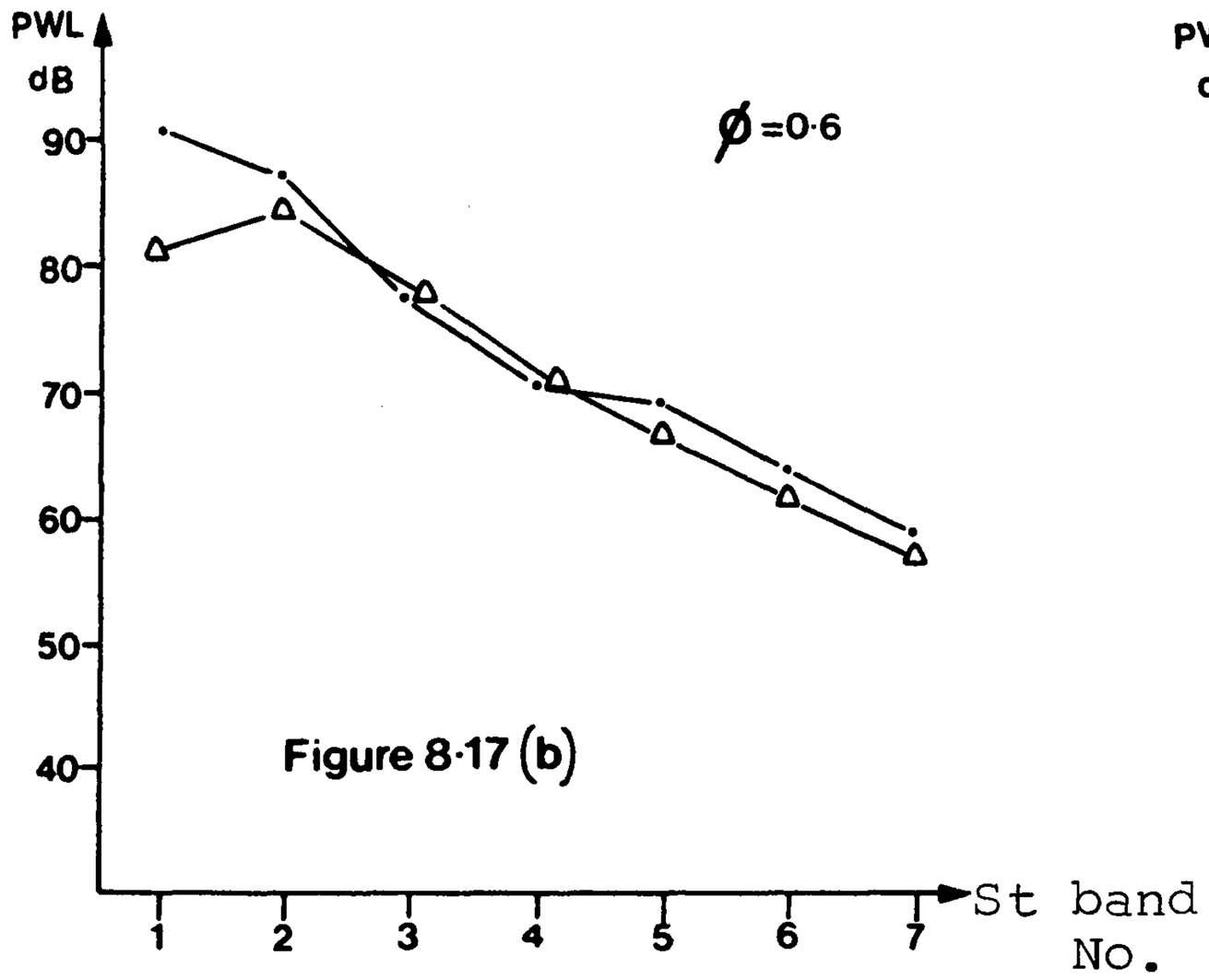

Figure 8·17 (b)

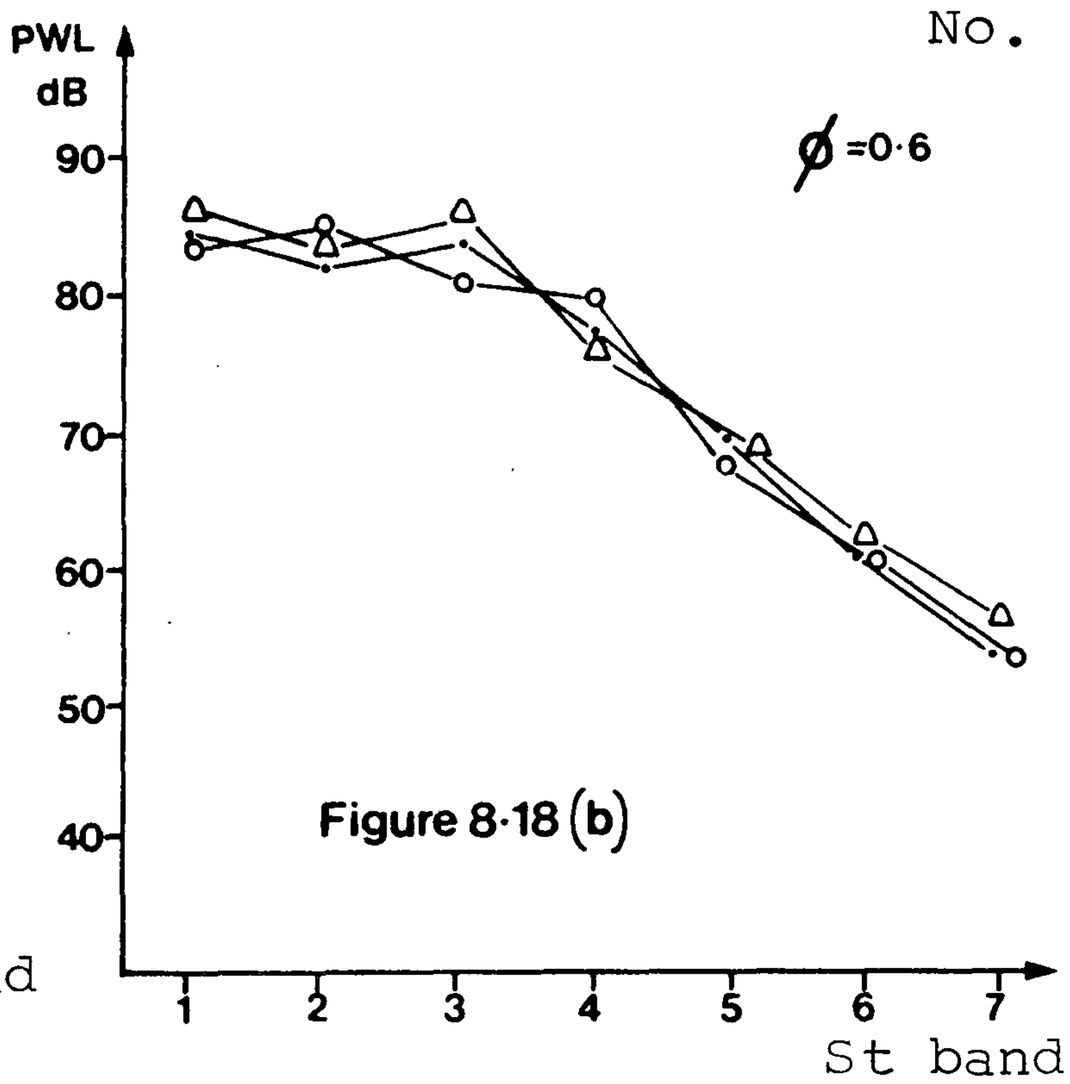

Figure 8·18 (b)

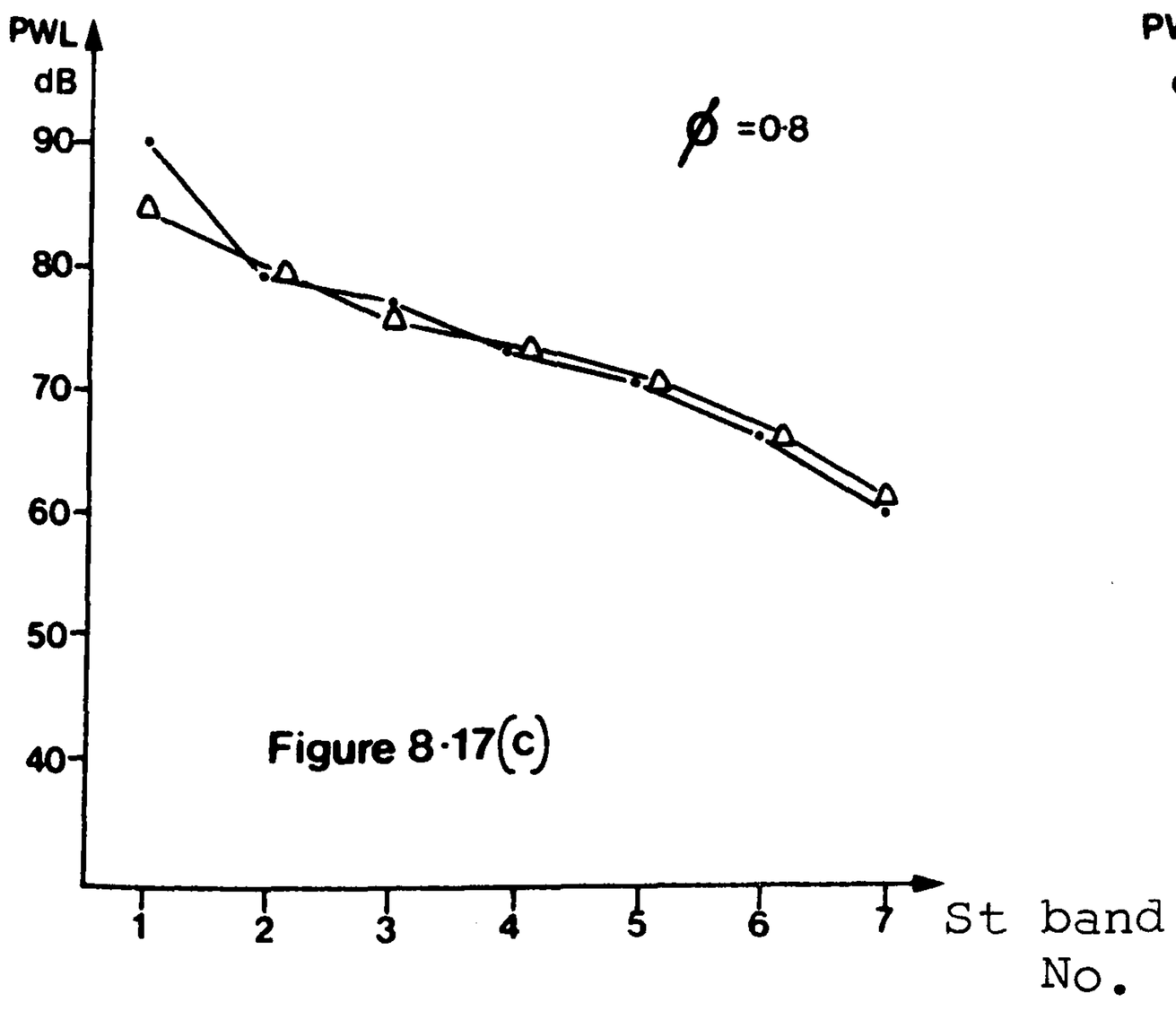

Figure 8·17(c)

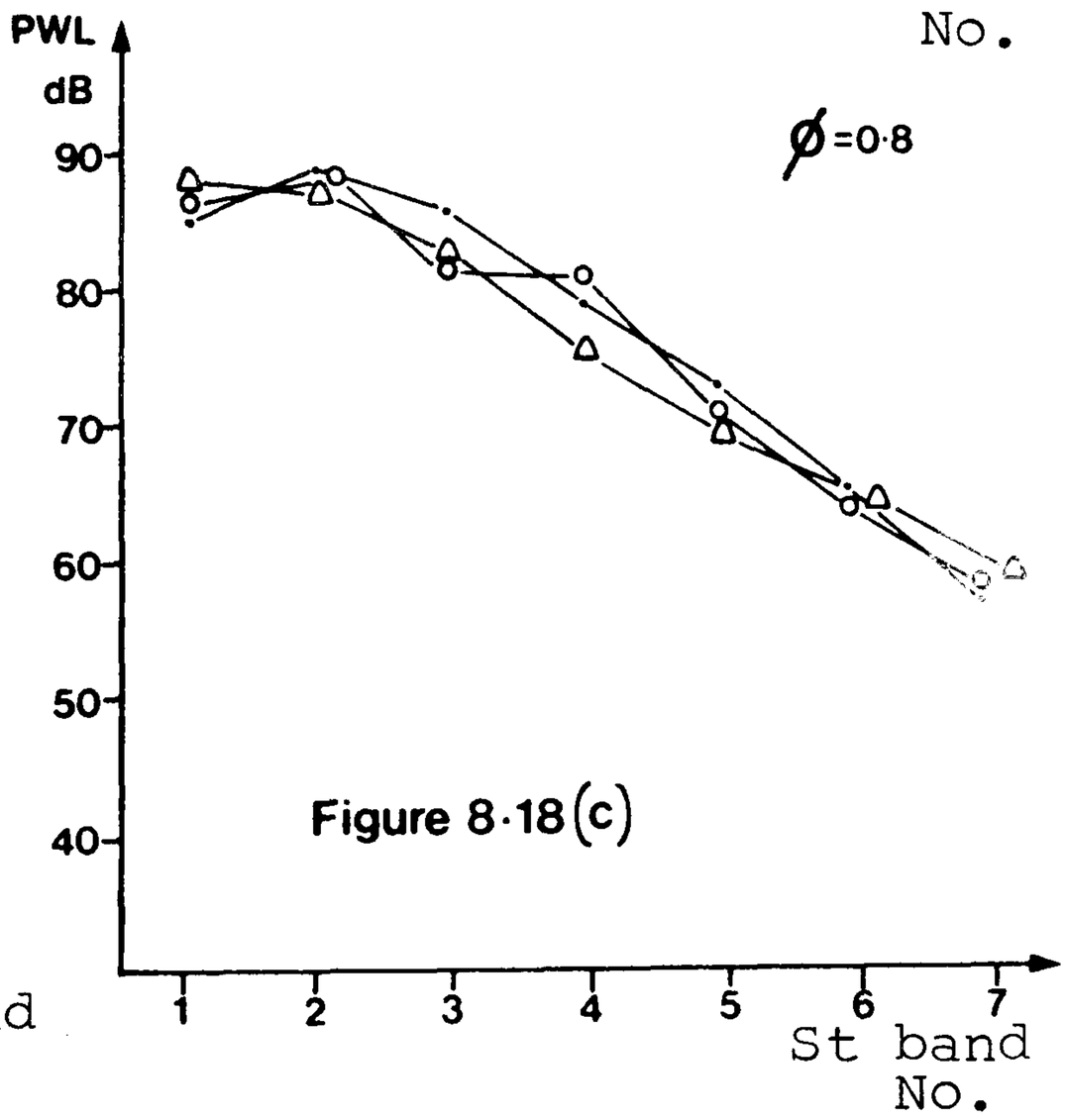

Figure 8·18(c)

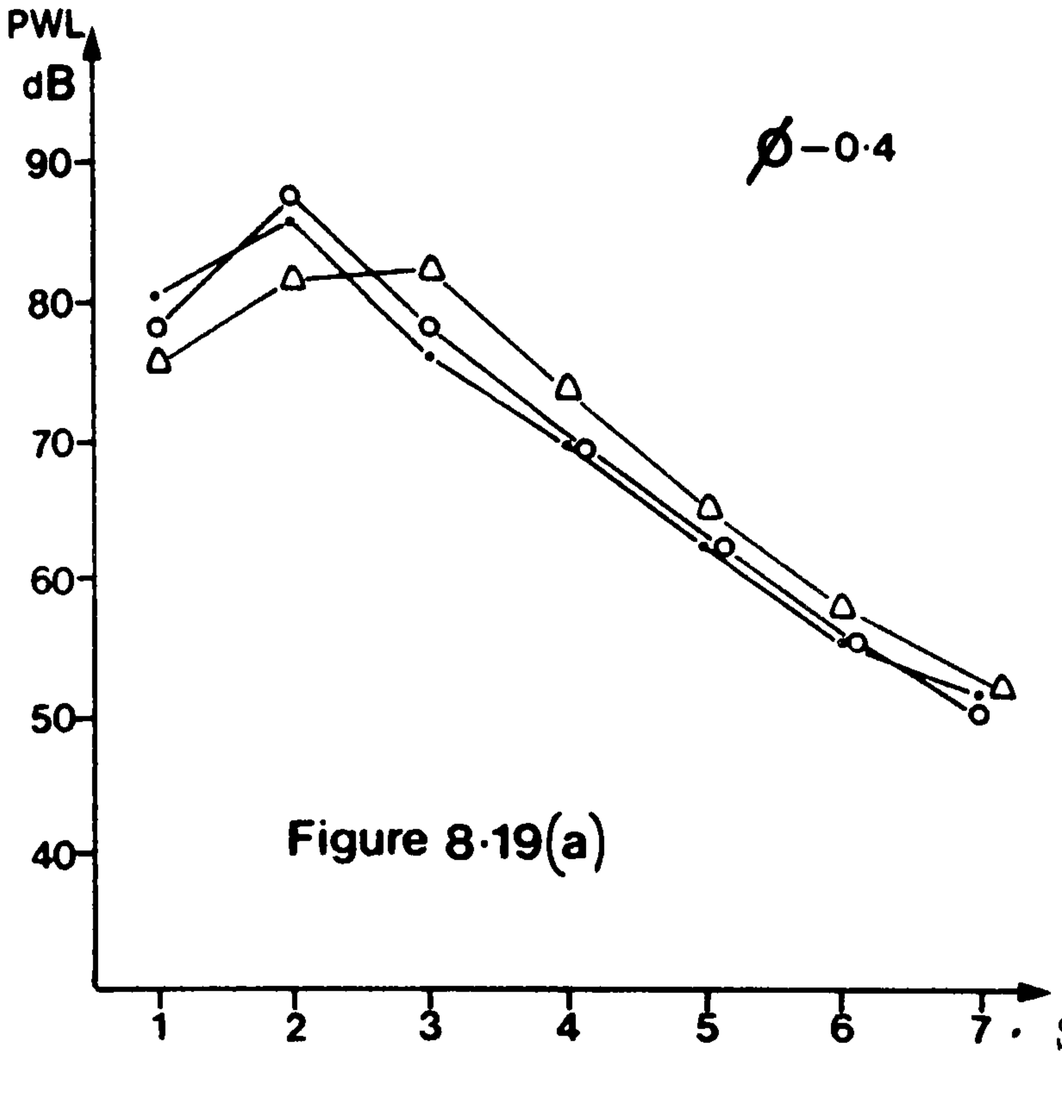

Figure 8·19(a)

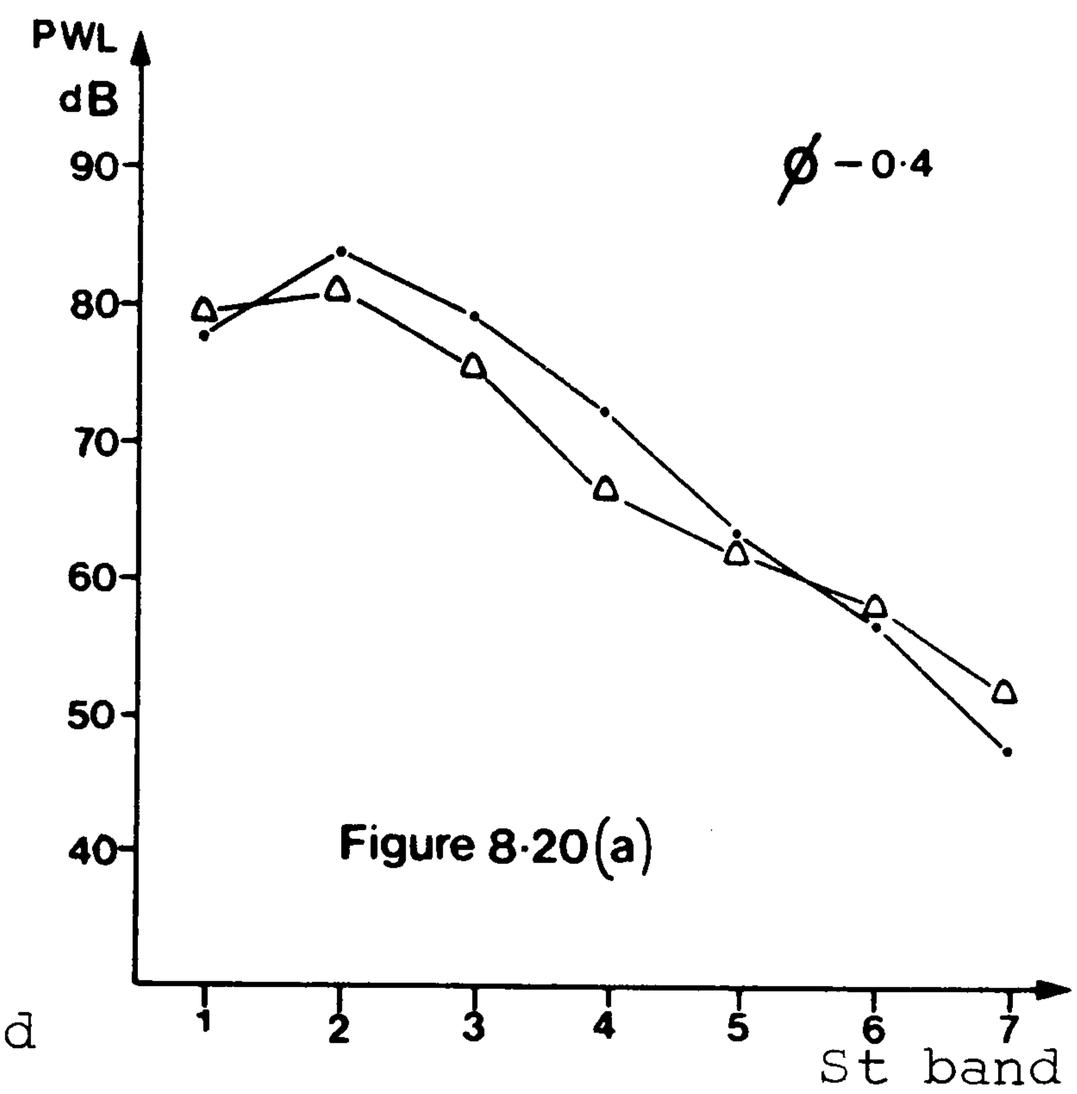

Figure 8·20(a)

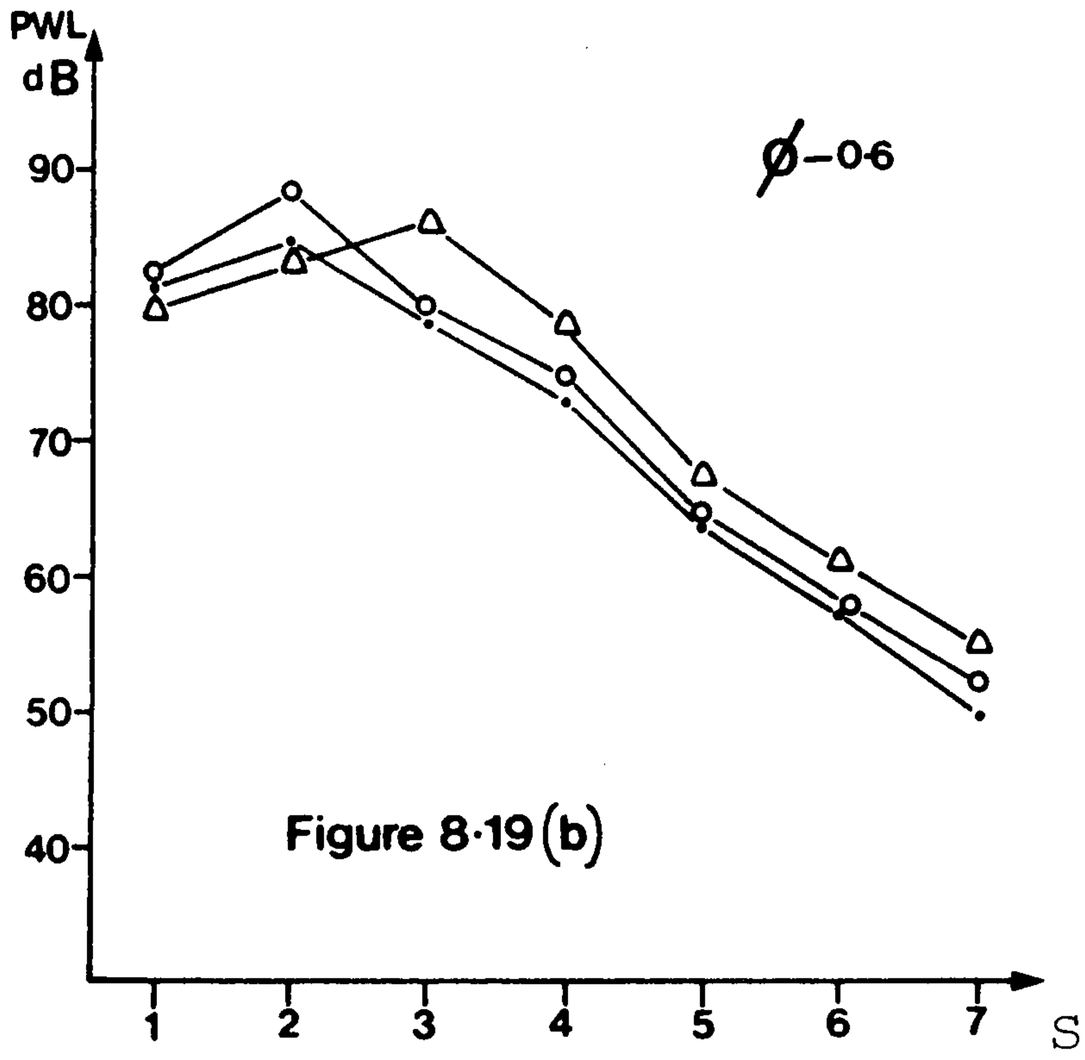

Figure 8·19(b)

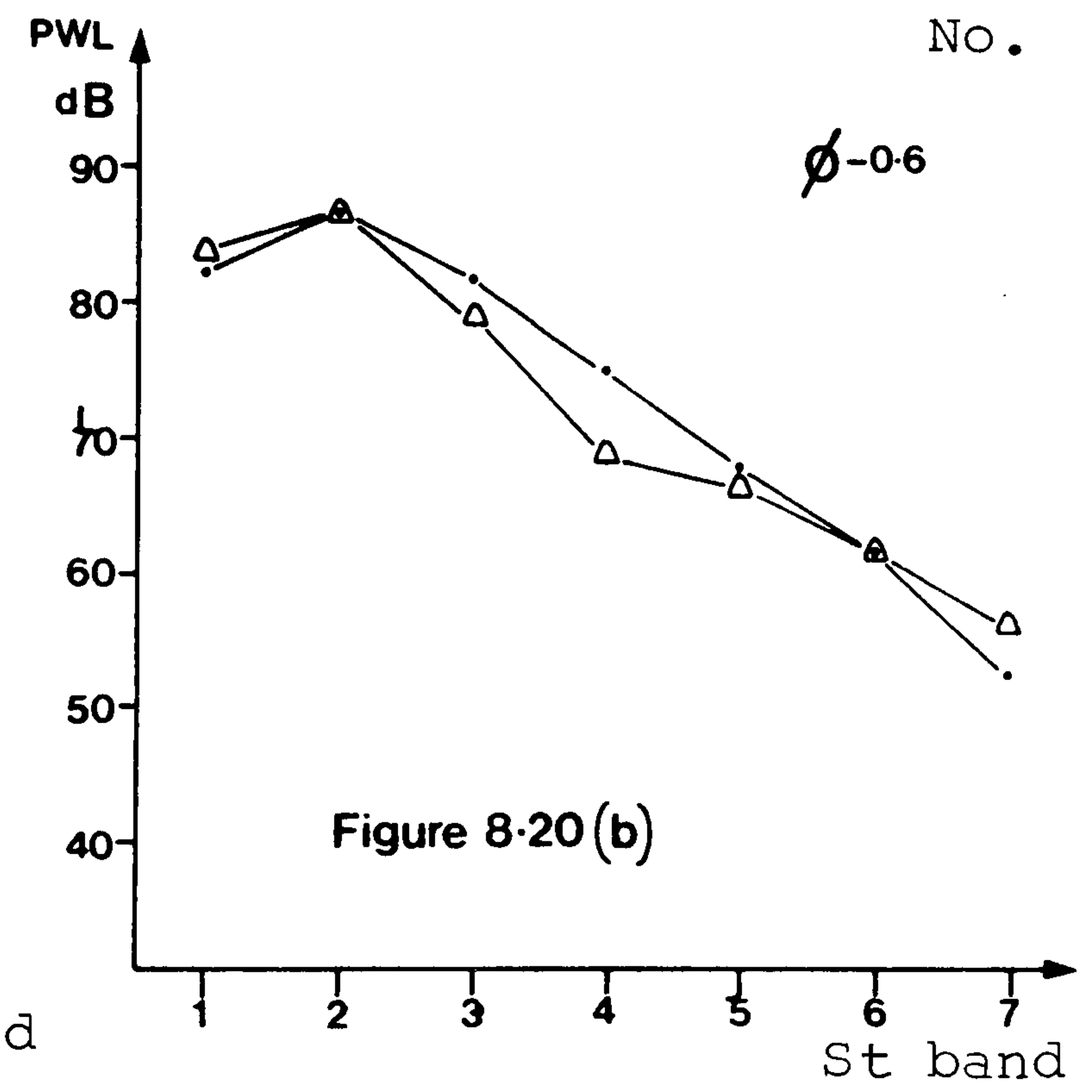

Figure 8·20(b)

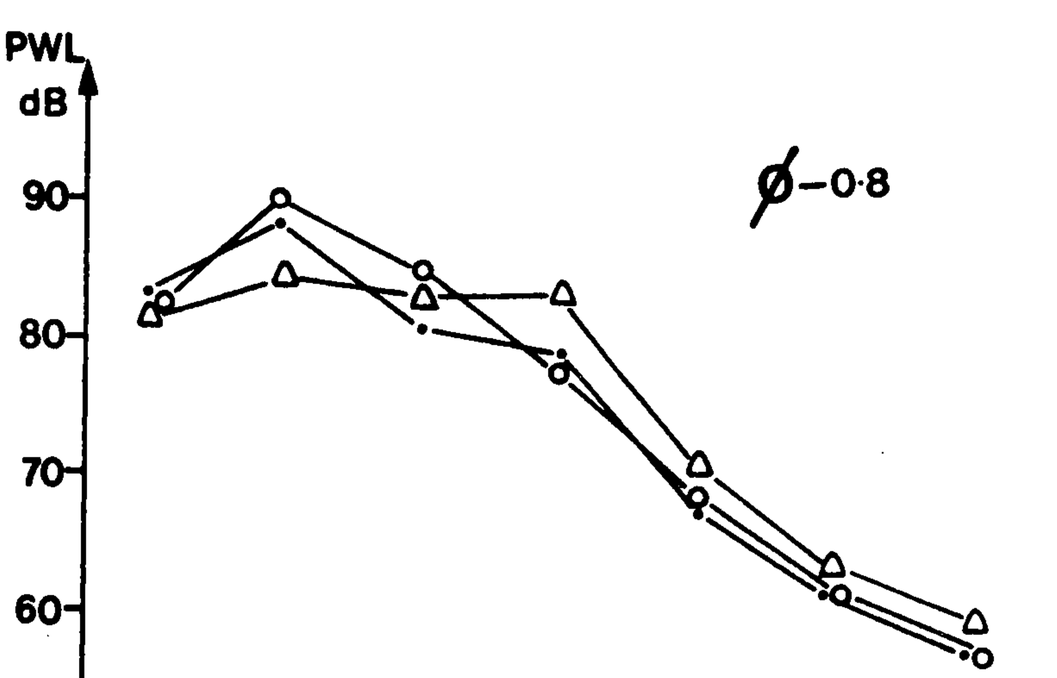

Figure 8·19(c)

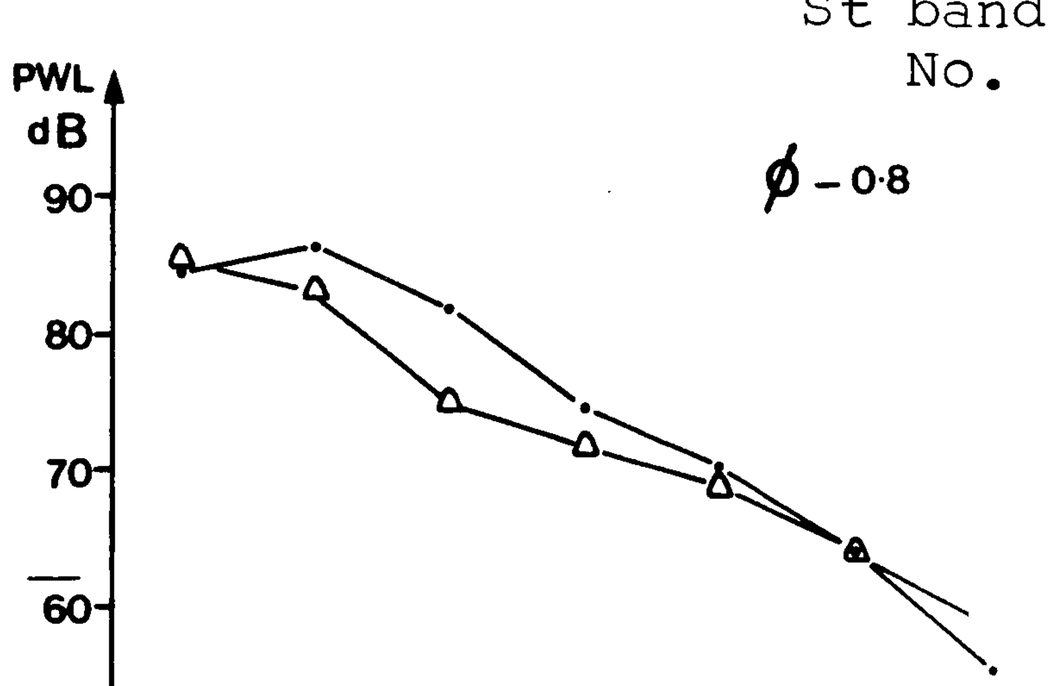

Figure 8·20(c)

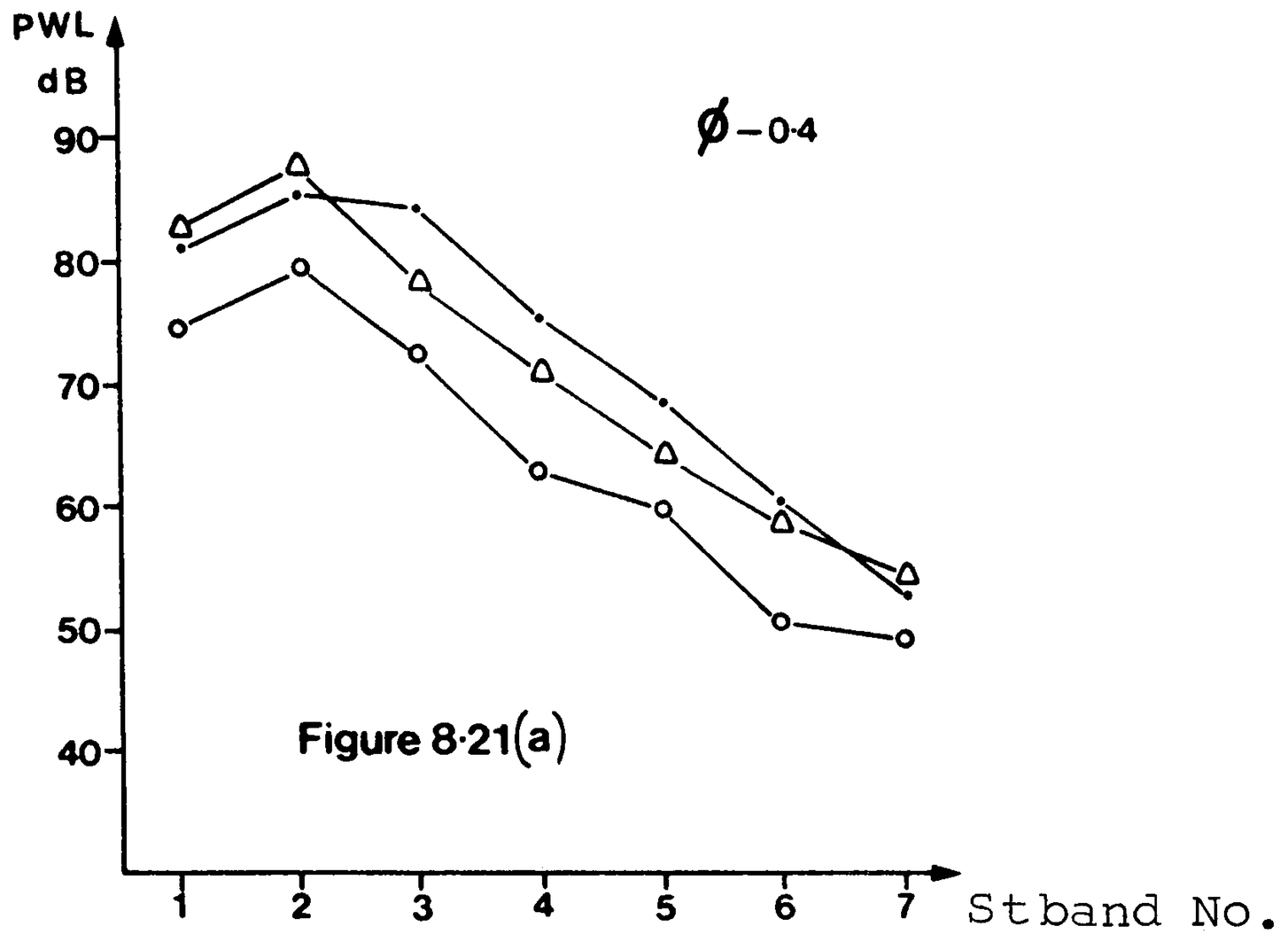

Figure 8·21(a)

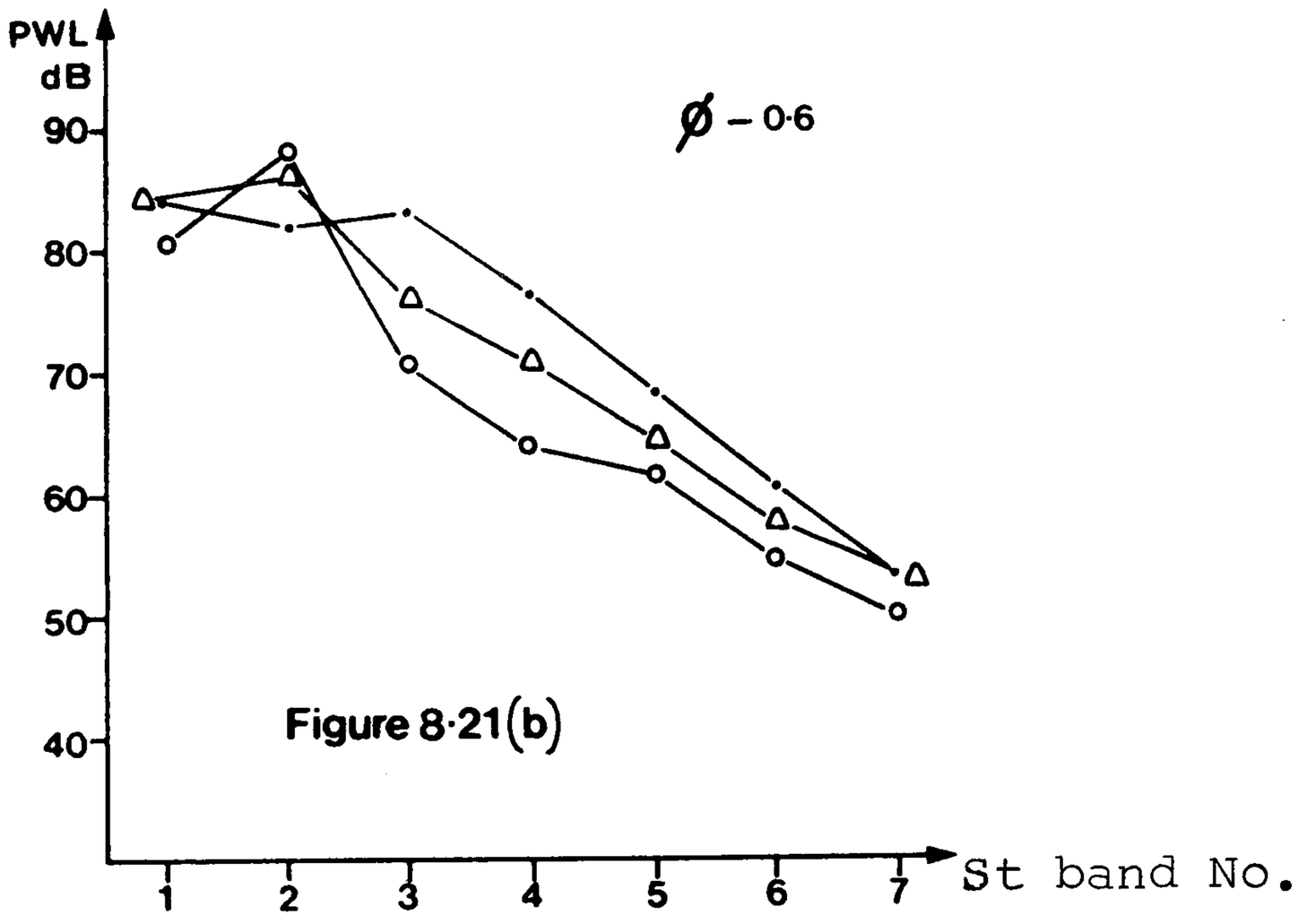

Figure 8·21(b)

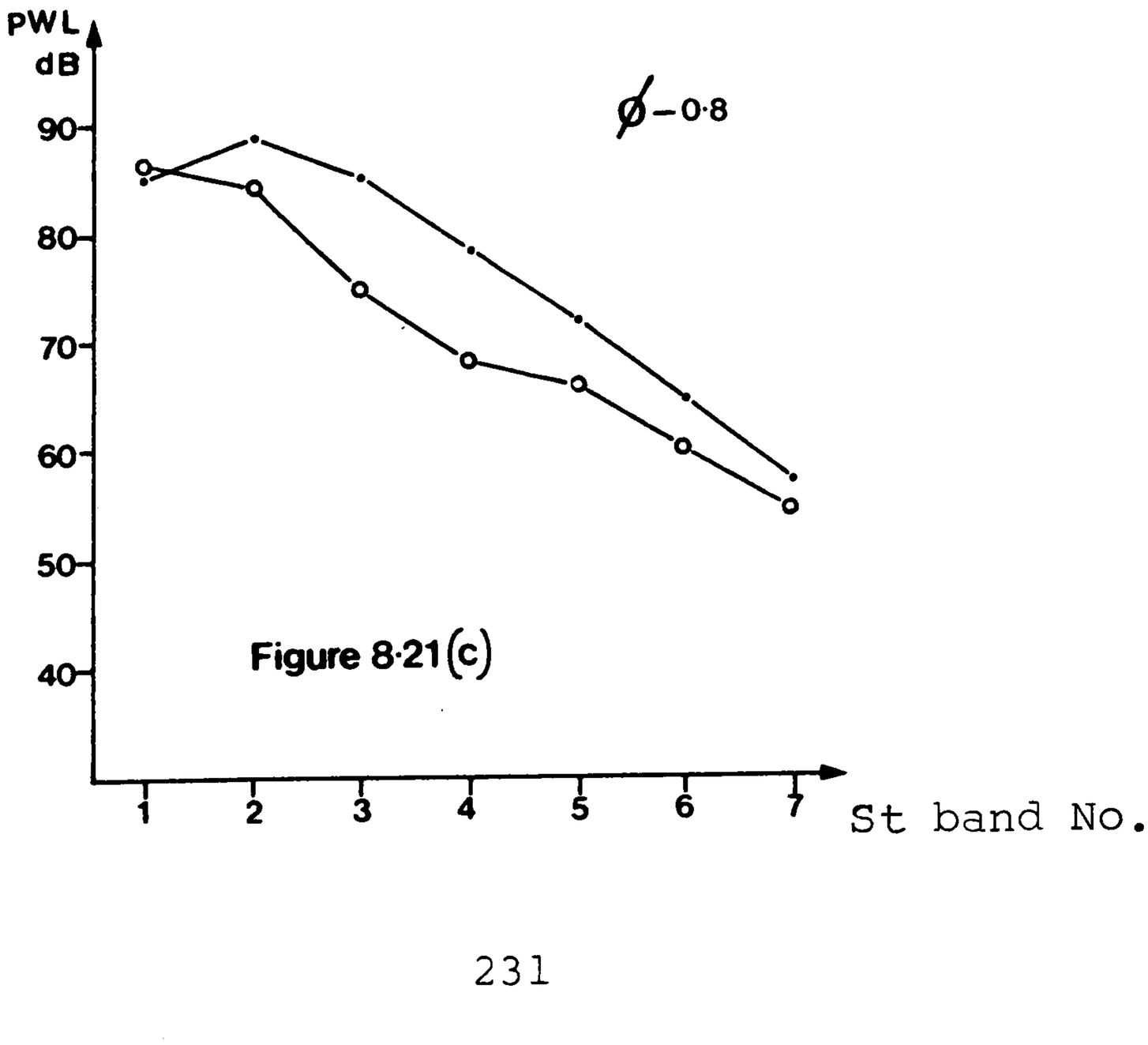

Figure 8·21(c)

CHAPTER NINE - CONCLUSIONS

9.1 DISCUSSION OF RESULTS

The best cross-flow fan design consists of a plain vortex wall, unobstructed suction arc, plain discharge and a rear wall with a profile governed by other primary design variables.

A number of novel fan designs have been tested but these have mostly been unable to prove their worth, and frequently to affect the performance adversely. The casing should be kept simple and the geometry of this within the established design limits (Section 9.2).

The experimental results presented in Chapters 6, 7 and 8 and the theoretical results of Chapter 5 have been written to enable easy cross-referencing. The overall effects of any design parameter on performance may be determined by referring to the companion sections in each Chapter.

The aerodynamic performance is principally dependent on five design parameters. The vortex wall declineation and the diameter ratio have the greatest effect on performance; the angular position of the rear wall and the vortex wall clearance must be kept within limits for efficient operation. Losses are reduced if the rear wall shape is determined using the 'constant mean velocity' principle.

No single optimum design of a fan exists, but there is a range of values within which a moderately efficient fan may be constructed: for a fan designed within these guidelines improved performance is gained largely at the expense of increased power demand.

A cross-flow fan exhibits an inherent instability due to the nature of the flow field. Adopting an ECK-type 'vortex stabiliser' does reduce the level of these pulsations, but exhibits a reduced aerodynamic performance. More generally, a fan which gives good aerodynamic performance will also operate stably.

The eccentrically located vortex which enables high performance also causes a peripherally irregular flow distribution and high flow velocities close to the vortex wall. These conditions increase the sound power output and determine that cross-flow fans will be relatively noisy in operation. For a simple fan design the sound power output tends to increase with increasing aerodynamic performance.

Unless there are fairly severe constraints on noise and operational stability, there is no reason why cross-flow fans should not supplant centrifugal exhausting fans for size-restricted, non-intermittent applications where a total efficiency of between 45% and 55% is acceptable.

9.2 FAN SELECTION PROCEDURE

A selection procedure is outlined in this section to enable a cross-flow blower to be designed for an application where the size and shape offer advantages over conventional machines.

There are three primary constraints:-

i) The fan should generally be less than .25 m diameter.

ii) The length/diameter ratio should be less than ~ 2.5 - 3.0

iii) The suction arc should be unobstructed by ducting, especially close to the vortex wall. Ideally the fan should draw fluid from free space.

The following parameters have been tested by the author, see Figure 6.1 for an explanation of the terms.

PARAMETER	COMMENTARY
Vortex wall declineation, B.	The most important geometrical parameter. B/D should be in the range 25% $\leq$ B/D $\leq$ 30% for optimum performance. Quieter operation occurs below this value, but at the expense of aerodynamic performance.
Diameter ratio d/D.	Ideally, 72% $\leq$ d/D $\leq$ 76% but acceptable in the range 70% $\leq$ d/D $\leq$ 80%.
Duct height, H.	The performance varies little in the range 70% $\leq$ H/D $\leq$ 85%.
Rear wall circumferential angle, δ.	This should be of the order of 20^{o}, efficiency is not compromised if δ is increased to 40^{o}.
Vortex wall clearance, E.	From performance considerations and ease of manufacture, the ratio of vortex wall clearance to diameter, E/D, should be about 3%.
Tongue thickness, T.	This will generally be determined by stiffness or material thickness considerations. A flat wall is recommended with a thickness in the range 0.8% $\leq$ T/D $\leq$ 4%.
Rear wall clearance, E_2.	The optimum clearance is a function of other design parameters, if an optimum clearance cannot be determined experimentally it should be kept within the range 9% $\leq$ E_2/D $\leq$ 12.5%.

A number of novel designs have been tested, see Figure 6.2, the results are documented in Sections 6.2.2, 7.5.2 and 8.6.2. A plain fan design is recommended. The effect of other design parameters on performance are reviewed in Section 6.2.3.

There are many options available for finessing the aerodynamic performance, noise and, to a lesser extent, stability: these options may be evaluated by studying Sections 6.2, 7.5, 8.6 and 8.5 (unshrouded rotor).

Example

Duty point: P_{st} = 1200 Pa

Q = 1.2 m^3/s

ρ = 1.2 kg/m^3, N = 2880

Try: Width = .5m, Diameter = .2 m. (U = 30.16 m/s)

$$\psi_{st} = \frac{1200}{1.2 \frac{1}{2} (30.16)^2} = 2.2.$$

It should be possible to achieve this coefficient using the recommended geometry, see for example Figure 6.9(a).

$$\phi = \frac{1.2}{.5 \quad .2 \quad 30.16} = 0.4.$$

Reduce the width to 330 mm and an achievable flow coefficient, ϕ, of 0.6 is required.

The coefficients may be modified by altering the fan diameter, width and rotational velocity - the fan performance may be manipulated by altering the geometrical design of the casing.

9.3 FUTURE WORK.

Further investigation into the effects of diameter ratio, length/diameter ratio and blade angles on performance would be valuable.

A worthwhile, purely theoretical analysis of the properties of the internal flow field would be extremely complicated, the complexity of the analysis not being commensurate with the assumption of a Laplacian field. The author performed an analysis which substantially ignored internal flow and where the external boundary conditions were established experimentally. This analysis successfully predicts most experimentally observed relationships between performance and casing design.

A thorough research programme investigating the flow field close to the blade passages would yield valuable information of general relevance to turbomachinery, and of particular interest to the study of cross-flow fans. These results could help to establish impeller boundary conditions and provide information helpful to an analysis of the flow field. It is arguable, however, whether complicated analytical treatments of the impeller flow-field are justified by the technical usefulness of the results they provide.

The noise analysis performed by the author isolated possible sound generating mechanisms and helped explain some of the observed dependence of noise on fan design. Future experimental work would be enhanced by a narrow-band or 1/3 octave analysis of the sound power output. Both cross-flow and centrifugal fan technologies would benefit from some

fundamental research on low speed sound radiation, and on the properties of tongue interaction mechanisms.

Modifying the shape of the vortex wall leading edge may be effective in reducing noise; the efficacy of a particular design can only, at present, be established experimentally.

REFERENCES

1 ALLEN C.H. 'Noise from air conditioning fans'. NOISE CONTROL 3 pp 28 - 34 (1957).

2 ANDERSON E.L. U.S. patent 1823 579 (1931).

3 ANDERSON E.L. U.S. patent 1838 169 (1931).

4 ANDERSON E.L. U.S. patent 1886 513 (1932).

5 ANDERSON E.L. U.S. patent 1920 952 (1933).

6 ARCTANDER C. 'Sound absorptive materials for aircraft noise control'. SOUND AND VIBRATION pp 12 - 16 (July 1976)

7 BENNINGER A.G. U.K. patent 830 362 (1960).

8 BOWERMAN R.D. and ACOSTA A.J. 'An experimental study of centrifugal pump impellers'. C.I.T. Hydrodynamics laboratory report E19-8 (August 1955).

9 BROCH J.T. Acoustic noise measurements 2nd Ed. published: Bruel and Kjaer (1971).

10 BRUEL and KJAER Instruction manuals for 4205 sound power source and HP1001 loudspeaker.

11 BUCK C.M. U.S. patent 1893 857 (1933).

12 BUCK C.M. U.S. patent 2033 273 (1936).

13 BUSH E.H. 'Cross-flow fans'.
Conference on fan technology and practice; I.Mech.E. London (18 - 19 April, 1972).

14 CHANDRASHEKHARA N. 'Sound radiation from inflow turbulence in axial fans'.
JOURNAL OF SOUND AND VIBRATION 19(2) pp 133 - 147 (1971).

15 COESTER R. U.S. patent 2965 284 (1960).

16 COESTER R. 'Remarks on the theory of cross-flow blowers'.
H.V.R.A. Translation No.39.

17 CREMER L. 'The treatment of fans as black boxes'.
JOURNAL OF SOUND AND VIBRATION 16(1) pp 1 - 17 (1971).

18 CURLE N. 'The influence of solid boundaries upon aerodynamic sound'.
PROC. ROYAL SOCIETY (London) A231 pp 505 - 514 (1955).

18b CURLE N. 'The generation of sound by aerodynamic means'.
JOURNAL OF THE ROYAL AERONAUTICAL SOCIETY 65 p 724 (1961).

19 DALIN H. U.K. patent 291 007 (1928).

20 DATWYLER G. U.K. patent 988 712 (1965).

21 DAVIES and FFOWCS-WILLIAMS 'Aerodynamic sound generation in a pipe'. JOURNAL OF FLUID MECHANICS 32 pp 765 - 778 (1968).

22 DE-FRIES J.R. '66 Jahre Querstrom ventilator'. UDI-Berichte uber betriebswissen scheftliche Arbeiten volume 38 pp 75 - 86 (1959).

23 ECK, B. Fans; design and operation of centrifugal, axial and cross-flow fans. translated: Azad and Scott Oxford, Pergaman Press (1973).

24 ECK, B. U.K. patent 757 543 (1954).

25 ECK, B. U.S. patent 2942 773 (1960).

26 EMBLETON T.F.W. 'Experimental study of noise reduction in centrifugal blowers'. J.A.S.A. 35(5) pp 700 - 705 (1963).

27 FFOWCS-WILLIAMS J.E. and HAWKINGS D.L. 'Theory relating to noise of rotating machinery'. JOURNAL OF SOUND AND VIBRATION 10(1) pp 10 - 21 (1969).

28 FIRTH-CLEVELAND LTD. U.K. patent 876 611 (1961).

29 FUKANO, KODOMA and SENOO. 'Noise generated by low pressure axial flow fans; (I) Modelling of turbulent noise'. JOURNAL OF SOUND AND VIBRATION 50(1) pp 63 - 75 (1977).

30 GORDON C.G. 'Fan noise and its prediction'. Conference of fan technology and practice. PROC. I.MECH.E. (London), paper 11 (1972).

31 GROFF G.C. 'Centrifugal fan sound power testing'. TRANS. A.S.H.R.A.E. 70 pp 269 - 277 (1964).

32 GUNTON M. and HOLGATE M.J. 'Research note: A twin rotor cross-flow fan'. JOURNAL OF MECHANICAL ENGINEERING SCIENCE, I.MECH.E. (1978).

33 GUTIN L. 'On the sound field of a rotating impeller'. NACA TM 1195 original paper: (1948).

34 HAINES P. and HOLGATE M.J. 'Scaling of cross-flow fans - an experimental comparison'. PROC. I.MECH.E., Stirling (1977).

35 HANSON D.B. 'Unified analysis of fan stator noise'. J.A.S.A. 54(6) pp 1571 - 1592 (1973).

36 HEINE-GELDERN R. U.S. patent 3 086 696 (1963).

37 HUBBARD H.H., LANSING D.L. and RUNYAN H.L. 'A review of rotating blade noise technology'. JOURNAL OF SOUND AND VIBRATION 19(3) pp 227 - 251 (1971).

38 IKEGAMI H. and MURATA S. 'A study of the cross-flow fan: Part 1: A theoretical analysis'. Technology Report. OSAKA University Volume 16 No.731.

39 IKEGAMI H. and MURATA S. 'Characteristics and problems of the cross-flow fan (2)'. SCIENCE OF MACHINES No.18-3 (1966).

40 ILBERG H. and SADEH W.Z. 'Flow theory and performance of tangential fans'. PROC. I.MECH.E., London 180 Part 1 No.19.

41 KEMP N.H. and SEARS W.R. 'The unsteady forces due to viscous wakes in turbomachines'. JOURNAL OF AERONATICAL SCIENCE 22 pp 478 - 483 (1955).

42 KESHAHAVEN N.R. 'Vortex shedding of aerofoils in smooth flow'. JOURNAL OF SOUND AND VIBRATION 52(3) pp 456 - 457 (1977).

43 KUROSAKA M. 'A note on multiple pure tone noise'. JOURNAL OF SOUND AND VIBRATION 19(4) pp 453 - 463 (1971).

44 LEVERTON J.W. and AMOR C.B. 'An investigation of impulsive noise of a model rotor'. JOURNAL OF SOUND AND VIBRATION 28(1) pp 55 - 71 (1973).

45 LIGHTHILL M.J. 'On sound generated aerodynamically : 1 GENERAL THEORY'. PROC. ROYAL SOCIETY (London) A211 pp 564 - 587 (1952).

46 LIGHTHILL M.J. 'On sound generated aerodynamically : 2 TURBULENCE AS A SOURCE OF SOUND'. PROC. ROYAL SOCIETY (London) A222 pp 1 - 32 (1954).

47 LOCKLEY D.J. The tangential fan. M.Sc. Thesis, Birmingham University 1966.

48 LOWSON M.V. and OLLERHEAD J.B. 'A theoretical study of helicopter rotor noise'. JOURNAL OF SOUND AND VIBRATION 9(2) pp 197 - 223 (1969).

49 LYONS L.A. and PLATTER S. 'Effect of cut-off configuration on pure tones generated by small centrifugal blowers'. J.A.S.A. 35 pp 1455 - 1456 (1963).

50 MØLLER A. 'How good are works noise standards?' NEW SCIENTIST pp 192 - 194 27/January 1977.

51 MOORE A. 'The tangential fan - analysis and design' Conference on fan technology and practice. PROC. I.MECH.E. (London), April 1972.

52 MORELAND J.B. 'Housing effects on centrifugal blower noise'. JOURNAL OF SOUND AND VIBRATION 36(2) pp 191 - 207 (1974).

53 MORELAND J.B. 'A note on the effect of operating point on centrifugal blower noise'. JOURNAL OF SOUND AND VIBRATION 46(3) pp 453 - 456 (1976).

54 MORFEY C.L. 'Rotating blades and aerodynamic sound'. JOURNAL OF SOUND AND VIBRATION 28(3) pp 587 - 617 (1973).

55 MORTIER P. U.S. patent 507 445 (1893).

56 MUGRIDGE B.D. 'The noise of cooling fans in heavy automotive vehicles'. JOURNAL OF SOUND AND VIBRATION 44(3) pp 349 - 369 (1976).

57 MURATA S. and NISHIHARA K. 'An experimental study of cross-flow fans'. Bulletin J.S.M.E. 19 (1976).

58 NEISE W. 'Application of similarity laws to blade passage sound of centrifugal fans'. JOURNAL OF SOUND AND VIBRATION 43(1) pp 61 - 75 (1975).

59 NEISE W. 'Noise reduction in centrifugal fans: A literature survey'. JOURNAL OF SOUND AND VIBRATION 45(3) pp 375 - 403 (1976).

60 PELHAM G. Inlet streamlines of the cross-flow fan. Final year project, DURHAM UNIVERSITY 1979.

61 PLONER B. and HERZ F. 'New design measures to reduce siren tones caused by centrifugal fans in rotating machines'. BROWN BOVERI REVUE 56 pp 280 - 287 (1969).

62 PORTER A.M. A study of the tangential fan. Ph.D Thesis, Queens University, Belfast 1969.

63 PORTER A.M. and MARKLAND E. 'A study of the cross-flow fan'. JOURNAL OF MECHANICAL ENGINEERING SCIENCE 12(6) pp 421 - 431 (1970).

64 PRAT E. U.K. patent 219 291 (1925).

65 PRESZLER L. and LAJOS T. 'Experiments for the development of the tangential flow fan'. PROC. 4th Conference on fluid machinery, Budapest. Akademiai Kiado, Budapest pp 1071 - 1082 (1972).

66 PURCELL W.E. 'Materials for noise and vibration control'. SOUND AND VIBRATION pp 6 - 33 July 1976.

67 RICHARDS E.J. and MEAD D.J. Editors. Noise and acoustic fatigue in aeronautics. London, Wiley 1968.

68 SCHMARJE J.E.F. German patent 242 076 (1910).

69 SCHMARJE J.E.F. U.K. patent 10 852 (1914).

70 STEPANOFF A.J. Turboblowers: theory, design and application of centrifugal and axial flow compressors and fans. New York, Wiley 1955.

71 TRAMPOSCH H. 'Cross-flow fan' Paper A.S.M.E. No. 64-WA FE-26 (1964).

72 TSEO G.G. 'Noise reduction of a miniature fan using blade treatment'. JOURNAL OF SOUND AND VIBRATION 32(2) pp 153 - 159 (1974).

73 TUCKEY P. The aerodynamics of the cross-flow fan. Ph.D Thesis, Durham University; In preparation.

74 WIEDEMANN J. 'Analysis of the relations between acoustic and aerodynamic parameters for a series of dimensionally similar centrifugal fan rotors'. NASA TT F-13, 798 August 1971.

75 WRIGHT S.E. 'Sound from a lifting rotor generated by asymmetric disk loading'. JOURNAL OF SOUND AND VIBRATION 9(2) pp 223 - 241 (1969).

76 WORSTER R.C. 'The flow in volutes and its effect on centrifugal pump performance'. PROC. I.MECH.E. 177 pp 843 - 875 (1963).

77 YAMAFUJI K. 'Studies on the flow of cross-flow impellers: (experimental study (I))'. Bulletin J.S.M.E. 18 No.123 (1975).

78 YEOW K.W. 'Acoustic modelling of ducted centrifugal rotors:- (1) The experimental acoustic characters of ducted centrifugal rotors'. JOURNAL OF SOUND AND VIBRATION 32(1) pp 143 - 152 (1974).

79 YEOW K.W. 'Acoustic modelling of ducted centrifugal rotors:- (II) The lumped impedence model'. JOURNAL OF SOUND AND VIBRATION 32(1) pp 203 - 227 (1974).

APPENDICES, A1 - A4

APPENDIX A1

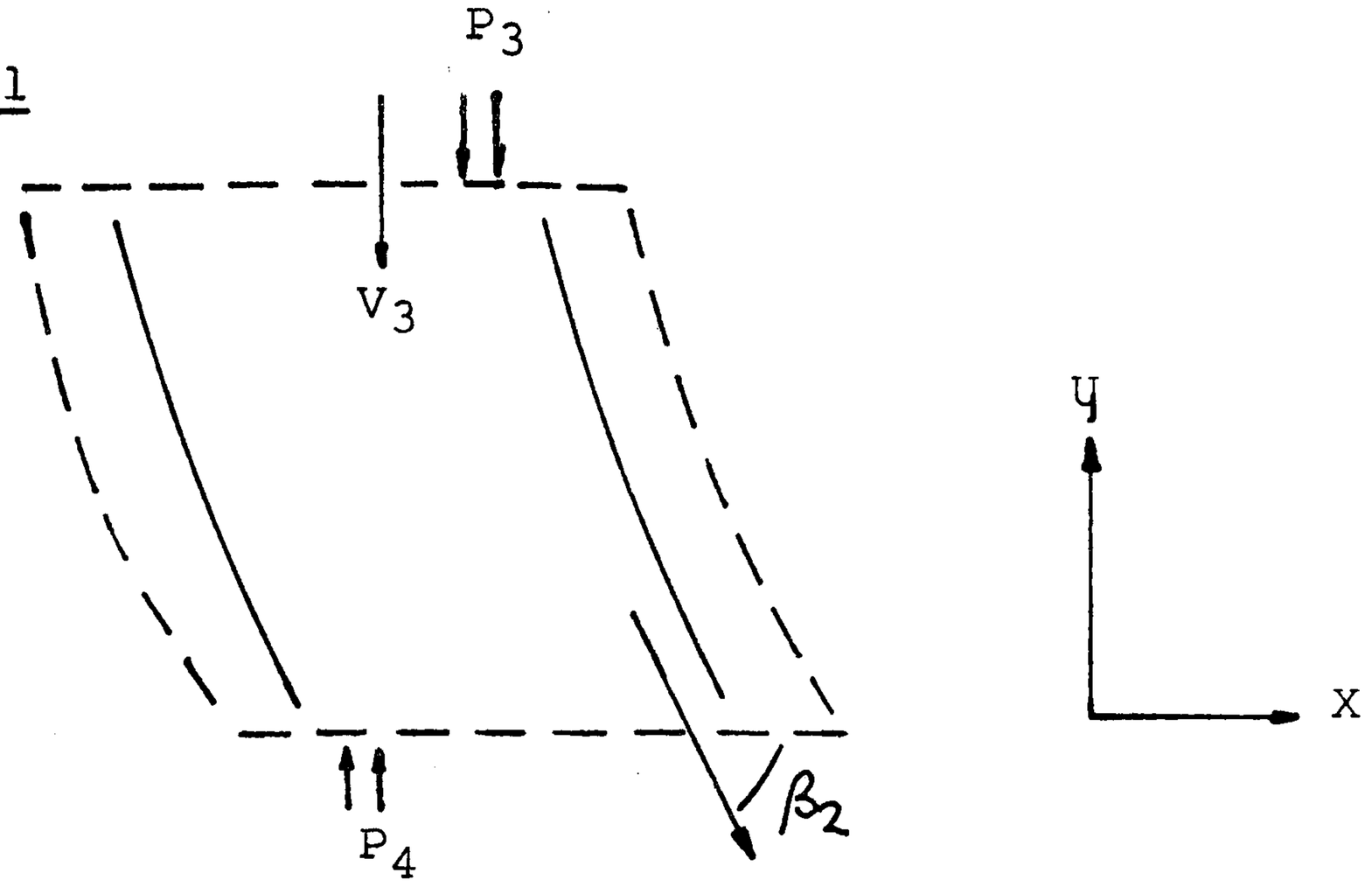

Figure A.1.1.

From Figure A.1.1:

$$P_{v4} = \tfrac{1}{2}\rho V_4^2 \qquad \text{A.1.1}$$

$$P_{v3} = \tfrac{1}{2}\rho V_3^2 \qquad \text{A.1.2}$$

Where:

$$V_4 = V_3 \times A_3/A_4 \qquad \text{A.1.3}$$

$$P_{v4} = \tfrac{1}{2}\rho V_3^2 \, (A_3/A_4)^2 \qquad \text{A.1.4}$$

There is an increase in total pressure across section 3 - 4:

$$P_{t4} = P_{t3} + 0.8\, P_t' \qquad \text{A.1.5}$$

P_t' - Total pressure rise across the fan.

Equate total pressures:

$$P_4 + P_{v4} = P_3 + P_{v3}^2 + 0.8\, P_t'$$

$$P_4 + \tfrac{1}{2}\rho V_3^2 \, (A_3/A_4)^2 = P_3 + \tfrac{1}{2}\rho V_3^2 + 0.8\, P_t'$$

$$P_3 = P_4 + \tfrac{1}{2}\rho V_3^2 \, (\, (A_3/A_4)^2 - 1) - 0.8\, P_t' \qquad \text{A.1.6}$$

P_4 is the 'ideal' static pressure, as calculated from the model formulated in section 3.3. From this value P_3, P_2 and P_1 may be calculated.

The total force exerted on the fluid within the control volume is the sum of the net static pressure force and the

net force due to the rate of increase of momentum:-

$$F_x = F_{xp} + F_{x\ mom} \qquad A.1.7$$

$$F_y = F_{yp} + F_{y\ mom} \qquad A.1.8$$

Pressure force in X-direction

$$F_{xp} = 0 \qquad A.1.9$$

Pressure force in Y-direction

$$F_{yp} = P_4A_4 - P_3A_3 \qquad A.1.10$$

Total force in the X-direction equals the rate of increase of Y-momentum:

$$F_x = \rho\, Q_n\ (V_4 \cos\beta_2 - 0) \qquad A.1.11$$

Where

$$Q_n = V_{r3(n)}A_3 \qquad A.1.12$$

Total force in the Y-direction equals the rate of increase of Y-momentum:

$$F_y - F_{yp} = \rho\, Q_n\ (V_4 \sin\beta_2 - V_3) \qquad A.1.13$$

$$F_y = \quad Q_n\ (V_4 \sin\beta_2 - V_3) + P_4A_4 - P_3A_3 \qquad A.1.14$$

(P_3 may be found from equation A.1.6)

Direction of the resultant force on the air:

$$\theta = \tan^{-1}(F_y/F_x) \qquad A.1.15$$

(The force on the blade is equal and opposite to the resultant force on the air)

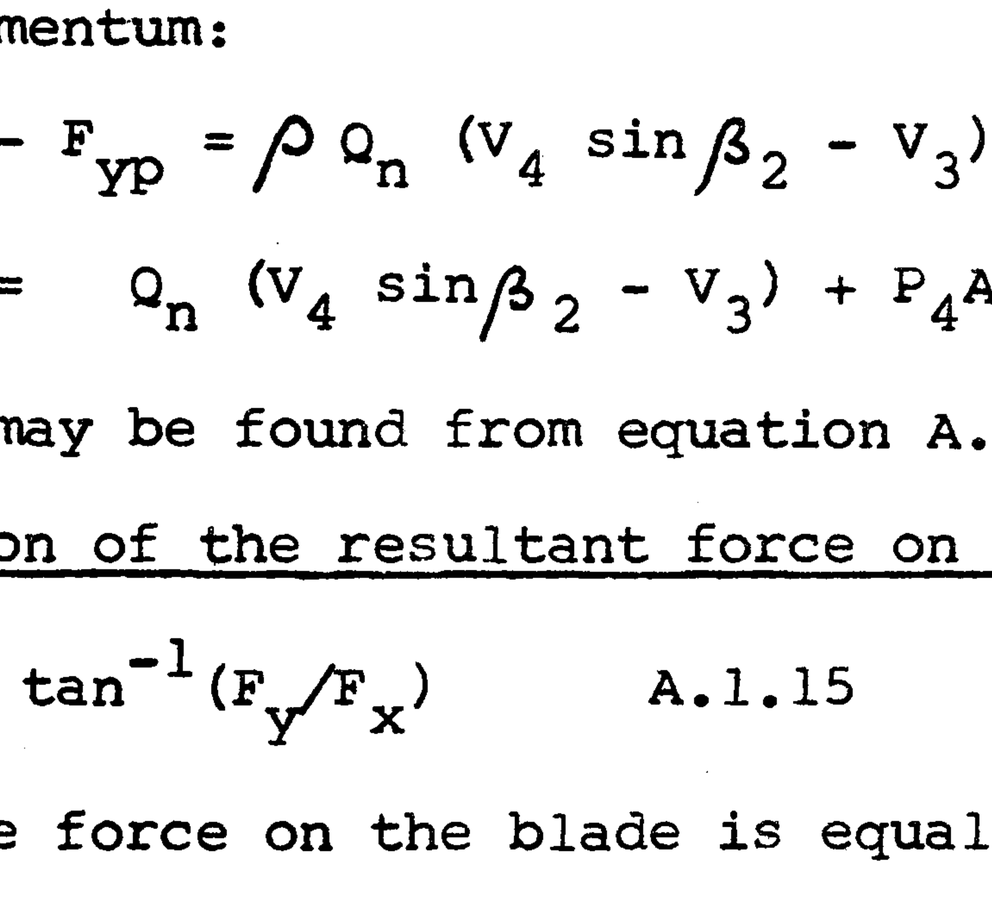

Figure A.1.2.

From Figure A.1.2:

Pressure force in the X-direction

$$F_{xp} = 0 \qquad \text{A.1.9(a)}$$

Pressure force in the Y-direction

$$F_{yp} = P_2A_2 - P_1A_1 \qquad \text{A.1.10(a)}$$

Total force in the X-direction:

$$F_x = \rho Q_n(0 - V_1 \cos\beta_2) \qquad \text{A.1.16}$$

Total force in the Y-direction:

$$F_y = \rho Q_n(V_2 - V_1 \sin\beta_2) + (P_2A_2 - P_1A_1) \qquad \text{A.1.17}$$

(P_2 is equal to P_3, and may be calculated from equation A.1.6)

Where 20% of the energy transfer occurs across the first blade row; (20% total pressire rise):

$$P_1 = P_2 + \tfrac{1}{2}\rho V_1^2 \left((A_1/A_2)^2 - 1) \right) - 0.2\, P_t' \qquad \text{A.1.18}$$

(Equation A.1.18 was derived in the same way as equation A.1.7)

In the recirculation zone the force on the blades, the 'blade loading', is assumed to be zero.

In the vortex zone:

$$F_x = 0$$

-- A.1.19

$$F_y = 0$$

Procedure for the solution of the 'blade loading' of a cross-flow fan.

From Figure A.1.3

$$S_1 = \theta/2\pi \times R1 \qquad \text{A.1.20}$$

$$S_2 = \theta/2\pi \times R2 \qquad \text{A.1.21}$$

$$A_1 = A_4 = S_1 \cdot \text{LENGTH}$$
$$A_2 = A_3 = S_2 \cdot \text{LENGTH} \qquad \text{-- A.1.22}$$

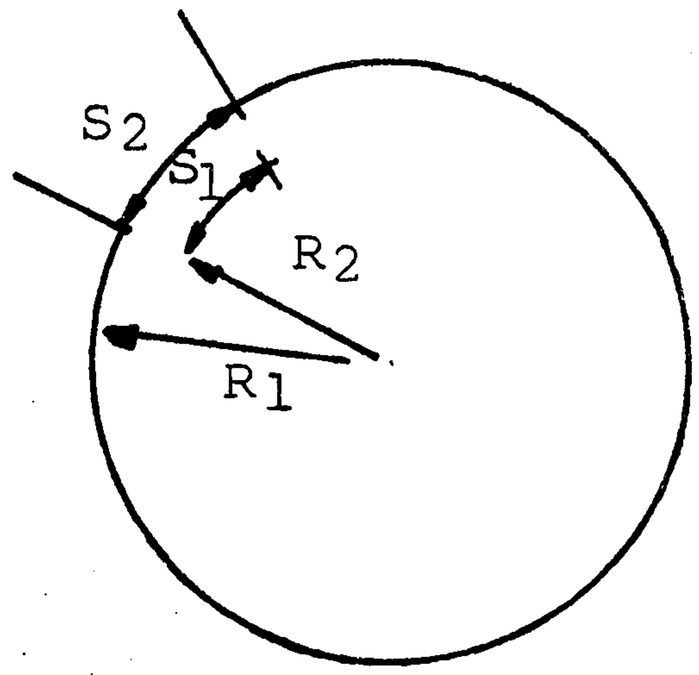

Figure A.1.3.

At each sector (θ_n); where n = 1, 2, 3 ....., $2\pi/\theta$.

A) Specify V_4 and V_{r3} (Discharge arc)

B) Specify V_1 and V_{r1} (Suction arc)

Knowing A_3, A_4, P_t', P_4, $_2$, A_1, A_2.

(P_1,P_2 and P_3 may be calculated from P_4)

- Equations A.1.1 - A.1.22 may be solved

Typical results are illustrated in Figures A.1.4 and A.1.5.

(F_x - Torque, (Q) F_y - Thrust, (T))

TORQUE

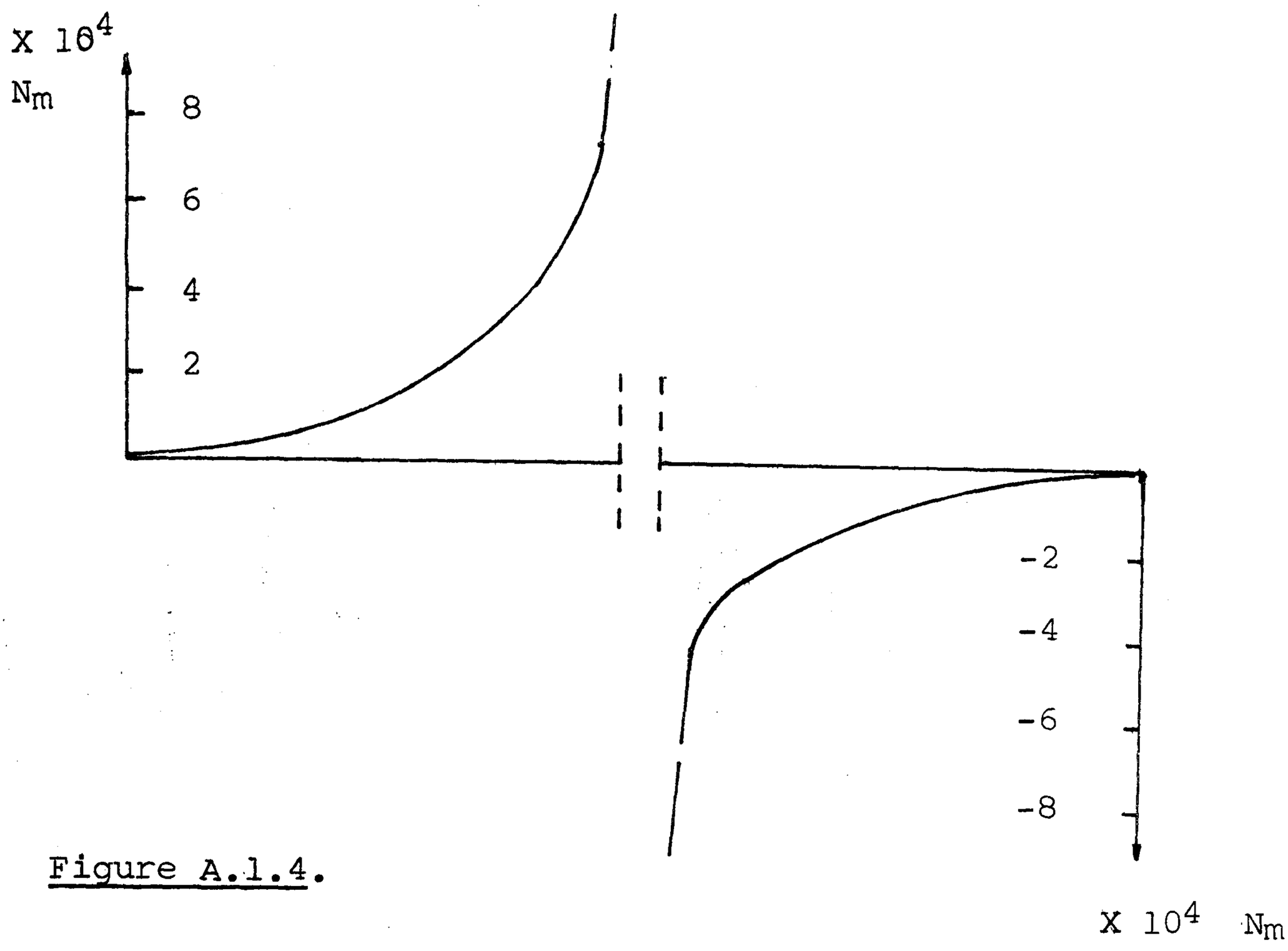

Figure A.1.4.

THRUST

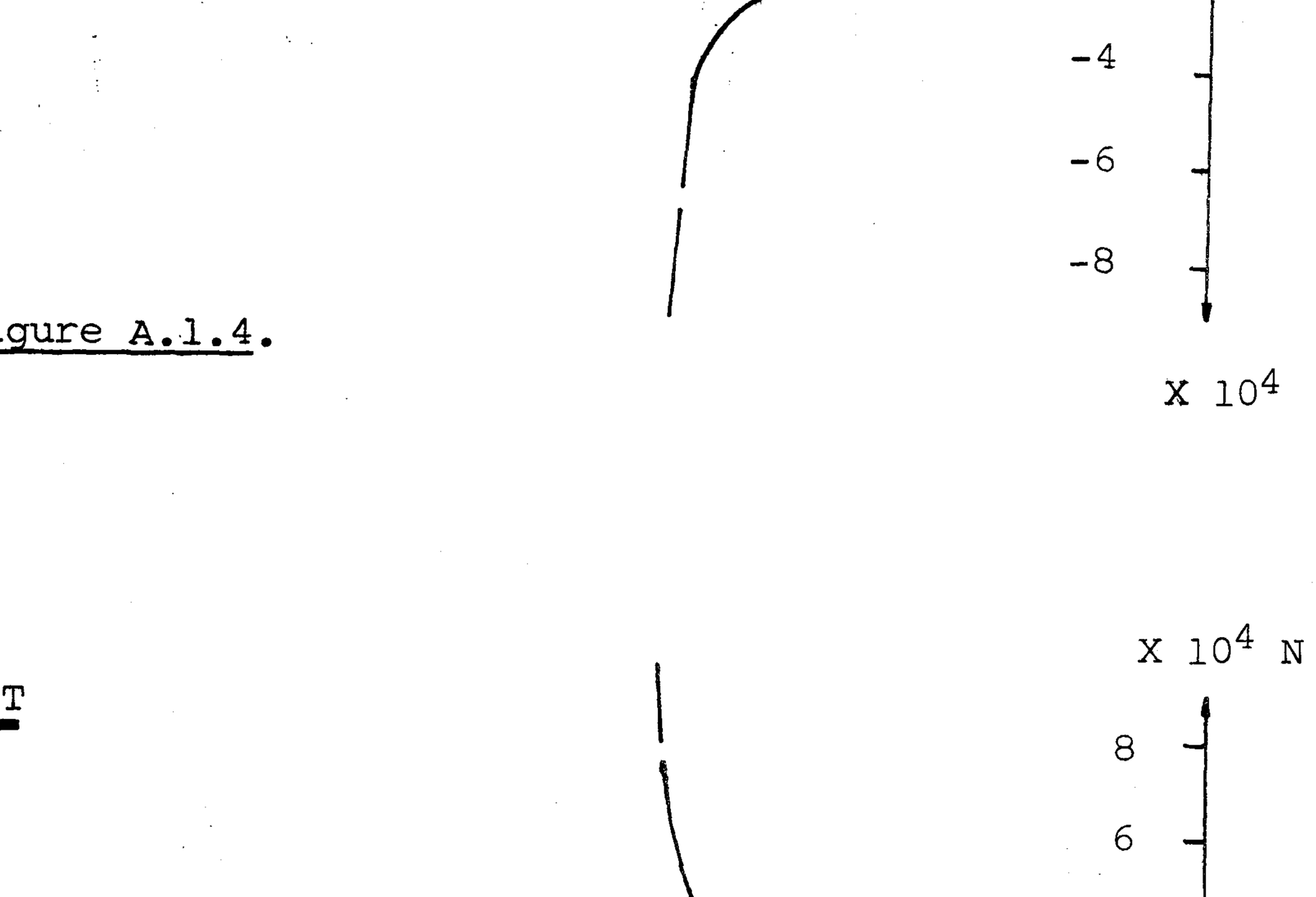

Figure A.1.5.

APPENDIX A2

SOLUTION OF A BESSEL FUNCTION OF THE FIRST KIND

Bessels' differential equation:

$$x^2y'' + xy' + (x^2 + \nu^2)y = 0 \qquad \text{A.2.1}$$

ν - A parameter, any given number.

A.2.1 has a solution of the form:

$$y(x) = \sum_{m=0}^{\infty} C_m x^{m+r} \qquad \text{A.2.2} \quad (C_0 \neq 0)$$

r - Any real number.

From Kreyszig(A1 ,page 127 equation 13):

The solution of equation A.2.1 for integer values of n may be expressed as a summation of powers and factorials.

$$J_n(x) = x^n \sum_{m=0}^{\infty} \frac{(-1)^m x^{2m}}{2^{2m+n}\, m!\, (n+m)!} \qquad \text{A.2.3}$$

and

$$J_{-n}(x) = (-1)^n J_n(x) \qquad \text{A.2.4}$$

The results of solutions to the Besselś' equation are Bessel numbers.

$J_n(x)$ and $J_{-n}(x)$ are particular solutions to the Bessel equation, the n term denotes an integer series.

REFERENCES

A 1 KREYSZIG, E. Advanced engineering mathematics
3rd edition
New York, (Wiley 1972)

ANALYTICAL SOLUTION TO EQUATION 4.7

(Sound power due to blade loading)

$$P_n(R) = \frac{1}{2\pi c R} \sum_{\lambda=-\infty}^{\infty} n Z \Omega T_\lambda \cos\psi - \frac{\Omega Q_\lambda (nZ-\lambda)}{M_t R_{eff}} J_{nZ-\lambda}(nZ M_t \sin\psi) e^{i\lambda\theta} \qquad 4.7$$

LET;

$$A = 2\pi c R$$

$$B = nZ\Omega T_\lambda$$

$$C = (nZ-\lambda)\frac{\Omega_\lambda}{M_t R_{eff}}$$

$$D = nZ M_t$$

Equation 4.7, for constant , may be integrated over a sphere:

$$P_n = \frac{1}{A} \int_0^{2\pi}\int_0^{2\pi} (B\cos\psi - C)(J_k(D\sin\psi)) e^{i\lambda\theta} d\psi d\theta \qquad A.2.5$$

Evaluate inner integral:

$$I_\psi = \int_0^{2\pi} (B\cos\psi - C) J_k(D\sin\psi) \qquad A.2.6$$

A.2.6 may be separated into two parts

$$I\psi = \int_0^{2\pi} B\cos\psi J_k(D\sin\psi) d\psi - \int_0^{2\pi} C J_k(D\sin\psi) d\psi \qquad A.2.7$$

Around 2π the first integral of A.2.7 equals zero

$$I\psi = \int_0^{2\pi} -C J_k(D\sin\psi) d\psi \qquad A.2.8$$

Expand A.2.8, using the factorial approximation of A.2.3:

$$I_\psi = \int_0^{2\pi} -C \left\{ \sum_{r=0}^{\infty} \frac{(-1)^r}{r!\,(k+r)!} \left(\frac{D}{2}\sin\psi\right)^{k+2r} \right\} d\psi$$

$$= \int_0^{2\pi} -C \left\{ \sum_{r=0}^{\infty} \frac{(-1)^r}{r!\ (k+r)!} \ (D/2)^{k+2r} \ \sin^{k+2r}\psi \right\} d\psi$$

$$= \int_0^{2\pi} -C \sum_{r=0}^{\infty} \frac{(-1)^r}{r!\ (k+r)!} \ (D/2)^{k+2r} \cdot \int_0^{2\pi} \sin^{k+2r}\psi \ d\psi \qquad \text{A.2.9}$$

<u>For odd k</u> $\int_0^{2\pi} \sin^{k+2r}\psi \ d\psi = 0$

Where $s = -n, -(n-1), \ldots\ldots, -1, 0, 1, 2, \ldots\ldots, n-1, n.$

Consider $k = 2s$:

$$I_\psi = -C \sum_{r=0}^{\infty} \frac{(-1)^r}{r!\ (2s+r)!} \ (D/2)^{2(s+r)} \int_0^{2\pi} \sin^{2(s+r)}\psi \ d\psi \qquad \text{A.2.10}$$

Equation A.2.11 is a particular representation of a BETA FUNCTION :

$$\beta(m,n) = 2\int_0^{\pi/2} \sin^{2m-1}\psi \cos^{2n-1}\psi \ d\psi \qquad \text{A.2.11}$$

Express $\int_0^{2\pi} \sin^{2(s+r)}\psi \ d\psi$ in the form of a Beta Function

$$2m-1 = 2s + 2r \qquad \text{A.2.11(a)}$$

$$m = s + r + \tfrac{1}{2} \qquad \text{A.2.11(b)}$$

<u>and:</u>

$$\int_0^{2\pi} \sin^{2(s+r)}\psi \ d\psi = 4 \int_0^{\pi/2} \sin^{2(s+r)}\psi \ d\psi \qquad \text{A.2.11(c)}$$

<u>The Beta Function:</u>

$$\beta(s+r+\tfrac{1}{2}, \tfrac{1}{2}) = \frac{(s+r-\frac{1}{2}) \times (s+r) \times \ldots\ldots\ldots \times \frac{1}{2}\,\beta(\frac{1}{2}, \frac{1}{2})}{(s+r)!}$$

Where: $\beta(\frac{1}{2}, \frac{1}{2}) = \pi$ (From A.2.11)

$$\beta(s+r+\tfrac{1}{2}, \tfrac{1}{2}) = \frac{(s+r-\frac{1}{2}) \times (s+r) \times \ldots\ldots\ldots \times \frac{1}{2}}{(s+r) \times \ldots\ldots\ldots\ldots \times 1} \cdot \pi$$

<u>Multiply the top row by two and express as factorials:</u>

$$\beta\,(s+r+\tfrac{1}{2},\ \tfrac{1}{2}) = 4\ \frac{(2s+2r)!}{2^{2s+2r}\ (s+r)!\ (s+r)!}\ .\ \pi \qquad \text{A.2.12}$$

Substitute A.2.11, A.2.11(c) and A.2.10 into A.2.12:

$$I_{\psi} = -4\ C\pi \sum_{r=0}^{\infty} \frac{(-1)^r\ (2s+2r)!}{r!\ (2s+r)!\ (\ (s+r)!\ )^2}\ (D/4)^{2s+2r} \qquad \text{A.2.13}$$

$s = \frac{1}{2}k\ ;\ k = 0,\ 2,\ 4, \ldots\ldots\ldots\ldots,\ N.$

Equation A.2.5 may be re-expressed:

$$P_n(R) = \frac{1}{A} \int_0^{2\pi} I_{\psi} \cos(\lambda\theta)\ d\theta \qquad \text{(Real part of equation A.2.5)}$$

$$= \frac{1}{\lambda A}\ I_u \sin(2\pi\lambda) \qquad \text{A.2.14}$$

Substituting A.2.13 into A.2.14 gives $P_n(R)$, for constant λ

$$P_n(R) = \frac{4\pi C}{\lambda A} \left\{ \sum_{r=0}^{\infty} \frac{(-1)^r}{r!}\ \frac{(2s+2r)!}{(2s+r)!\ (\ (s+r)!\ )^2}\ (D/4)^{2s+2r} \right\} \times \sin(2\pi\lambda) \qquad \text{A.2.15}$$

For steady (θ-invariant) loading.

$$P_n(R) = \frac{8\pi^2 C'}{A'} \left\{ \sum_{r=0}^{\infty} \frac{(-1)^r}{r!}\ \frac{(2s+2r)!}{(2s+r)!\ (\ (s+r)!\ )^2}\ (D/4)^{2s+2r} \right. \qquad \text{A.2.16}$$

For unsteady (θ-variant) loading.

Where: $A' = \dfrac{2\pi\ c\ R}{n\ Z\ \Omega}$

$C' = Q/M_t\ R_{eff}$

$D' = nZ\ M_t$

Equations A.2.15 and A.2.16 have been found to converge for $\lambda = \pm 240$, and have been solved for various casing types, these solutions are found to compare reasonably well with experimentally observed trends, See Chapter 5.

For an explanation of the terms used, see Chapter 4.

The preceeding analysis yields two fundamental results:

i) The sound power due to blade-loading is independent of thrust (see Appendix A.1).

ii) The sound power due to blade-loading is zero in even harmonics.

APPENDIX A3

TIME-UNSTEADY FLOW

and approximation to Sears' function.

Lift and Momentum results developed for steady flow over a thin airfoil have to be modified to account for pulsing flow (i.e. with a rotor potential field pulsing turbulent wakes across the tongue).

The simple Joukowski formula:-

$$L = \rho u \Gamma_o \qquad \text{A.3.1.}$$

has to be modified, and is modified into a lift term incorporating three components.

$$L = L_0 + L_1 + L_2 \qquad \text{A.3.2.}$$

where;

$$L_0 = \rho u \Gamma_o$$

$$L_1 = -\rho \frac{d}{d\tau} \int_{-1}^{1} \gamma_o(x) \; x \; dx$$

$$L_2 = \rho u \int_{1}^{\infty} \gamma(\xi) \, d\xi \, / N\{\xi^2 - 1\}$$

u - convection velocity of air over tongue (airfoil)

Γ - circulation arising from vorticity $\gamma_o(x)$.

$\gamma_o(x)$ - vorticity bound to airfoil that would be produced by gust if the instantaneous velocity were maintained permanently.

x - coordinate along blade, rearward from mid-chord.

$\gamma(\xi)$ - vorticity in wake.

L_o - lift produced if instantaneous velocity and angle of attack were maintained.

L_1 - forces acting on the body in an ideal fluid, when no circulation is produced, because of the reaction of the accelerated fluid masses.

L_2 - contributions to lift from the wake.

The magnitude of overall lift (L) is found to decrease as the frequency of the gusts increase. Thus it is most for zero pulsation and $(-L_1 + L_2)$ must be subtractive.

from: AERODYNAMIC DESIGN OF AXIAL-FLOW COMPRESSORS.

N.A.S.A. N 65-23345-362

Washington 1965

Page 382 - 385 'TIME-UNSTEADY FLOW'.

In the developed analysis it is assumed that the frequency of pulsation will not change over small E.

APPENDIX A4

FINITE FOURIER SERIES

The fourier series:-

$$f(x) = \frac{a_o}{2} + \sum_{k=1}^{\infty} (a_k \cos kx + b_k \sin kx) \qquad \text{A.4.1.}$$

where
$$a_k = \frac{1}{\pi} \int_0^{2\pi} f(x) \cos Kx \, dx. \qquad \text{A.4.2.}$$

$$b_k = \frac{1}{\pi} \int_0^{2\pi} f(x) \sin kx \, dx. \qquad \text{A.4.3.}$$

$$a_o = \frac{1}{\pi} \int_0^{2\pi} f(x) \, dx = 2\bar{x}. \qquad \text{A.4.4.}$$

f(x) here is defined on (O, 2π), but in general may be defined on any arbitrary interval. For a Fourier series to be applicable as an approximation, the function f(x) must satisfy the DIRICHLET conditions:

1. Be absolutely integrable over the interval.
2. Have a finite number of discontinuities.
3. Have a finite number of maxima and minima.

When applying FOURIER analysis to a discrete time series the function f(t) is defined only by a number of discrete points.

The finite fourier series:-

$$f(x) = \frac{a_o}{2} + \sum_{k=1}^{M/2-1} \left(a_k \cos\left(\frac{2\pi}{M} kx\right) + b_k \sin\left(\frac{2\pi}{M} kx\right)\right)$$

$$+ a_{M/2} \cos \pi x \qquad \text{A.4.5.}$$

where f(x) defined over 2π

M observation points. (x = 1, 2, ..., M)

The coefficients are of the same form as A.4.1, A.4.2 and A.4.3.

$$a_k = \frac{2}{M} \sum_{x=1}^{M} f(x) \cos\left(\frac{2\pi}{M} kx\right) \qquad \text{A.4.6.}$$

$$b_k = \frac{2}{M} \sum_{x=1}^{M} f(x) \sin\left(\frac{2\pi}{M} kx\right) \qquad \text{A.4.7.}$$

$$a_o = \frac{1}{M} \sum_{x=1}^{M} f(x) \qquad \text{A.4.8.}$$

$$a_{M/2} = \frac{1}{M} \sum_{x=1}^{M} (-1)^x f(x) \qquad \text{A.4.9.}$$